

NASA Contractor Report 3478

NASA
CR
3478
c. 1

F-15 Rotary Balance Data for an Angle-of-Attack Range of 8° to 90°

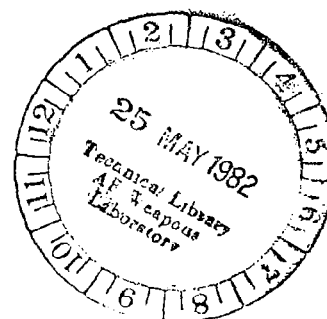
Billy Barnhart

CONTRACT NAS1-16205
MAY 1982

NASA

TECH LIBRARY KAFB, NM
0062242

LOAN COPY: RETURN TO
AFSC TECHNICAL LIBRARY
COLUMBUS, OH, 43208





0062242

NASA Contractor Report 3478

F-15 Rotary Balance Data for an Angle-of-Attack Range of 8° to 90°

Billy Barnhart

*Bihrl Applied Research, Inc.
Jericho, New York*

Prepared for
Langley Research Center
under Contract NAS1-16205



National Aeronautics
and Space Administration

**Scientific and Technical
Information Branch**

1982

SUMMARY

Aerodynamic characteristics obtained in a rotational flow environment, utilizing a rotary balance located in the Langley Spin Tunnel, are presented in plotted form for a 1/12-scale F-15 airplane model. The configurations tested included the build-up of airplane components and the basic airplane with various control deflections. Data are presented for all configurations without analysis for an angle-of-attack range of 8° to 90° , and clockwise and counter-clockwise rotations covering an $\Omega b/2V$ range from 0 to 0.4. Selected configurations are presented over an extended $\Omega b/2V$ range from 0 to 0.9. Analysis of these data is presented in another report.

INTRODUCTION

The NASA Langley Research Center is conducting an investigation to determine the influence of the addition of conformal fuel tanks on the spin and recovery characteristics of the Air Force/McDonnell Douglas F-15 airplane. As a part of this effort, rotary balance wind tunnel force tests of the F-15 airplane were conducted to establish a data base for analysis of the free-spinning model results. A rotary balance is used to measure the forces and moments acting on an airplane while it is subjected to steady rotational flow conditions.

A 1/12-scale model of the F-15 was tested on the rotary balance located in the Langley Spin Tunnel. Data were obtained for the basic airplane with various control settings and for build-up of airplane components. This report presents the data obtained for these configurations without analysis. Reference 1

presents an analysis of the influence of conformal fuel tanks on the aerodynamic characteristics of the basic airplane, as presented herein, as well as the effect of control deflections, component build-up, and predicted spin modes.

SYMBOLS

The units for physical quantities used herein are presented in the International System of Units and U.S. Customary Units. The measurements were all made in the U.S. Customary Units; equivalent dimensions were determined by using the conversion factors found in reference 2.

b	wing span, m (ft)
\bar{c}	mean aerodynamic chord, m (ft)
C_A	axial-force coefficient, $\frac{\text{Axial force}}{qS}$
C_N	normal-force coefficient, $\frac{\text{Normal force}}{qS}$
C_Y	side-force coefficient, $\frac{\text{Side force}}{qS}$
C_ℓ	rolling-moment coefficient, $\frac{\text{Rolling moment}}{qSb}$
C_m	pitching-moment coefficient, $\frac{\text{Pitching moment}}{qS\bar{c}}$
C_n	yawing-moment coefficient, $\frac{\text{Yawing moment}}{qSb}$
q	free-stream dynamic pressure, N/m ² (lb/ft ²)
S	wing area, m ² (ft ²)
V	free-stream velocity, m/sec (ft/sec)
α	angle of attack, deg
β	angle of sideslip, deg
Ω	angular velocity about spin axis, rad/sec

$\frac{\Omega b}{2V}$ spin coefficient, positive for clockwise spin
 δ_a aileron deflection, positive when right aileron is down
 $(\delta_{a_{right}} - \delta_{a_{left}})/2$, deg
 δ_d differential horizontal tail deflection, positive when
right surface is down, $(\delta_{d_{right}} - \delta_{d_{left}})/2$, deg
 δ_e symmetrical horizontal tail deflection, positive when
trailing edge is down, deg
 δ_r rudder deflection, positive when trailing edge is to the
left, deg

Abbreviations:

cg center of gravity
rpm revolutions per minute
SR spin radius
TE trailing edge

TEST EQUIPMENT

A rotary balance measures the forces and moments acting on a model while it is subjected to rotational flow conditions. The historical background for this apparatus is discussed in reference 3. A photograph and sketch of the rotary balance apparatus installed in the Langley Spin Tunnel are shown in figures 1 and 2, respectively. The system's rotary arm, which rotates about a vertical axis at the tunnel center, is supported by a horizontal boom and is driven by a motor mounted external to the test section.

The test model is mounted on a strain gauge balance affixed to the bottom of the rotary balance apparatus. Controls located outside of the tunnel are used to activate motors on the rig, which position the model to the desired attitude. The angle-of-attack range of the rig is 0° to 90° , and the sideslip angle range is ± 15 degrees. Spin radius and lateral displacement motors are used to position the moment center of the balance on, or a specific distance from, the spin axis. (This is done for each combination of angle of attack and sideslip angle.) It is customary to mount the balance to the model such that its moment center is at the location about which the aerodynamic moments are desired. Electrical current from the balance and to the motors on the rig is conducted through slip-rings located in the rig head. Figure 2 shows how the rig is positioned in angle of attack and sideslip.

The rig is capable of rotating up to 90 rpm in either direction. A range of $\frac{\Omega b}{2V}$ values can be obtained by adjusting rotational speed and/or tunnel air flow velocity. (Static aerodynamic forces and moments are obtained when $\Omega=0$.)

A NASA six-component strain gauge balance, mounted inside the model, is used to measure the normal, lateral, and longitudinal forces, and the yawing, rolling, and pitching moments acting about the model body axis.

The data acquisition, reduction, and presentation system is composed of a 12-channel scanner/voltmeter, a mini-computer, a plotter, and a CRT display. This equipment permits data to

be presented via on-line digital print-outs and/or graphical plots.

TEST PROCEDURES

Rotary aerodynamic data are obtained in two steps. First, the inertial forces and moments (tares) acting on the model at different attitudes and rotational speeds are measured. To accomplish this, the model is enclosed in a sealed spherical structure, which rotates with the model without touching it. In this manner, the air immediately surrounding the model is constrained to rotate with it, thus eliminating any aerodynamic forces and moments as would be present if the model were moving through a stationary air mass. As the rig is rotated at the desired attitude and rate, the inertial forces and moments generated by the model are measured and stored on magnetic tape for later use.

The second step is to record force and moment data with the air on and with the enclosure removed. The tares, measured in step one, are then subtracted from these data, leaving only the aerodynamic forces and moments, which are converted to coefficient form and stored on magnetic tape.

MODEL

A 1/12-scale model of the Air Force/McDonnell Douglas F-15 fighter airplane was constructed of balsa and plywood. A three-view drawing of the model is shown in figure 3, dimensional characteristics of the basic model are listed in Table I, and a photo-

graph of the model installed on the rotary balance located in the Langley Spin Tunnel is presented in figure 1.

The model was constructed such that the various airplane components were removable for component build-up tests. The model control surfaces could be set at any position prior to testing. The maximum deflections for the control surfaces were:

Rudder, deg	30 right, 30 left
Horizontal tail (TE)	25 up, 15 down
Aileron	20 up, 20 down

TEST CONDITIONS

The tests were conducted in the spin tunnel at a free-stream velocity of 7.62 m/sec (25 ft/sec), which corresponds to a Reynolds number of approximately 211,000 based on model wing chord. All the configurations were tested through an angle-of-attack range of 8° to 90° , unless noted otherwise in Table II. The component build-up tests were all performed at a zero sideslip angle, while the basic airplane tests were performed at both zero and ten degrees sideslip angles. For all tests, the spin axis passed through the full-scale airplane nominal cg location for angles of attack above 30° . For angles of attack below 35° , the spin axis was set 0.28 $b/2$ forward of the cg location. For each angle of attack, data were obtained for $\frac{\Omega b}{2V}$ values of 0.1, 0.2, 0.3, and 0.4 in both clockwise and counter-clockwise directions, as well as for $\frac{\Omega b}{2V} = 0$ (static value). In addition, data were obtained for an $\frac{\Omega b}{2V}$ range through 0.9

for selected configurations.

DATA PRESENTATION

Table II identifies the configurations tested and the corresponding appendix figure numbers which present the aerodynamic data. The body-axis aerodynamic coefficients, plotted as a function of $\frac{\Omega b}{2V}$, are presented for each configuration in six sequentially numbered figures in the following order: C_n , C_ℓ , C_m , C_N , C_Y , C_A . Each figure, in turn, consists of four pages which present the subject aerodynamic coefficient vs. $\frac{\Omega b}{2V}$ for the following angles of attack and spin radii, unless noted otherwise in Table II.

- a) $\alpha = 8, 10, 12, 14, 16$ deg SR = 0.28 b/2
- b) $\alpha = 18, 20, 25, 30, 35$ deg SR = 0.28 b/2
- c) $\alpha = 30, 35, 40, 45, 50$ deg SR = 0
- d) $\alpha = 55, 60, 70, 80, 90$ deg SR = 0

All the moment data are presented for a cg position of $0.26\bar{c}$.

REFERENCES

1. Barnhart, B.: Analysis of Rotary Balance Data for the F-15 Airplane Including the Effect of Conformal Fuel Tanks. NASA CR-3479, 1982.
2. Standard for Metric Practice. E 380-79, American Society for Testing and Materials, c. 1980.
3. Bihrlle, William, Jr.; Bowman, James S., Jr.: The Influence of Wing, Fuselage, and Tail Design on Rotational Flow, Journal of Aircraft, Vol. 18, November 1981.

TABLE I.- DIMENSIONAL CHARACTERISTICS OF THE BASIC MODEL

Overall length, m (ft)	1.59 (5.21)
Wing:	
Area, m ² (ft ²)	0.39 (4.16)
Span, m (ft)	1.09 (3.57)
Mean aerodynamic chord, m (ft)	0.41 (1.33)
Leading edge of \bar{c} , distance rearward of leading edge of theoretical root chord, m (ft)	0.22 (0.71)
Aspect ratio	3.01
Taper ratio	0.25
Leading edge sweep, deg	45
Dihedral, deg	-1
Incidence, deg	0
Airfoil section:	
Root	NACA 64A006.6
Tip	NACA 64A203
Ailerons:	
Area (each), m ² (ft ²)	0.009 (0.092)
Span (percent b/2)	25.3
Horizontal tails:	
Area (each), m ² (ft ²)	0.036 (0.39)
Span (each), m (ft)	0.21 (0.68)
Mean aerodynamic chord, m (ft)	0.21 (0.69)
Aspect ratio	2.05
Taper ratio	0.34
Leading edge sweep, deg	50
Dihedral, deg	0
Hinge-line location, percent root chord	60.9
Airfoil section:	
Root	NACA 0005.5-64 (Mod)
Tip	NACA 0002.5-64
Vertical tails:	
Area (each), m ² (ft ²)	0.04 (0.43)
Span, m (ft)	0.26 (0.86)
Taper ratio	0.27
Leading edge sweep, deg	36.57
Airfoil section:	
Root	NACA 0005-64
Tip	NACA 0003.5-64
Rudders:	
Area (each), m ² (ft ²)	0.006 (0.069)
Hinge-line location, percent chord	71.75

TABLE II.- CONFIGURATIONS TESTED AND FIGURE INDEX
 (Unless noted otherwise, all configurations tested through $\alpha = 8$ to 90° .)

FIGURE NO.	CONFIGURATION	β deg	δ_e deg	δ_d deg	δ_a deg	δ_r deg	REMARKS
A1-A6	Body alone	0	off	off	off	off	
A7-A12	Body, wing	↓	↓	↓	0	↓	
A13-A18	Body, wing, vertical tail	↓	↓	↓	↓	0	
A19-A24	Body, wing, horizontal tail	↓	0	0	↓	↓	
A25-A30	Basic	↓	↓	↓	↓	↓	*
A31-A36	↓	+10	↓	↓	↓	↓	
A37-A42	↓	-10	↓	↓	↓	↓	
A43-A48	↓	0	-25	↓	↓	↓	* $\alpha = 30$ to 90° only
A49-A54	↓	+10	↓	↓	↓	↓	* ↓
A55-A60	↓	0	0	+6	↓	↓	
A61-A66	↓	+10	↓	↓	↓	↓	
A67-A72	↓	0	↓	+11	↓	↓	
A73-A78	↓	+10	↓	↓	↓	↓	
A79-A84	↓	0	↓	+6	+20	↓	* $\alpha = 30$ to 90° only
A85-A90	↓	+10	↓	↓	↓	↓	* ↓
A91-A96	↓	0	↓	↓	↓	-15	
A97-A102	↓	+10	↓	↓	↓	↓	
A103-A108	↓	0	↓	-6	-20	+30	
A109-A114	↓	+10	↓	↓	↓	↓	↓

* Not tested at $\alpha = 35^\circ$ and 45° with $SR=0$.

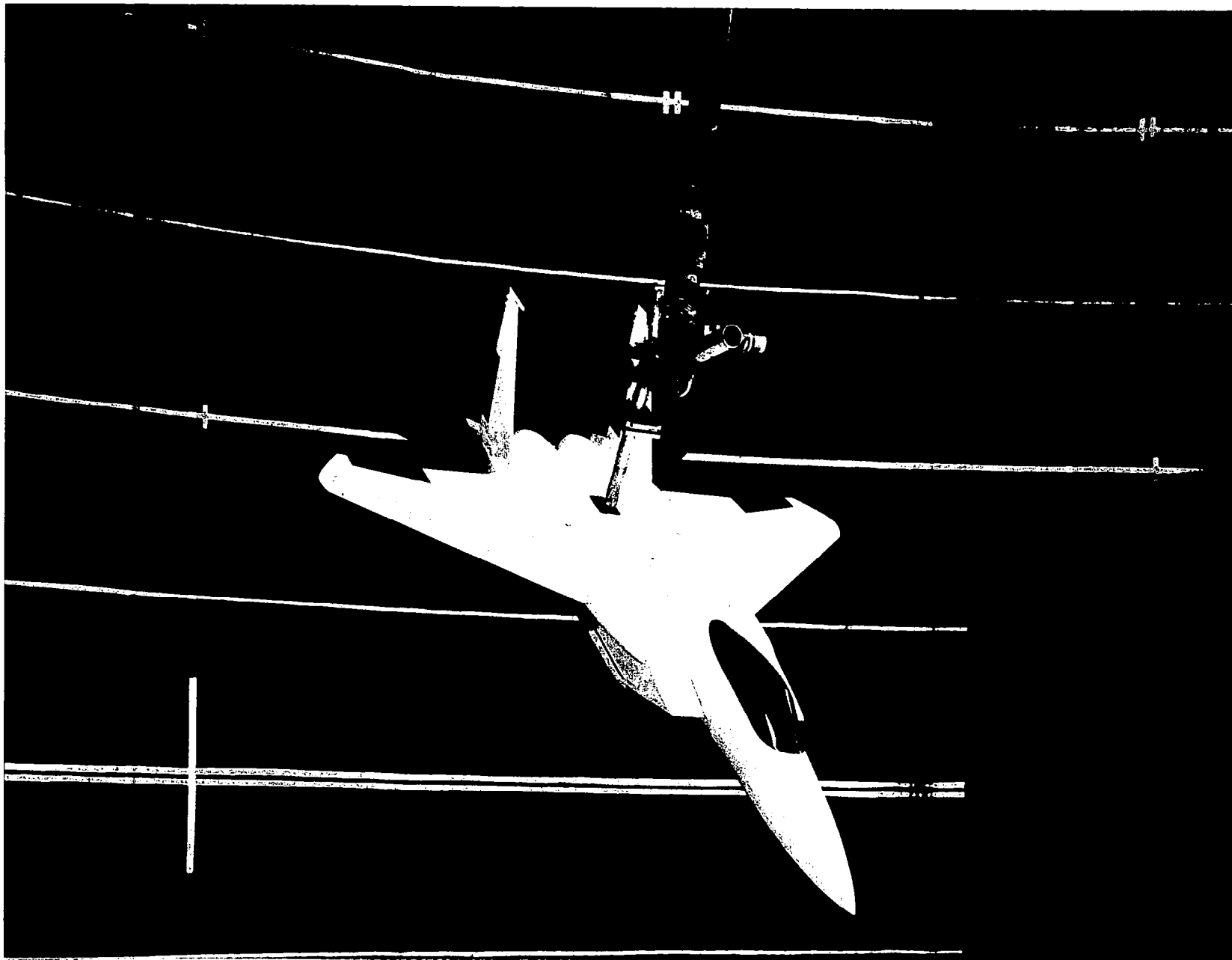
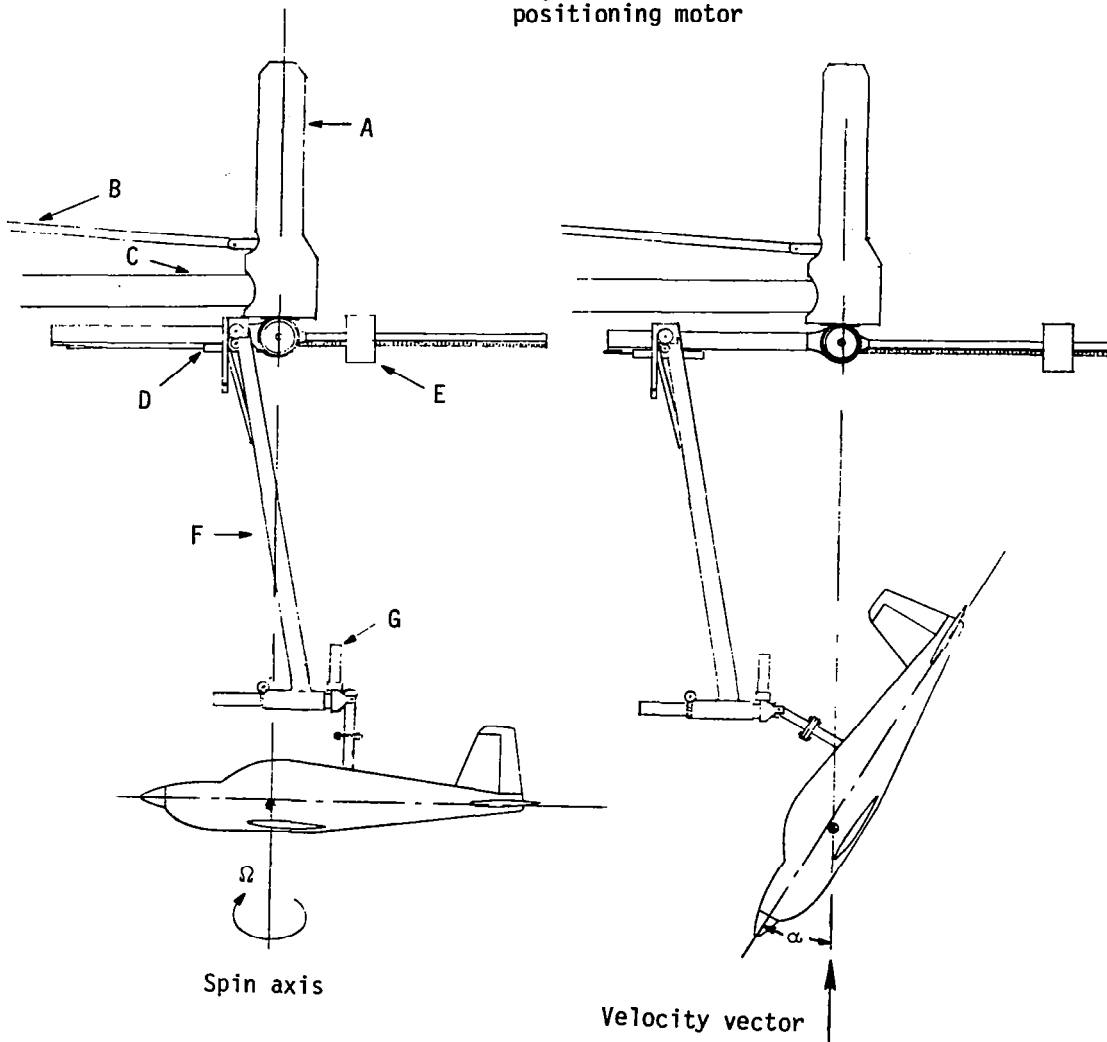


Figure 1.- Photograph of 1/12-scale model installed on
rotary balance apparatus.

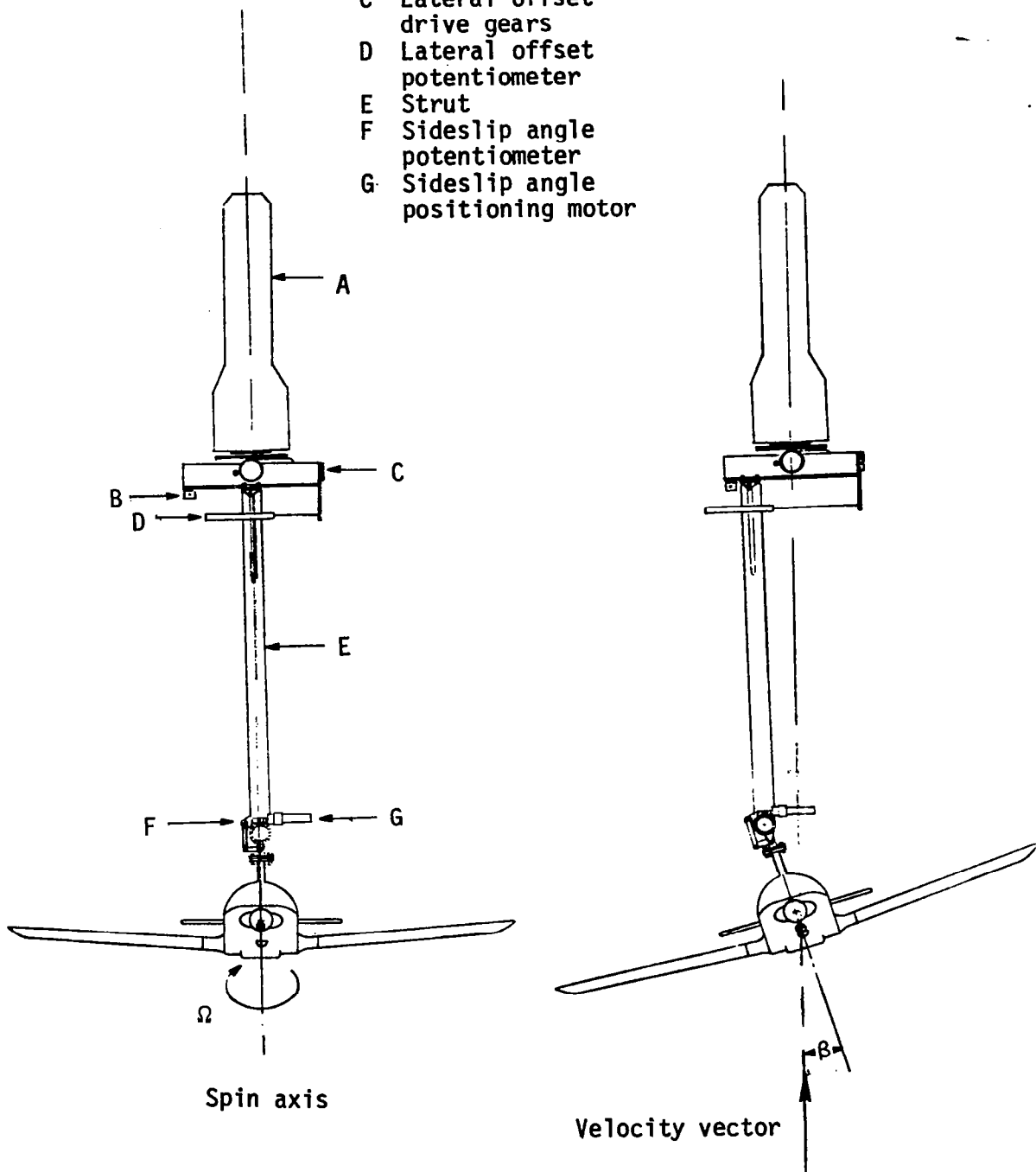
- A Slip ring housing
- B Drive shaft
- C Support boom
- D Spin radius offset potentiometer
- E Counterweight
- F Strut
- G Angle of attack positioning motor



(a) Side view of model.

Figure 2.- Sketch of rotary balance apparatus.

- A Slip ring housing
- B Spin radius offset potentiometer
- C Lateral offset drive gears
- D Lateral offset potentiometer
- E Strut
- F Sideslip angle potentiometer
- G Sideslip angle positioning motor



(b) Front view of model.

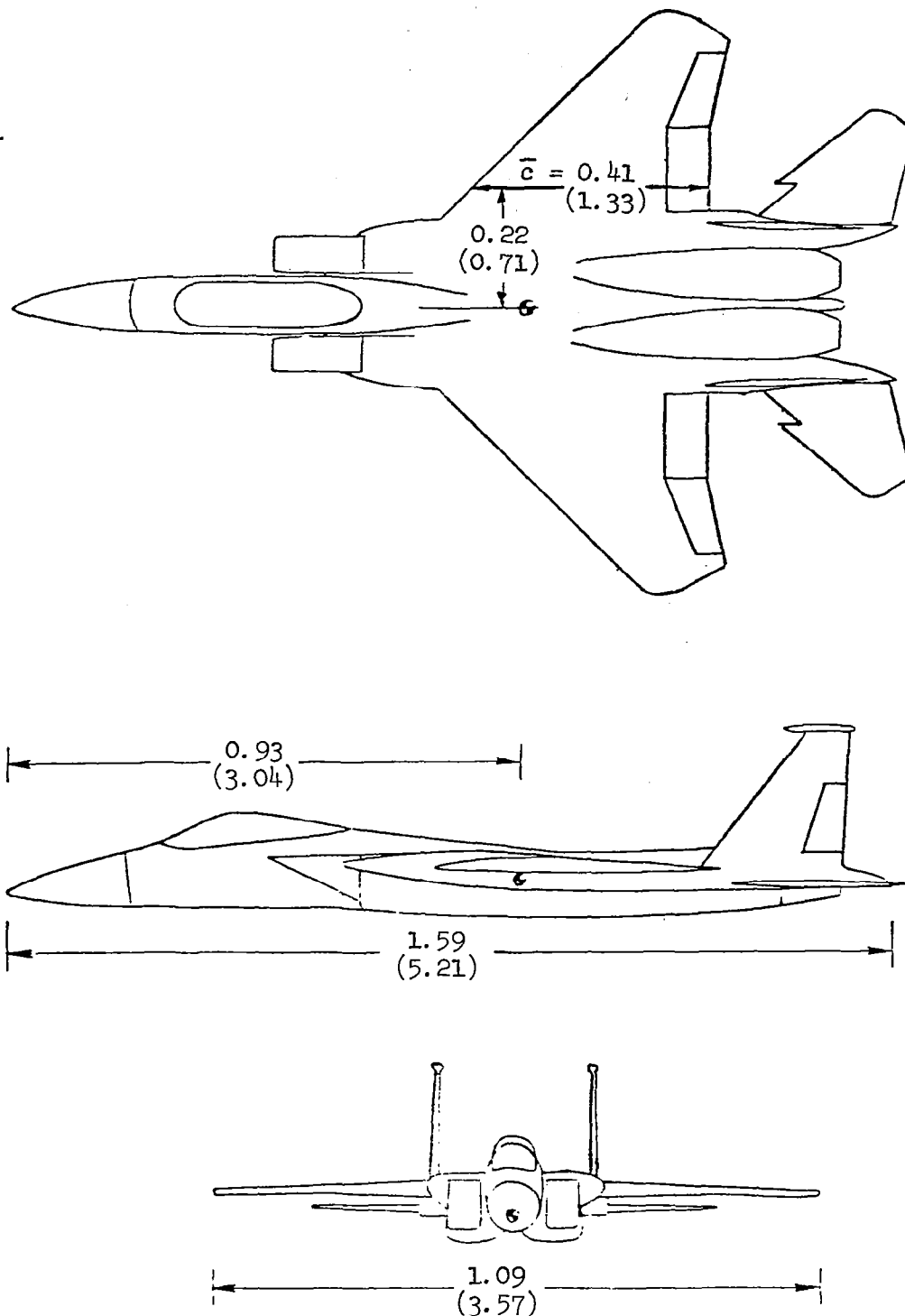
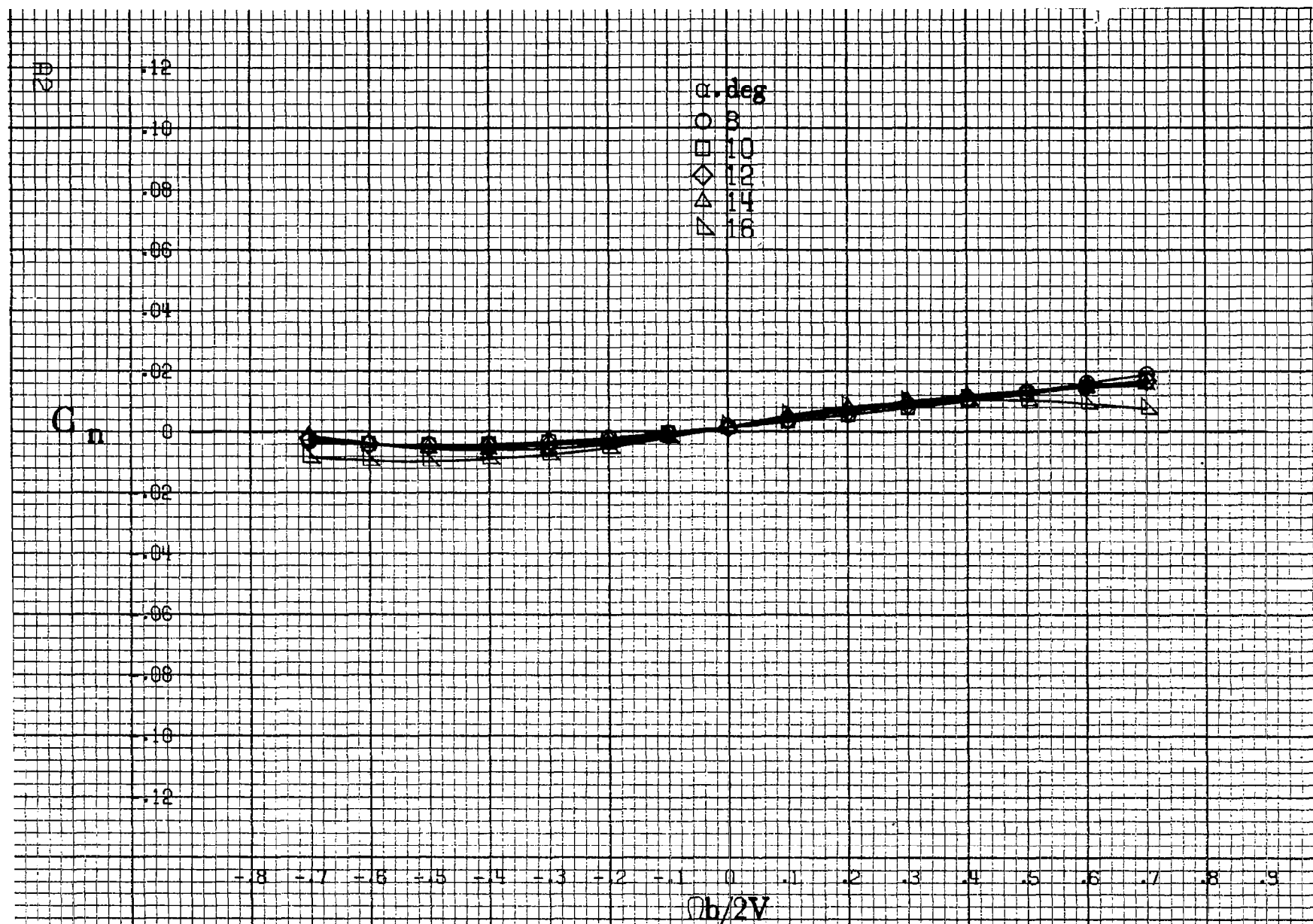


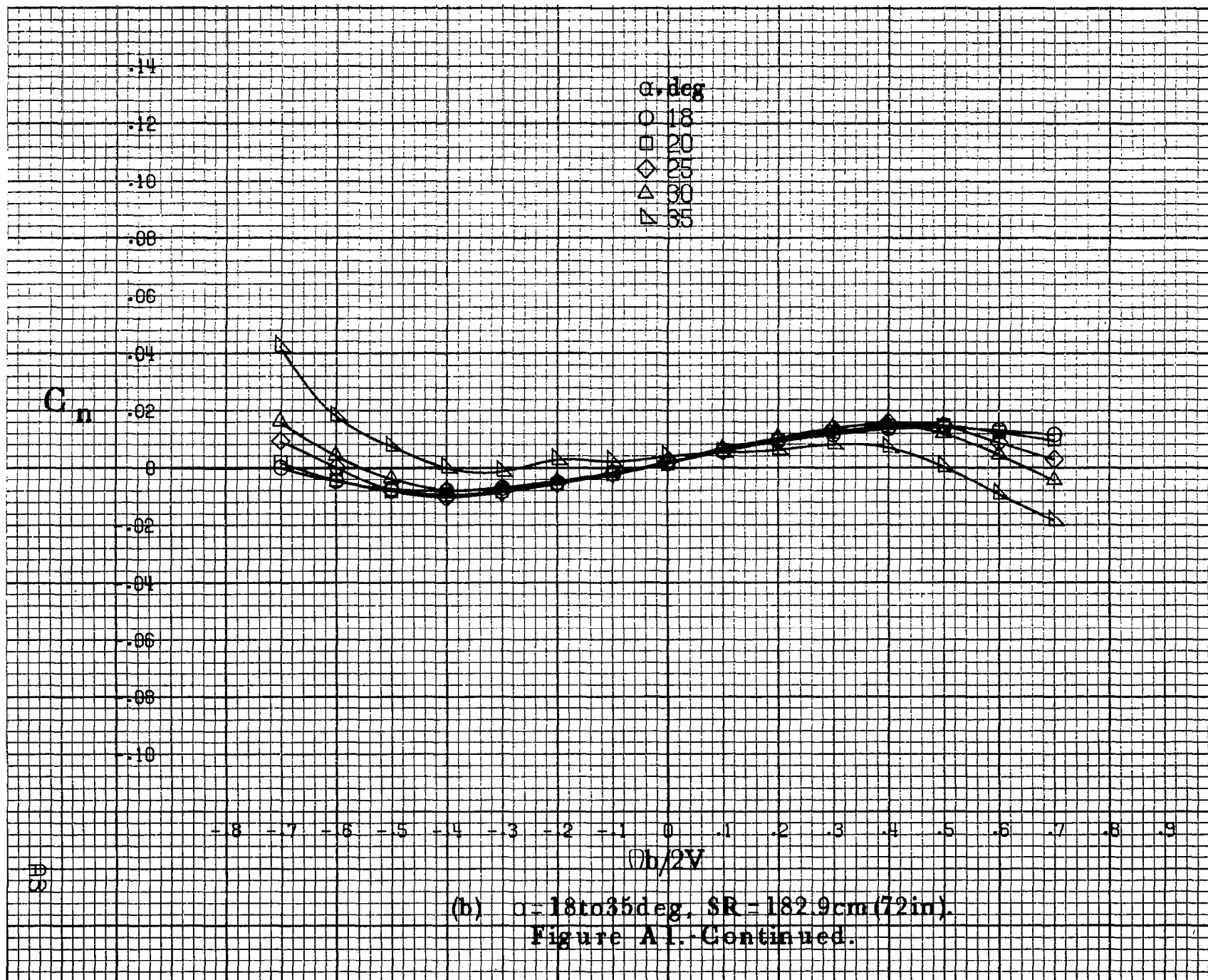
Figure 3.- Three-view sketch of 1/12-scale model. Dimensions are given in meters(feet).

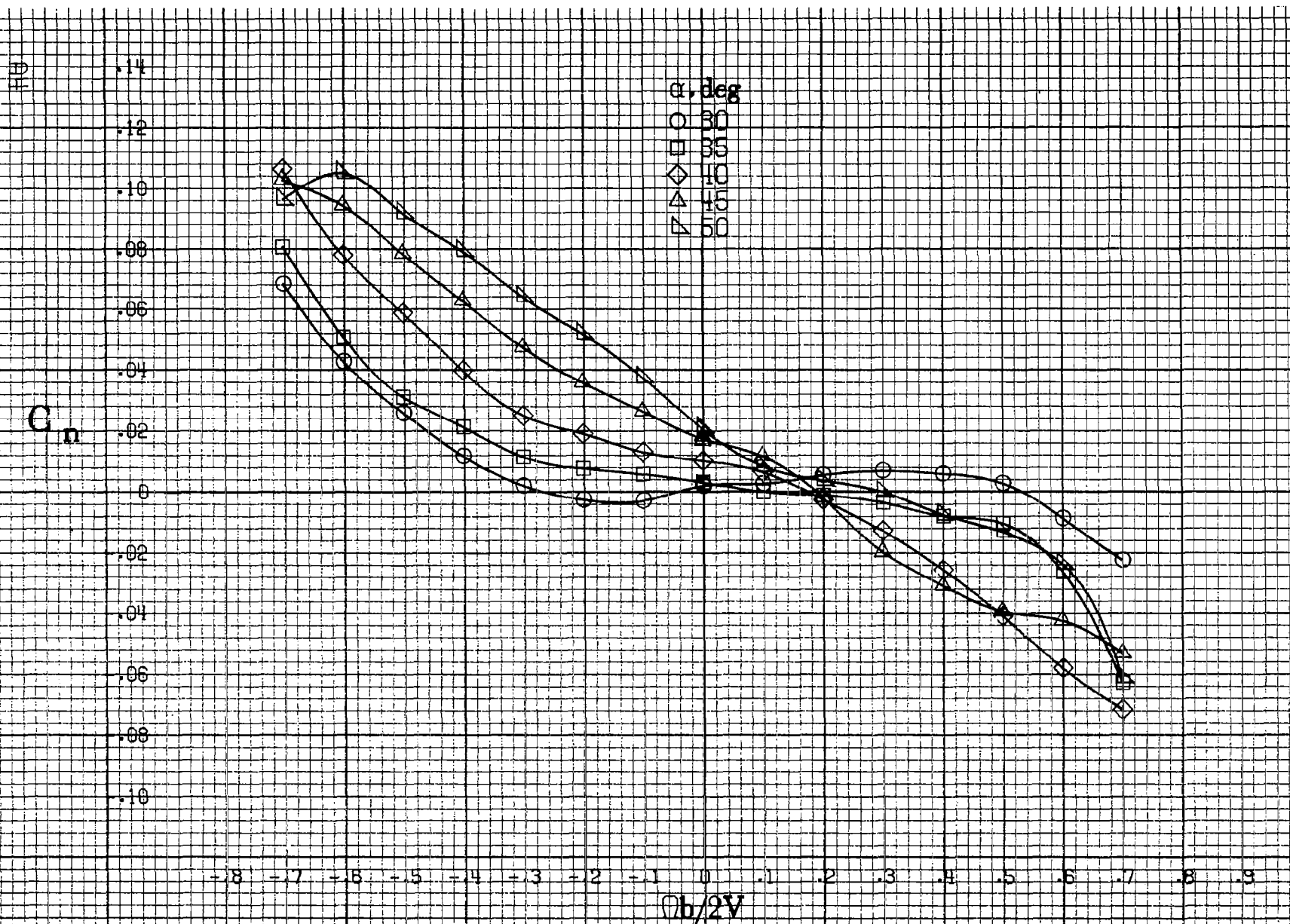
APPENDIX



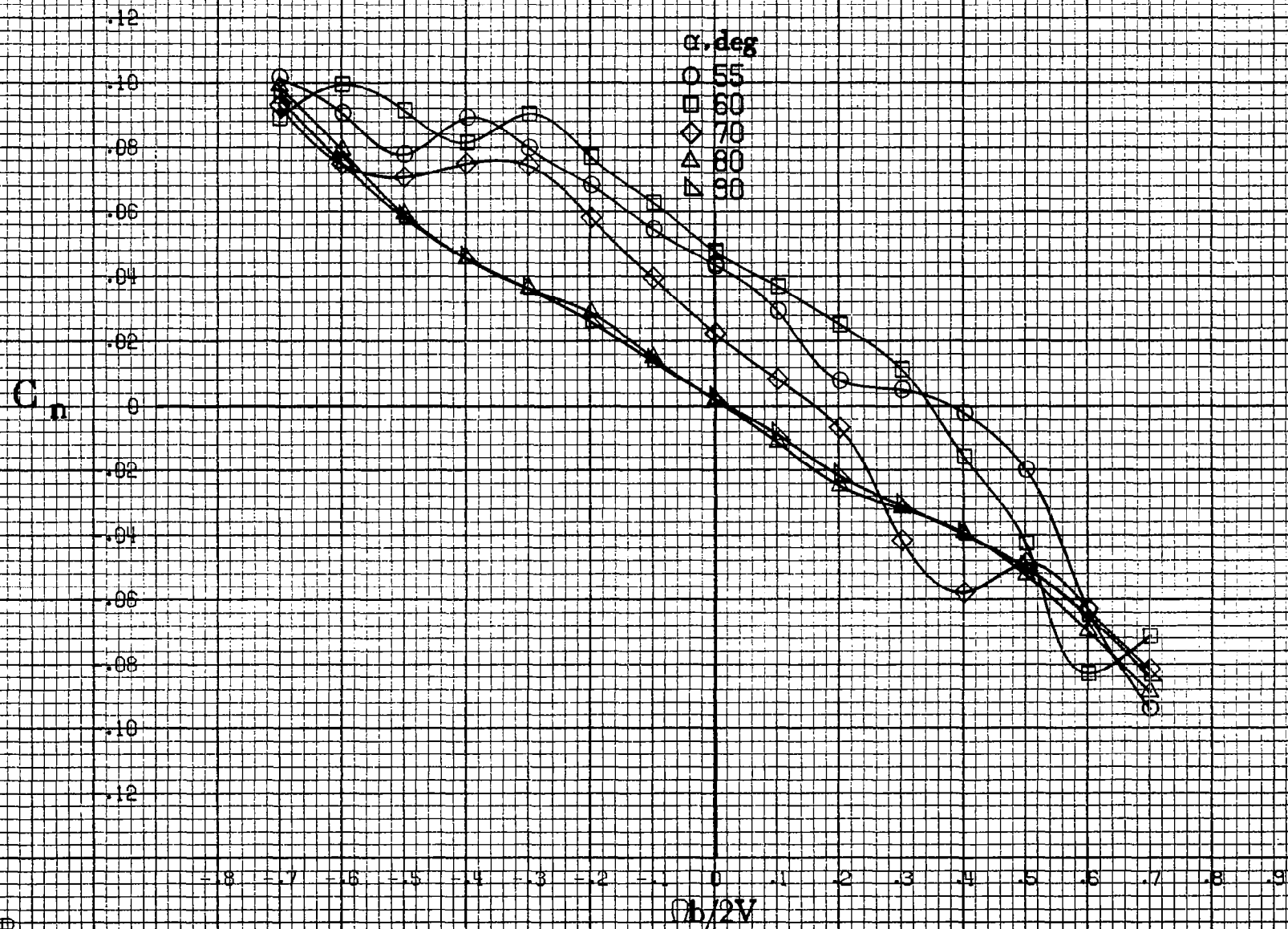
(a) $\alpha = 8$ to 16° , $SR = 182.9\text{cm (72in)}$.

Figure A1. Effect of rotation rate and angle of attack on yawing-moment coefficient for body alone configuration. $\delta_e = 0^\circ$, $\delta_a = 0^\circ$, $\delta_r = 0^\circ$, $\beta = 0^\circ$.



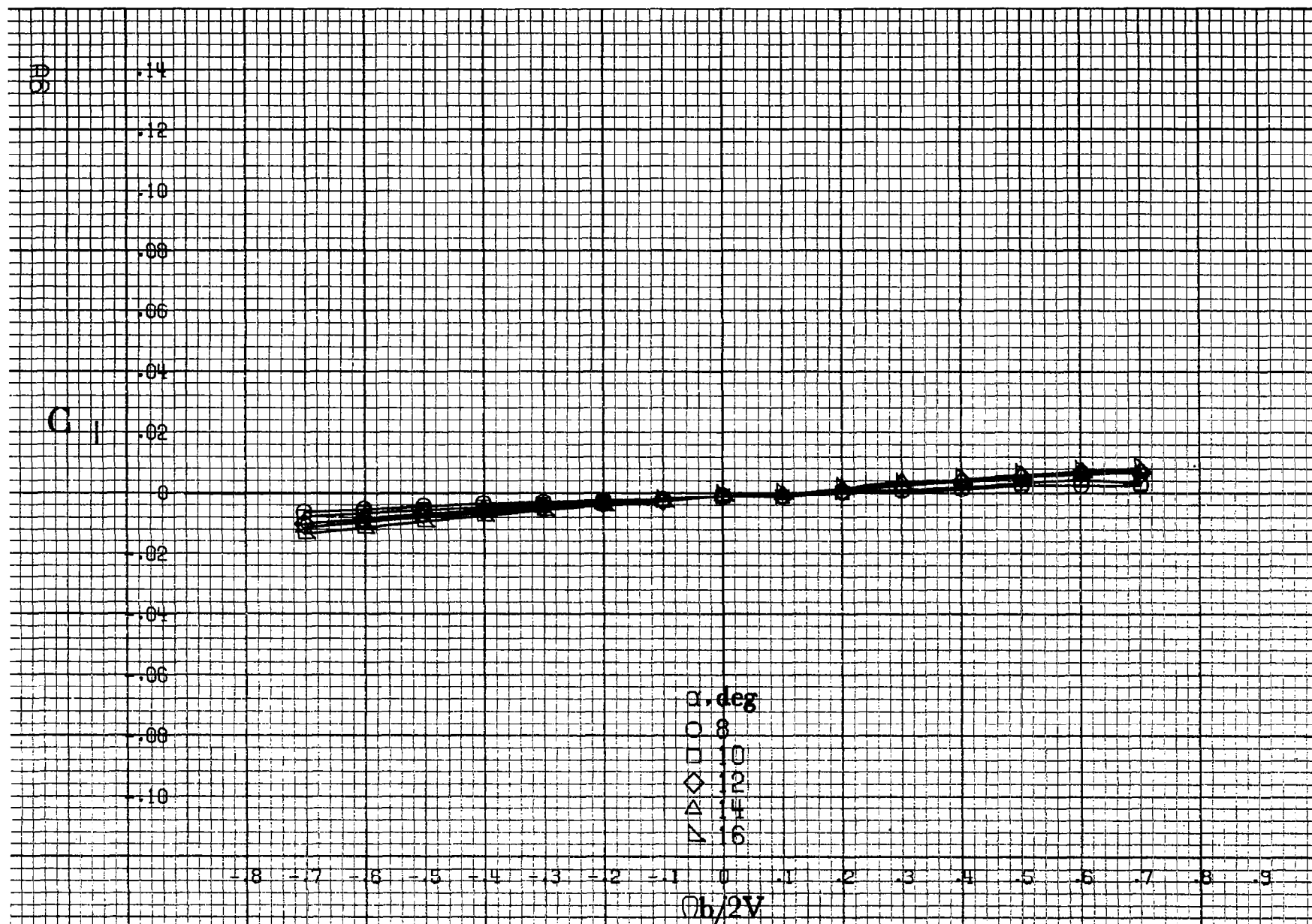


(c) $\alpha=30$ to 50 deg, $SR=0$.
Figure A1. Continued.



(d) $\alpha = 55$ to 90 deg, $SR = 0$.

Figure A1.-Concluded.



(a) $\alpha = 8$ to 16 deg, $SR = 182.9$ cm (72 in).

Figure A2: Effect of rotation rate and angle of attack on rolling-moment coefficient for body alone configuration. $\delta_e = 0^\circ$, $\delta_a = 0^\circ$, $\delta_r = 0^\circ$, $\beta = 0^\circ$.

C_1

.14
.12
.10
.08
.06
.04
0
-.02
-.04
-.06
-.08
-.10

-8 -7 -6 -5 -4 -3 -2 -1 0 .1 .2 .3 .4 .5 .6 .7 .8 .9

α, deg
○ 18
□ 20
◇ 25
△ 30
▽ 35

$\phi h/2V$

(b) $\alpha = 18 \text{ to } 35 \text{ deg}$, SR = 182.9 cm (72 in).
Figure A2.-Continued.

88

C

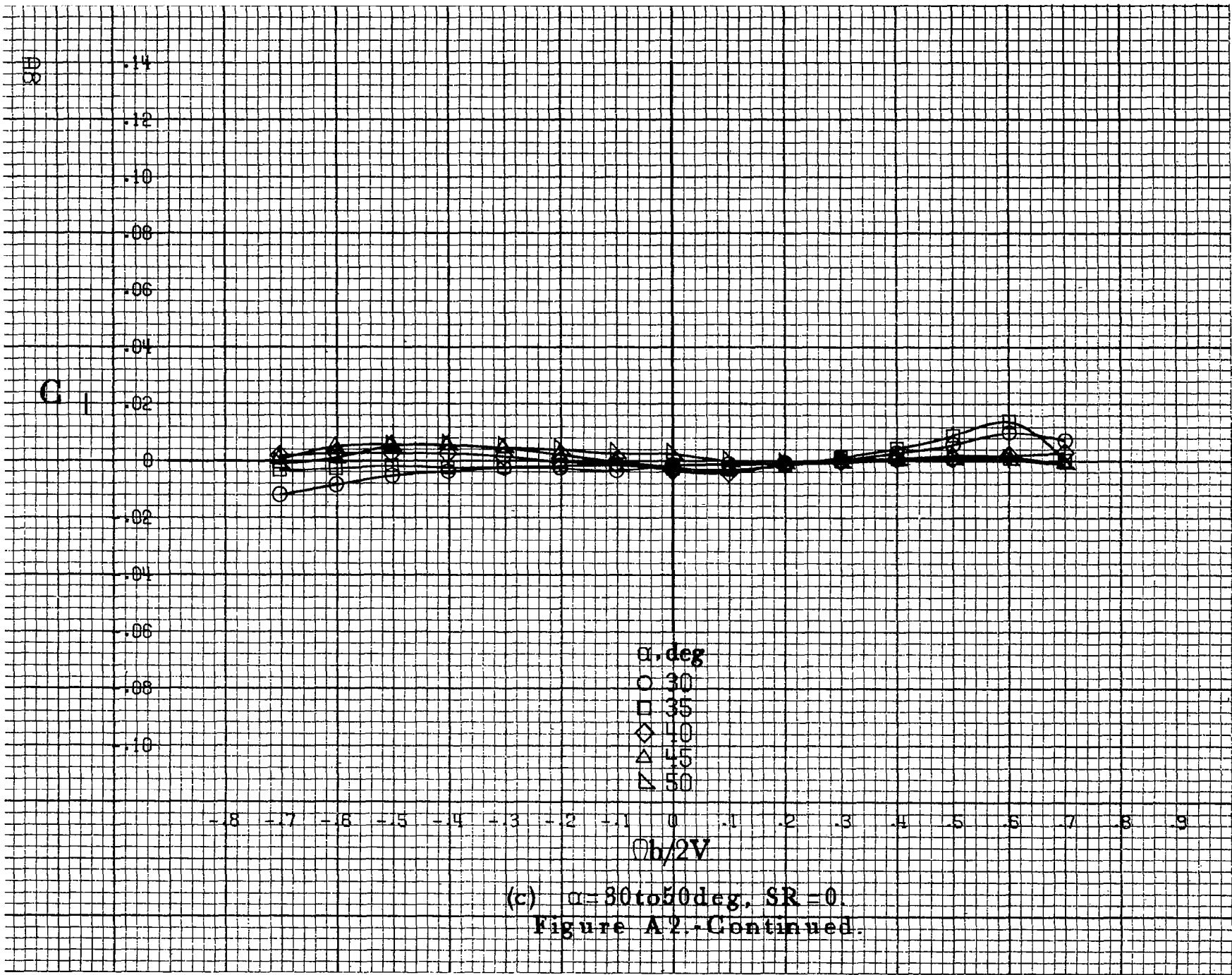
.14
.12
.10
.08
.06
.04
.02
0
-.02
-.04
-.06
-.08
-.10

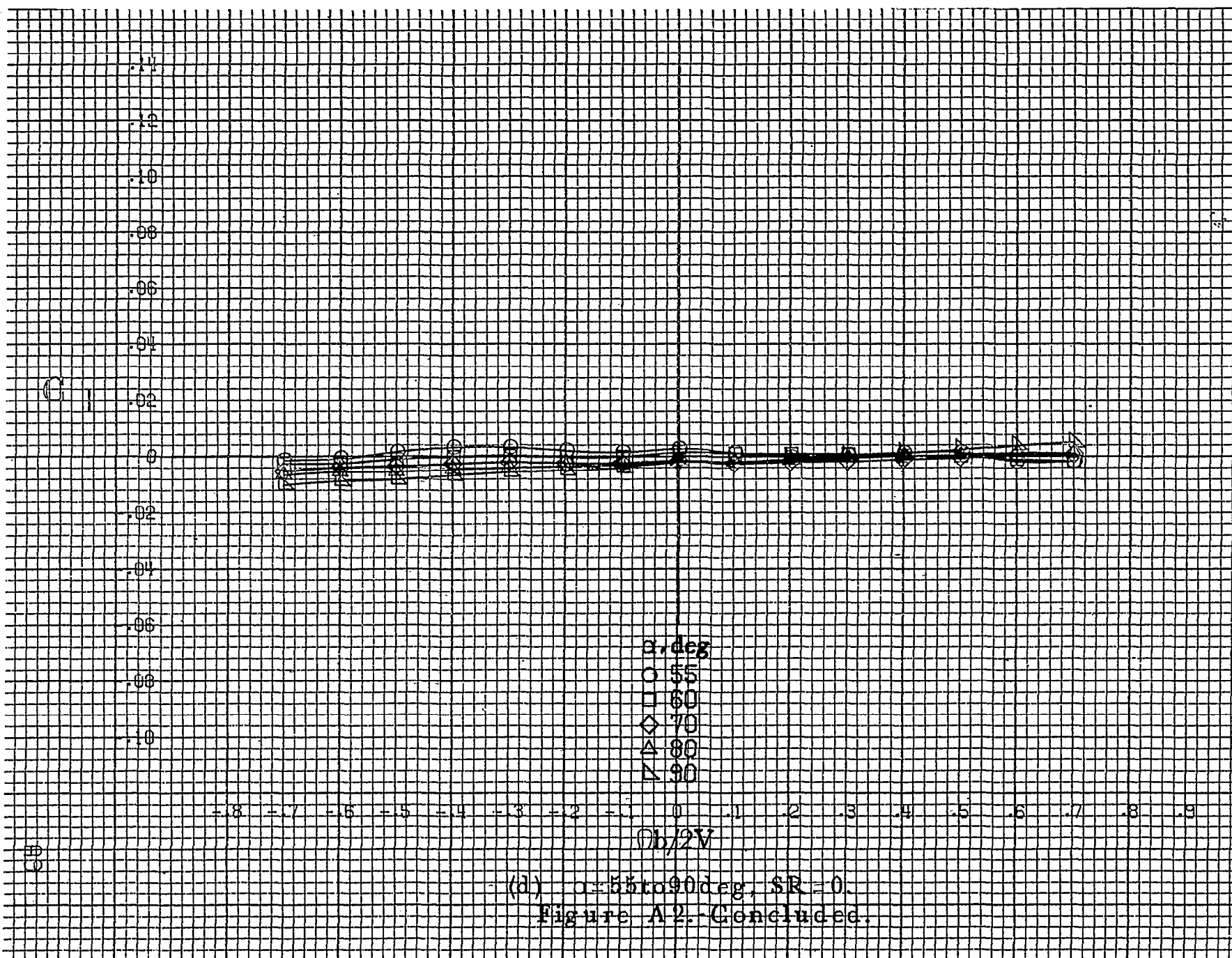
-8 -7 -6 -5 -4 -3 -2 -1 0 .1 .2 .3 .4 .5 .6 .7 8 9

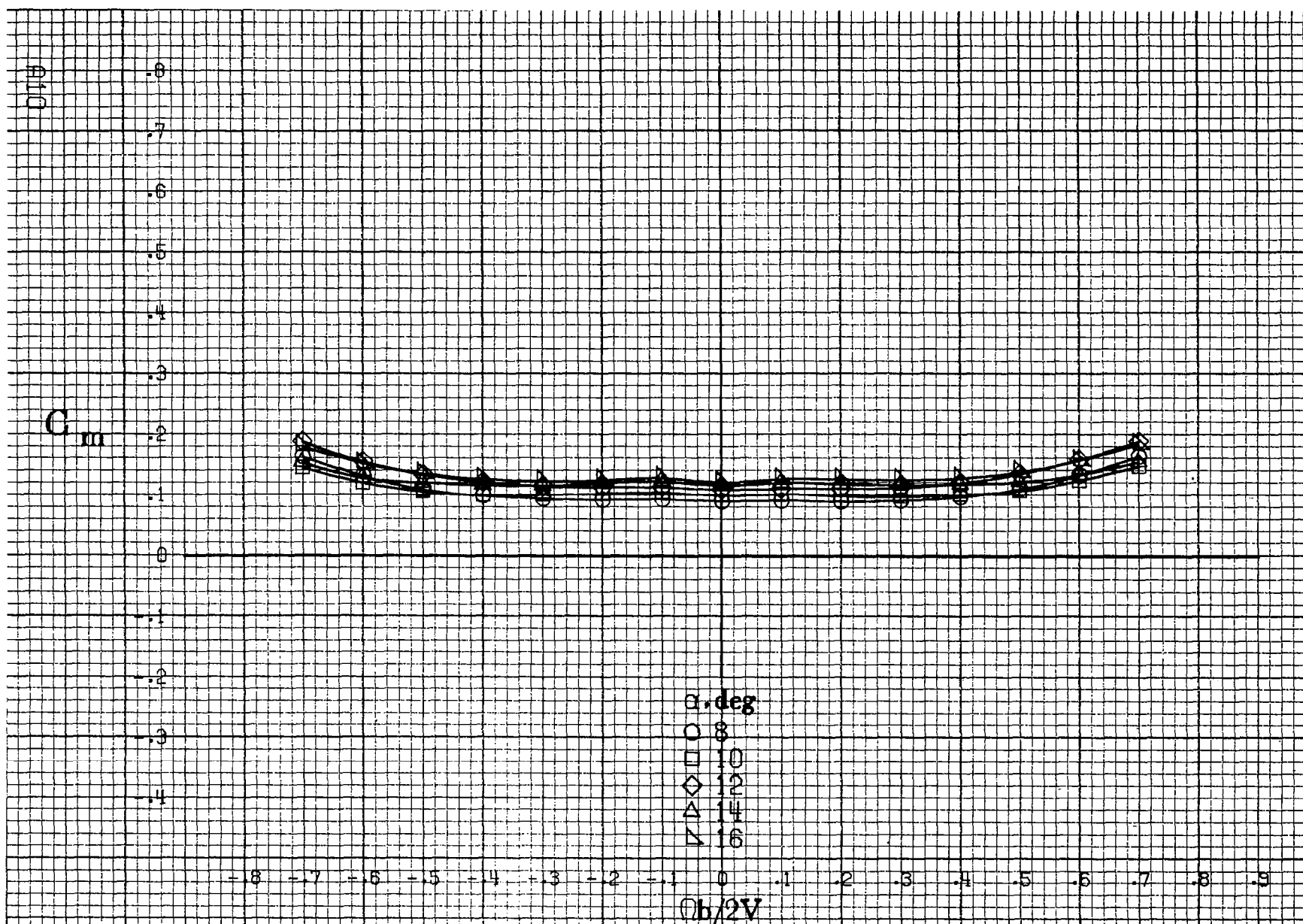
α, deg
○ 30
□ 35
◇ 40
△ 45
▽ 50

$Ob/2V$

(c) $\alpha=30\text{ to }50\text{ deg. SR}=0.$
Figure A2.-Continued.







(a) $\alpha = 8$ to 16 deg, $SR = 182.9 \text{ cm (72 in)}$.

Figure A3: Effect of rotation rate and angle of attack on pitching-moment coefficient for body alone configuration. $\delta_e = 0^\circ$, $\delta_a = 0^\circ$, $\delta_r = 0^\circ$, $\beta = 0^\circ$.

C_m

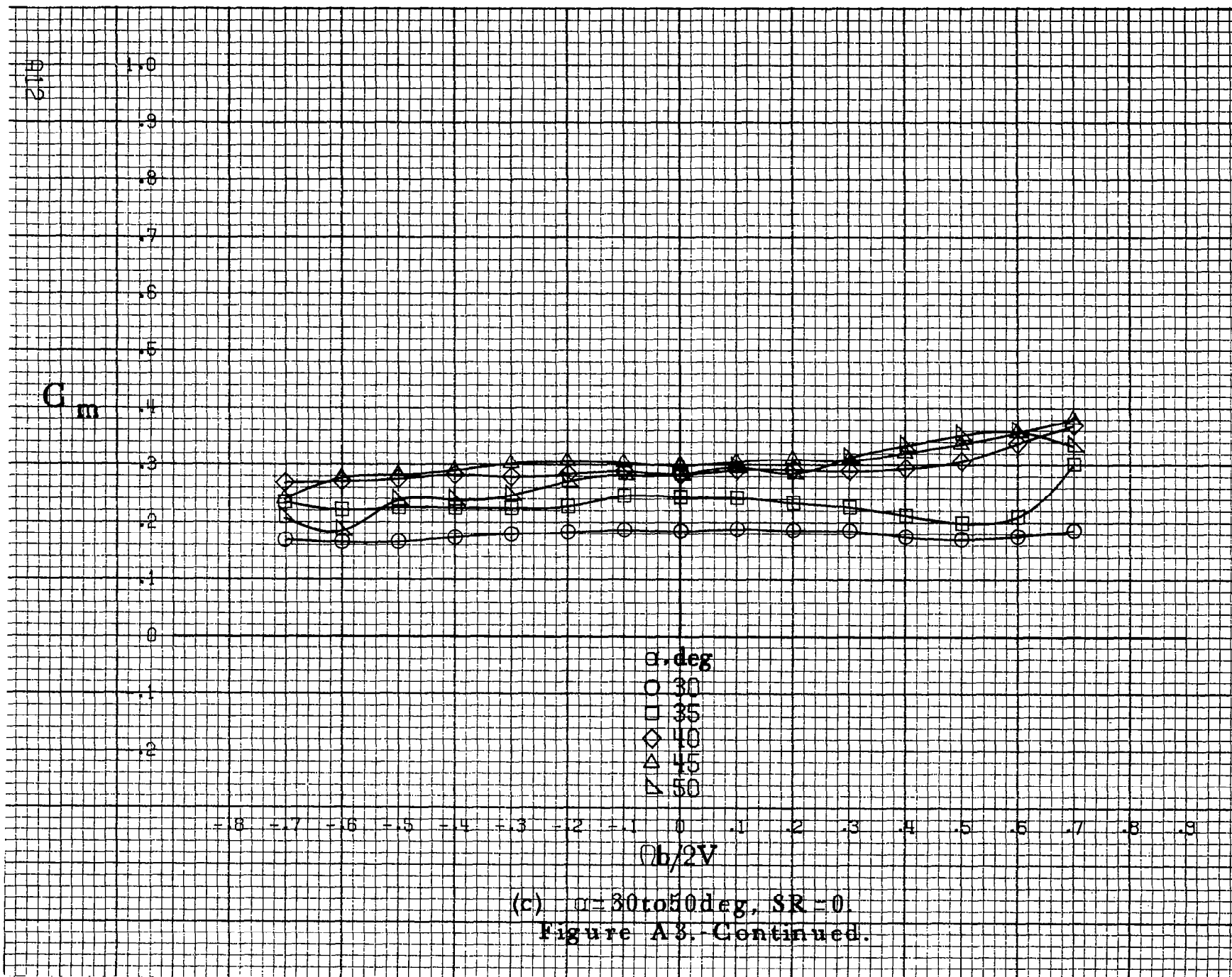
.9
.8
.7
.6
.5
.4
.3
.2
.1
0
-.1
-.2
-.3

-0.8 -0.7 -0.6 -0.5 -0.4 -0.3 -0.2 -0.1 0 0.1 0.2 0.3 0.4 0.5 0.6 0.7 0.8 0.9

α , deg
○ 18
□ 20
◇ 25
△ 30
▽ 35

$b/2V$

(b) $\alpha = 18$ to 35 deg, $SR = 182.9$ cm (72 in).
Figure A3.-Continued.



C_m

α, deg

○ 55

□ 60

◇ 70

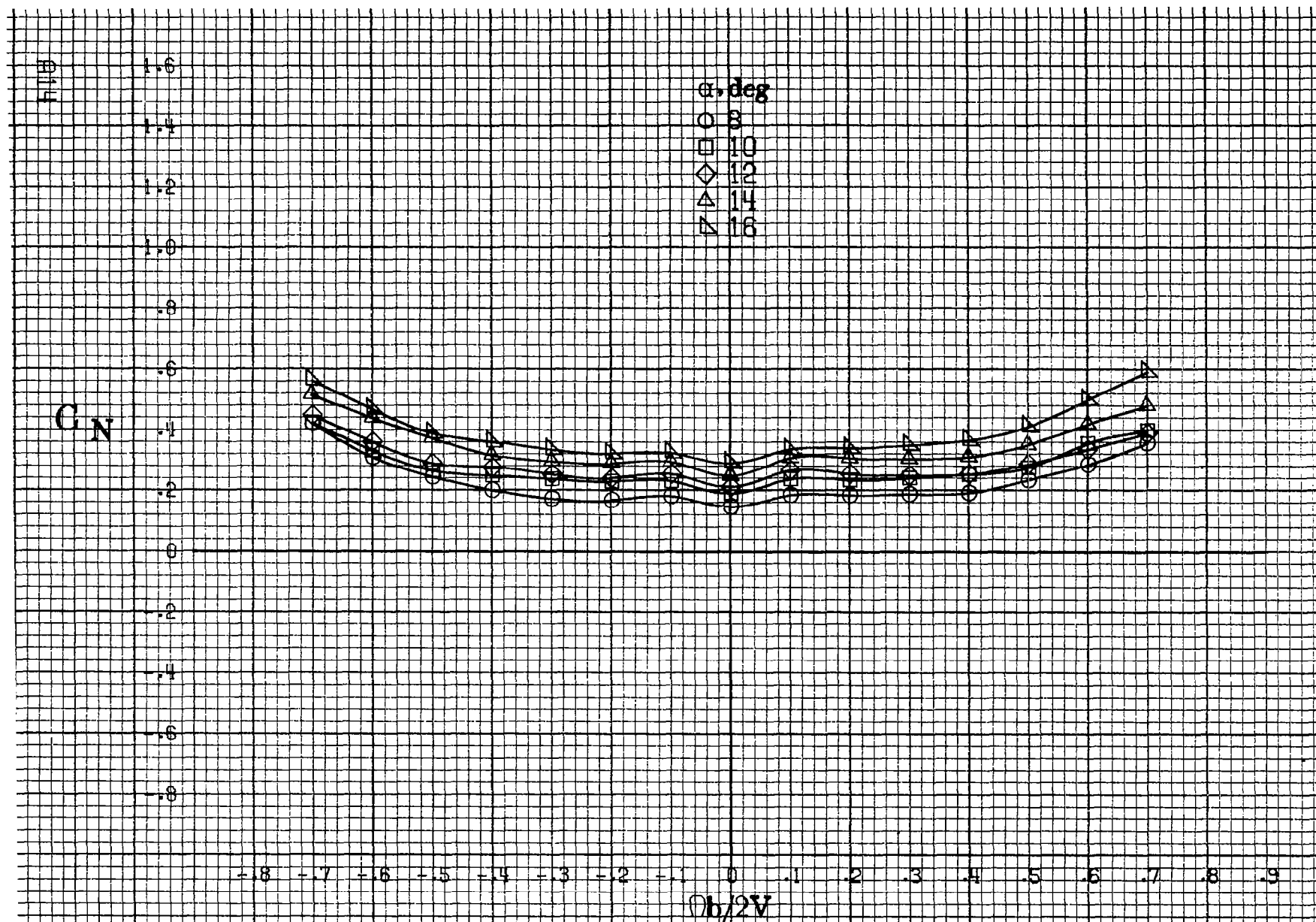
△ 80

▽ 90

$\phi b/2V$

(d) $\alpha=55\text{ to }90\text{ deg}, SR=0.$

Figure A3.- Concluded.



(a) $\alpha = 8$ to 16 deg, $SR = 182.9$ cm (72 in).

Figure A4. Effect of rotation rate and angle of attack on normal-force coefficient for body alone configuration. $\delta_a = 0^\circ$, $\delta_s = 0^\circ$, $\delta_r = 0^\circ$. $\beta = 0^\circ$.

C_N

α, deg

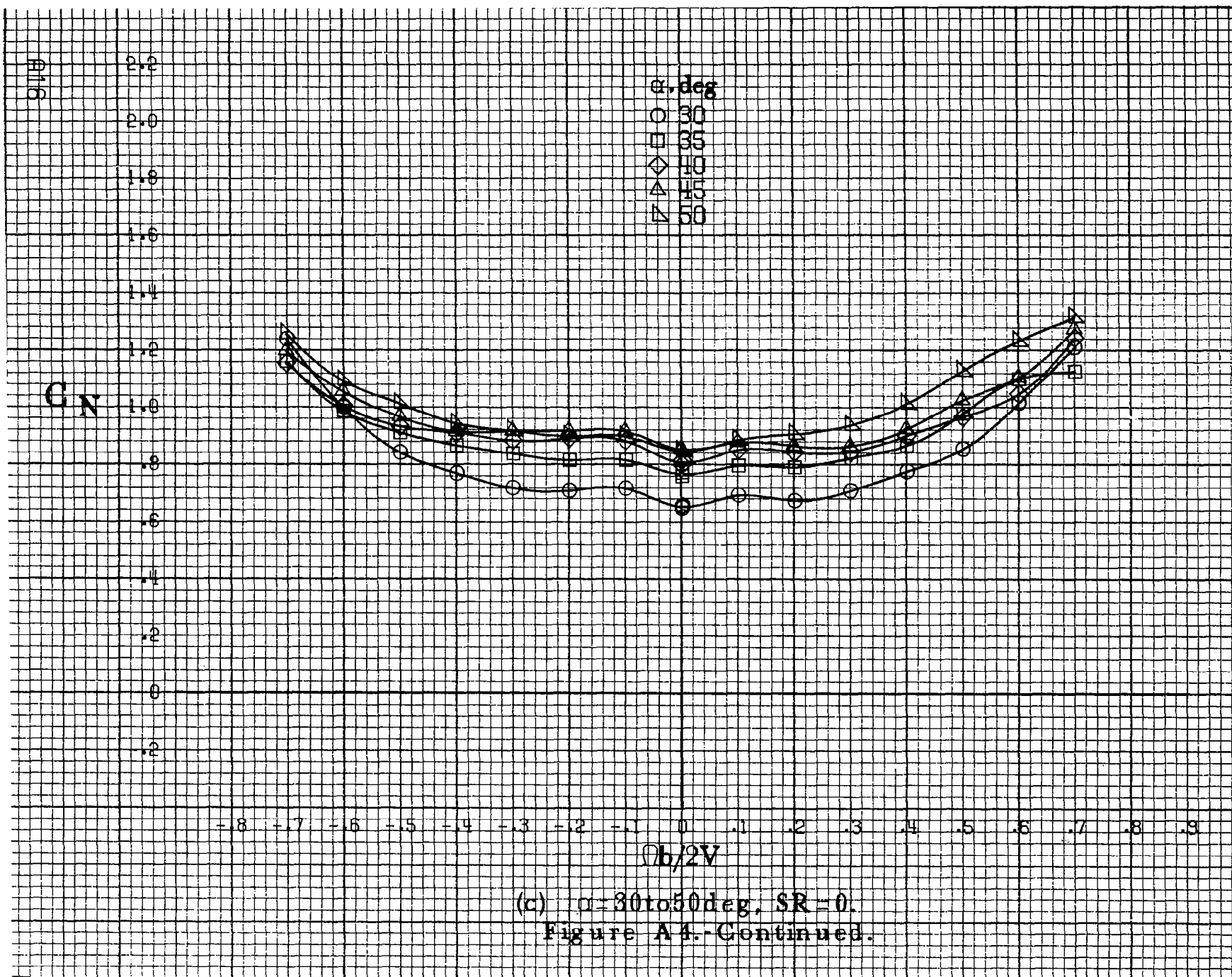
- 18
- 20
- ◇ 25
- △ 30
- ▽ 35

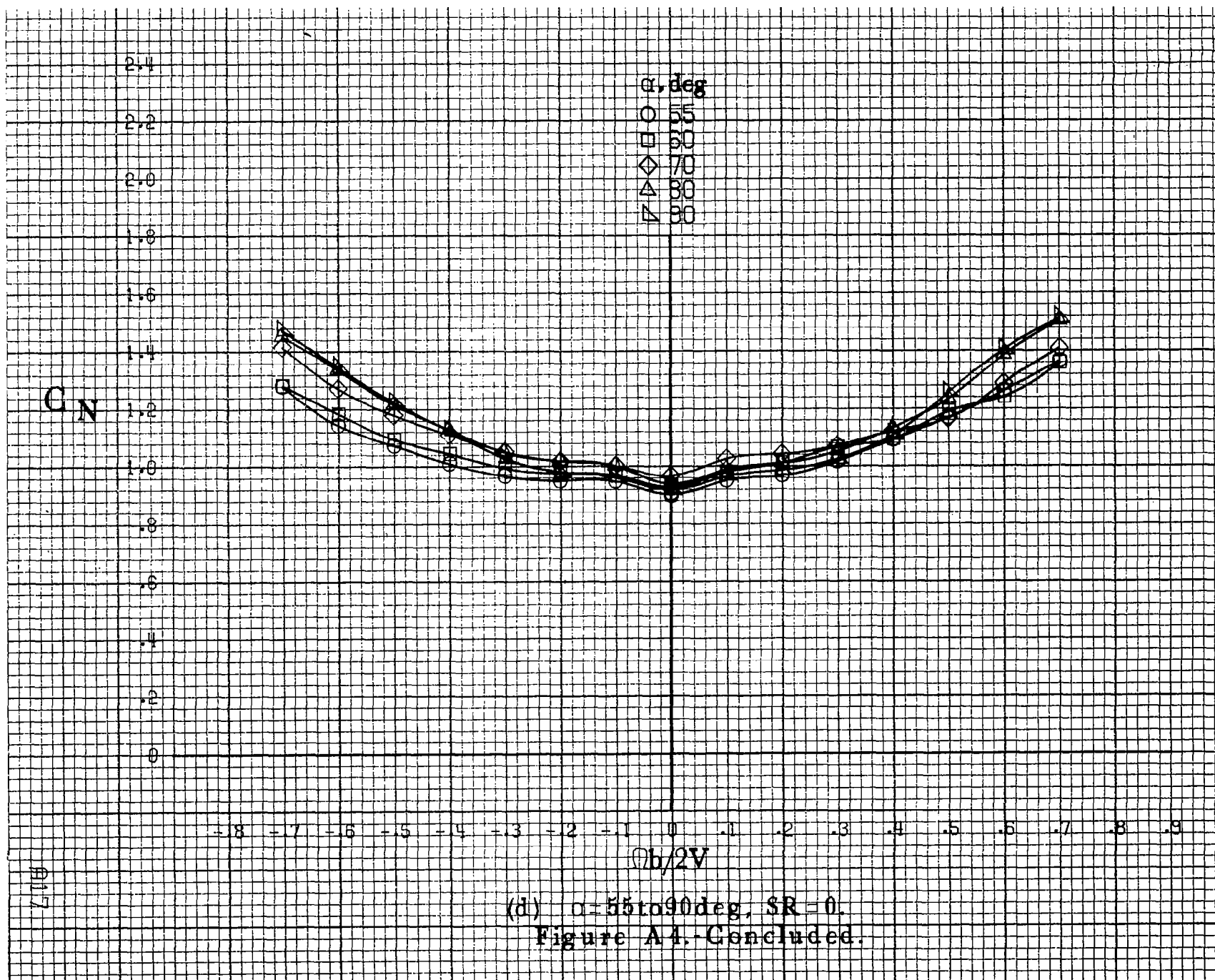
-0.8 -0.7 -0.6 -0.5 -0.4 -0.3 -0.2 -0.1 0 .1 .2 .3 .4 .5 .6 .7 .8 .9

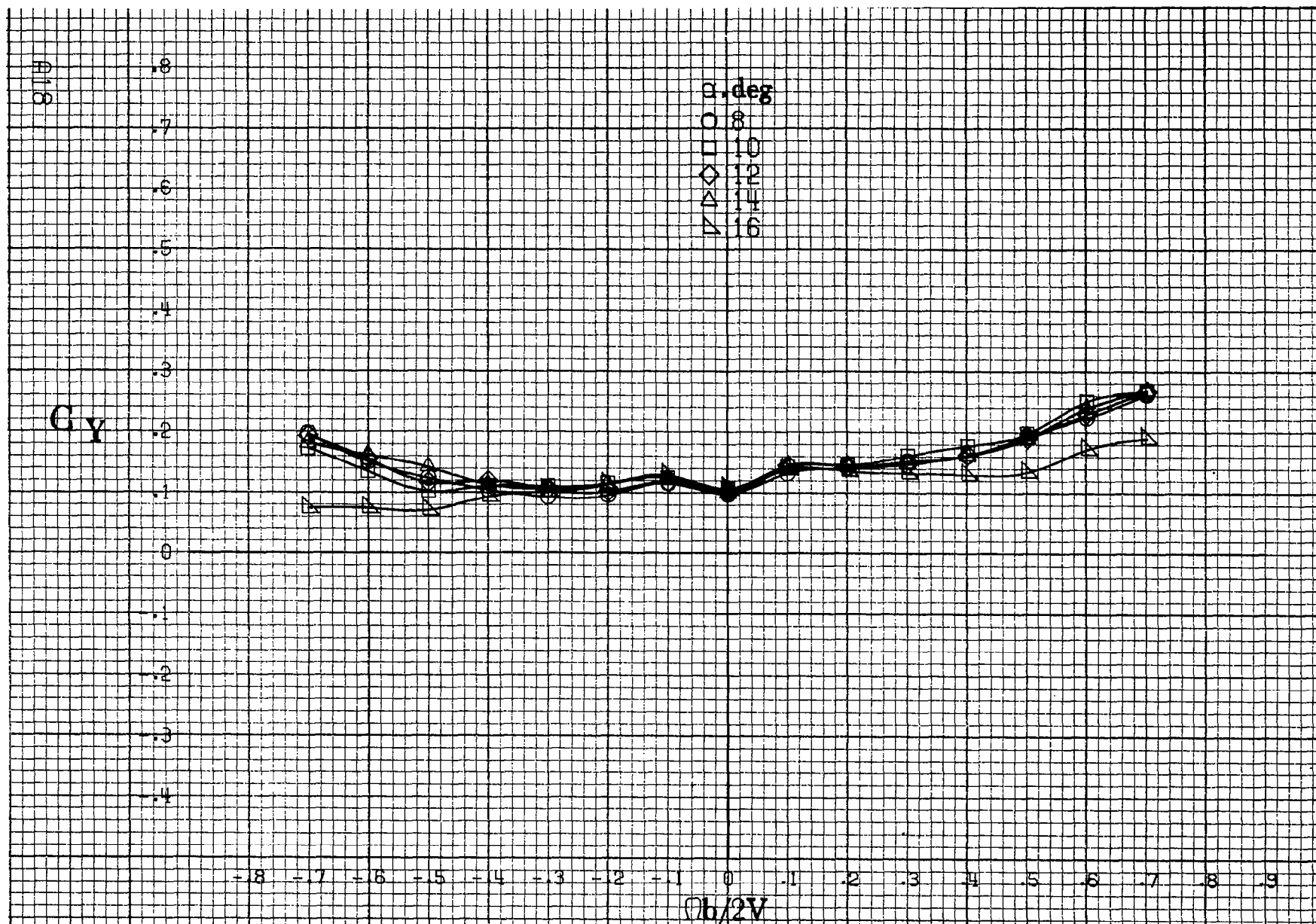
$\phi b/2V$

(b) $\alpha = 18 \text{ to } 35 \text{ deg. SR} = 182.9 \text{ cm (72 in.)}$

Figure A4.-Continued.







(a) $\alpha = 8$ to 16 deg, $SR = 182.9$ cm (72 in).

Figure A5 - Effect of rotation rate and angle of attack on side-force coefficient for body alone configuration. $\delta_a = 0^\circ$, $\delta_s = 0^\circ$, $\delta_r = 0^\circ$, $\beta = 0^\circ$.

C_Y

α, deg

○ 18

□ 20

◇ 25

△ 30

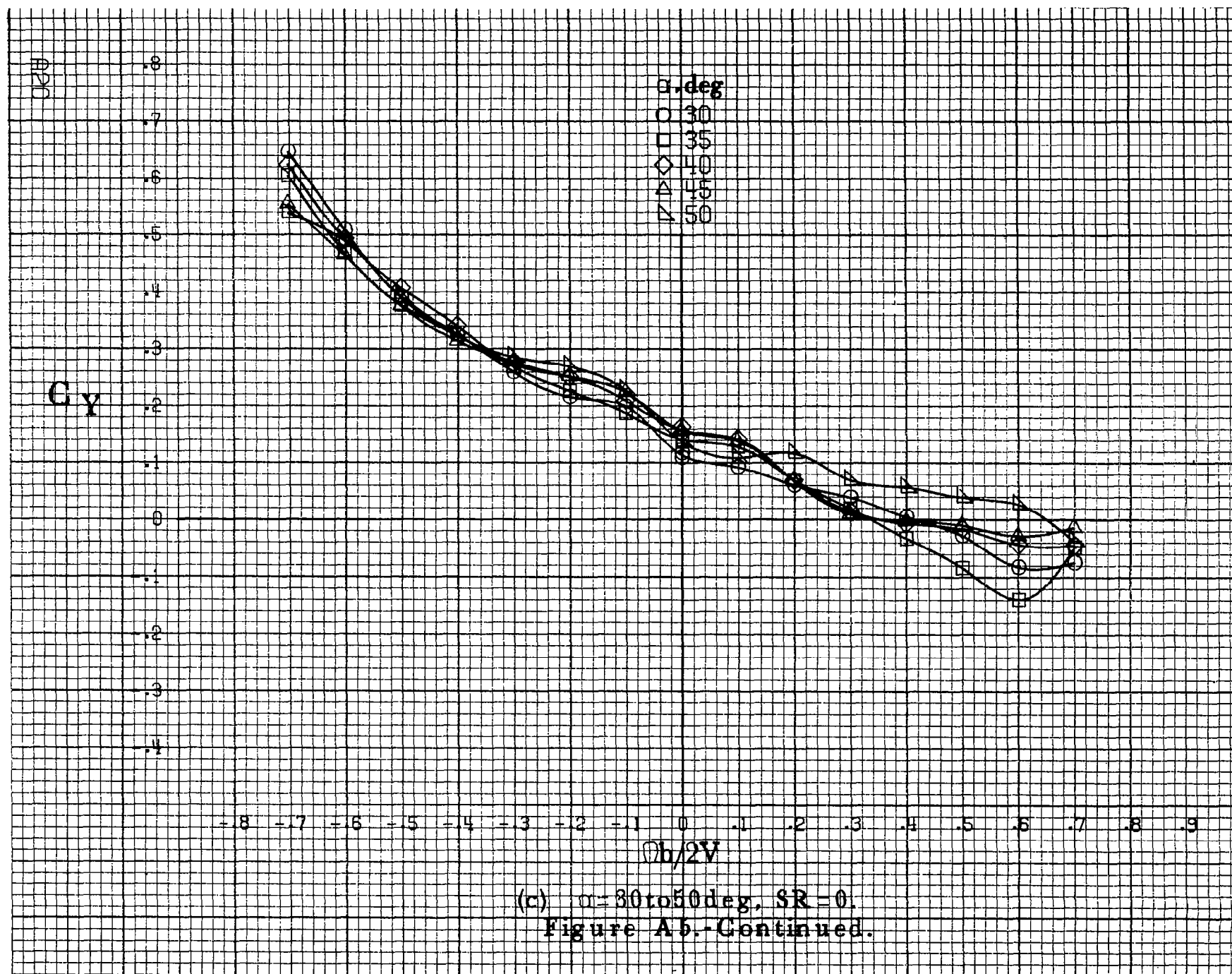
▽ 35

-0.8 -0.7 -0.6 -0.5 -0.4 -0.3 -0.2 -0.1 0 .1 .2 .3 .4 .5 .6 .7 .8 .9

$Ob/2V$

019

(b) $\alpha = 18 \text{ to } 35 \text{ deg}$, $SR = 182.9 \text{ cm (72 in)}$.
Figure A6. Continued.



(c) $\alpha=30$ to 50 deg, $SR=0$.
Figure A5.-Continued.

C_Y

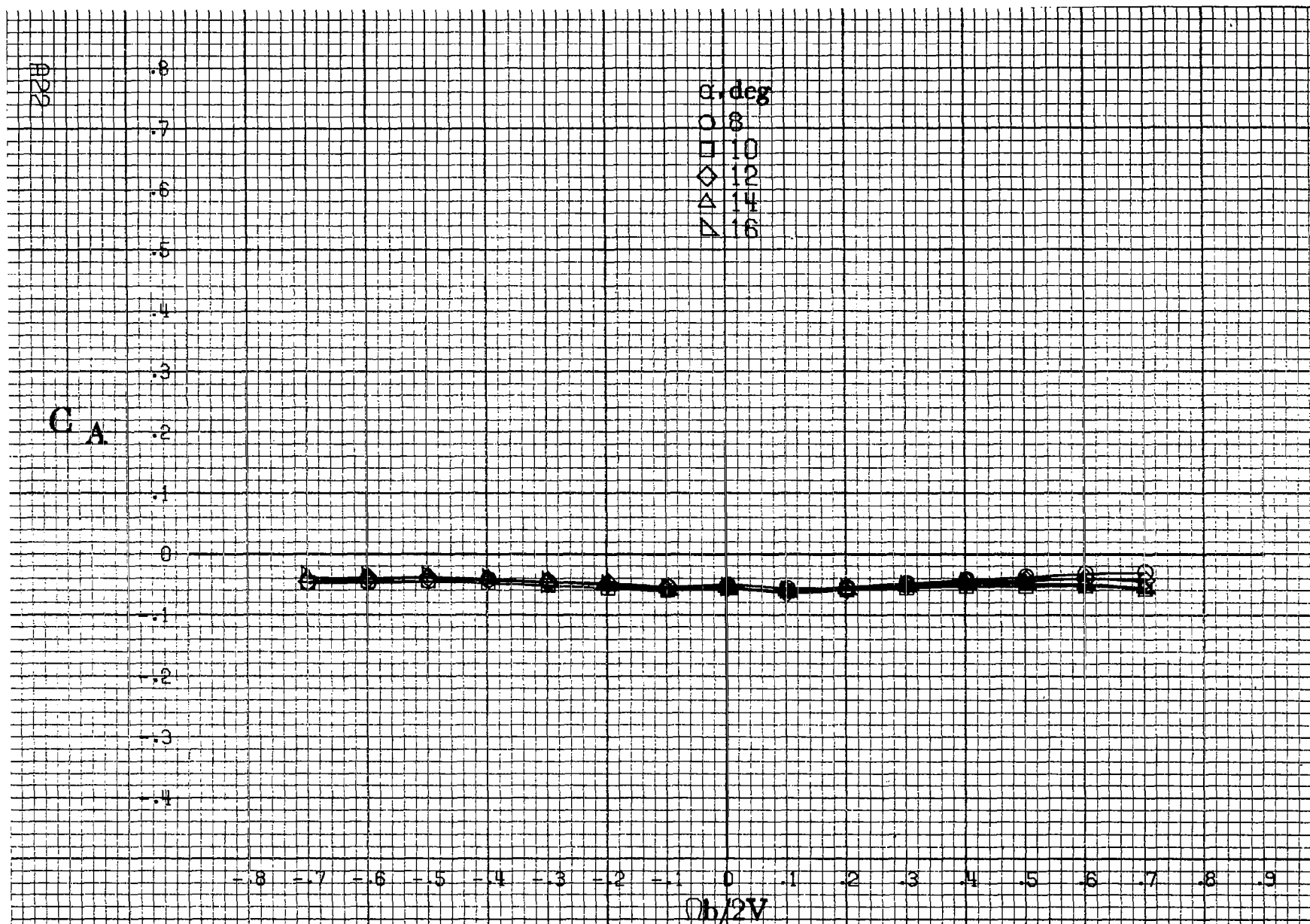
α, deg

- 55
- 60
- ◇ 70
- △ 80
- ▽ 90

-0.8 -0.7 -0.6 -0.5 -0.4 -0.3 -0.2 -0.1 0 0.1 0.2 0.3 0.4 0.5 0.6 0.7 0.8 0.9

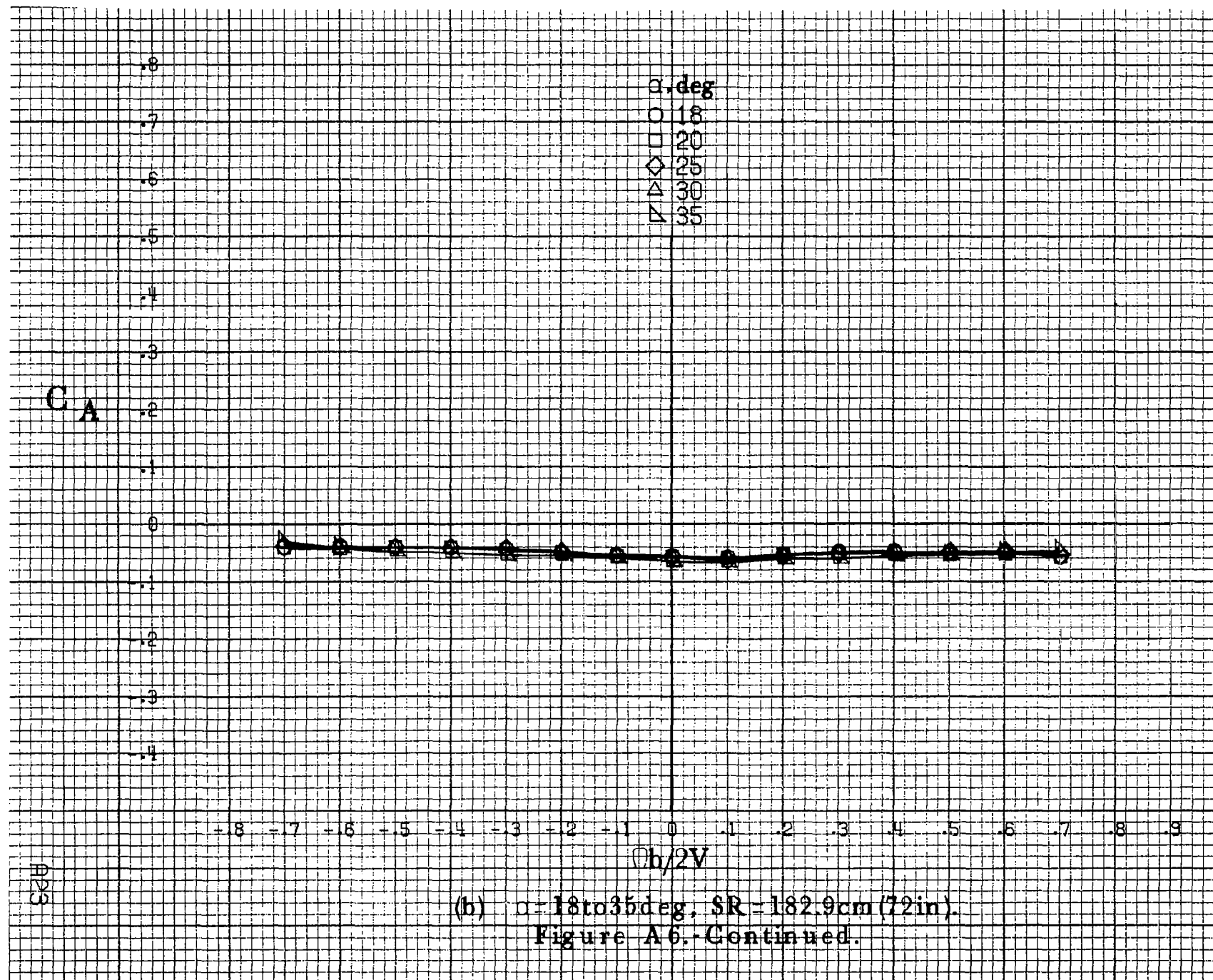
$Ob/2V$

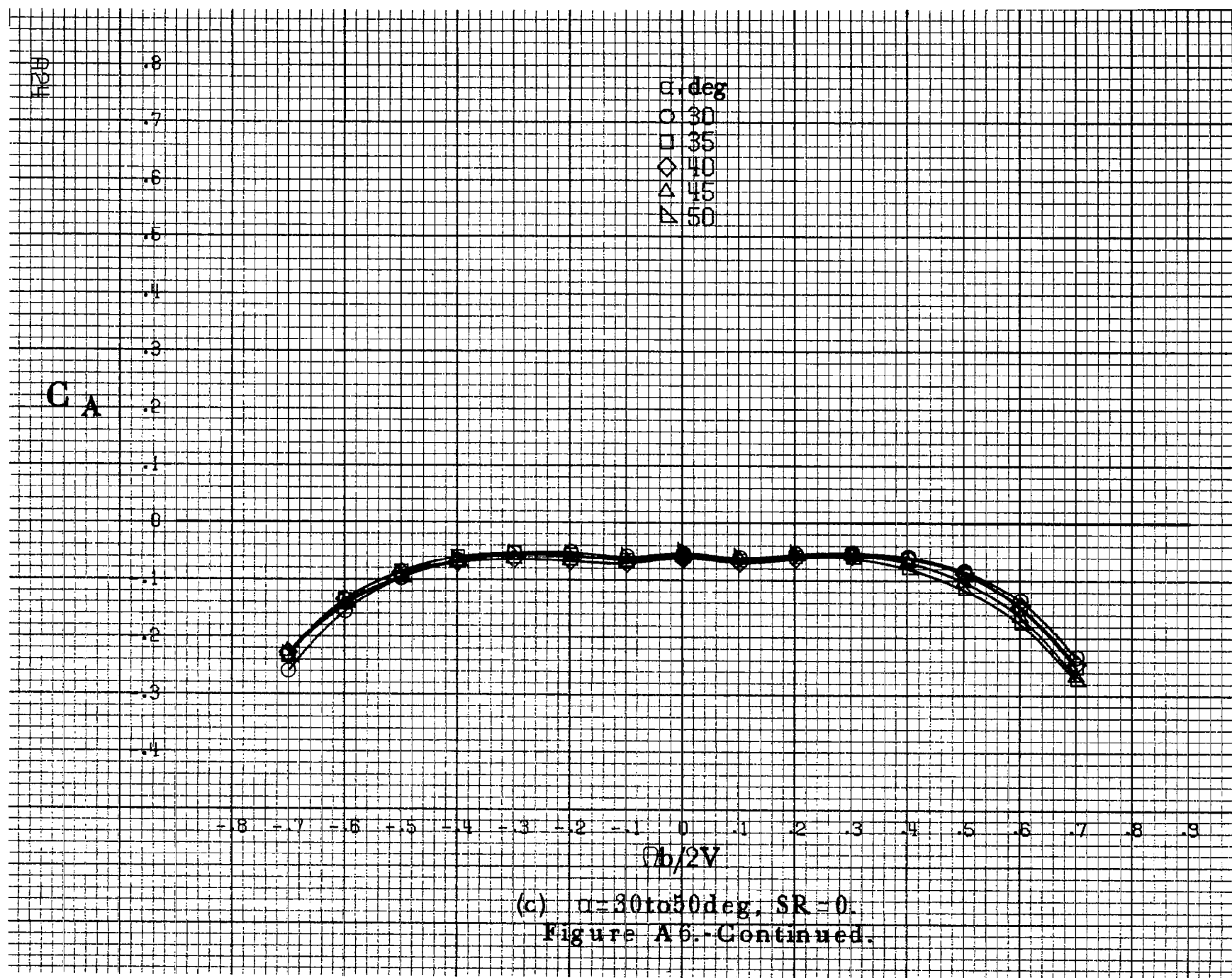
(d) $\alpha=55\text{ to }90\text{ deg. SR}=0.$
Figure A5.-Concluded.

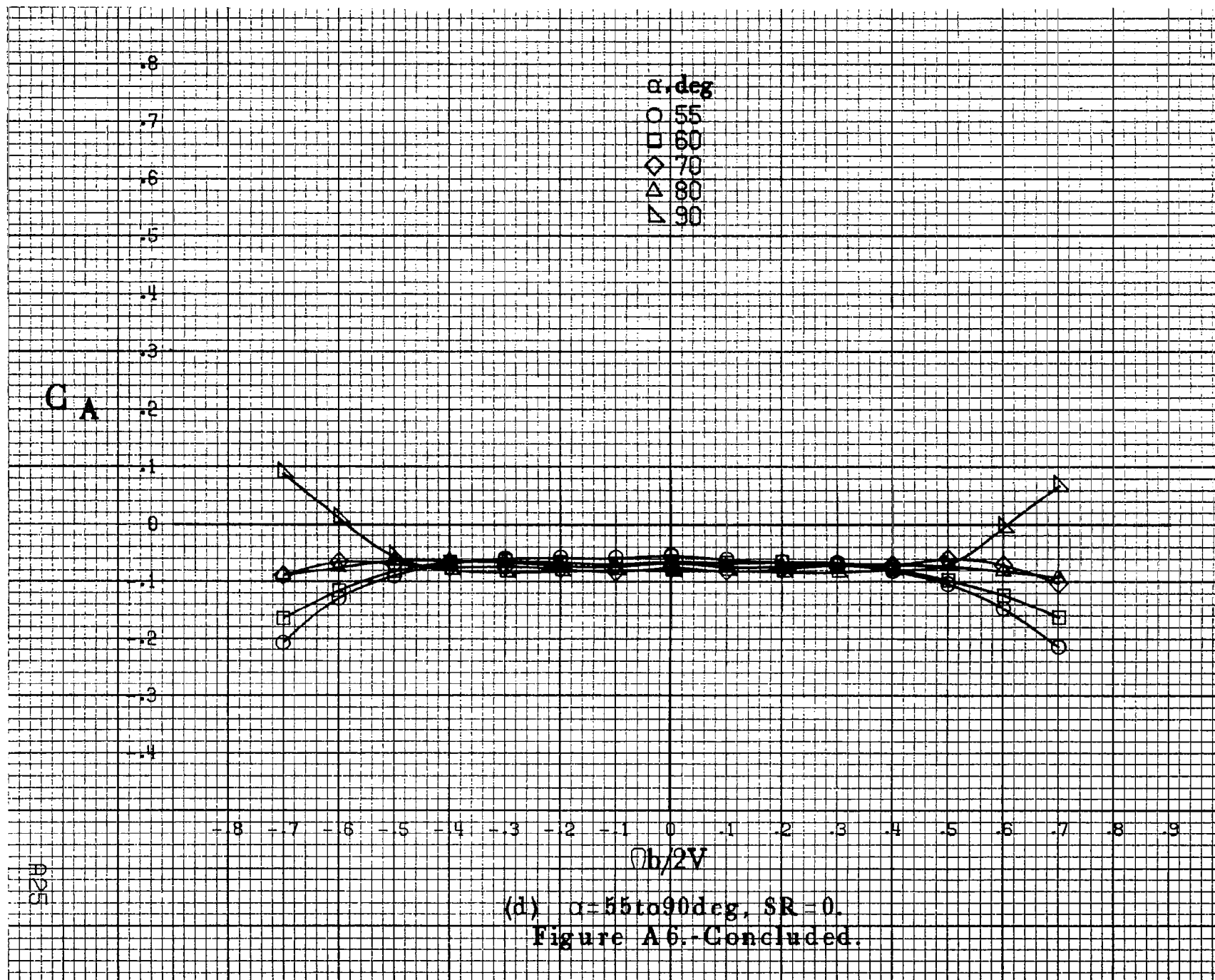


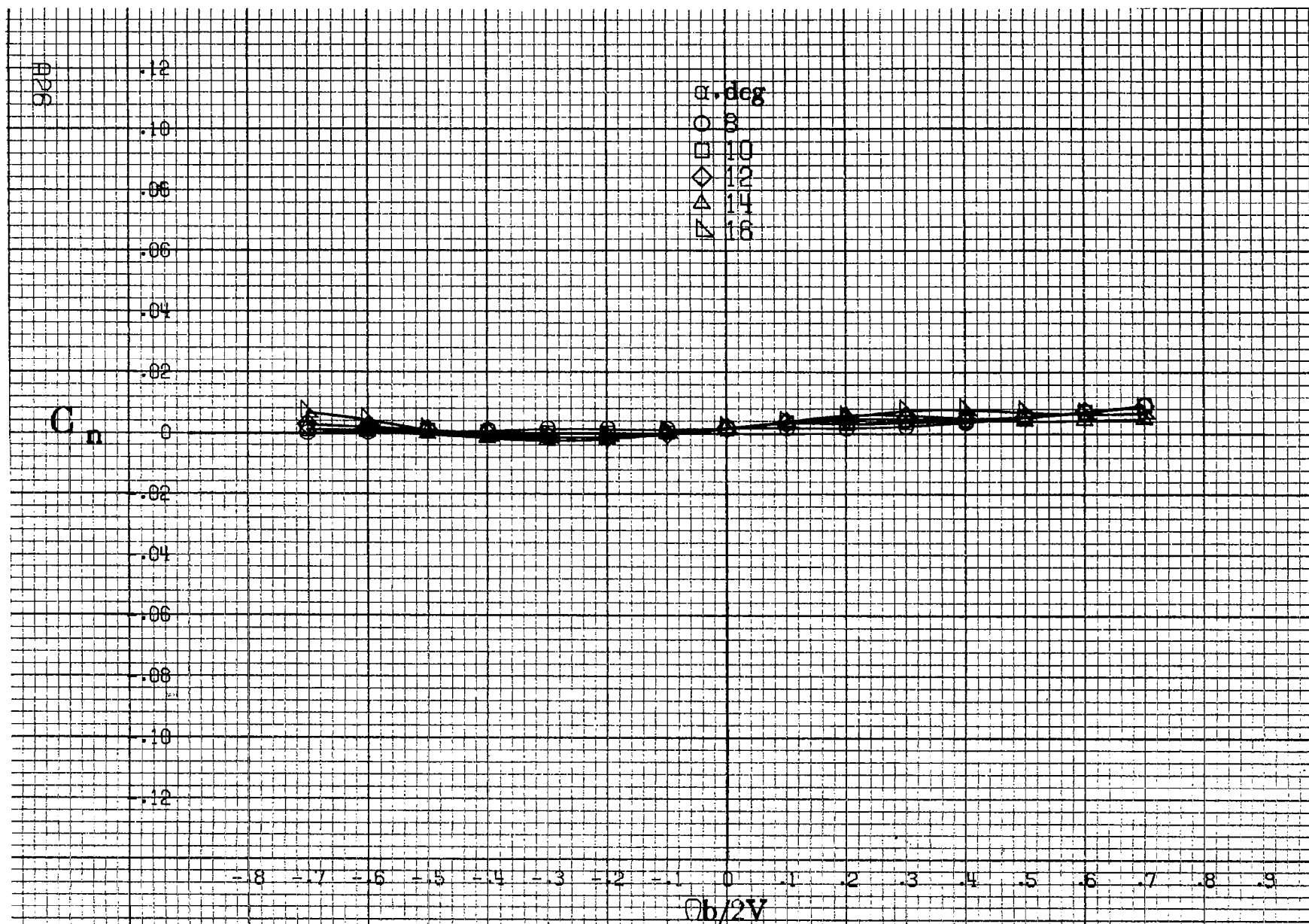
(a) $\alpha=8$ to 16° , $SR=182.9\text{cm}(72\text{in})$.

Figure A6. Effect of rotation rate and angle of attack on axial force coefficient for body alone configuration. $\delta_a=0^\circ$, $\delta_s=0^\circ$, $\delta_r=0^\circ$, $\delta=0^\circ$.









(a) $\alpha=8$ to 16° , $SR=182.9\text{cm}$ (72 in).

Figure A7.-Effect of rotation rate and angle of attack on yawing-moment coefficient for body wing configuration. $\delta_e=0^\circ$, $\delta_a=0^\circ$, $\delta_r=0^\circ$, $\beta=0^\circ$.

C_n

α, deg
 ○ 18
 □ 20
 ◇ 25
 △ 30
 ▴ 35

.14
 .12
 .10
 .08
 .06
 .04
 .02
 0
 .02
 .04
 .06
 .08
 .10

-8 -7 -6 -5 -4 -3 -2 -1 0 .1 .2 .3 .4 .5 .6 .7 .8 .9

$b/2V$

(b) $\alpha = 18 \text{ to } 35 \text{ deg}$, $SR = 182.9 \text{ cm (72 in)}$.

Figure A7.- Continued.

AP7

C_n

.14
.12
.10
.08
.06
.04
.02
0
.02
.04
.06
.08
.10

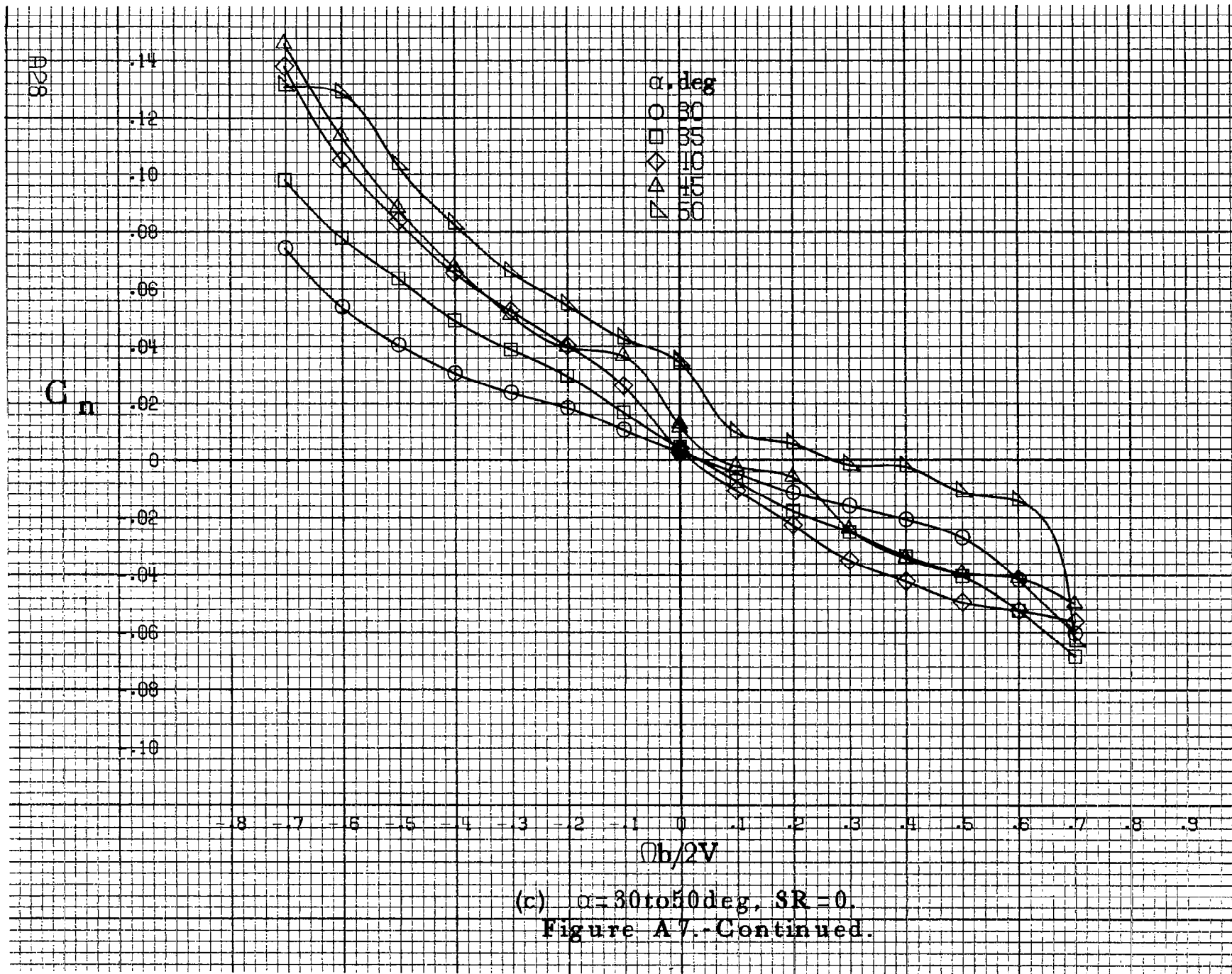
α, deg

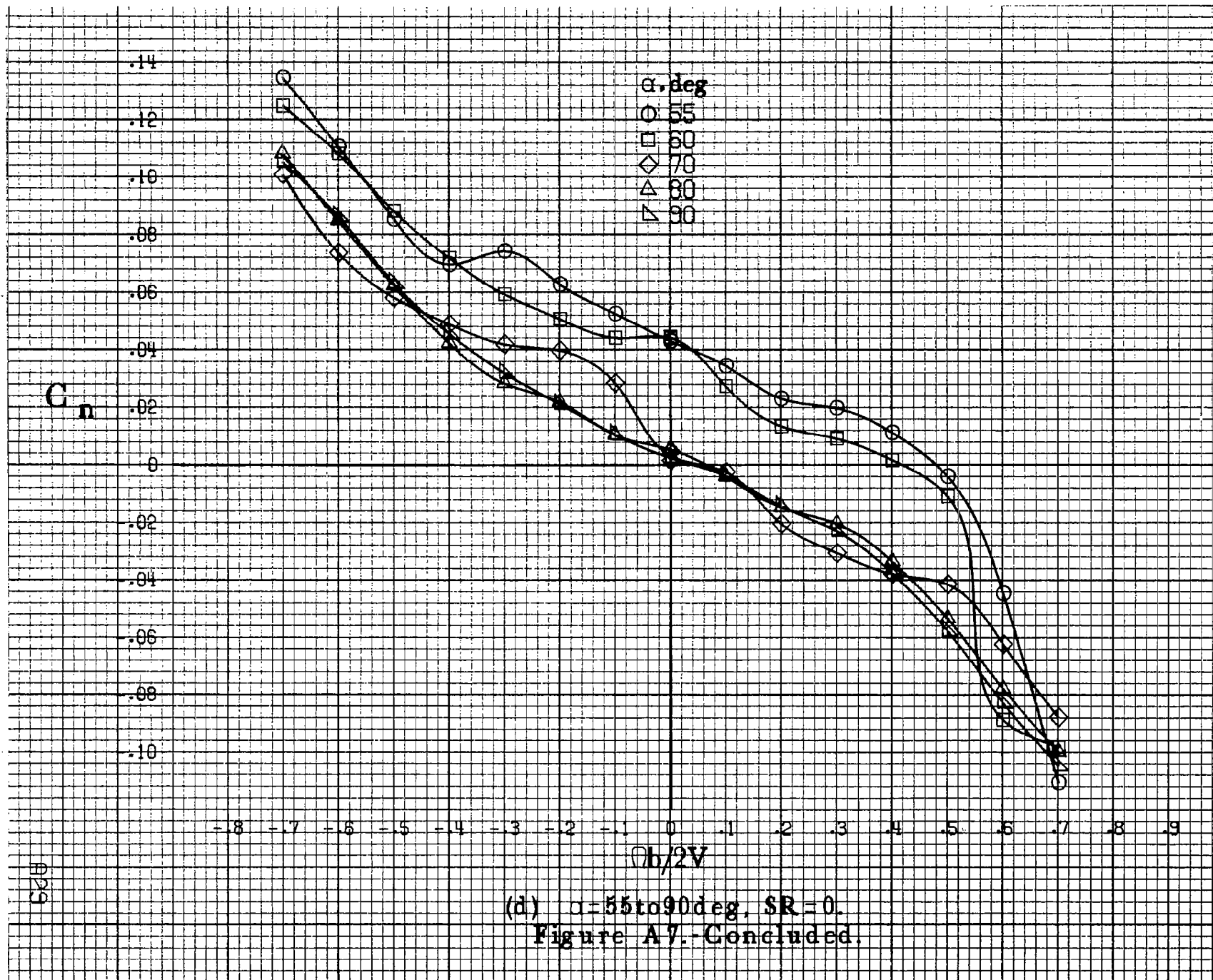
- 30
- 35
- ◇ 40
- △ 45
- ▽ 50

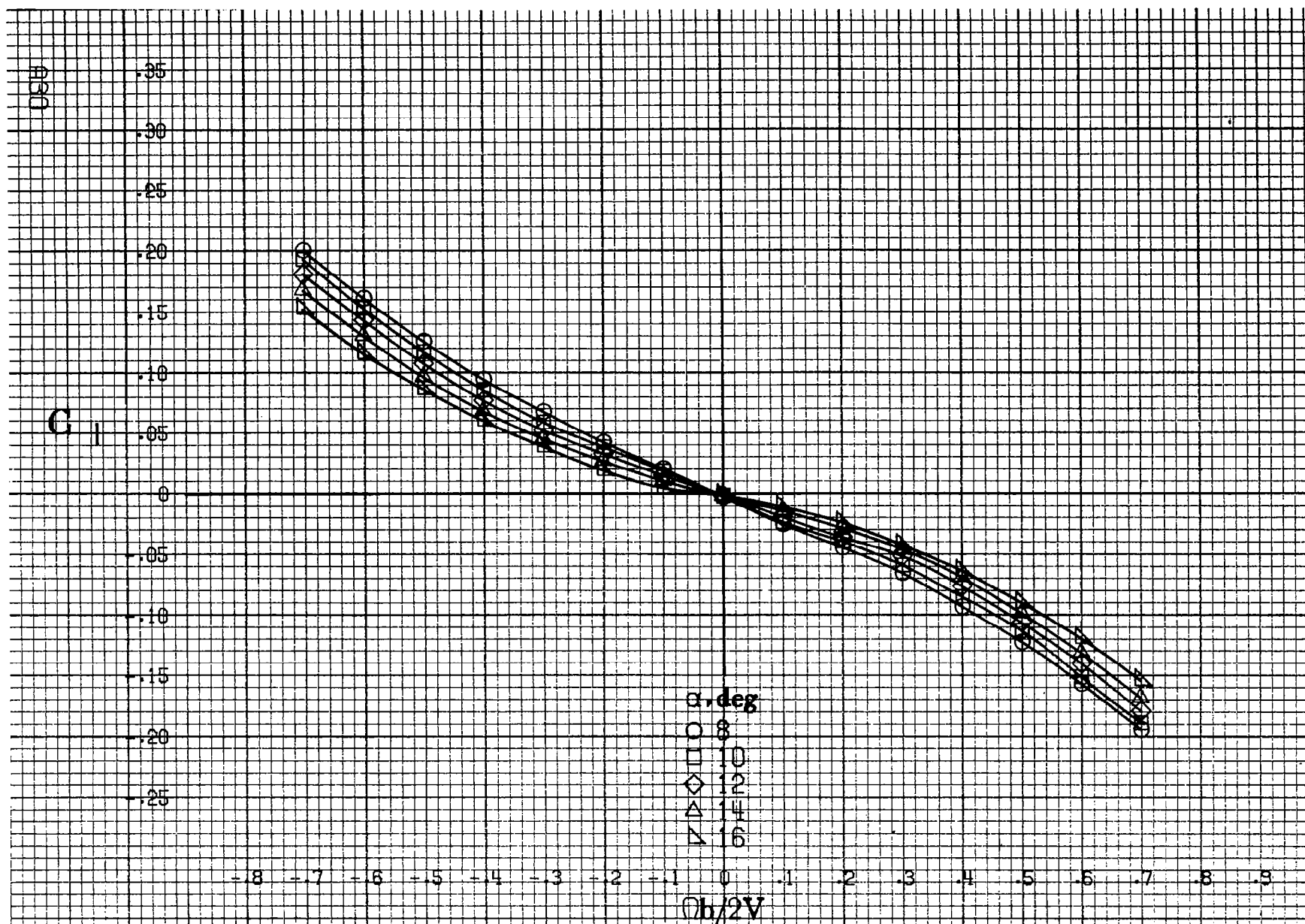
-.8 -.7 -.6 -.5 -.4 -.3 -.2 -.1 0 .1 .2 .3 .4 .5 .6 .7 .8 .9

$Ob/2V$

(c) $\alpha=30\text{ to }50\text{deg}$, $SR=0$.
Figure A7.-Continued.







(a) $\alpha=8$ to 16° , $SR=182.9\text{cm}(72\text{in})$.

Figure A8.-Effect of rotation rate and angle of attack on rolling-moment coefficient for body wing configuration. $\delta_e=0^\circ$, $\delta_a=0^\circ$, $\delta_r=0^\circ$, $\delta=0^\circ$.

C_1

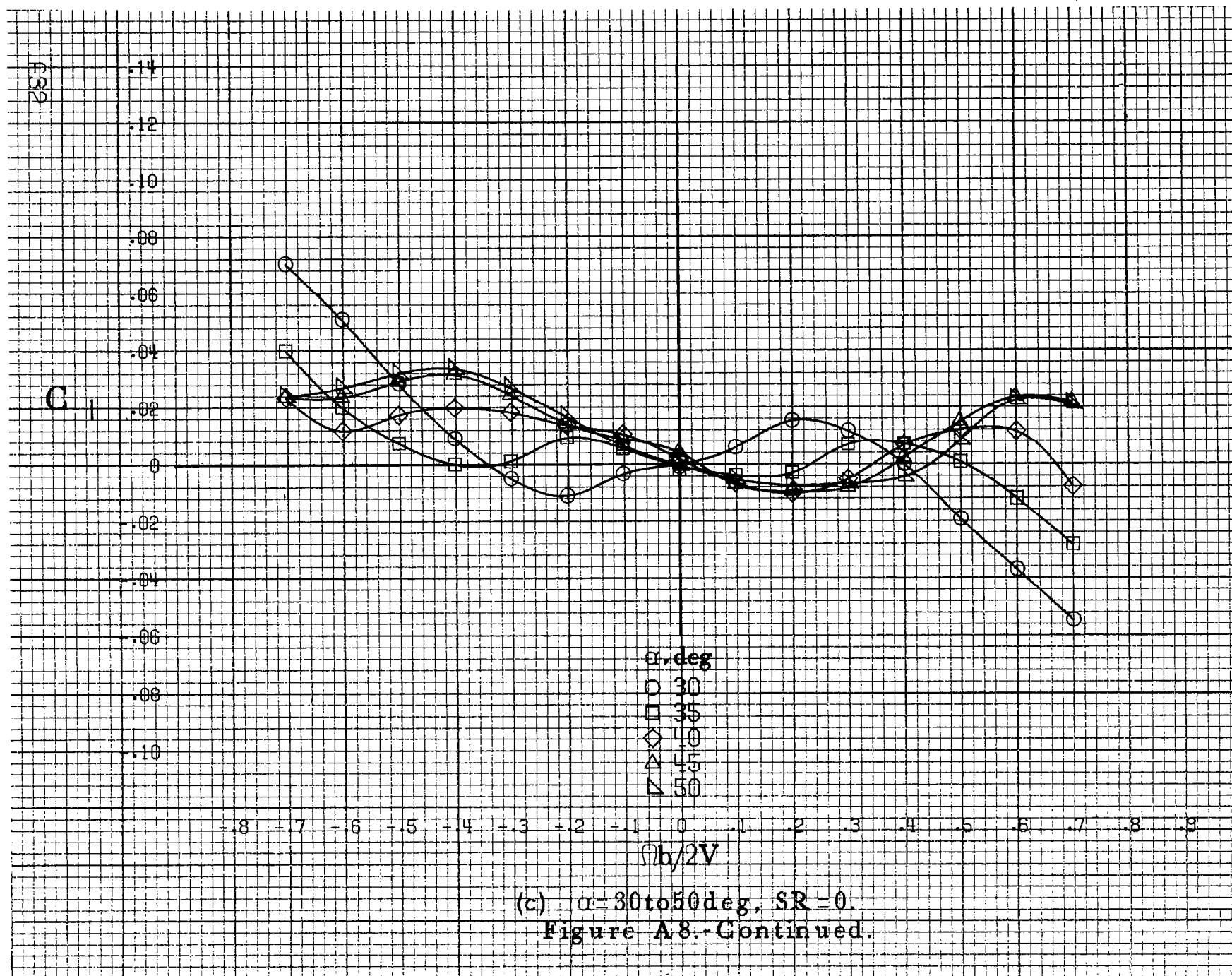
.14
.12
.10
.08
.06
.04
.02
0
-.02
-.04
-.06
-.08
-.10

α, deg
○ 18
□ 20
◇ 25
△ 30
▽ 35

-8 -7 -6 -5 -4 -3 -2 -1 0 .1 .2 .3 .4 .5 .6 .7 .8 .9

$b/2V$

(b) $\alpha = 18 \text{ to } 35 \text{ deg}$, SR = 182.9 cm (72 in).
Figure A8. Continued.



C_1

.14
 .12
 .10
 .08
 .06
 .04
 .02
 0
 -.02
 -.04
 -.06
 -.08
 -.10

 α, deg

○ 55

□ 60

◇ 70

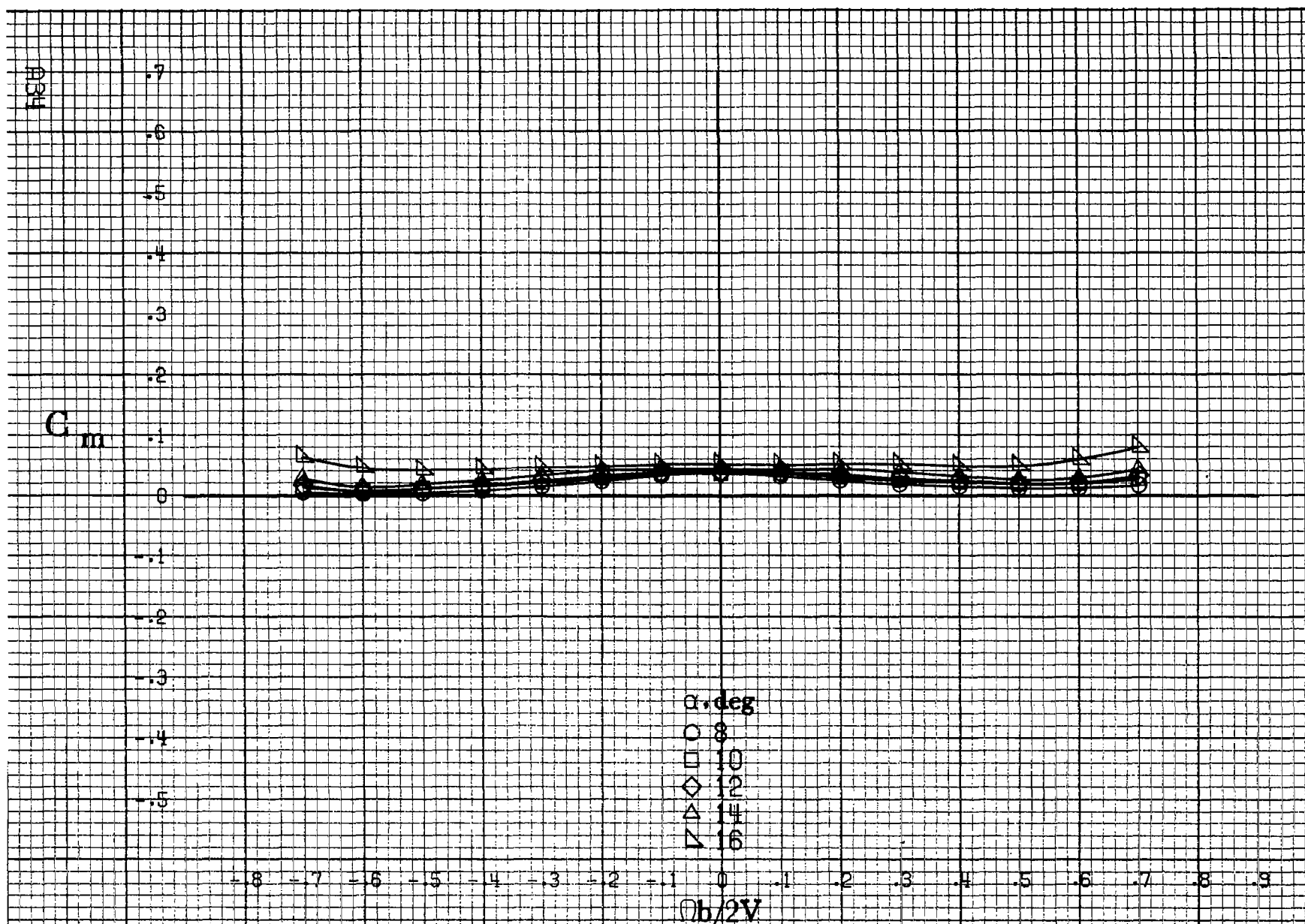
△ 80

▽ 90

 $Ob/2V$

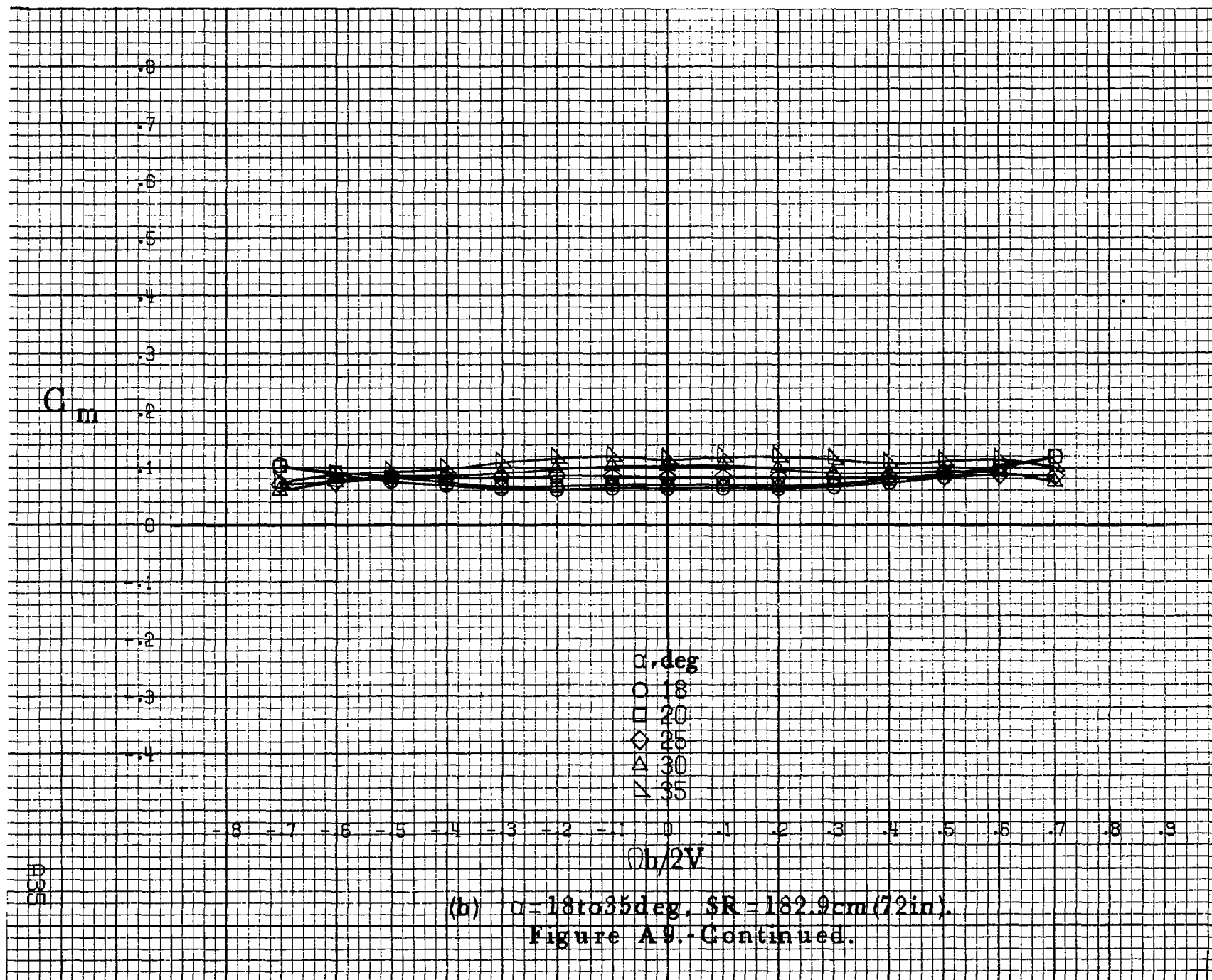
-0.8 -0.7 -0.6 -0.5 -0.4 -0.3 -0.2 -0.1 0 .1 .2 .3 .4 .5 .6 .7 .8 .9

(d) $\alpha=55$ to 90 deg, $SR=0$.
 Figure A8.- Concluded.

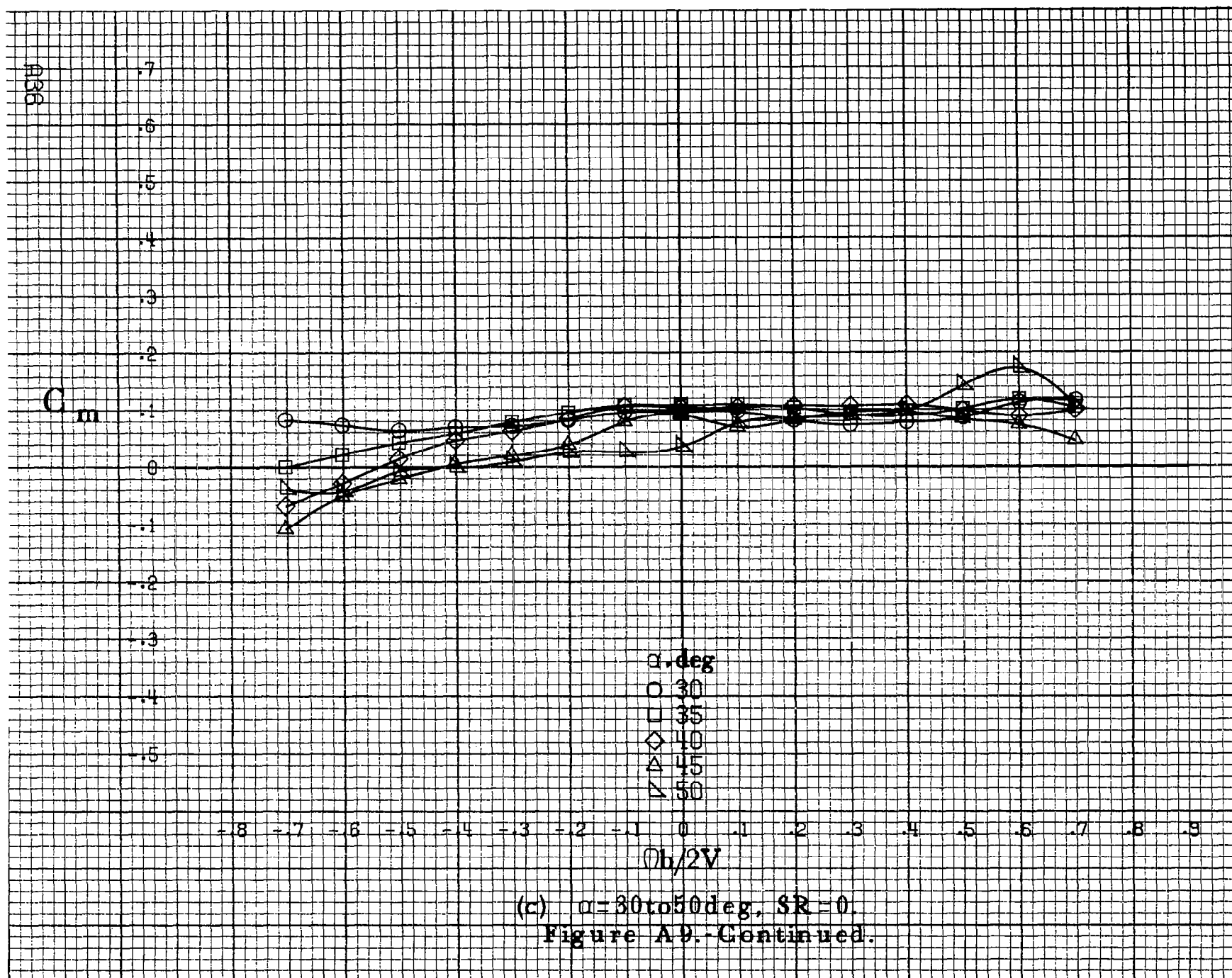


(a) $\alpha = 8$ to 16° , $SR = 182.9 \text{ cm (72 in)}$.

Figure A.9. Effect of rotation rate and angle of attack on pitching-moment coefficient for body wing configuration. $\delta_e = 0^\circ$, $\delta_a = 0^\circ$, $\delta_r = 0^\circ$, $\beta = 0^\circ$.



(b) $\alpha=18$ to 35° , $SR=182.9\text{cm}(72\text{in})$.
Figure A9.-Continued.



C_m

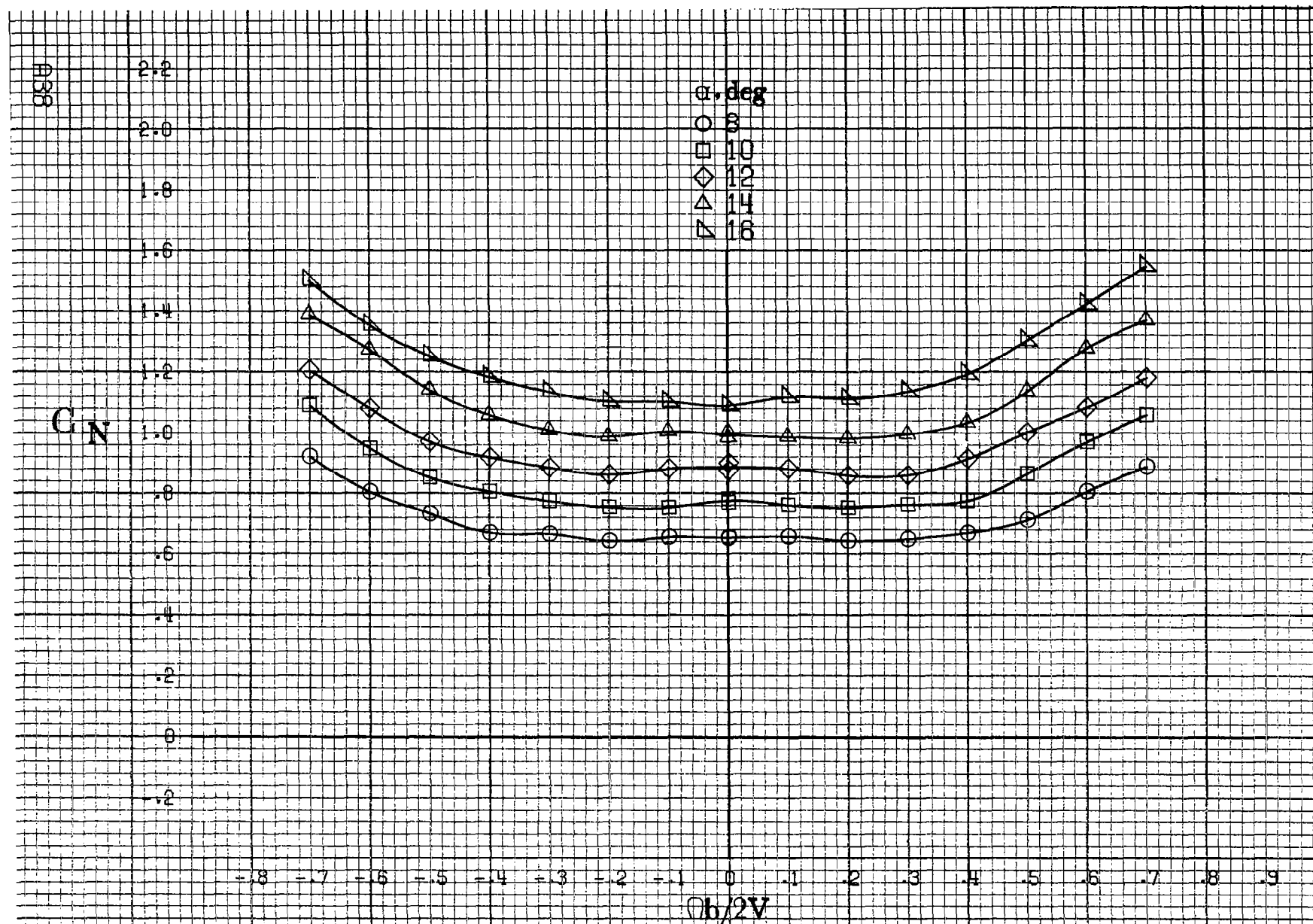
.6
.5
.4
.3
.2
.1
0
-.1
-.2
-.3
-.4
-.5
-.6

-8 -7 -6 -5 -4 -3 -2 -1 0 .1 .2 .3 .4 .5 .6 .7 .8 .9

α, deg
○ 55
□ 60
◇ 70
△ 80
▽ 90

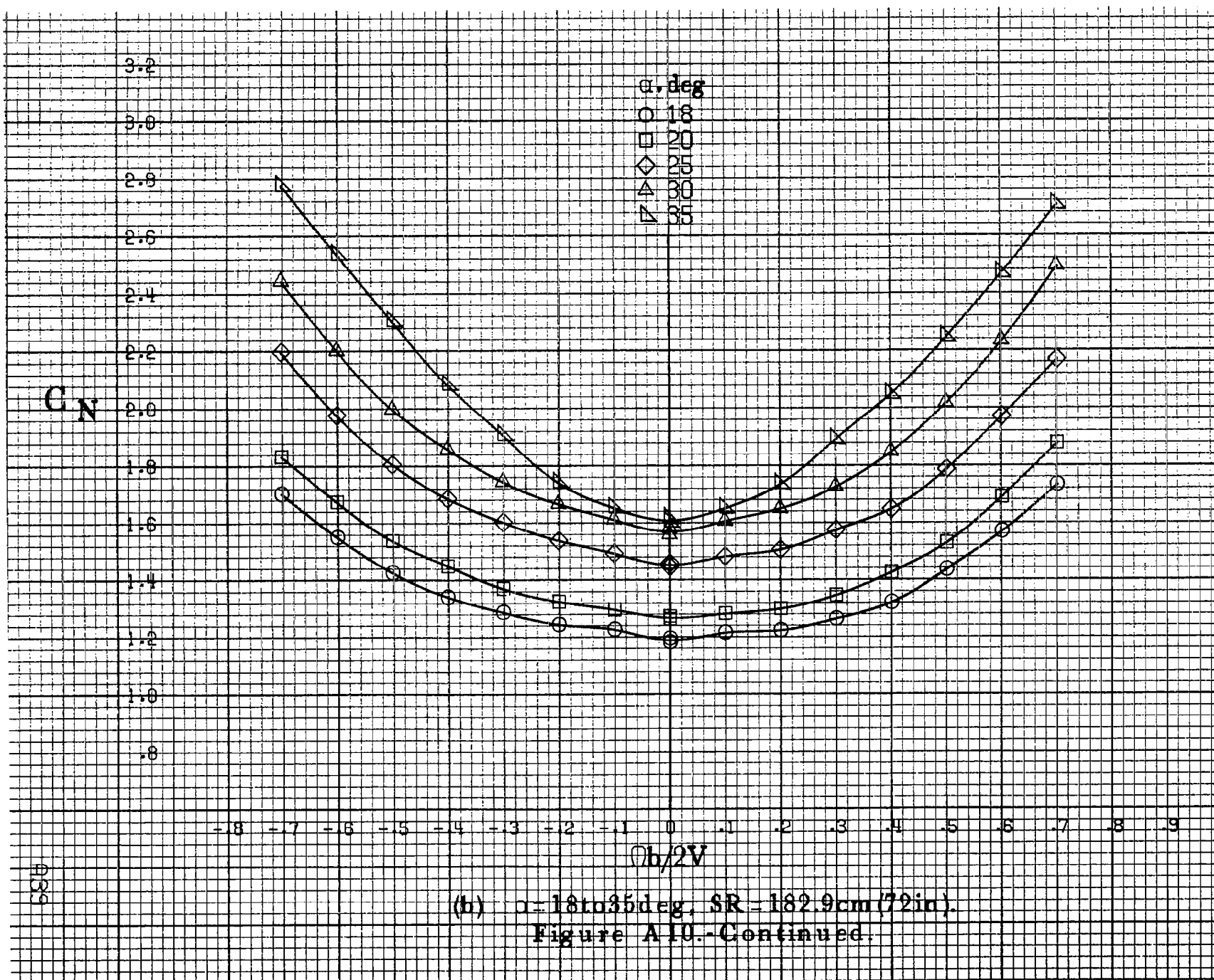
$Ob/2V$

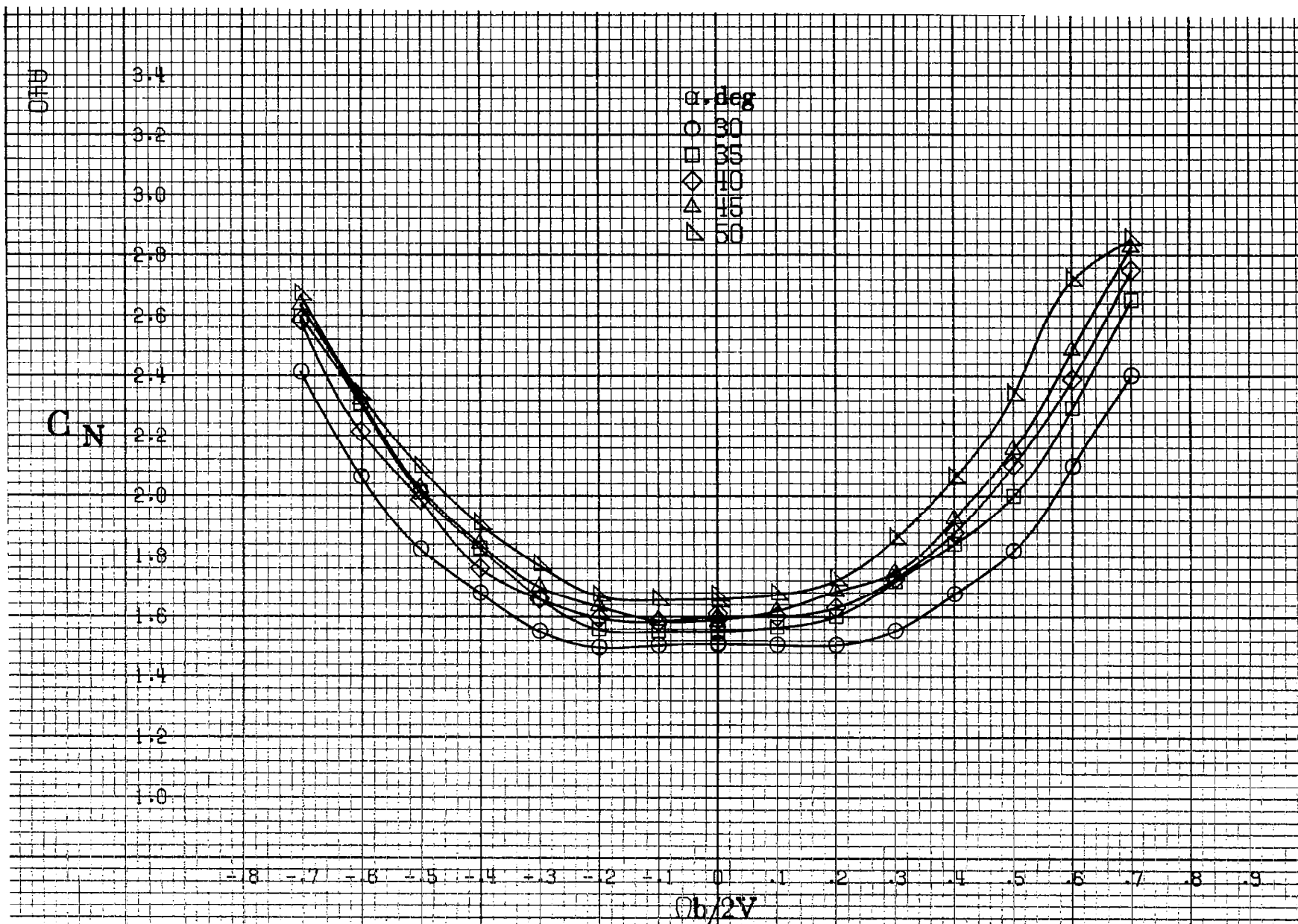
(d) $\alpha=55\text{to}90\text{deg}, SR=0.$
Figure A9.-Concluded.



(a) $\alpha = 8$ to 16° , $SR = 182.9\text{ cm (72 in.)}$.

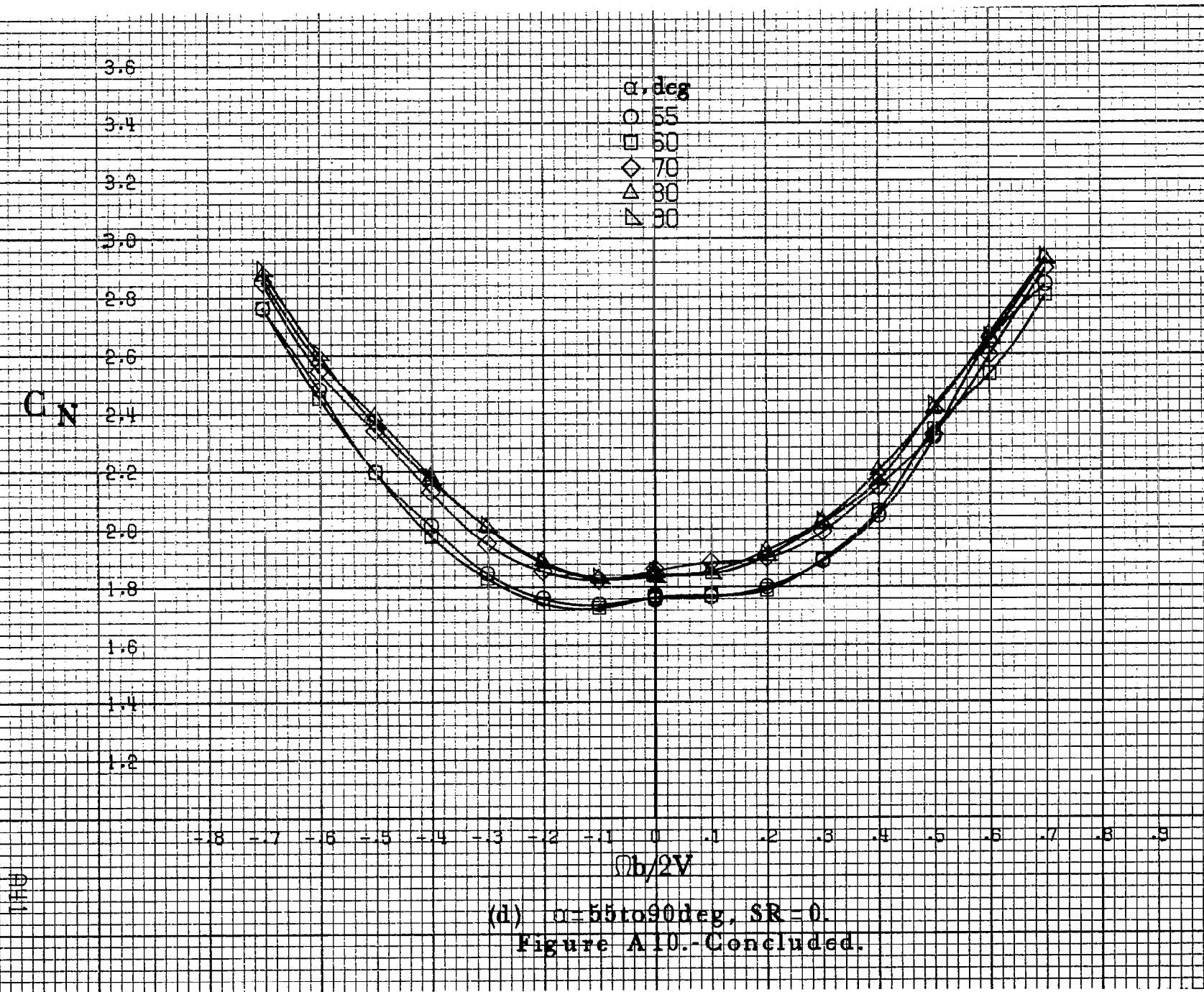
Figure A10.-Effect of rotation rate and angle of attack on normal-force coefficient for body wing configuration. $\delta_e = 0^\circ$, $\delta_a = 0^\circ$, $\delta_r = 0^\circ$, $\beta = 0^\circ$.

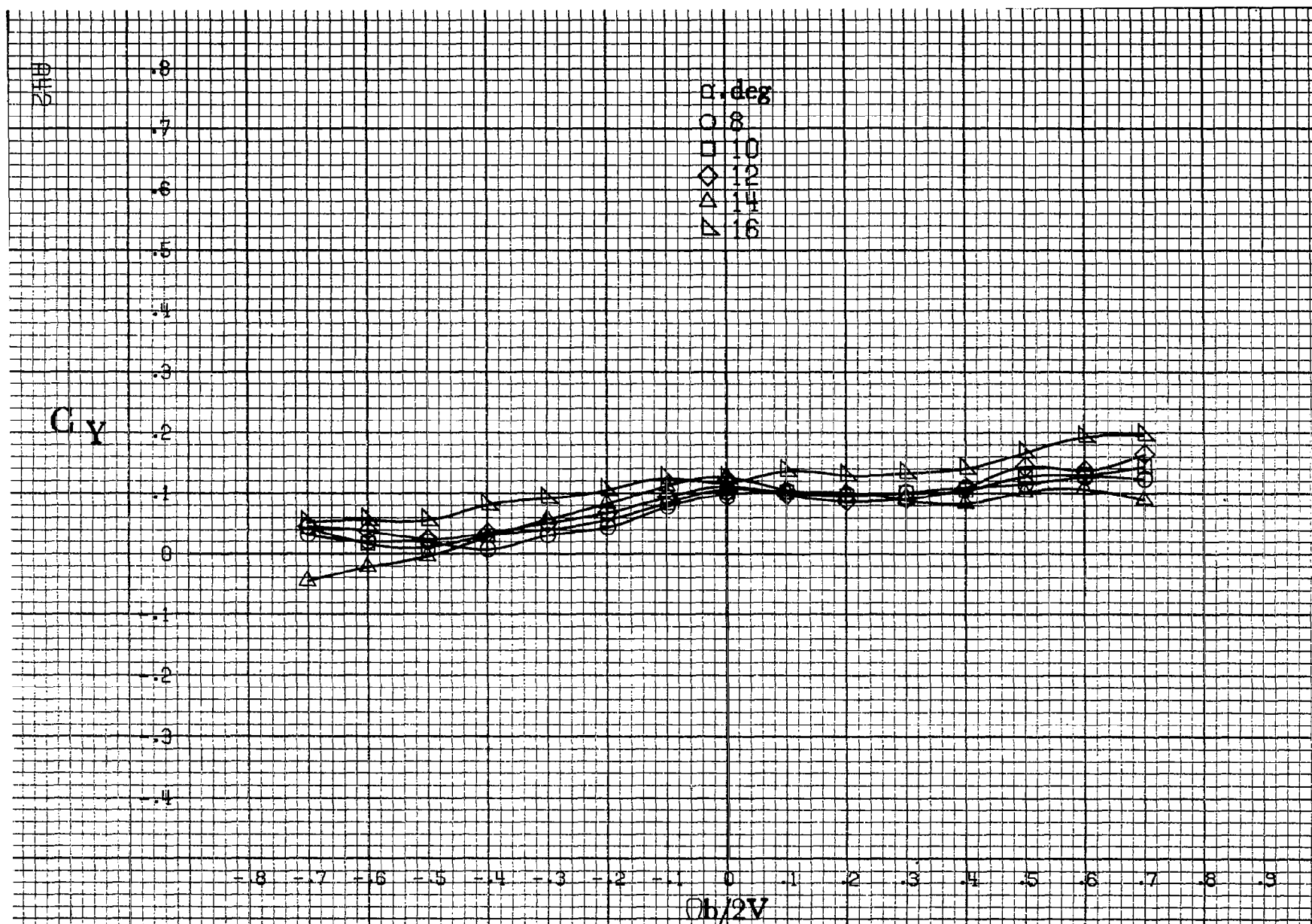




(c) $\alpha = 30$ to 50 deg, $SR = 0$.

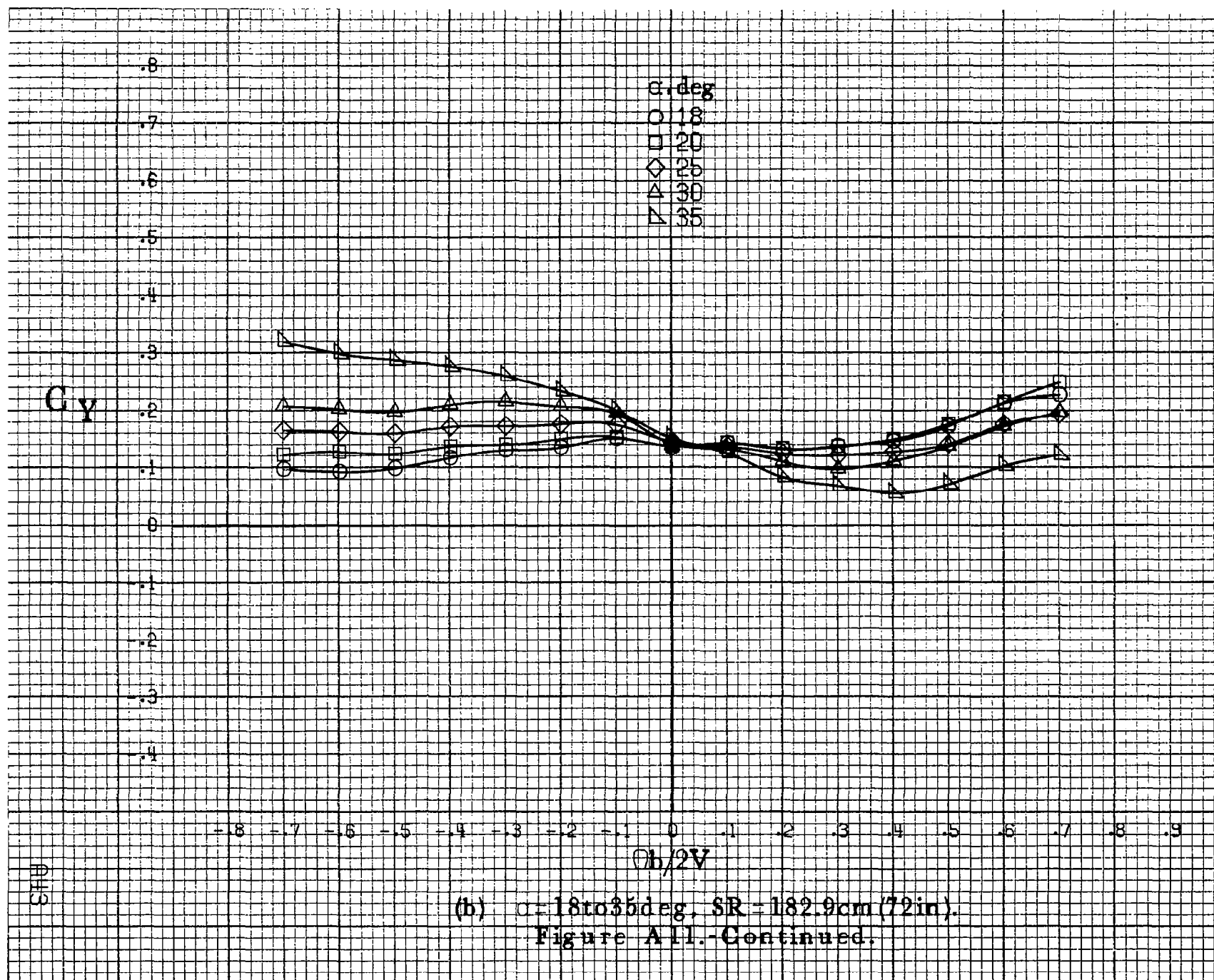
Figure A10.-Continued.

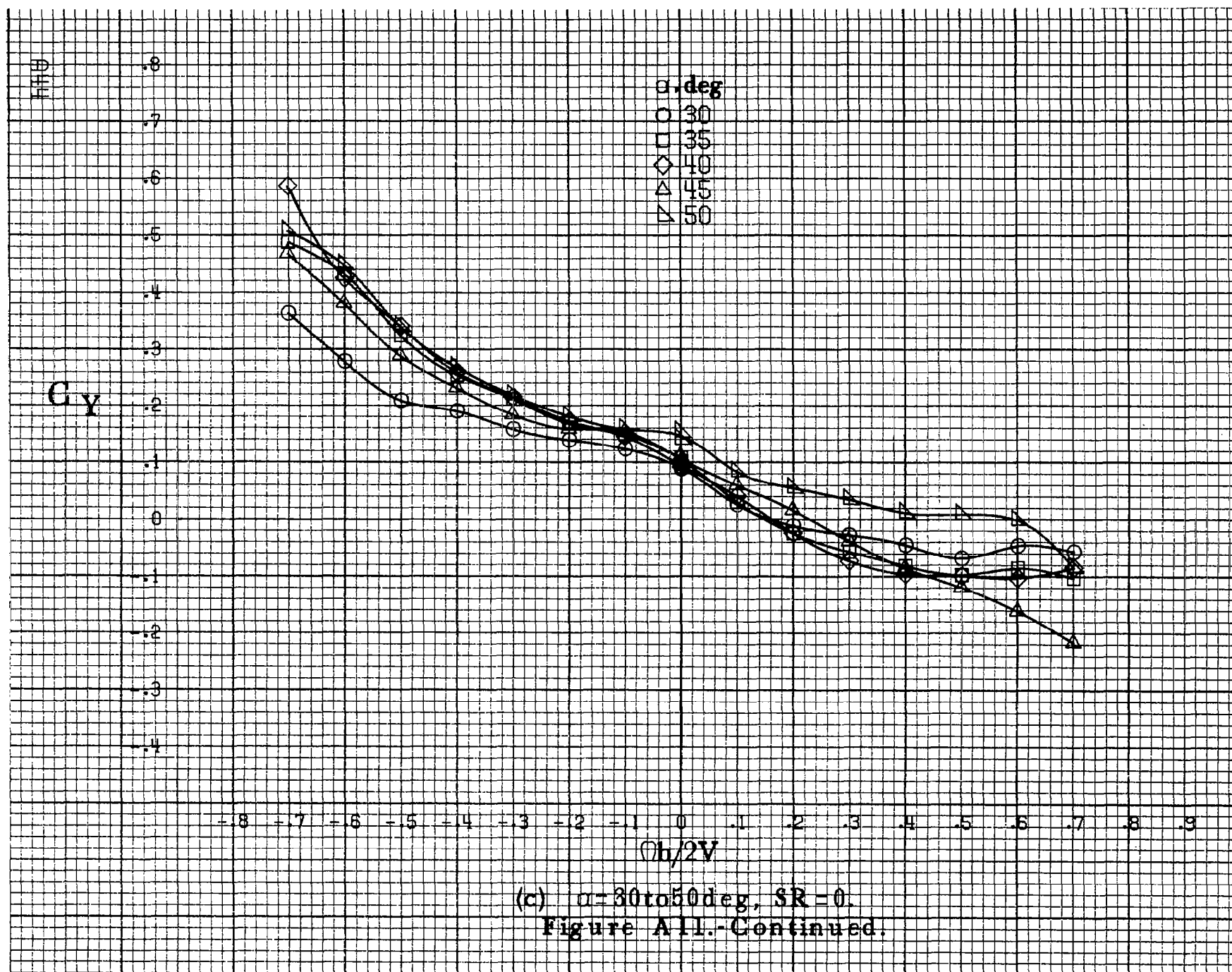


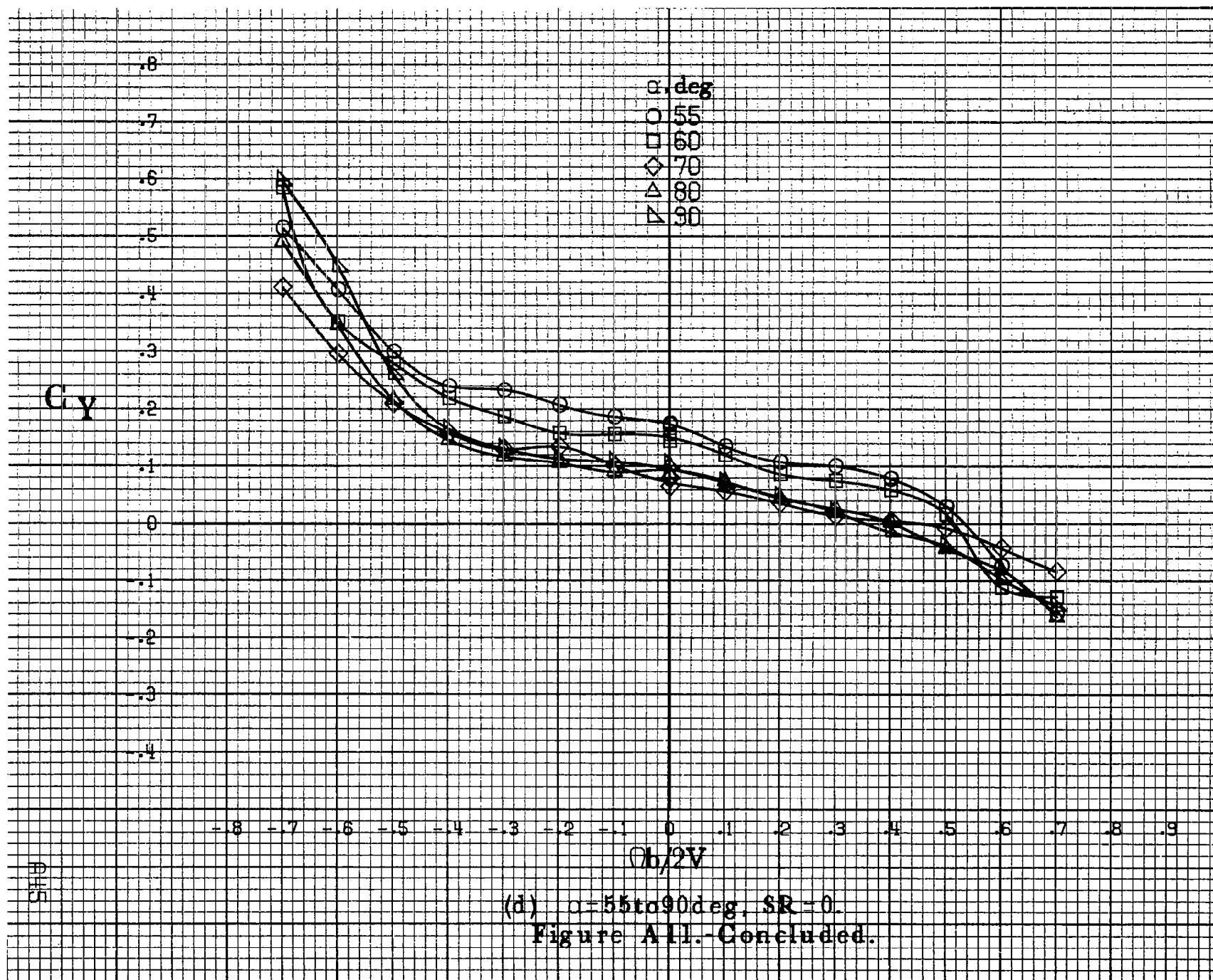


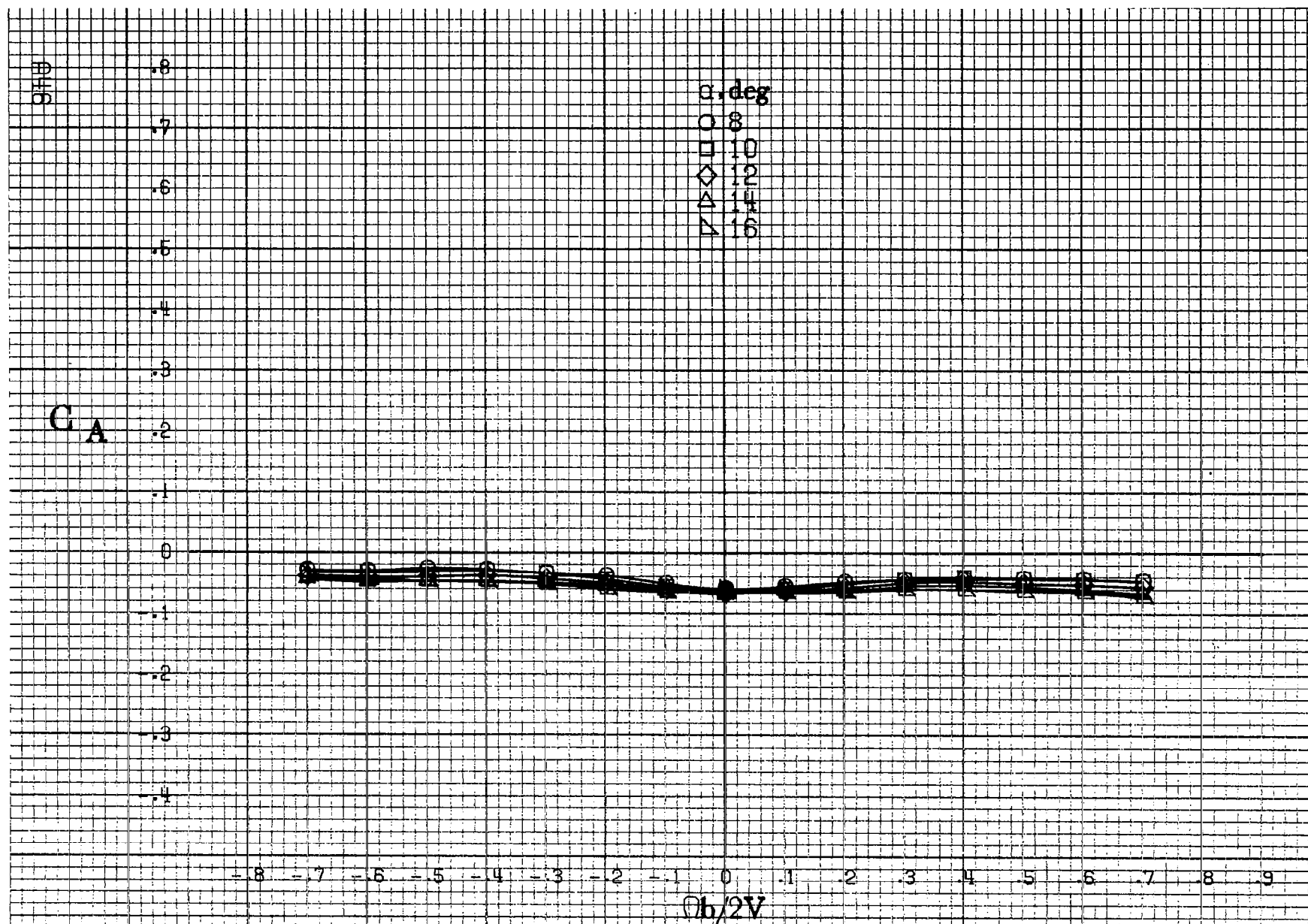
(a) $\alpha = 8$ to 16 deg, $SR = 182.9$ cm (72 in).

Figure A11.-Effect of rotation rate and angle of attack on side force coefficient for body wing configuration. $\delta_e = 0^\circ$, $\delta_a = 0^\circ$, $\delta_r = 0^\circ$, $\beta = 0^\circ$.



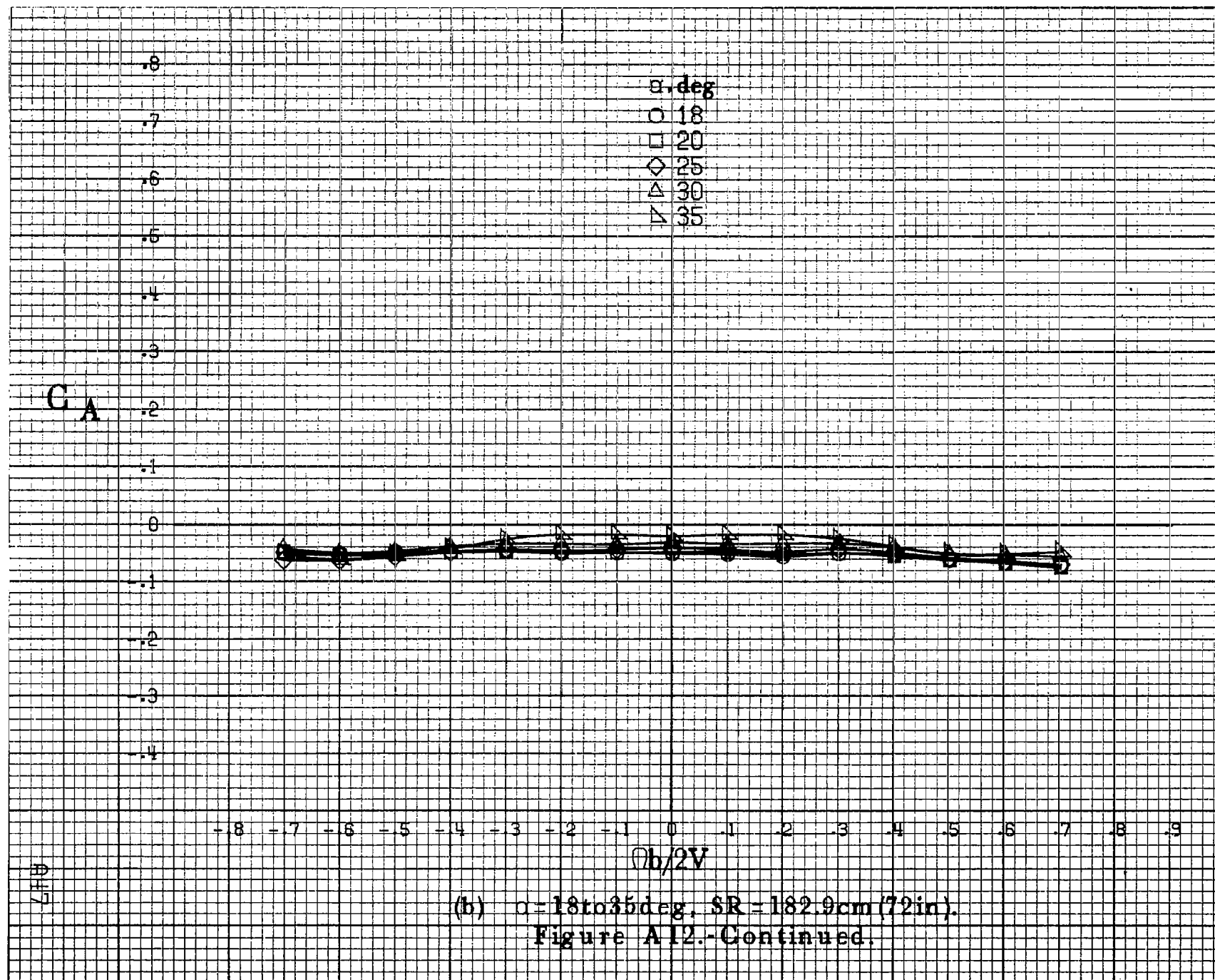


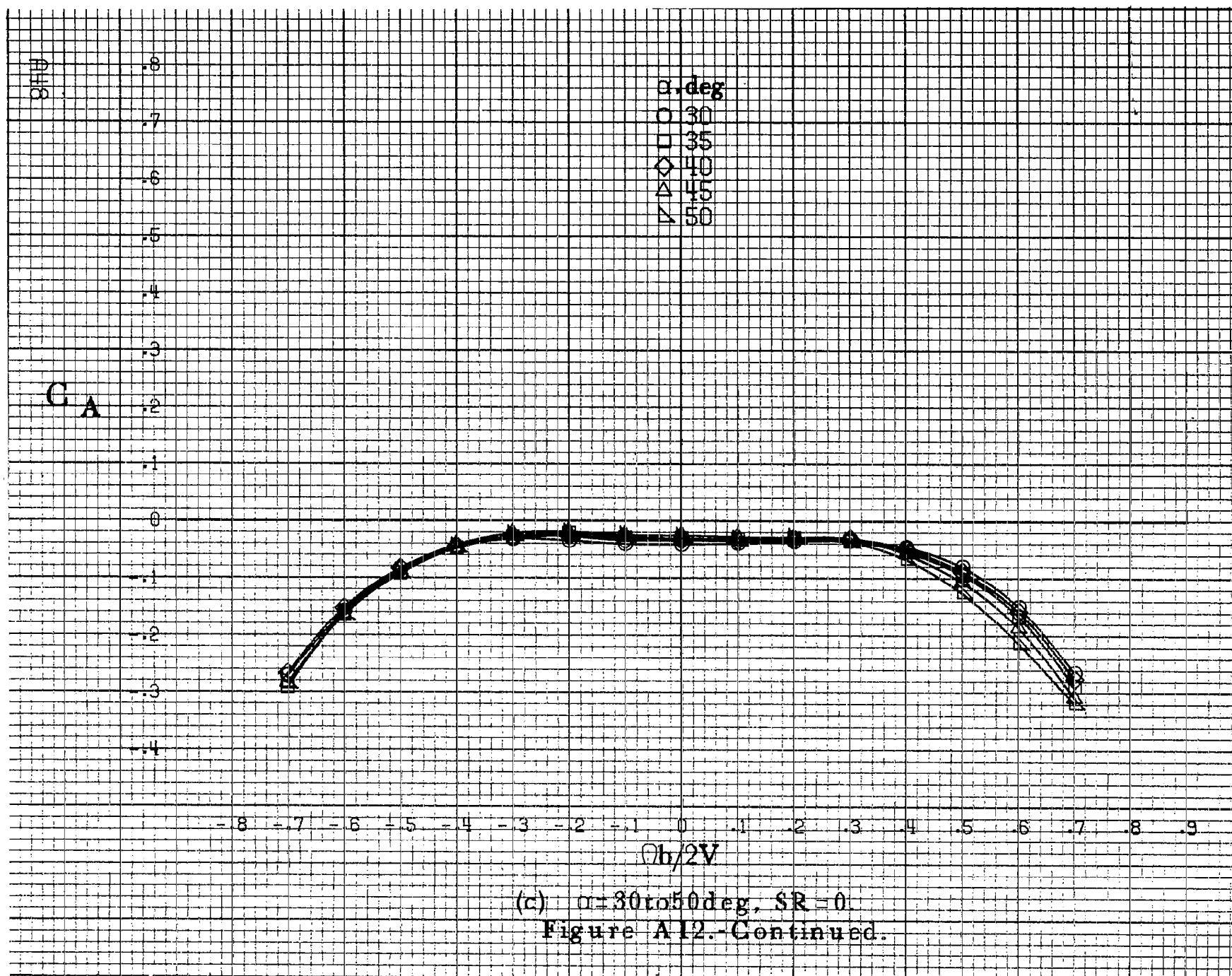


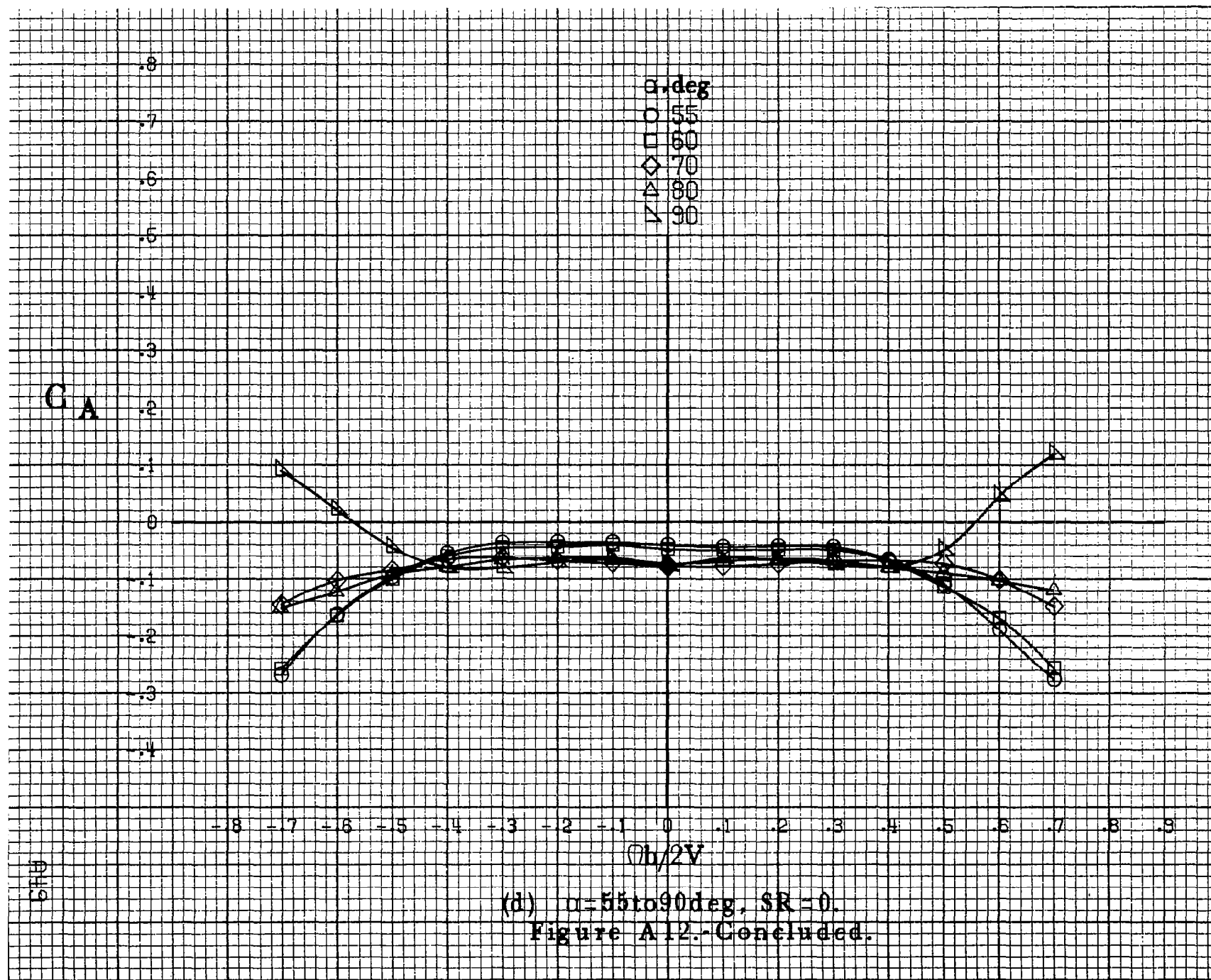


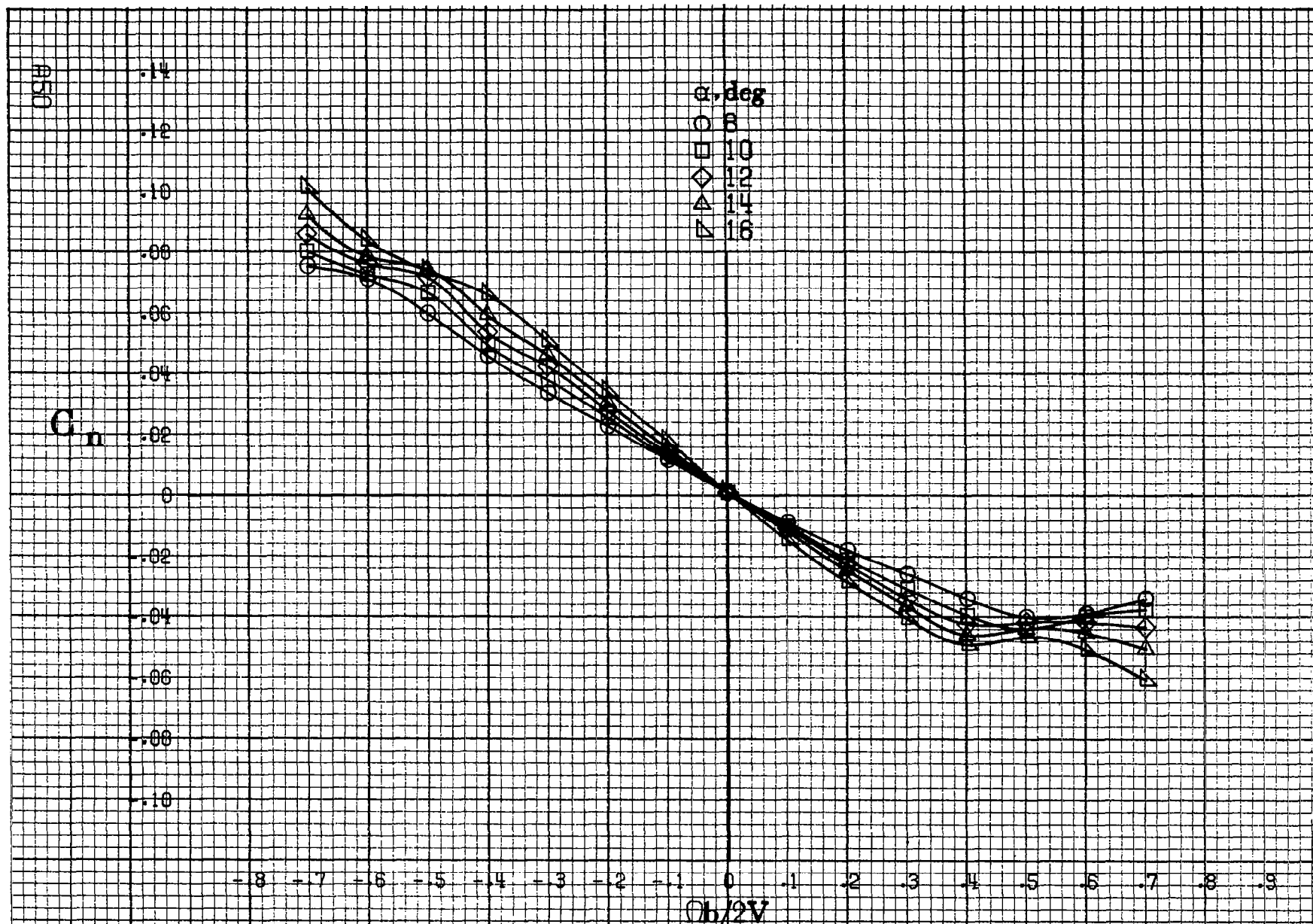
(a) $\alpha=8$ to 16° , $SR=182.9\text{cm}(72\text{in})$.

Figure A12.-Effect of rotation rate and angle of attack on axial-force coefficient for body wing configuration. $\delta_a=0^\circ$, $\delta_s=0^\circ$, $\delta_r=0^\circ$, $\beta=0^\circ$.









(a) $\alpha = 8$ to 16° , $SR = 182.9 \text{ cm (72 in)}$.

Figure A13.-Effect of rotation rate and angle of attack on yawing-moment coefficient for body wing vertical tail configuration $\delta_a = 10^\circ$, $\delta_e = 10^\circ$, $\delta_r = 0^\circ$, $\delta = 10^\circ$.

C_n

α, deg

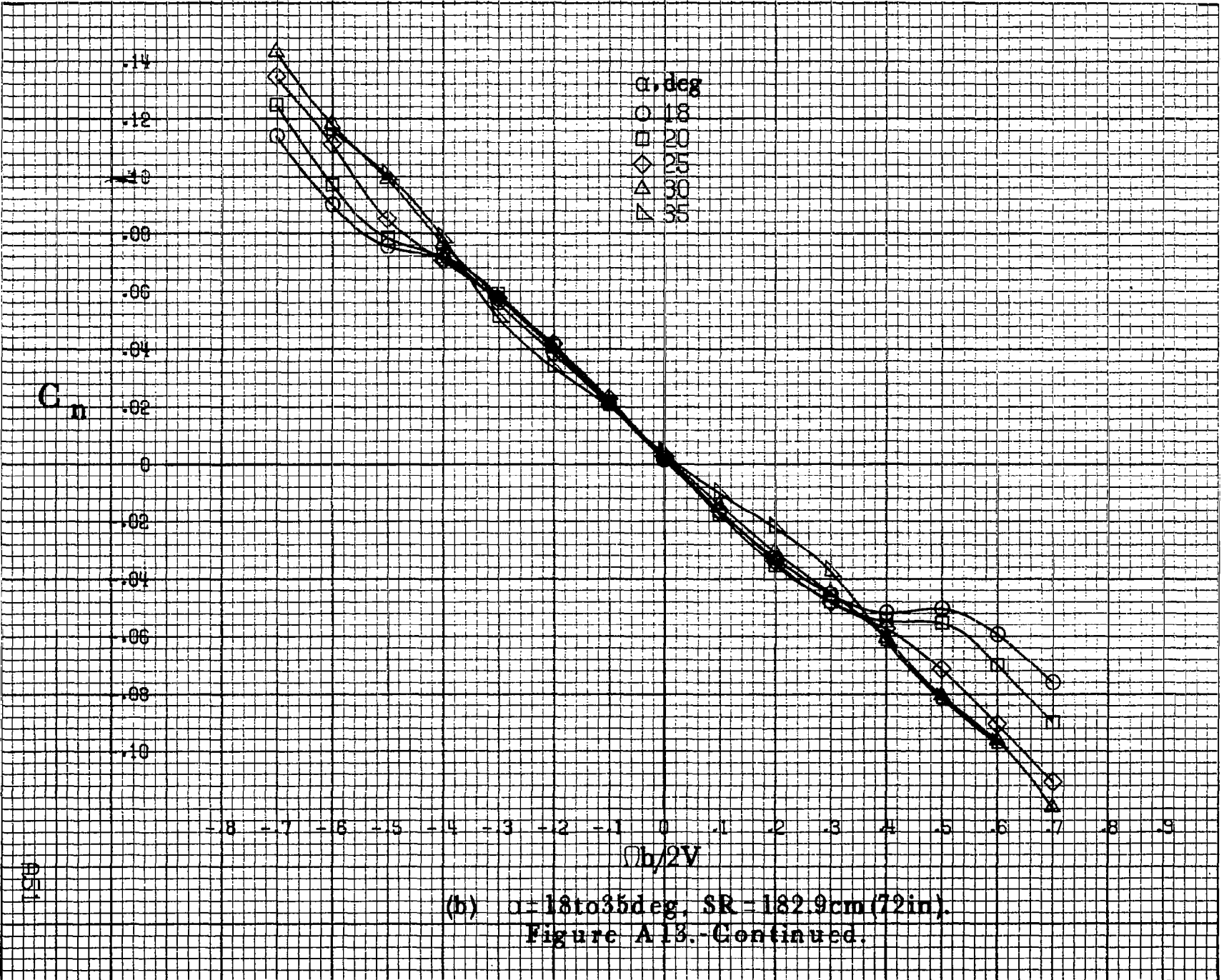
- 18
- 20
- ◇ 25
- △ 30
- ▽ 35

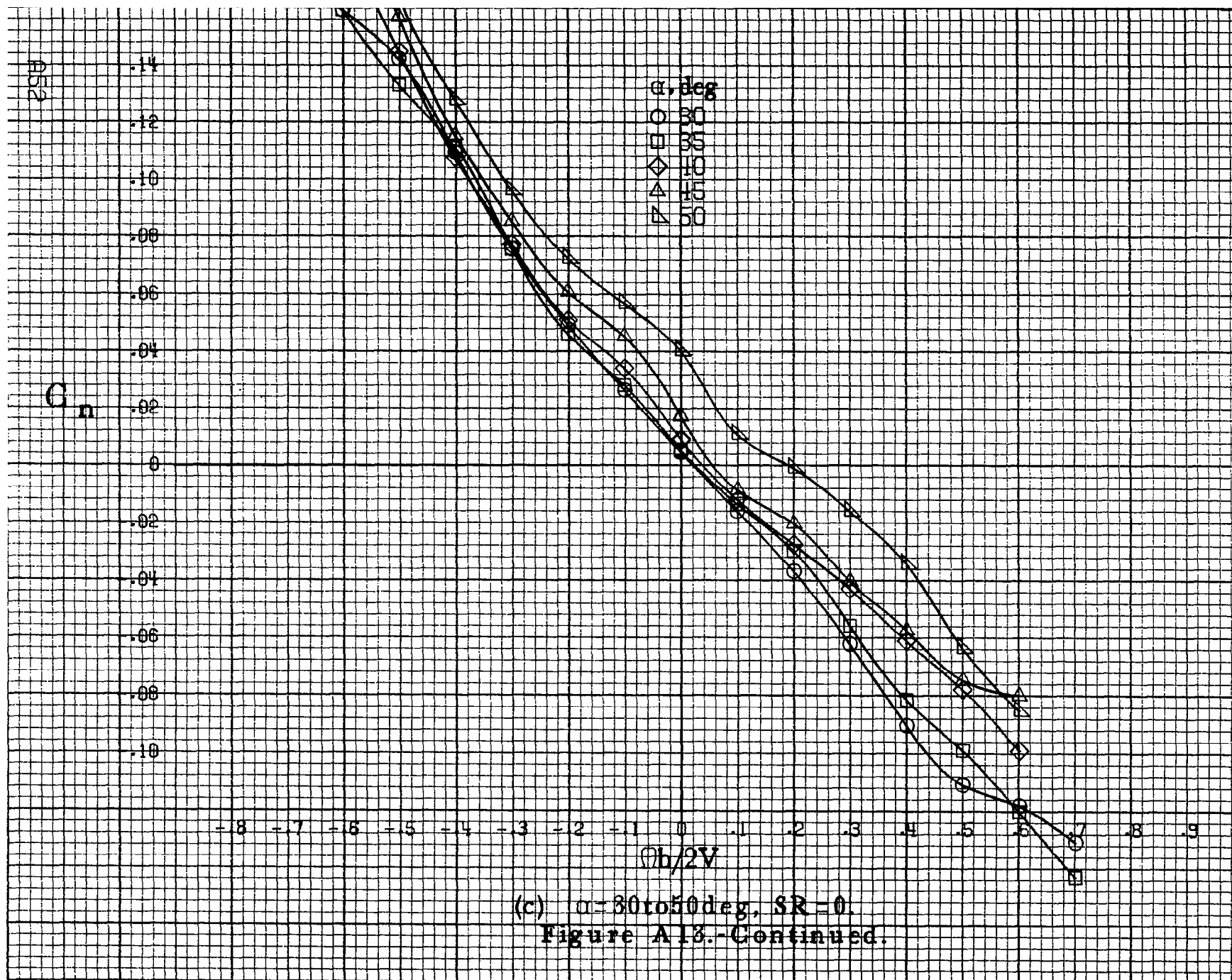
051

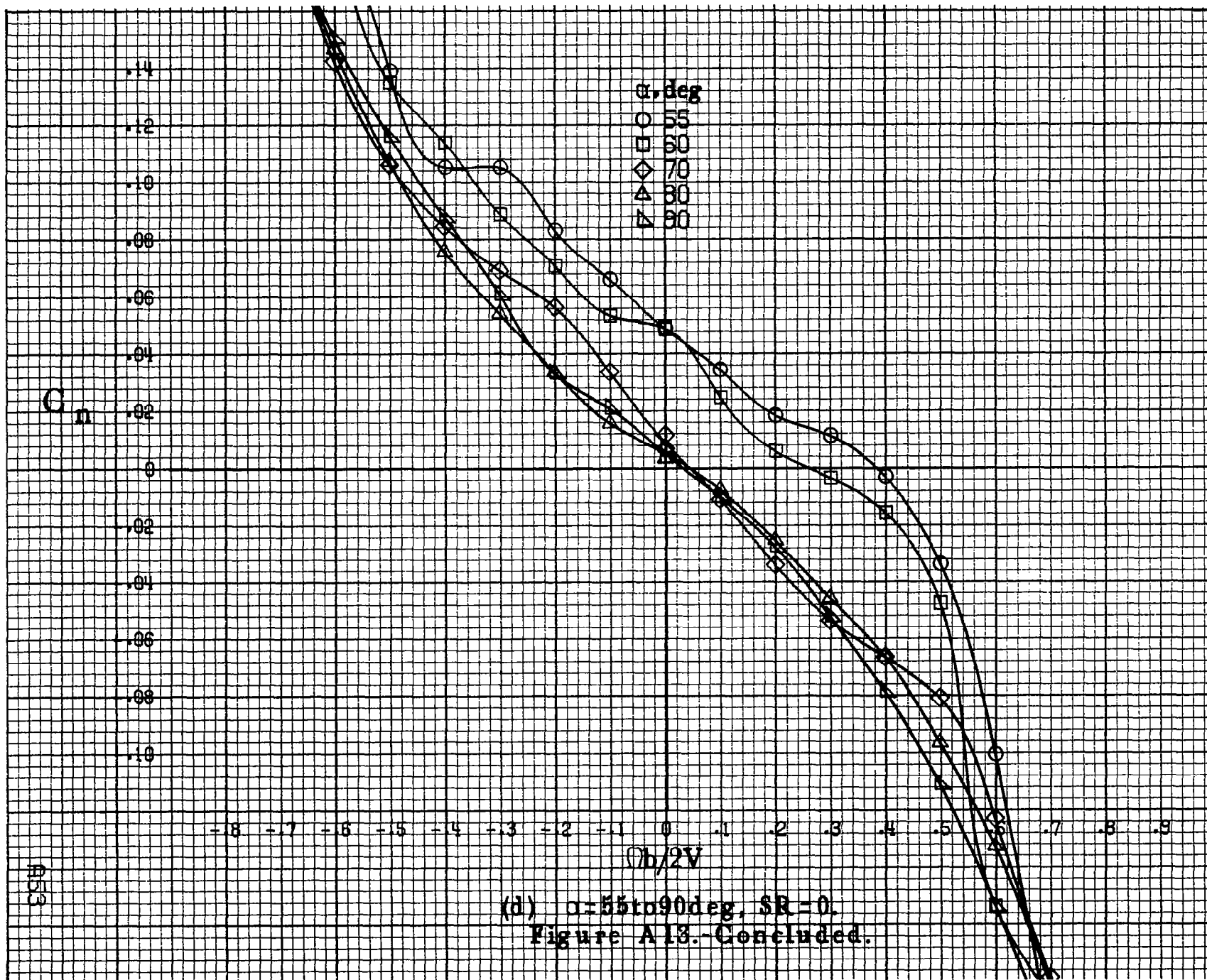
$\Omega b/2V$

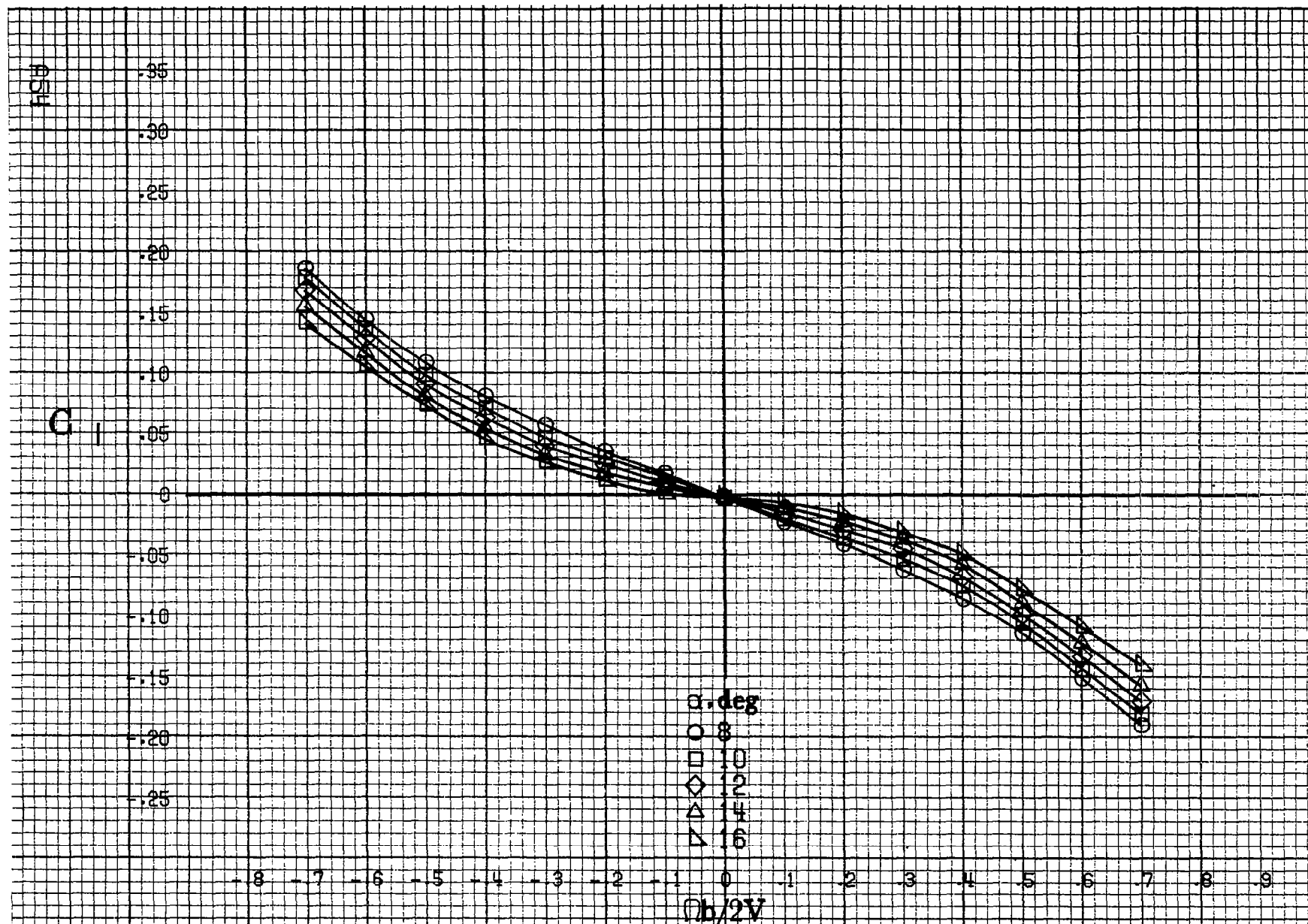
(b) $\alpha=18$ to 35 deg, SR = 182.9 cm (72 in).

Figure A13.-Continued.









(a) $\alpha=8$ to 16° , $SR=182.9\text{cm}(72\text{in})$.

Figure A14.-Effect of rotation rate and angle of attack on rolling-moment coefficient for body wing vertical tail configuration $\delta_a = 0^\circ$, $\delta_e = 0^\circ$, $\delta_r = 0^\circ$, $\delta = 0^\circ$.

C

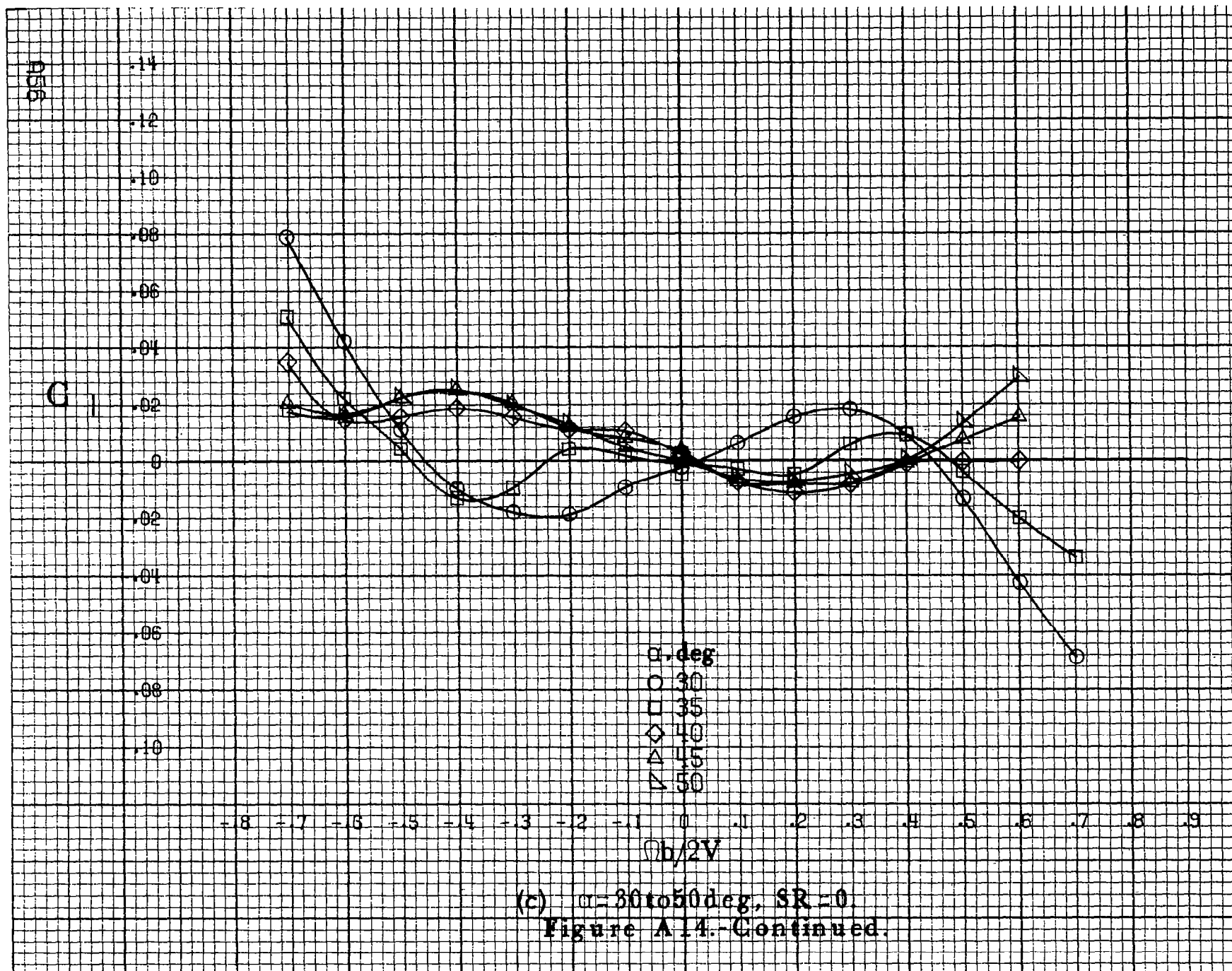
.14
.12
.10
.08
.06
.04
.02
0
-.02
-.04
-.06
-.08
-.10

α , deg
○ 18
□ 20
◇ 25
△ 30
△ 35

-0.8 -0.7 -0.6 -0.5 -0.4 -0.3 -0.2 -0.1 0 0.1 0.2 0.3 0.4 0.5 0.6 0.7 0.8 0.9
 $b/2V$

055

(b) $\alpha = 18$ to 35 deg, $SR = 182.9$ cm (72 in).
Figure A14. Continued.



C₁

.14
.12
.10
.08
.06
.04
.02
0
.02
.04
.06
.08
.10

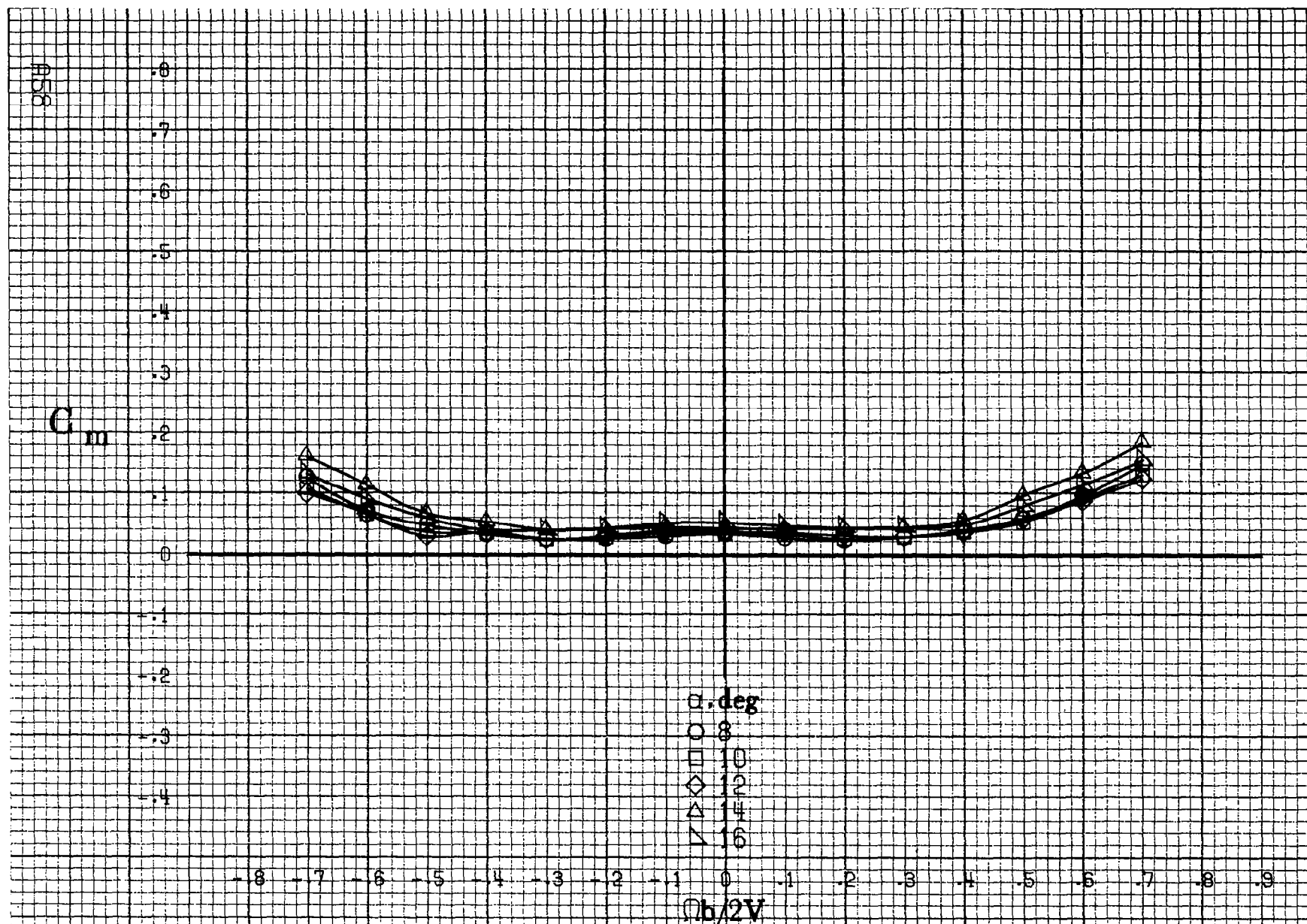
-0.8 -0.7 -0.6 -0.5 -0.4 -0.3 -0.2 -0.1 0 .1 .2 .3 .4 .5 .6 .7 .8 .9

α .deg
○ 55
□ 60
◇ 70
△ 80
▽ 90

$Ob/2V$

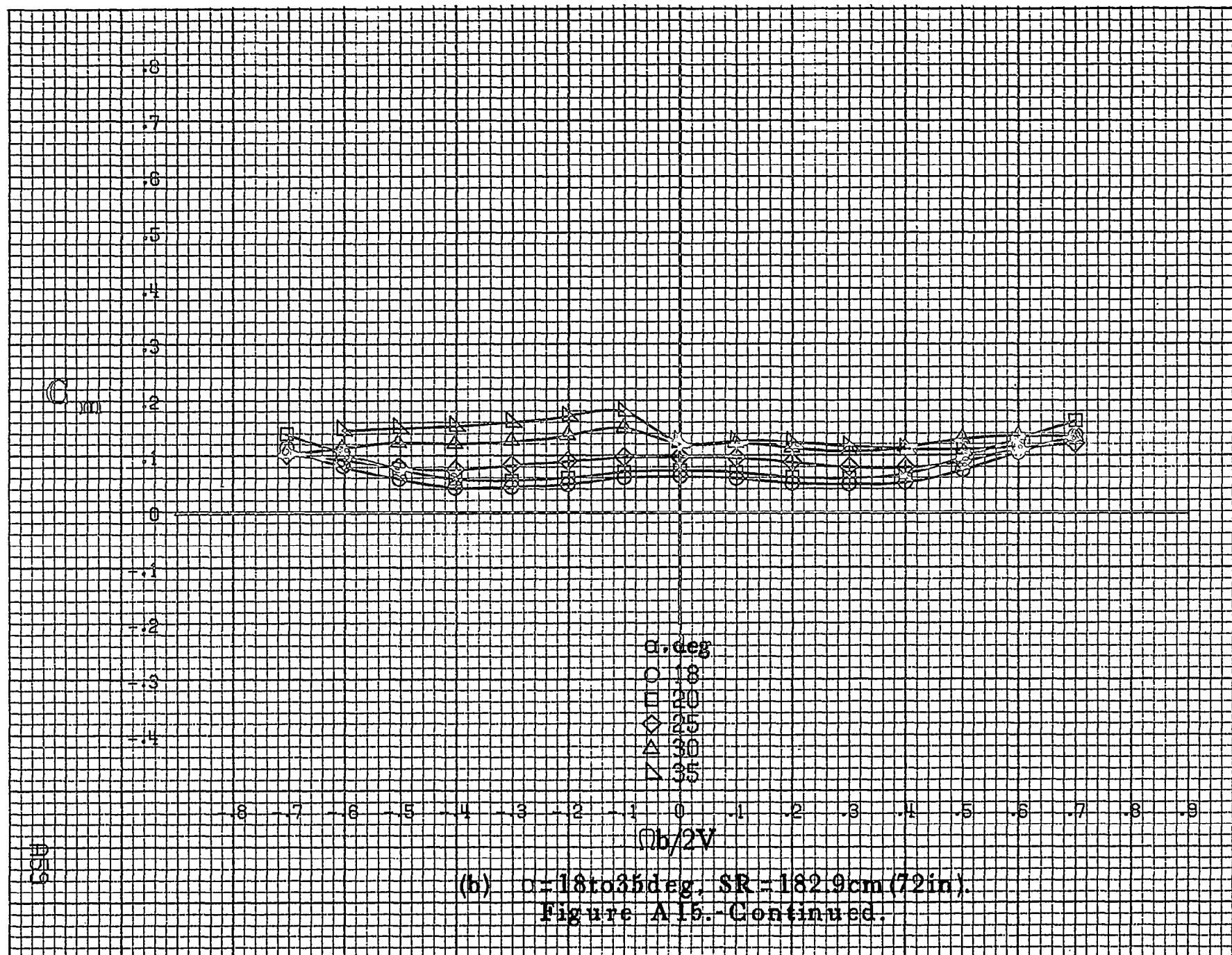
(d) $\alpha=55$ to 90 deg, $SR=0$.
Figure A14.-Concluded.

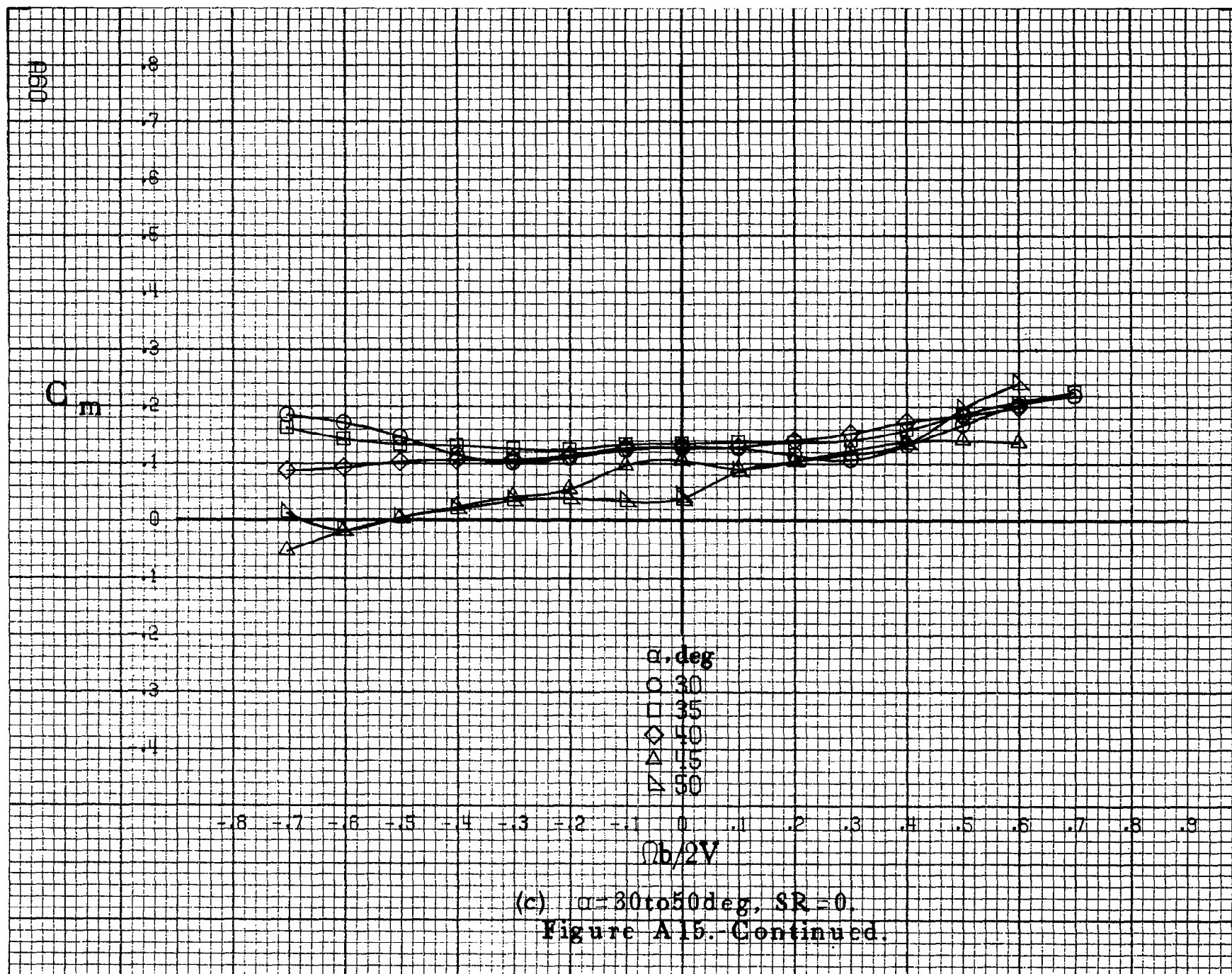
AS7

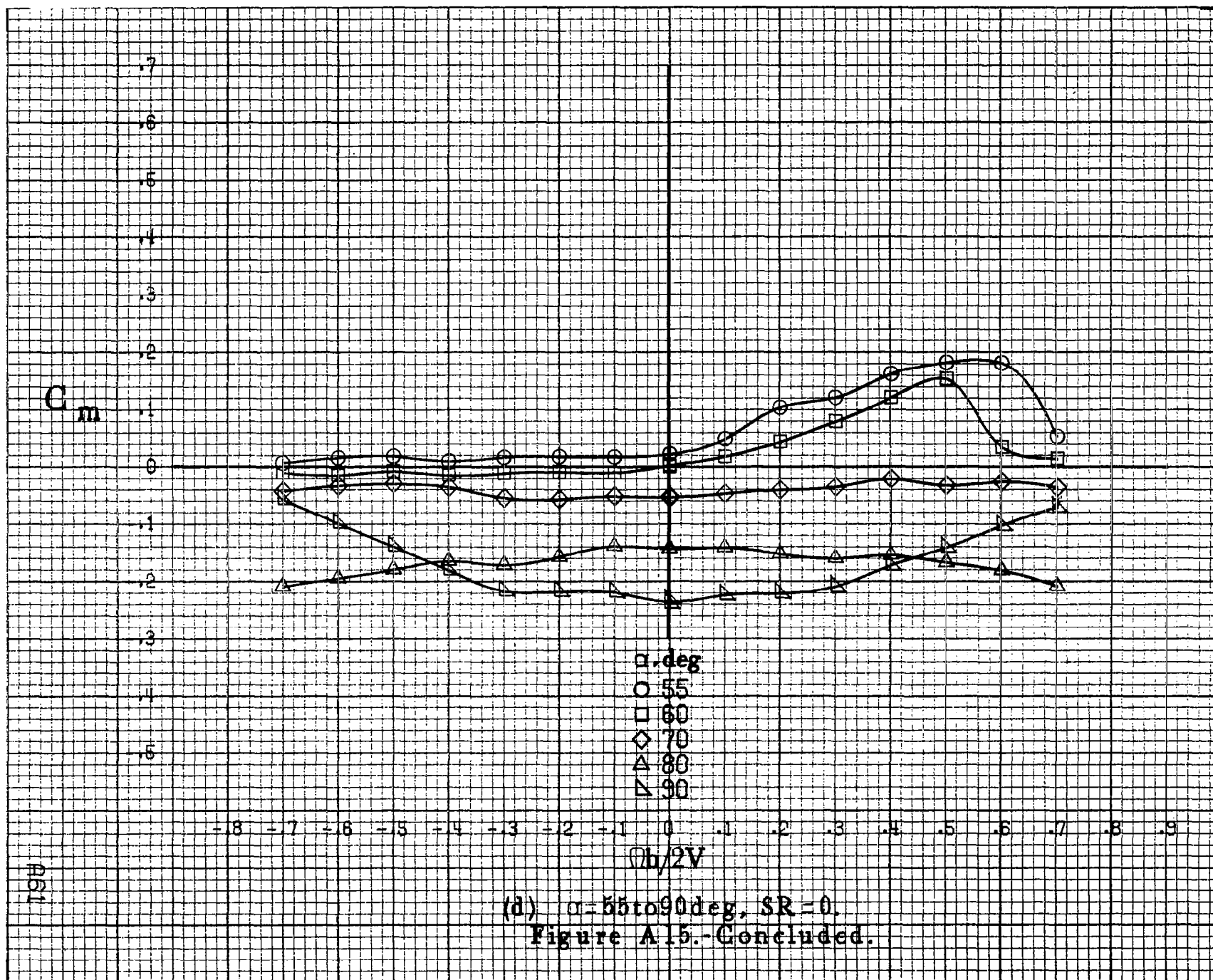


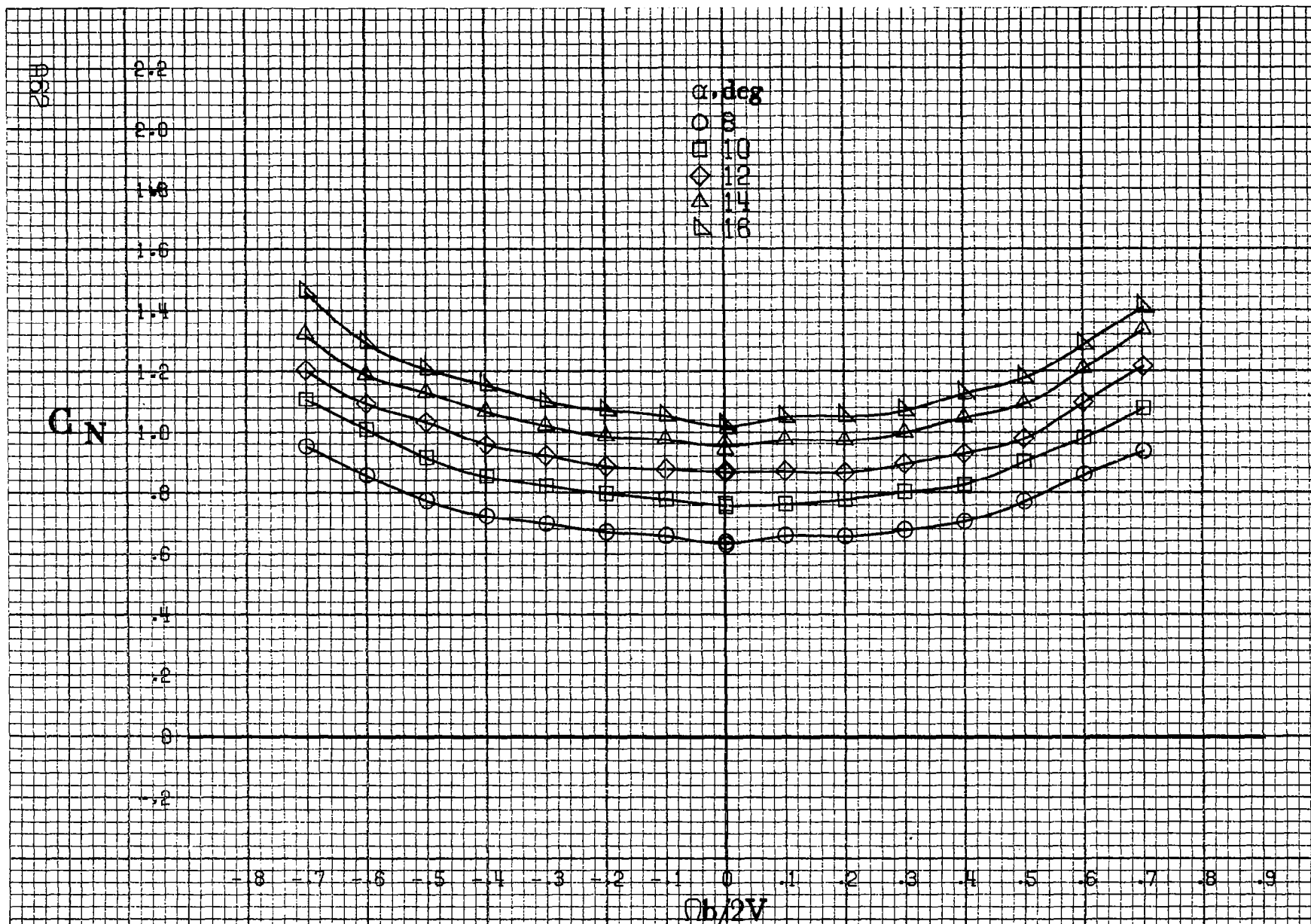
(a) $\alpha = 8$ to 16 deg, $SR = 182.9 \text{ cm (72 in)}$.

Figure A15.-Effect of rotation rate and angle of attack on pitching-moment coefficient for body wing vertical tail configuration $\delta_e = 0^\circ$, $\delta_a = 0^\circ$, $\delta_r = 0^\circ$, $\beta = 0^\circ$.









(a) $\alpha = 8$ to 16° , $SR = 182.9 \text{ cm (72 in.)}$.

Figure A16.-Effect of rotation rate and angle of attack on normal-force coefficient for body wing vertical tail configuration $\delta_e = 0^\circ$, $\delta_s = 0^\circ$, $\delta_r = 0^\circ$, $\beta = 0^\circ$.

C_N

α, deg
 ○ 18
 □ 20
 ◇ 25
 △ 30
 ▽ 35

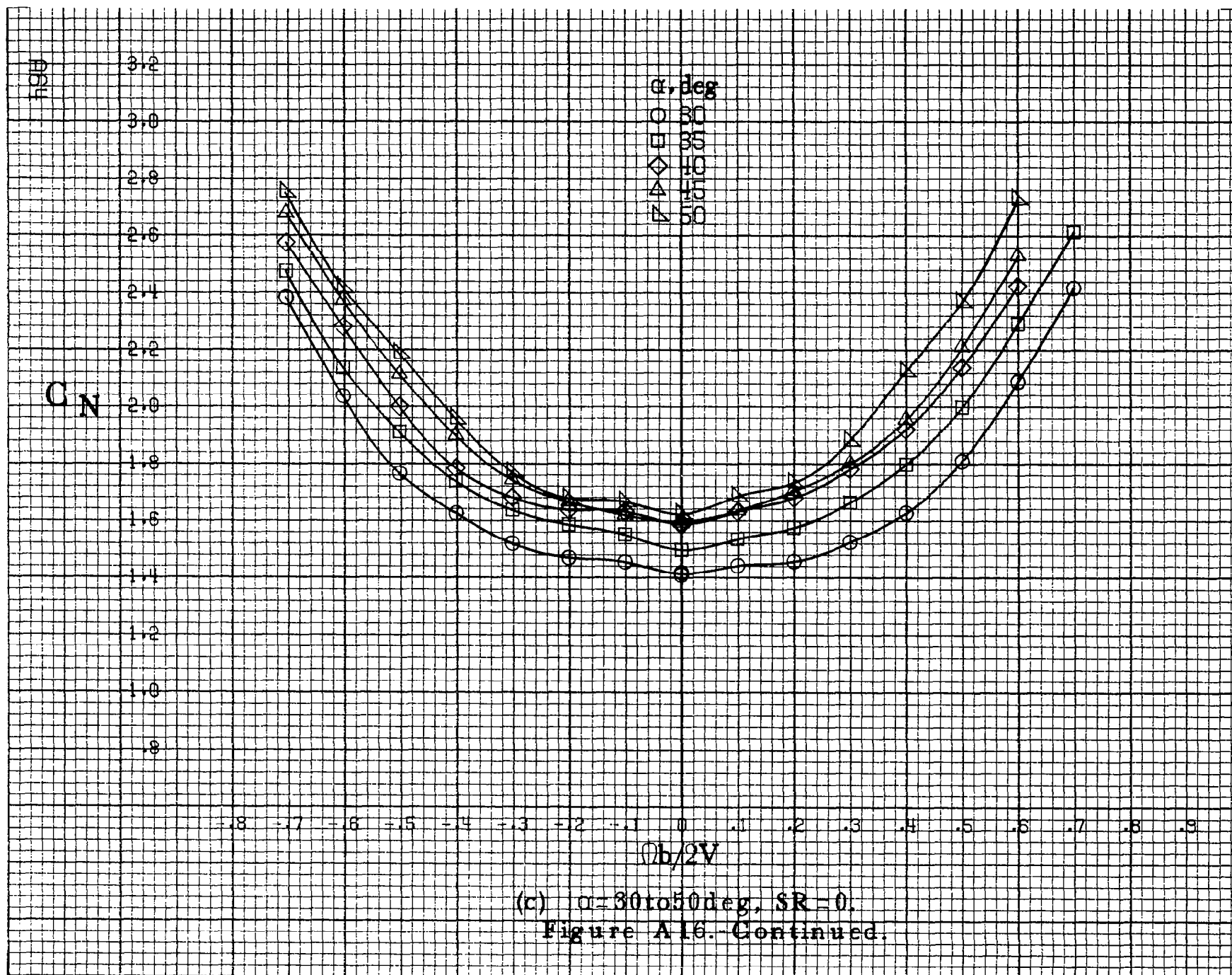
-8 -7 -6 -5 -4 -3 -2 -1 0 .1 .2 .3 .4 .5 .6 .7 .8 .9

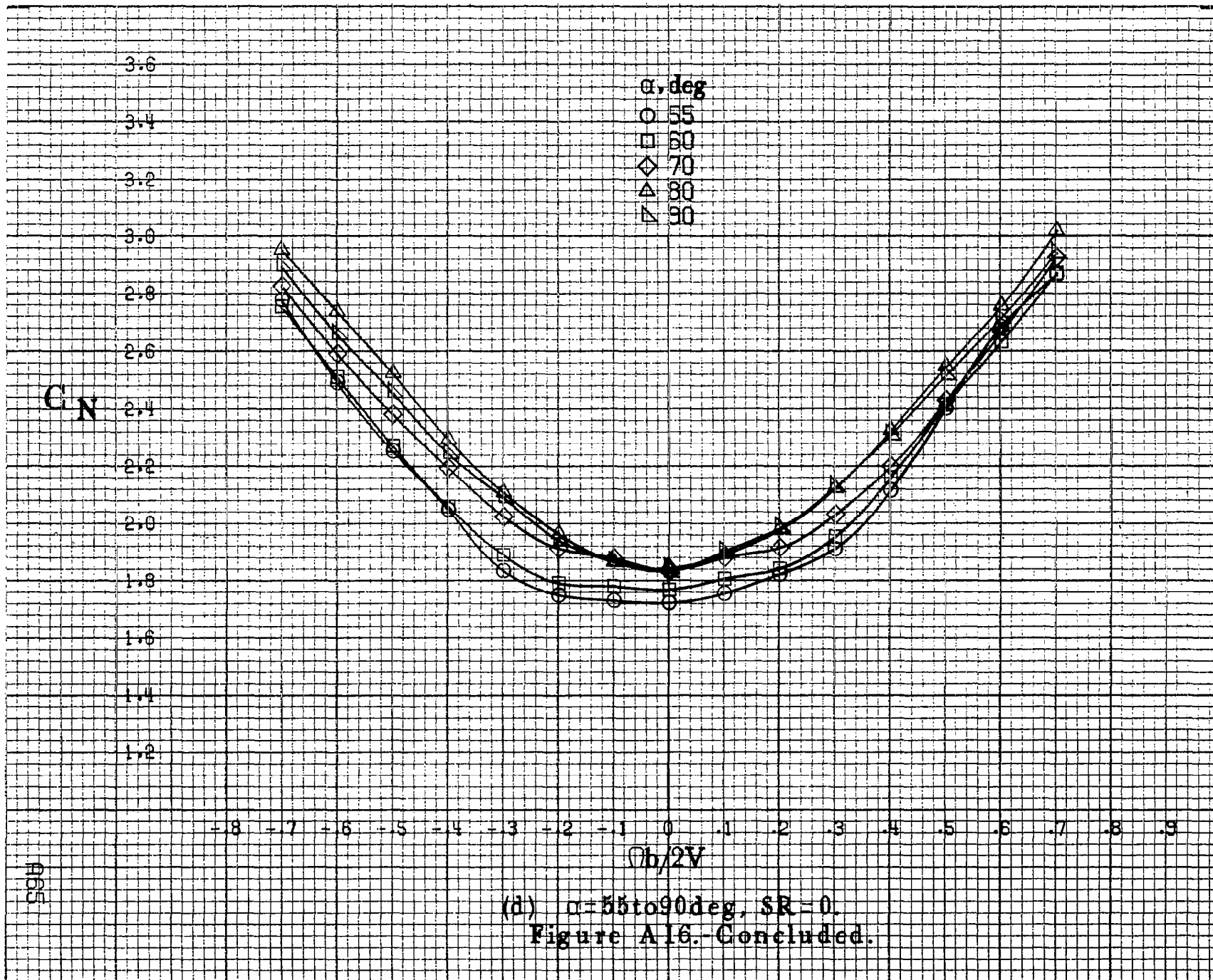
$Qh/2V$

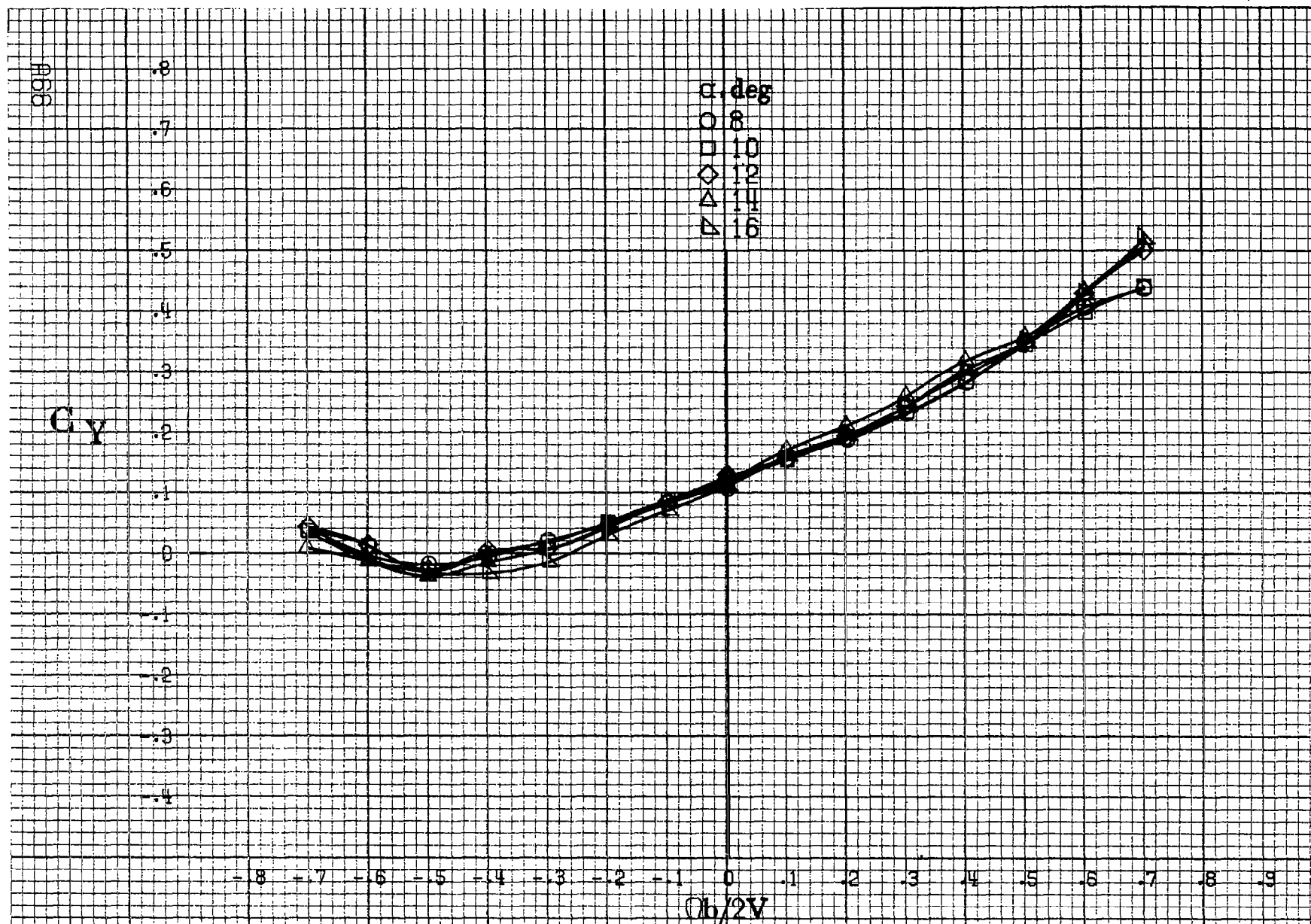
(b) $\alpha = 18 \text{ to } 35 \text{ deg}$, $SR = 182.9 \text{ cm (72 in)}$.

Figure A16.-Continued.

163

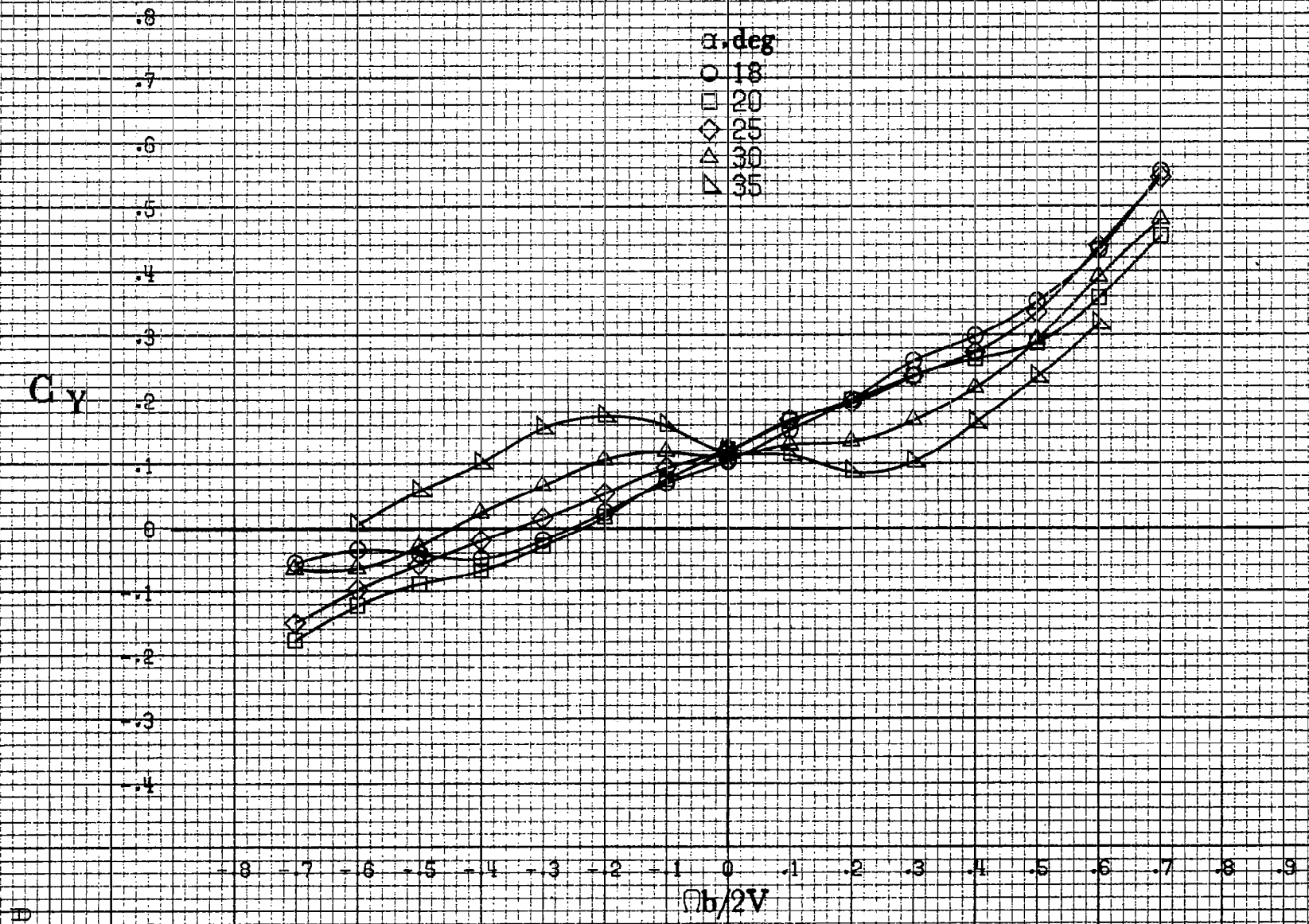






(a) $\alpha = 8$ to 16° , $SR = 182.9 \text{ cm (72 in.)}$.

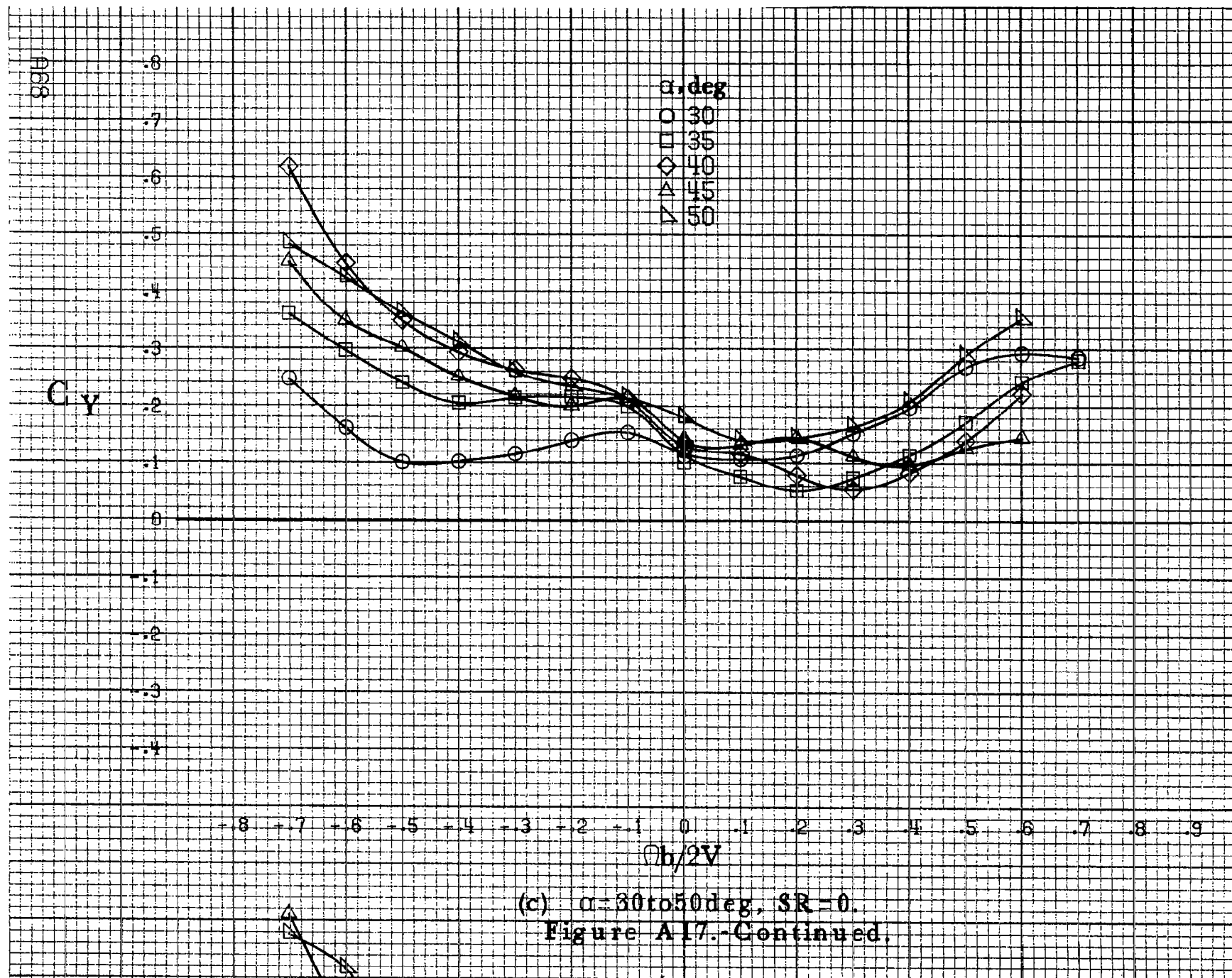
Figure A17 - Effect of rotation rate and angle of attack on side-force coefficient for body wing vertical tail configuration $\delta_a = 0^\circ$, $\delta_s = 0^\circ$, $\delta_r = 0^\circ$, $\delta = 0^\circ$.

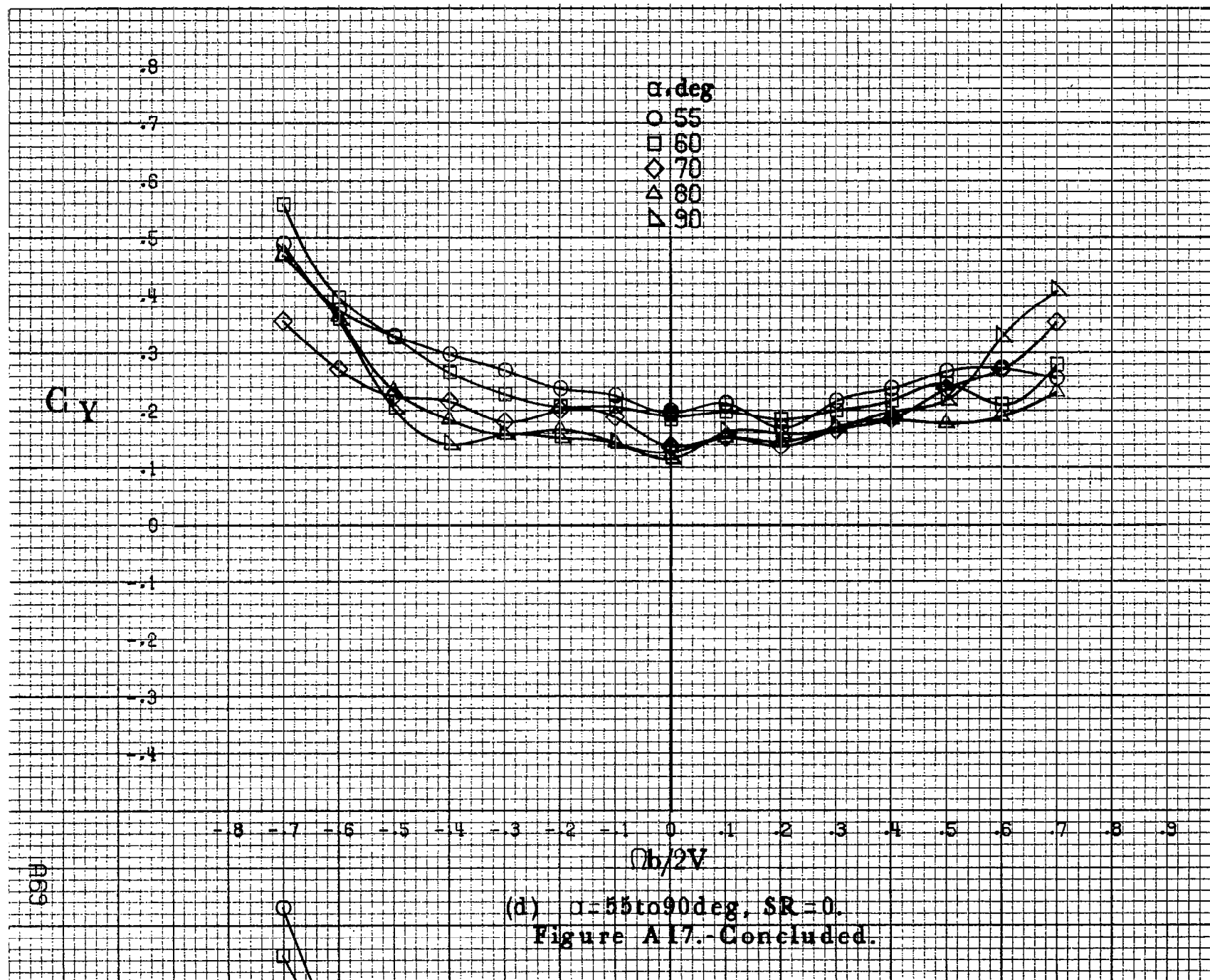


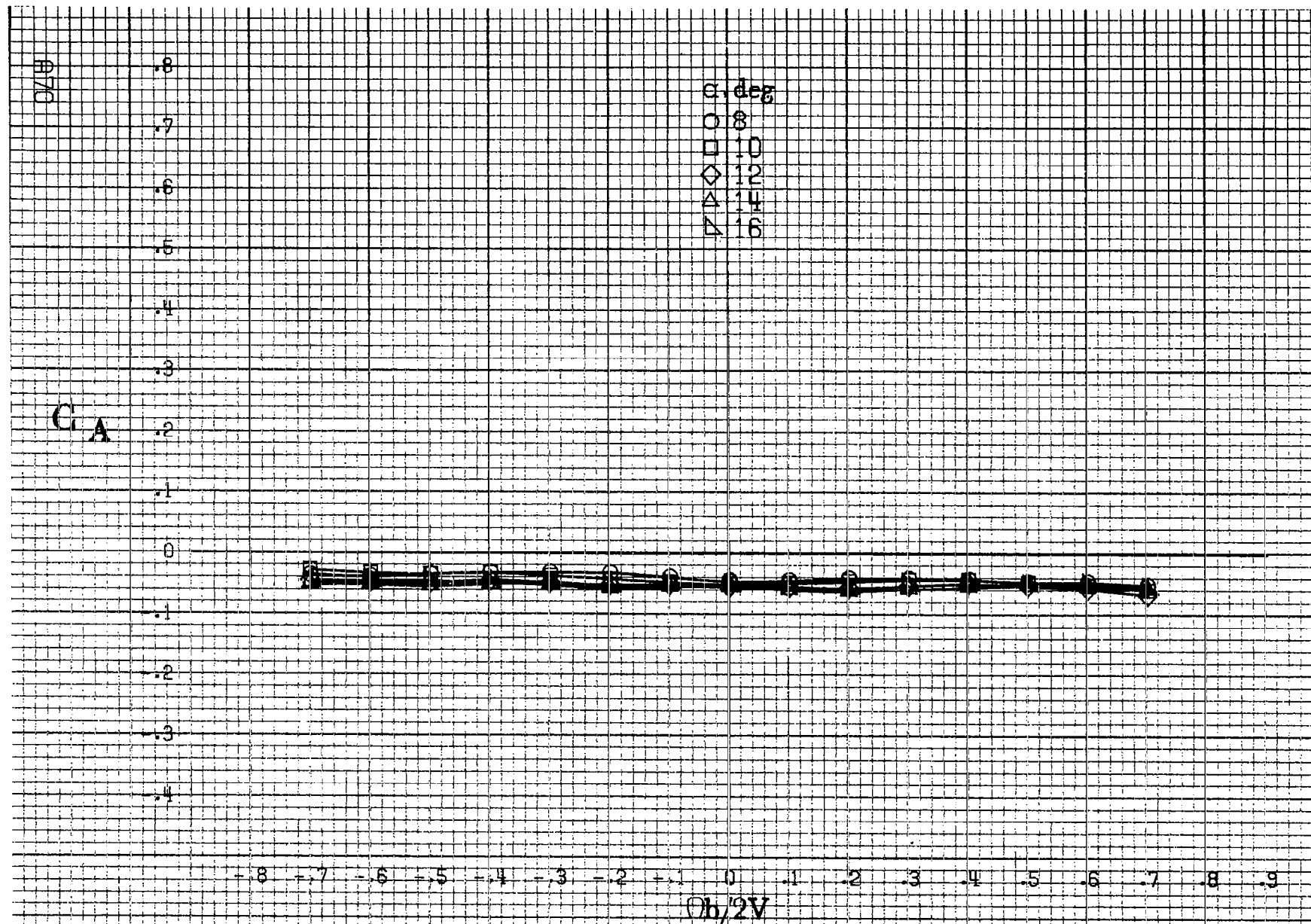
(b) $\alpha = 18$ to 35° , SR = 182.9 cm (72 in).

Figure A17.-Continued.

1057

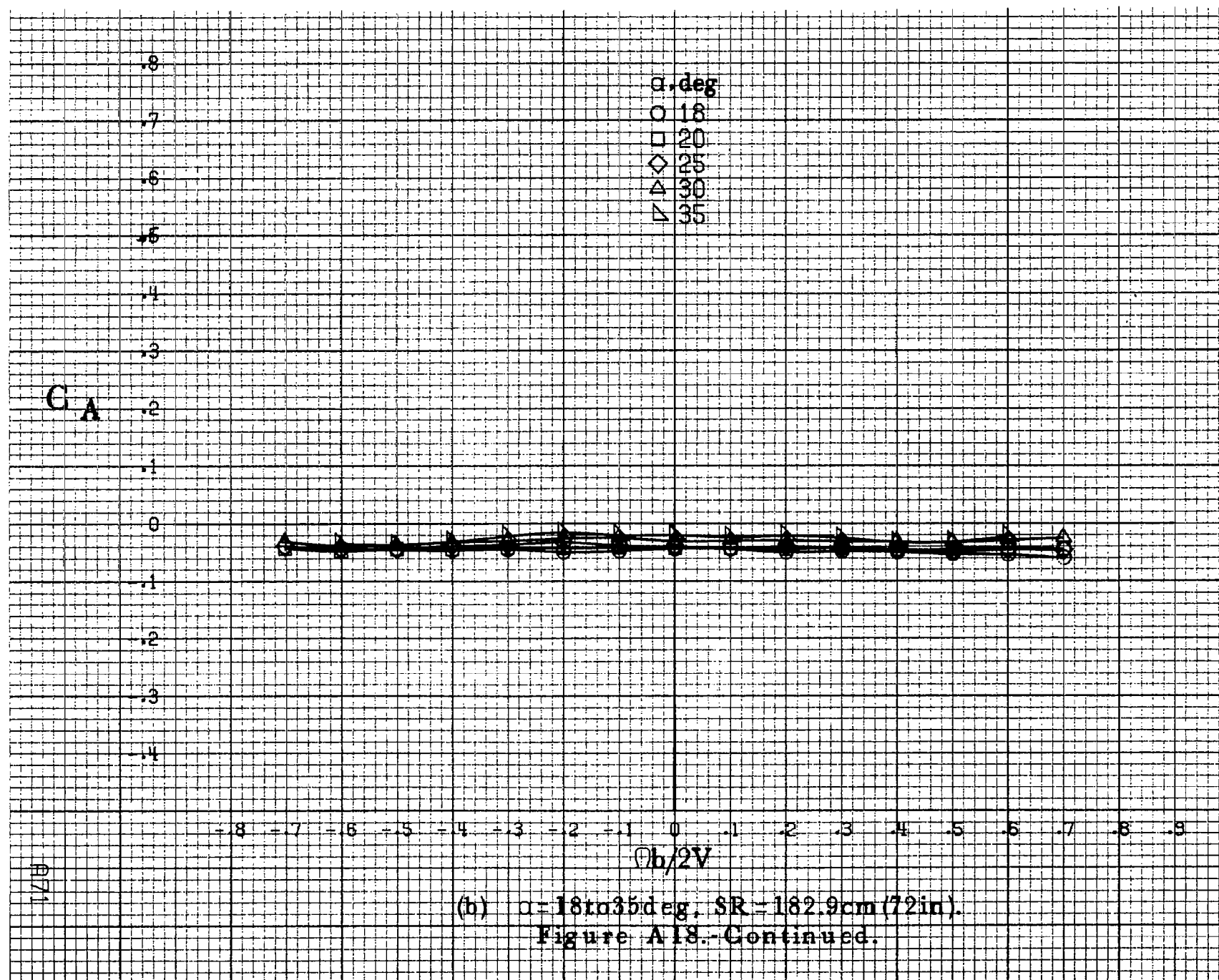




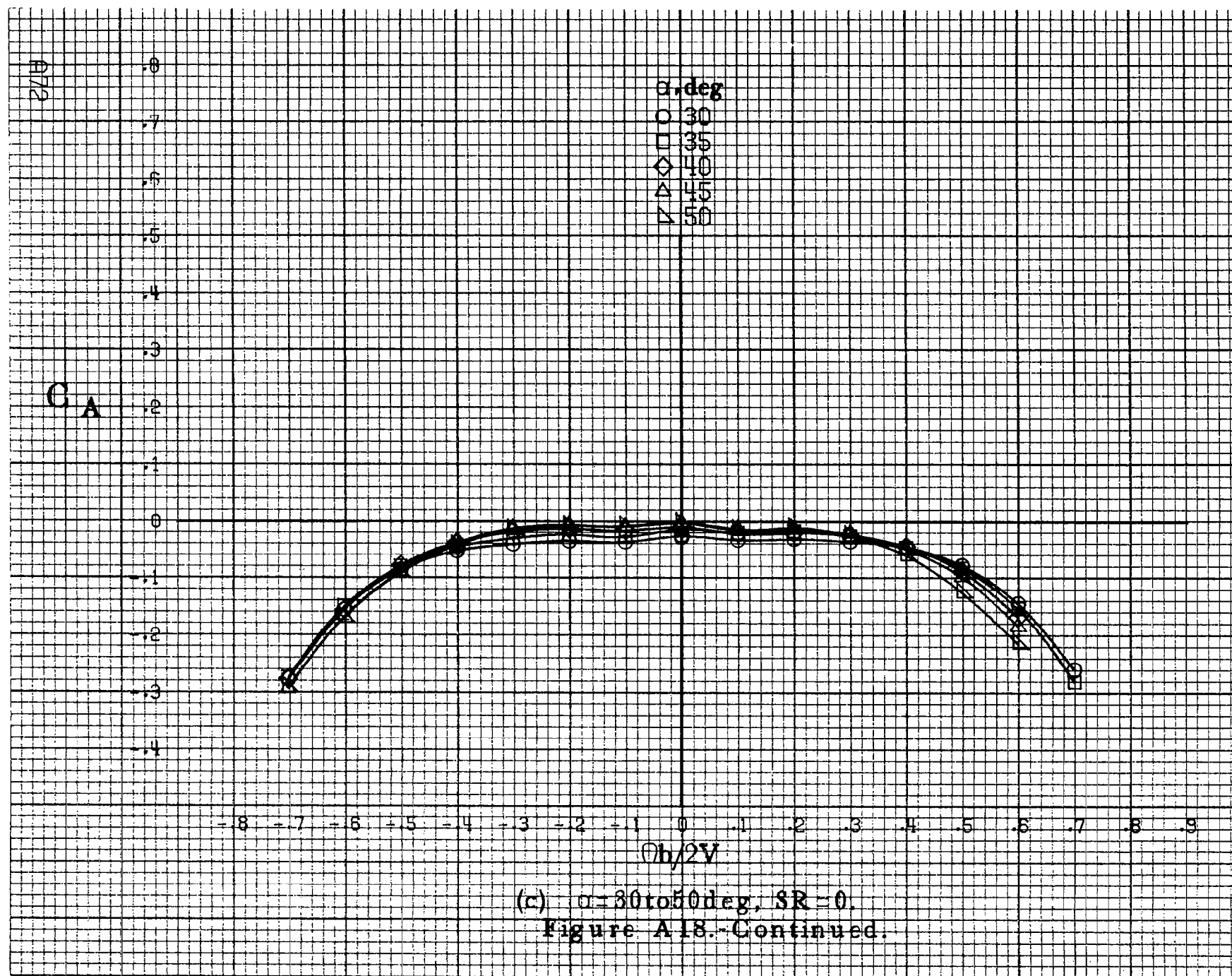


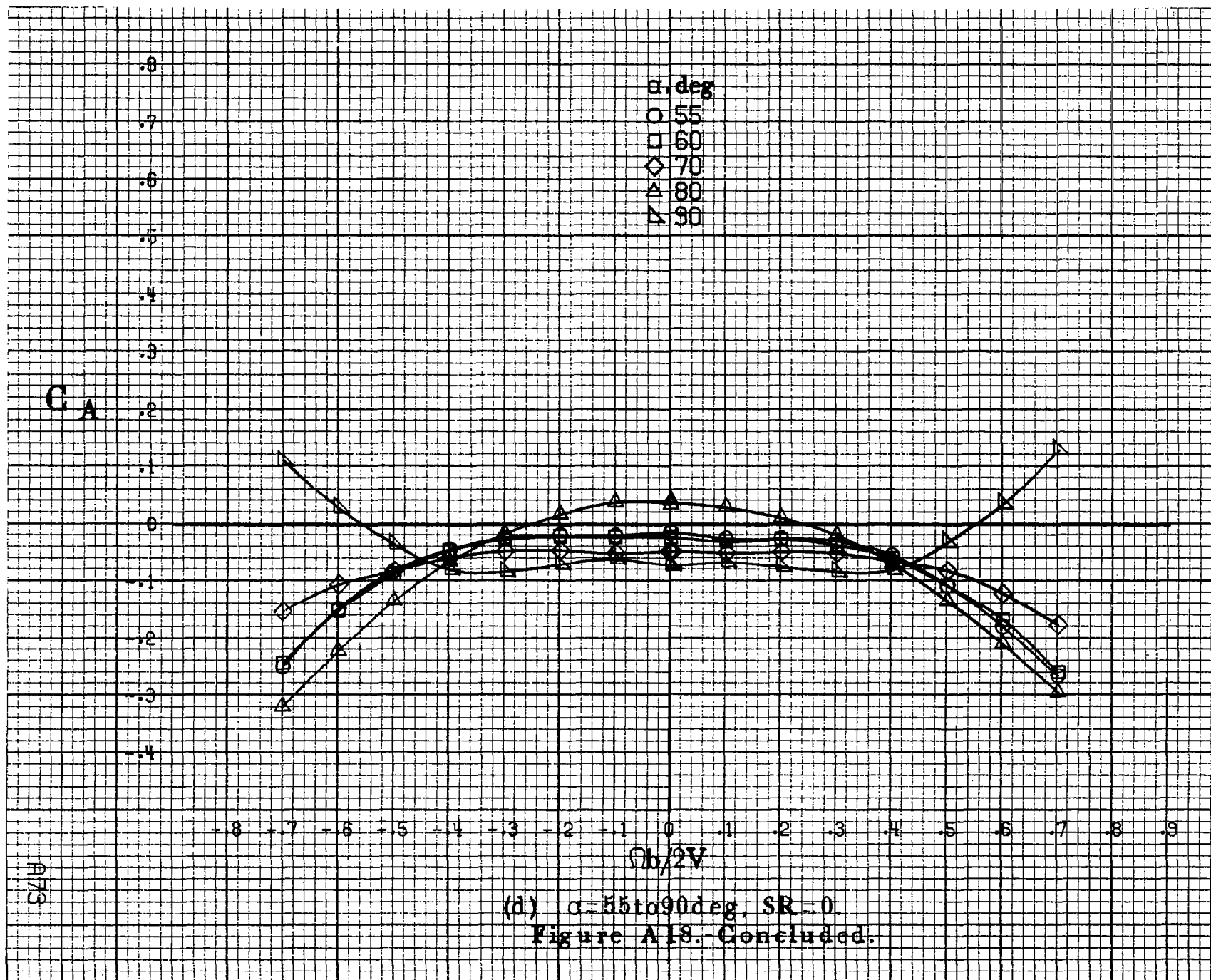
(a) $\alpha = 8$ to 16° , $SR = 182.9 \text{ cm (72 in)}$.

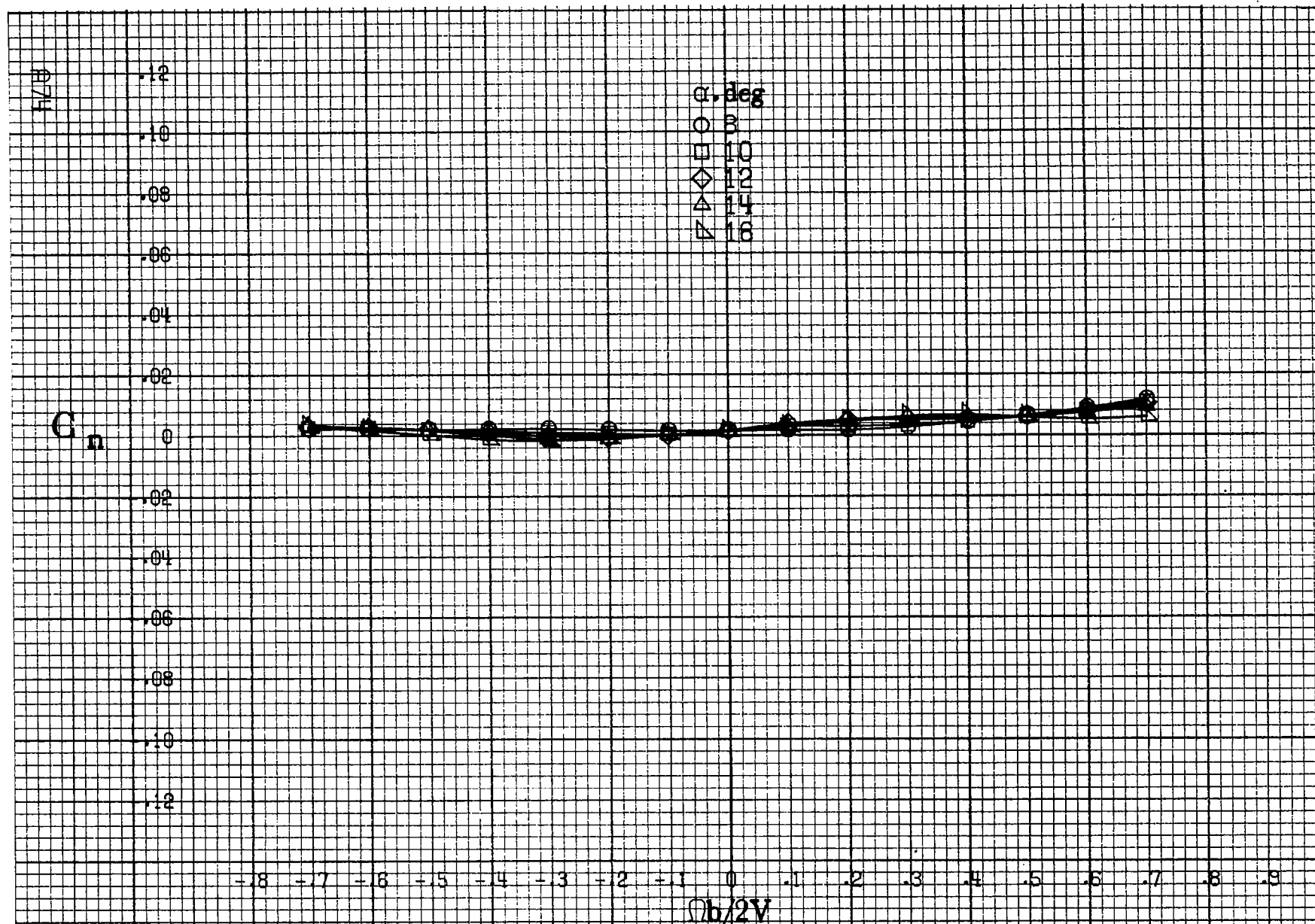
Figure A18 - Effect of rotation rate and angle of attack on axial-force coefficient for body wing vertical tail configuration $\delta_e = 0^\circ$, $\delta_a = 0^\circ$, $\delta_r = 0^\circ$, $\beta = 0^\circ$.



(b) $\alpha=18$ to 35° , $SR=162.9\text{cm}(72\text{in})$.
Figure A18.-Continued.

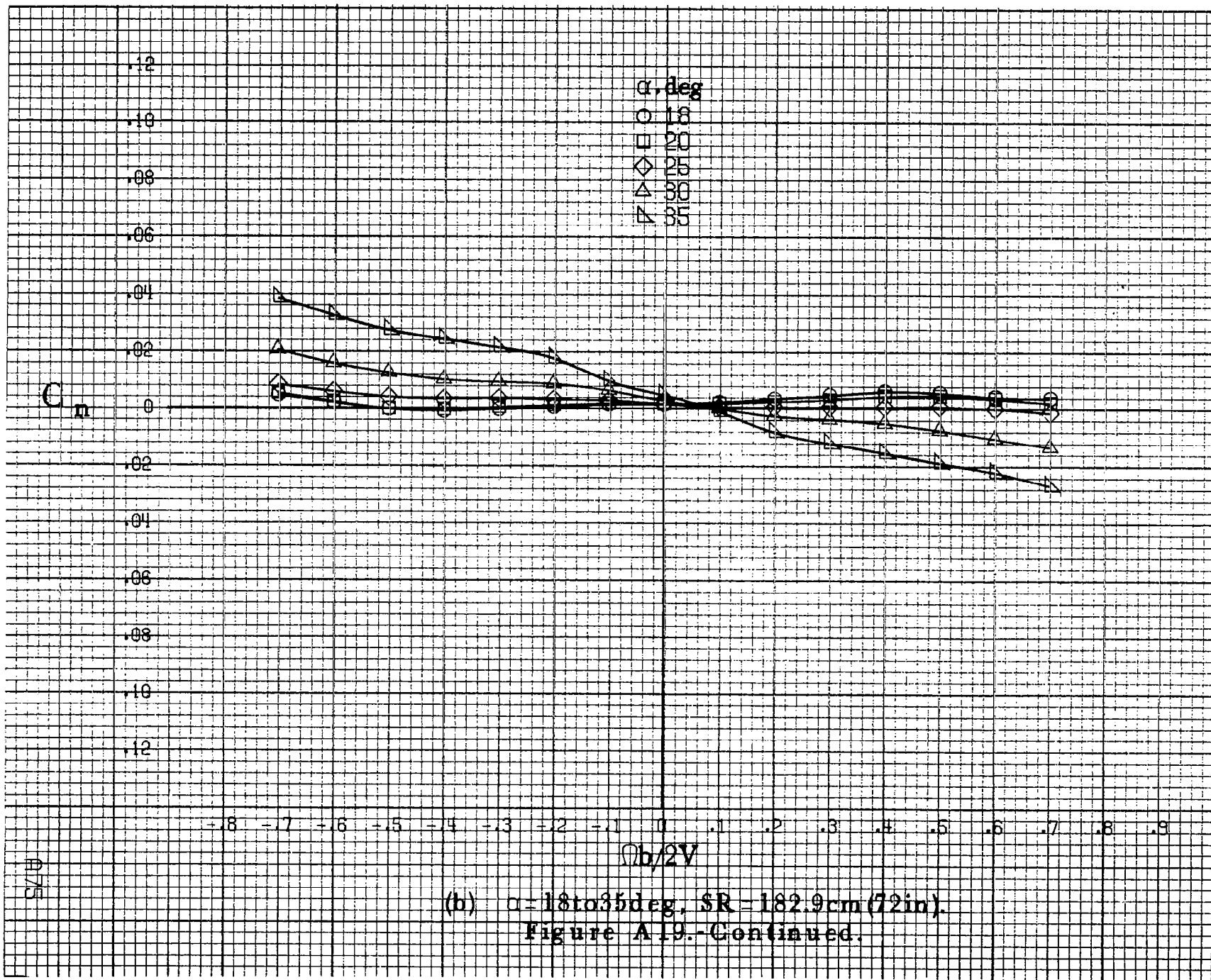




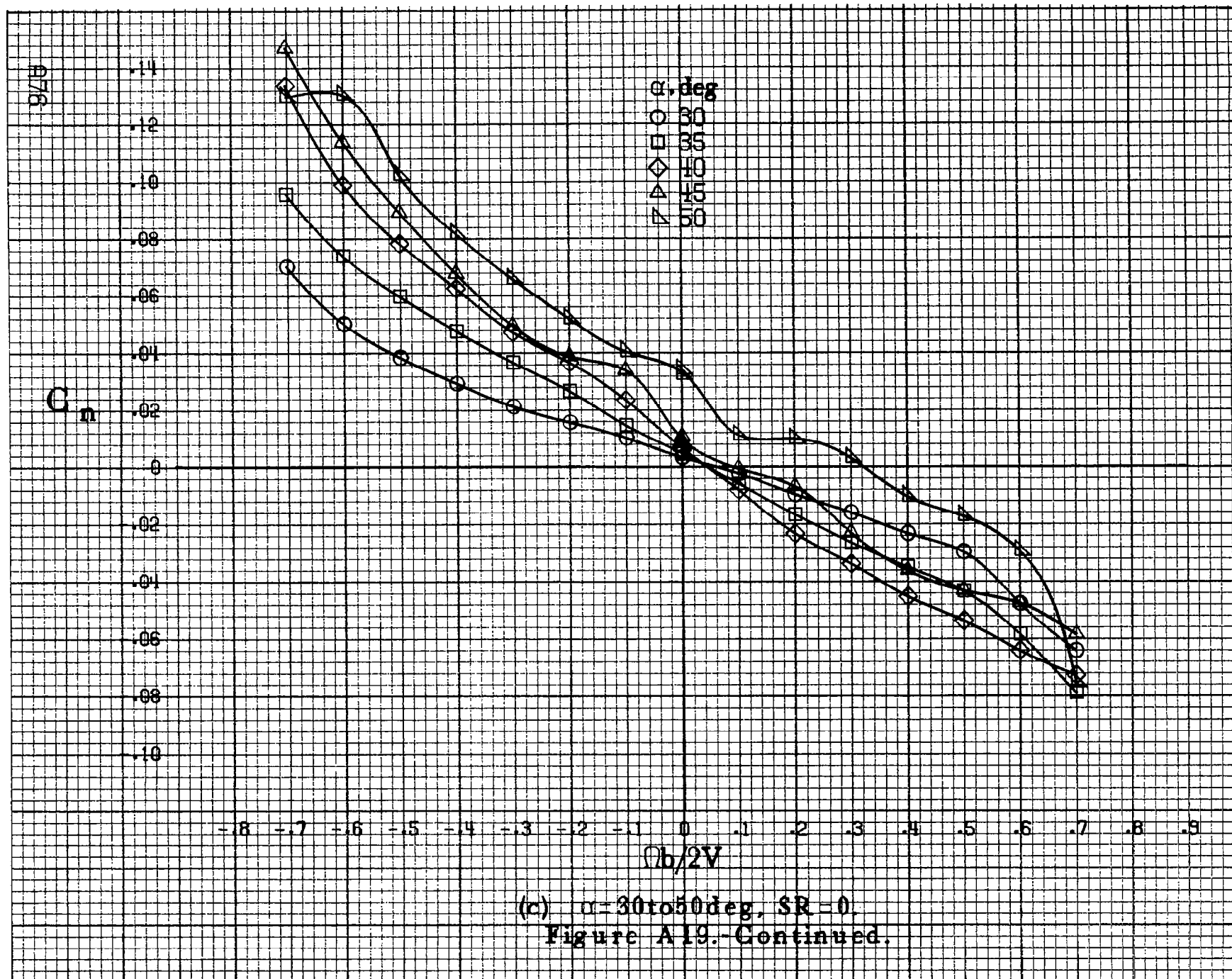


(a) $\alpha=8$ to 16° , $SR=182.9\text{cm}(72\text{in})$.

Figure A19.-Effect of rotation rate and angle of attack on yawing-moment coefficient for body wing horizontal tail configuration $\delta_e=0^\circ$, $\delta_a=0^\circ$, $\delta_r=0^\circ$, $\beta=0^\circ$.



(b) $\alpha=18$ to 35° , $SR=182.9\text{cm}(72\text{in})$.
Figure A19.-Continued.



C_n

α, deg

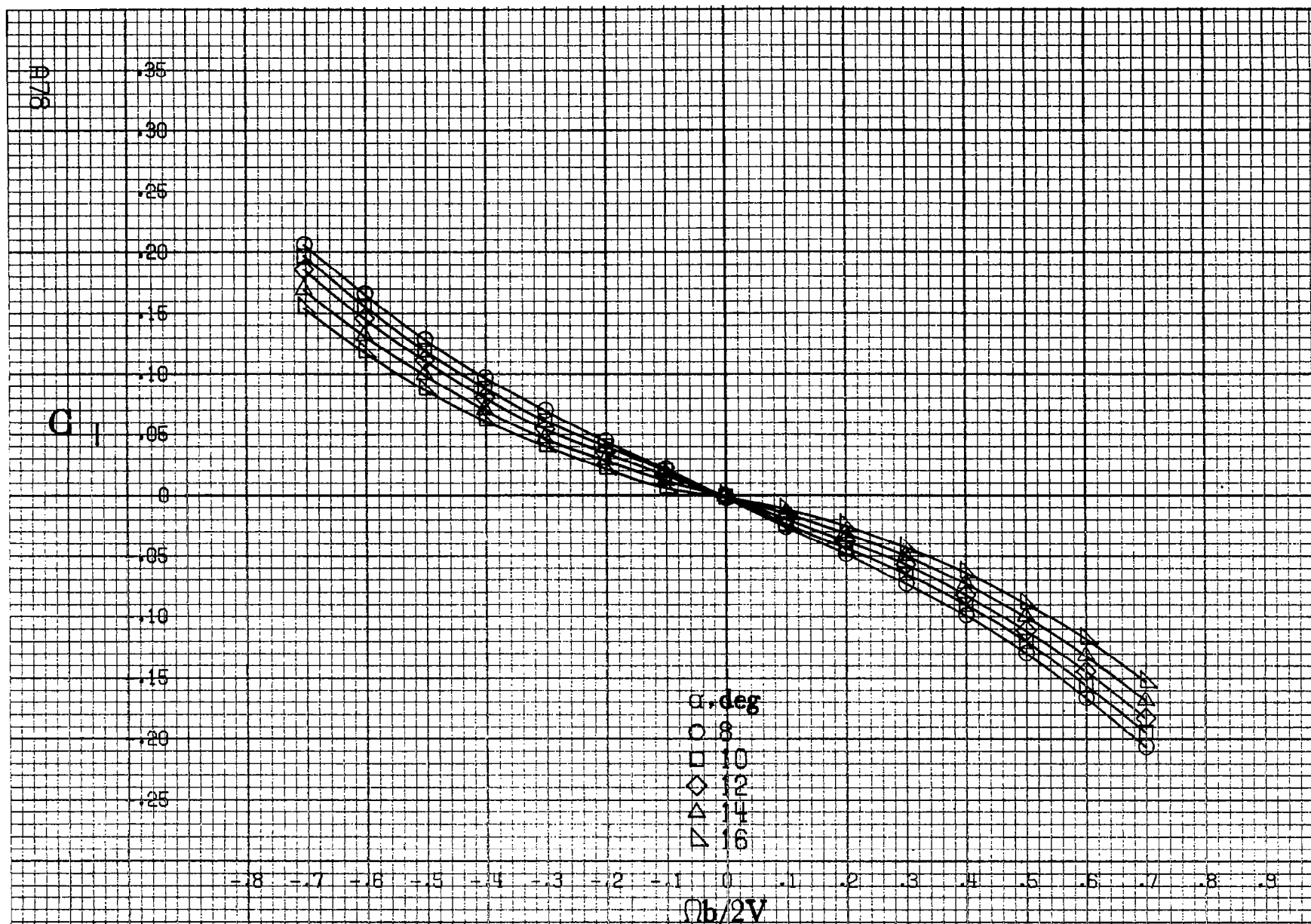
- 55
- 60
- ◇ 70
- △ 80
- ▽ 90

.14
.12
.10
.08
.06
.04
.02
0
-.02
-.04
-.06
-.08
-.10

-.8 -.7 -.6 -.5 -.4 -.3 -.2 -.1 0 .1 .2 .3 .4 .5 .6 .7 .8 .9

$Ob/2V$

(d) $\alpha = 55 \text{ to } 90 \text{ deg}, SR = 0.$
Figure A19.-Concluded.



(a) $\alpha=8\text{ to }16\text{deg}$, $SR=182.9\text{cm (72in)}$.

Figure A20.-Effect of rotation rate and angle of attack on rolling-moment coefficient for body wing horizontal tail configuration $\delta_a=0^\circ$, $\delta_h=0^\circ$, $\delta_r=0^\circ$, $\beta=0^\circ$.

C_1

.14
.12
.10
.08
.06
.04
0
.02
.04
.06
.08
.10

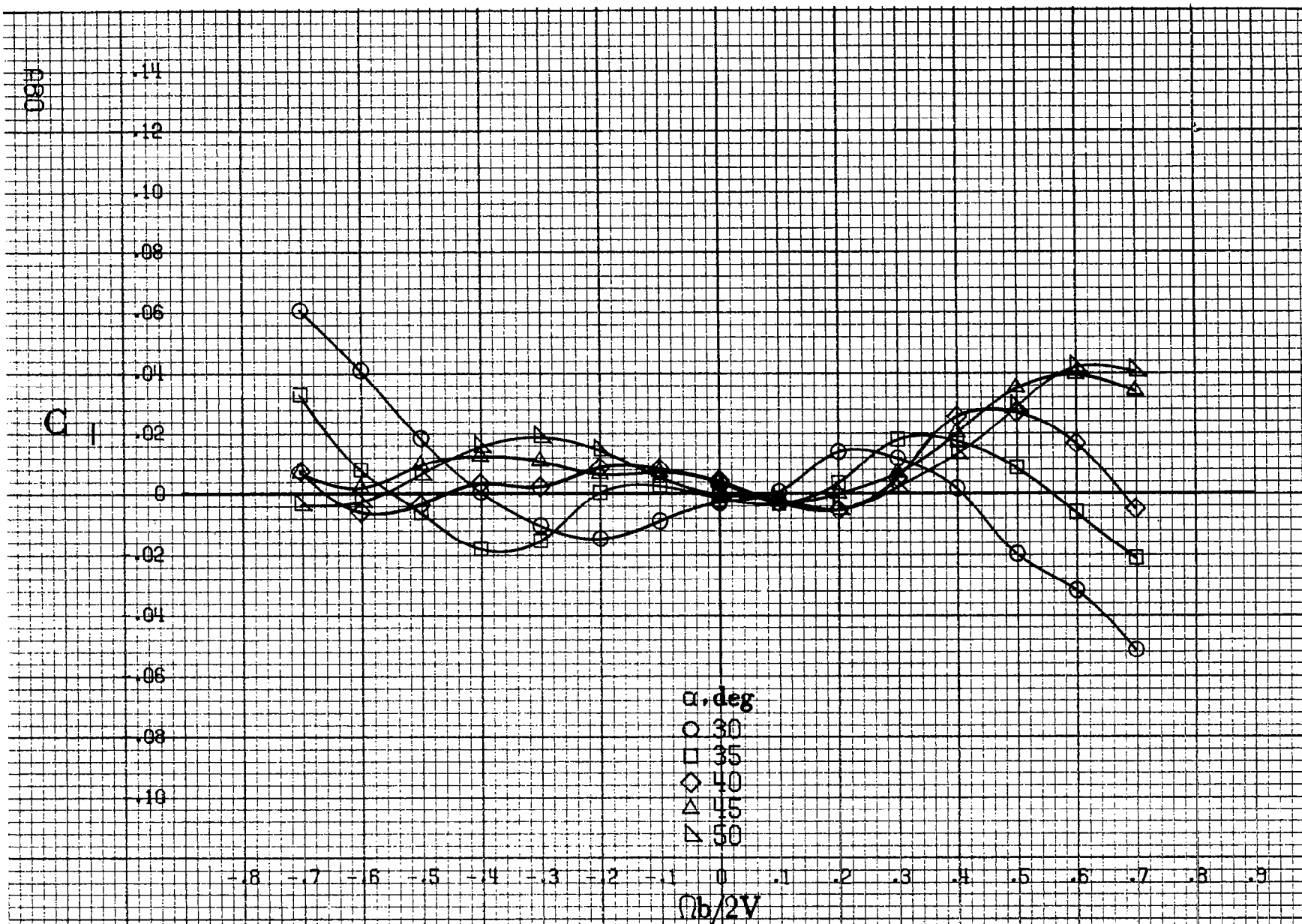
α, deg
○ 18
□ 20
◇ 25
△ 30
▲ 35

$Ob/2V$

.8 .7 .6 .5 .4 .3 .2 .1 0 .1 .2 .3 .4 .5 .6 .7 .8 .9

0.79

(b) $\alpha = 18 \text{ to } 35 \text{ deg. SR} = 182.9 \text{ cm (72 in).}$
Figure A20.-Continued.



(c) $\alpha=30$ to 50° , $SR=0$.
Figure A20.-Continued.

C₁

.14
.12
.10
.08
.06
.04
.02
0
-.02
-.04
-.06
-.08
-.10

-0.8 -0.7 -0.6 -0.5 -0.4 -0.3 -0.2 -0.1 0 .1 .2 .3 .4 .5 .6 .7 .8 .9

α , deg

○ 55
□ 60
◇ 70
△ 80
▽ 90

$Ob/2V$

(d) $\alpha=55$ to 90 deg, $SR=0$.
Figure A20.-Concluded.

C_m .6
.5
.4
.3
.2
.1
0
.1
.2
.3
.4
.5
.6 α , deg

○ 8

□ 10

◇ 12

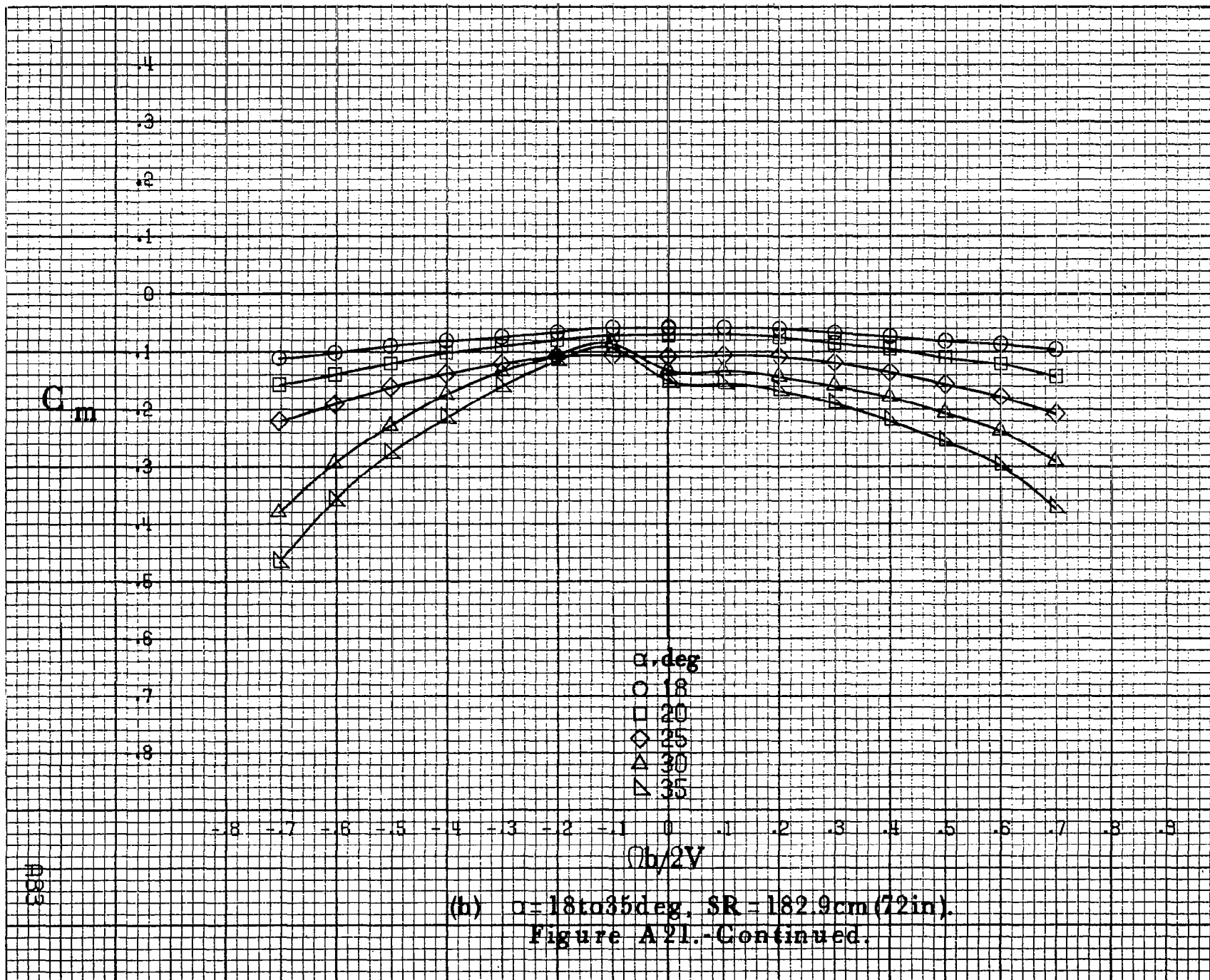
△ 14

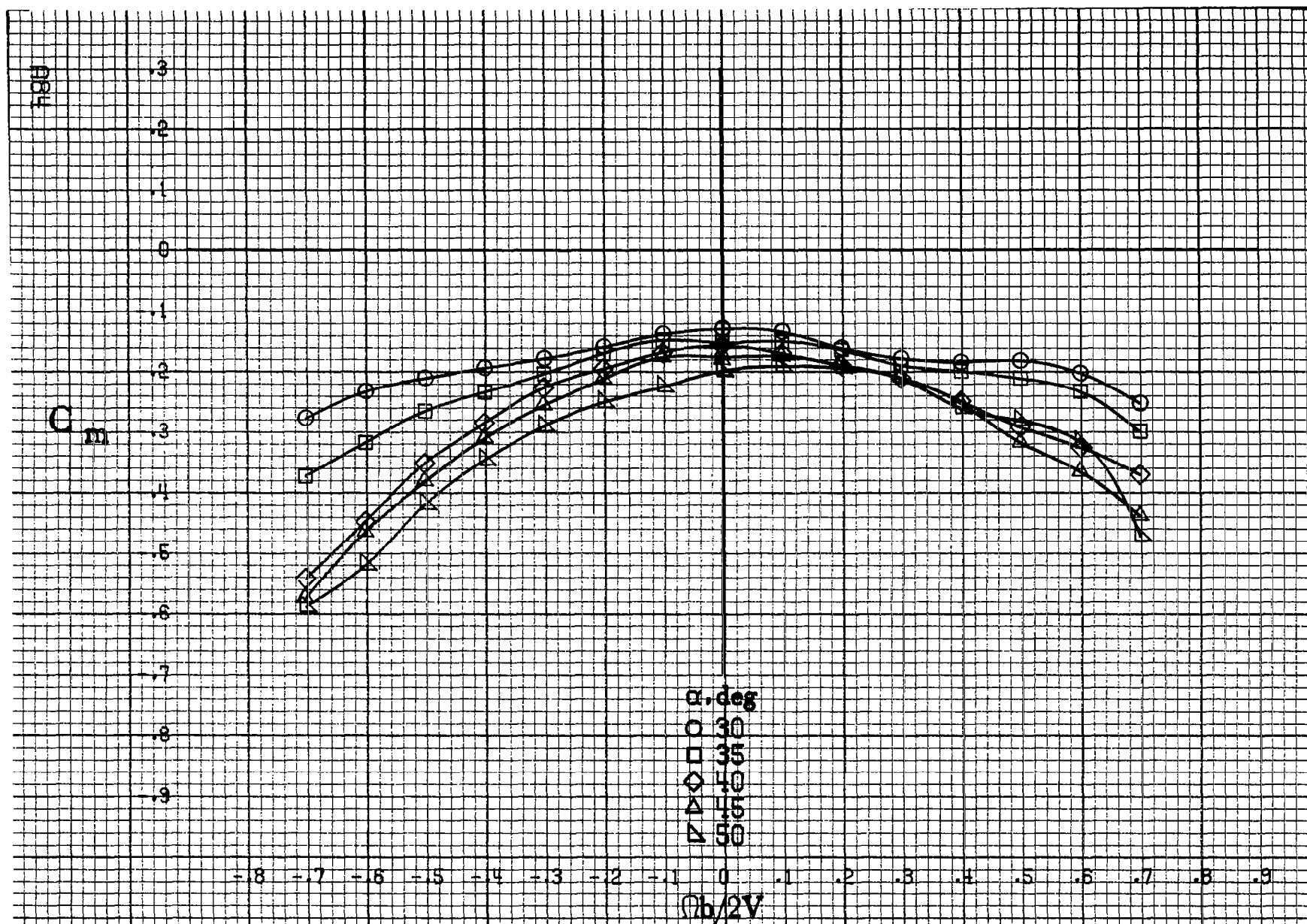
▽ 16

-0.8 -0.7 -0.6 -0.5 -0.4 -0.3 -0.2 -0.1 0 .1 .2 .3 .4 .5 .6 .7 .8 .9

 $\Omega b/2V$ (a) $\alpha = 8$ to 16 deg, $SR = 132.9$ cm (72 in).

Figure A21.-Effect of rotation rate and angle of attack on pitching-moment coefficient for body wing horizontal tail configuration $\delta_e = 0^\circ$, $\delta_a = 0^\circ$, $\delta_r = 0^\circ$, $\beta = 0^\circ$.





(c) $\alpha = 30$ to 50 deg, $SR = 0$
 Figure A21.-Continued.

C_m

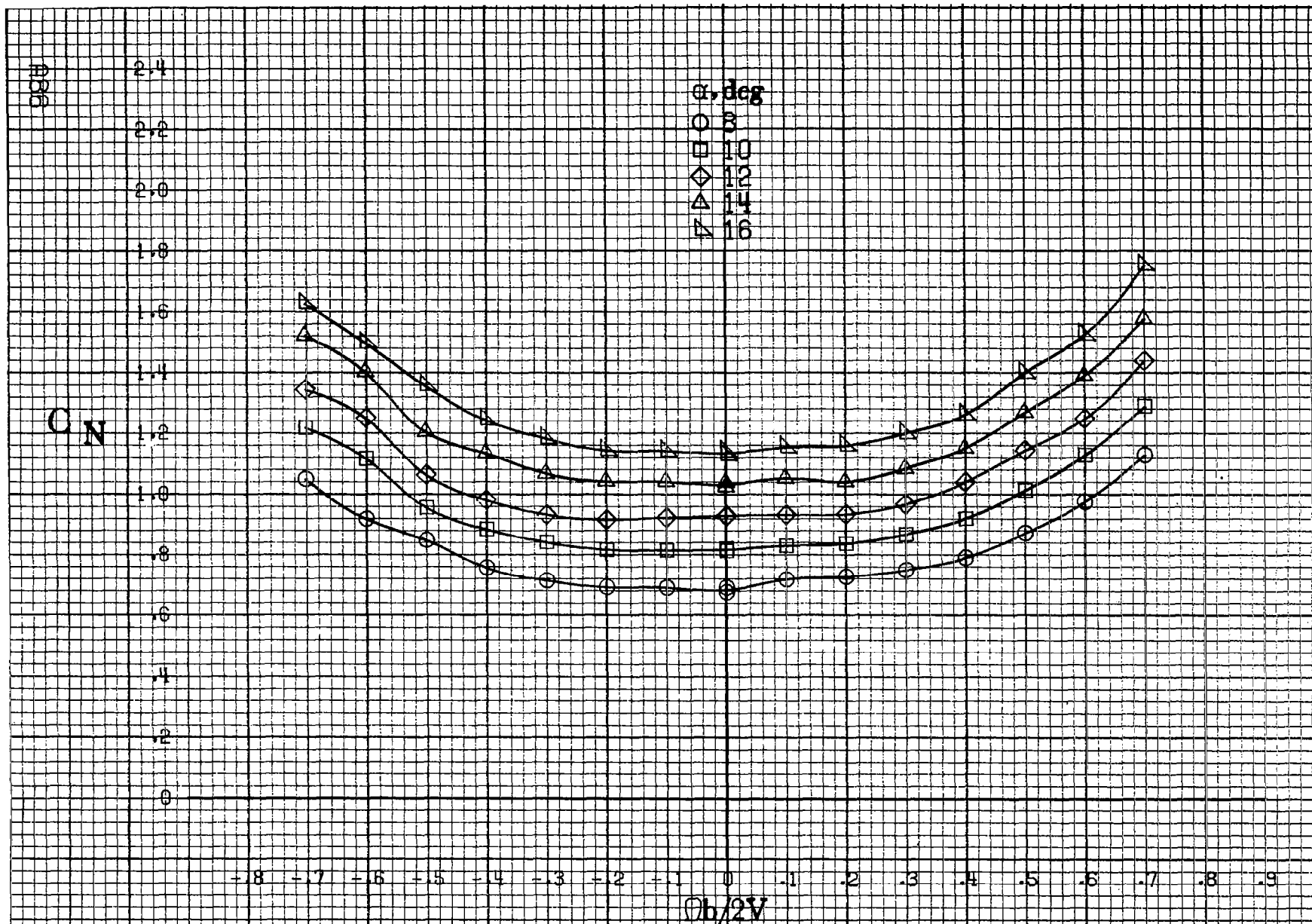
α, deg

- 55
- 60
- ◇ 70
- △ 80
- ▽ 90

$Ob/2V$

(d) $\alpha=55\text{ to }90\text{ deg, }SR=0.$

Figure A21.-Concluded.



(a) $\alpha = 8$ to 16 deg, $SR = 182.9$ cm (72 in).

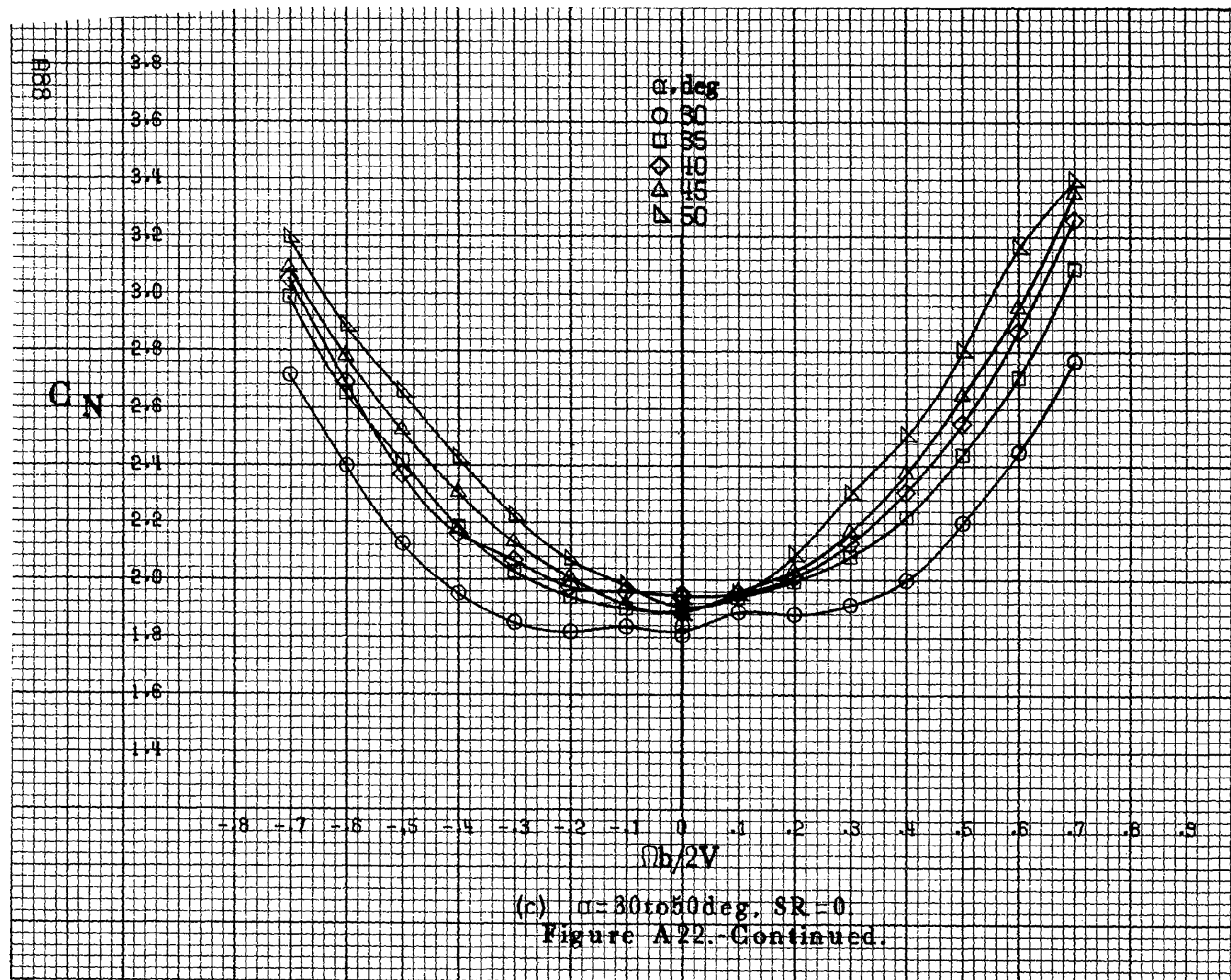
Figure A22.-Effect of rotation rate and angle of attack on normal-force coefficient for body wing horizontal tail configuration $\delta_a = 0^\circ$, $\delta_s = 0^\circ$, $\delta_r = 0^\circ$, $\beta = 0^\circ$.

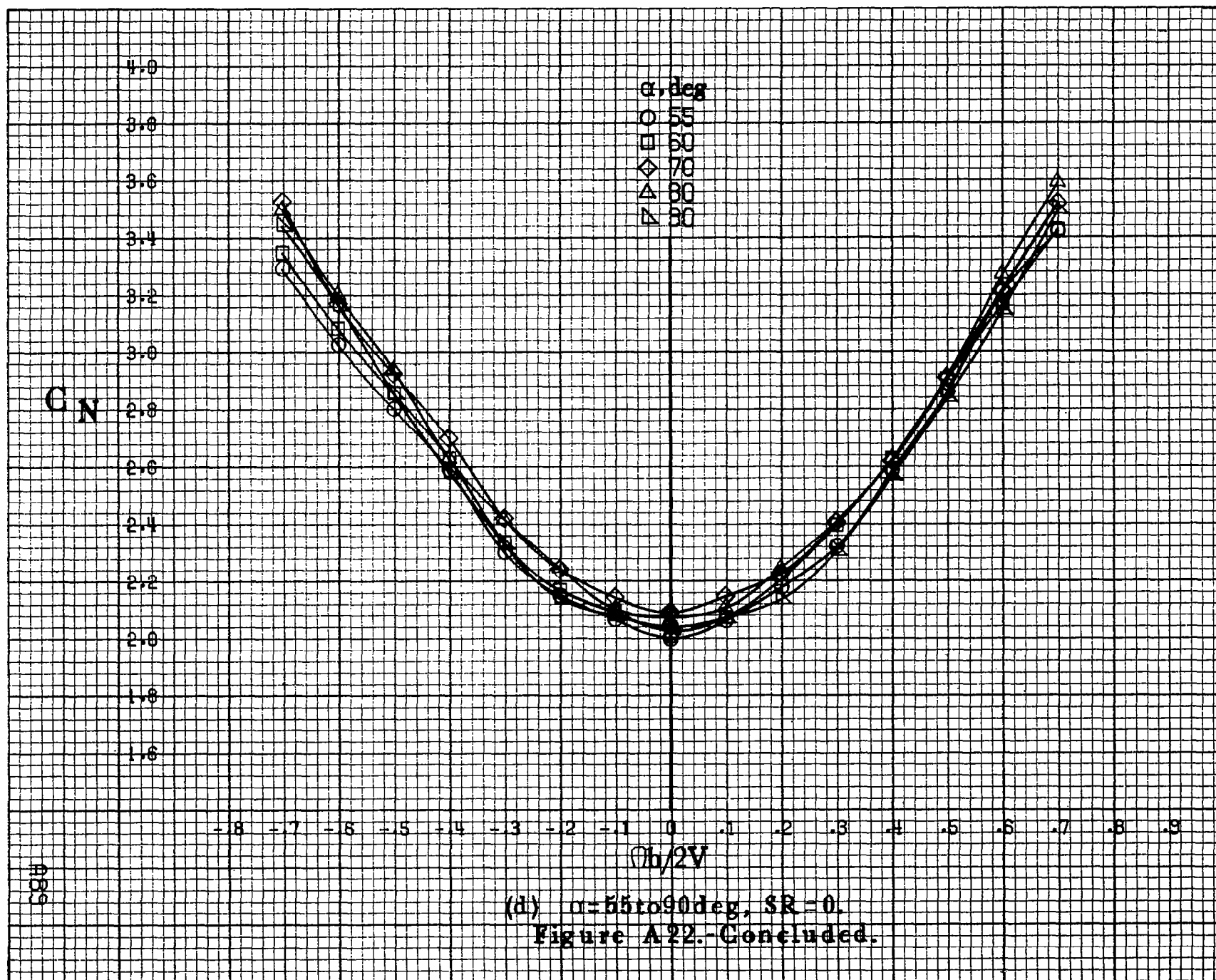
C_N

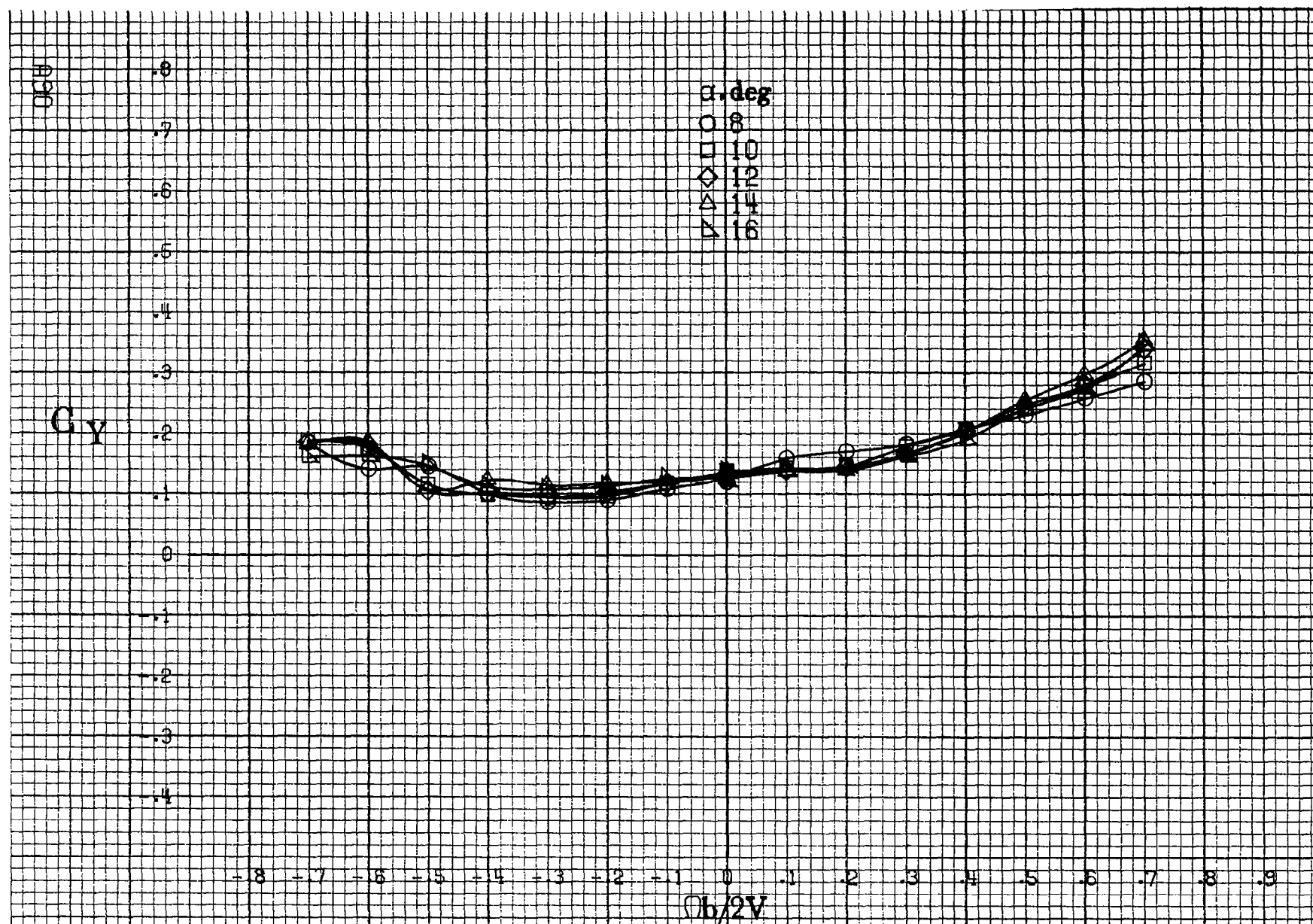
α, deg
 ○ 18
 □ 20
 ◇ 25
 △ 30
 ▽ 35

$\Omega b/2V$

(b) $\alpha = 18 \text{ to } 35 \text{ deg}$, $SR = 182.9 \text{ cm (72 in)}$.
 Figure A22.-Continued.

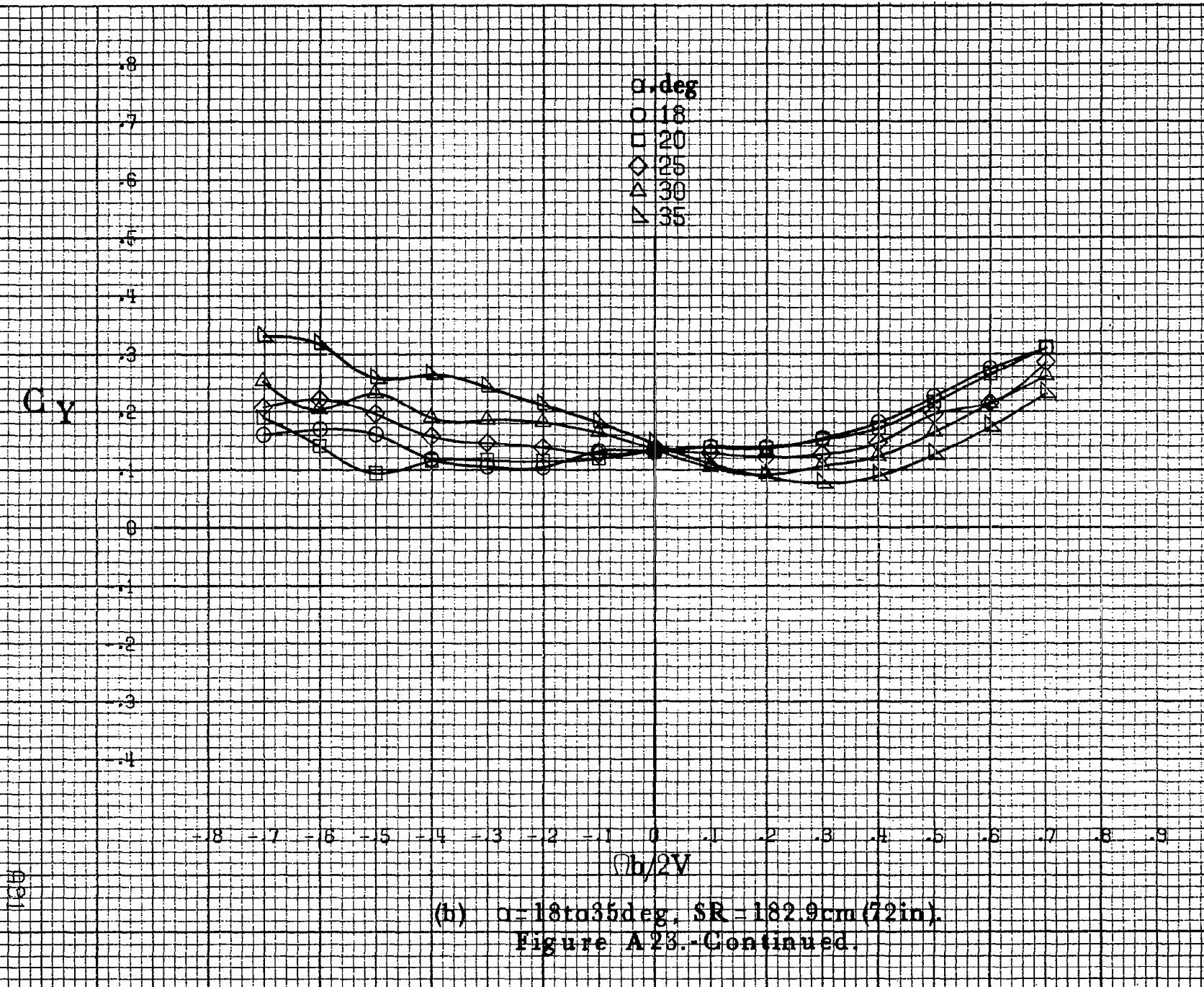


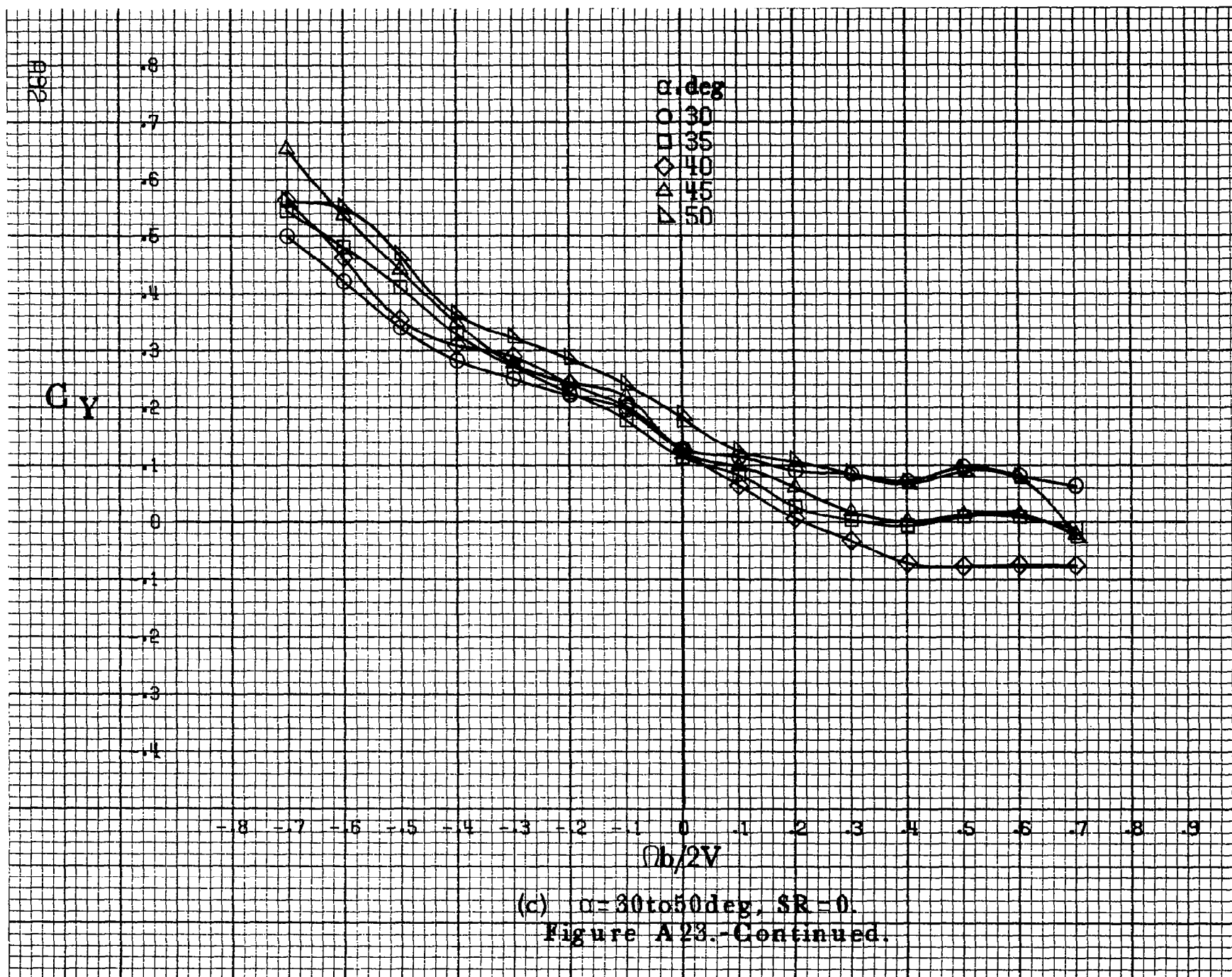


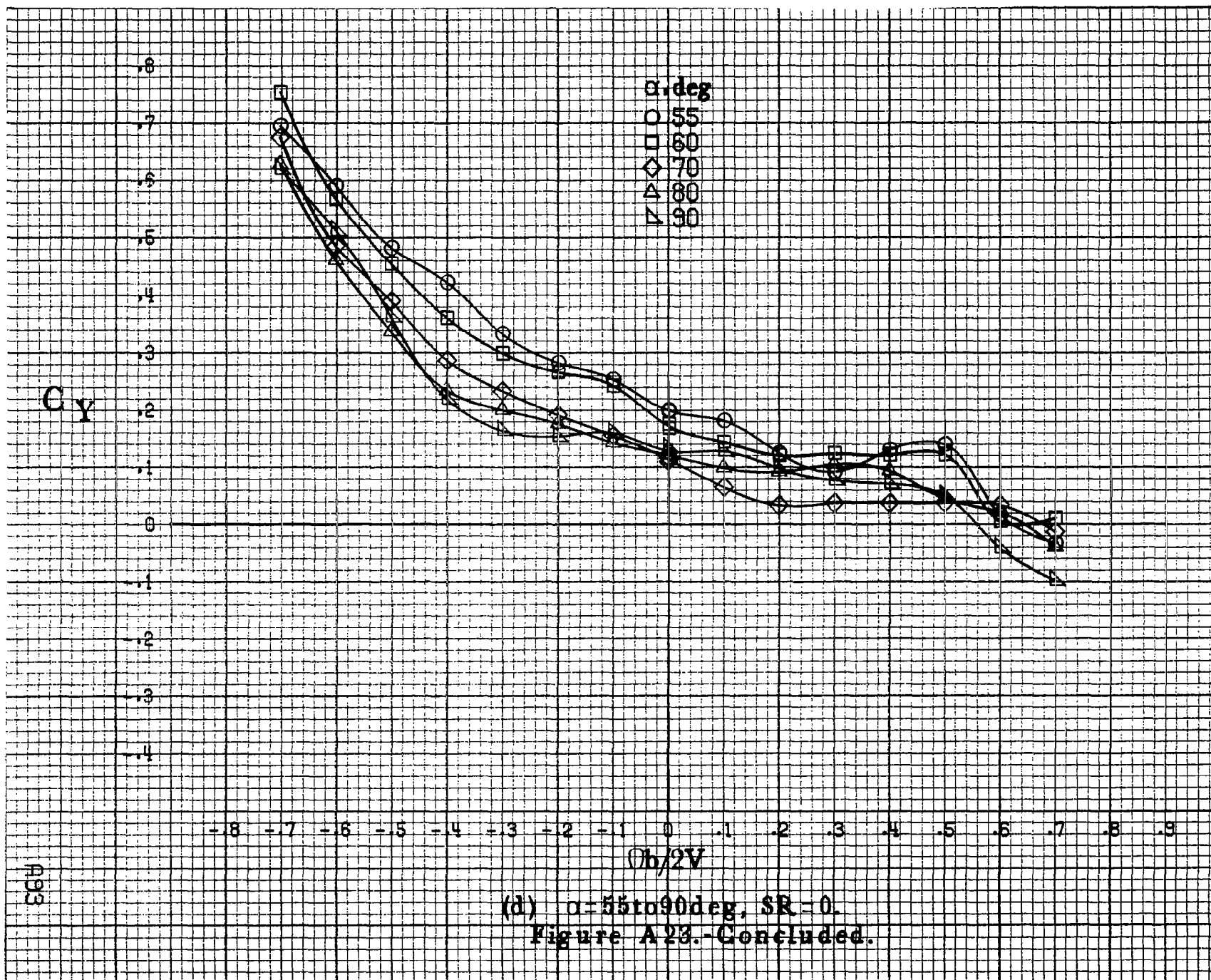


(a) $\alpha = 8$ to 16° , $SR = 182.9 \text{ cm (72 in)}$.

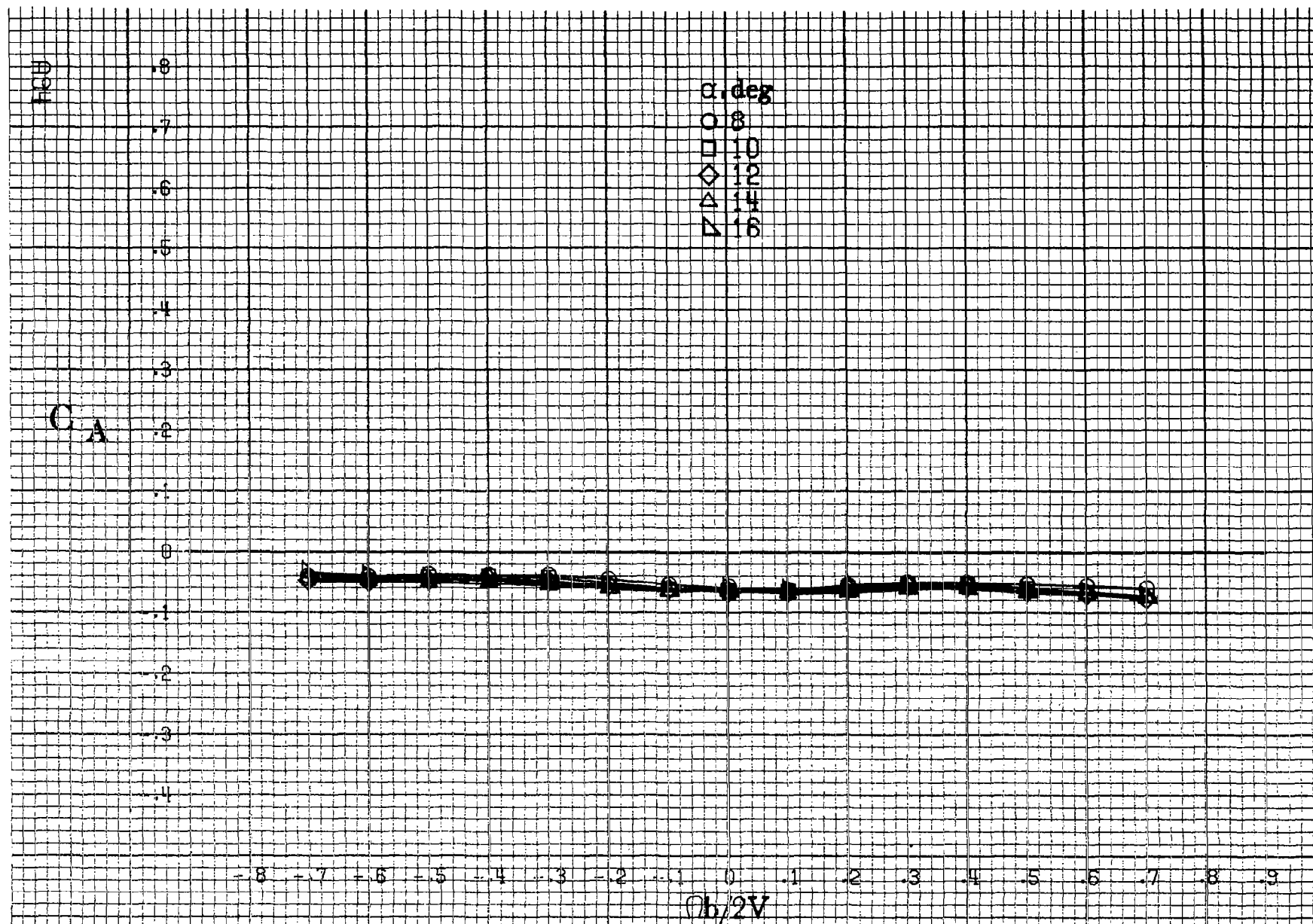
Figure A23.-Effect of rotation rate and angle of attack on side-force coefficient for body wing horizontal tail configuration $\delta_e = 0^\circ$, $\delta_a = 0^\circ$, $\delta_r = 0^\circ$, $\delta = 0^\circ$.





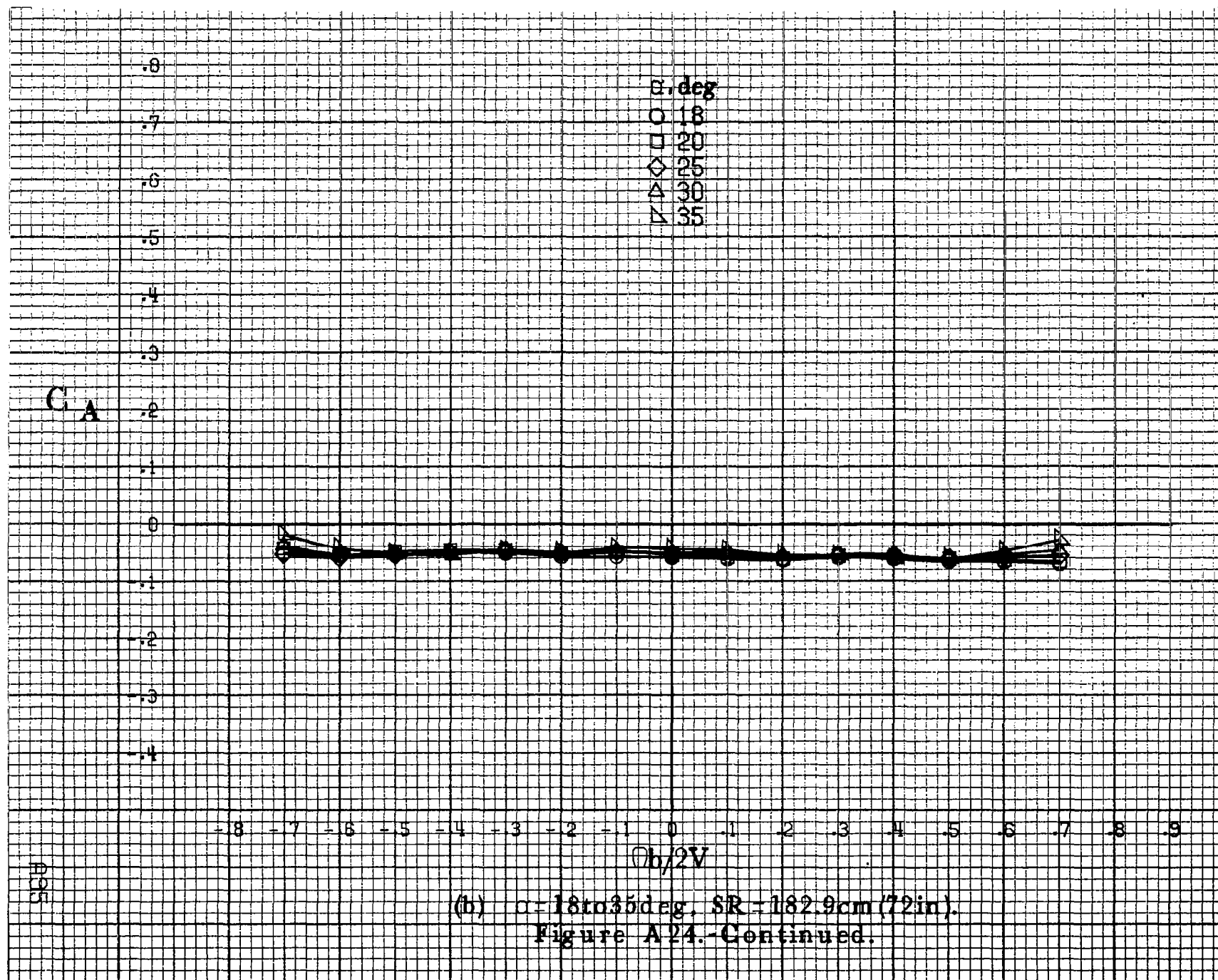


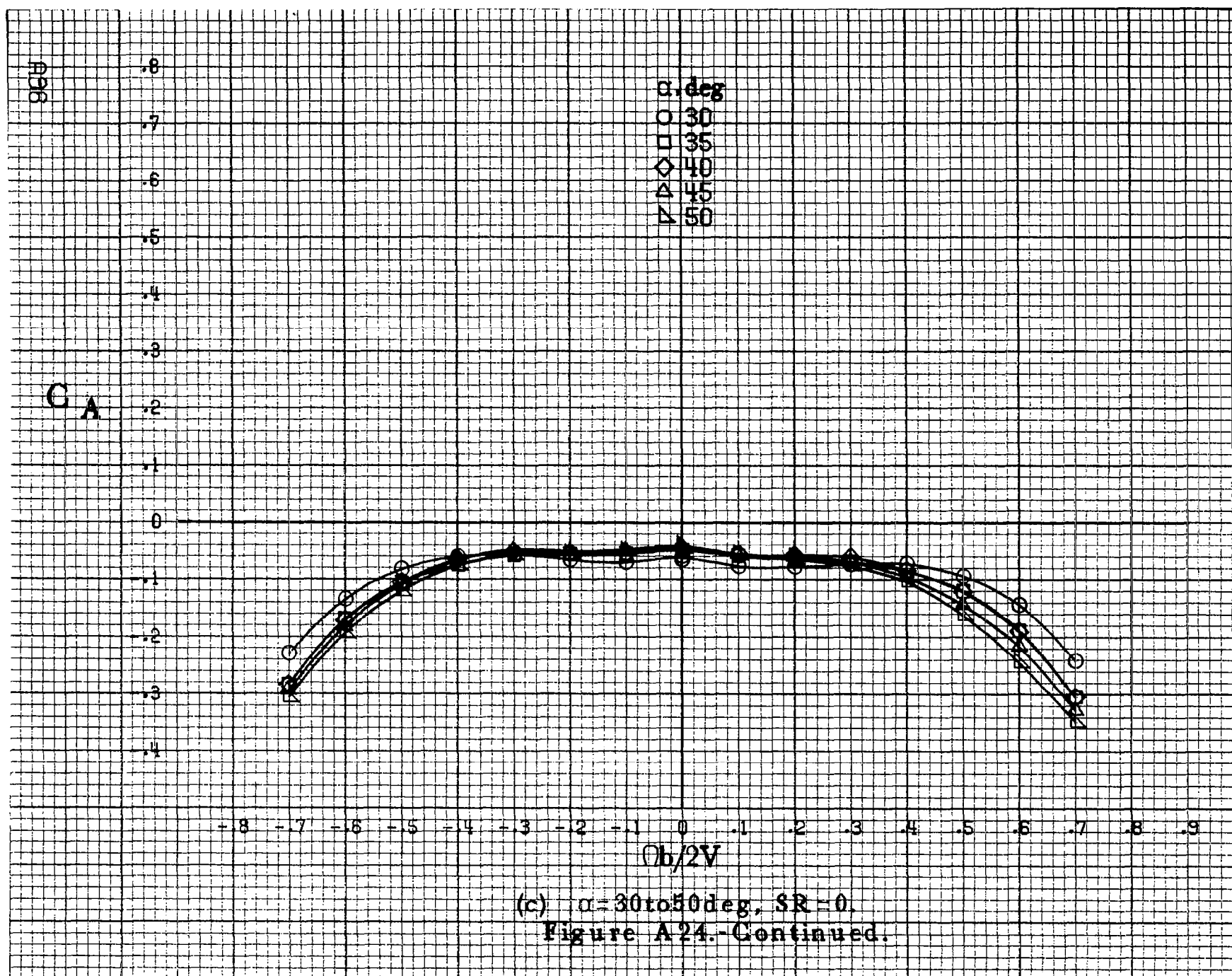
(d) $\alpha=55$ to 90° , $SR=0$.
Figure A23.-Concluded.



(a) $\alpha = 8$ to 16° , $SR = 182.9\text{cm (72in)}$.

Figure A24. Effect of rotation rate and angle of attack on axial force coefficient for body wing horizontal tail configuration $\delta_e = 0^\circ$, $\delta_a = 0^\circ$, $\delta_r = 0^\circ$, $\beta = 0^\circ$.





C_A

α, deg

○ 55

□ 60

◇ 70

△ 80

▽ 90

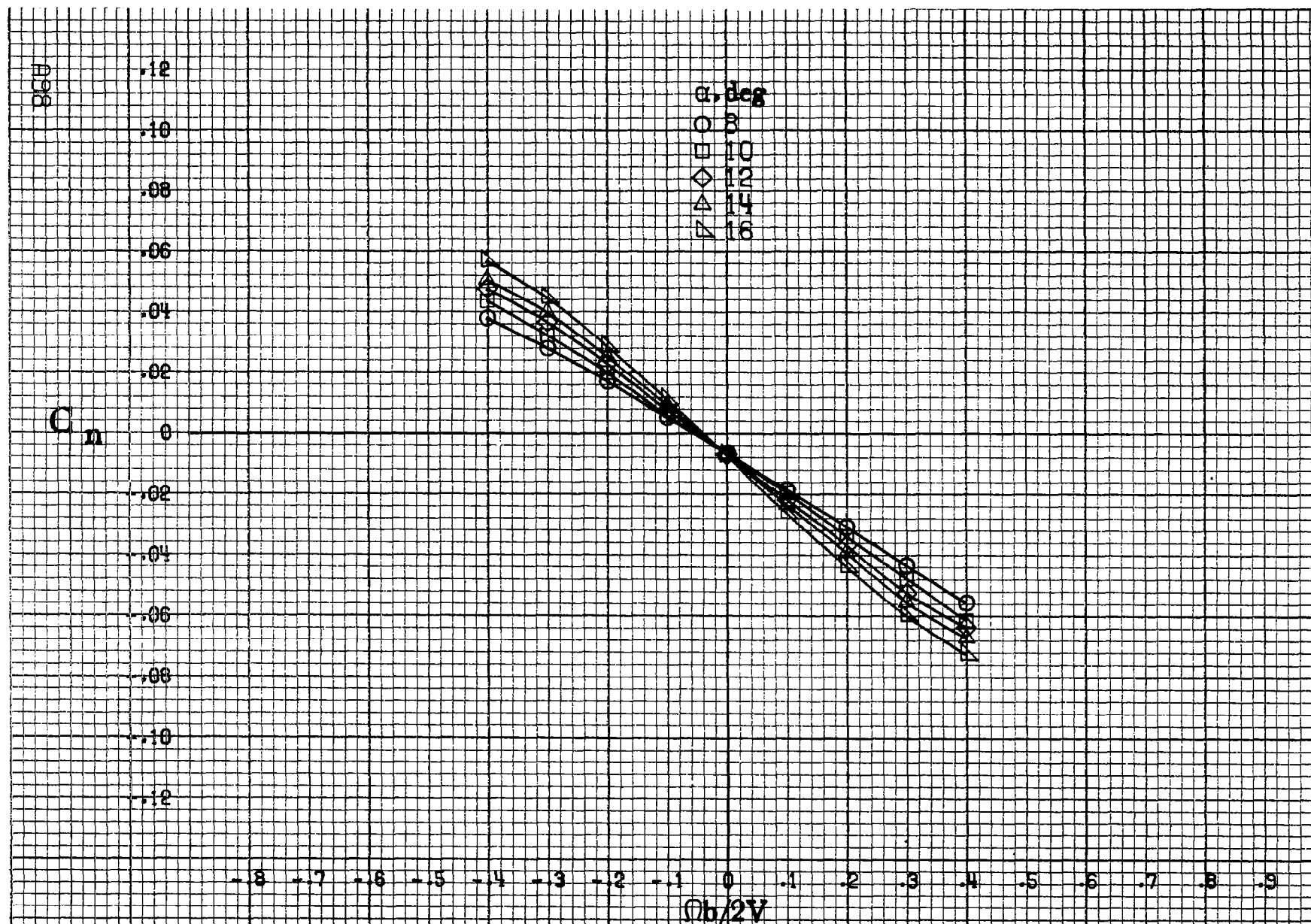
-8 -7 -6 -5 -4 -3 -2 -1 0 .1 .2 .3 .4 .5 .6 .7 .8 .9

$b/2V$

(d) $\alpha=55$ to 90° , $SR=0$.

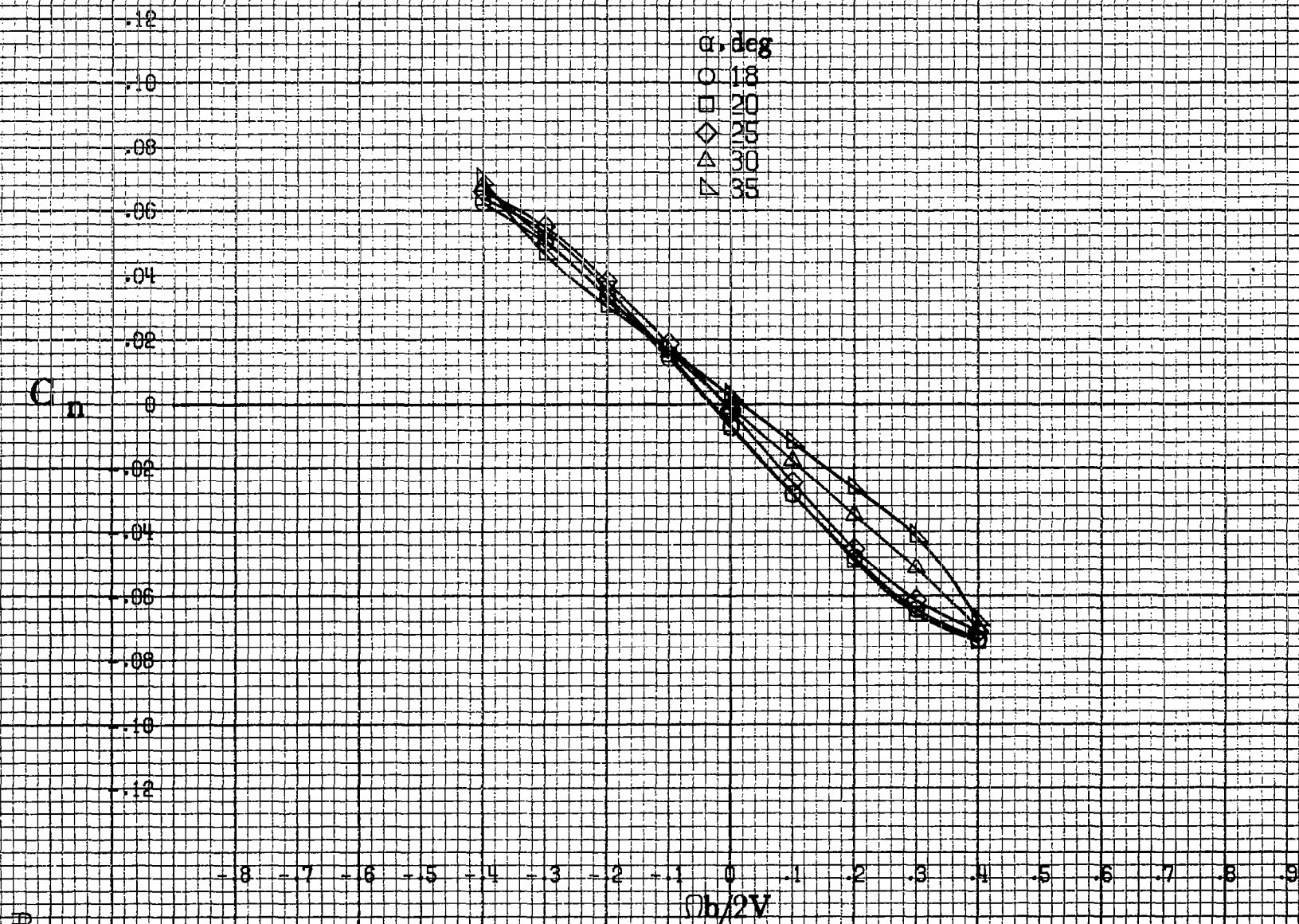
Figure A24.-Concluded.

897

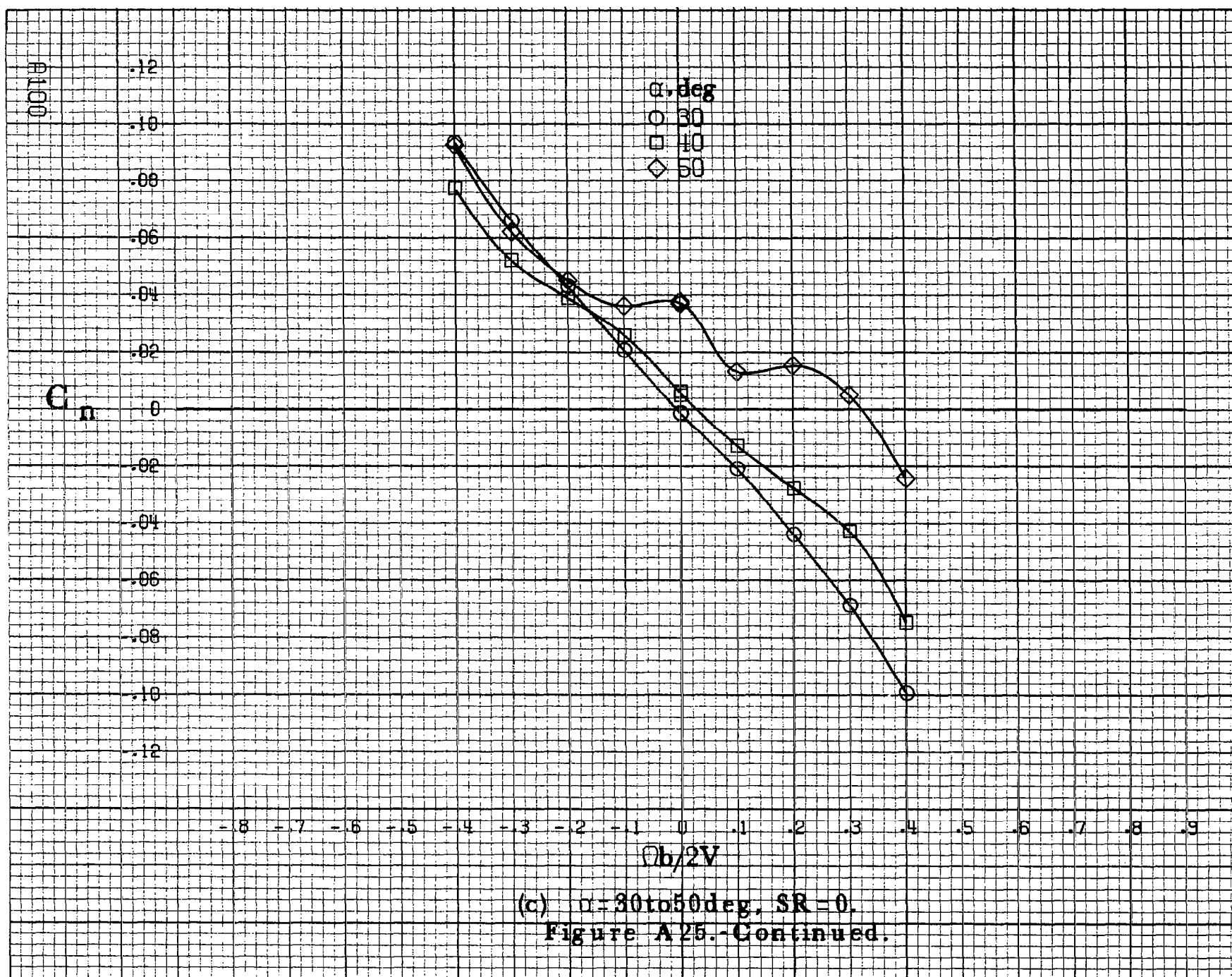


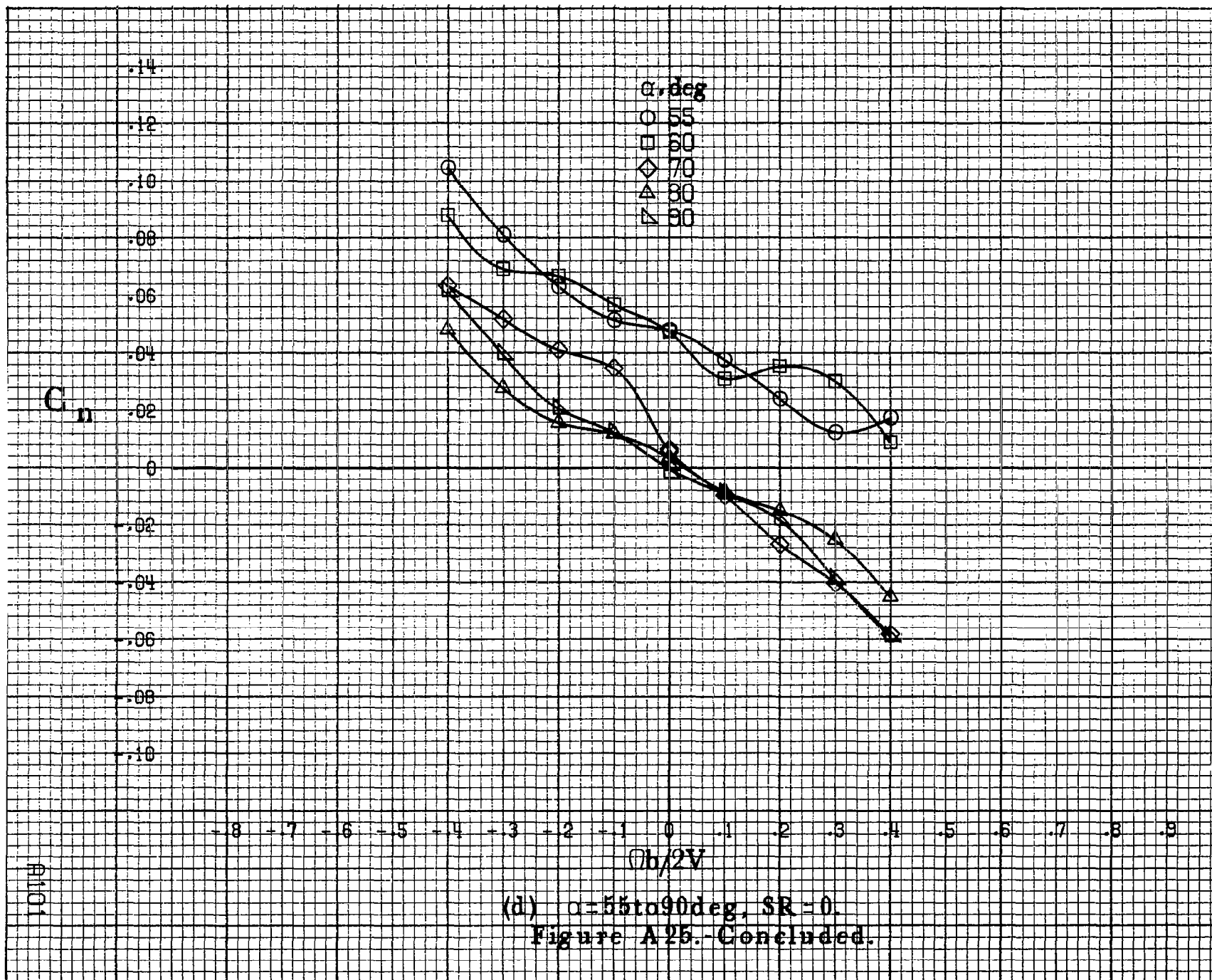
(a) $\alpha = 8$ to 16° , $SR = 182.9 \text{ cm (72 in)}$.

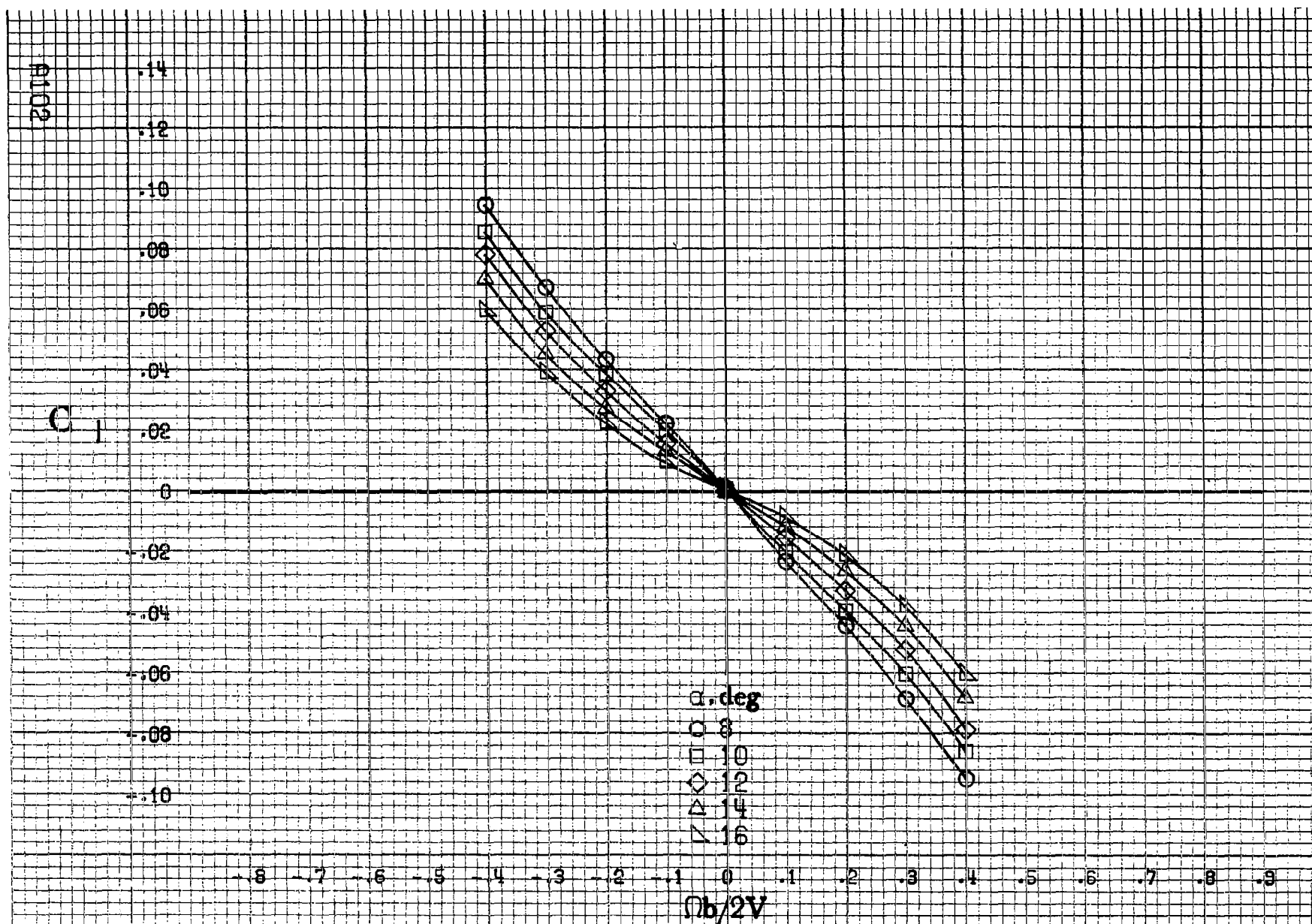
Figure A25.-Effect of rotation rate and angle of attack on yawing-moment coefficient for basic configuration. $\delta_e = 0^\circ$, $\delta_a = 0^\circ$, $\delta_1 = 0^\circ$, $\delta_2 = 0^\circ$, $\beta = 0^\circ$.



(b) $\alpha=18$ to 35° , SR = 182.9 cm (72 in).
Figure A25.-Continued.

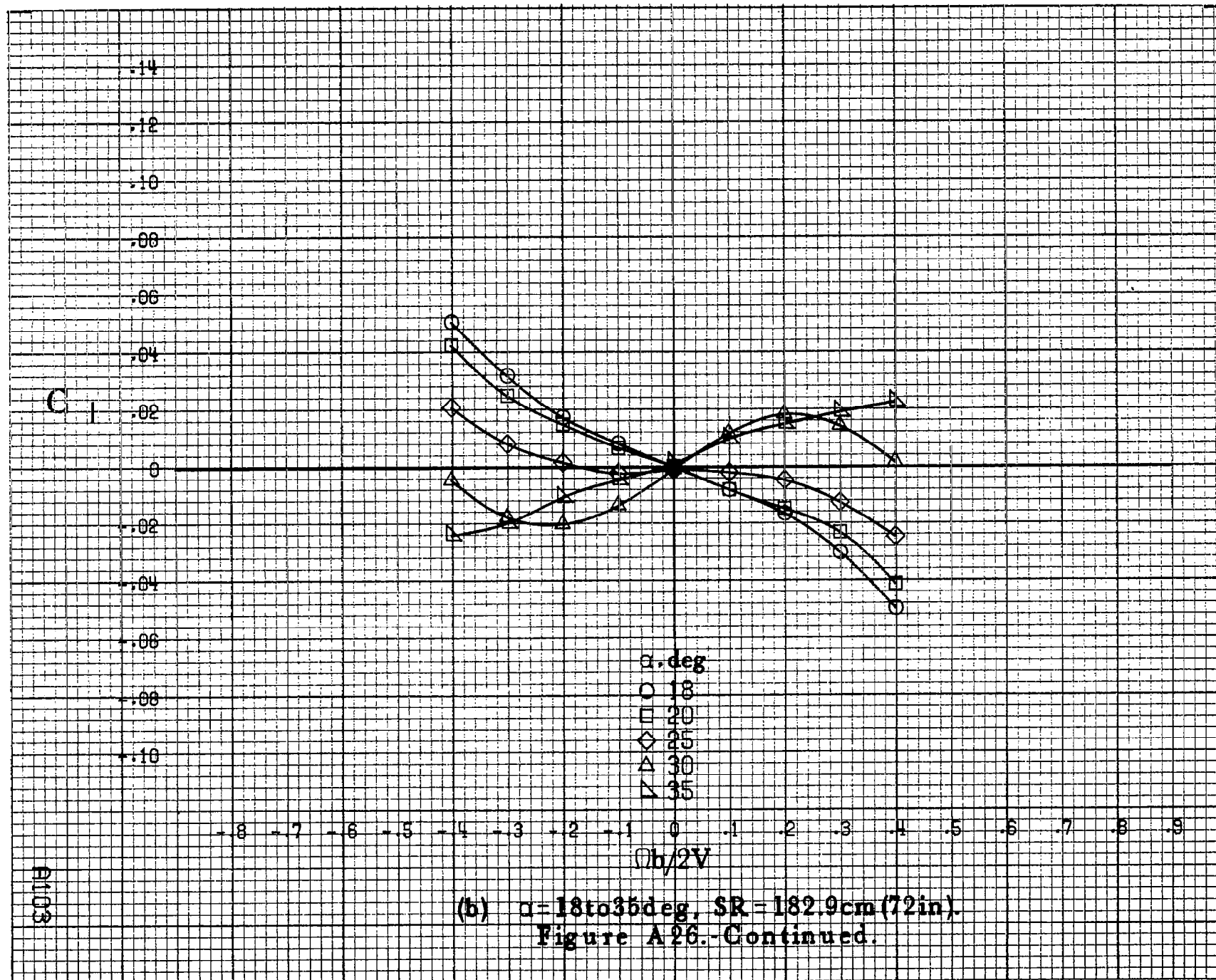


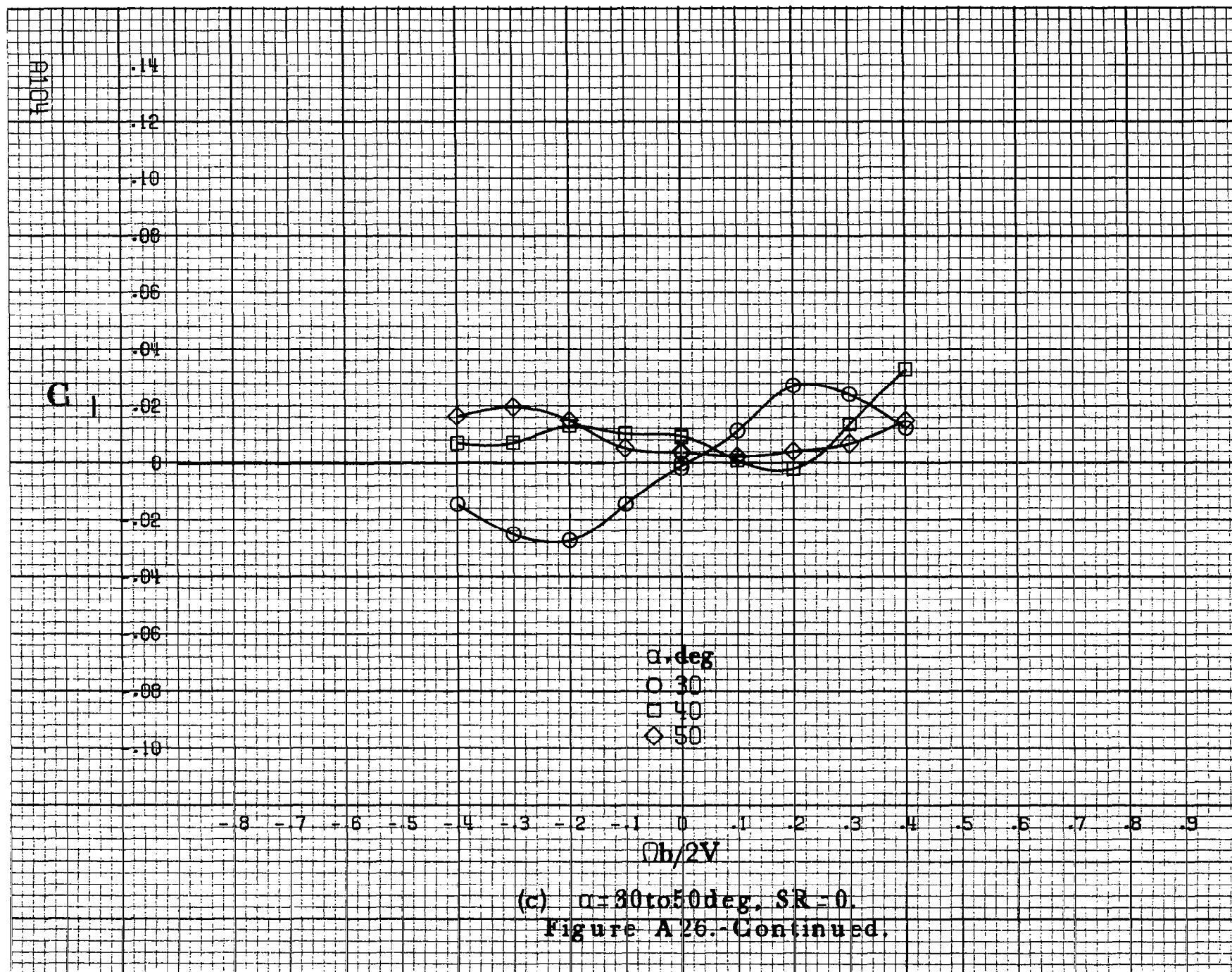


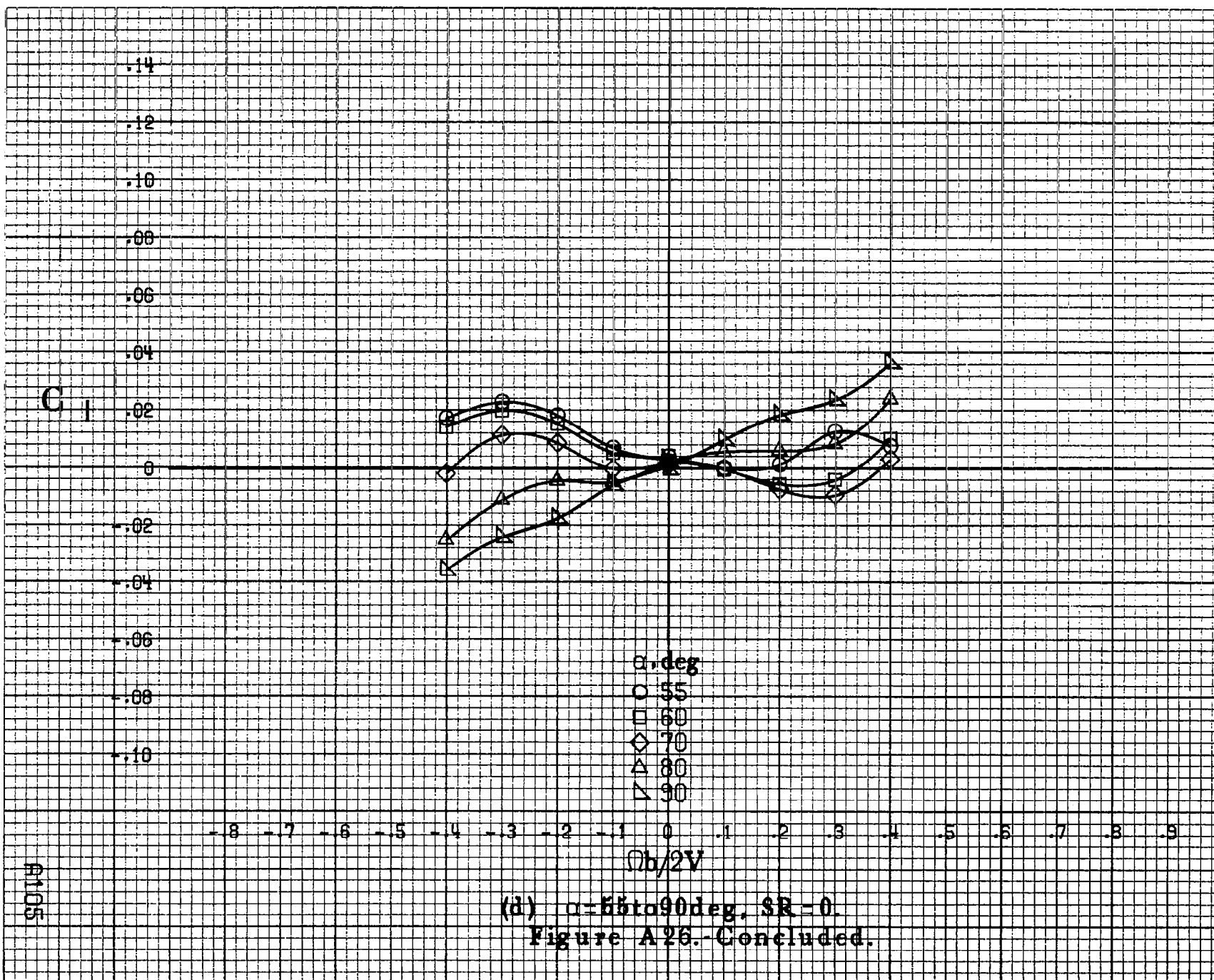


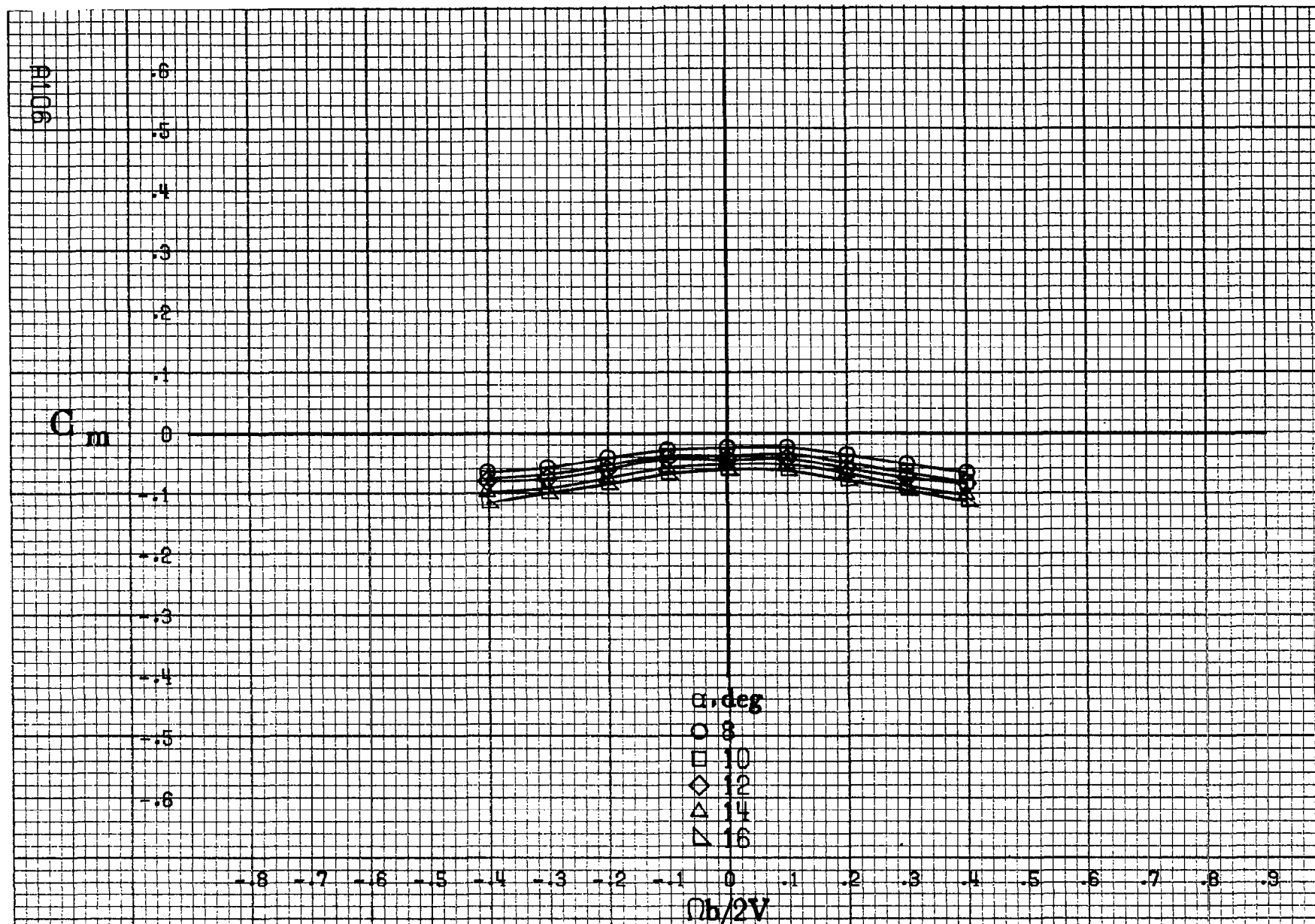
(a) $\alpha = 8$ to 16 deg, $SR = 182.9$ cm (72 in).

Figure A26.-Effect of rotation rate and angle of attack on rolling-moment coefficient for basic configuration. $\delta_e = 0^\circ$, $\delta_a = 0^\circ$, $\delta_r = 0^\circ$, $\beta = 0^\circ$.









(a) $\alpha = 8$ to 16° , $SR = 182.9 \text{ cm (72 in)}$.

Figure A27.- Effect of rotation rate and angle of attack on pitching-moment coefficient for basic configuration. $\delta_e = 0^\circ$, $\delta_a = 0^\circ$, $\delta_d = 0^\circ$, $\delta_r = 0^\circ$, $\beta = 0^\circ$.

C_m

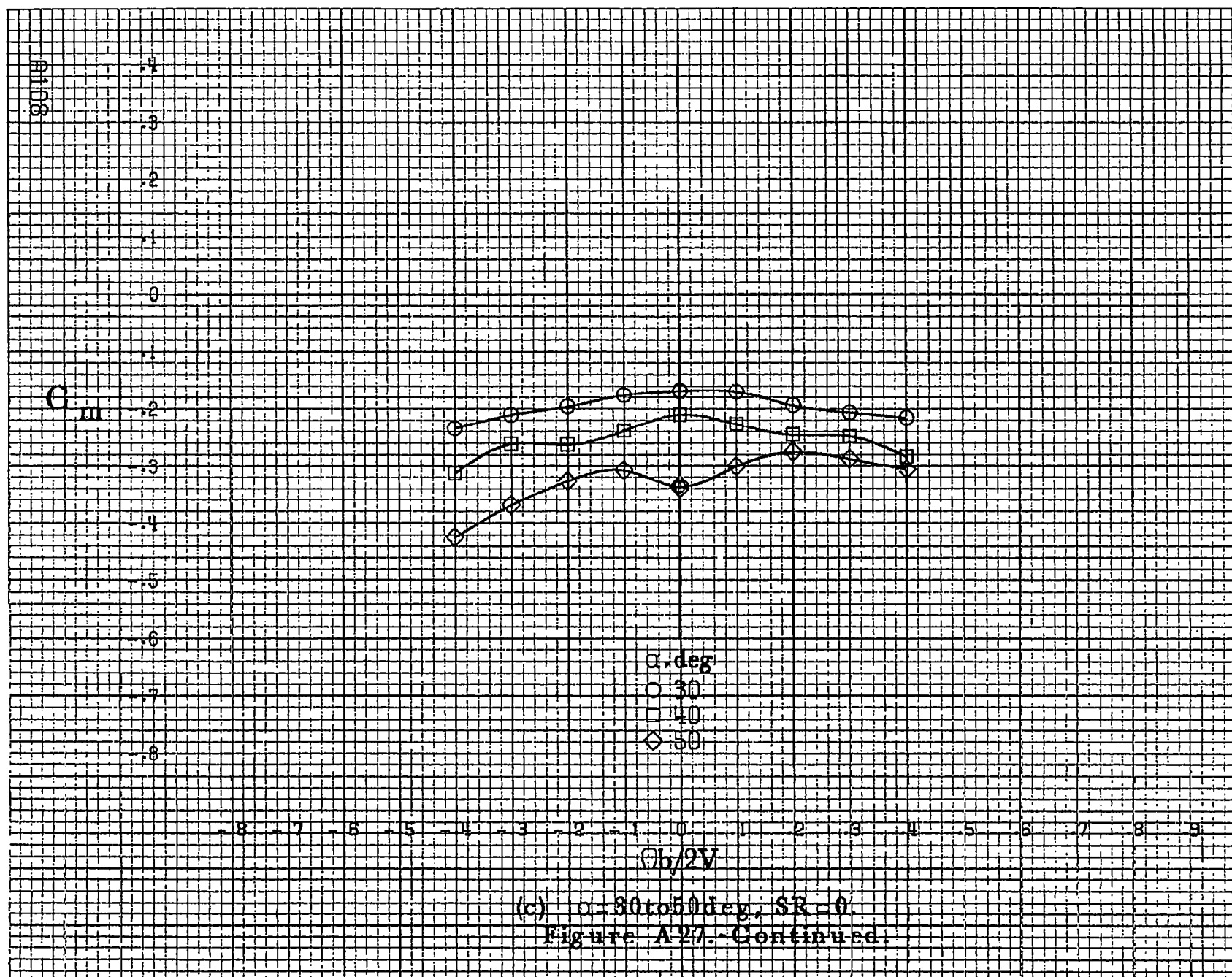
.5
.4
.3
.2
.1
0
-.1
-.2
-.3
-.4
-.5
-.6
-.7

α, deg
○ 18
□ 20
◇ 25
△ 30
▽ 35

-8 -7 -6 -5 -4 -3 -2 -1 0 .1 .2 .3 .4 .5 .6 .7 .8 .9
 $b/2V$

(b) $\alpha = 18 \text{ to } 35 \text{ deg}$, $SR = 182.9 \text{ cm (72 in)}$.
Figure A27.-Continued.

AI107



C_m

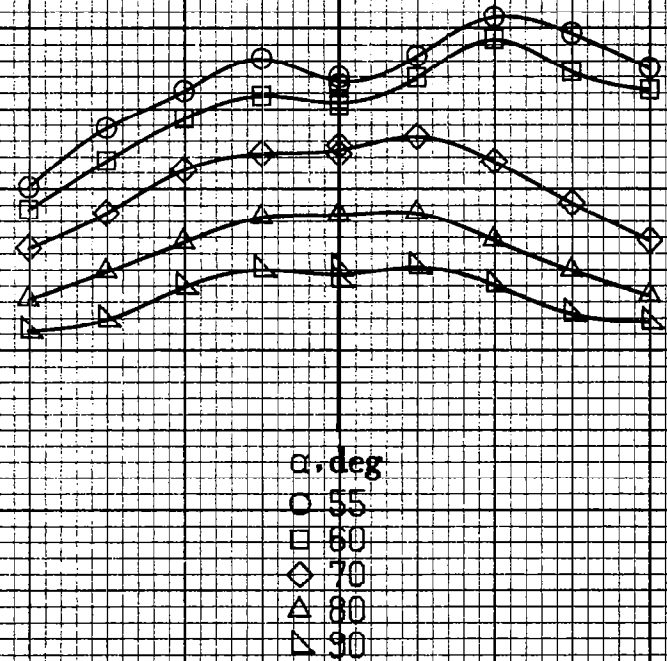
.2
.1
0
-.1
-.2
-.3
-.4
-.5
-.6
-.7
-.8
-.9
-1.0

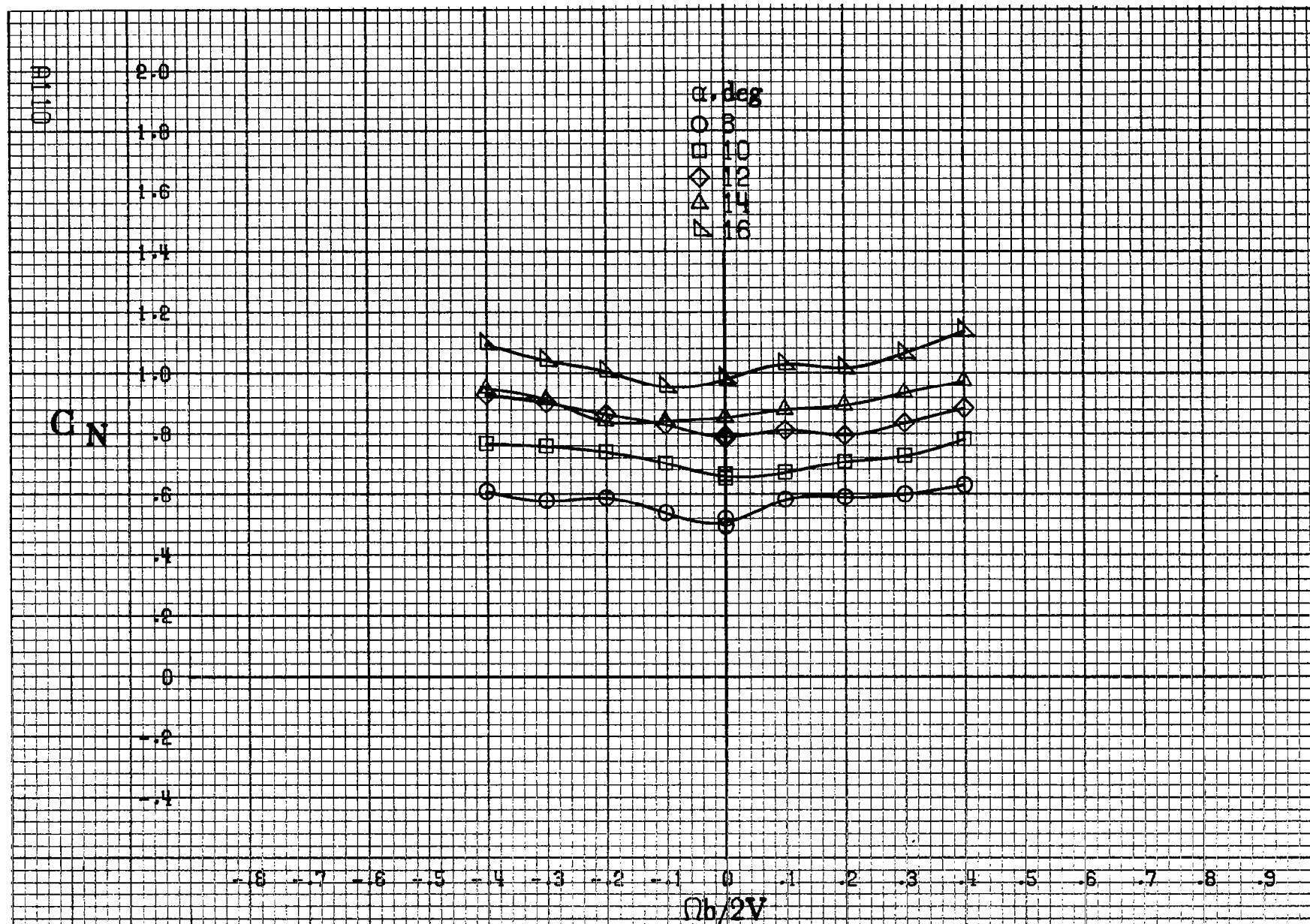
-8 -7 -6 -5 -4 -3 -2 -1 0 .1 .2 .3 .4 .5 .6 .7 .8 .9
 $\phi b/2V$

α, deg
○ 55
□ 60
◇ 70
△ 80
▽ 90

A109

(d) $\alpha=55$ to 90 deg, $SR=0$.
Figure A27.-Concluded.





(a) $\alpha = 8$ to 16° , $SR = 132.9 \text{ cm (72 in)}$.

Figure A28.-Effect of rotation rate and angle of attack on normal force coefficient for basic configuration. $\delta_a = 0^\circ$, $\delta_s = 0^\circ$, $\delta_{sa} = 0^\circ$, $\delta_r = 0^\circ$, $\beta = 0^\circ$.

C_N

α, deg

- 18
- 20
- ◇ 25
- △ 30
- ▽ 35

2.80
2.60
2.40
2.20
2.00
1.80
1.60
1.40
1.20
1.00
.80
.60
.40

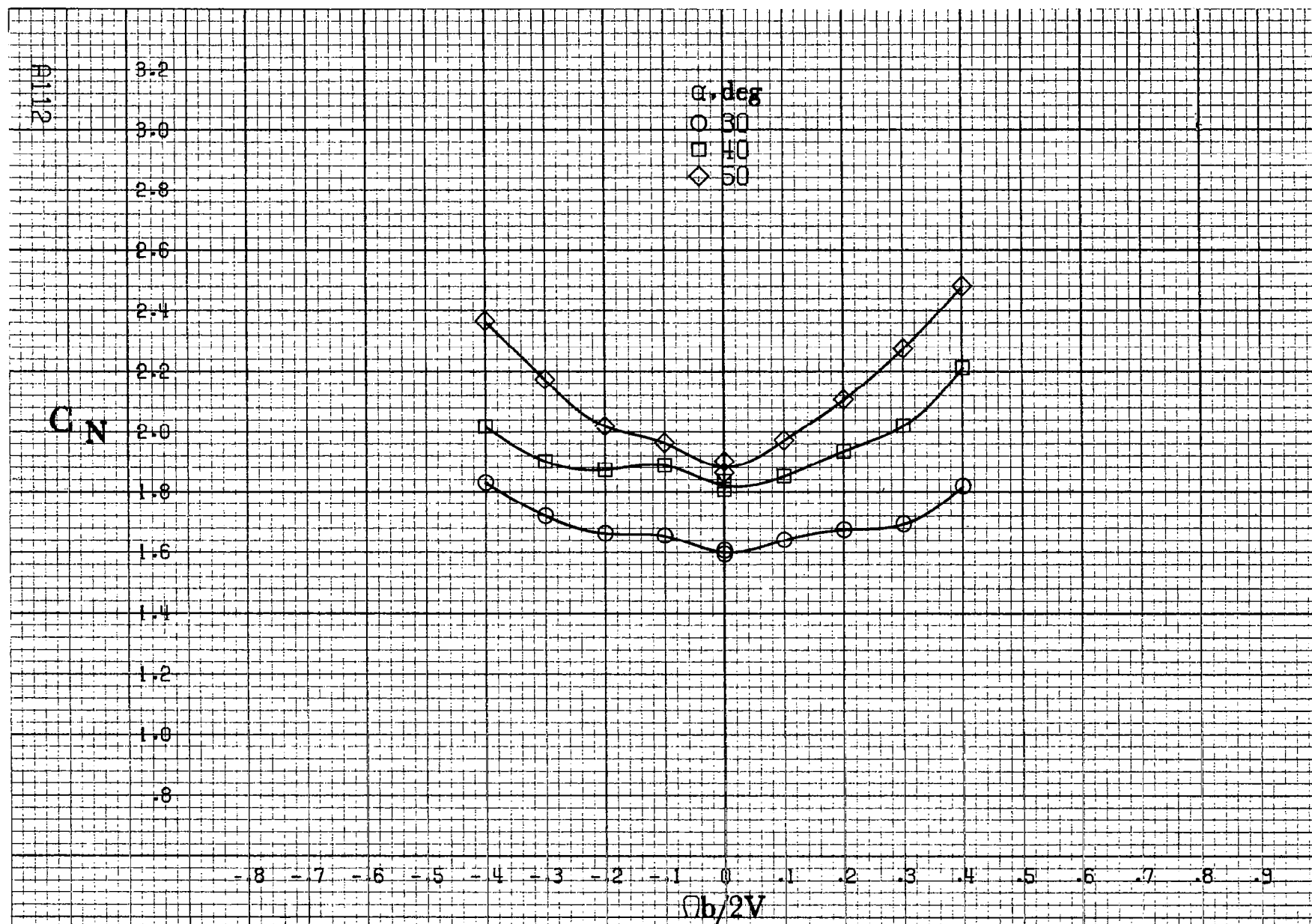
-8 -7 -6 -5 -4 -3 -2 -1 0 .1 .2 .3 .4 .5 .6 .7 .8 .9

$\Omega b/2V$

01111

(b) $\alpha = 18 \text{ to } 35 \text{ deg}$, $SR = 182.9 \text{ cm (72 in)}$.

Figure A28. Continued.



(c) $\alpha = 30$ to 50 deg. $SR = 0$.

Figure A 28.-Continued.

C_N

α, deg

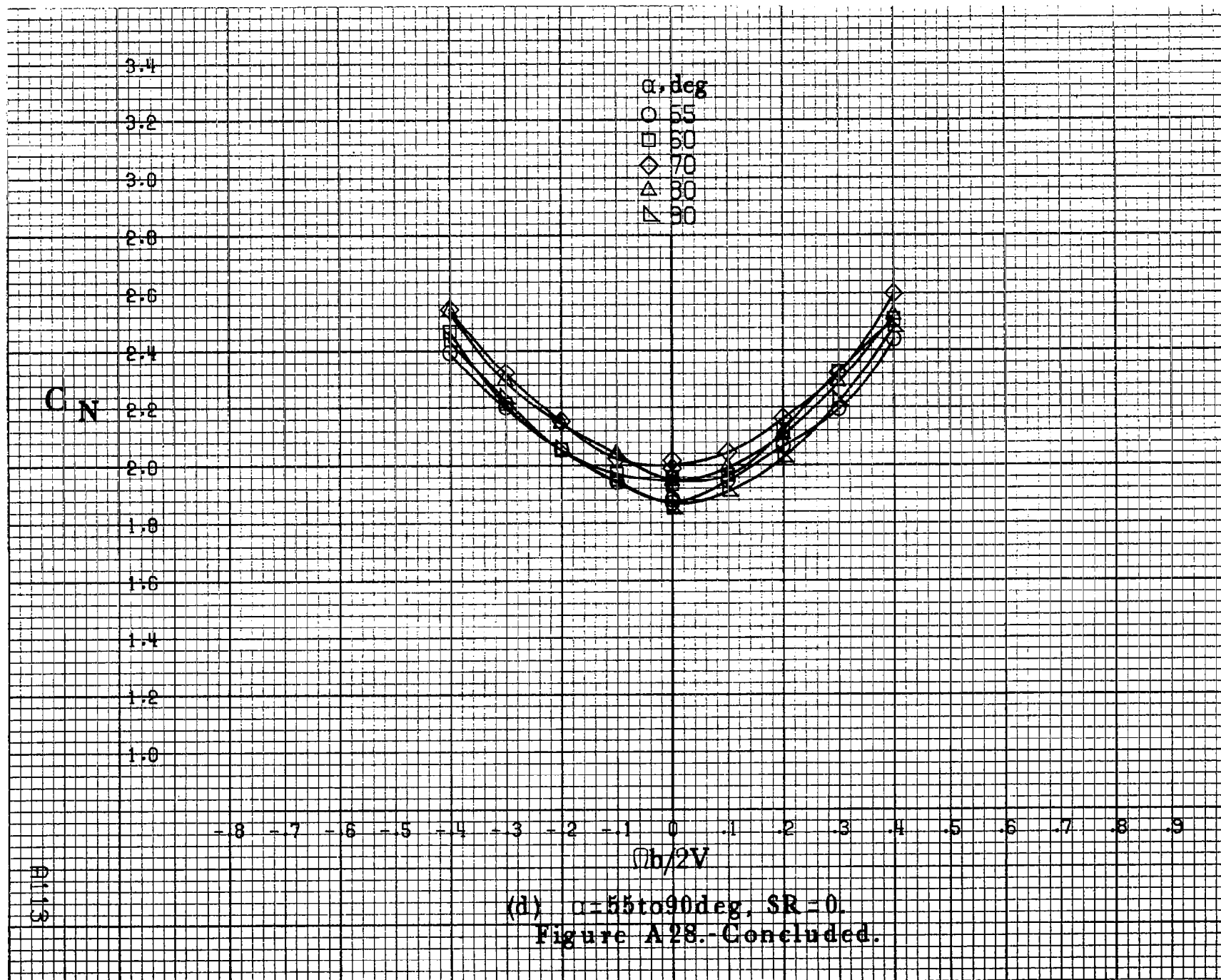
- 55
- 60
- ◇ 70
- △ 80
- ▽ 90

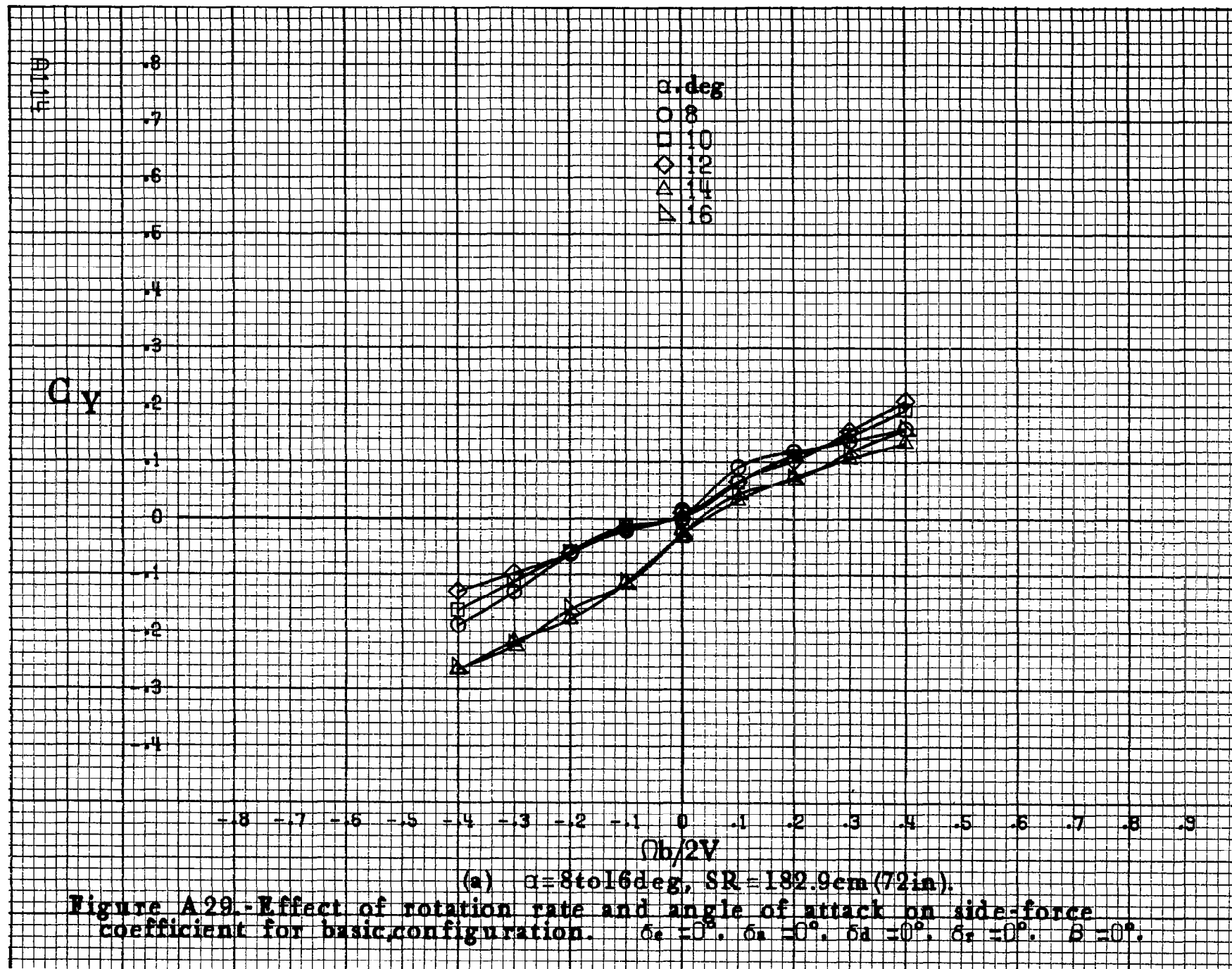
-8 -7 -6 -5 -4 -3 -2 -1 0 .1 .2 .3 .4 .5 .6 .7 .8 .9

$\phi b/2V$

Alt 15

(d) $\alpha=55\text{ to }90\text{deg}$, $SR=0$.
Figure A28.-Concluded.





C_y

α, deg

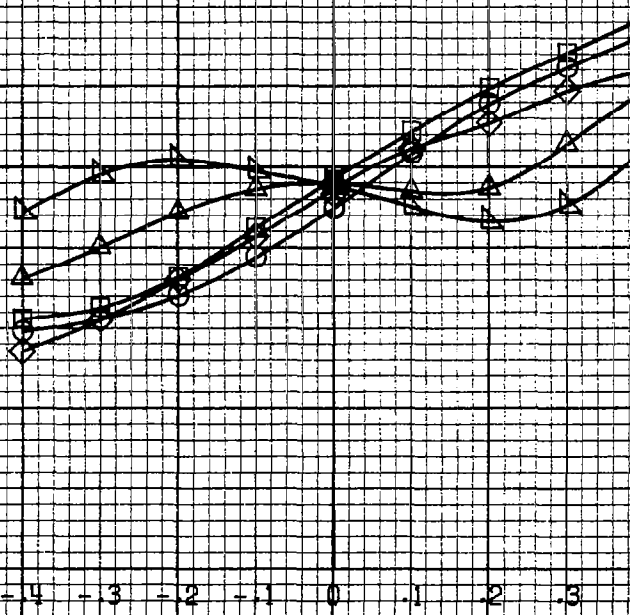
- 18
- 20
- ◇ 25
- △ 30
- ▽ 35

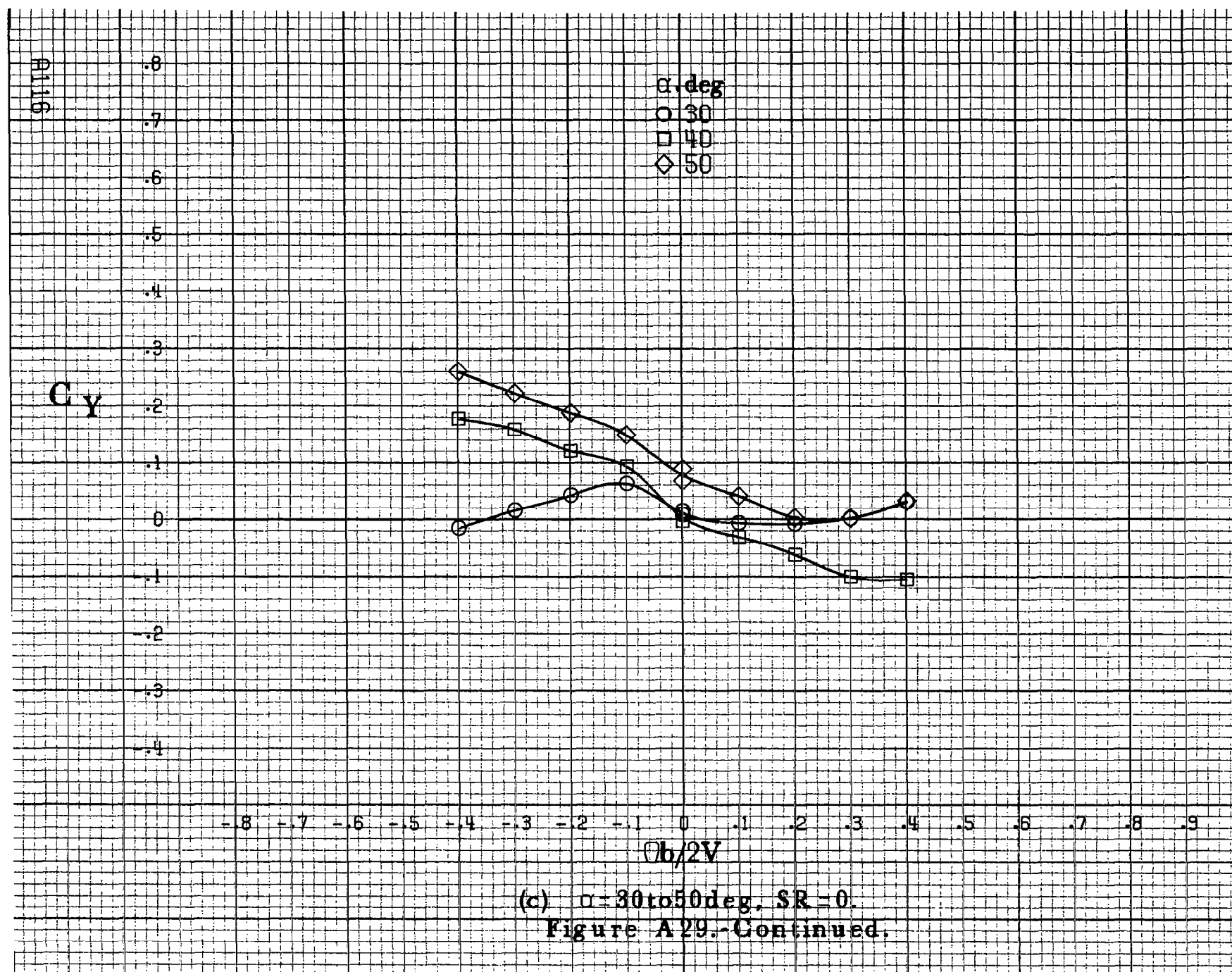
4115

- .8 - .7 - .6 - .5 - .4 - .3 - .2 - .1 - 0 .1 .2 .3 .4 .5 .6 .7 .8 .9

$Ob/2V$

(b) $\alpha = 18 \text{ to } 35 \text{ deg}$, $SR = 182.9 \text{ cm (72 in)}$.
Figure A29.-Continued.





C_y

α, deg

○ 55

□ 60

◇ 70

△ 80

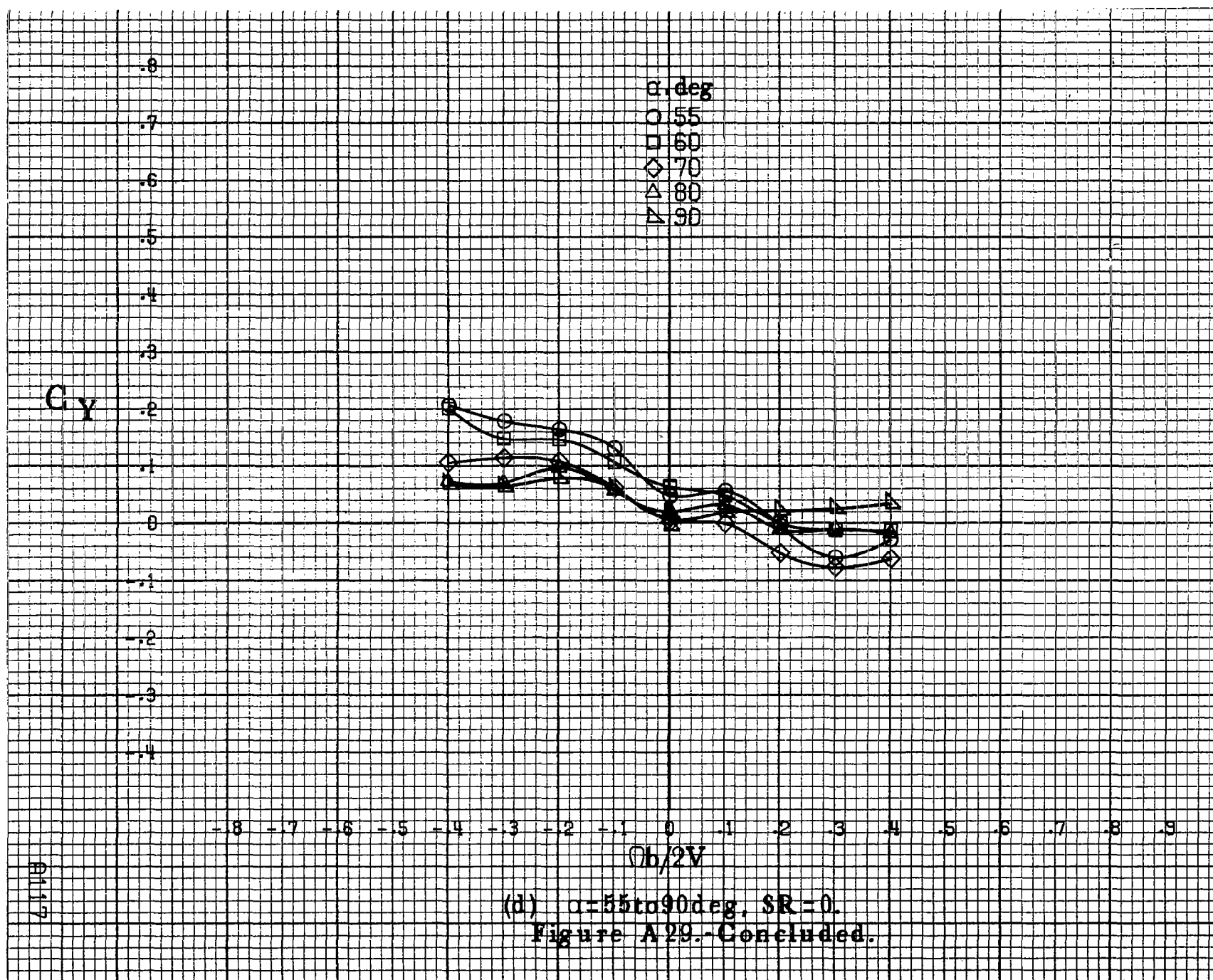
△ 90

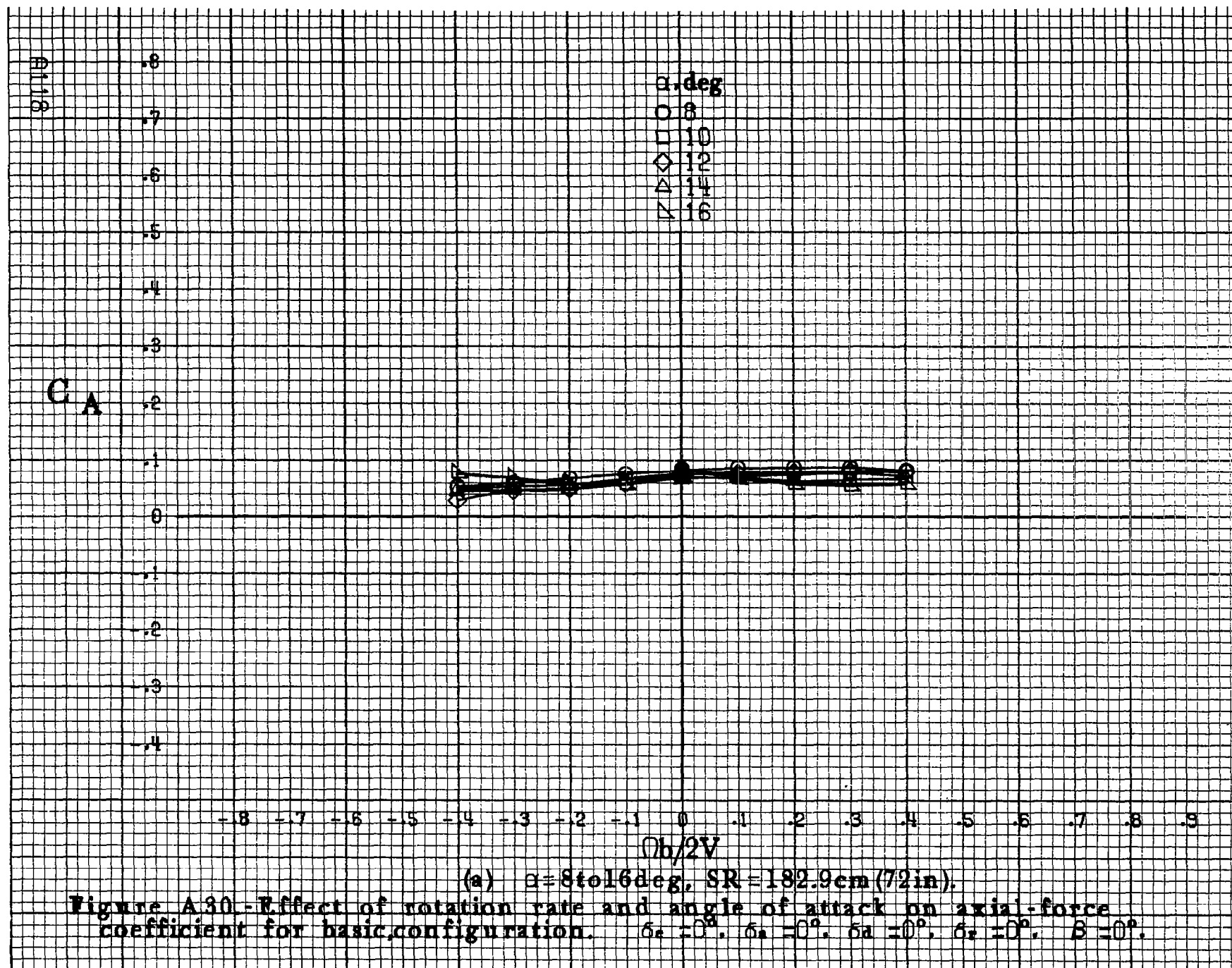
0117

$Ob/2V$

(d) $\alpha=55$ to 90 deg. $SR=0$.

Figure A29.-Concluded.





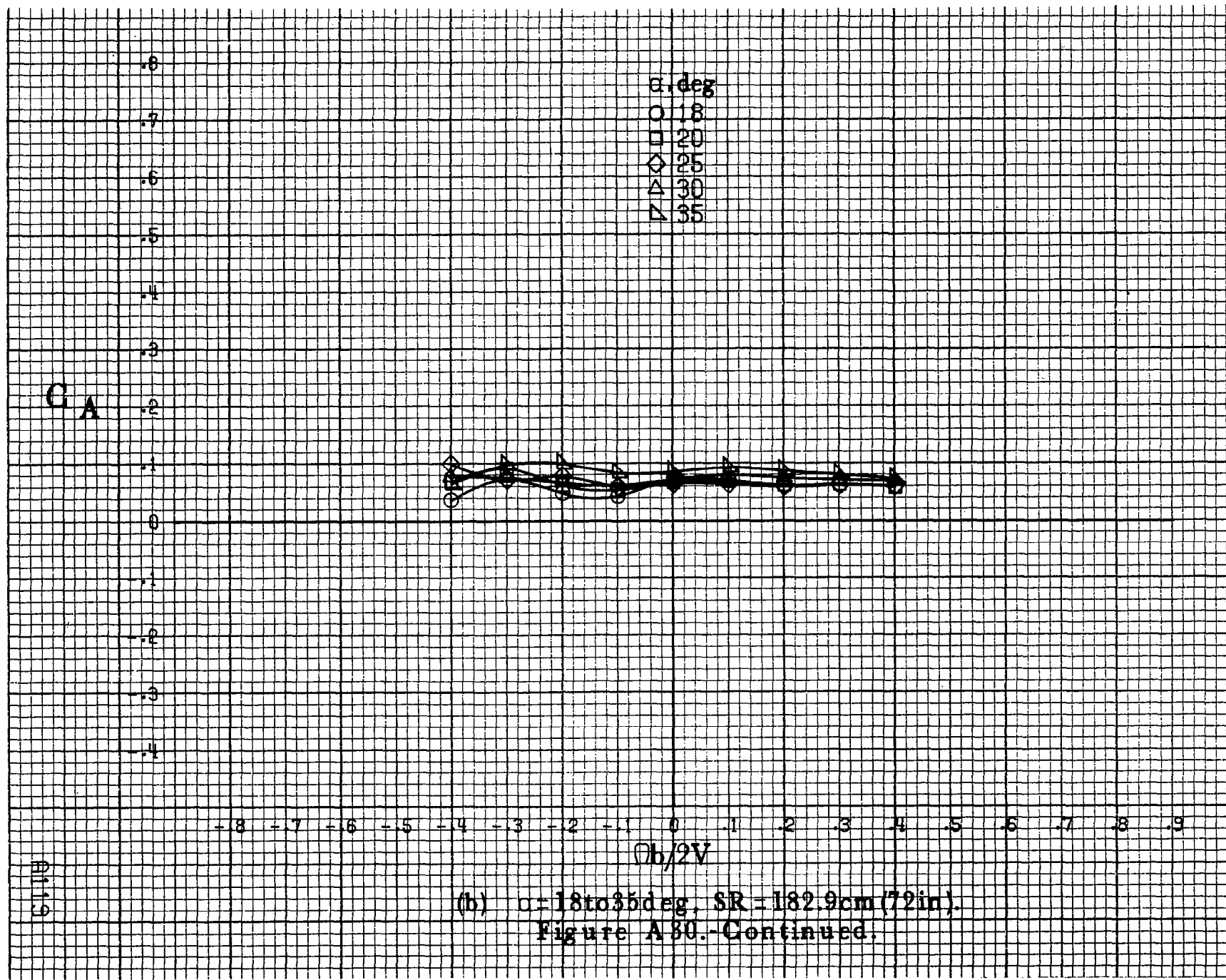
C_A

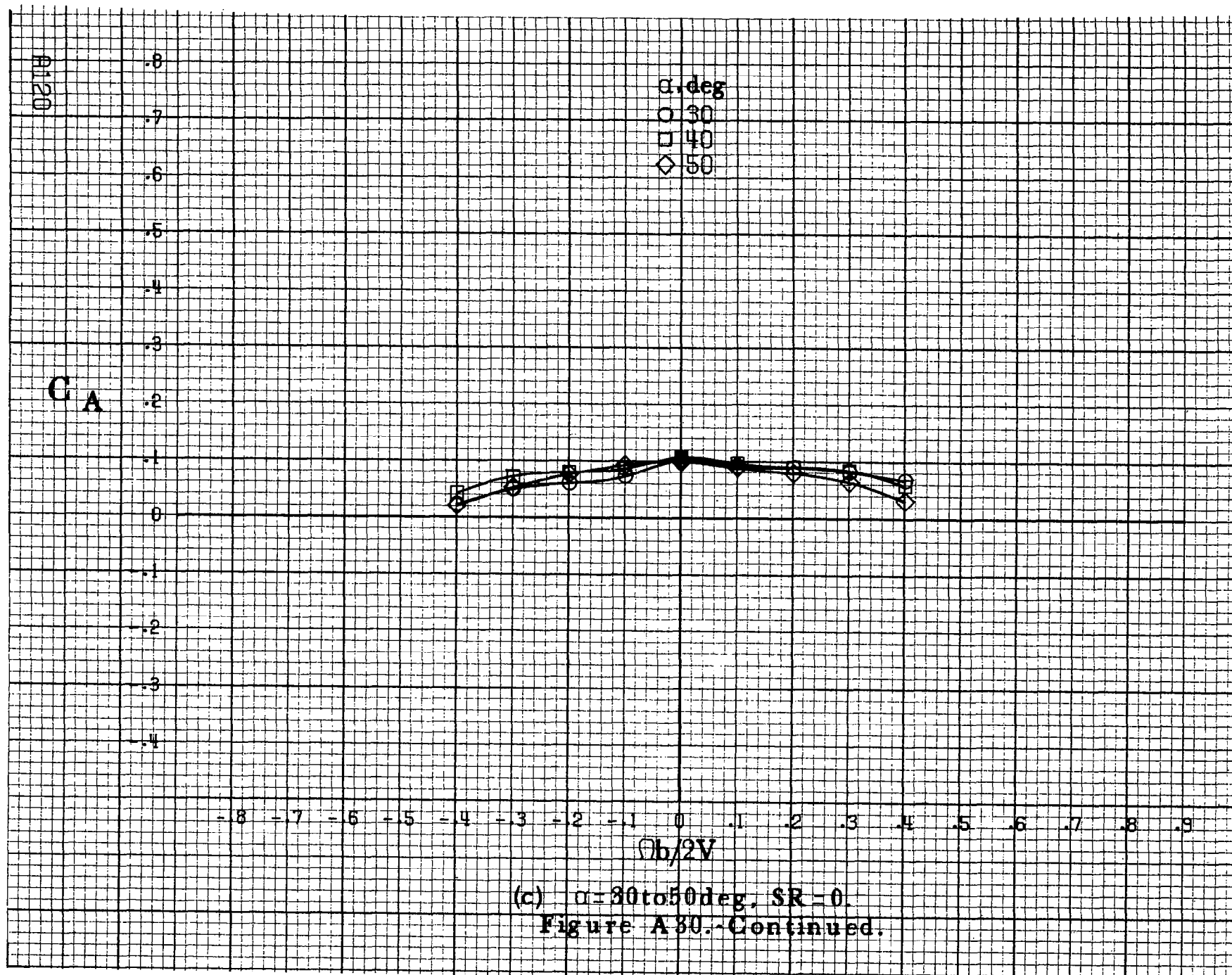
α, deg
 ○ 18
 □ 20
 ◇ 25
 △ 30
 ▽ 35

Al19

$Ob/2V$

(b) $\alpha = 18 \text{ to } 35 \text{ deg}$, $SR = 182.9 \text{ cm (72 in)}$.
 Figure A 80.-Continued.





C_A

α, deg
 ○ 55
 □ 60
 ◇ 70
 △ 80
 ▽ 90

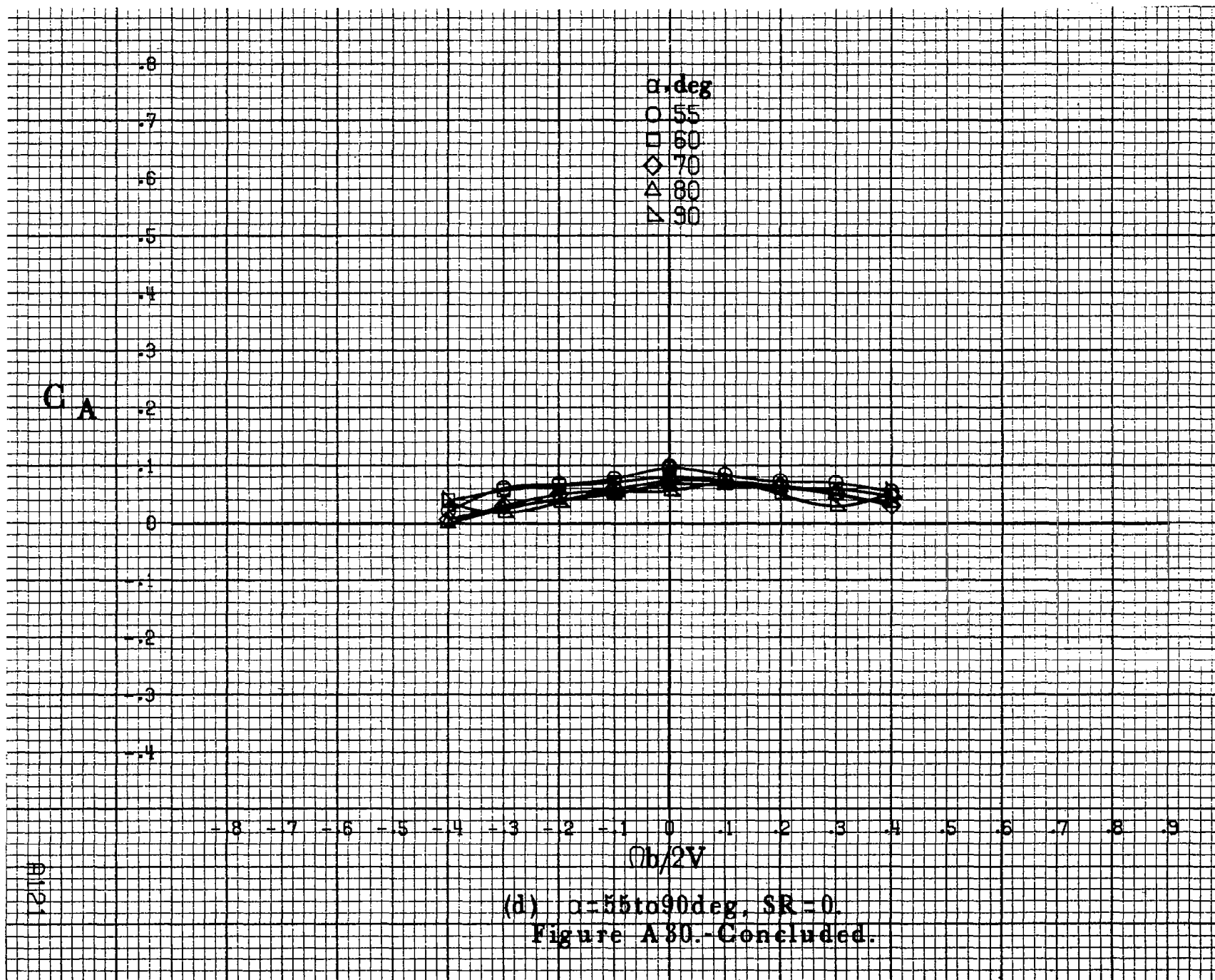
-8
-7
-6
-5
-4
-3
-2
-1
0
-1
-2
-3
-4

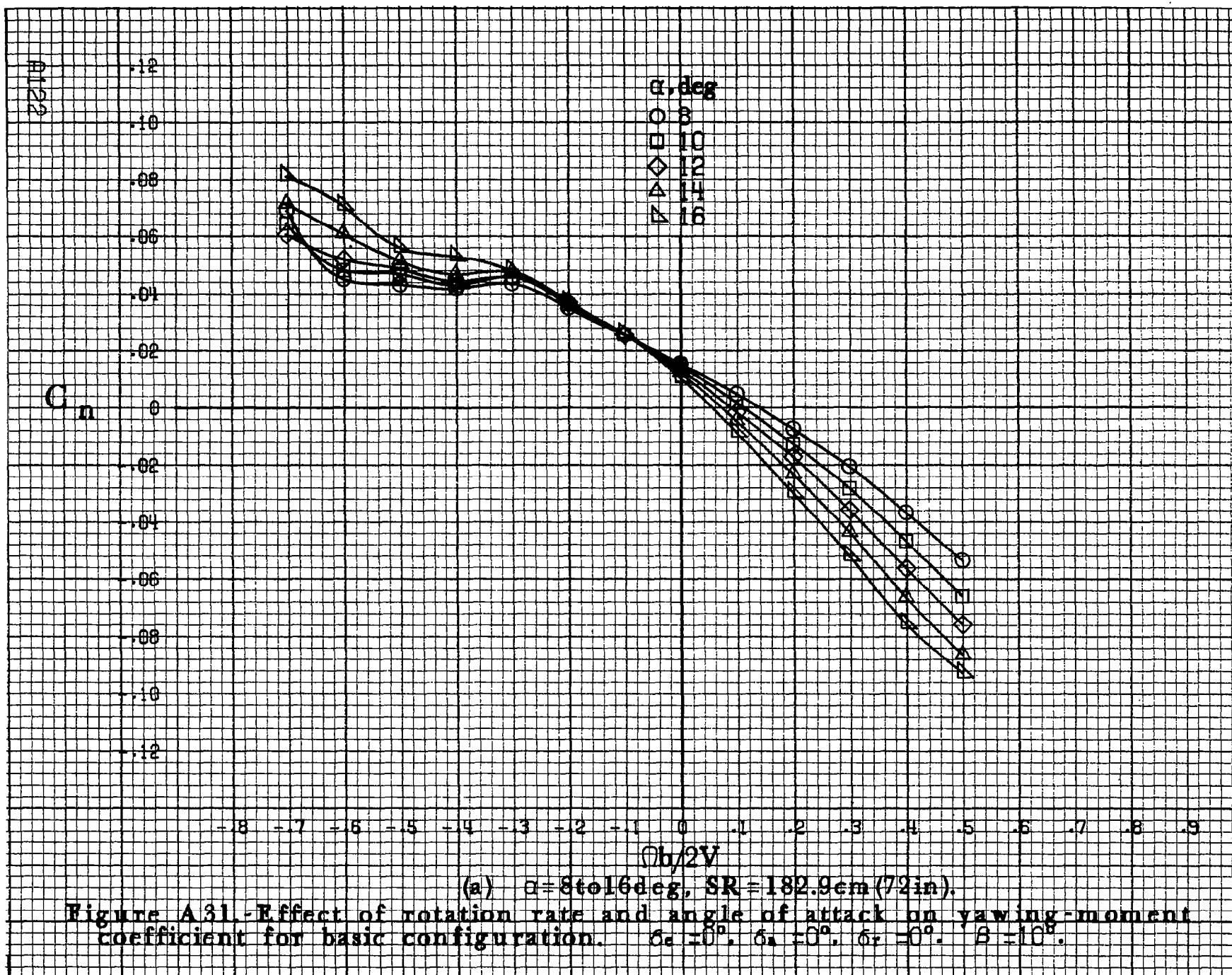
-8 -7 -6 -5 -4 -3 -2 -1 0 -1 -2 -3 -4 .5 .6 .7 .8 .9

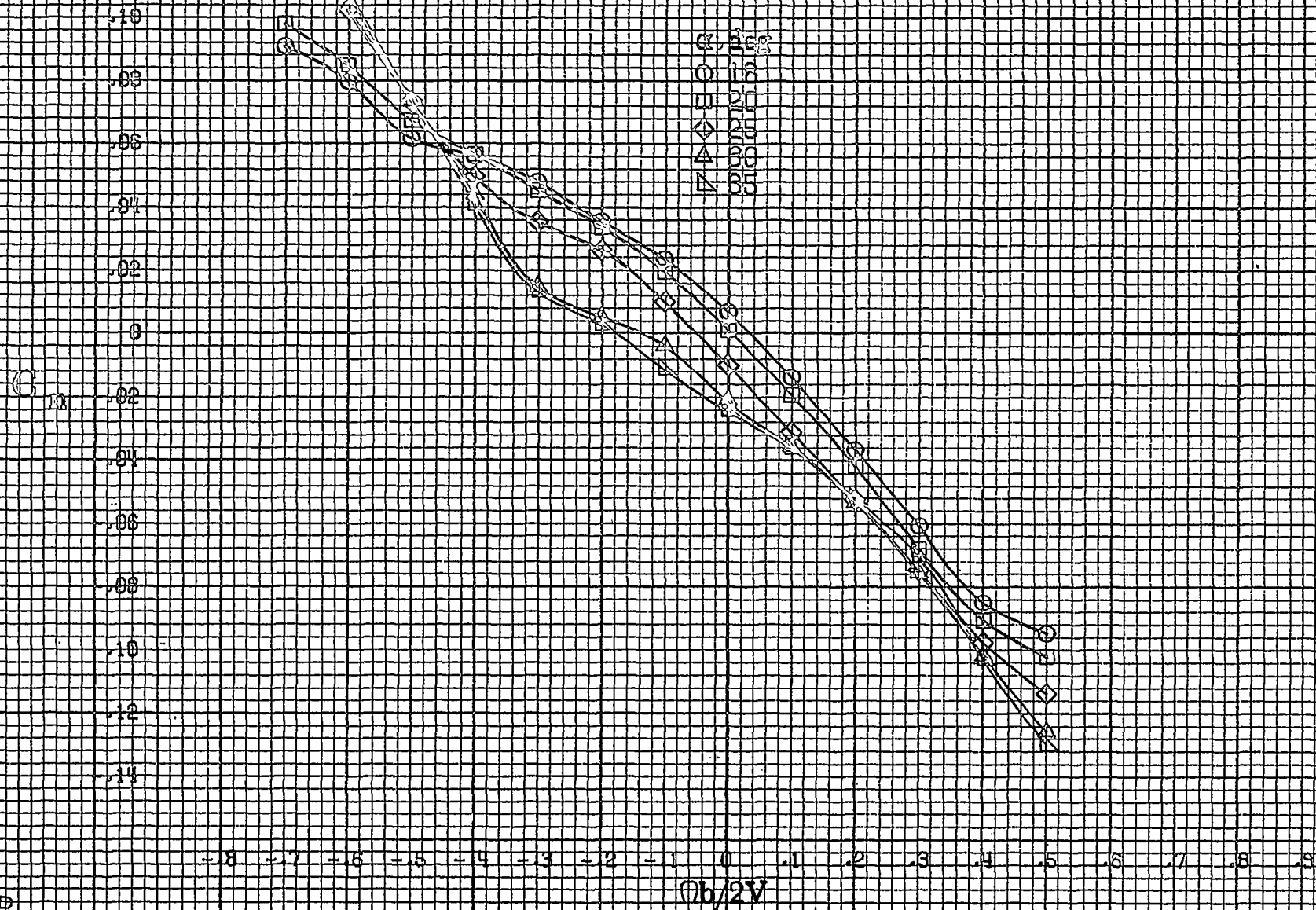
$\eta_b/2V$

(d) $\alpha=55\text{to}90\text{deg}, SR=0.$
 Figure A30.-Concluded.

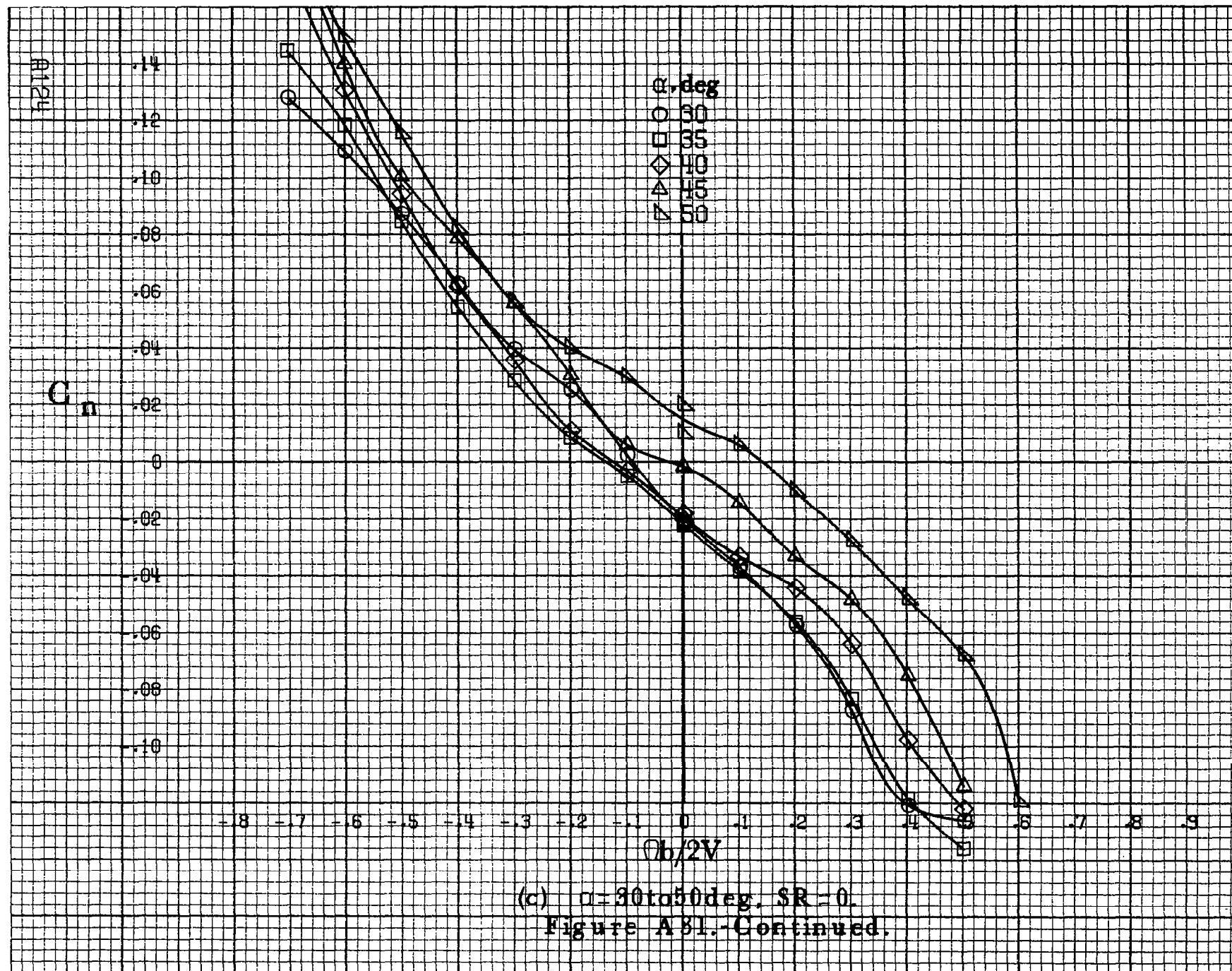
0121

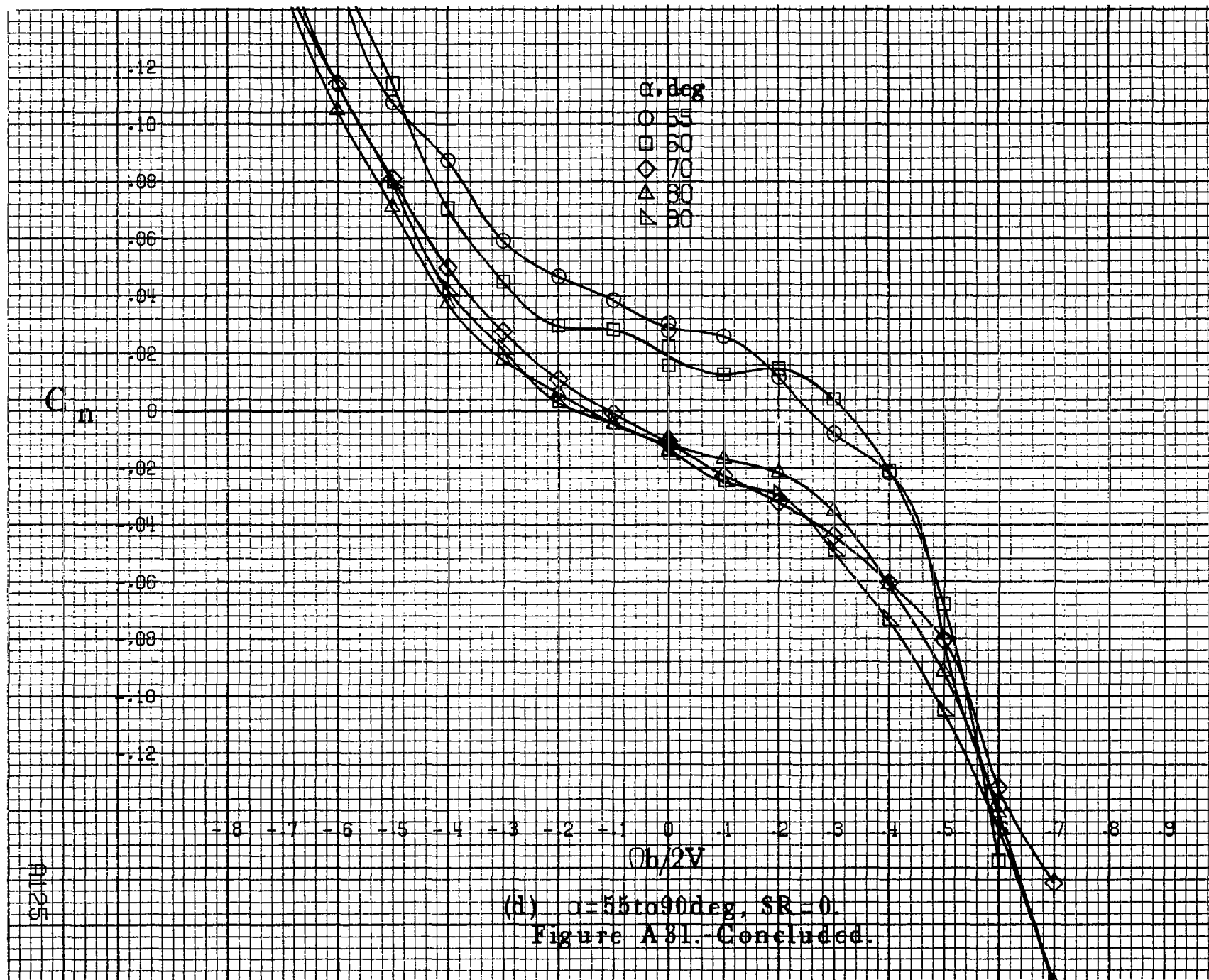






(b) $\alpha = 18$ to 35° , $SR = 182.9\text{cm (72in.)}$.
Figure A 31.-Continued.





A126

 C_l

.40
 .35
 .30
 .25
 .20
 .15
 .10
 .05
 0
 .05
 .10
 .15
 .20

 α, deg

○ 8
 □ 10
 ◇ 12
 △ 14
 ▴ 16

.8 .7 .6 .5 .4 .3 .2 .1 0 .1 .2 .3 .4 .5 .6 .7 .8 .9

 $\Omega b/2V$ (a) $\alpha = 8 \text{ to } 16 \text{ deg}$, $SR = 182.9 \text{ cm (72 in)}$.

Figure A32.-Effect of rotation rate and angle of attack on rolling-moment coefficient for basic configuration. $\delta_e = 0^\circ$, $\delta_a = 0^\circ$, $\delta_r = 0^\circ$, $\delta = 10^\circ$.

C_1

.16
.14
.12
.10
.08
.06
.04
0
-.02
-.04
-.06
-.08

α , deg

○ 18
□ 20
◇ 25
△ 30
▽ 35

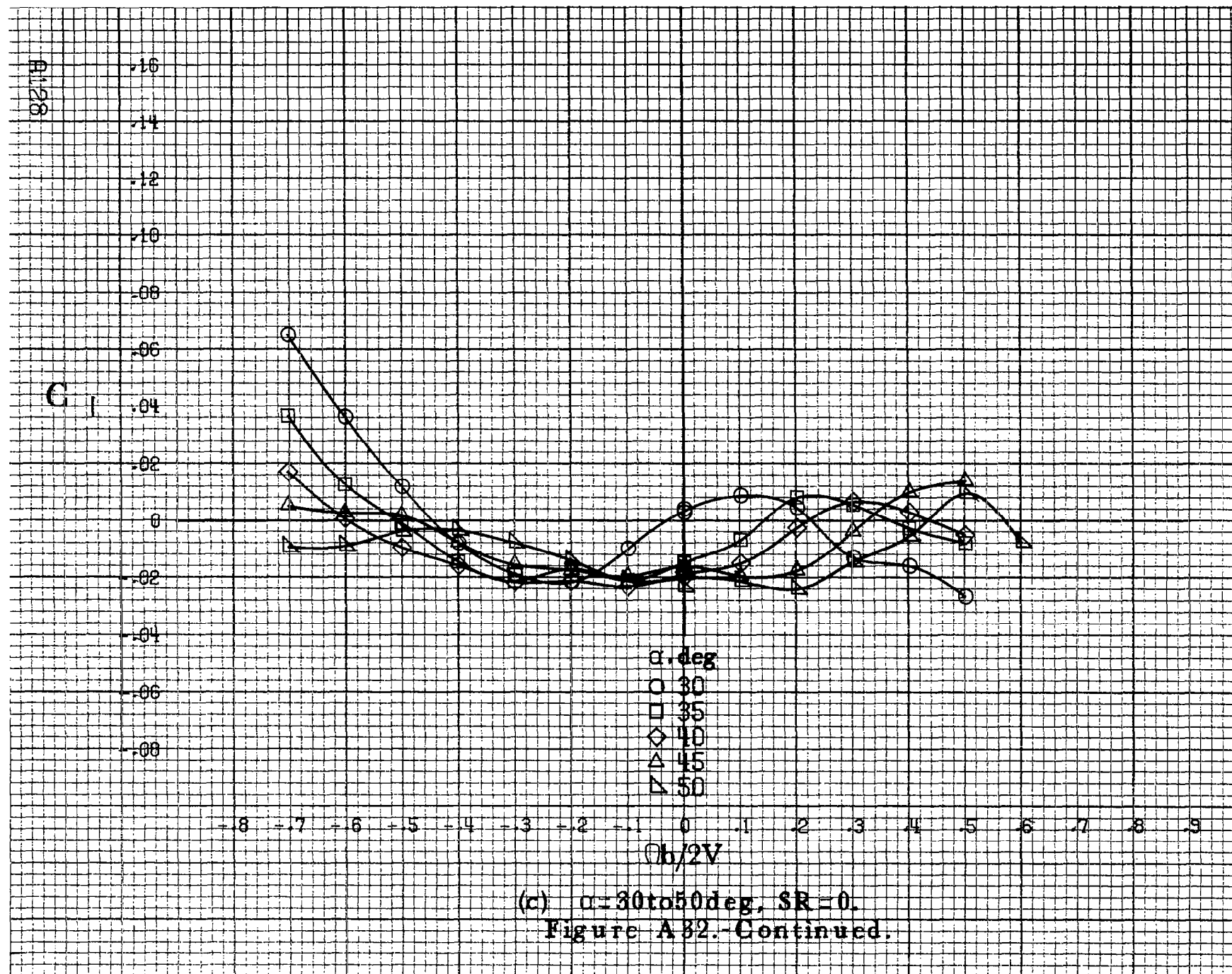
-.8 -.7 -.6 -.5 -.4 -.3 -.2 -.1 0 .1 .2 .3 .4 .5 .6 .7 .8 .9

$h/2V$

(b) $\alpha = 18$ to 35 deg, SR = 182.9 cm (72 in).

Figure A32.-Continued.

#127



C_1

.14
.12
.10
.08
.06
.04
.02
0
-.02
-.04
-.06
-.08
-.10

-8 -7 -6 -5 -4 -3 -2 -1 0 1 2 3 4 5 6 7 8 9

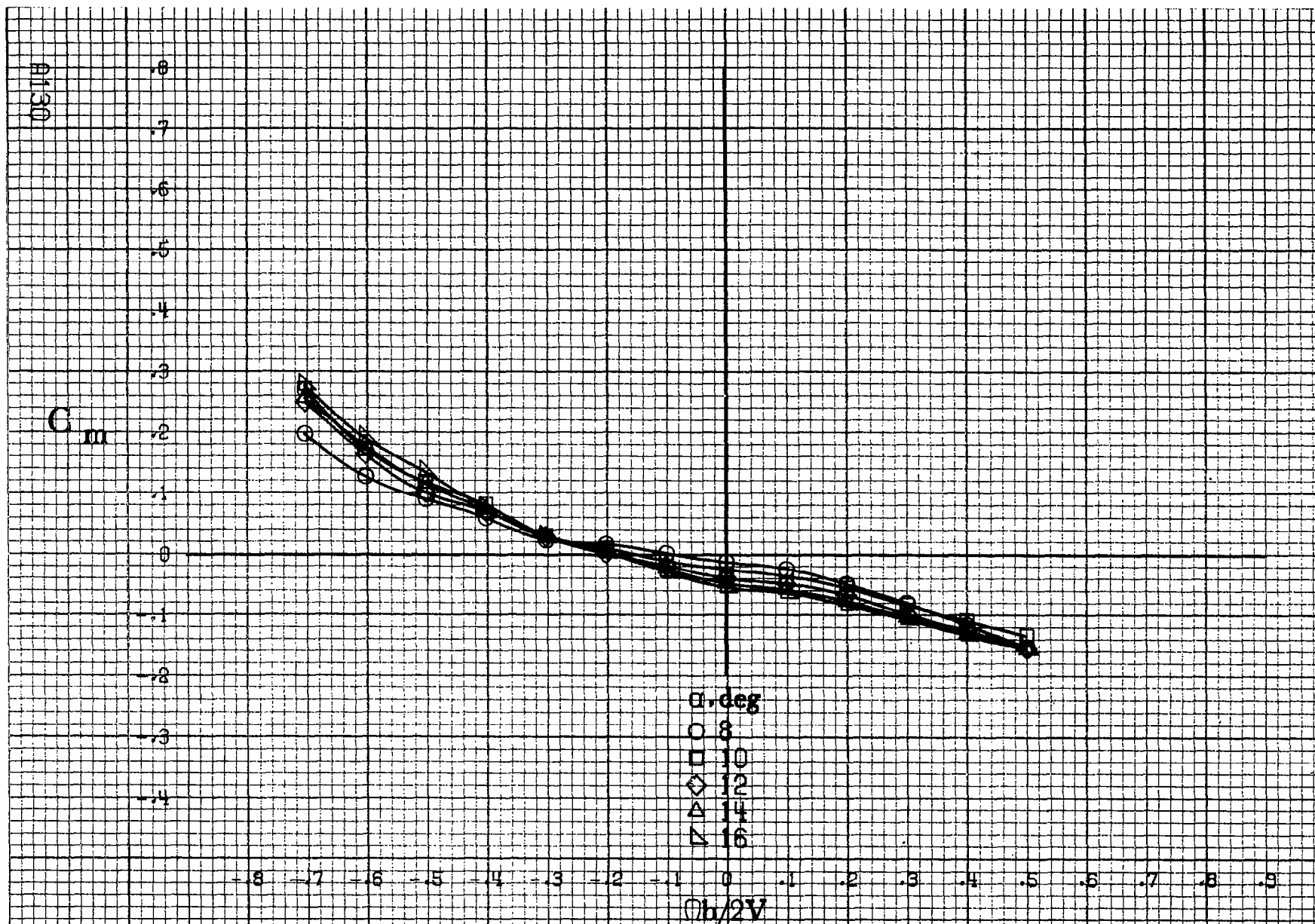
α, deg

○ 55
□ 60
◇ 70
△ 80
▽ 90

$\Phi h/2V$

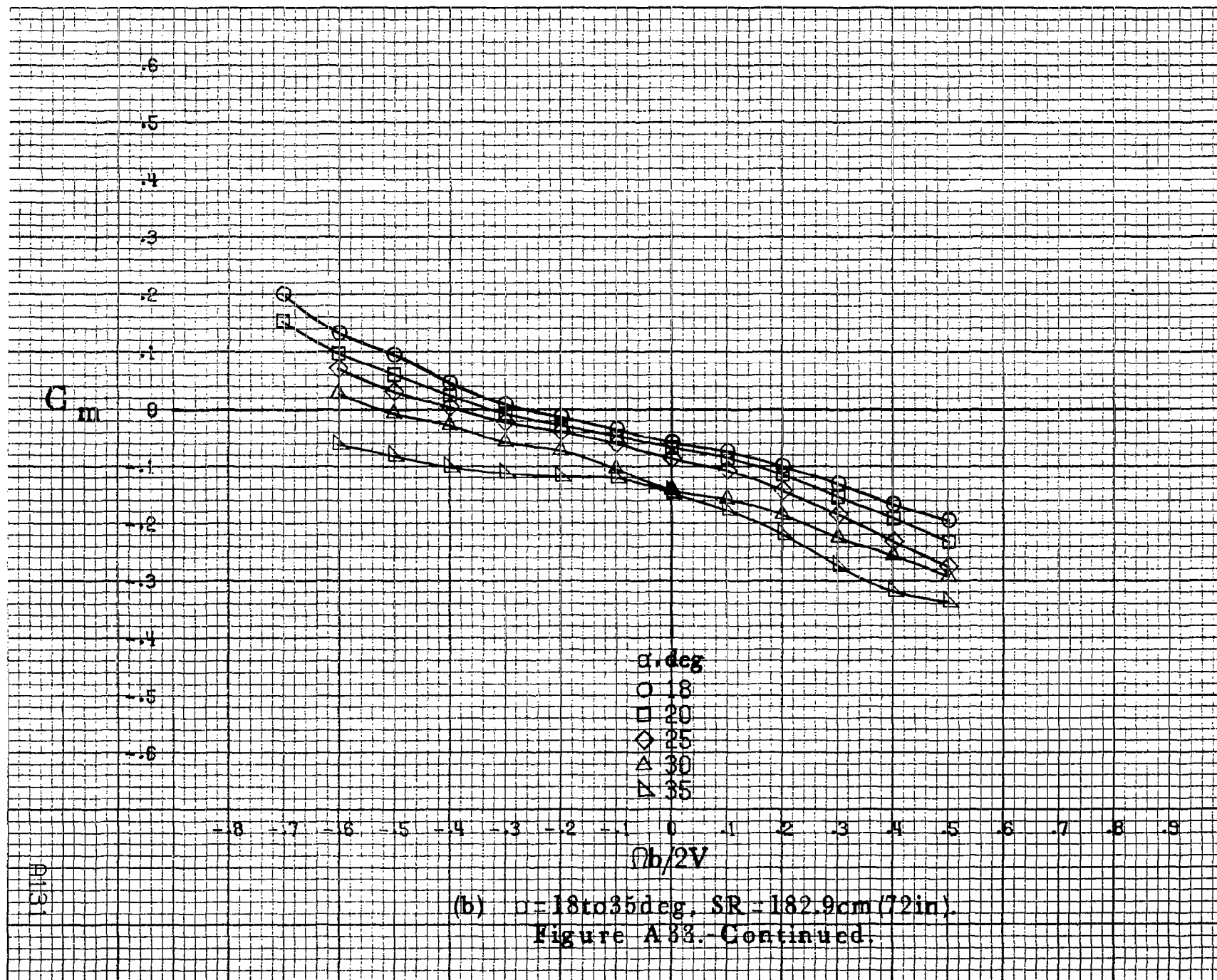
(d) $\alpha=55$ to 90 deg, $SR=0$
Figure A32.- Concluded.

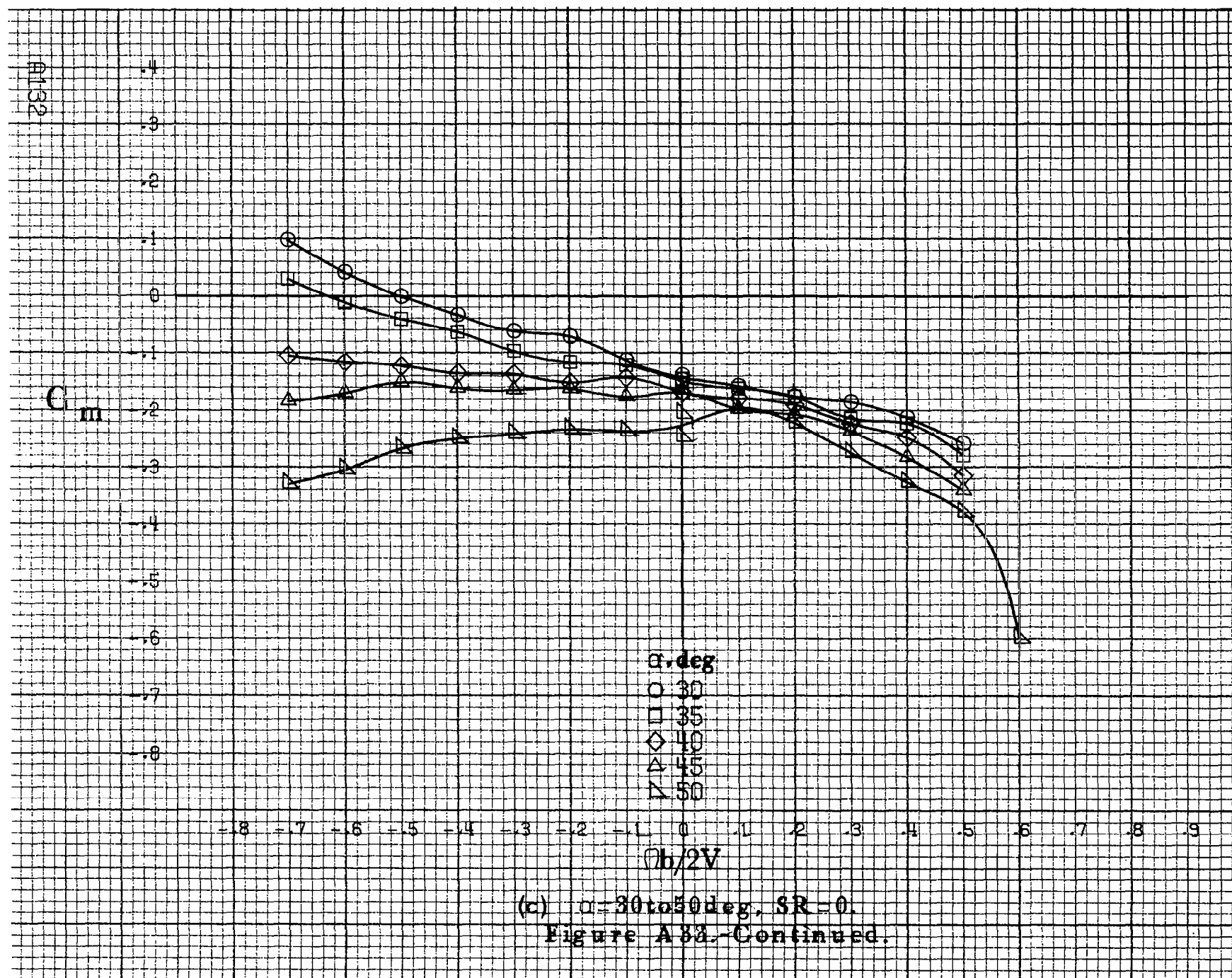
A1129



(a) $\alpha=8\text{ to }16^\circ$, $SR=182.9\text{ cm (72 in.)}$.

Figure A33.-Effect of rotation rate and angle of attack on pitching-moment coefficient for basic configuration. $\delta_a=0^\circ$, $\delta_s=0^\circ$, $\delta_r=0^\circ$, $\beta=10^\circ$.





C_m

α, deg

○ 55

□ 60

◇ 70

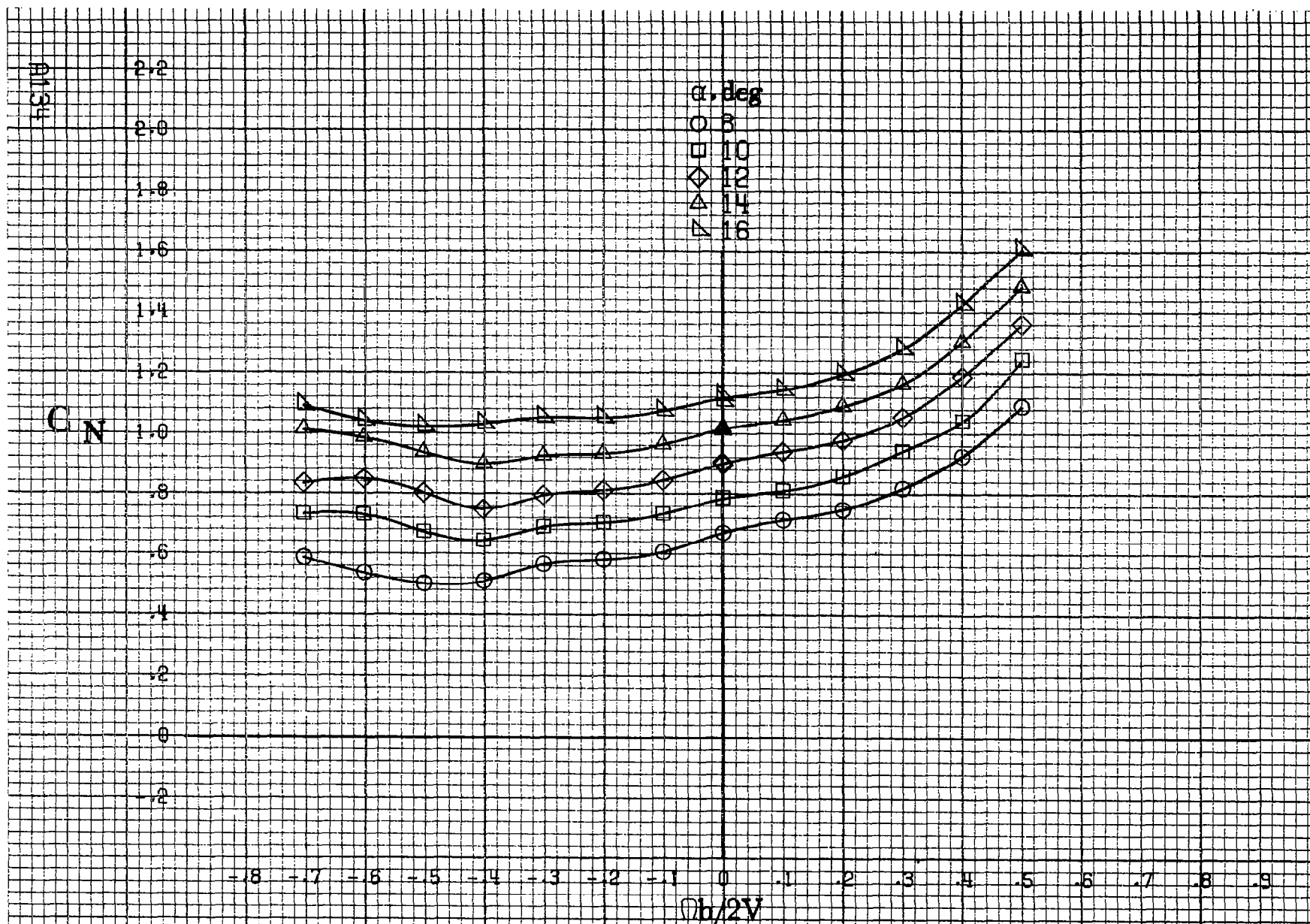
△ 80

▽ 90

$b/2V$

(d) $\alpha = 55 \text{ to } 90 \text{ deg}, SR = 0.$
Figure A33.-Concluded.

A133



(a) $\alpha = 8$ to 16° , $SR = 182.9$ cm (72 in).

Figure A34 - Effect of rotation rate and angle of attack on normal-force coefficient for basic configuration. $\delta_e = 0^\circ$, $\delta_a = 0^\circ$, $\delta_r = 0^\circ$, $\beta = 10^\circ$.

C_N

α, deg

- 18
- 20
- ◇ 25
- △ 30
- ▽ 35

$Ob/2V$

(b) $\alpha = 18 \text{ to } 35 \text{ deg}$, $SR = 182.9 \text{ cm (72 in)}$.

Figure A 84.-Continued.

81135

C_N

3.6
3.4
3.2
3.0
2.8
2.6
2.4
2.2
2.0
1.8
1.6
1.4
1.2

 α, deg

○ 30
□ 35
◇ 40
△ 45
▽ 50

-0.8 -0.7 -0.6 -0.5 -0.4 -0.3 -0.2 -0.1 0 .1 .2 .3 .4 .5 .6 .7 .8 .9

$Ob/2V$

(c) $\alpha = 30 \text{ to } 50 \text{ deg. SR} = 0.$
Figure A 84.-Continued.

C_N

α, deg

○ 55

□ 60

◇ 70

△ 80

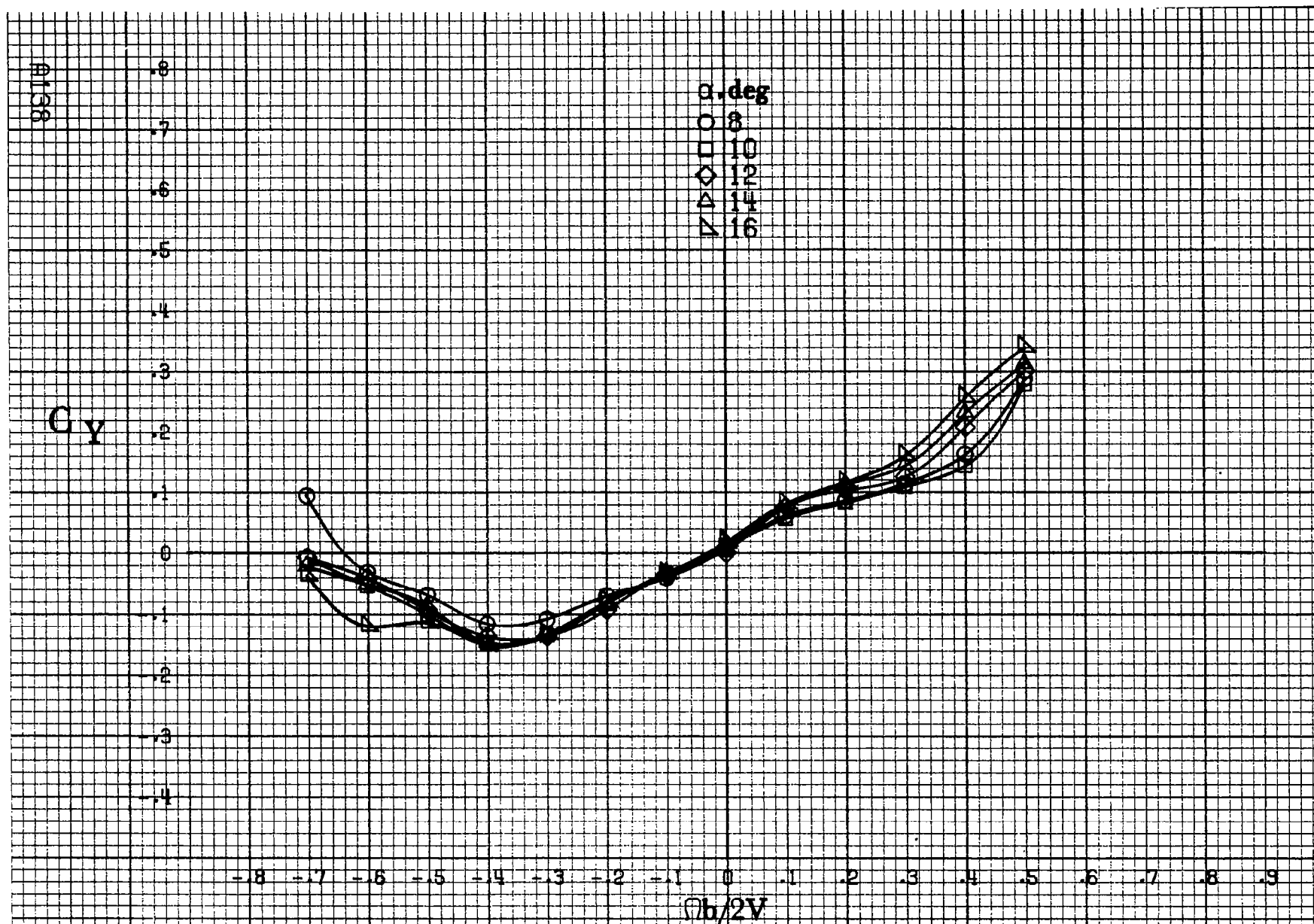
▽ 90

$Ob/2V$

(d) $\alpha=55$ to 90 deg, $SR=0$.

Figure A34.-Concluded.

A137



(a) $\alpha = 8$ to 16° , $SR = 182.9$ cm (72 in).

Figure A35.-Effect of rotation rate and angle of attack on side-force coefficient for basic configuration. $\delta_e = 0^\circ$, $\delta_s = 0^\circ$, $\delta_r = 0^\circ$, $\beta = 10^\circ$.

C_y

α, deg
 ○ 18
 □ 20
 ◇ 25
 △ 30
 ▽ 35

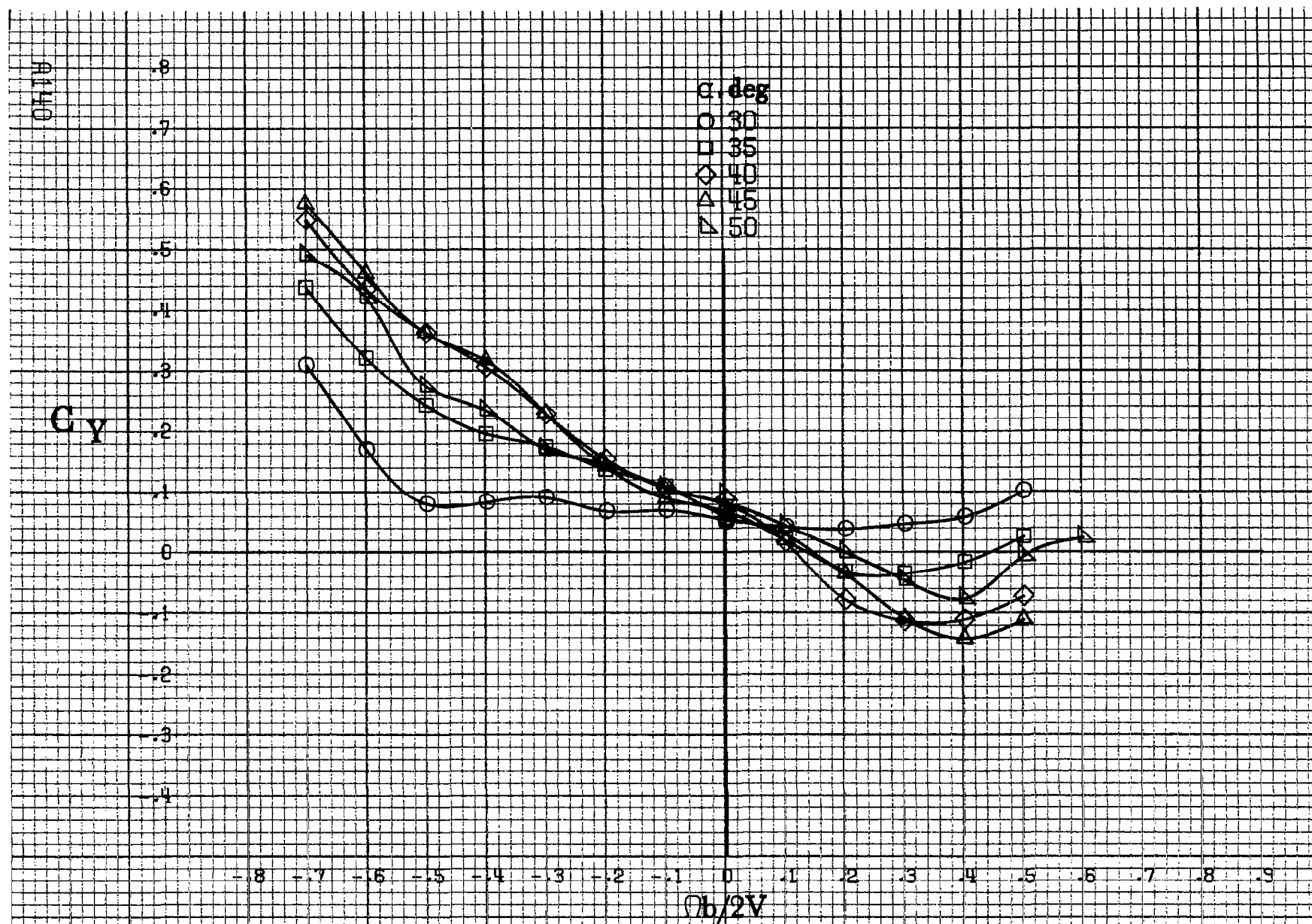
.8
.7
.6
.5
.4
.3
.2
.1
0
.1
.2
.3
.4

-0.8 -0.7 -0.6 -0.5 -0.4 -0.3 -0.2 -0.1 0 .1 .2 .3 .4 .5 .6 .7 .8 .9

$Qb/2V$

#159

(b) $\alpha = 18 \text{ to } 35 \text{ deg. SR} = 182.9 \text{ cm (72 in).}$
 Figure A35.-Continued.



(c) $\alpha=30$ to 50 deg, $SR=0$.

Figure A35.-Continued.

C_y

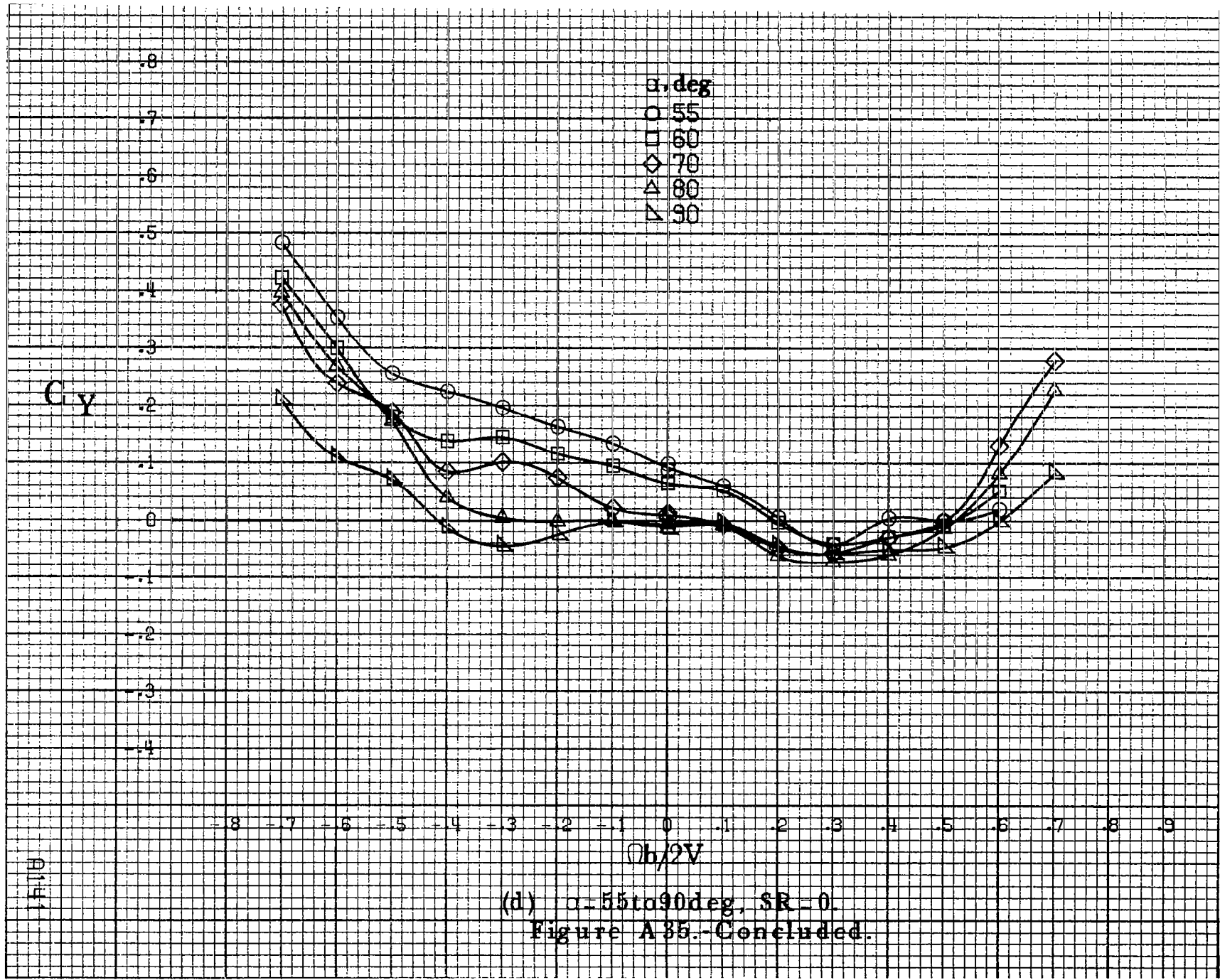
α, deg

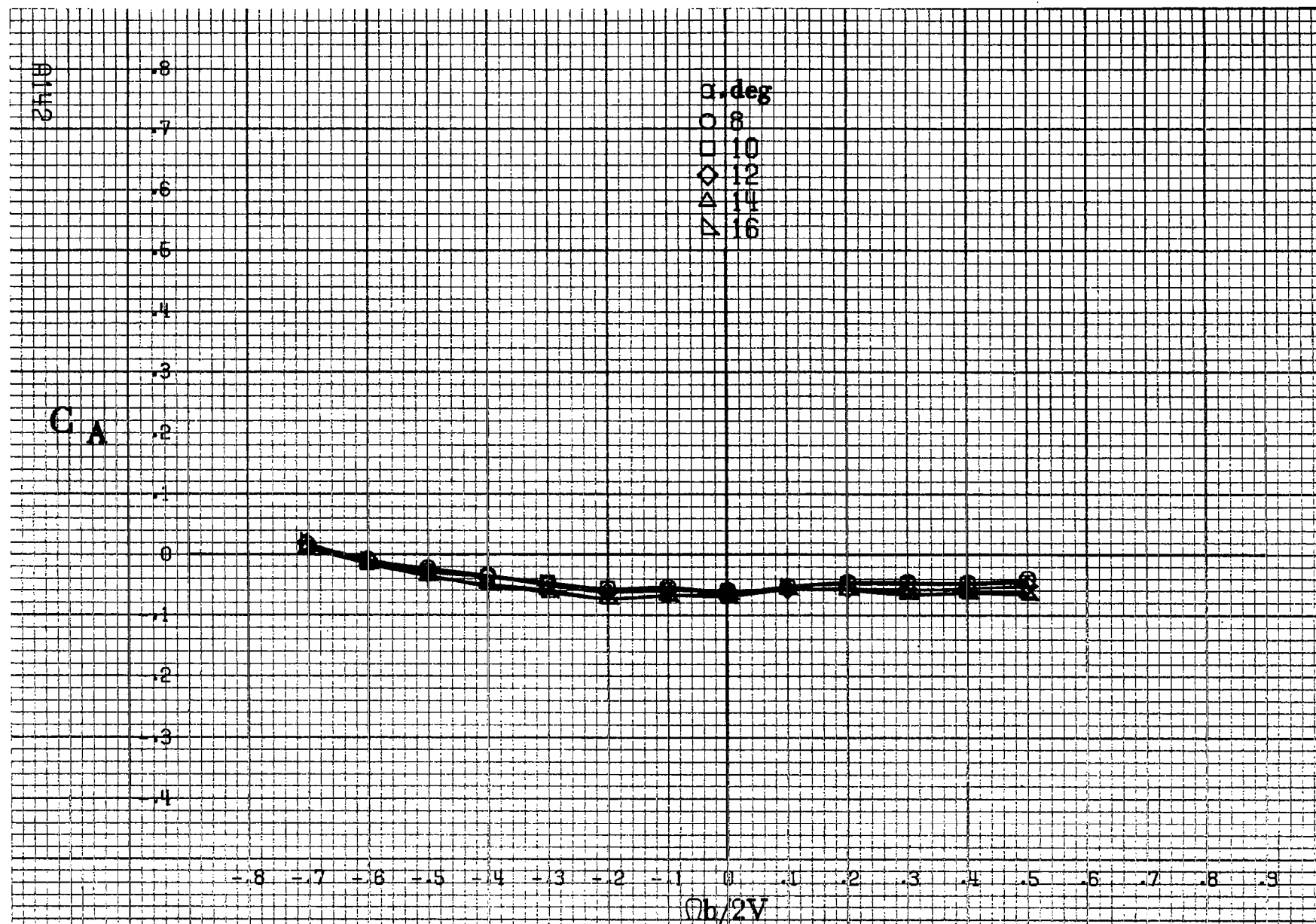
- 55
- 60
- ◇ 70
- △ 80
- ▽ 90

01141

$Ob/2V$

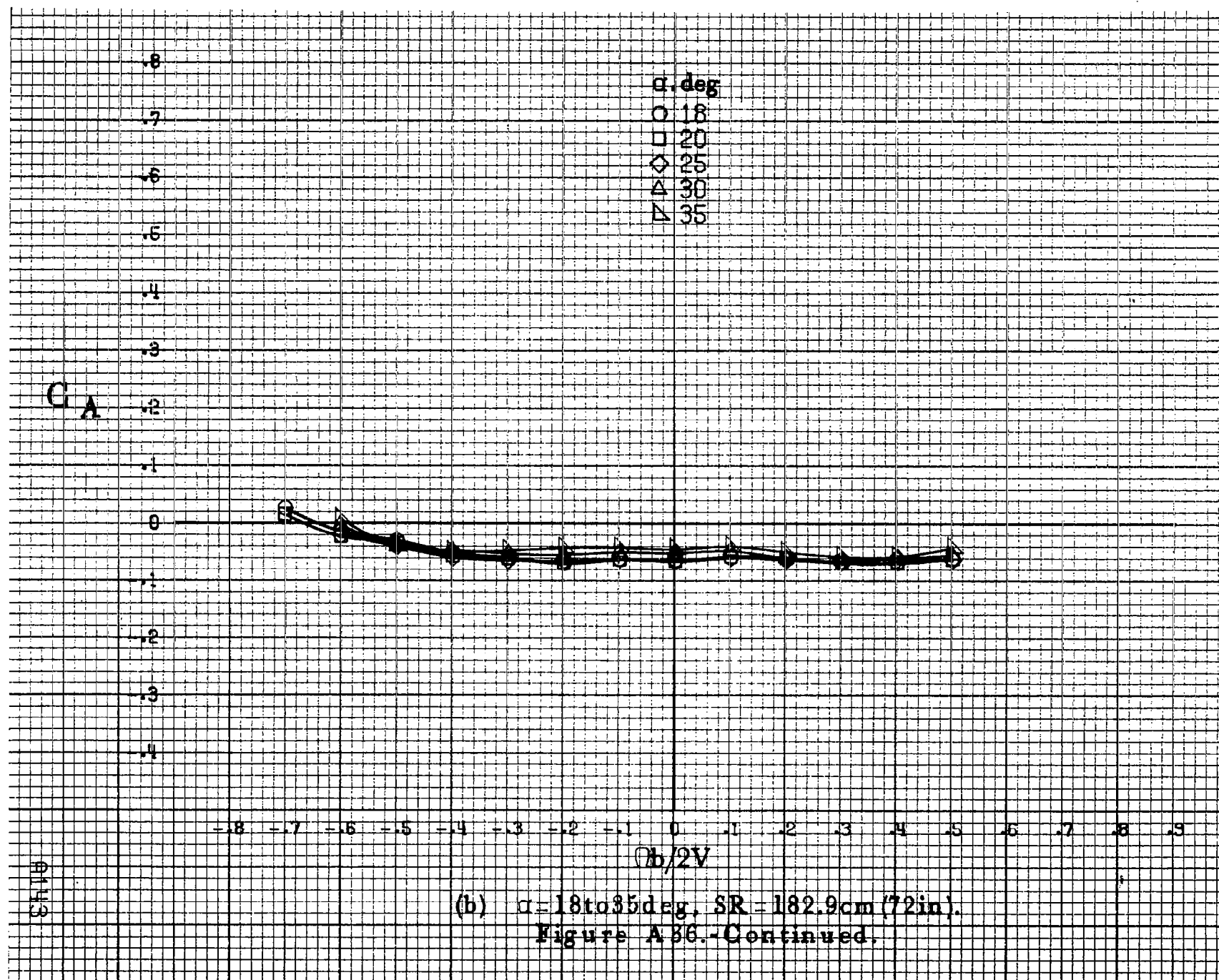
(d) $\alpha = 55 \text{ to } 90 \text{ deg}, SR = 0$.
Figure A35.- Concluded.

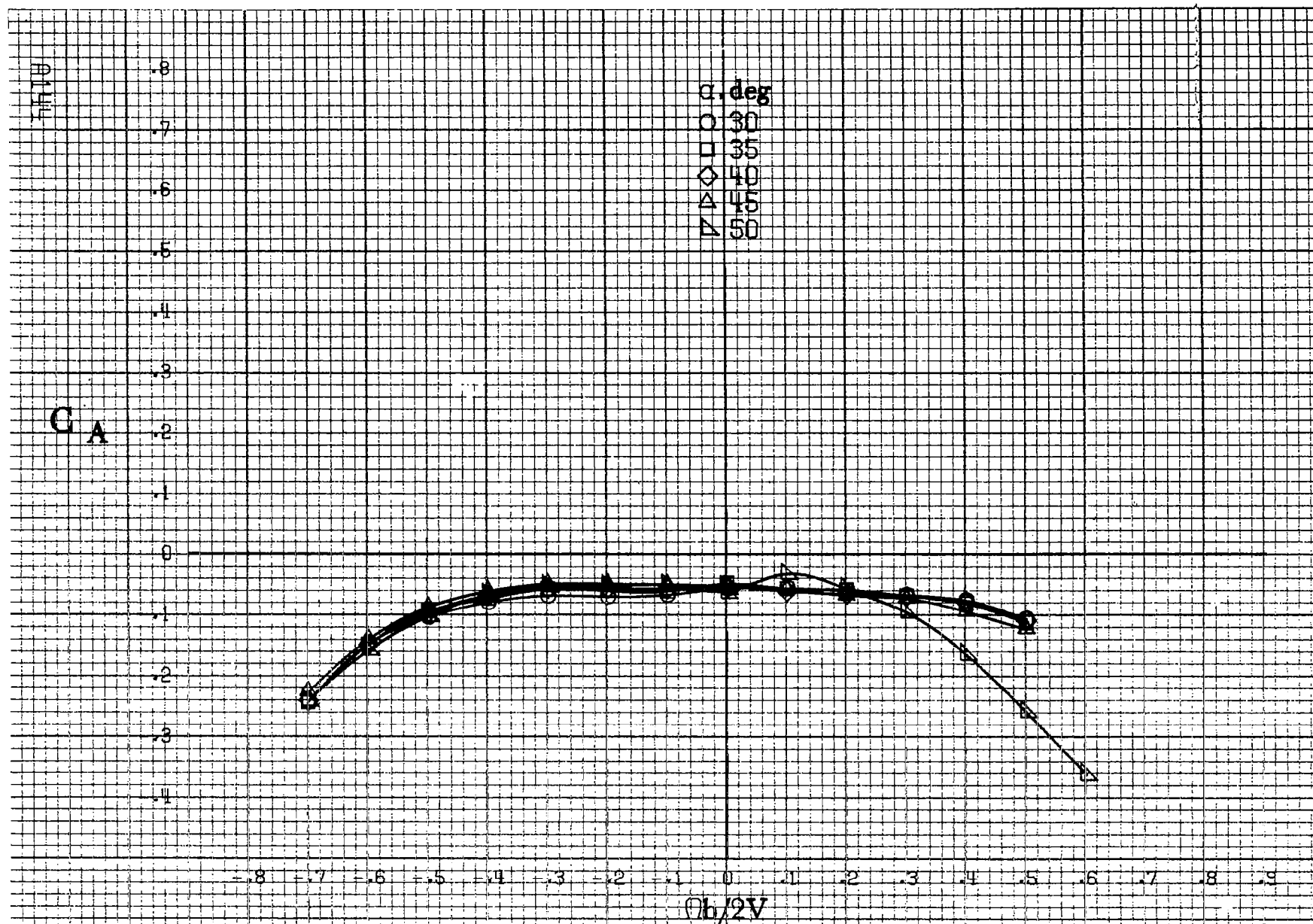




(a) $\alpha = 8$ to 16 deg, $SR = 182.9$ cm (72 in).

Figure A36.-Effect of rotation rate and angle of attack on axial-force coefficient for basic configuration. $\delta_z = 0^\circ$, $\delta_a = 0^\circ$, $\delta_r = 0^\circ$. $\theta = 10^\circ$.





(c) $\alpha = 30$ to 50 deg, $SR = 0$.

Figure A 36.-Continued.

C_A

0145

α, deg

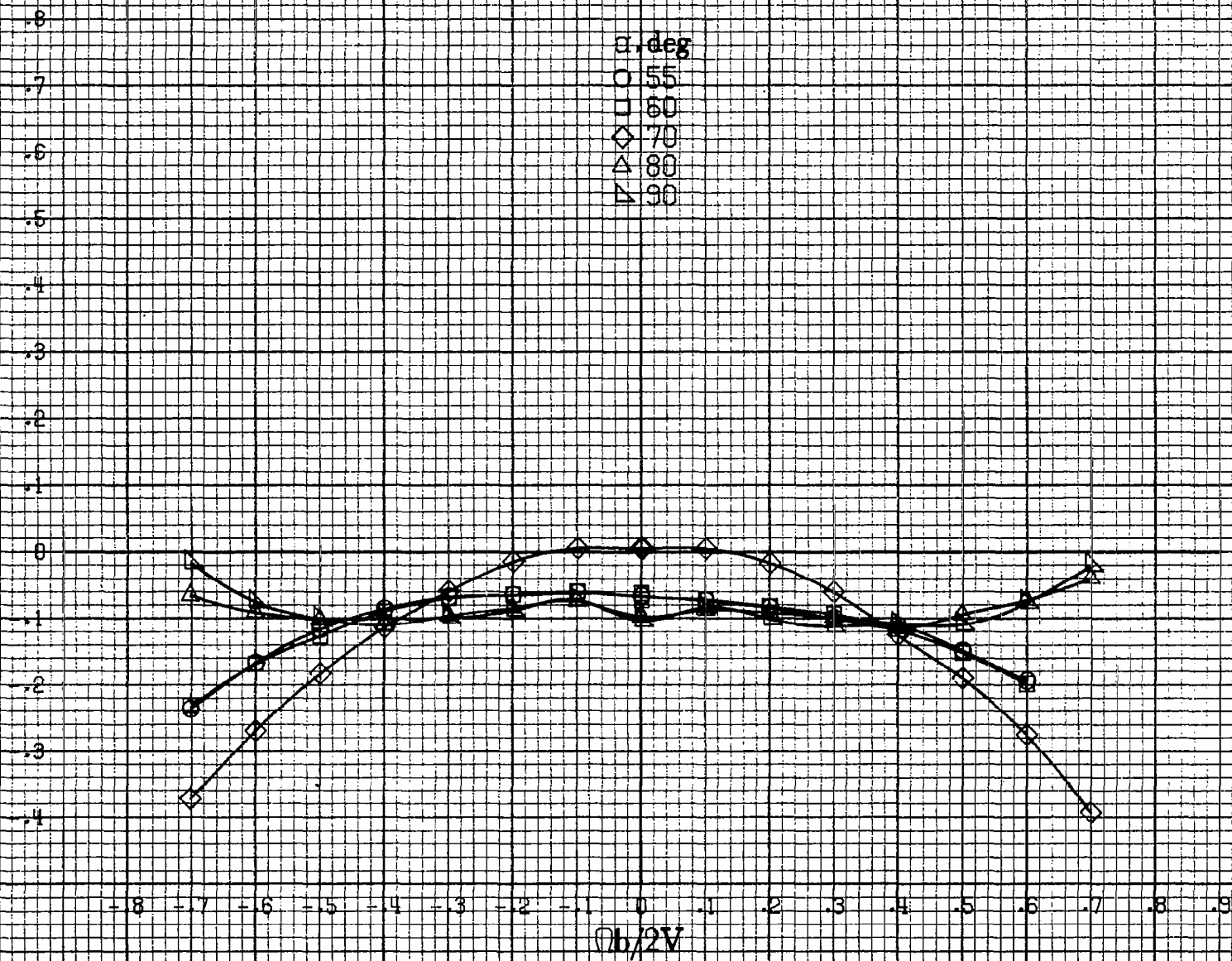
○ 55

□ 60

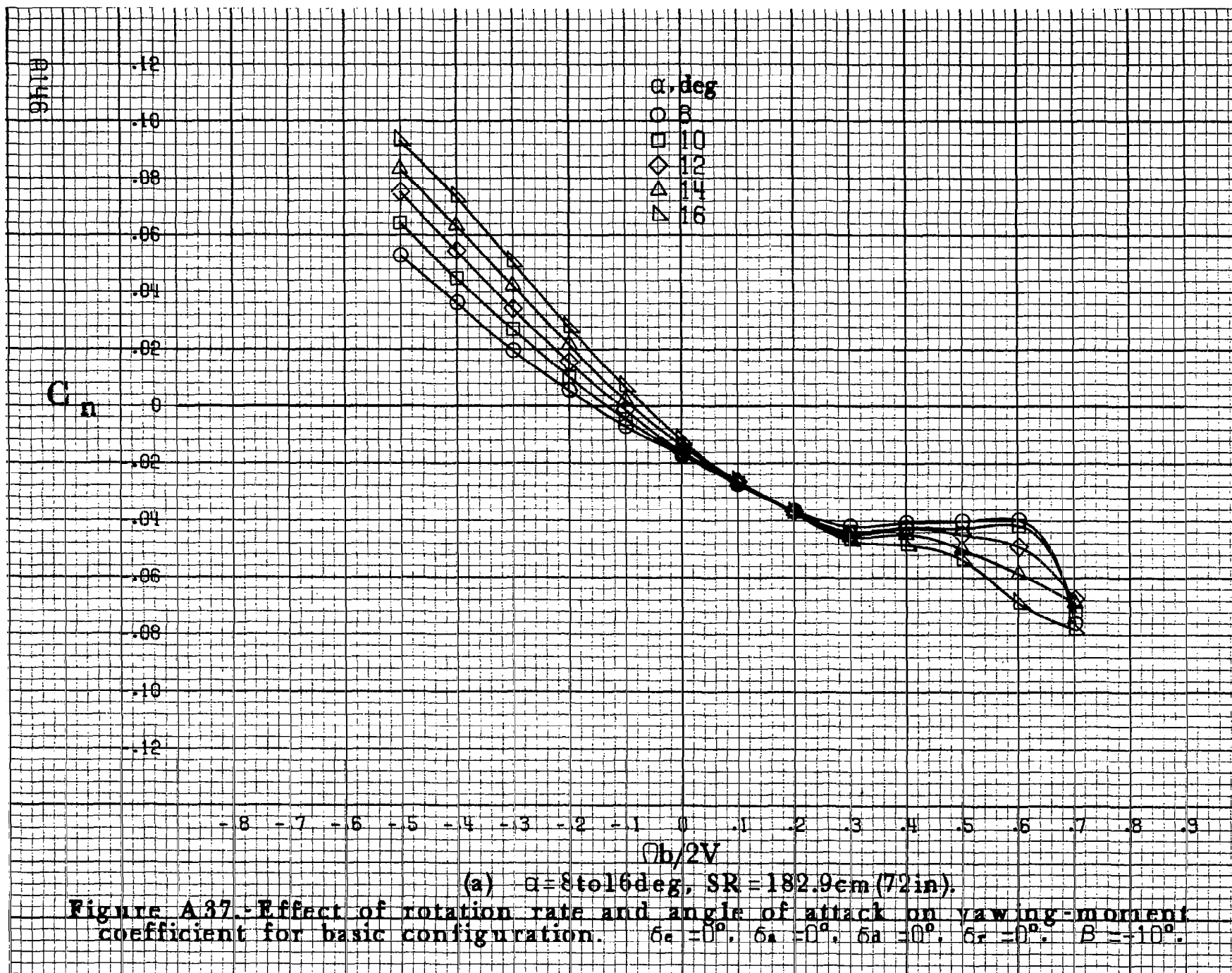
◇ 70

△ 80

▽ 90

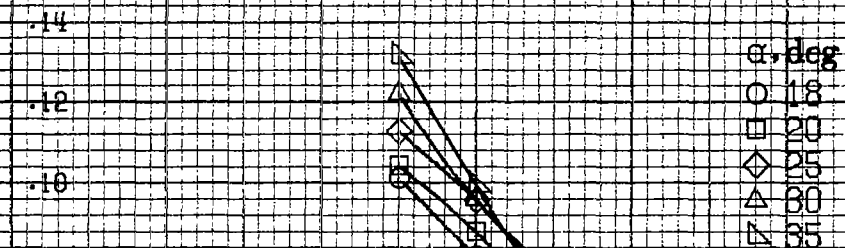


(d) $\alpha = 55$ to 90° , $SR = 0$.
Figure A86.-Concluded.



C_n

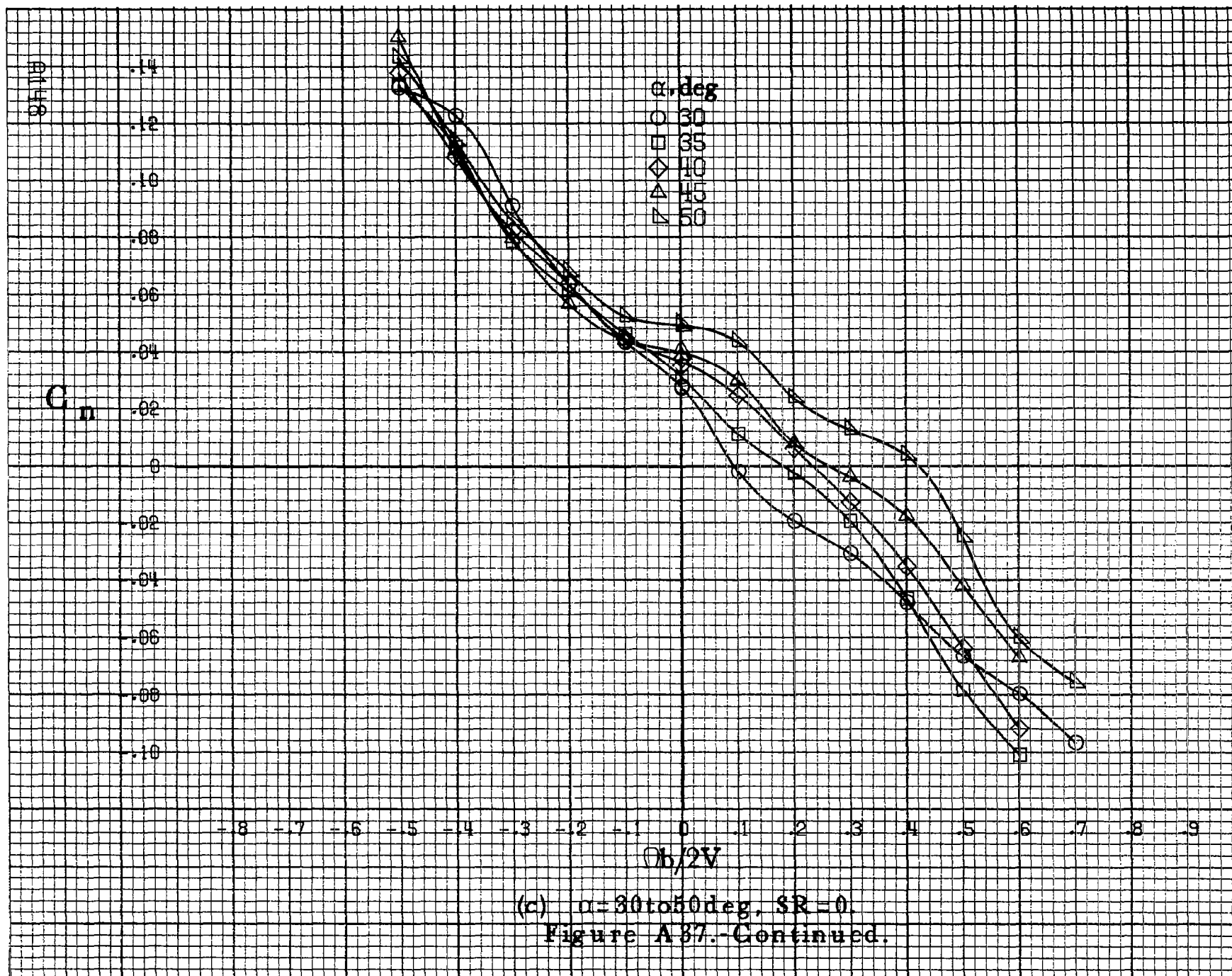
01147



-0.8 -0.7 -0.6 -0.5 -0.4 -0.3 -0.2 -0.1 0 0.1 0.2 0.3 0.4 0.5 0.6 0.7 0.8 0.9

$Oh/2V$

(b) $\alpha = 18 \text{ to } 35 \text{ deg}$, $SR = 182.9 \text{ cm (72 in)}$.
Figure A 37. Continued.



C_n

α, deg

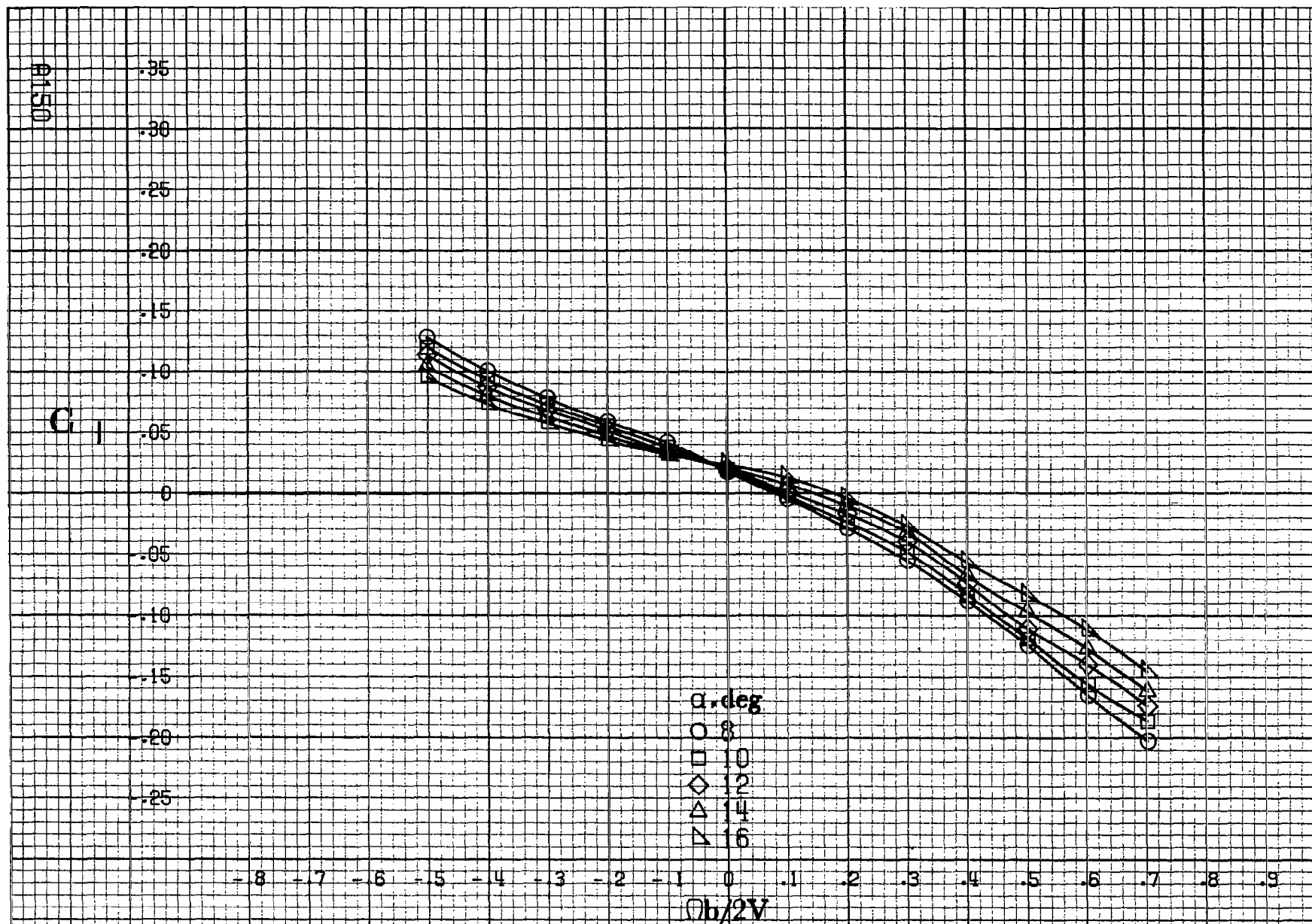
- 55
- 60
- ◇ 70
- △ 80
- ▽ 90

-0.8 -0.7 -0.6 -0.5 -0.4 -0.3 -0.2 -0.1 0 0.1 0.2 0.3 0.4 0.5 0.6 0.7 0.8 0.9

$Ob/2V$

(d) $\alpha=55\text{ to }90\text{ deg, }SR=0.$
Figure A37.-Concluded.

0149



(a) $\alpha = 8$ to 16 deg, $SR = 182.9$ cm (72 in).

Figure A38.-Effect of rotation rate and angle of attack on rolling-moment coefficient for basic configuration. $\delta_e = 0^\circ$, $\delta_a = 0^\circ$, $\delta_d = 0^\circ$, $\delta_r = 0^\circ$, $B = -10^\circ$.

C₁

.14
.12
.10
.08
.06
.04
0
-.02
-.04
-.06
-.08
-.10

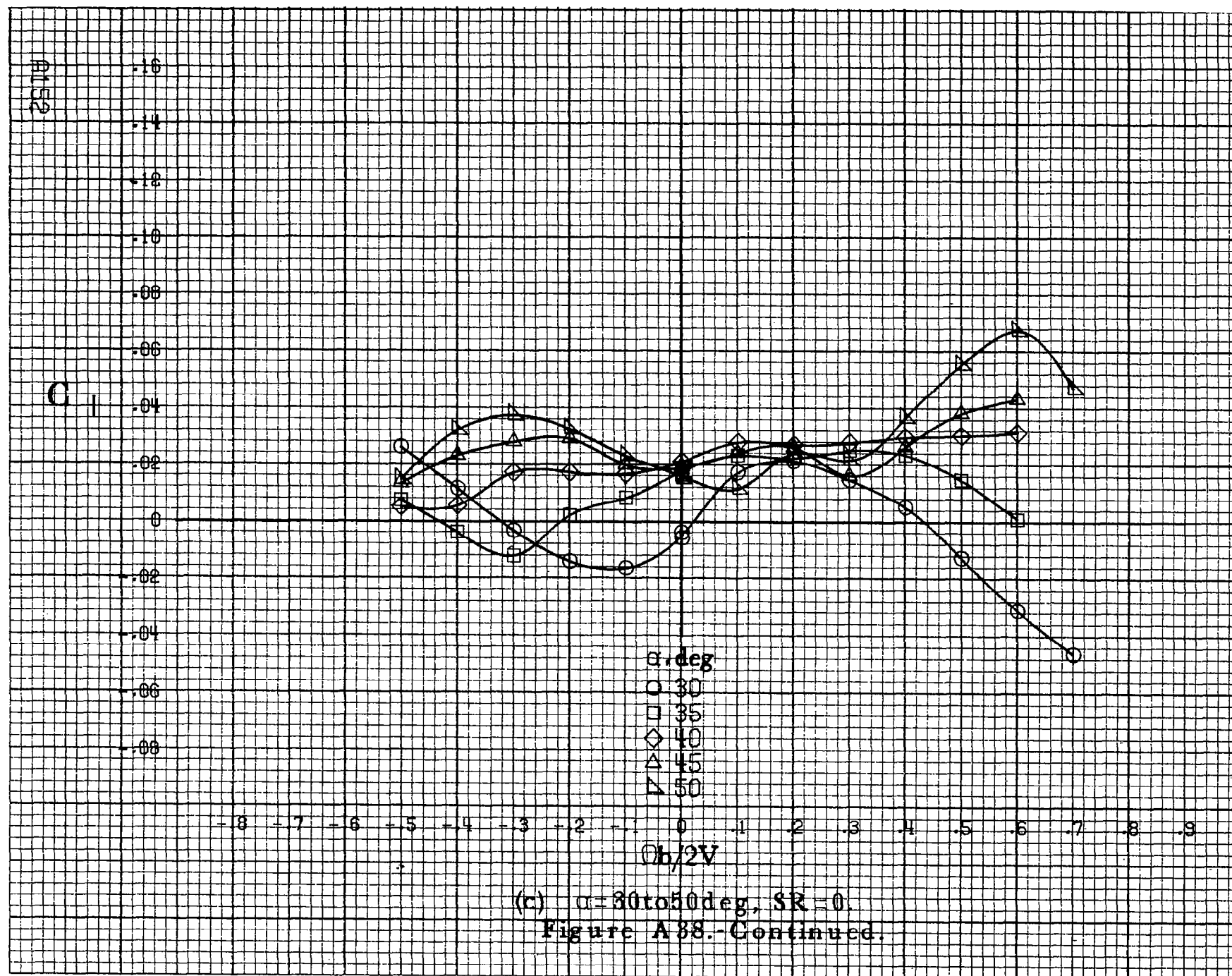
α , deg
○ 18
□ 20
◇ 25
△ 30
▽ 35

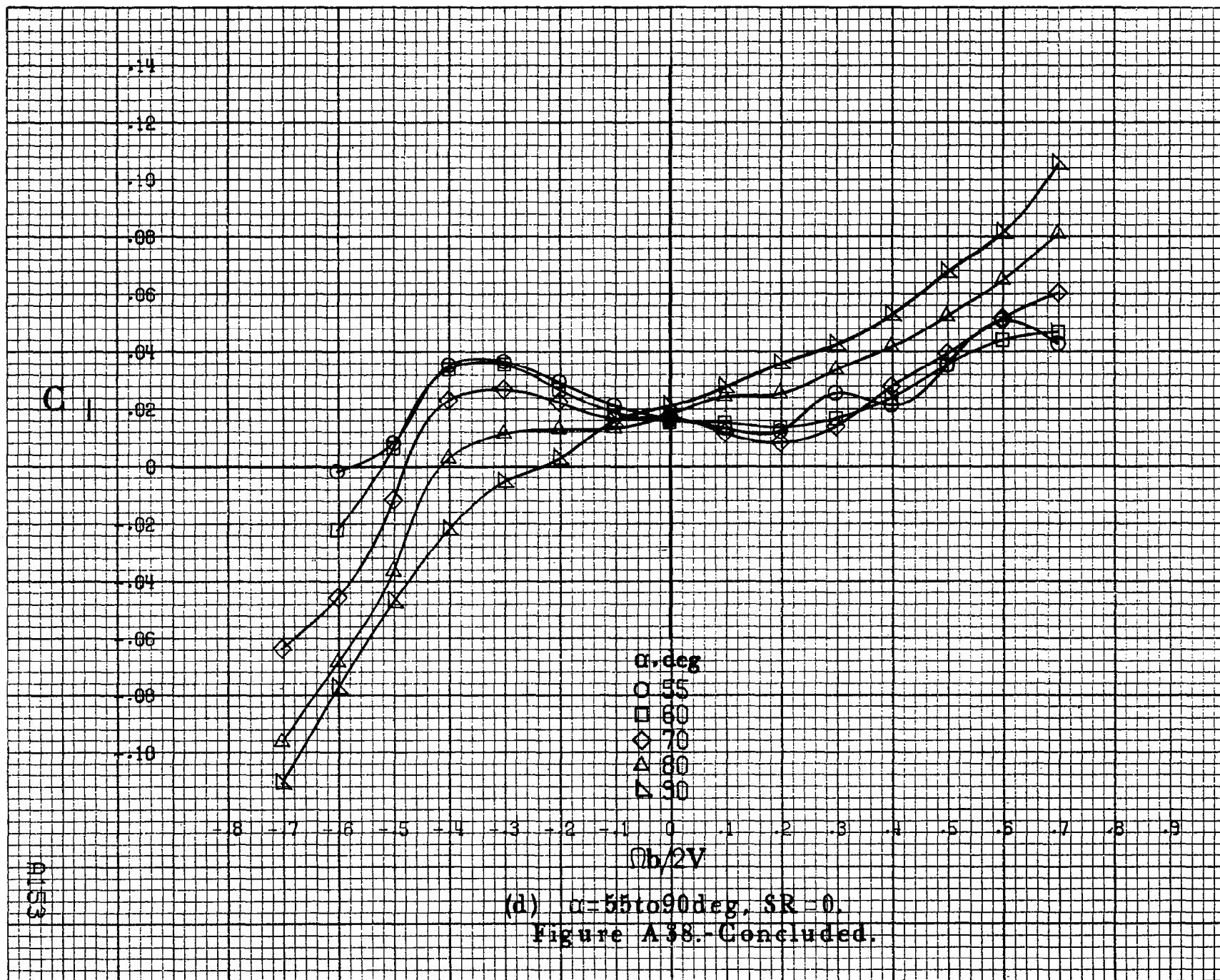
-8 -7 -6 -5 -4 -3 -2 -1 0 .1 .2 .3 .4 .5 .6 .7 .8 .9
 $Qh/2V$

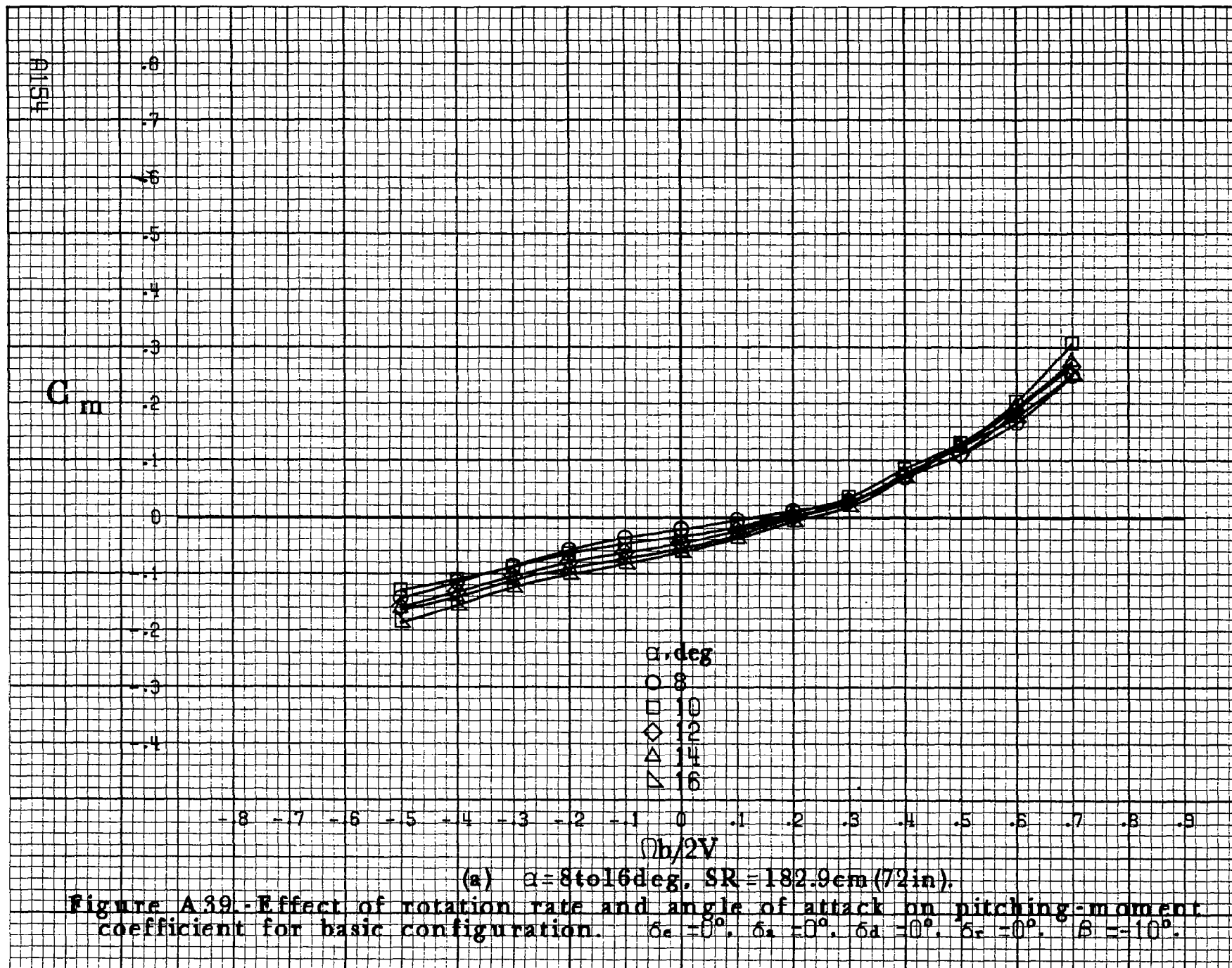
(b) $\alpha = 18$ to 35 deg, $SR = 182.9$ cm (72 in).

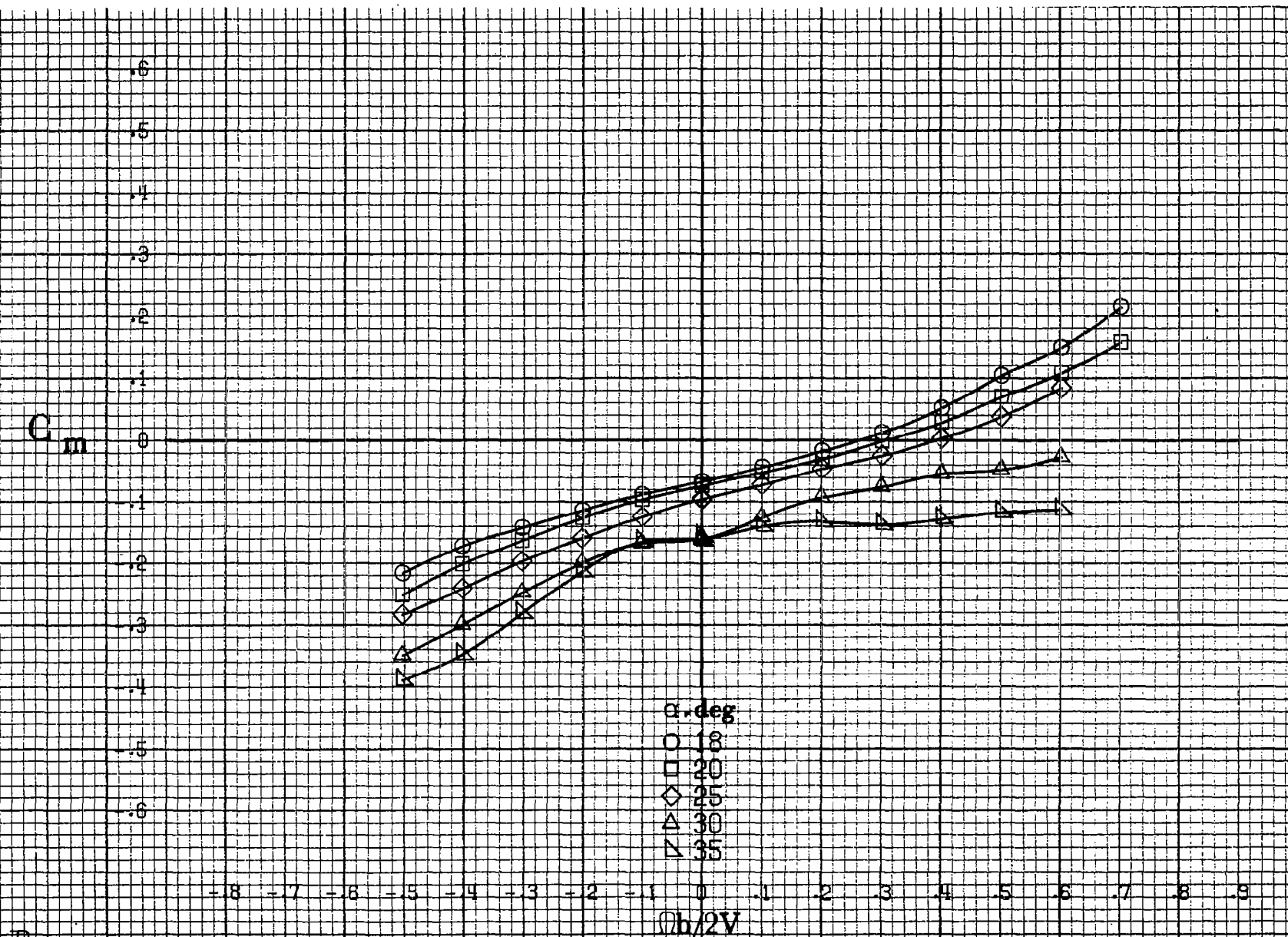
Figure A38.-Continued.

1151



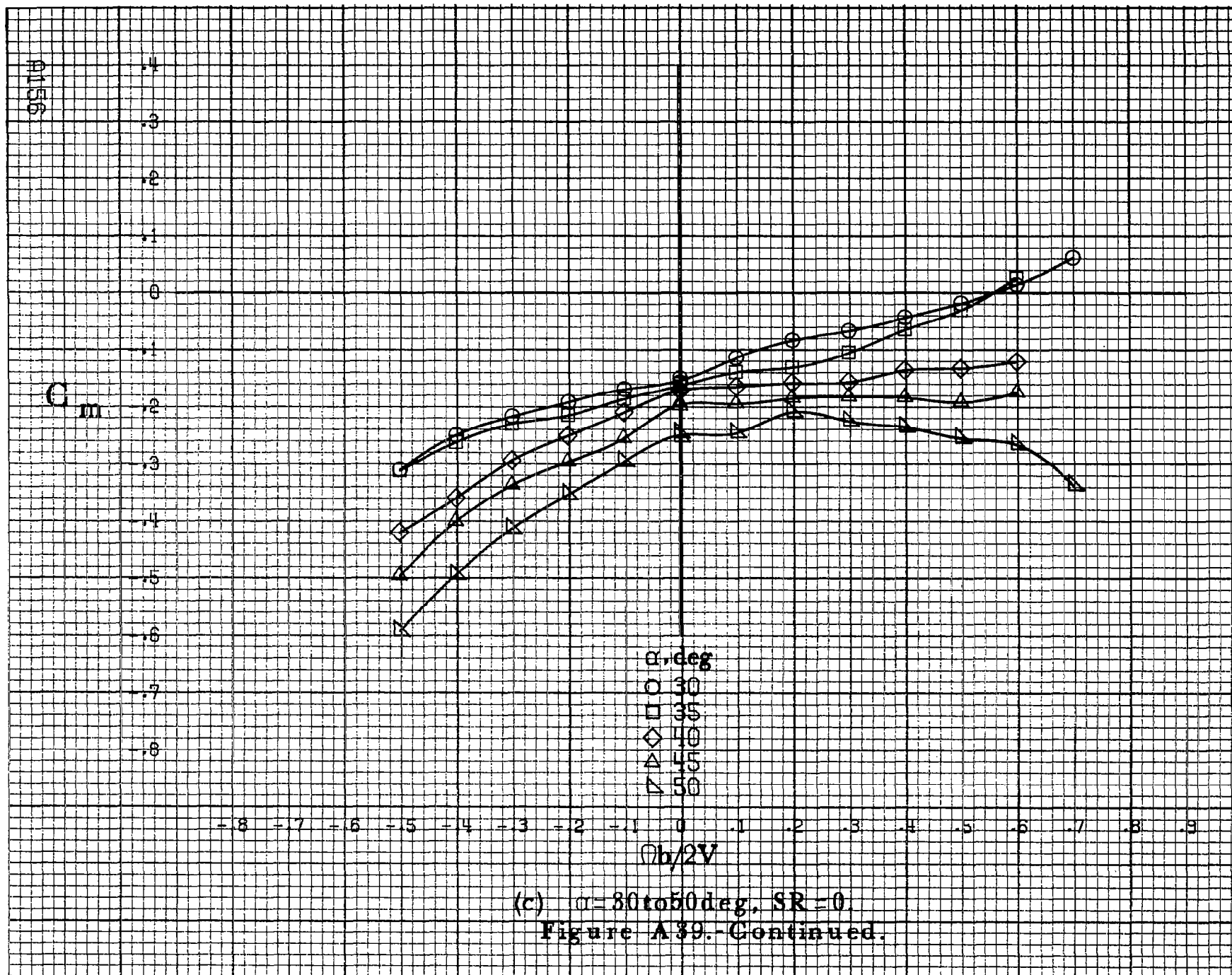






(b) $\alpha = 18$ to 35° , $SR = 182.9\text{cm (72in.)}$.
Figure A39.-Continued.

91555



C_m

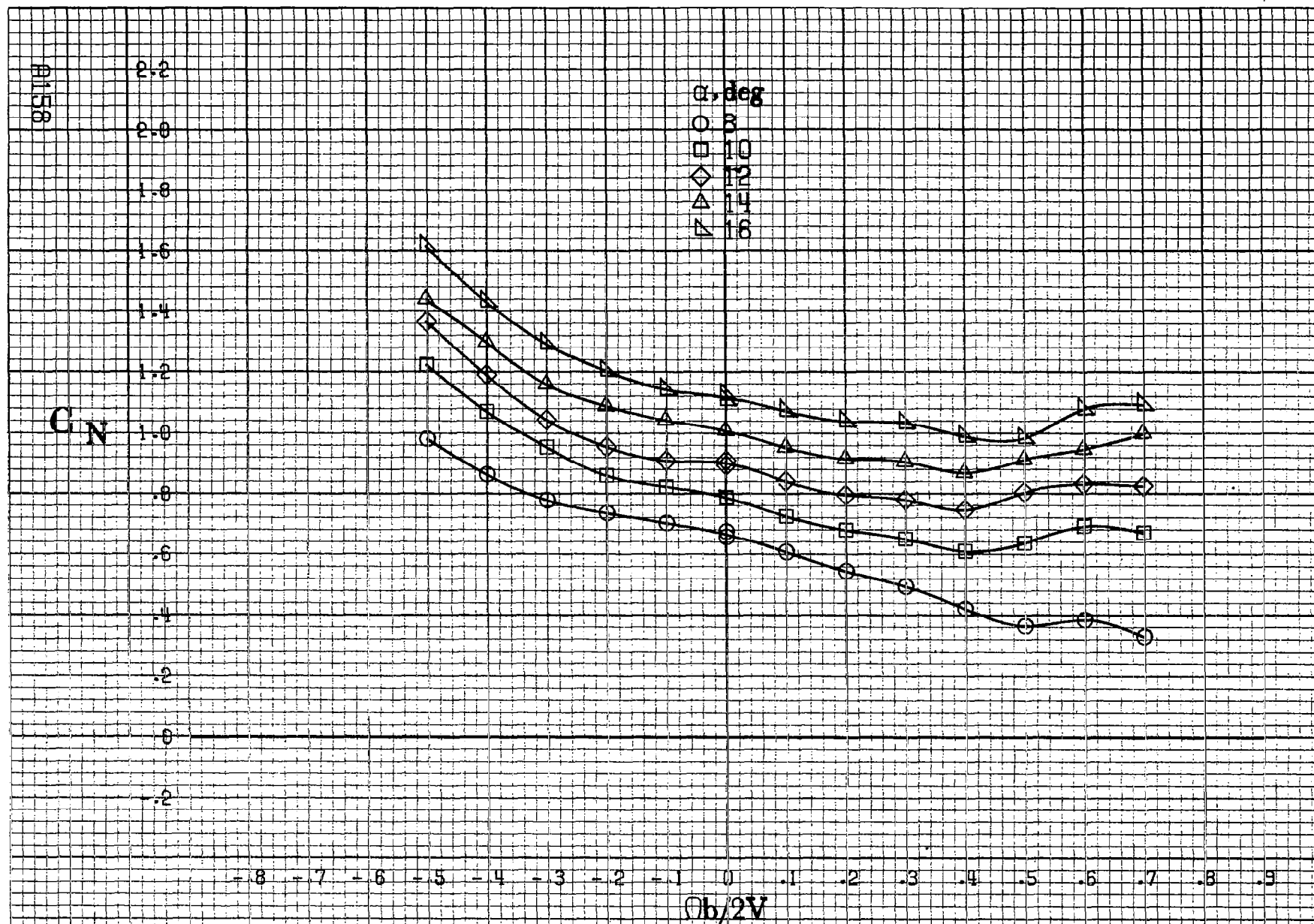
.1
0
.1
.2
.3
.4
.5
.6
.7
.8
.9
1.0
1.1

α, deg
○ 55
□ 60
◇ 70
△ 80
▽ 90

-0.8 -0.7 -0.6 -0.5 -0.4 -0.3 -0.2 -0.1 0 0.1 0.2 0.3 0.4 0.5 0.6 0.7 0.8 0.9
 $Ob/2V$

AI 57

(d) $\alpha=55$ to 90 deg. $SR=0$.
Figure A39.-Concluded.



(a) $\alpha = 8 \text{ to } 16 \text{ deg}$, $SR = 182.9 \text{ cm (72 in)}$.

Figure A 40.-Effect of rotation rate and angle of attack on normal-force coefficient for basic configuration. $\delta_a = 0^\circ$, $\delta_s = 0^\circ$, $\delta_a = 0^\circ$, $\delta_s = 0^\circ$, $\beta = -10^\circ$.

C_N

α, deg
 ○ 18
 □ 20
 ◇ 25
 △ 30
 ▽ 35

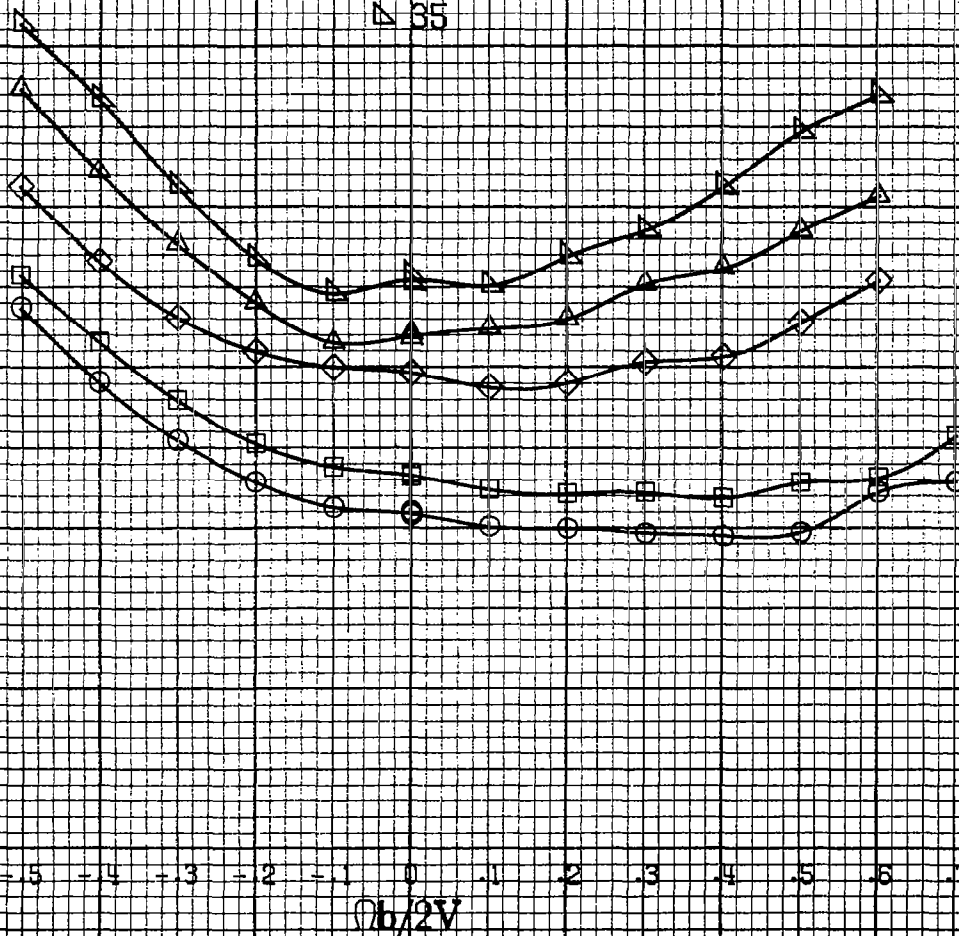
3.0
2.8
2.6
2.4
2.2
2.0
1.8
1.6
1.4
1.2
1.0
.8
.6

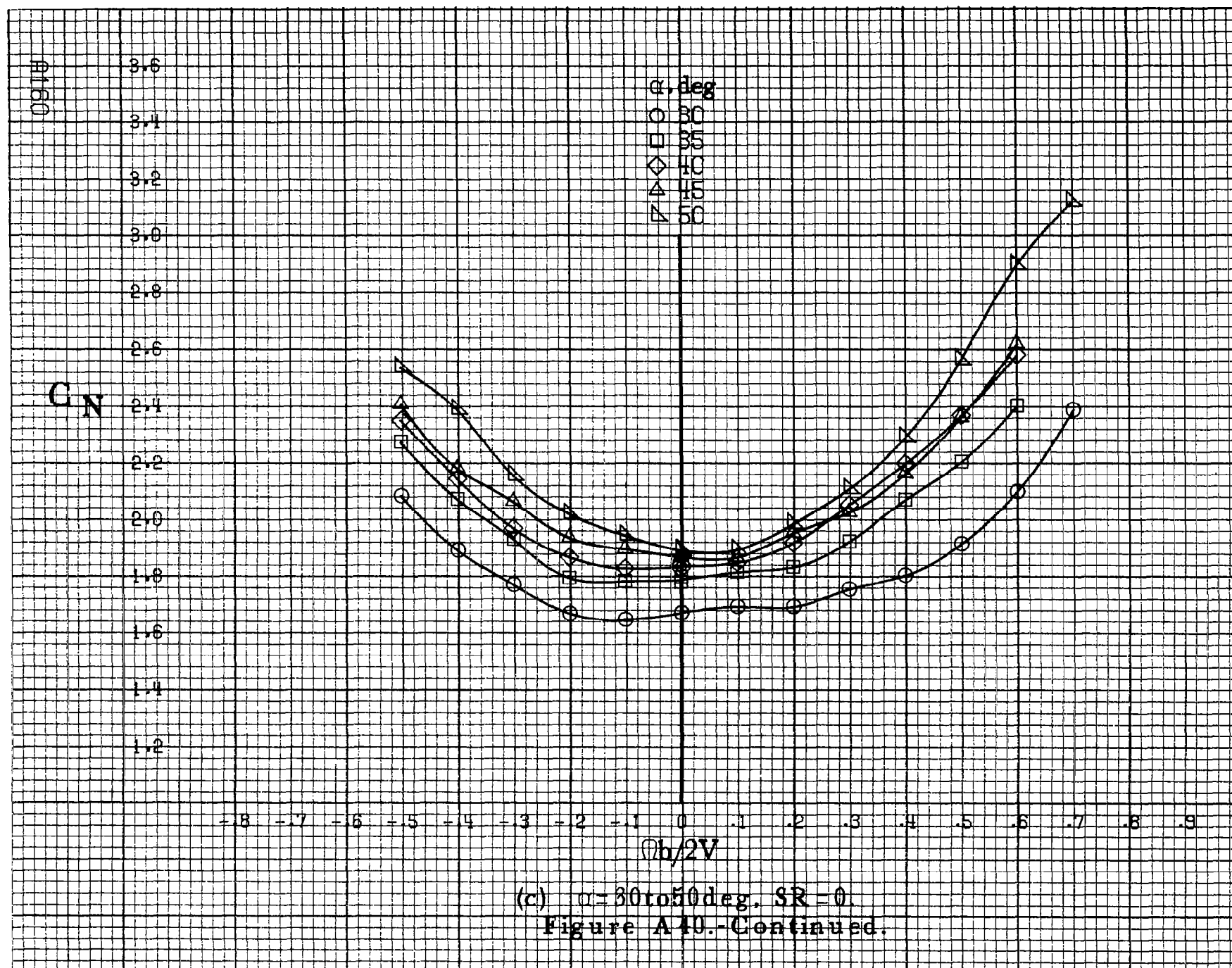
- .8 - .7 - .6 - .5 - .4 - .3 - .2 - .1 0 .1 .2 .3 .4 .5 .6 .7 .8 .9

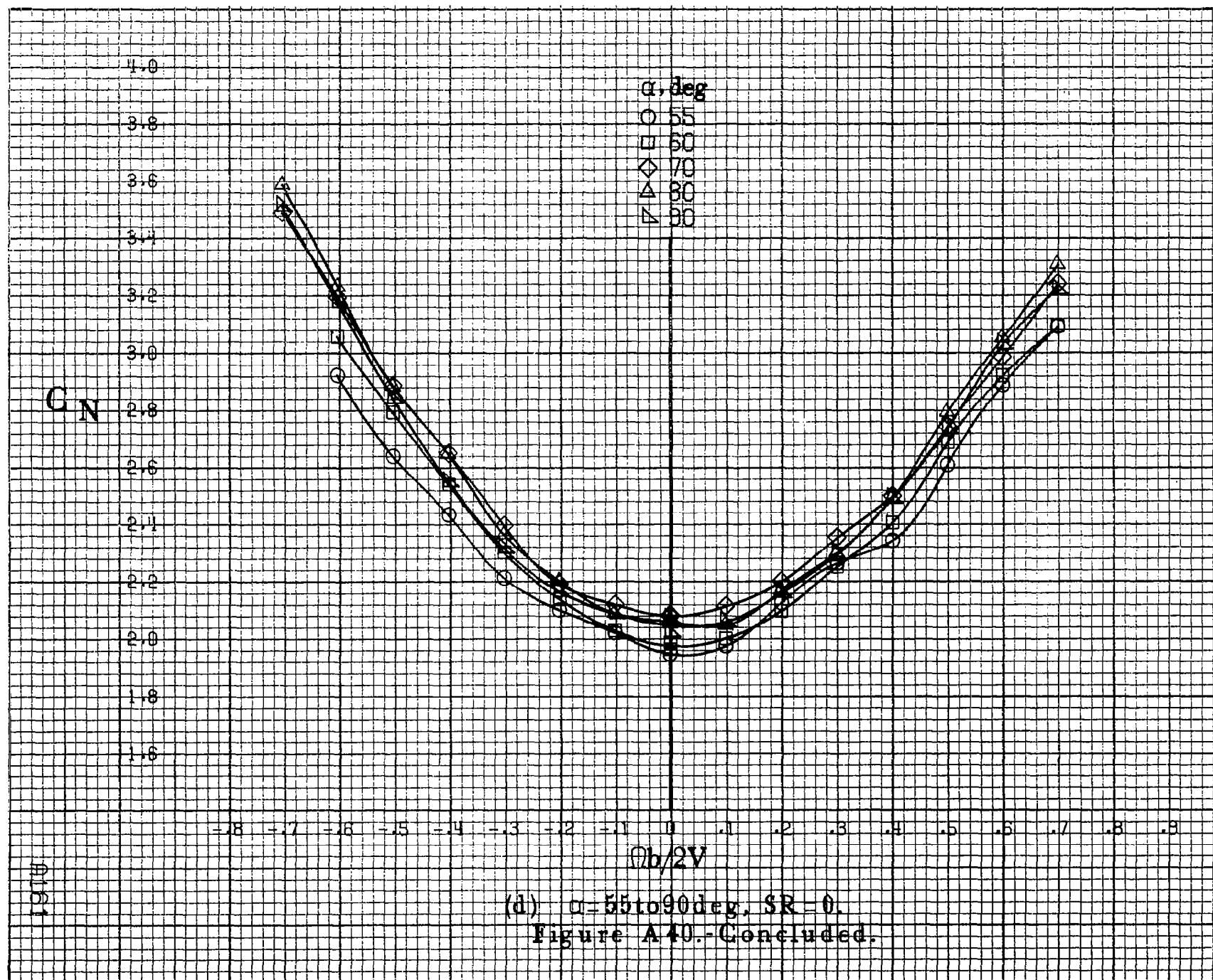
$Ob/2V$

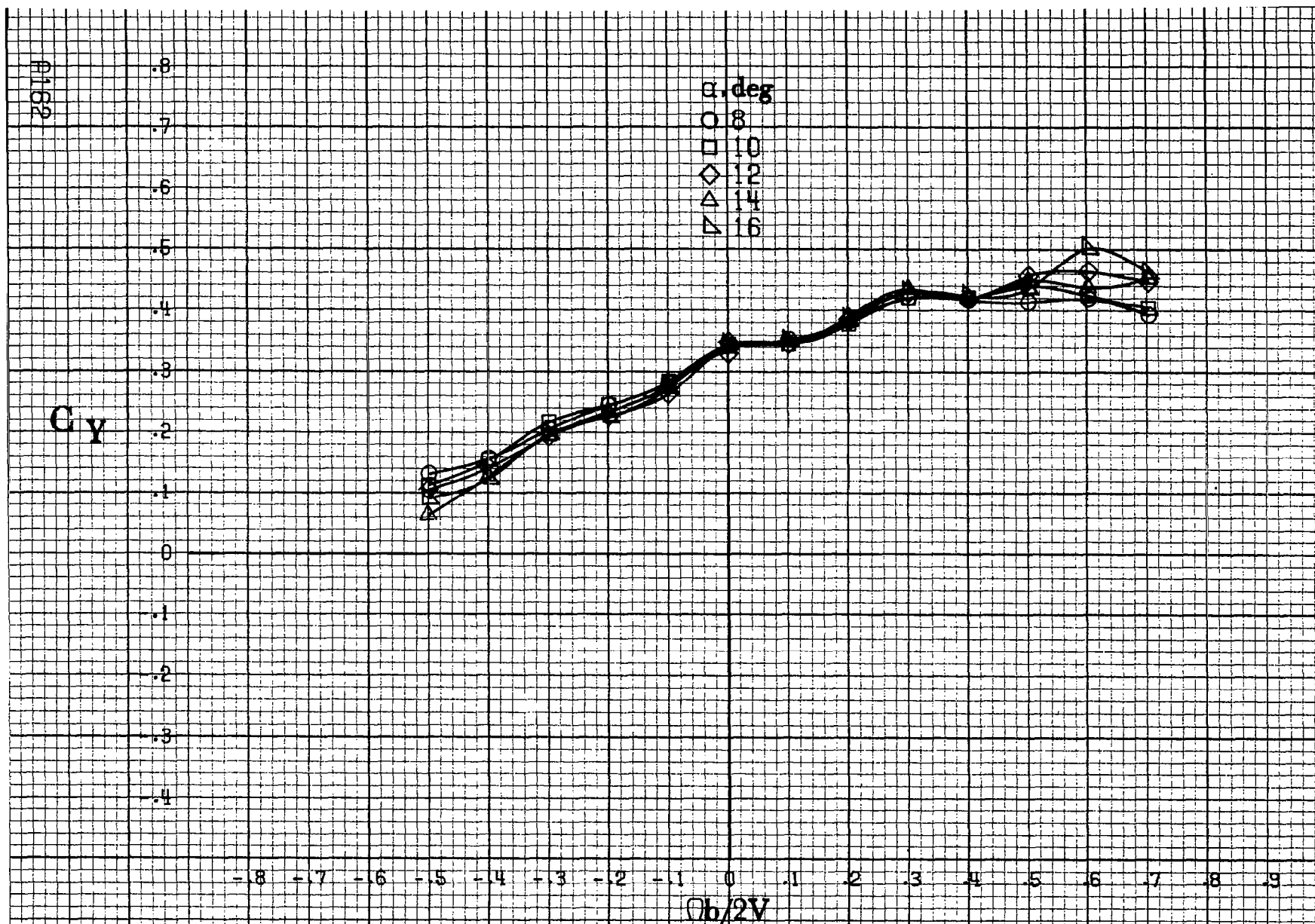
A1591

(b) $\alpha = 18 \text{ to } 35 \text{ deg}$, $SR = 182.9 \text{ cm (72 in)}$.
 Figure A40.-Continued.









(a) $\alpha = 8$ to 16° , $SR = 182.9 \text{ cm (72 in.)}$.

Figure A41.- Effect of rotation rate and angle of attack on side-force coefficient for basic configuration. $\delta_e = 0^\circ$, $\delta_a = 0^\circ$, $\delta_d = 0^\circ$, $\delta_r = 0^\circ$, $\beta = -10^\circ$.

C_{xy}

α, deg

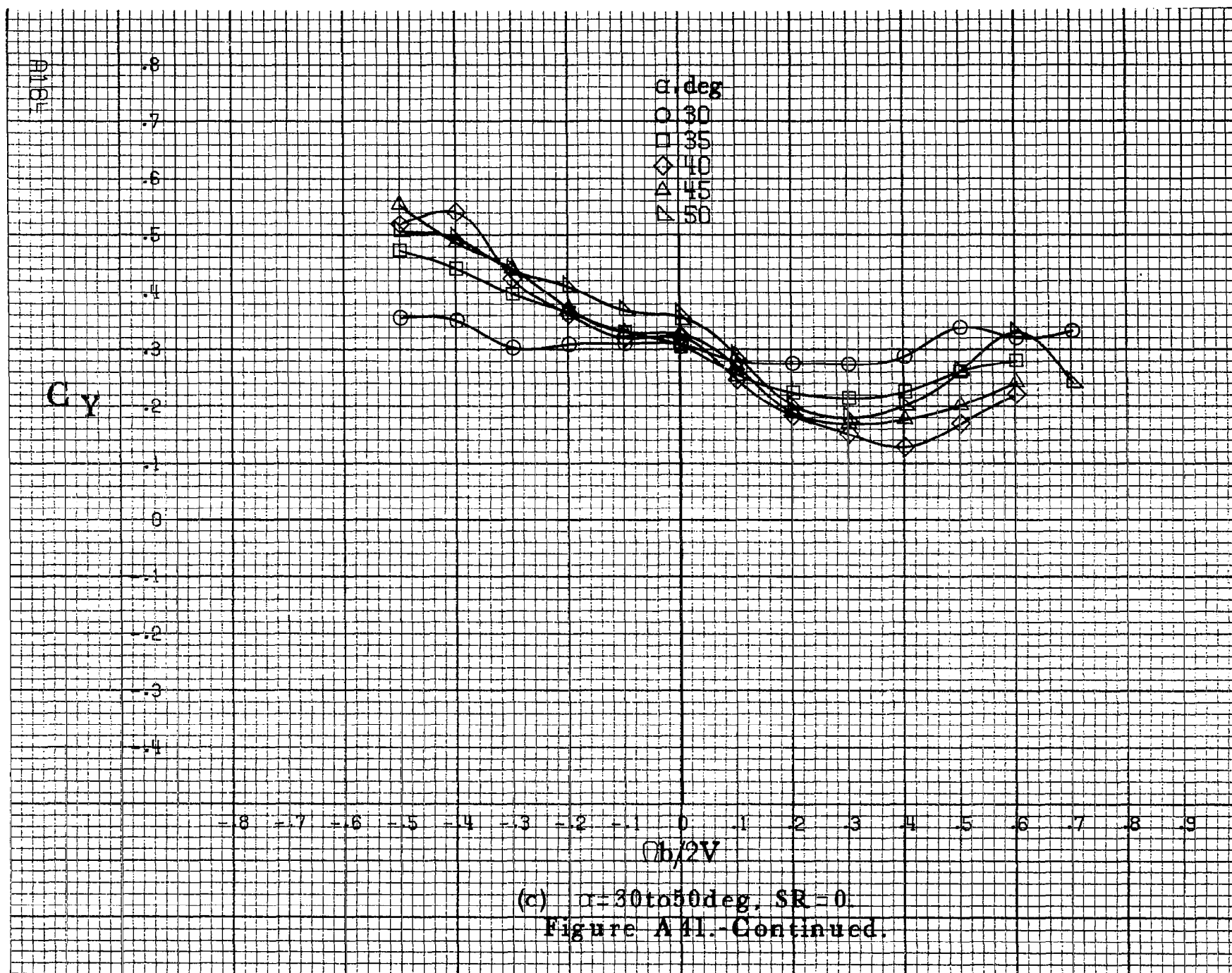
- 18
- 20
- ◇ 25
- △ 30
- ▽ 35

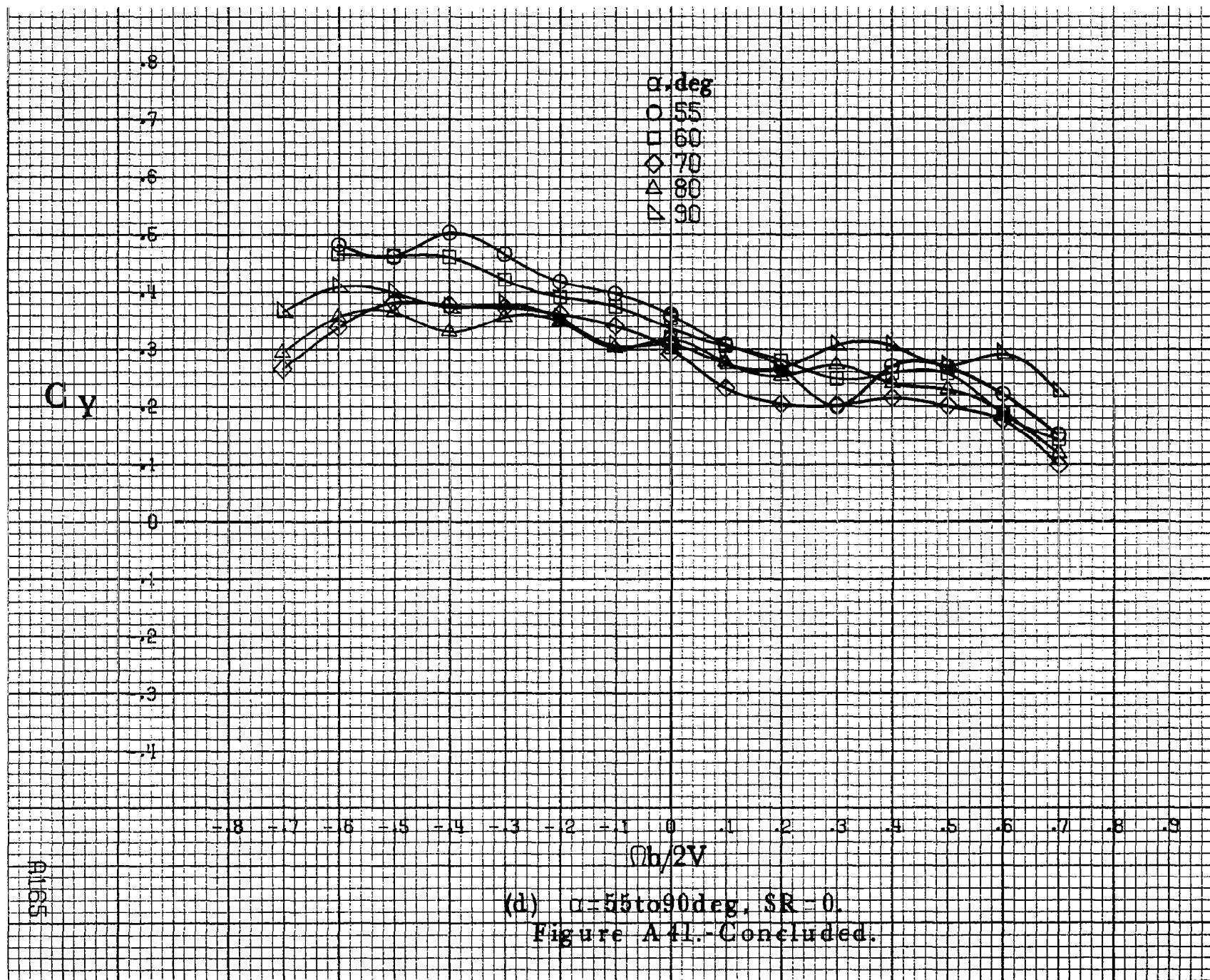
- .8 - .7 - .6 - .5 - .4 - .3 - .2 - .1 - 0 - .1 - .2 - .3 - .4

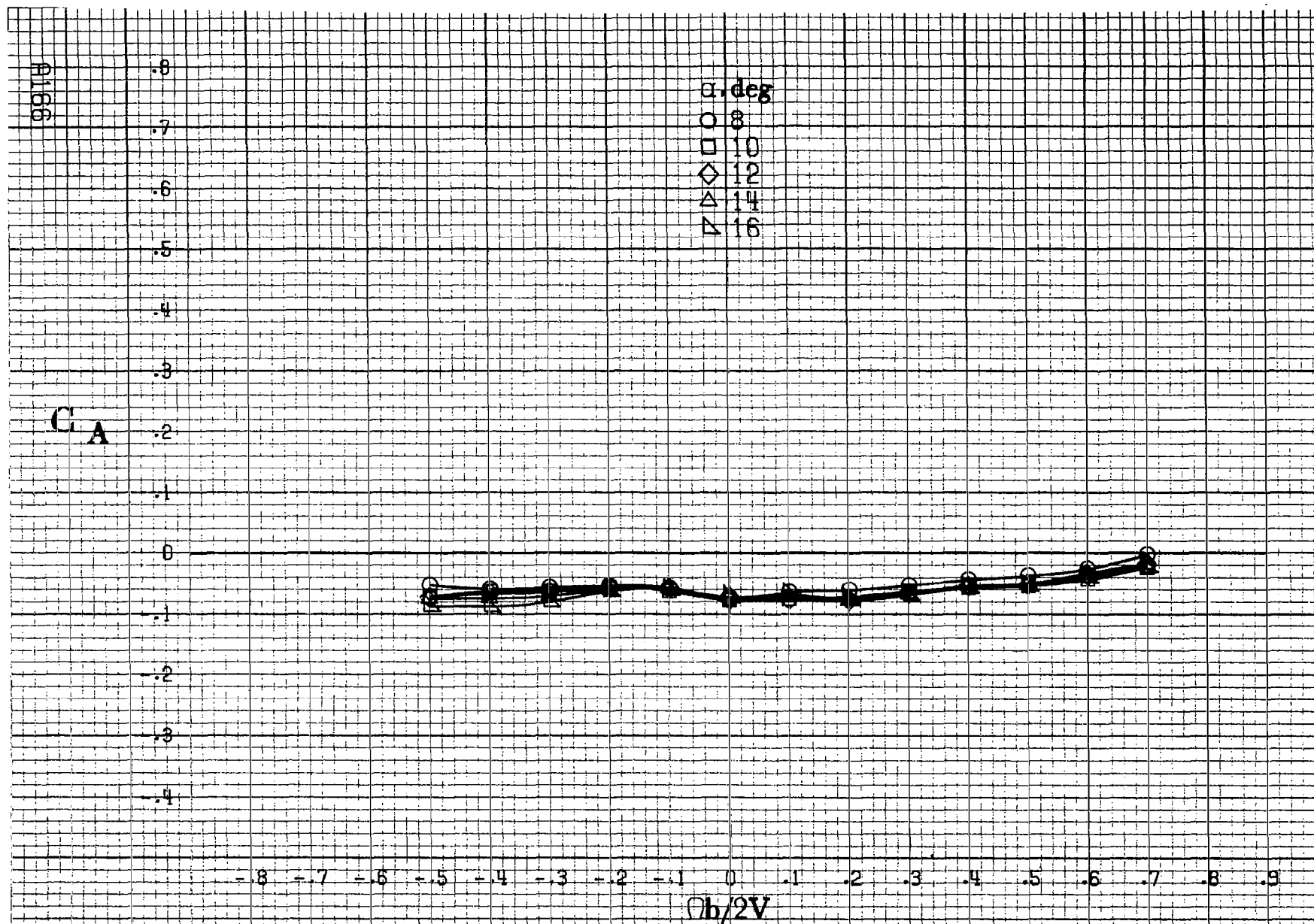
$b/2V$

A163

(b) $\alpha = 18$ to 35 deg, $SR = 182.9 \text{ cm (72 in.)}$.
Figure A41.-Continued.







(a) $\alpha = 8 \text{ to } 16 \text{ deg}$, $SR = 182.9 \text{ cm (72 in)}$.

Figure A42.-Effect of rotation rate and angle of attack on axial force coefficient for basic configuration. $\delta_e = 0^\circ$, $\delta_a = 0^\circ$, $\delta_d = 0^\circ$, $\delta_r = 0^\circ$, $\beta = -10^\circ$.

C_A

α , deg
 ○ 18
 □ 20
 ◇ 25
 △ 30
 ▴ 35

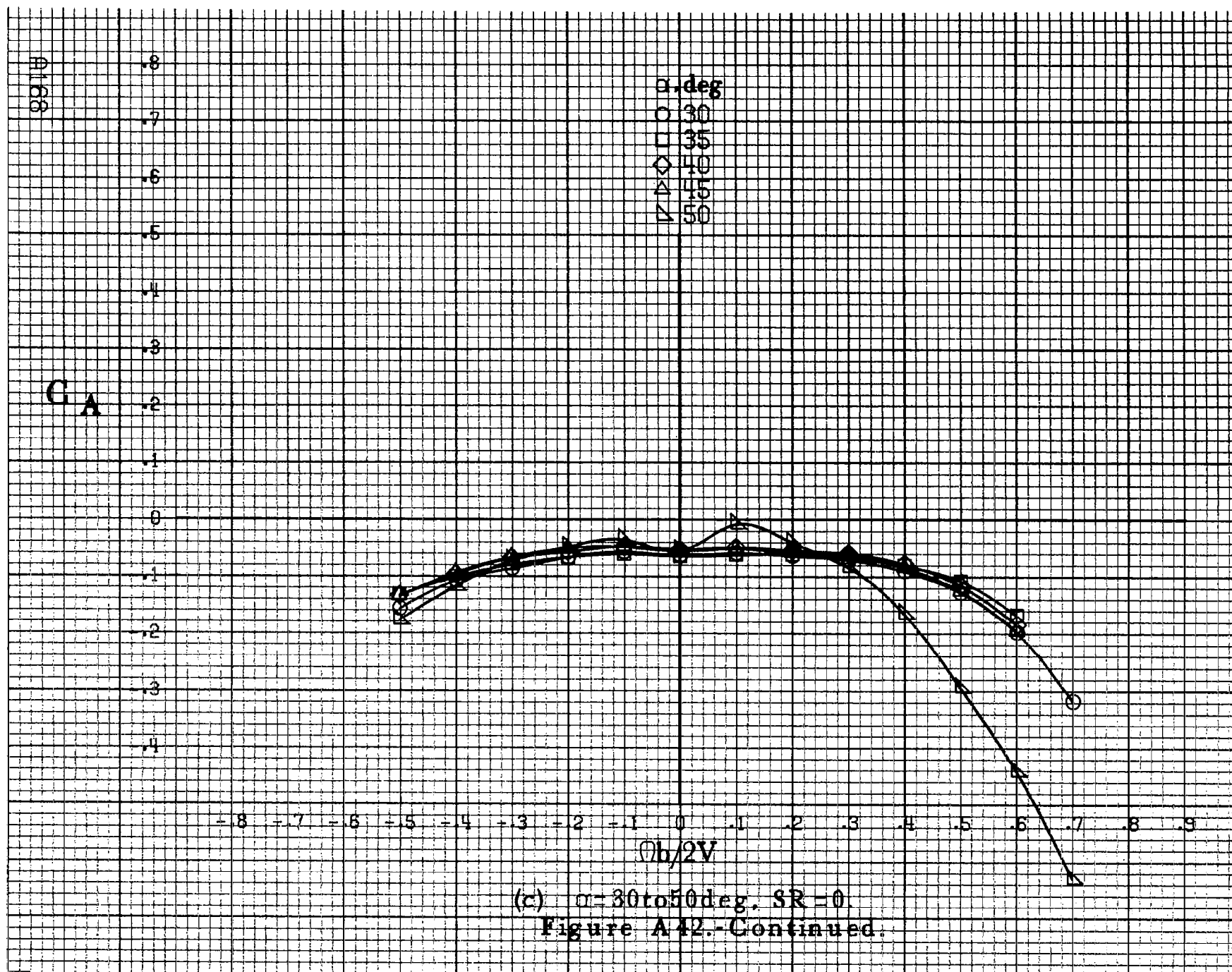
.8
.7
.6
.5
.4
.3
.2
.1
0
.1
.2
.3
.4

-18 -17 -16 -15 -14 -13 -12 -11 -10 -9 -8 -7 -6 -5 -4 -3 -2 -1 0 1 2 3 4 5 6 7 8 9

$b/2V$

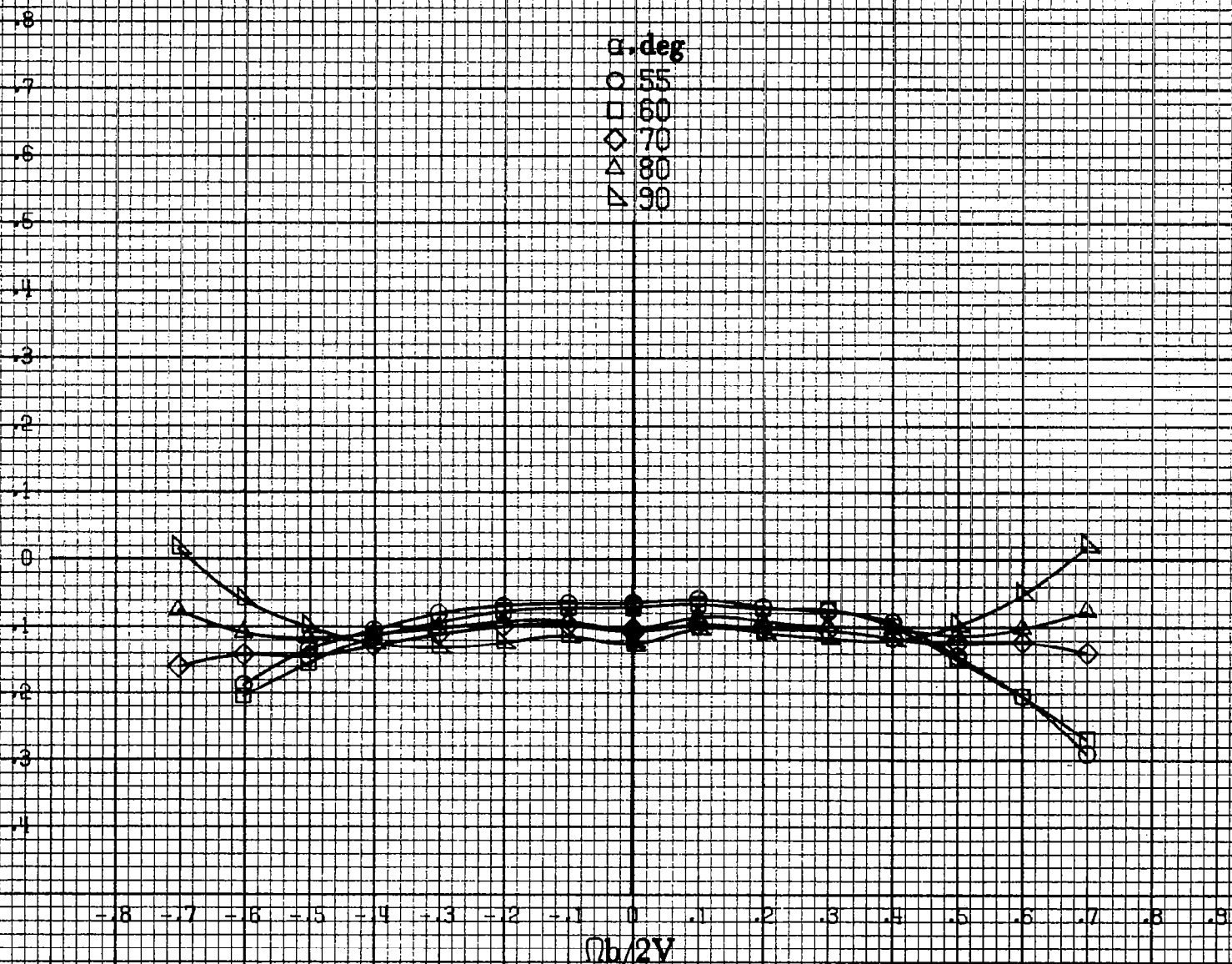
(b) $\alpha = 18$ to 35 deg, $SR = 182.9$ cm (72 in).
 Figure A42.-Continued.

A167

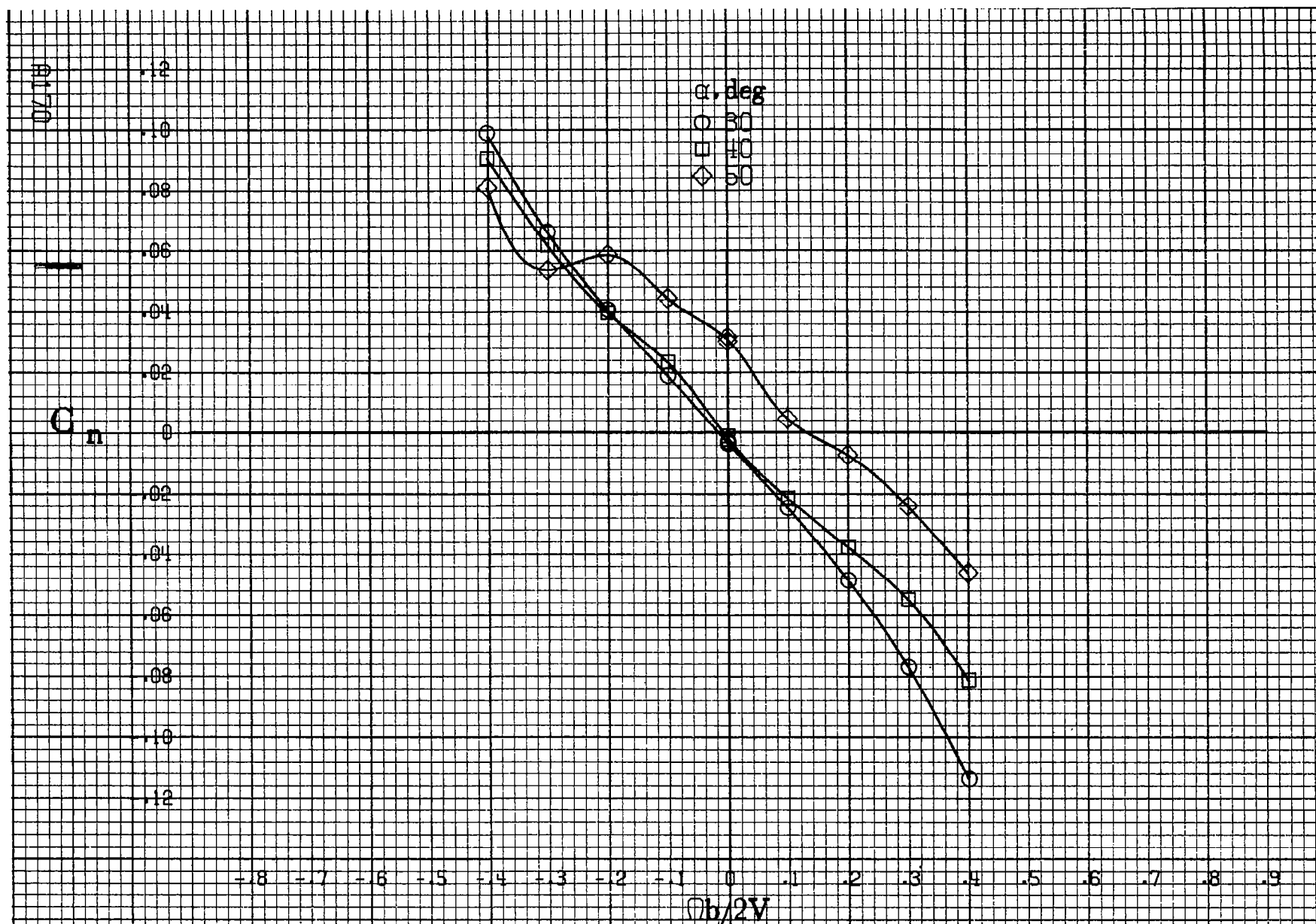


C_A

α, deg
 ○ 55
 □ 60
 ◇ 70
 △ 80
 ▴ 90



(d) $\alpha = 55$ to 90° , $SR = 0$.
 Figure A42.-Concluded.



(a) $\alpha = 30$ to 50 deg, $SR = 0$.

Figure A43.- Effect of rotation rate and angle of attack on yawing-moment coefficient for basic configuration. $\delta_e = -25^\circ$, $\delta_a = 0^\circ$, $\delta_d = 0^\circ$, $\delta_r = 0^\circ$, $\beta = 0^\circ$.

C_n

α, deg

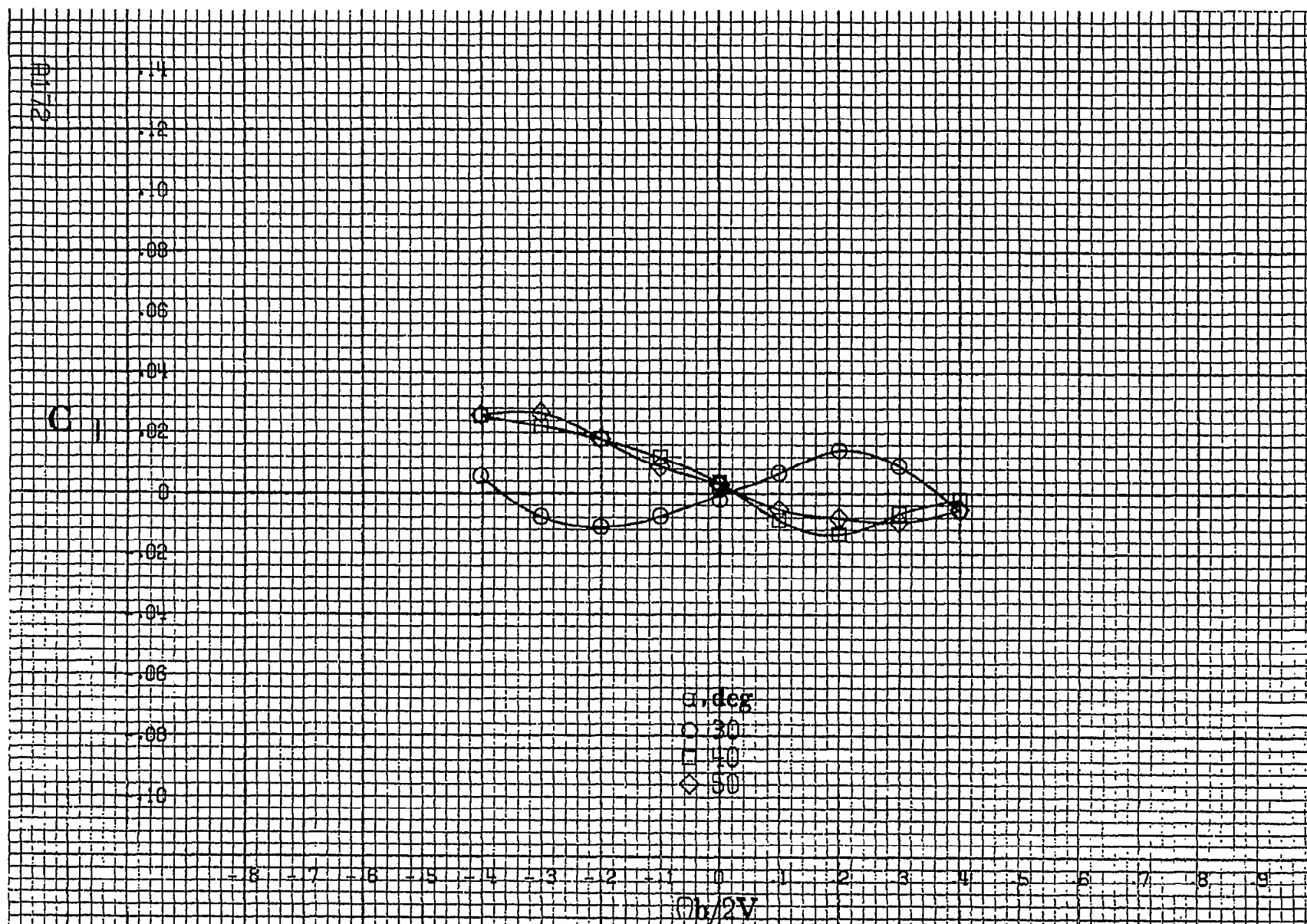
- 55
- 60
- ◇ 70
- △ 80
- ▽ 90

-0.8 -0.7 -0.6 -0.5 -0.4 -0.3 -0.2 -0.1 0 0.1 0.2 0.3 0.4 0.5 0.6 0.7 0.8 0.9

$Ob/2V$

(b) $\alpha=55$ to 90 deg, $SR=0$.
Figure A 43.-Concluded.

81171



(a) $\alpha = 30$ to 60 deg, $SR = 0$.

Figure A44. Effect of rotation rate and angle of attack on rolling-moment coefficient for basic configuration. $\delta_e = 25^\circ$, $\delta_a = 0^\circ$, $\delta_d = 0^\circ$, $\delta_r = 0^\circ$, $\delta = 0^\circ$.

C₁

.14
.12
.10
.08
.06
.04
0
-.02
-.04
-.06
-.08
-.10

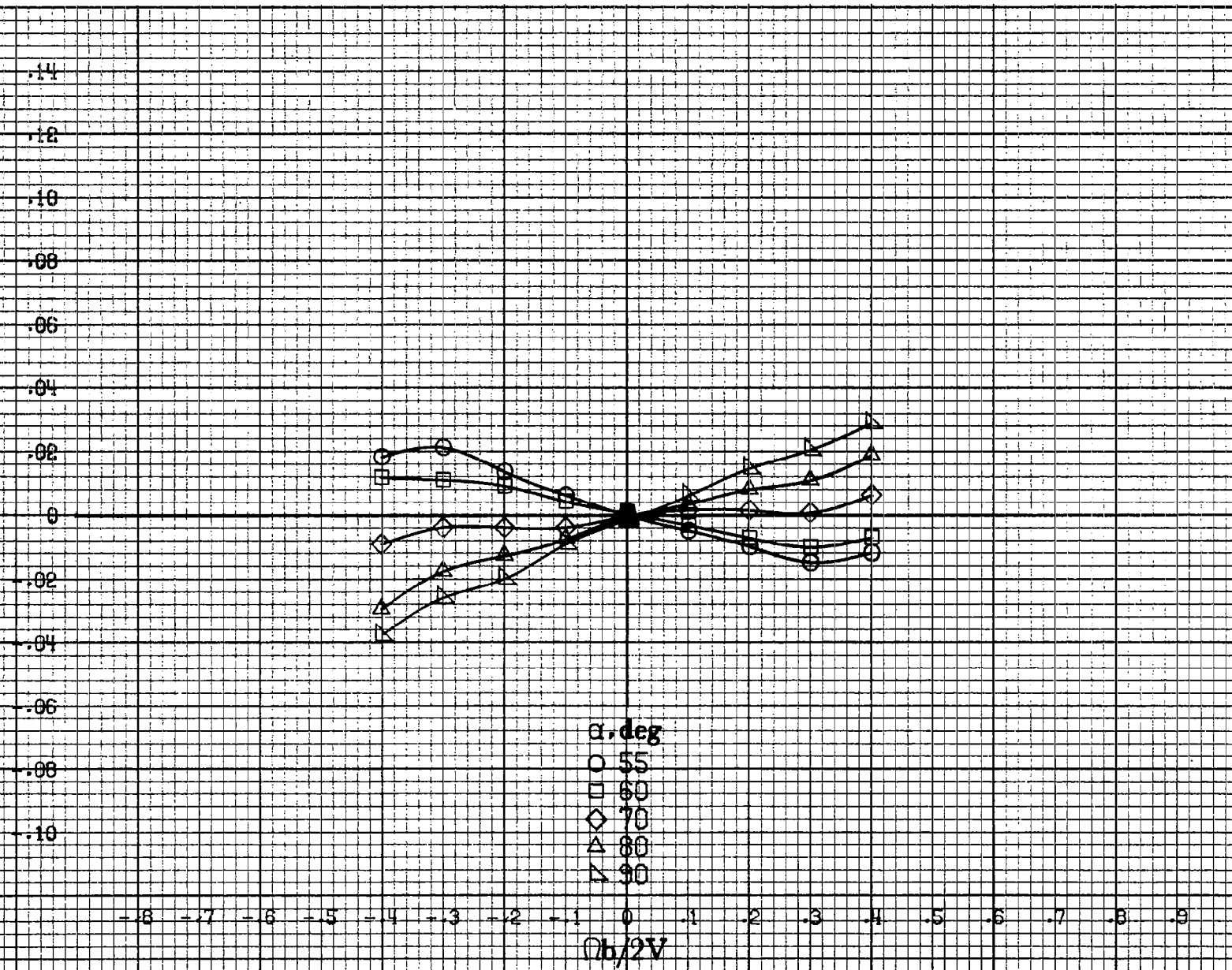
-8 -7 -6 -5 -4 -3 -2 -1 0 -1 -2 -3 -4 -5 -6 -7 -8 -9

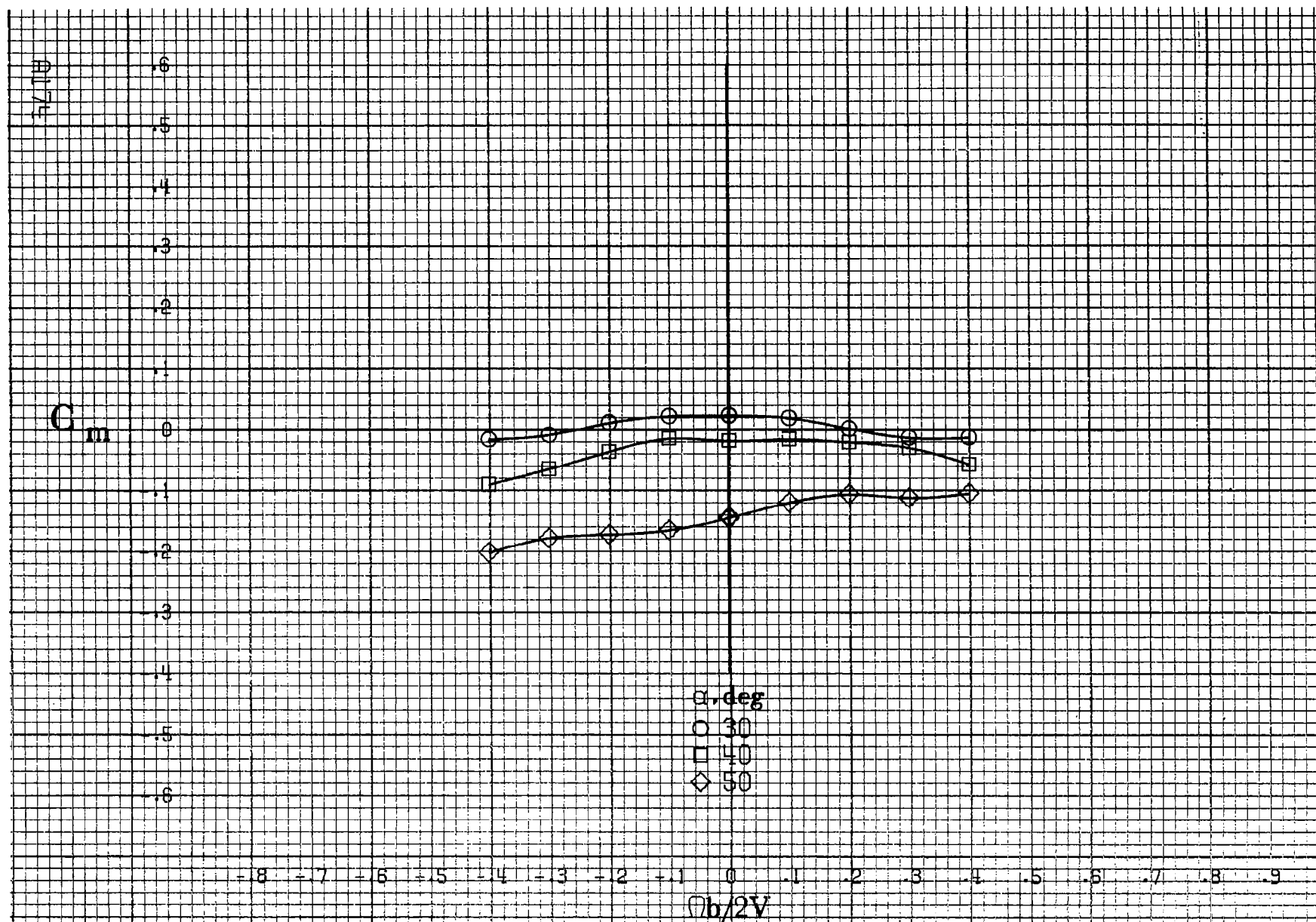
α, deg
○ 55
□ 60
◇ 70
△ 80
▽ 90

$\phi b/2V$

A173

(b) $\alpha=55$ to 90 deg, $SR=0$.
Figure A44.-Concluded.





(a) $\alpha = 30$ to 50° , $SR = 0$.

Figure A45 - Effect of rotation rate and angle of attack on pitching-moment coefficient for basic configuration. $\delta_e = -25^\circ$, $\delta_a = 0^\circ$, $\delta_d = 0^\circ$, $\delta_r = 0^\circ$, $\delta = 0^\circ$.

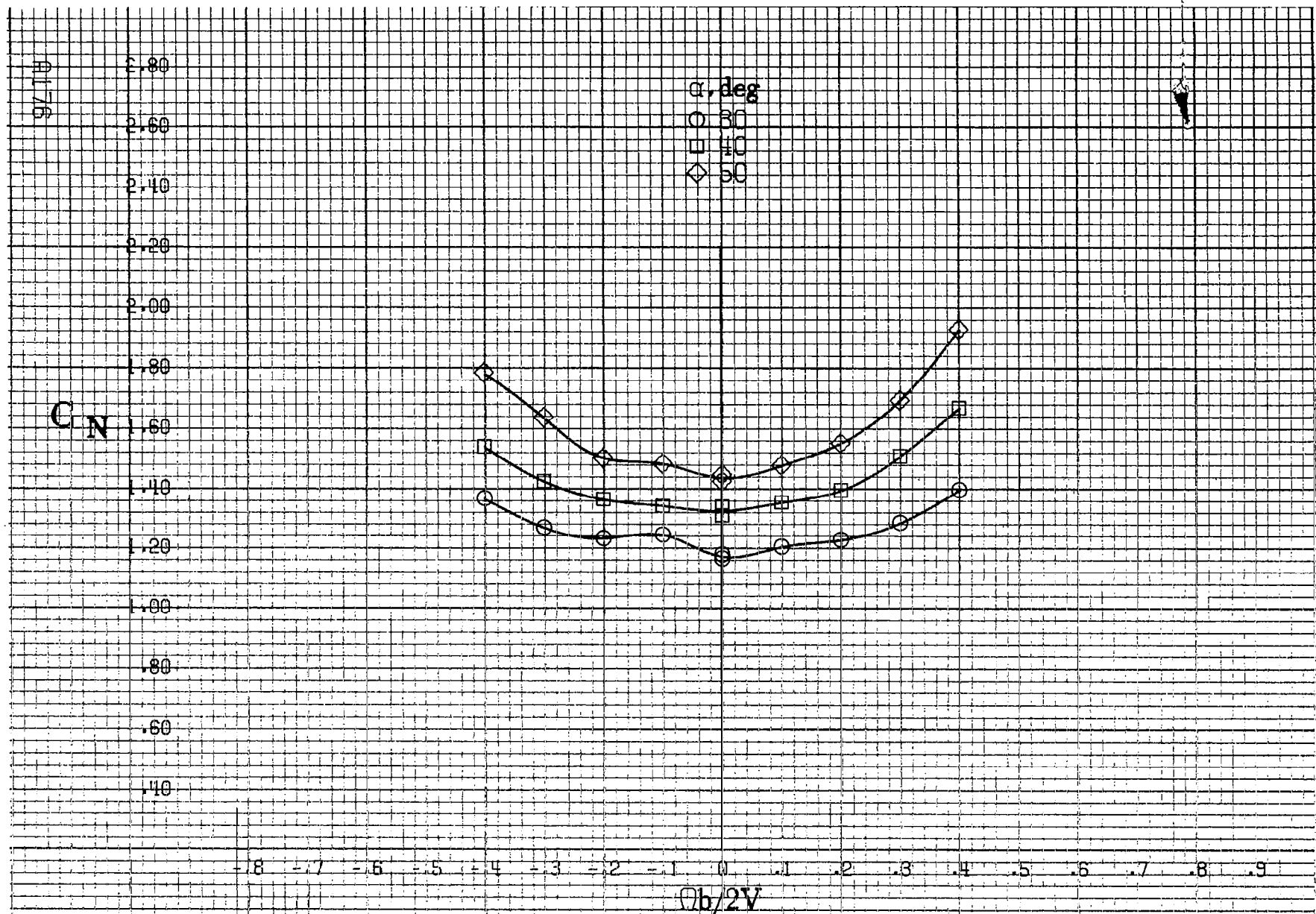
C_m

-.3
-.2
-.1
0
-.1
-.2
-.3
-.4
-.5
-.6
-.7
-.8
-.9

α, deg
○ 55
□ 60
◇ 70
△ 80
▽ 90

-8 -7 -6 -5 -4 -3 -2 -1 0 .1 .2 .3 .4 .5 .6 .7 .8 .9
 $Ob/2V$

(b) $\alpha=55$ to 90 deg, $SR=0$.
Figure A45.- Concluded.



(a) $\alpha = 30$ to 50 deg, $SR = 0$.

Figure A46.-Effect of rotation rate and angle of attack on normal-force coefficient for basic configuration. $\delta_e = -25^\circ$, $\delta_a = 0^\circ$, $\delta_d = 0^\circ$, $\delta_r = 0^\circ$, $\delta = 0^\circ$.

C_N

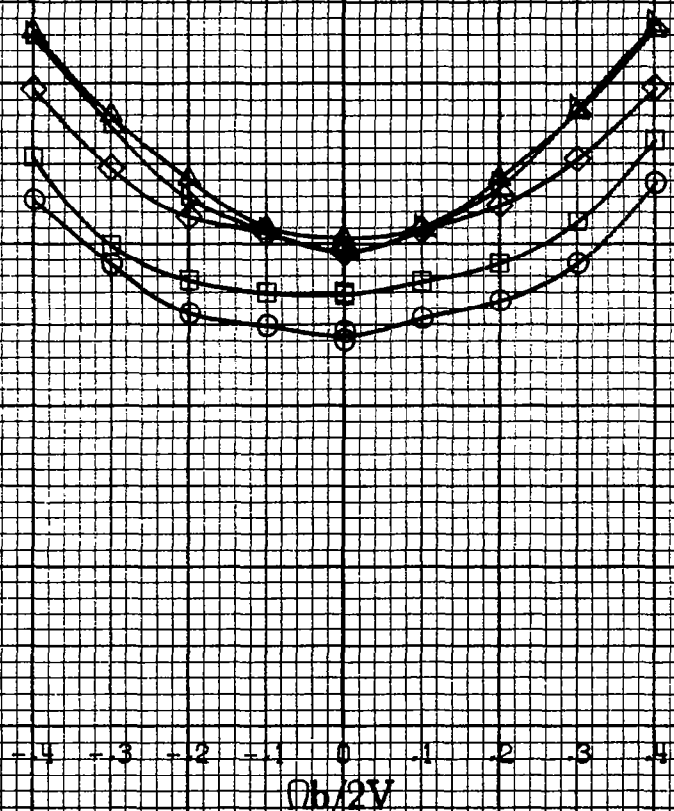
α, deg
 ○ 55
 □ 60
 ◇ 70
 △ 80
 ▽ 90

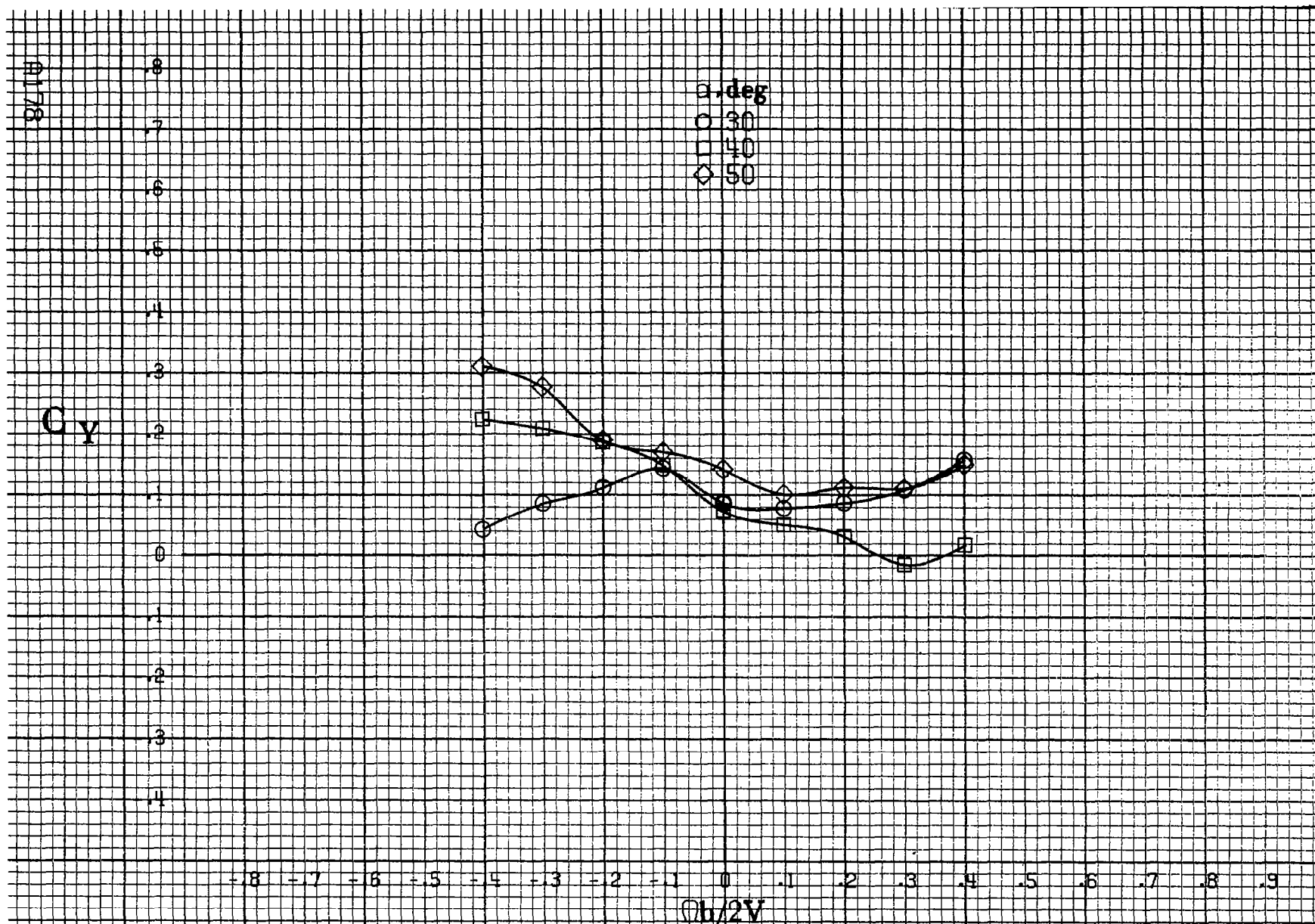
3.2
3.0
2.8
2.6
2.4
2.2
2.0
1.8
1.6
1.4
1.2
1.0
.8

-8 -7 -6 -5 -4 -3 -2 -1 0 .1 .2 .3 .4 .5 .6 .7 .8 .9
 $Ob/2V$

AI 77

(b) $\alpha=55$ to 90 deg, $SR=0$.
 Figure A16.-Concluded.





(a) $\alpha = 30$ to 50° , $SR = 0$.

Figure A47.- Effect of rotation rate and angle of attack on side-force coefficient for basic configuration. $\delta_e = -25^\circ$, $\delta_a = 0^\circ$, $\delta_d = 0^\circ$, $\delta_r = 0^\circ$, $\beta = 0^\circ$.

C_y

α, deg

○ 55

□ 60

◇ 70

△ 80

▽ 90

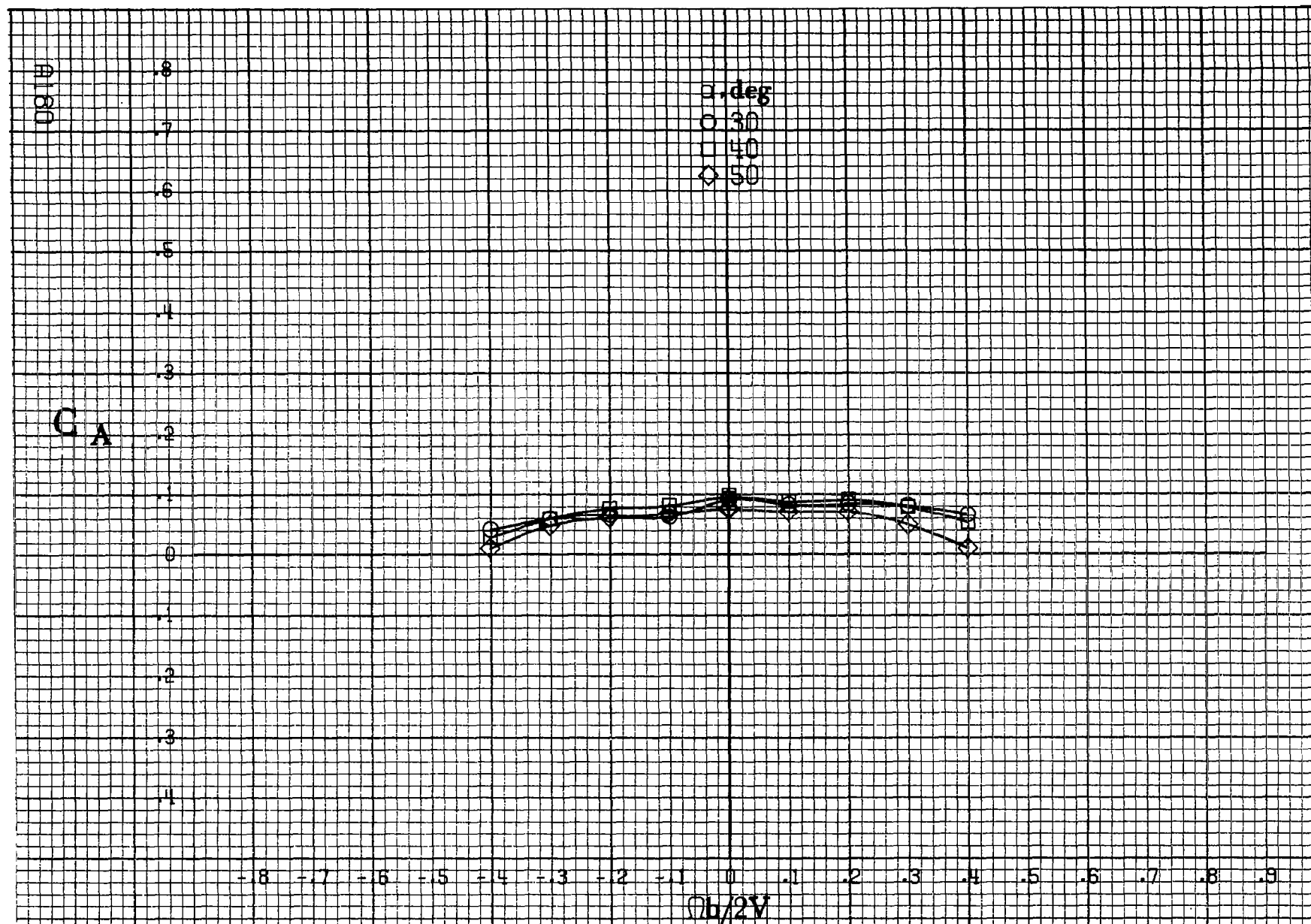
-0.8 -0.7 -0.6 -0.5 -0.4 -0.3 -0.2 -0.1 0 0.1 0.2 0.3 0.4 0.5 0.6 0.7 0.8 0.9

$Ob/2V$

(b) $\alpha = 55 \text{ to } 90 \text{ deg}, SR = 0.$

Figure A47.-Concluded.

A179



(a) $\alpha = 30$ to 50° , $SR = 0$.

Figure A48.-Effect of rotation rate and angle of attack on axial-force coefficient for basic configuration. $\delta_e = -25^\circ$, $\delta_a = 0^\circ$, $\delta_d = 0^\circ$, $\delta_r = 0^\circ$. $\beta = 0^\circ$.

C_A

α, deg
 ○ 55
 □ 60
 ◇ 70
 △ 80
 ▽ 90

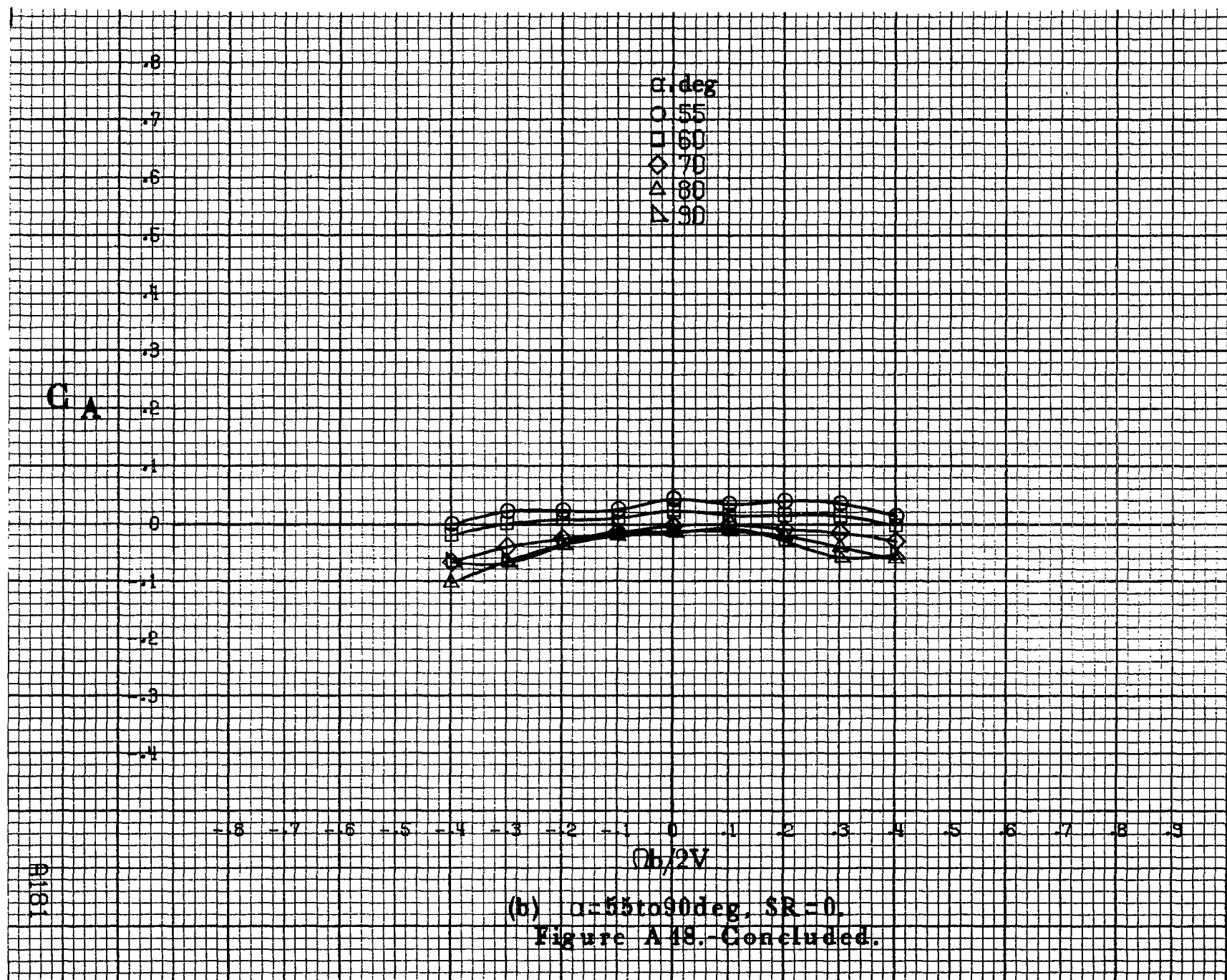
.8
.7
.6
.5
.4
.3
.2
.1
0
-.1
-.2
-.3
-.4

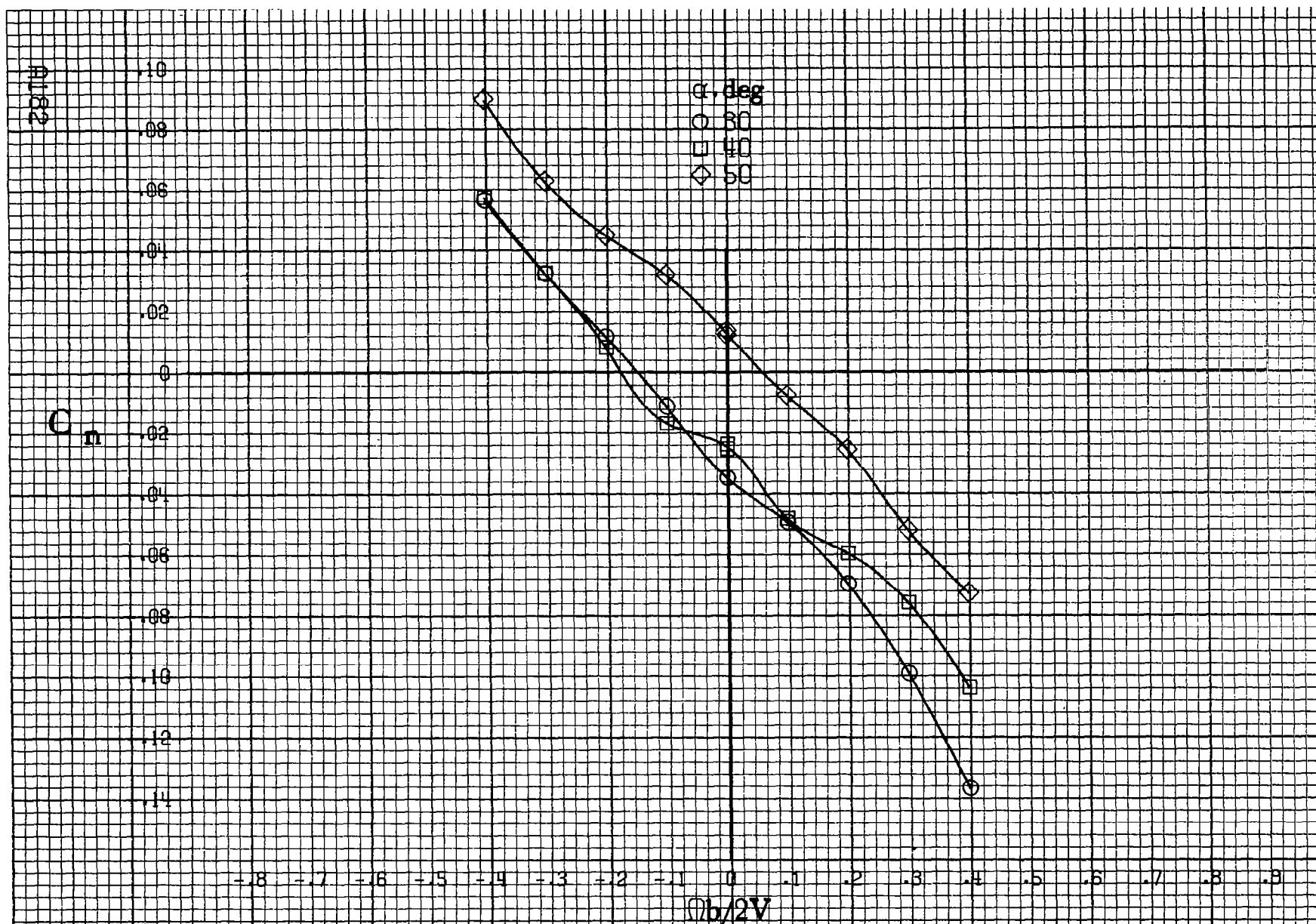
-8 -7 -6 -5 -4 -3 -2 -1 0 .1 .2 .3 .4 .5 .6 .7 .8 .9

$Ob/2V$

8181

(b) $\alpha=55$ to 90 deg, $SR=0$.
 Figure A48.- Concluded.





(a) $\alpha = 30$ to 50° , $SR = 0$.

Figure A 49. Effect of rotation rate and angle of attack on yawing-moment coefficient for basic configuration. $\delta_a = -25^\circ$, $\delta_n = 0^\circ$, $\delta_d = 0^\circ$, $\delta_r = 0^\circ$, $\delta = 10^\circ$.

AI 63

C_n

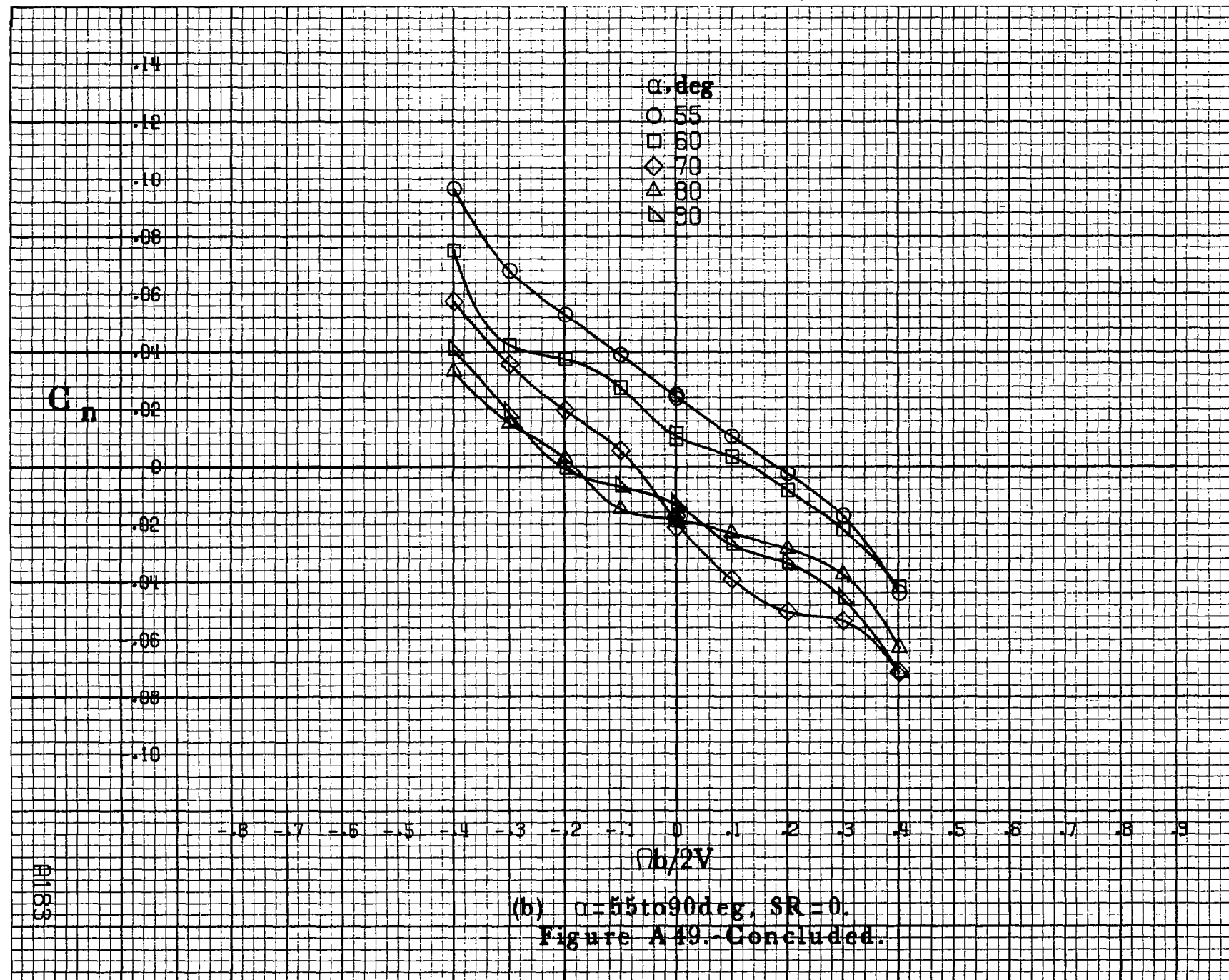
.14
.12
.10
.08
.06
.04
0
.02
.04
.06
.08
.10

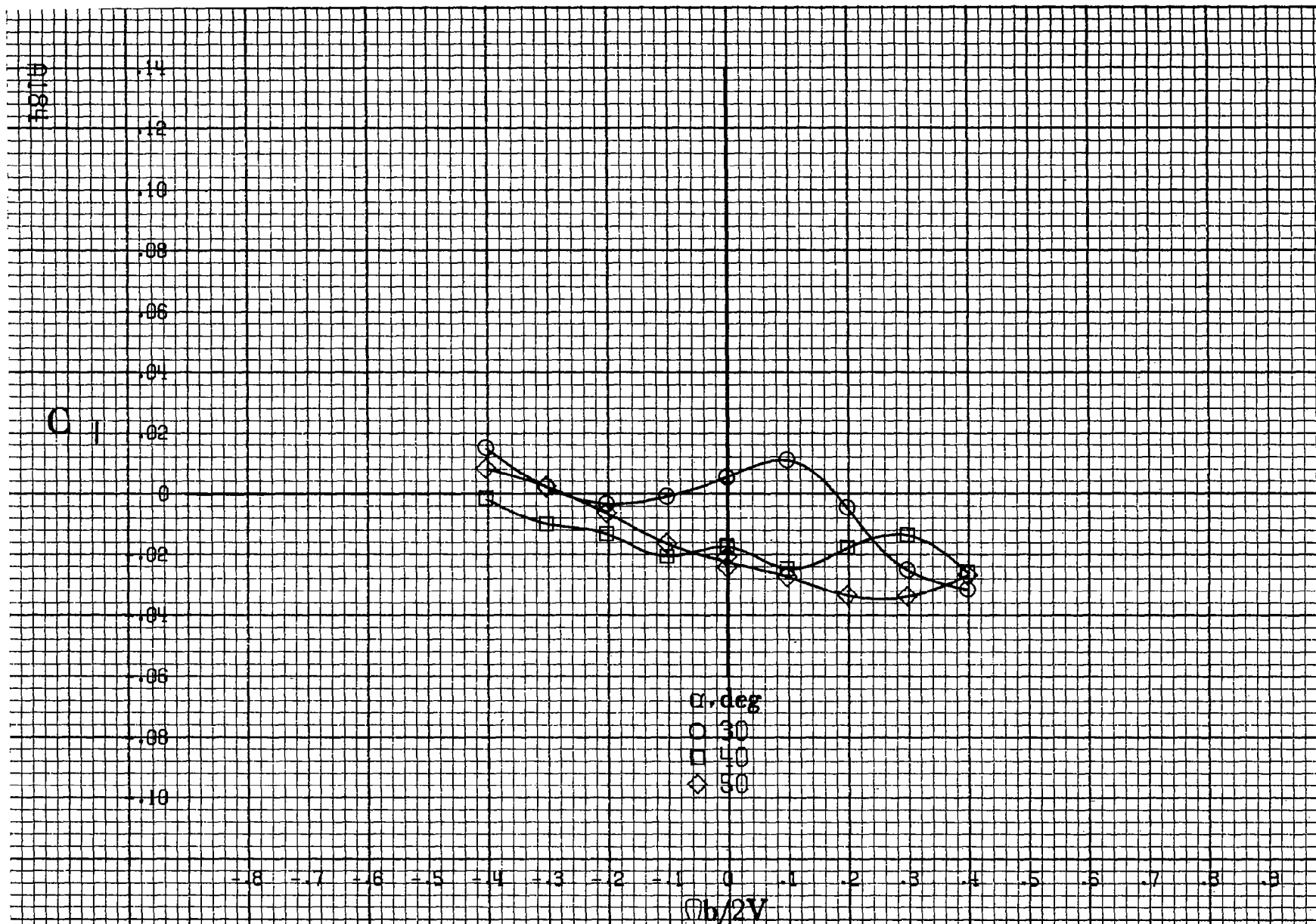
α, deg
○ 55
□ 60
◇ 70
△ 80
▽ 85

-8 -7 -6 -5 -4 -3 -2 -1 0 .1 .2 .3 .4 .5 .6 .7 .8 .9

$Ob/2V$

(b) $\alpha=55\text{to}90\text{deg}$, $SR=0$.
Figure A 49.-Concluded.





(a) $\alpha = 30$ to 50 deg, $SR = 0$.

Figure A.50 - Effect of rotation rate and angle of attack on rolling-moment coefficient for basic configuration. $\delta_c = -25^\circ$, $\delta_a = 0^\circ$, $\delta_d = 0^\circ$, $\delta_r = 0^\circ$, $\delta = 10^\circ$.

G₁

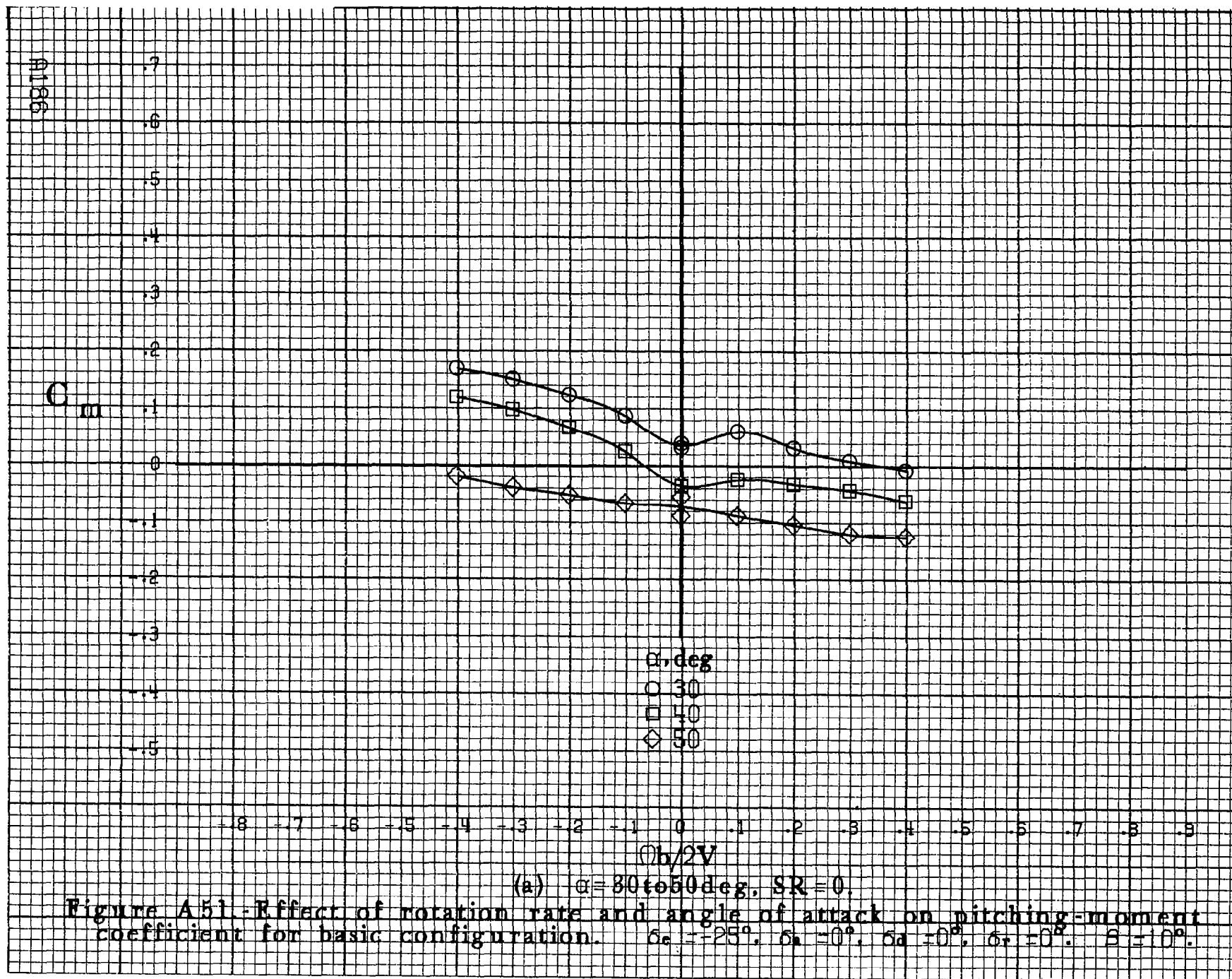
.14
.12
.10
.08
.06
.04
.02
0
-.02
-.04
-.06
-.08
-.10

α, deg
○ 55
□ 60
◇ 70
△ 80
▽ 90

-.8 -.7 -.6 -.5 -.4 -.3 -.2 -.1 0 .1 .2 .3 .4 .5 .6 .7 .8 .9
 $b/2V$

0165

(b) $\alpha=55\text{ to }90\text{ deg, SR}=0$.
Figure A50.-Concluded.



C_m

α, deg

○ 55

□ 60

◇ 70

△ 80

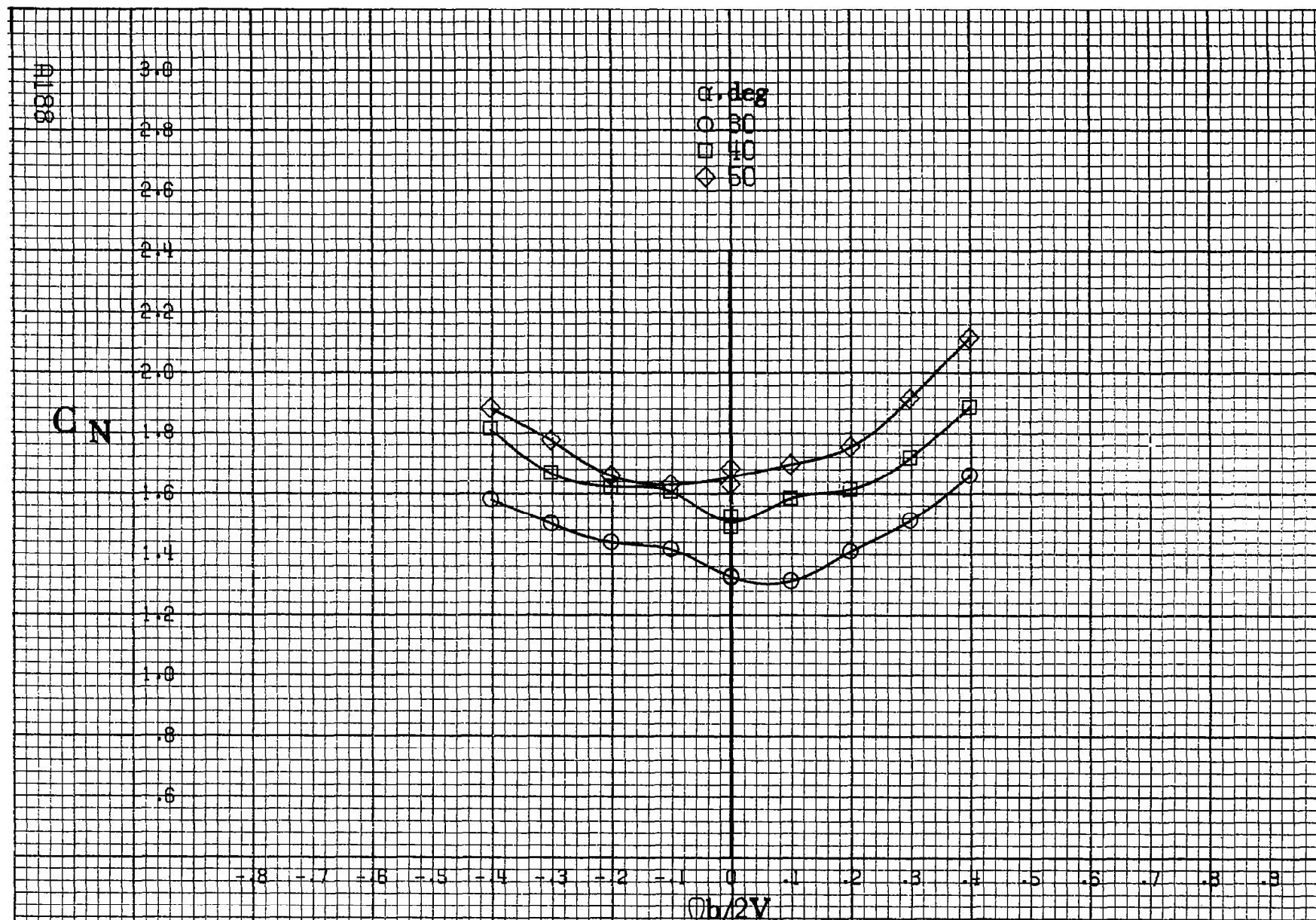
▽ 90

$Ob/2V$

(b) $\alpha=55$ to 90 deg, $SR=0$.

Figure A51.- Concluded.

A167



(a) $\alpha = 30$ to 50 deg, $SR = 0$.

Figure A52. Effect of rotation rate and angle of attack on normal-force coefficient for basic configuration. $\delta_e = \pm 25^\circ$, $\delta_a = 0^\circ$, $\delta_d = 0^\circ$, $\delta_r = 0^\circ$, $\beta = 10^\circ$.

C_N

α, deg

- 55
- 60
- ◇ 70
- △ 80
- ▽ 90

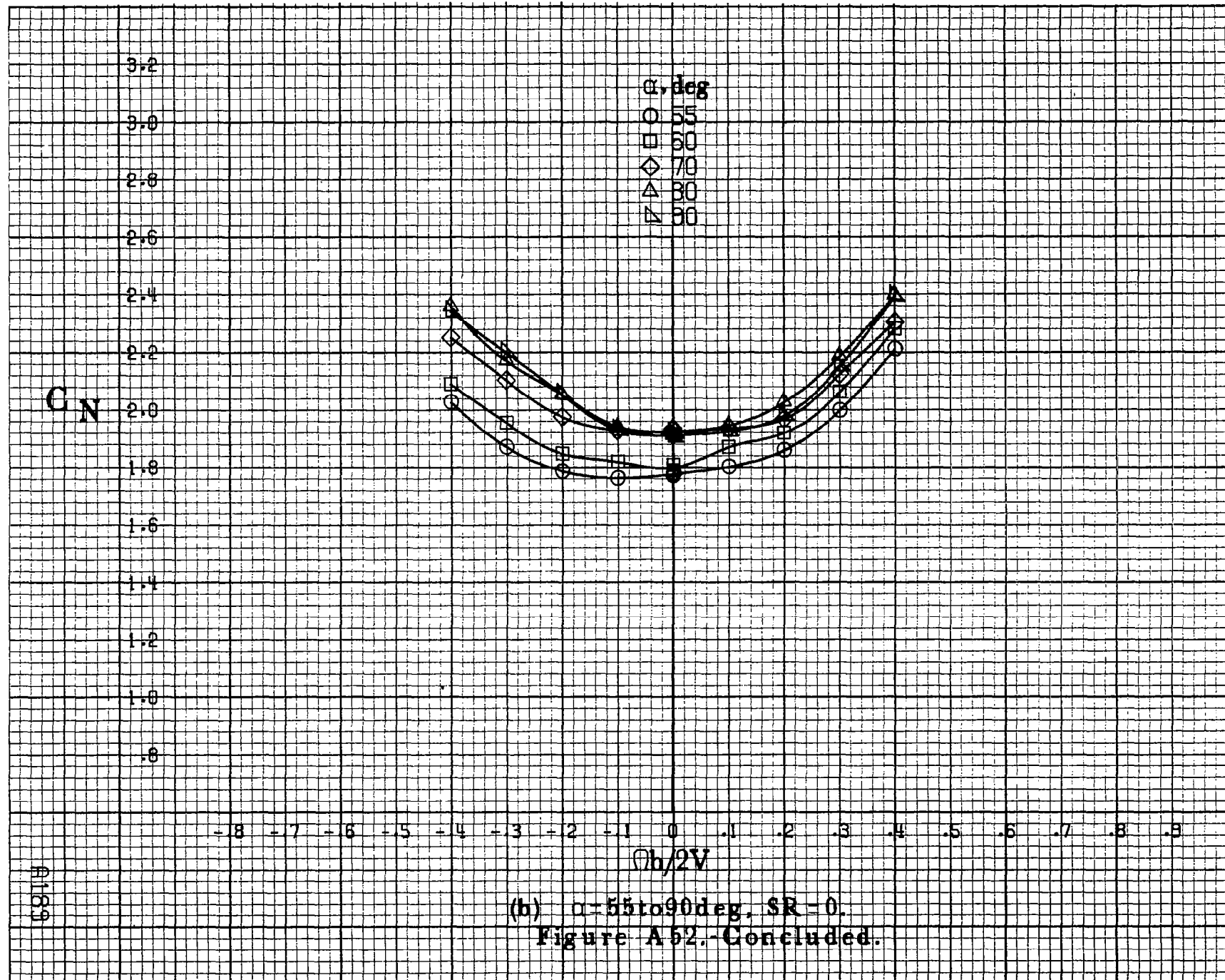
-8 -7 -6 -5 -4 -3 -2 -1 0 .1 .2 .3 .4 .5 .6 .7 .8 .9

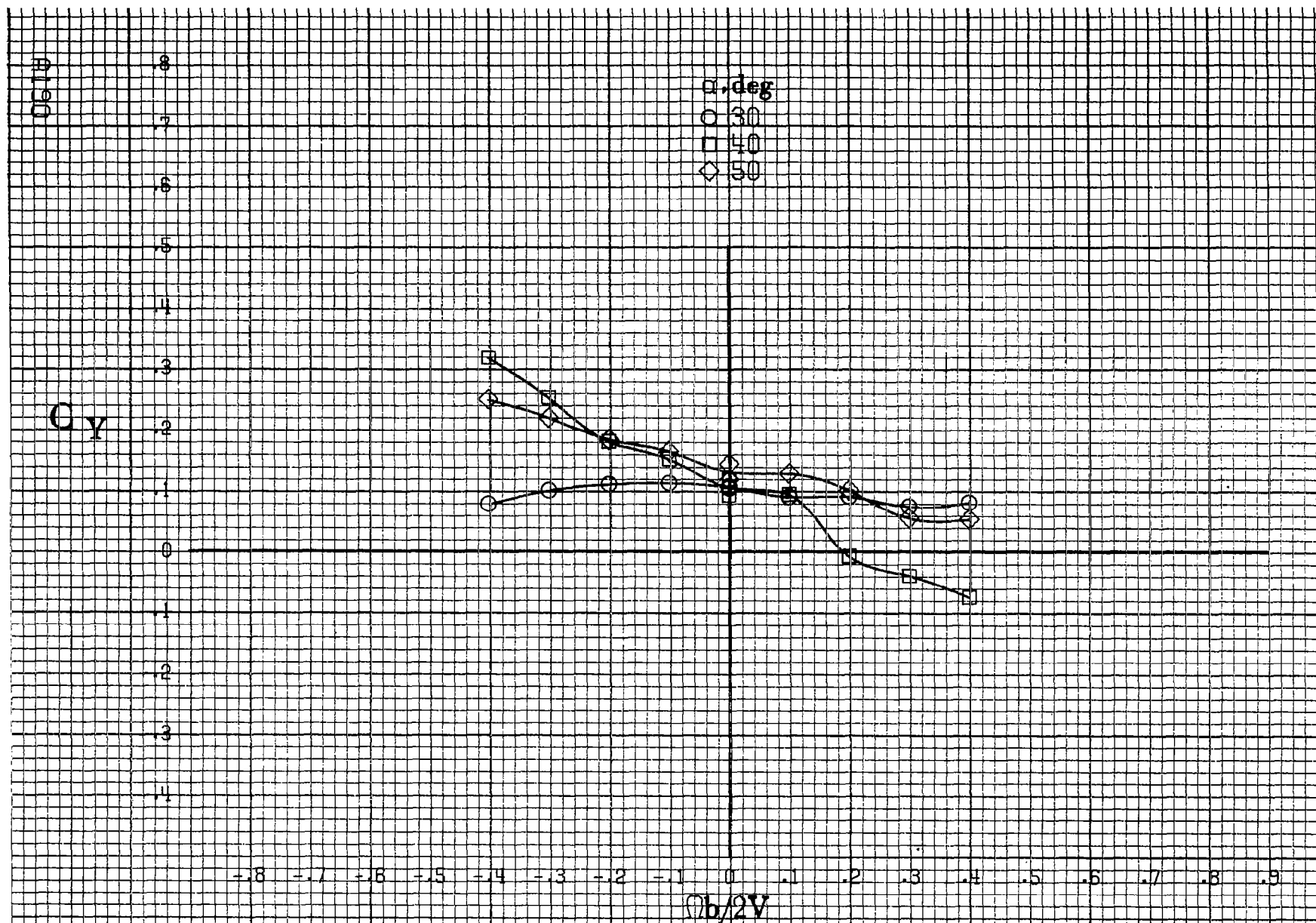
$\phi h/2V$

(b) $\alpha=55\text{to}90\text{deg}$, $SR=0$.

Figure A52.-Concluded.

A169





(a) $\alpha = 30$ to 50 deg, $SR = 0$.

Figure A53. Effect of rotation rate and angle of attack on side-force coefficient for basic configuration. $\delta_e = -25^\circ$, $\delta_a = 0^\circ$, $\delta_d = 0^\circ$, $\delta_r = 0^\circ$. $\beta = 10^\circ$.

C_y

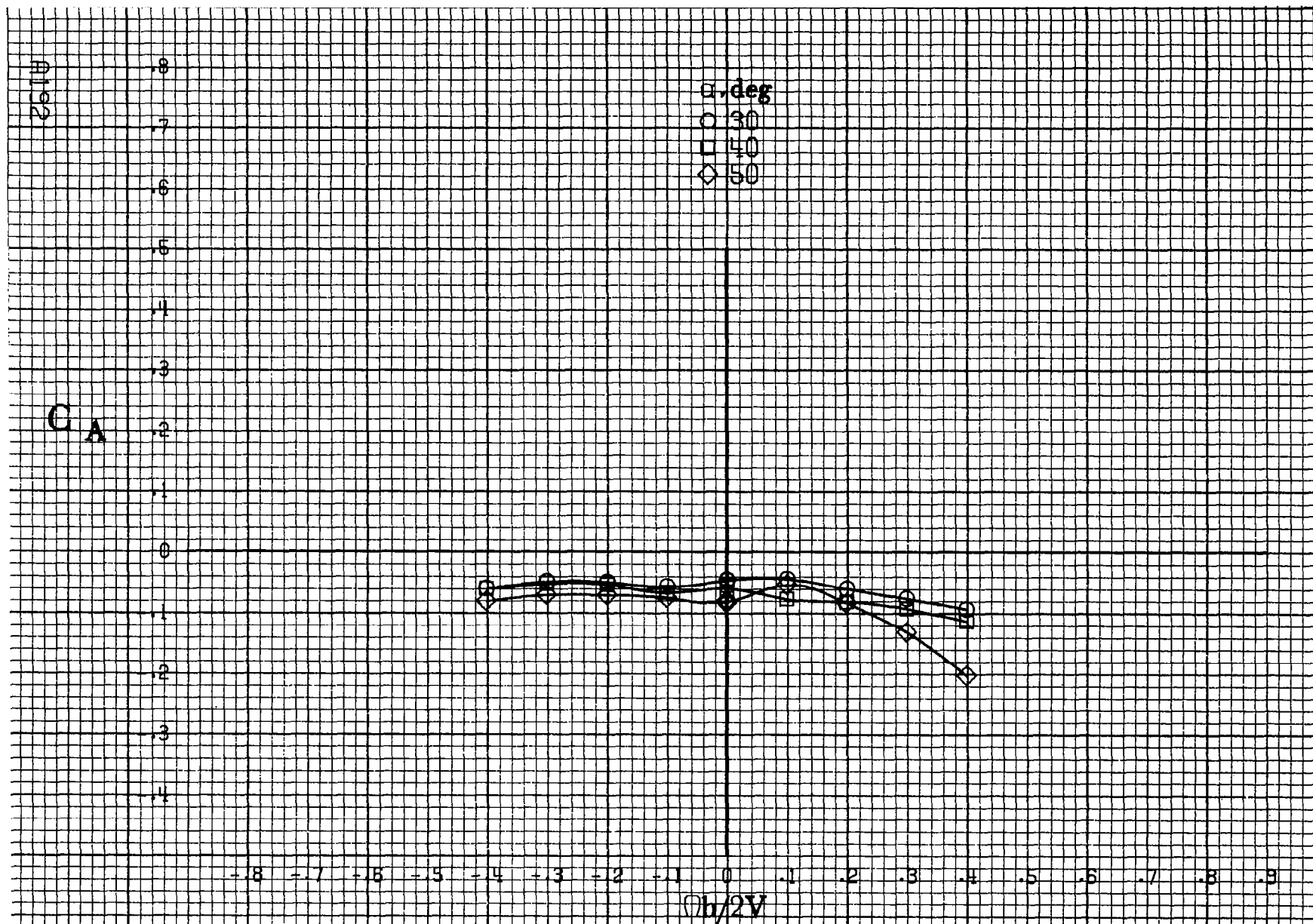
α, deg
 ○ 55
 □ 60
 ◇ 70
 △ 80
 ▽ 90

-0.8 -0.7 -0.6 -0.5 -0.4 -0.3 -0.2 -0.1 0 .1 .2 .3 .4 .5 .6 .7 .8 .9

$b/2V$

(b) $\alpha=55$ to 90° , $SR=0$.
 Figure A53.-Concluded.

4191



(a) $\alpha = 30$ to 50° , $SR = 0$.

Figure A54 - Effect of rotation rate and angle of attack on axial-force coefficient for basic configuration. $\delta_c = -25^\circ$, $\delta_a = 0^\circ$, $\delta_d = 0^\circ$, $\delta_r = 0^\circ$, $\delta = 10^\circ$.

C_A

α, deg

○ 55

□ 60

◇ 70

△ 80

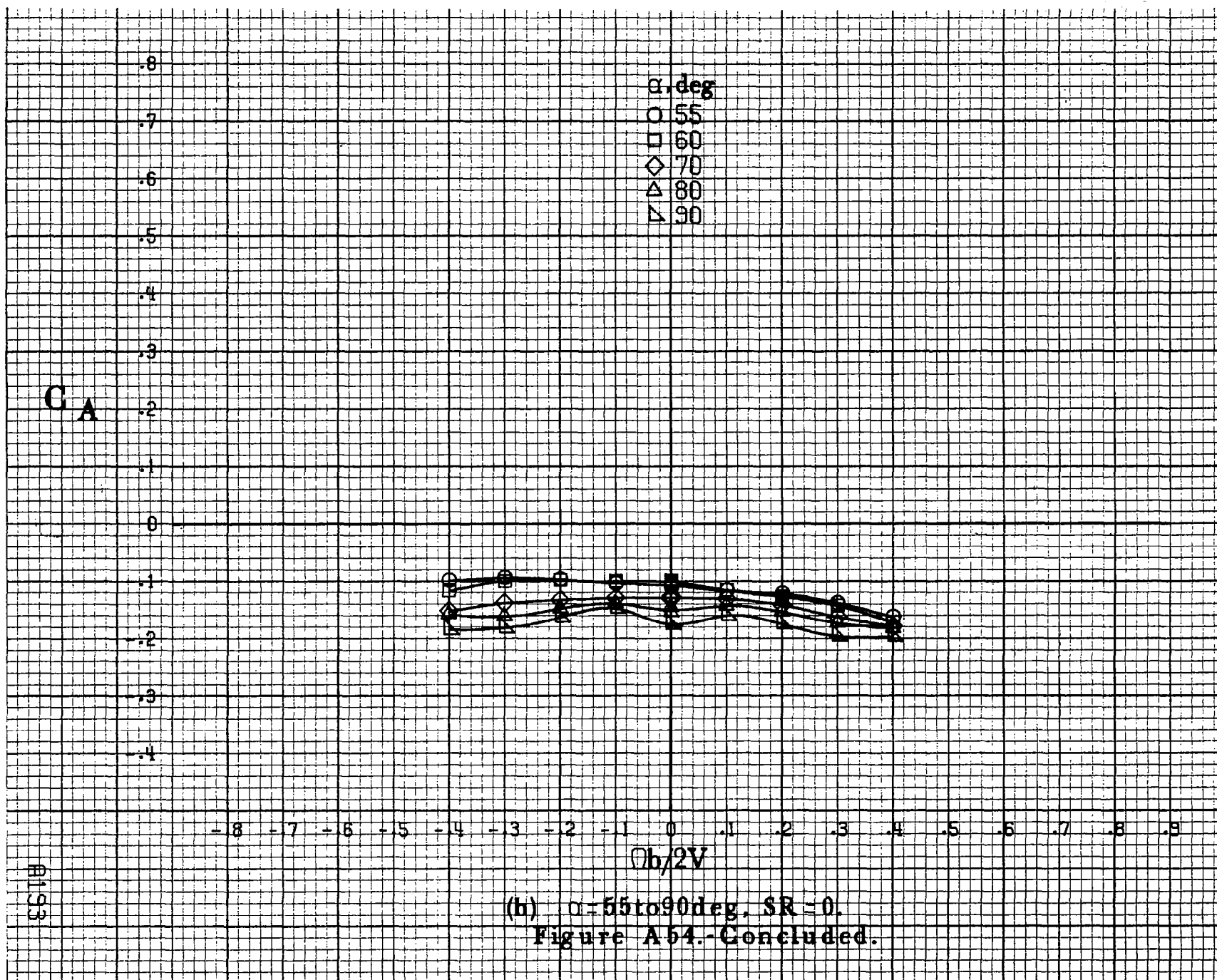
▽ 90

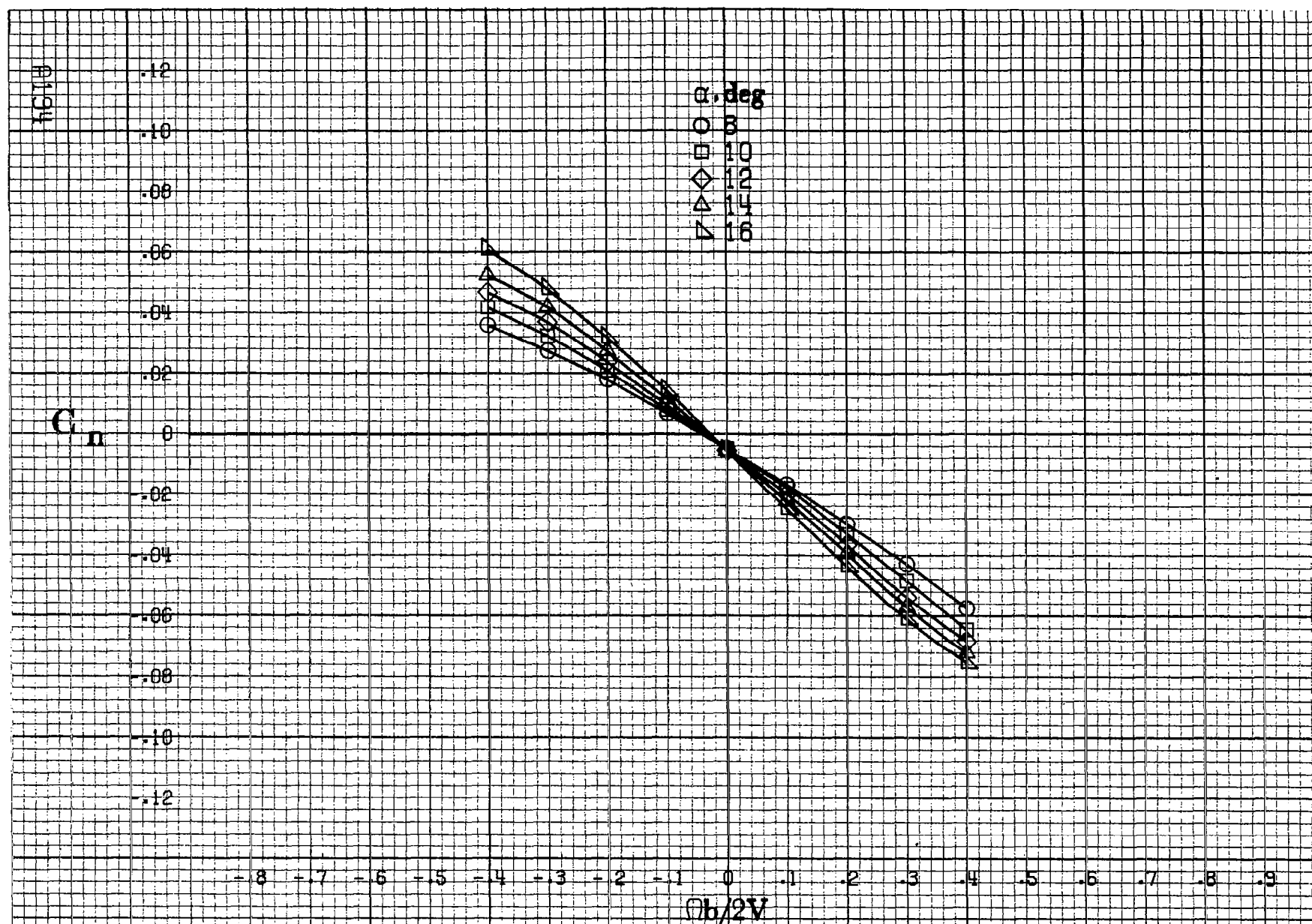
8193

$b/2V$

(h) $\alpha = 55 \text{ to } 90 \text{ deg}, SR = 0.$

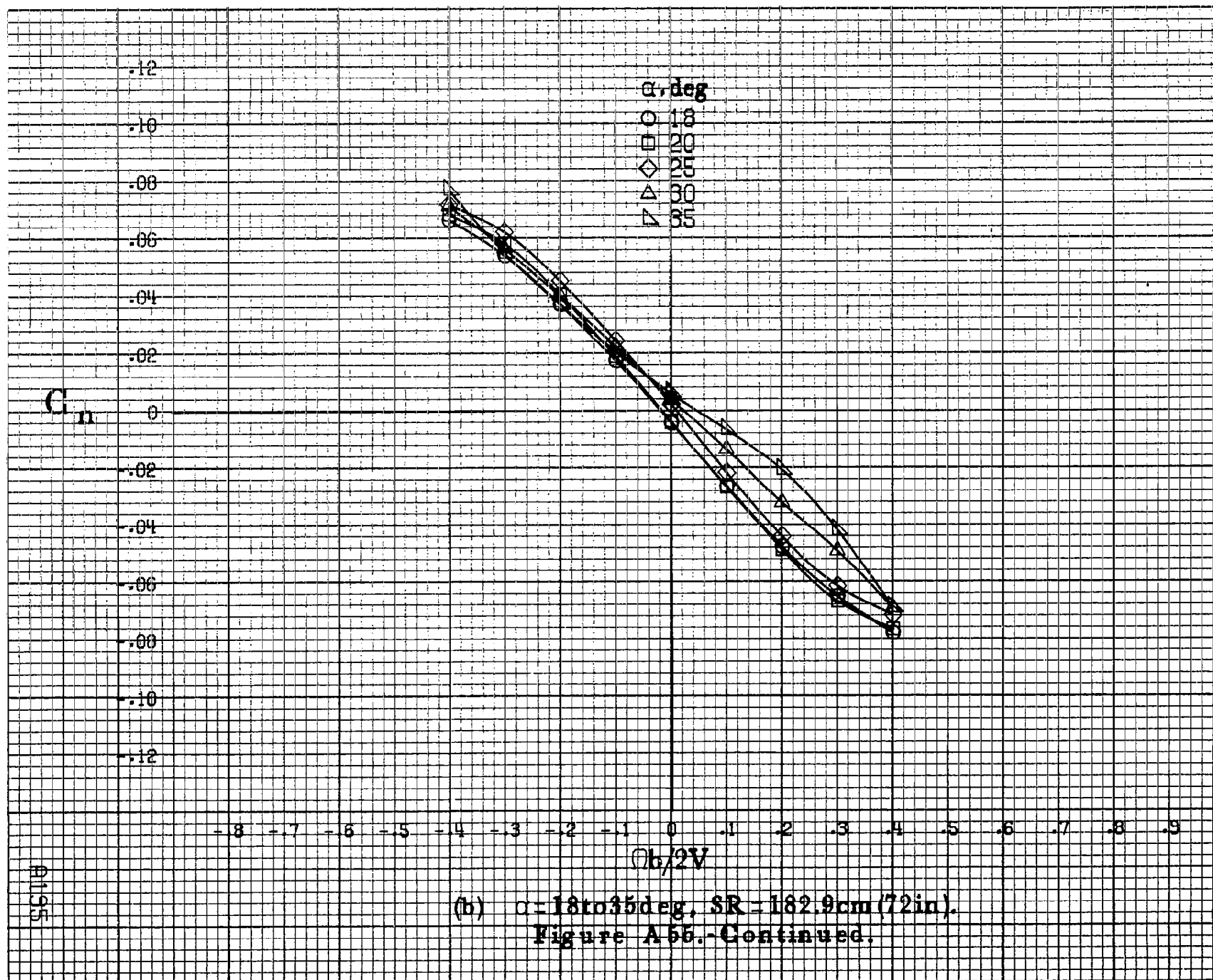
Figure A54.-Concluded.

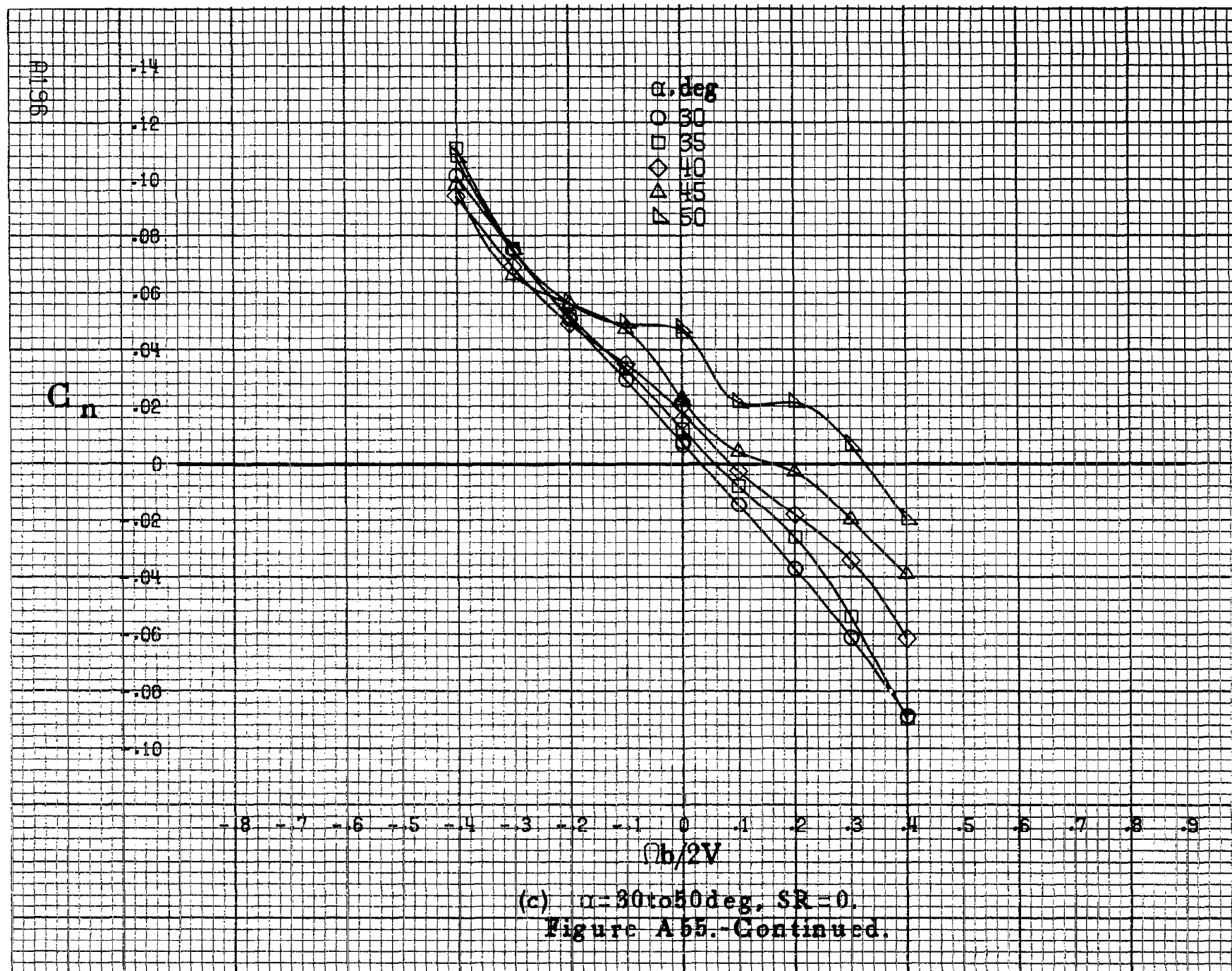


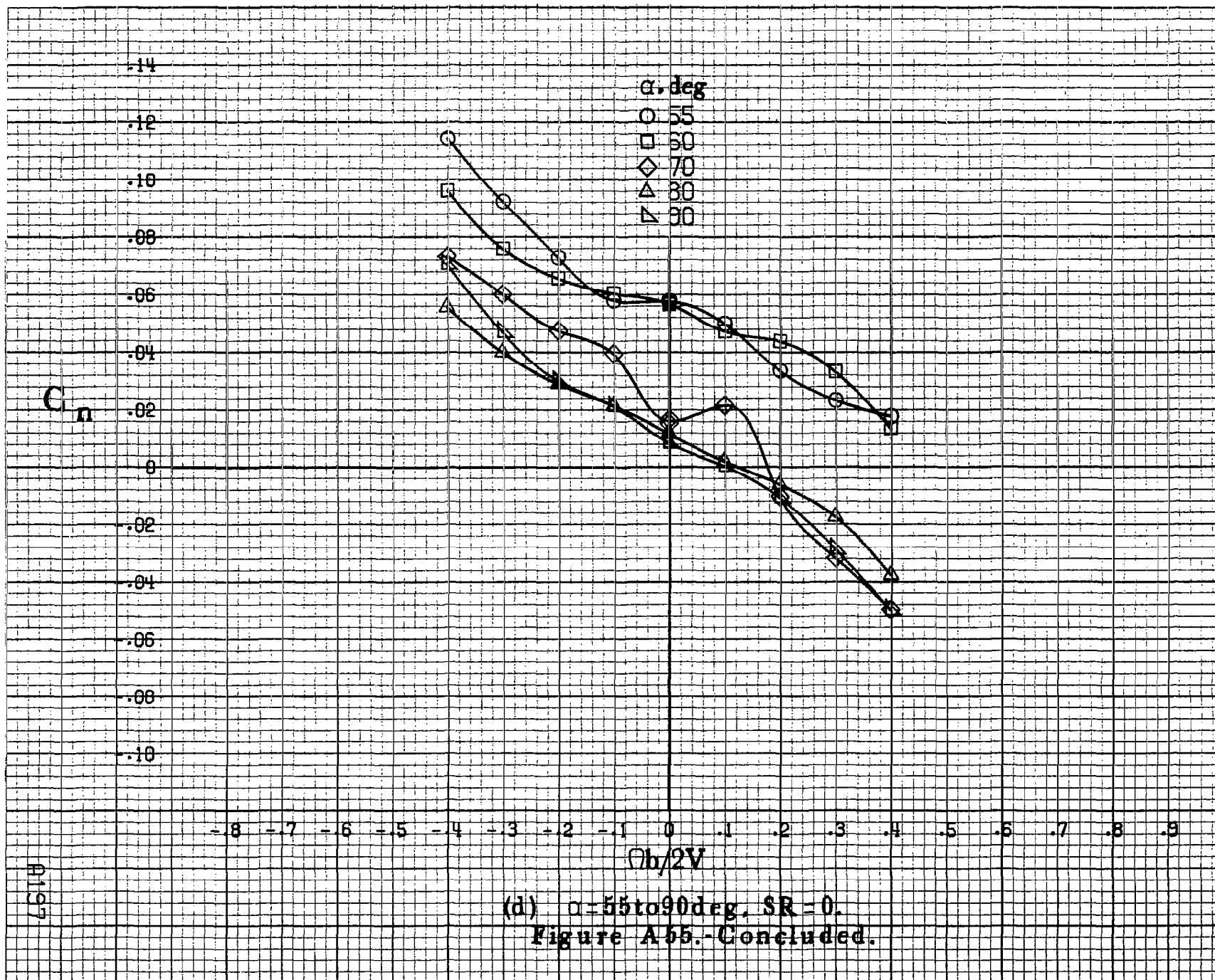


(a) $\alpha=8$ to 16° , $SR=182.9\text{cm}$ (72 in).

Figure A55 - Effect of rotation rate and angle of attack on yawing-moment coefficient for basic configuration. $\delta_e=0^\circ$, $\delta_a=0^\circ$, $\delta_d=6^\circ$, $\delta_r=0^\circ$, $\beta=0^\circ$.

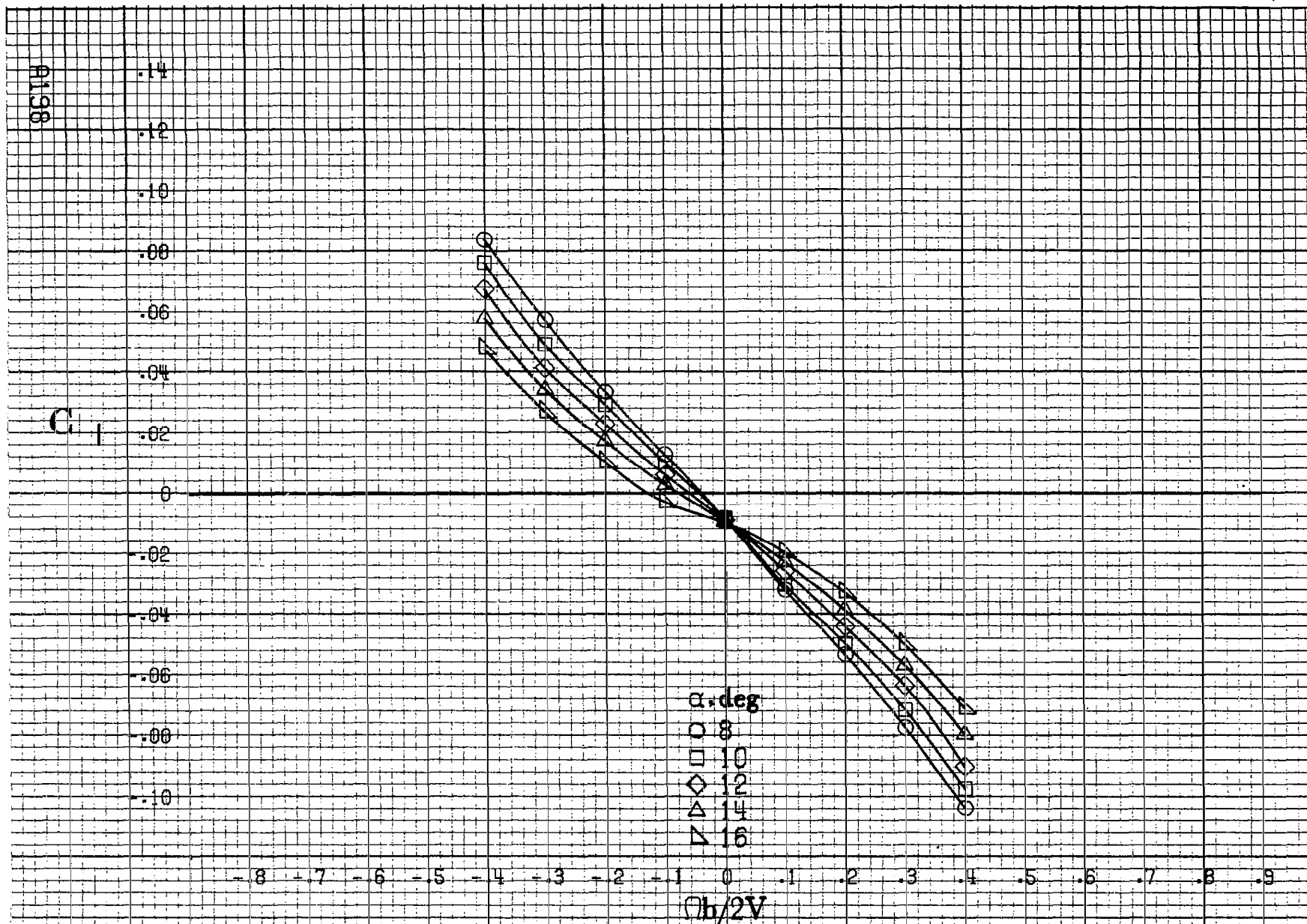






(d) $\alpha = 55$ to 90 deg, $SR = 0$.

Figure A55.-Concluded.



(a) $\alpha = 8$ to 16° , $SR = 182.9$ cm (72 in).

Figure A56.-Effect of rotation rate and angle of attack on rolling-moment coefficient for basic configuration. $\delta_a = 0^\circ$, $\delta_s = 0^\circ$, $\delta_d = 6^\circ$, $\delta_r = 0^\circ$, $\beta = 0^\circ$.

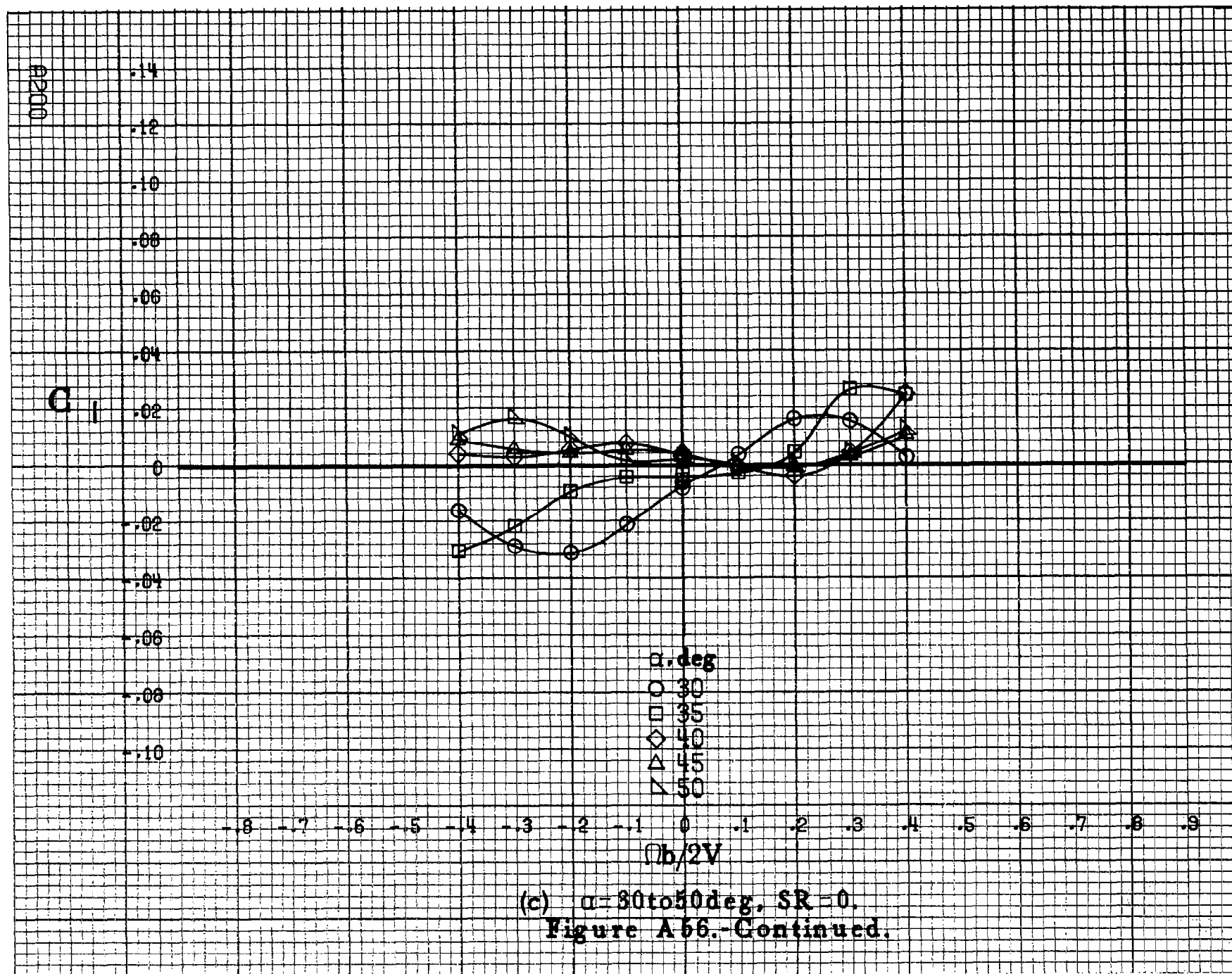
C_1

.14
.12
.10
.08
.06
.04
.02
0
-.02
-.04
-.06
-.08
-.10

α, deg
○ 18
□ 20
◇ 25
△ 30
▽ 35

-0.8 -0.7 -0.6 -0.5 -0.4 -0.3 -0.2 -0.1 0 -0.1 -0.2 -0.3 -0.4 -0.5 -0.6 -0.7 -0.8 -0.9
 $b/2V$

(b) $\alpha = 18 \text{ to } 35 \text{ deg}$, $SR = 162.9 \text{ cm (72 in)}$.
Figure A56.-Continued.



C₁

.14
.12
.10
.08
.06
.04
.02
0
-.02
-.04
-.06
-.08
-.10

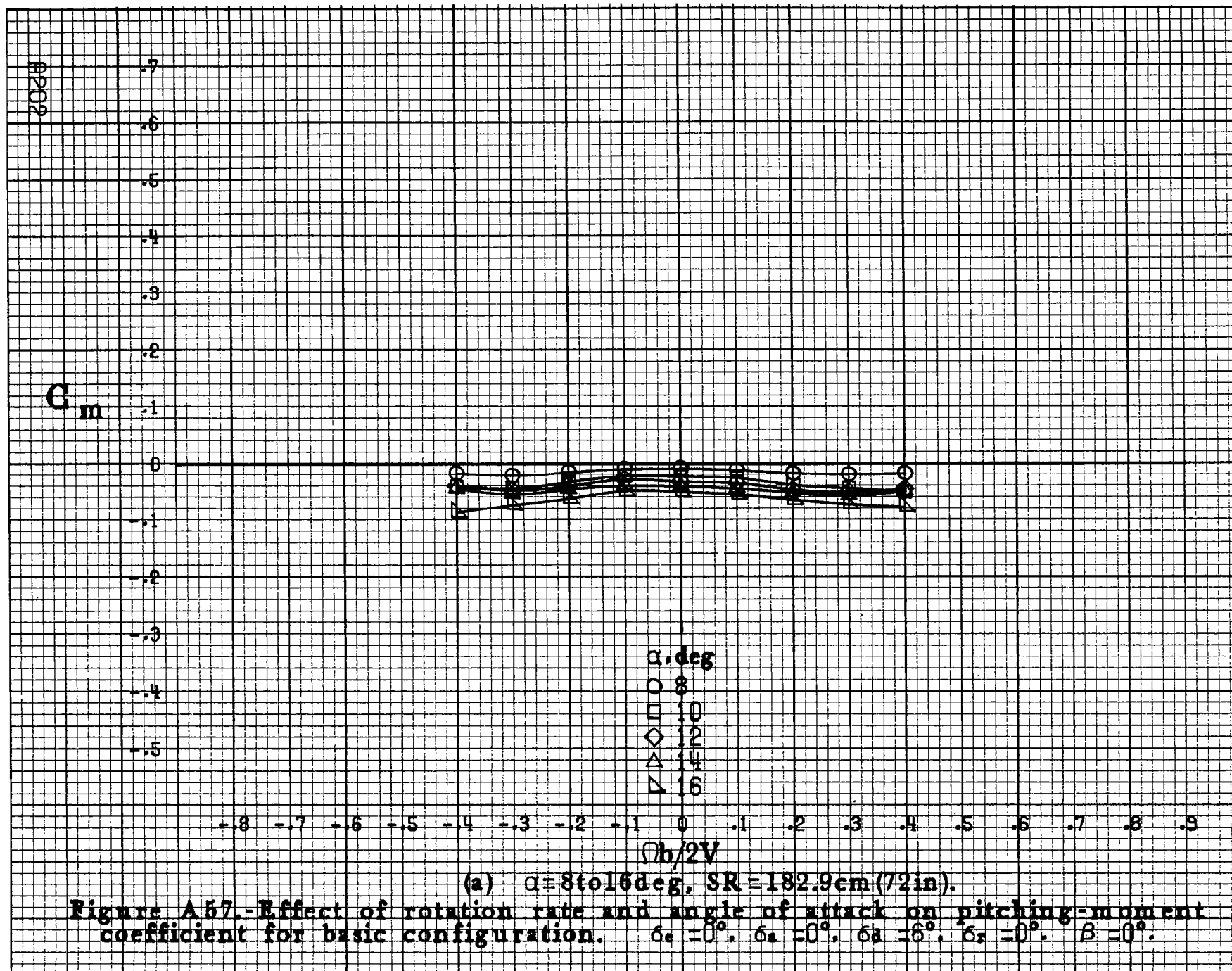
α, deg
○ 55
□ 60
◇ 70
△ 80
▽ 90

-0.8 -0.7 -0.6 -0.5 -0.4 -0.3 -0.2 -0.1 0 0.1 0.2 0.3 0.4 0.5 0.6 0.7 0.8 0.9

$Qb/2V$

(d) $\alpha=55$ to 90 deg, $SR=0$.
Figure A56.-Concluded.

A201



C_m

.6
.5
.4
.3
.2
.1
0
-.1
-.2
-.3
-.4
-.5
-.6

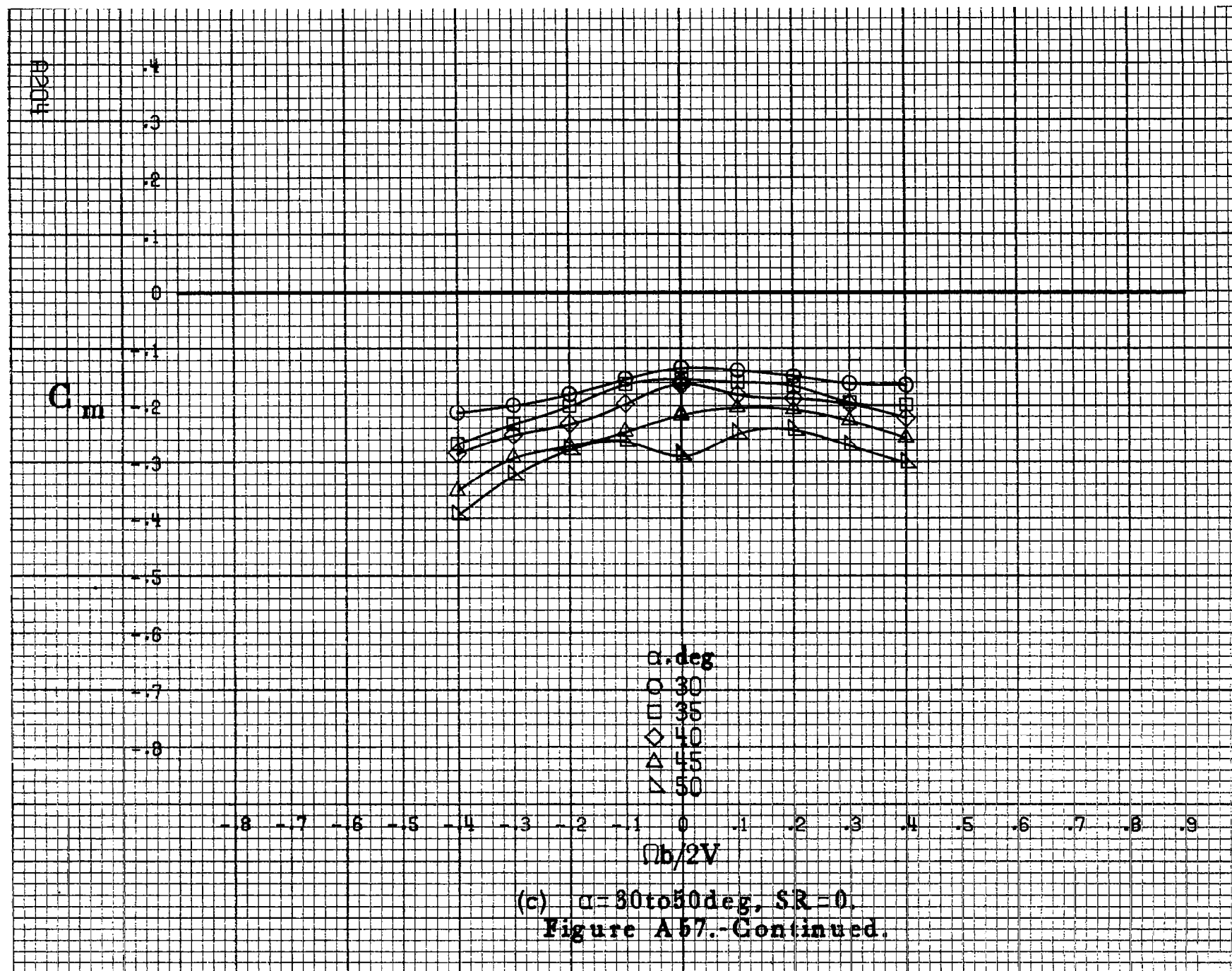
α , deg
○ 18
□ 20
◇ 25
△ 30
▽ 35

$\Omega b/2V$

-.8 -.7 -.6 -.5 -.4 -.3 -.2 -.1 0 .1 .2 .3 .4 .5 .6 .7 .8 .9

(b) $\alpha = 18$ to 35 deg, $SR = 182.9$ cm (72 in).
Figure A57.-Continued.

A203



C_m

α, deg

○ 55

□ 60

◇ 70

△ 80

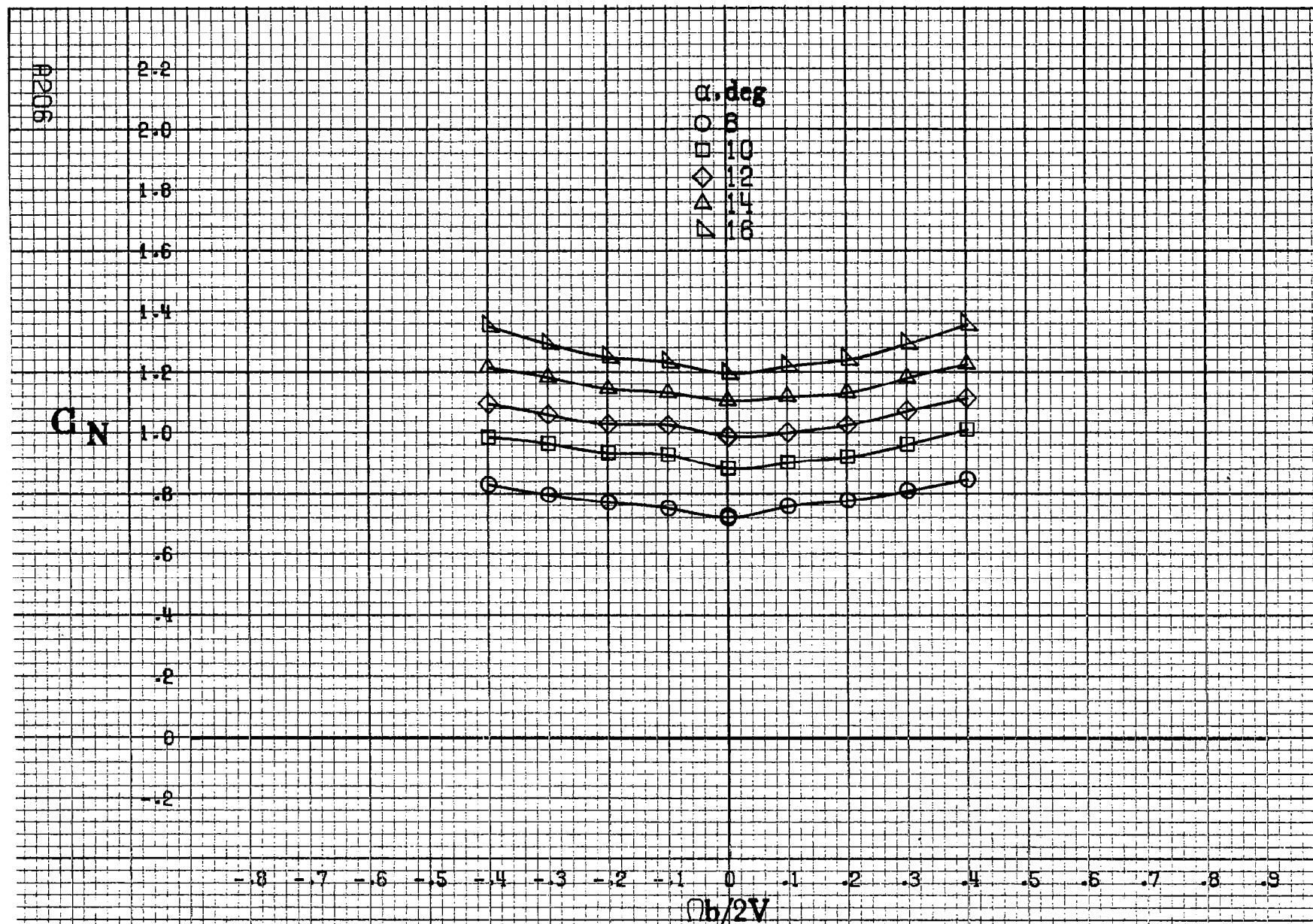
▽ 90

$Ob/2V$

(d) $\alpha=55\text{to}90\text{deg}, SR=0.$

Figure A 67.- Concluded.

A205



(a) $\alpha = 8 \text{ to } 16^\circ$, $SR = 182.9 \text{ cm (72 in.)}$.

Figure A58.-Effect of rotation rate and angle of attack on normal-force coefficient for basic configuration. $\delta_e = 0^\circ$, $\delta_a = 0^\circ$, $\delta_d = 6^\circ$, $\delta_r = 0^\circ$, $\beta = 0^\circ$.

C_N

α, deg

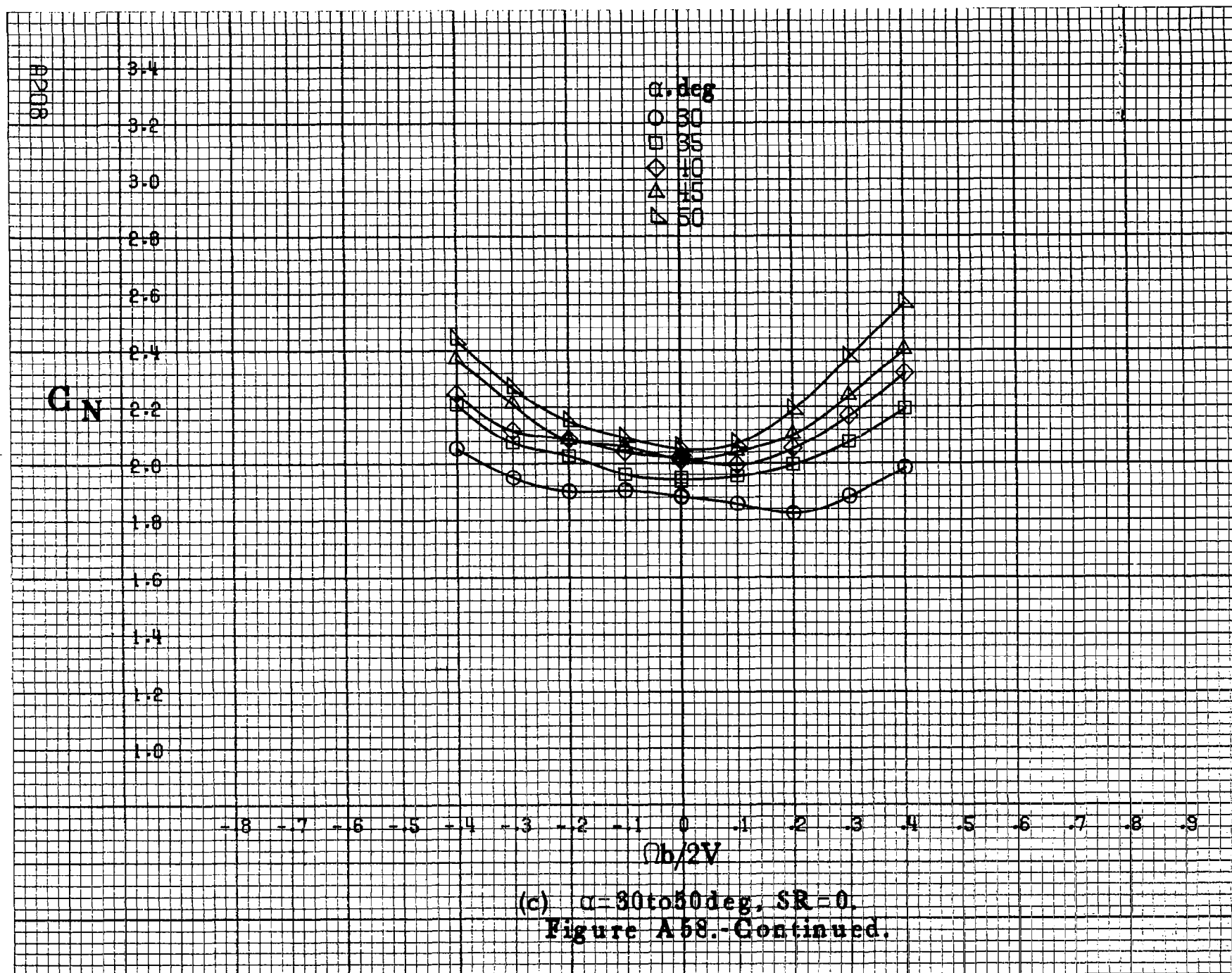
- 18
- 20
- ◇ 25
- △ 30
- ▽ 35

-8 -7 -6 -5 -4 -3 -2 -1 0 .1 .2 .3 .4 .5 .6 .7 .8 .9

$b/2V$

(b) $\alpha = 18 \text{ to } 35 \text{ deg}$, $SR = 182.9 \text{ cm (72 in)}$.
Figure A58.-Continued.

AP07



C_N

α, deg

- 55
- 60
- ◇ 70
- △ 80
- ▽ 90

3.6
3.4
3.2
3.0
2.8
2.6
2.4
2.2
2.0
1.8
1.6
1.4
1.2

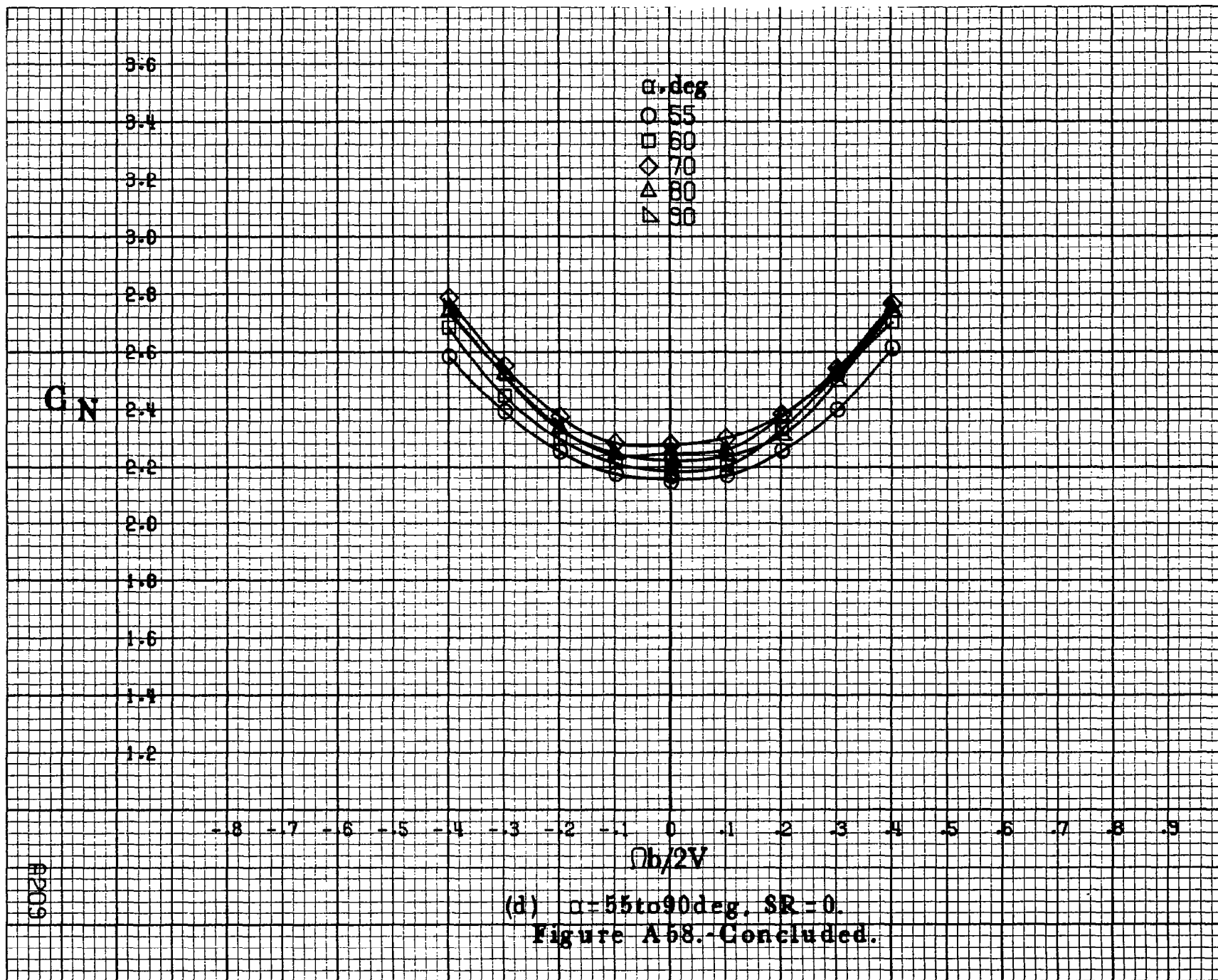
-8 -7 -6 -5 -4 -3 -2 -1 0 .1 .2 .3 .4 .5 .6 .7 .8 .9

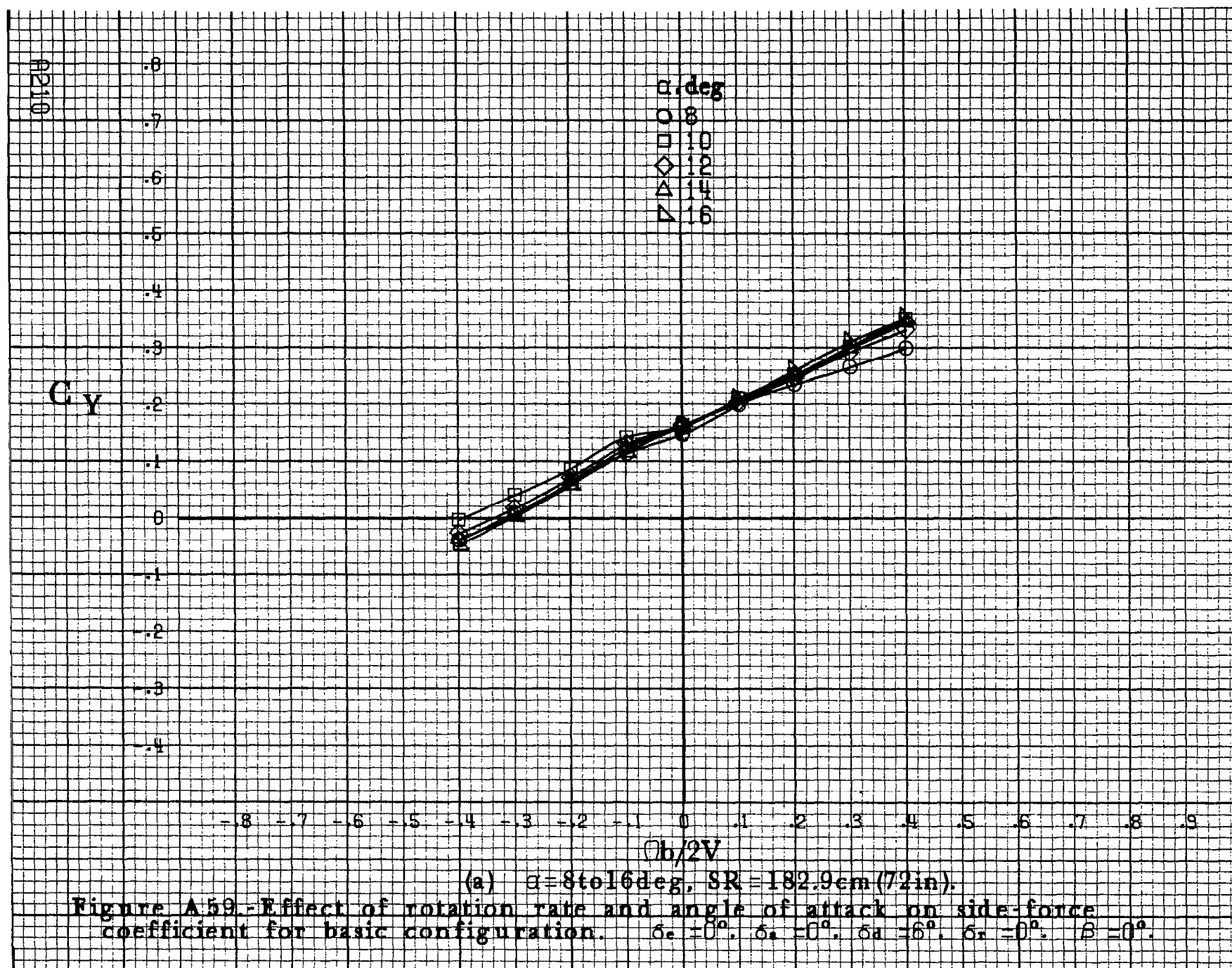
$\Omega b/2V$

#209

(d) $\alpha=55\text{to}90\text{deg. SR}=0.$

Figure A58.-Concluded.





C_y

α, deg

○ 18

□ 20

◇ 25

△ 30

▽ 35

42111

-8 -7 -6 -5 -4 -3 -2 -1 0 .1 .2 .3 .4 .5 .6 .7 .8 .9

$\Omega b/2V$

(b) $\alpha = 18 \text{ to } 35 \text{ deg. SR} = 182.9 \text{ cm (72 in.)}$

Figure A59.-Continued.

#212

C_y

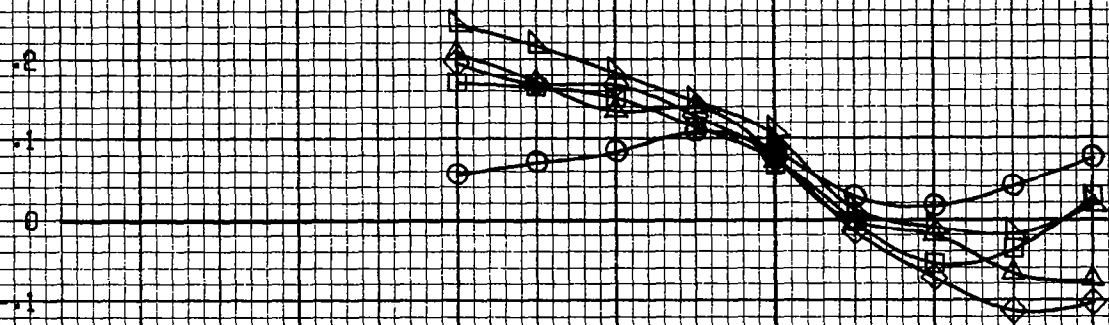
α, deg
 ○ 30
 □ 35
 ◇ 40
 △ 45
 ▽ 50

0.8
0.7
0.6
0.5
0.4
0.3
0.2
0.1
0
-0.1
-0.2
-0.3
-0.4

-0.8 -0.7 -0.6 -0.5 -0.4 -0.3 -0.2 -0.1 0 0.1 0.2 0.3 0.4 0.5 0.6 0.7 0.8 0.9

$\Omega b/2V$

(c) $\alpha=30$ to 50 deg, $SR=0$.
 Figure A59.-Continued.



C_Y

α, deg

○ 55

□ 60

◇ 70

△ 80

▽ 90

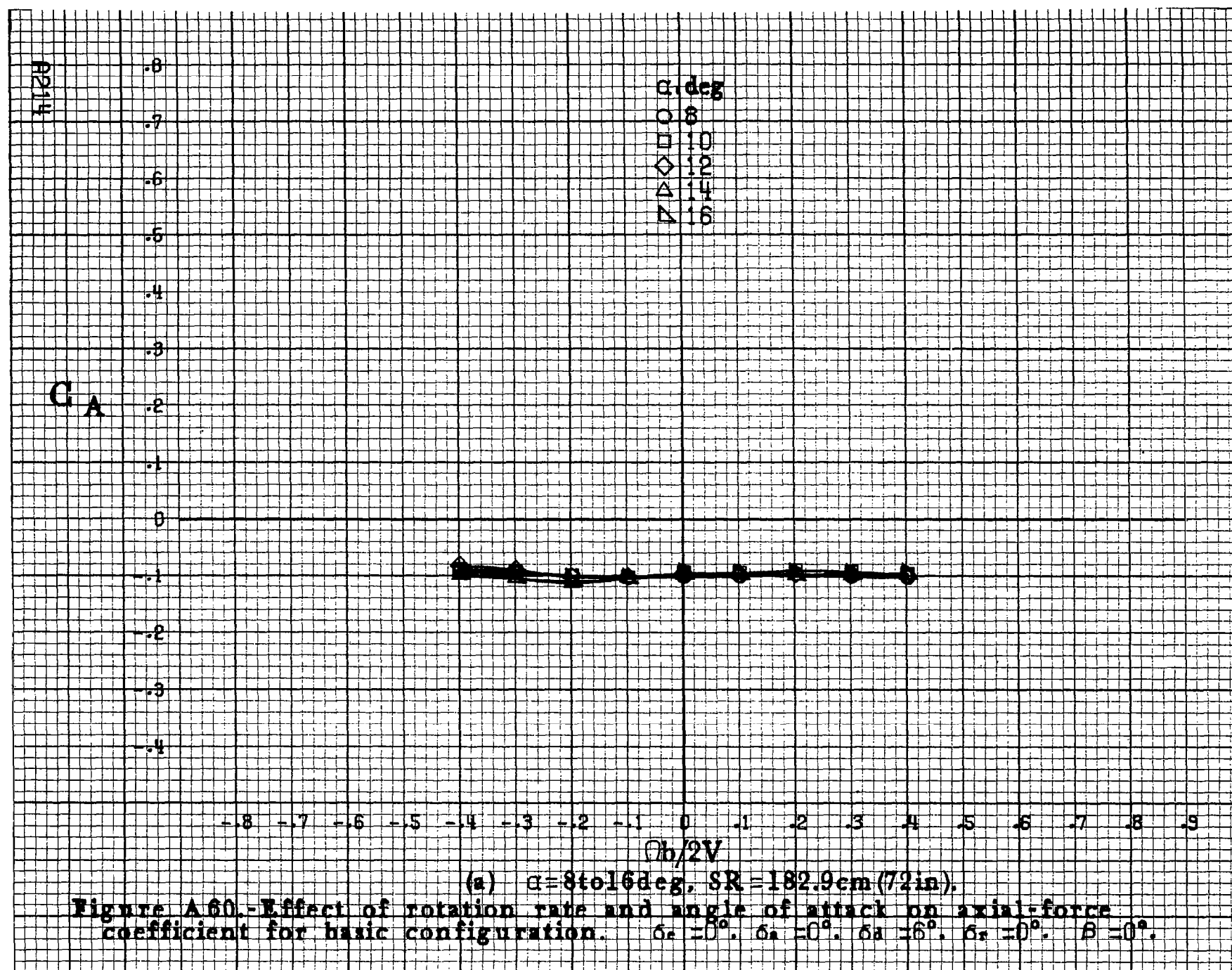
-8 -7 -6 -5 -4 -3 -2 -1 0 -1 -2 -3 -4 .5 .6 .7 .8 .9

$Ob/2V$

A213

(d) $\alpha=55\text{to}90\text{deg}$, $SR=0$.

Figure A59.-Concluded.



C_A

0
.1
.2
.3
.4
.5
.6
.7
.8

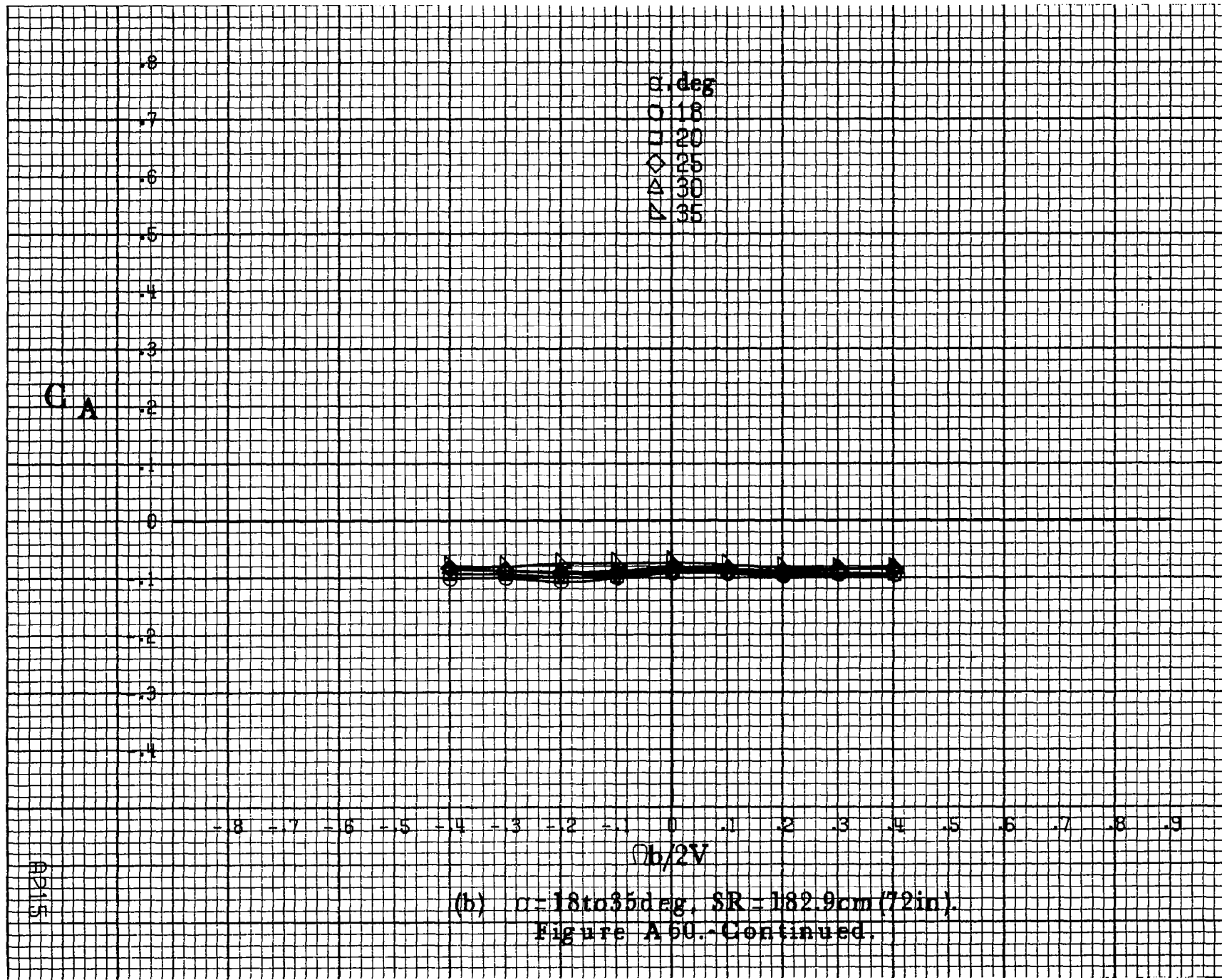
α , deg
18
20
25
30
35

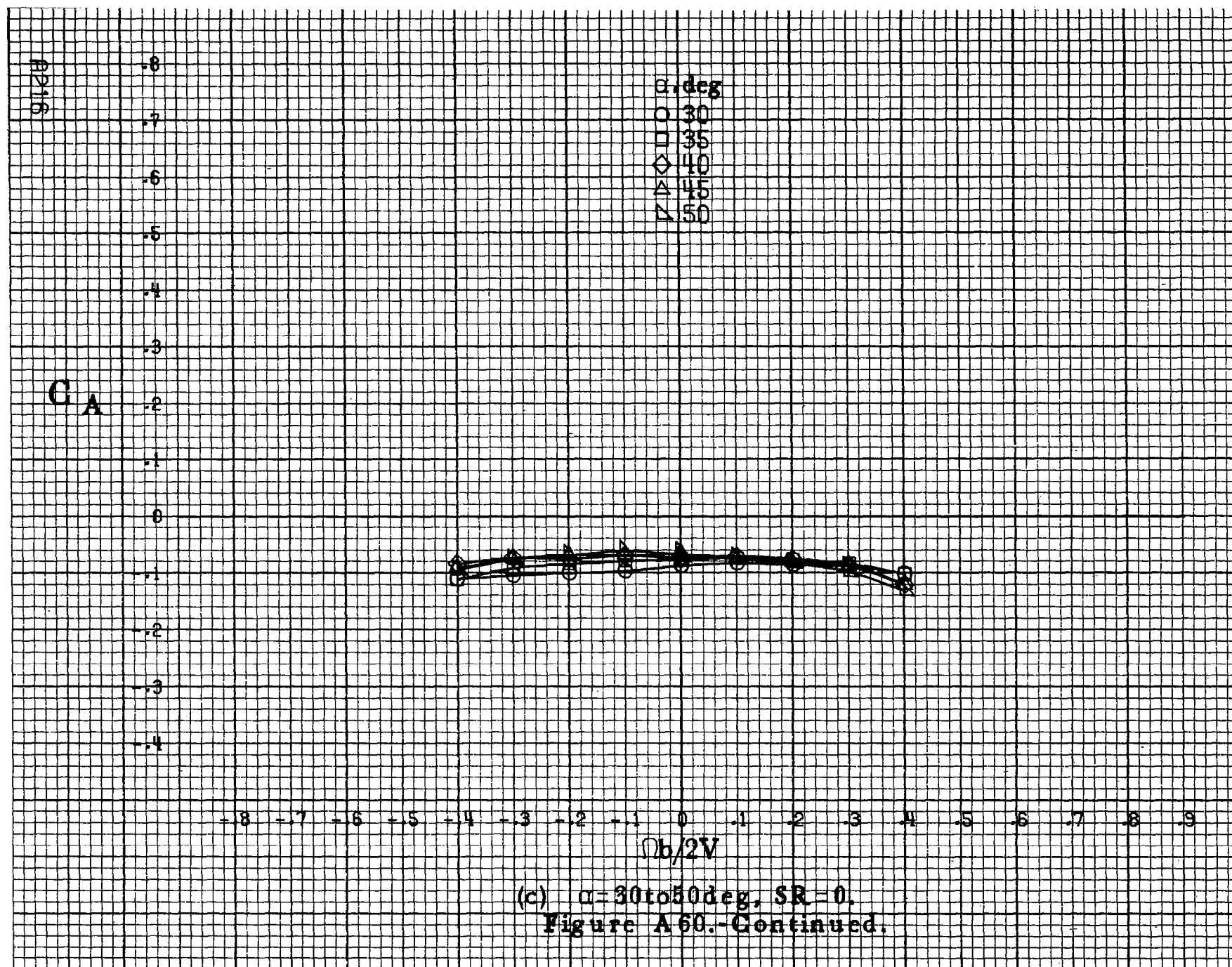
-1.8 -1.7 -1.6 -1.5 -1.4 -1.3 -1.2 -1.1 -1.0 -0.9 -0.8 -0.7 -0.6 -0.5 -0.4 -0.3 -0.2 -0.1 0 .1 .2 .3 .4 .5 .6 .7 .8 .9

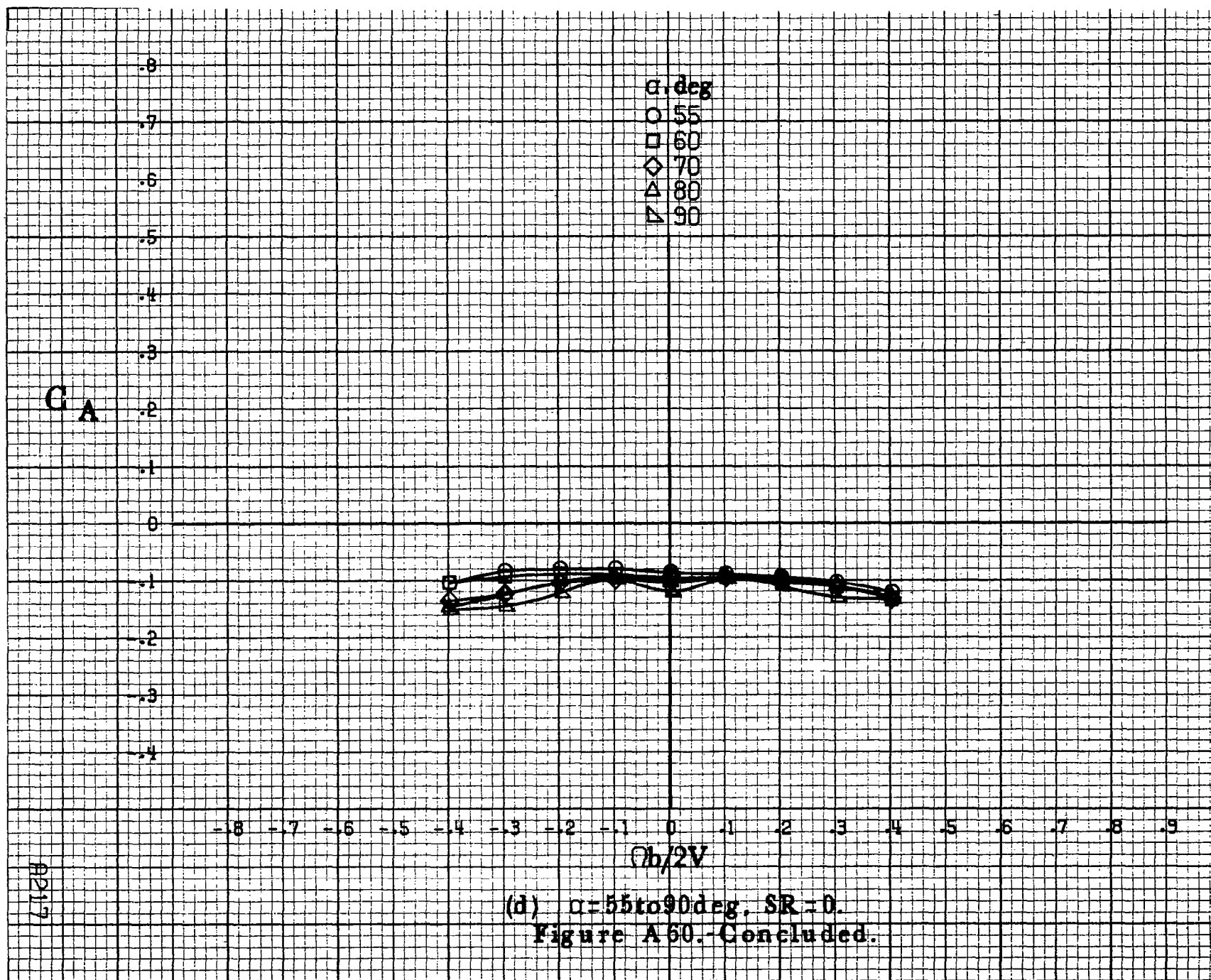
$b/2V$

(b) $\alpha = 18$ to 35 deg, $SR = 182.9$ cm (72 in).
Figure A 60.-Continued.

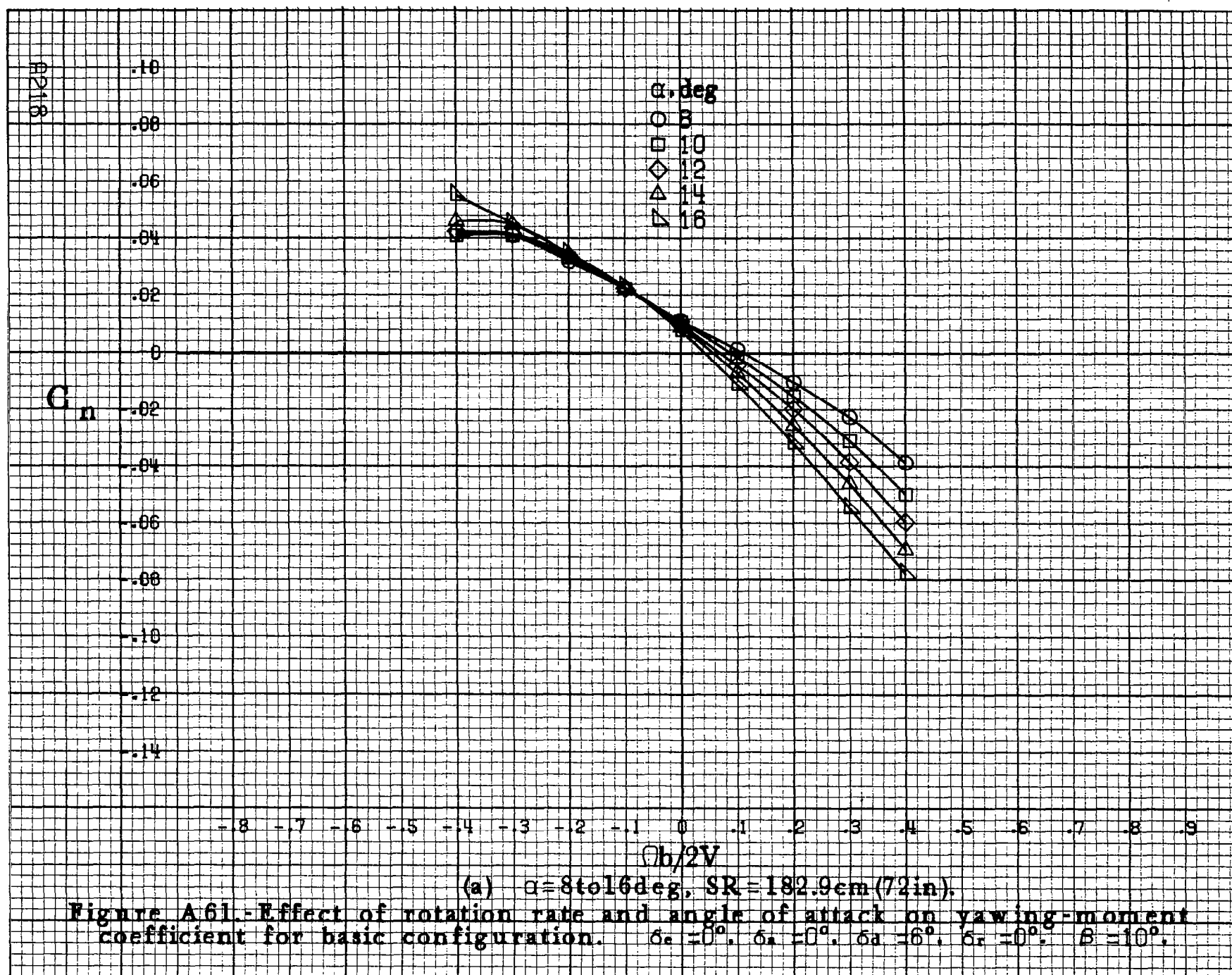
A215

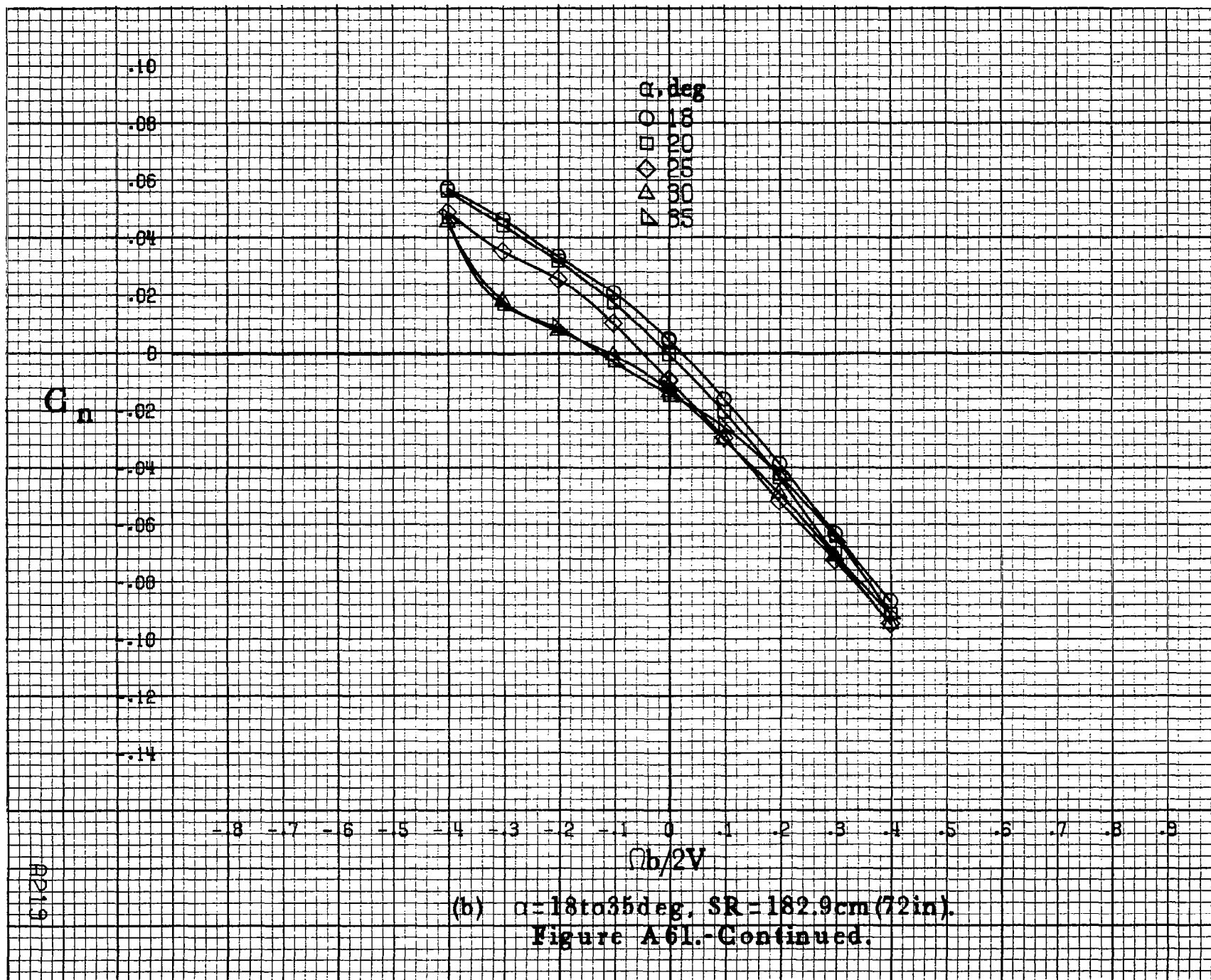


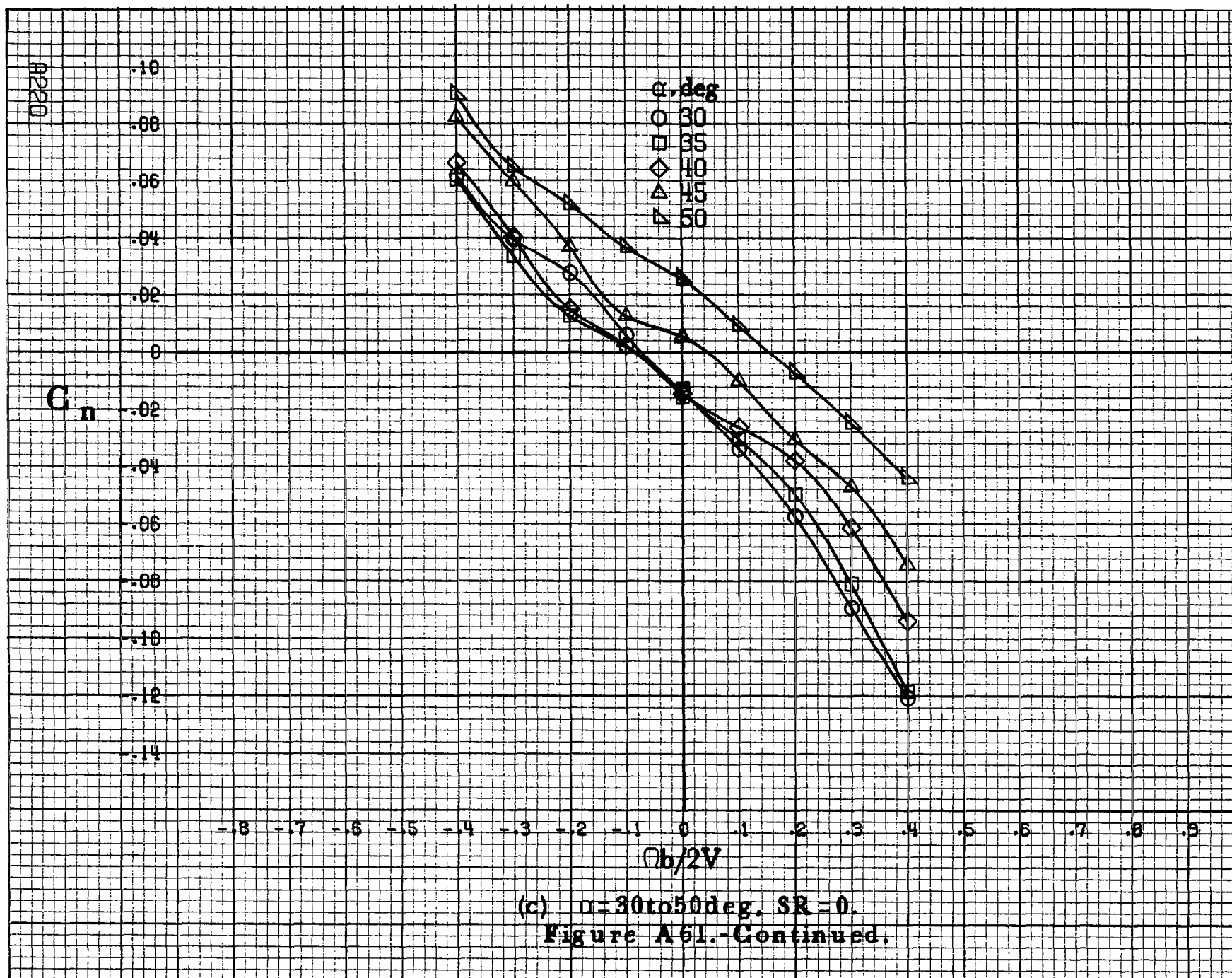




(d) $\alpha = 55$ to 90 deg. $SR = 0$.
Figure A 60.-Concluded.







C_n

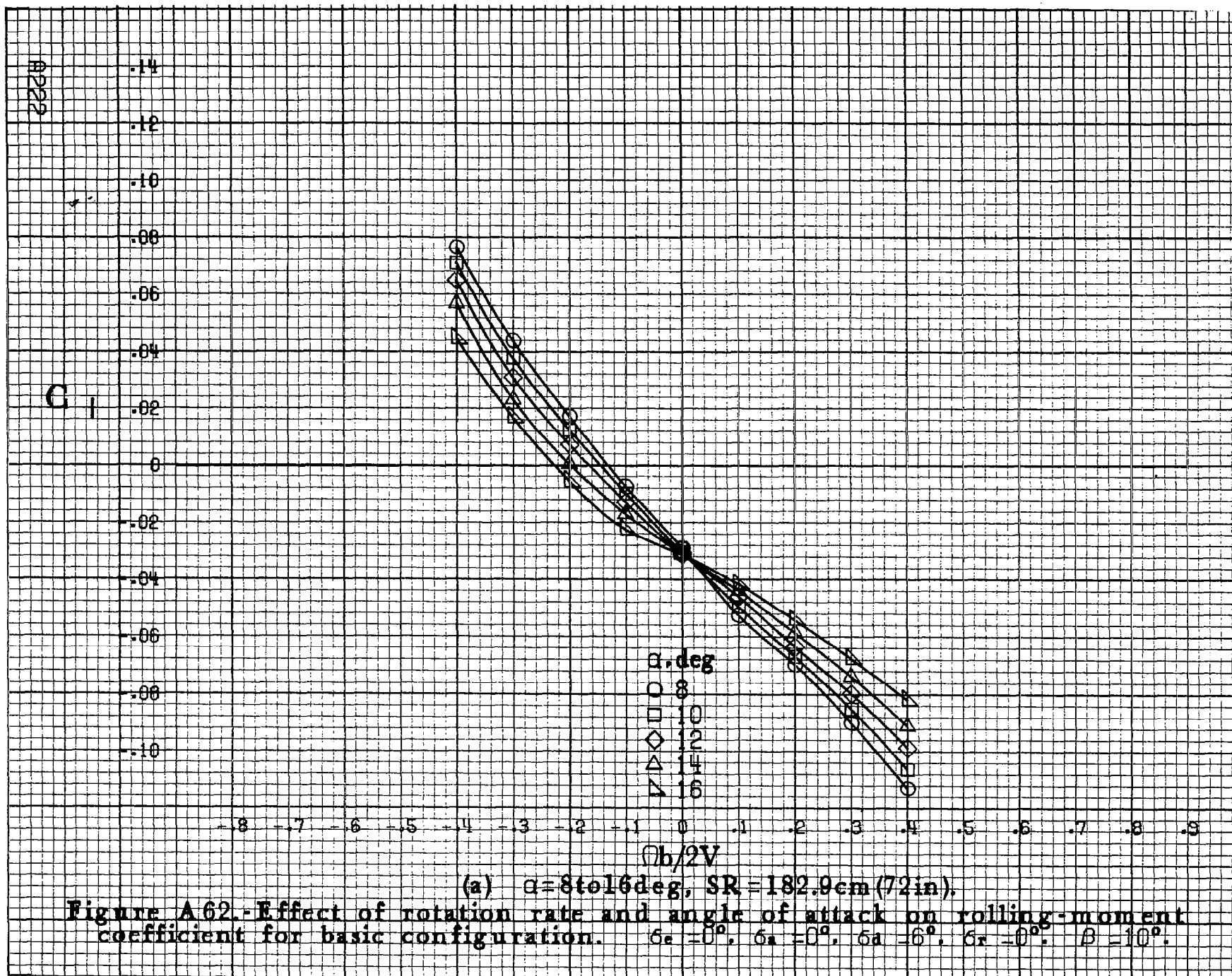
α, deg
○ 55
□ 60
◇ 70
△ 80
▽ 90

-8 -7 -6 -5 -4 -3 -2 -1 0 .1 .2 .3 .4 .5 .6 .7 .8 .9

$Ob/2V$

(d) $\alpha=55\text{to}90\text{deg}$, $SR=0$.
Figure A61.-Concluded.

A2221



C_1

.14
.12
.10
.08
.06
.04
.02
0
-.02
-.04
-.06
-.08
-.10

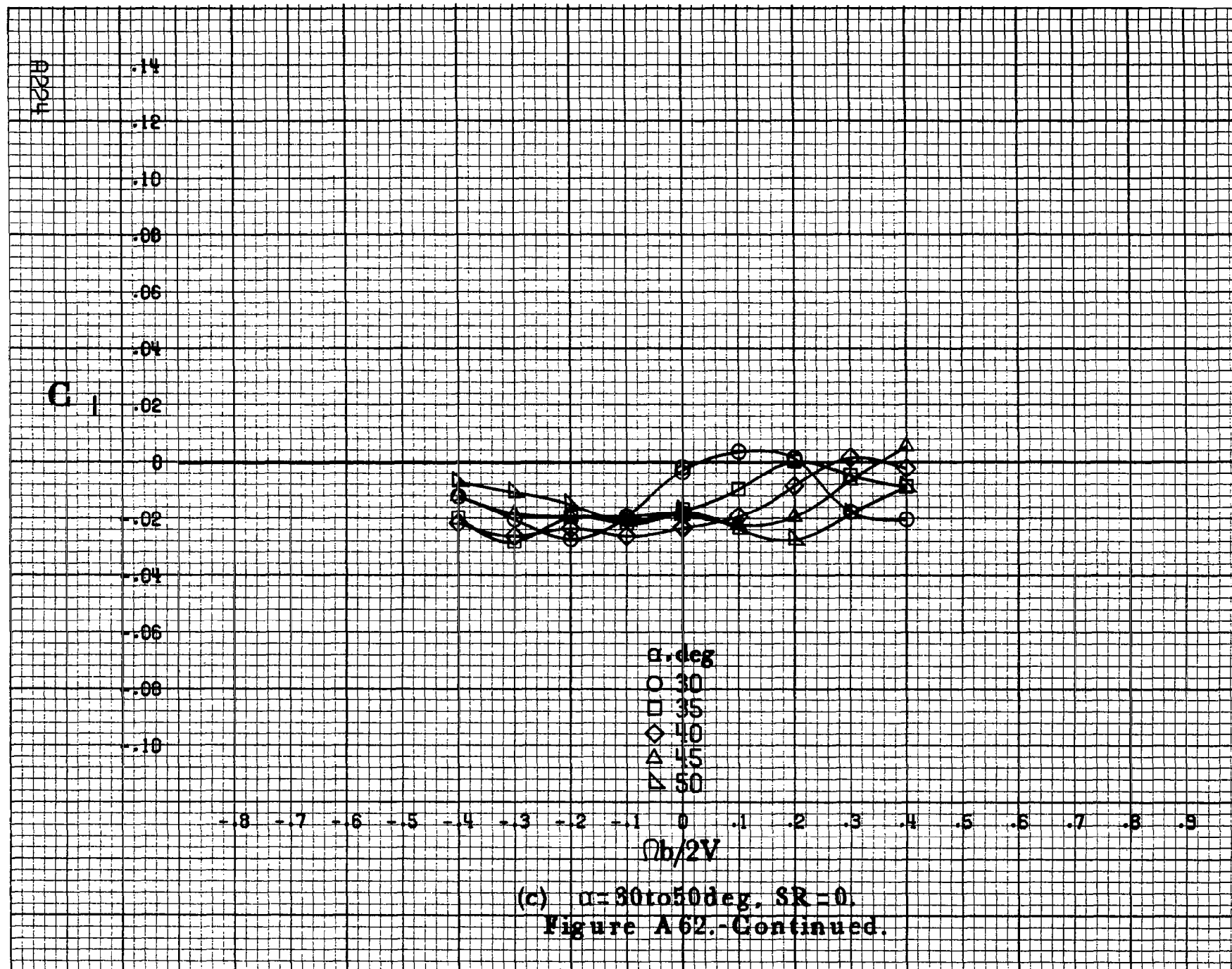
α, deg
○ 18
□ 20
◇ 25
△ 30
▽ 35

-8 -7 -6 -5 -4 -3 -2 -1 0 .1 .2 .3 .4 .5 .6 .7 .8 .9

$\Omega b/2V$

A223

(b) $\alpha = 18 \text{ to } 35 \text{ deg}$, $SR = 182.9 \text{ cm (72 in)}$.
Figure A 62.-Continued.



(c) $\alpha=30$ to 50° , $SR=0$.
Figure A62.-Continued.

C₁

.14
.12
.10
.08
.06
.04
.02
0
-.02
-.04
-.06
-.08
-.10

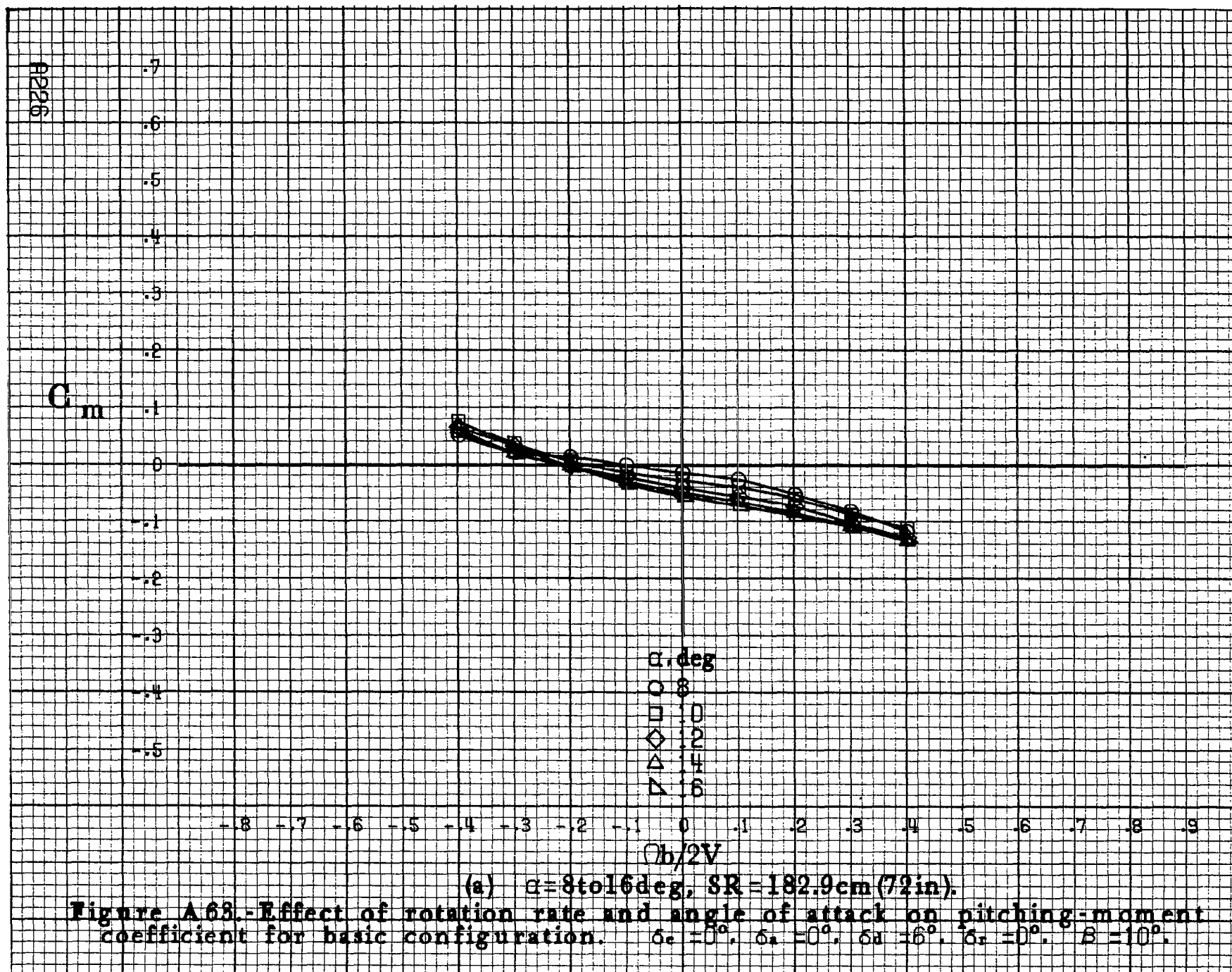
+8 -7 -6 -5 -4 -3 -2 -1 0 .1 .2 .3 .4 .5 .6 .7 .8 .9

α, deg
○ 55
□ 60
◇ 70
△ 80
▽ 90

$\Omega h/2V$

(d) $\alpha=55$ to 90 deg, $SR=0$.
Figure A62.-Concluded.

82251



C_m

0.6
0.5
0.4
0.3
0.2
0.1
0
-0.1
-0.2
-0.3
-0.4
-0.5
-0.6

-0.8 -0.7 -0.6 -0.5 -0.4 -0.3 -0.2 -0.1 0 0.1 0.2 0.3 0.4 0.5 0.6 0.7 0.8 0.9

α, deg
○ 18
□ 20
◇ 25
△ 30
▽ 35

$b/2V$

(b) $\alpha = 18 \text{ to } 35 \text{ deg}$, $SR = 182.9 \text{ cm (72 in)}$.

Figure A68.-Continued.

10227

A9228

 C_m

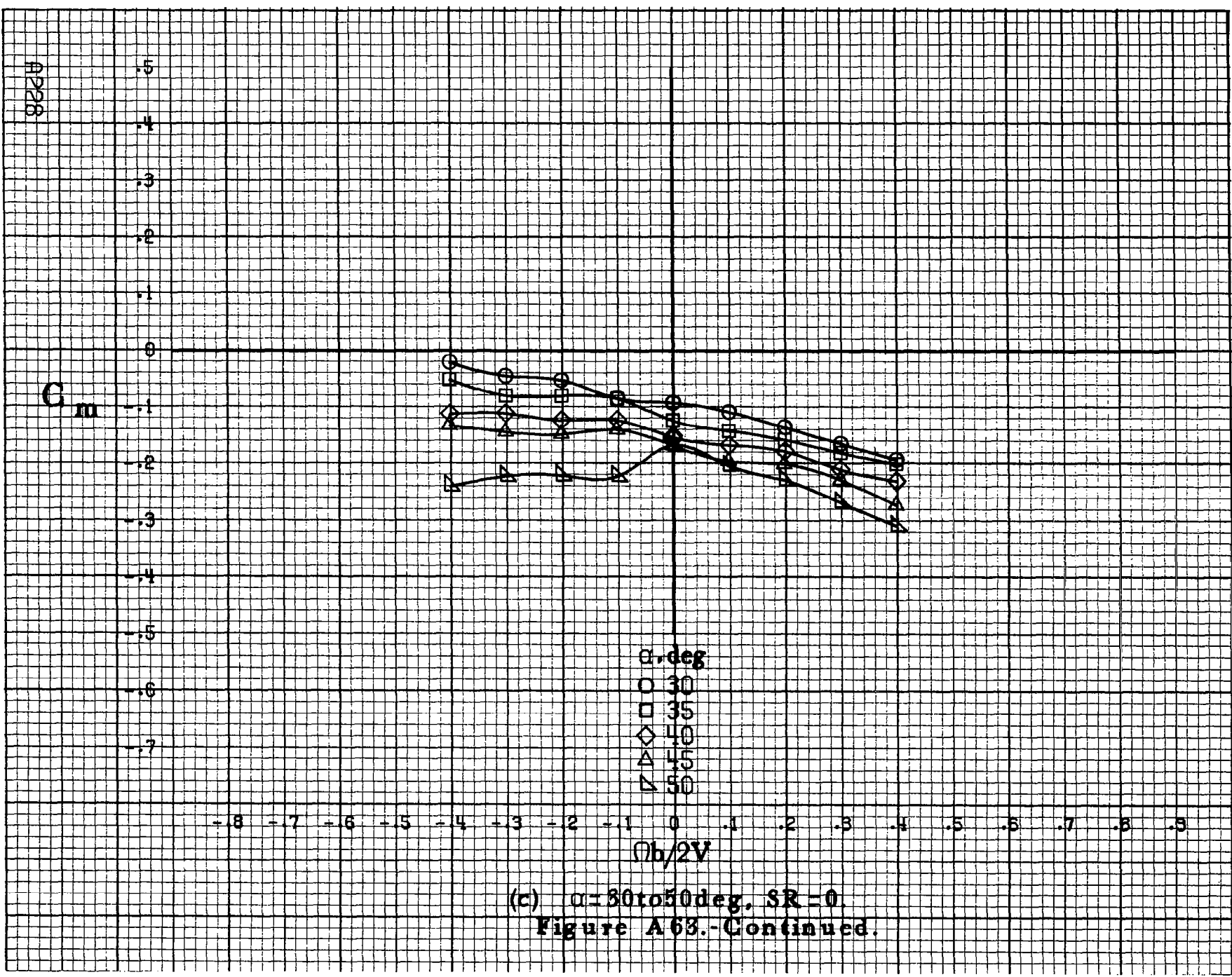
.5
.4
.3
.2
.1
0
-.1
-.2
-.3
-.4
-.5
-.6
-.7

-8 -7 -6 -5 -4 -3 -2 -1 0 .1 .2 .3 .4 .5 .6 .7 .8 .9

α, deg
○ 30
□ 35
◇ 40
△ 45
▽ 50

$nb/2V$

(c) $\alpha=30$ to 50 deg, $SR=0$.
Figure A63.-Continued.



C_m

.2
.1
0
-.1
-.2
-.3
-.4
-.5
-.6
-.7
-.8
-.9
-1.0

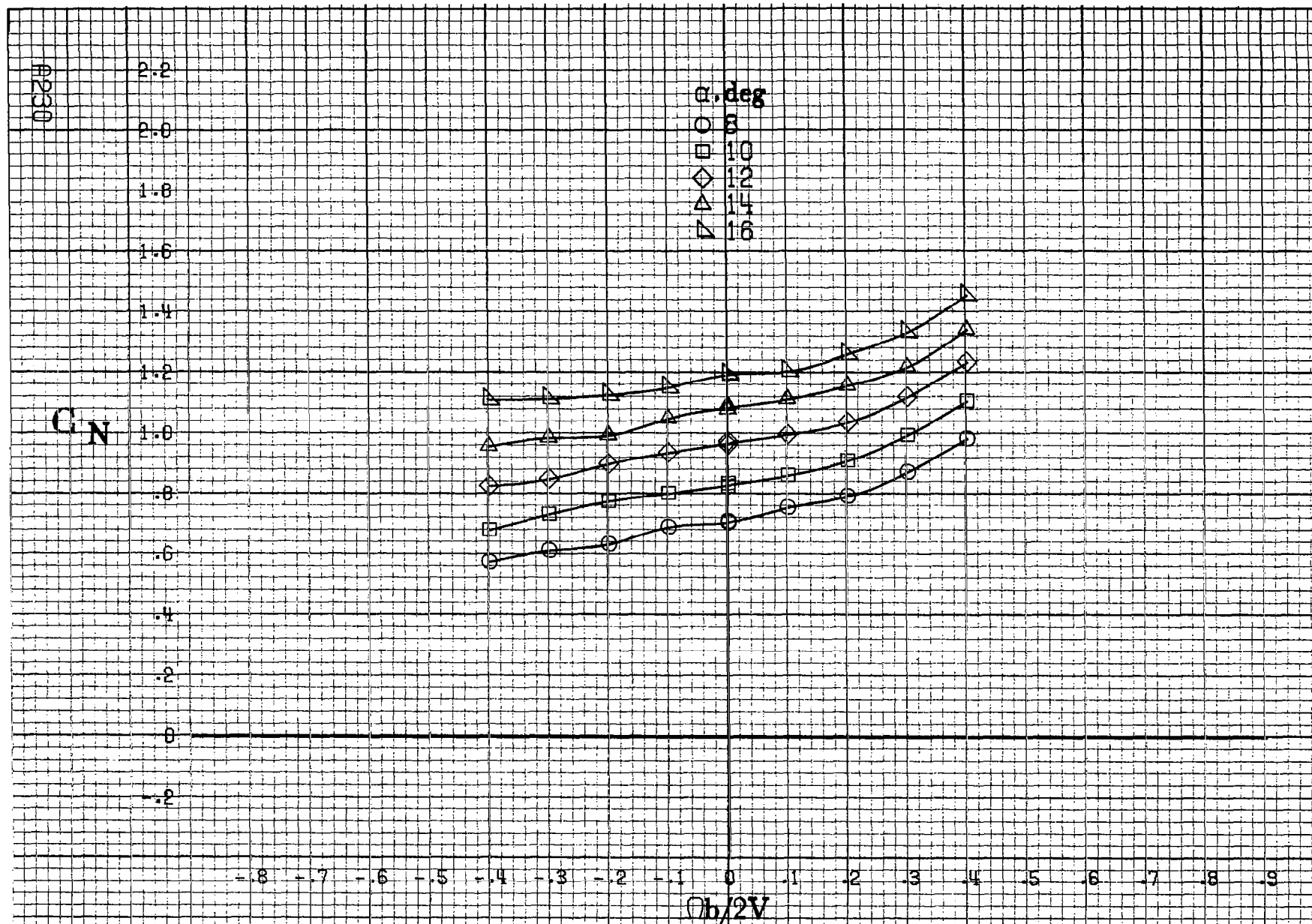
α, deg
○ 55
□ 60
◇ 70
△ 80
▽ 90

$b/2V$

-8 -7 -6 -5 -4 -3 -2 -1 0 .1 .2 .3 .4 .5 .6 .7 .8 .9

(d) $\alpha=55\text{ to }90\text{ deg, SR}=0.$
Figure A63.-Concluded.

A229



(a) $\alpha = 8$ to 16 deg, $SR = 182.9$ cm (72 in).

Figure A64.-Effect of rotation rate and angle of attack on normal-force coefficient for basic configuration. $\delta_e = 0^\circ$, $\delta_a = 0^\circ$, $\delta_d = 6^\circ$, $\delta_r = 0^\circ$, $\beta = 10^\circ$.

C_N

α, deg

- 18
- 20
- ◇ 25
- △ 30
- ▽ 35

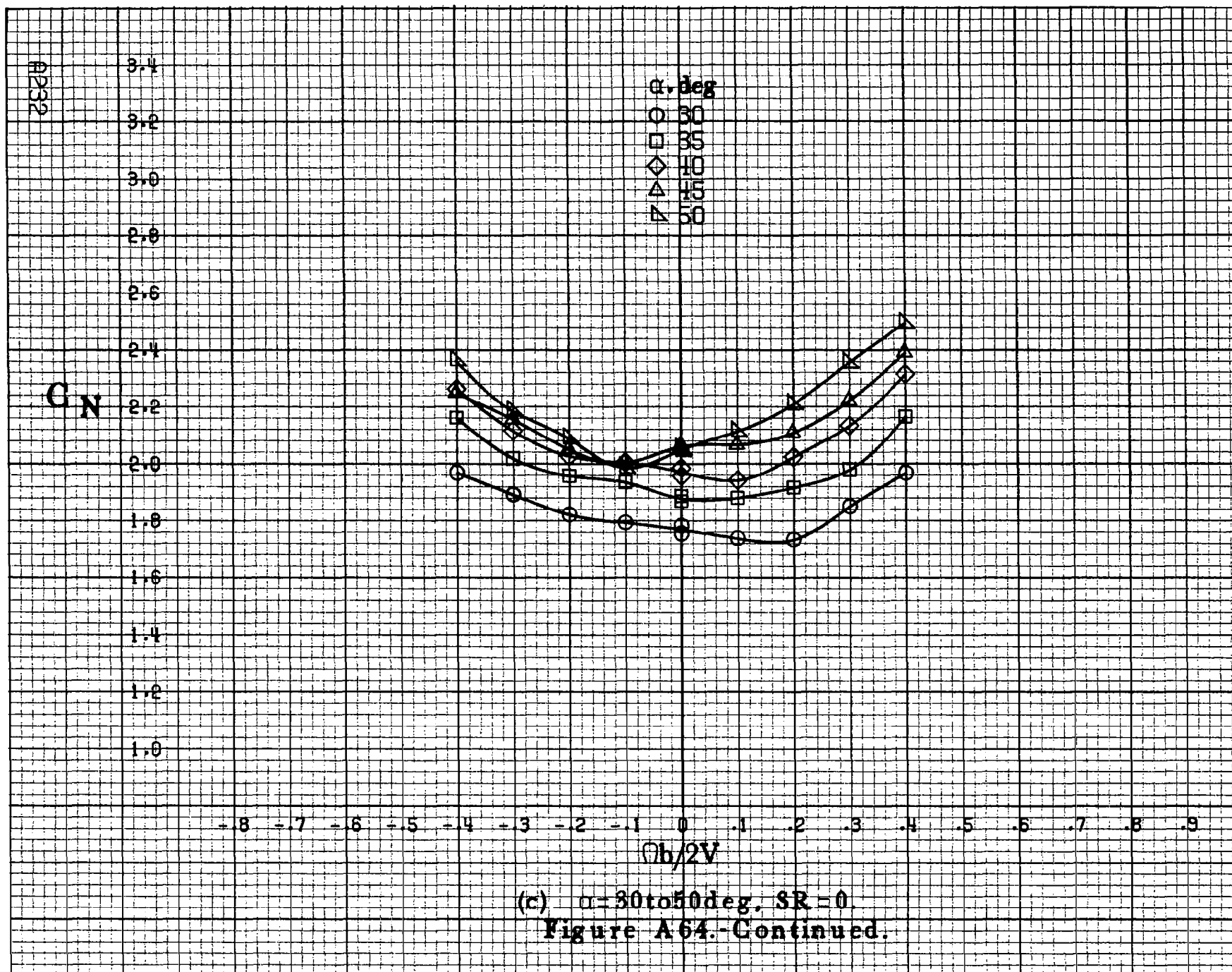
-0.8 -0.7 -0.6 -0.5 -0.4 -0.3 -0.2 -0.1 0 .1 .2 .3 .4 .5 .6 .7 .8 .9

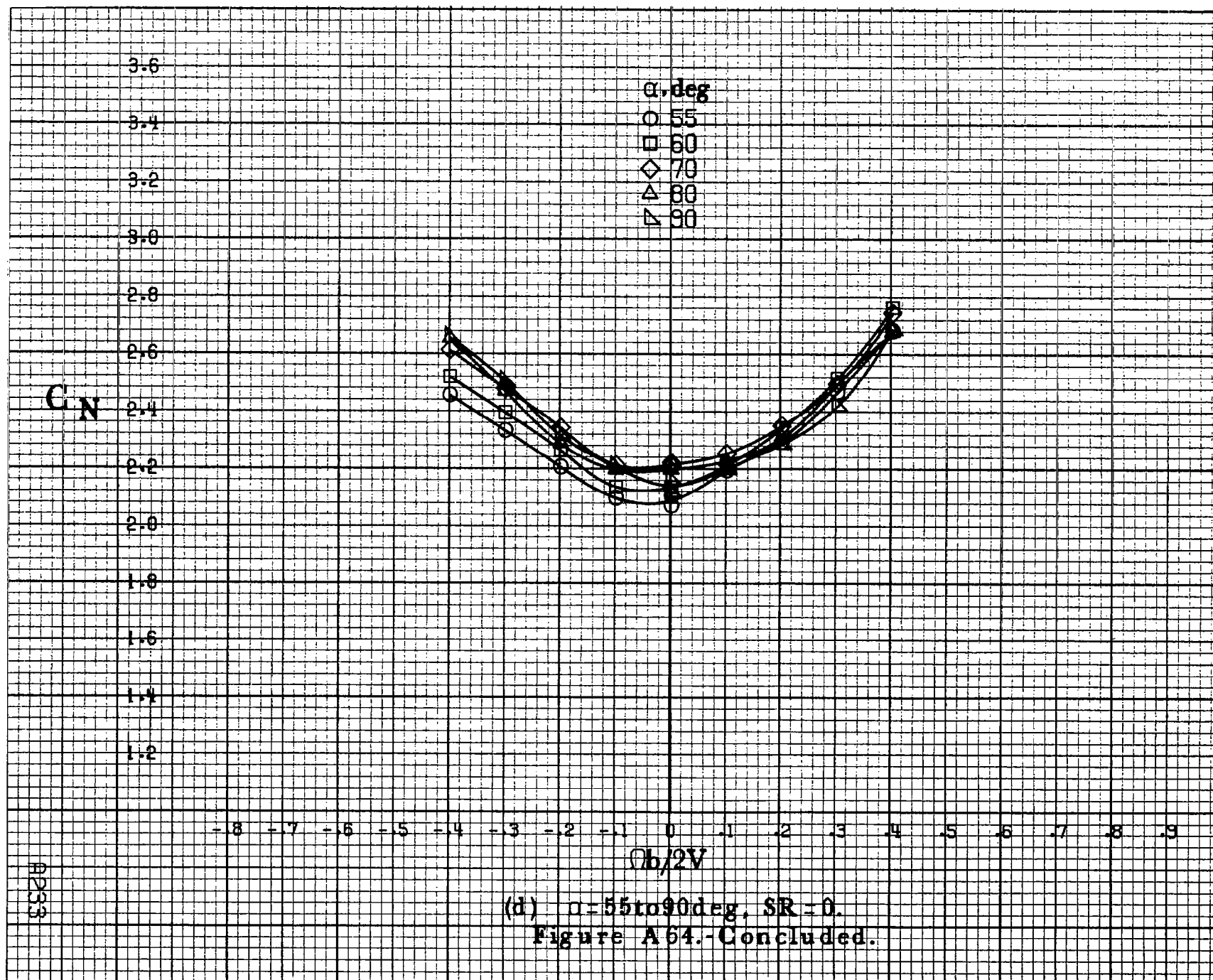
$Ob/2V$

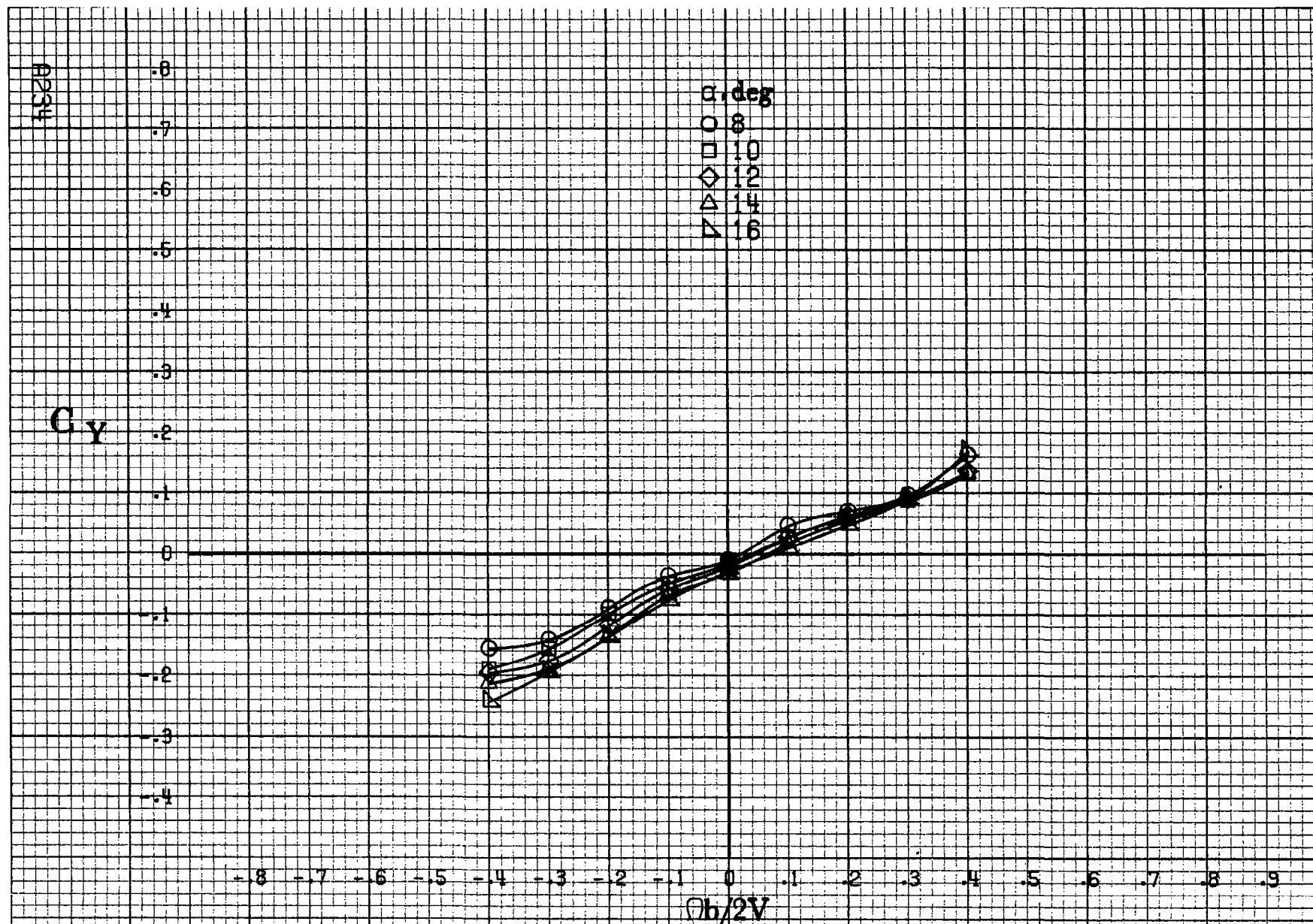
(b) $\alpha = 18 \text{ to } 35 \text{ deg}$, $SR = 182.9 \text{ cm (72 in)}$.

Figure A 64.-Continued.

#231

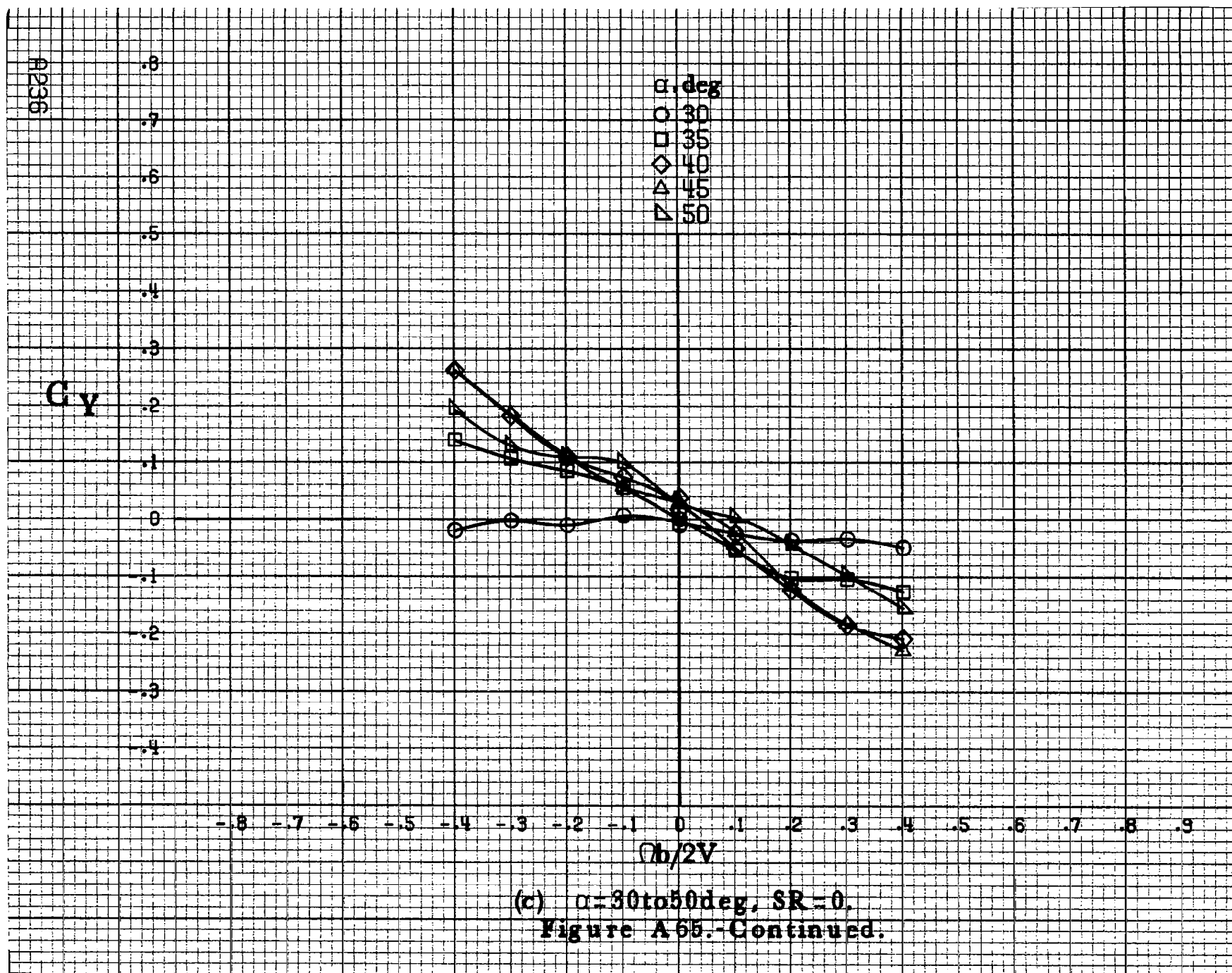






(a) $\alpha = 8 \text{ to } 16^\circ$, $SR = 182.9 \text{ cm (72 in.)}$.

Figure A65.-Effect of rotation rate and angle of attack on side-force coefficient for basic configuration. $\delta_c = 0^\circ$, $\delta_a = 0^\circ$, $\delta_d = 6^\circ$, $\delta_r = 0^\circ$, $\beta = 10^\circ$.



C_y

α, deg

○ 55

□ 60

◇ 70

△ 80

▽ 90

.8
.7
.6
.5
.4
.3
.2
.1
0
-.1
-.2
-.3
-.4

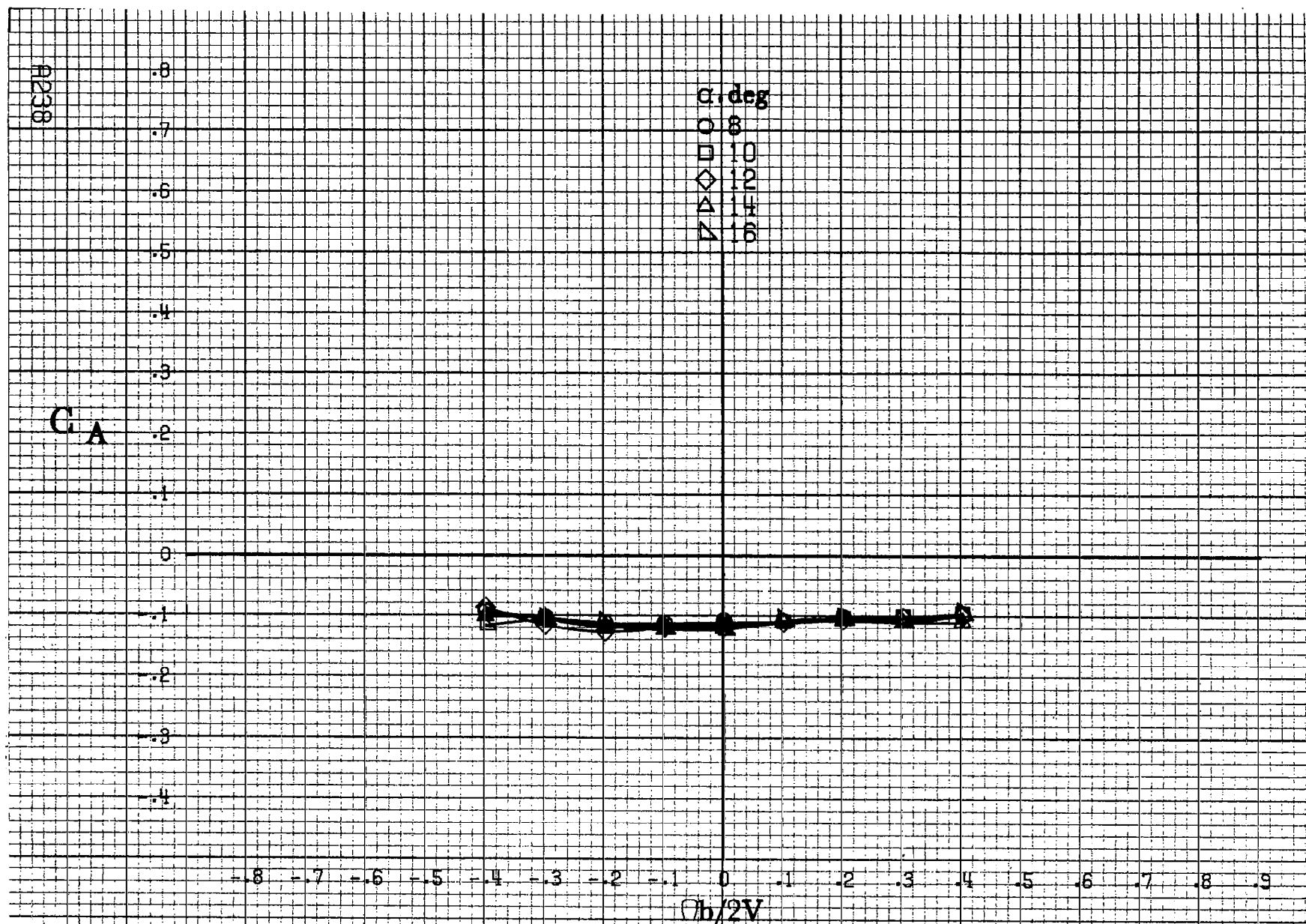
-8 -7 -6 -5 -4 -3 -2 -1 0 .1 .2 .3 .4 .5 .6 .7 .8 .9

$Ob/2V$

(d) $\alpha=55\text{to}90\text{deg}$, $SR=0$.

Figure A65.-Concluded.

#237



(a) $\alpha=8\text{ to }16\text{deg}$, $SR=182.9\text{cm}(72\text{in})$.

Figure A66.- Effect of rotation rate and angle of attack on axial-force coefficient for basic configuration. $\delta_e=0^\circ$, $\delta_a=0^\circ$, $\delta\alpha=6^\circ$, $\delta\tau=0^\circ$, $\beta=10^\circ$.

C_A

.8
.7
.6
.5
.4
.3
.2
.1
0
-.1
-.2
-.3
-.4

α , deg
○ 18
□ 20
◇ 25
△ 30
▽ 35

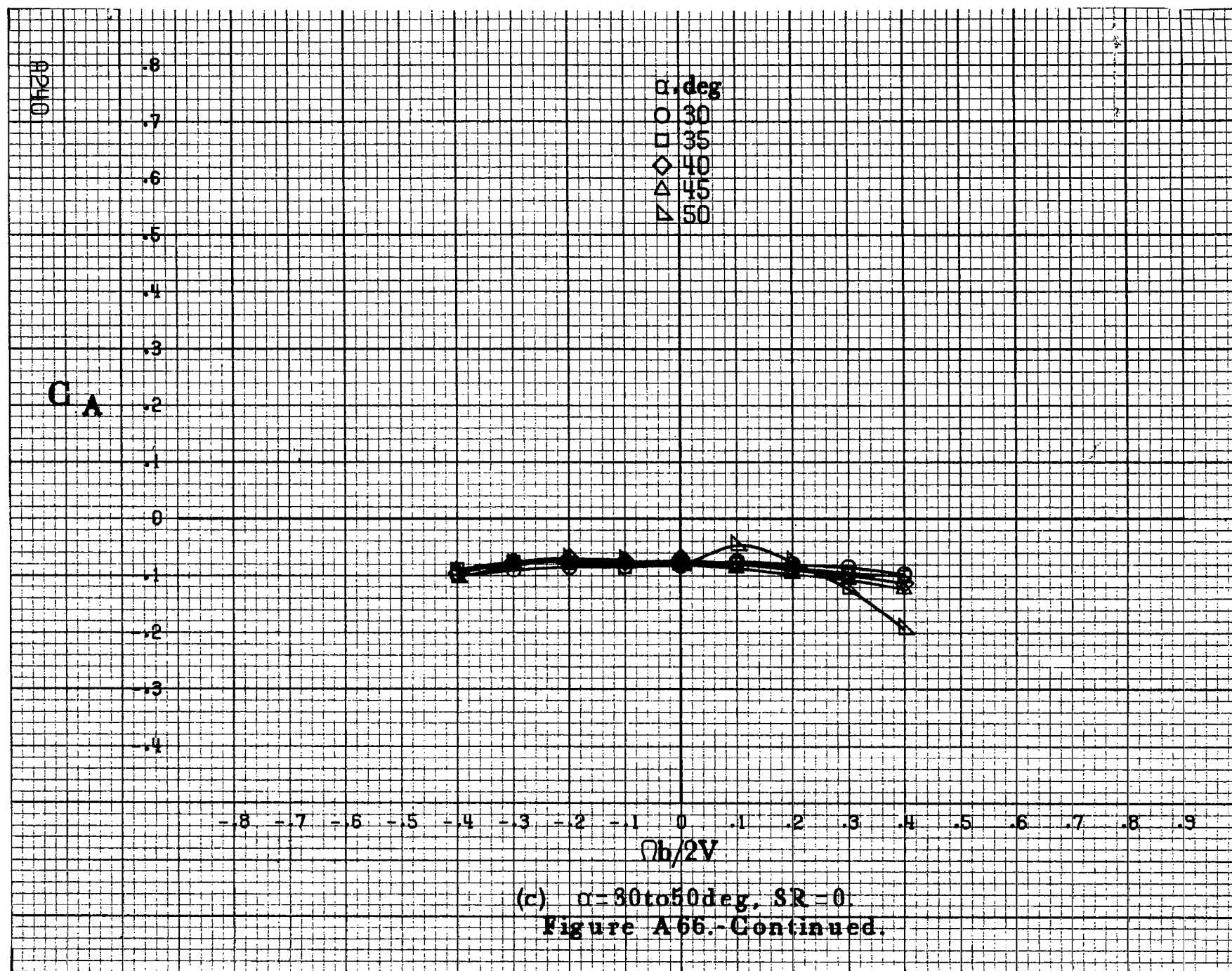
-.8 -.7 -.6 -.5 -.4 -.3 -.2 -.1 0 .1 .2 .3 .4 .5 .6 .7 .8 .9

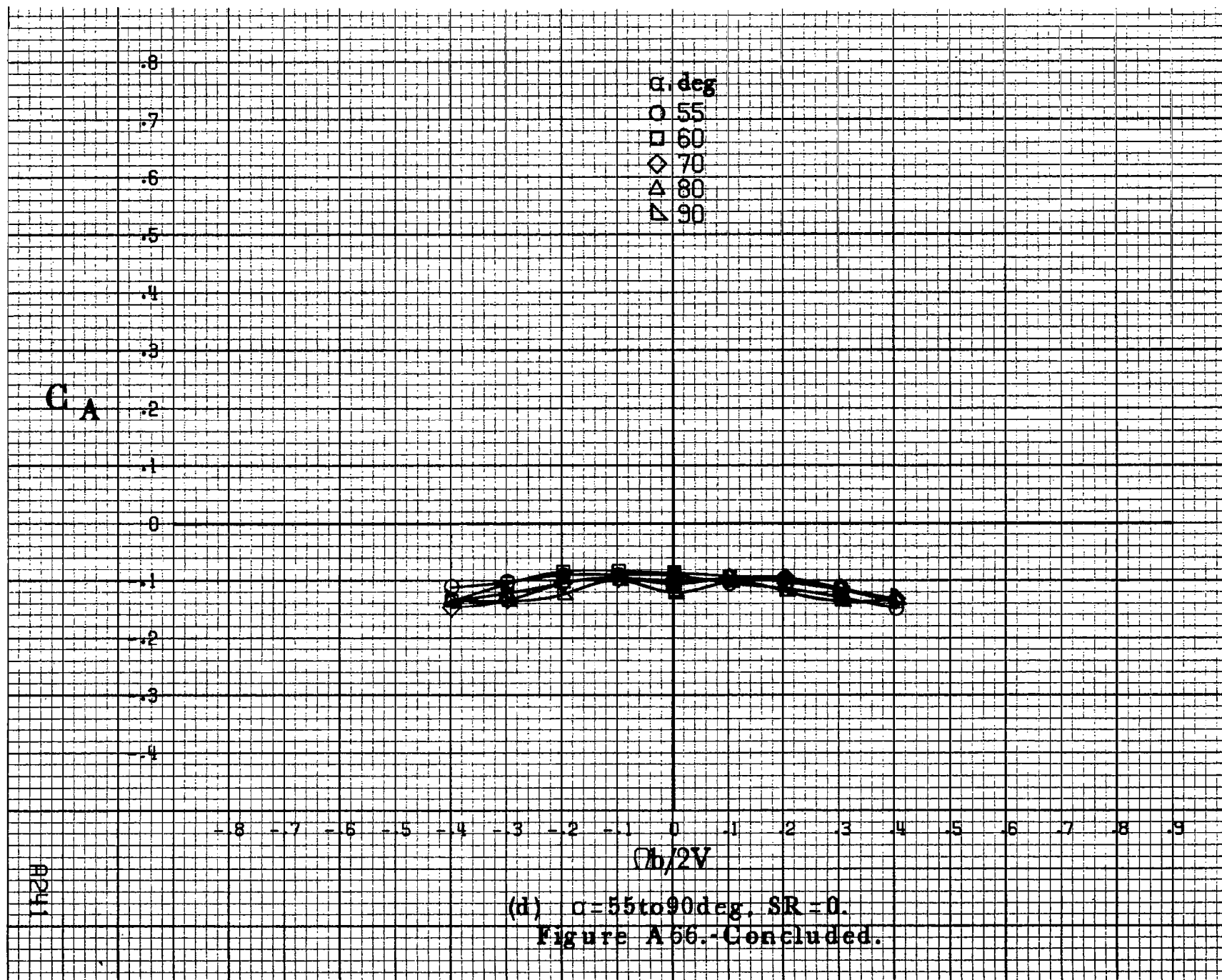
$Ob/2V$

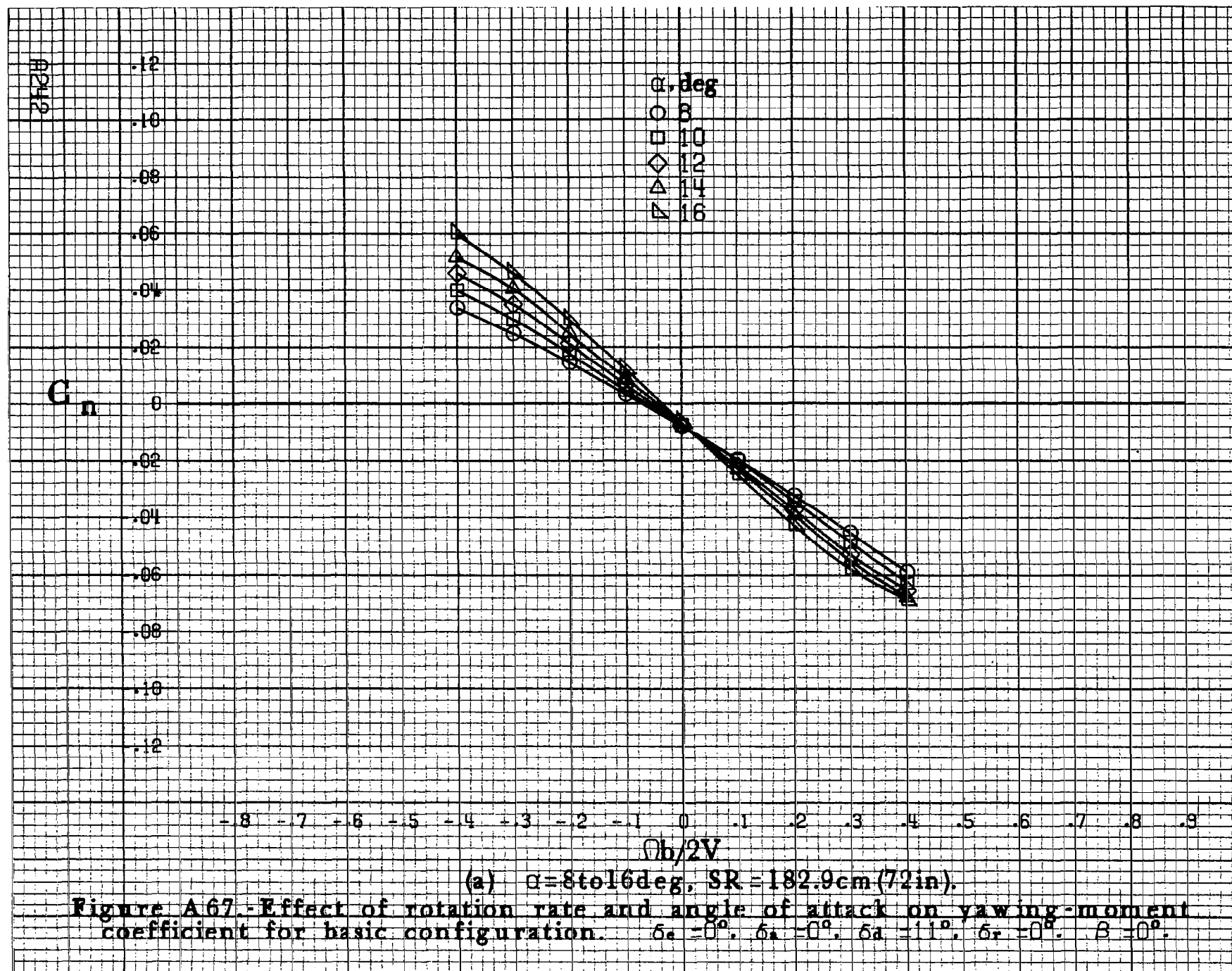
(b) $\alpha=18$ to 35 deg. $SR=182.9$ cm (72 in).

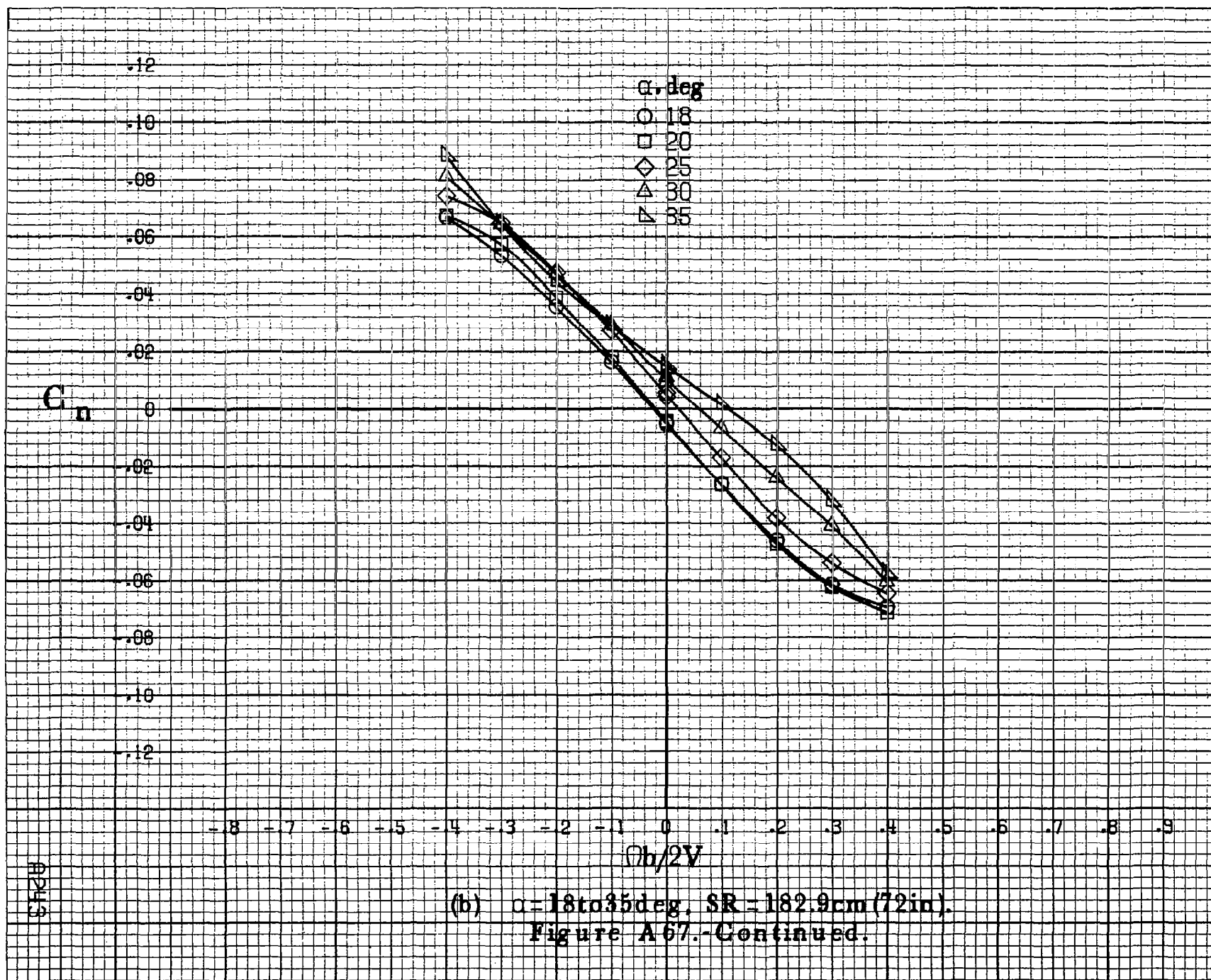
Figure A 66.-Continued.

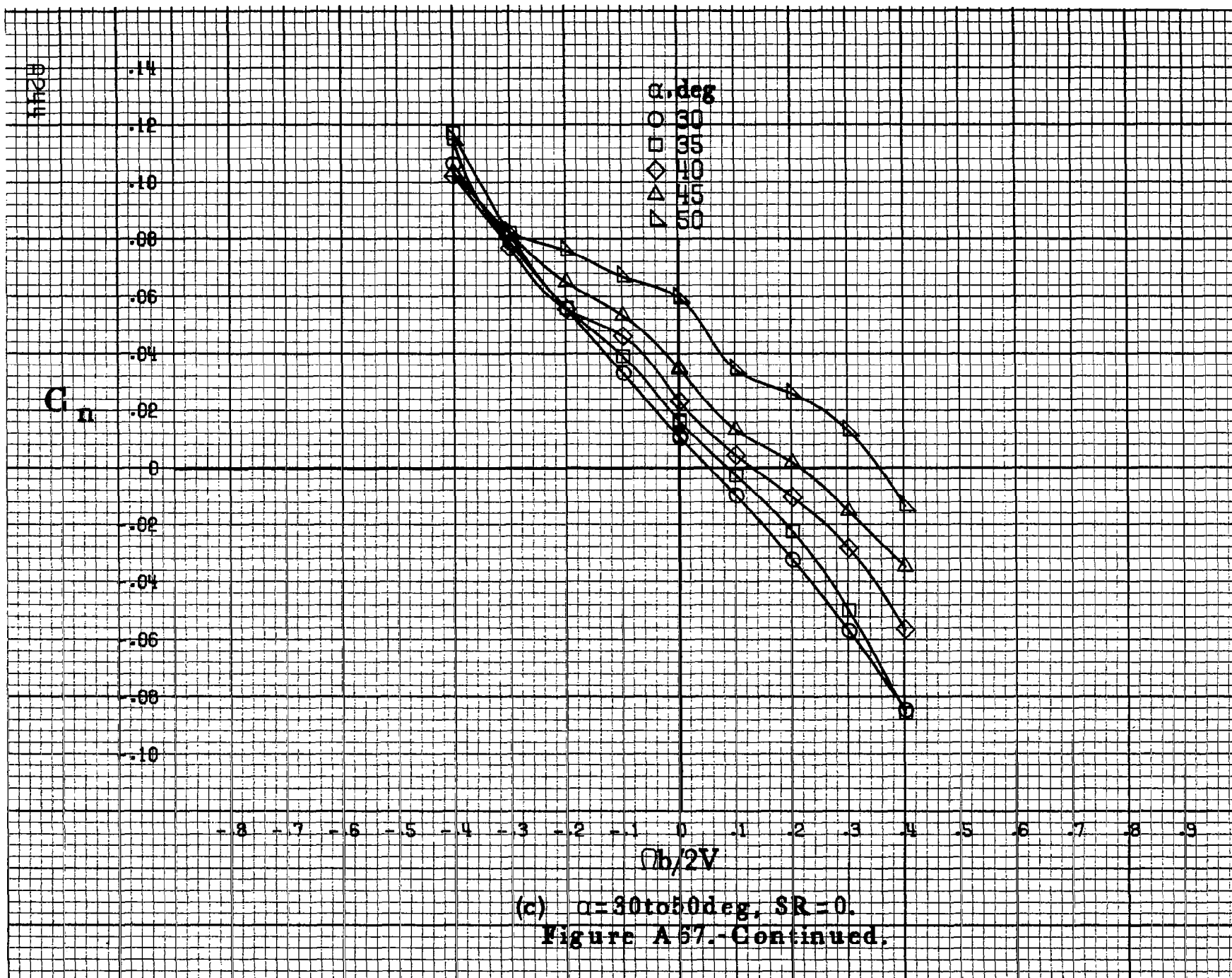
0259











C_n

α, deg
 ○ 55
 □ 60
 ◇ 70
 ▲ 80
 △ 90

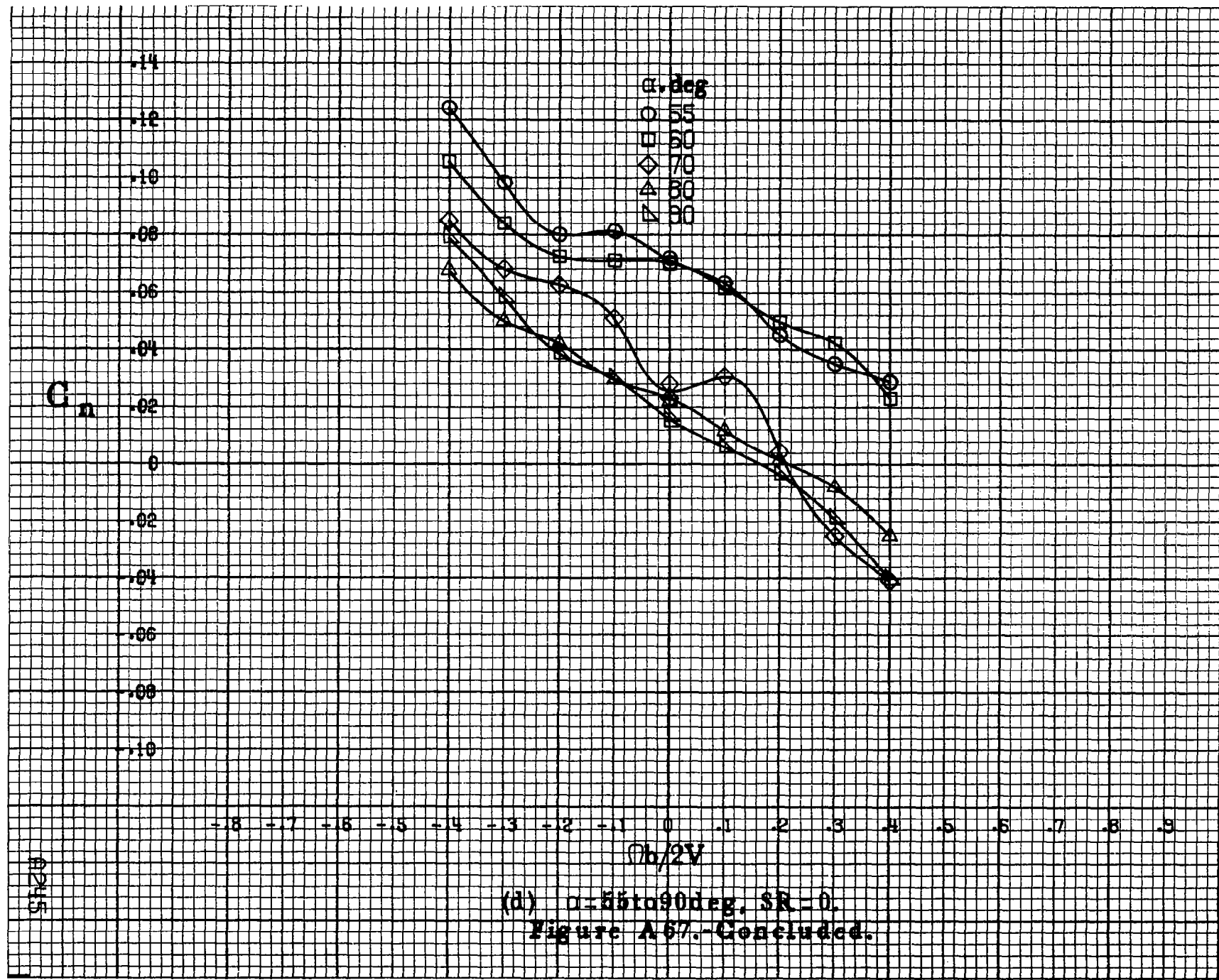
.14
.12
.10
.08
.06
.04
0
.02
.04
.06
.08
.10

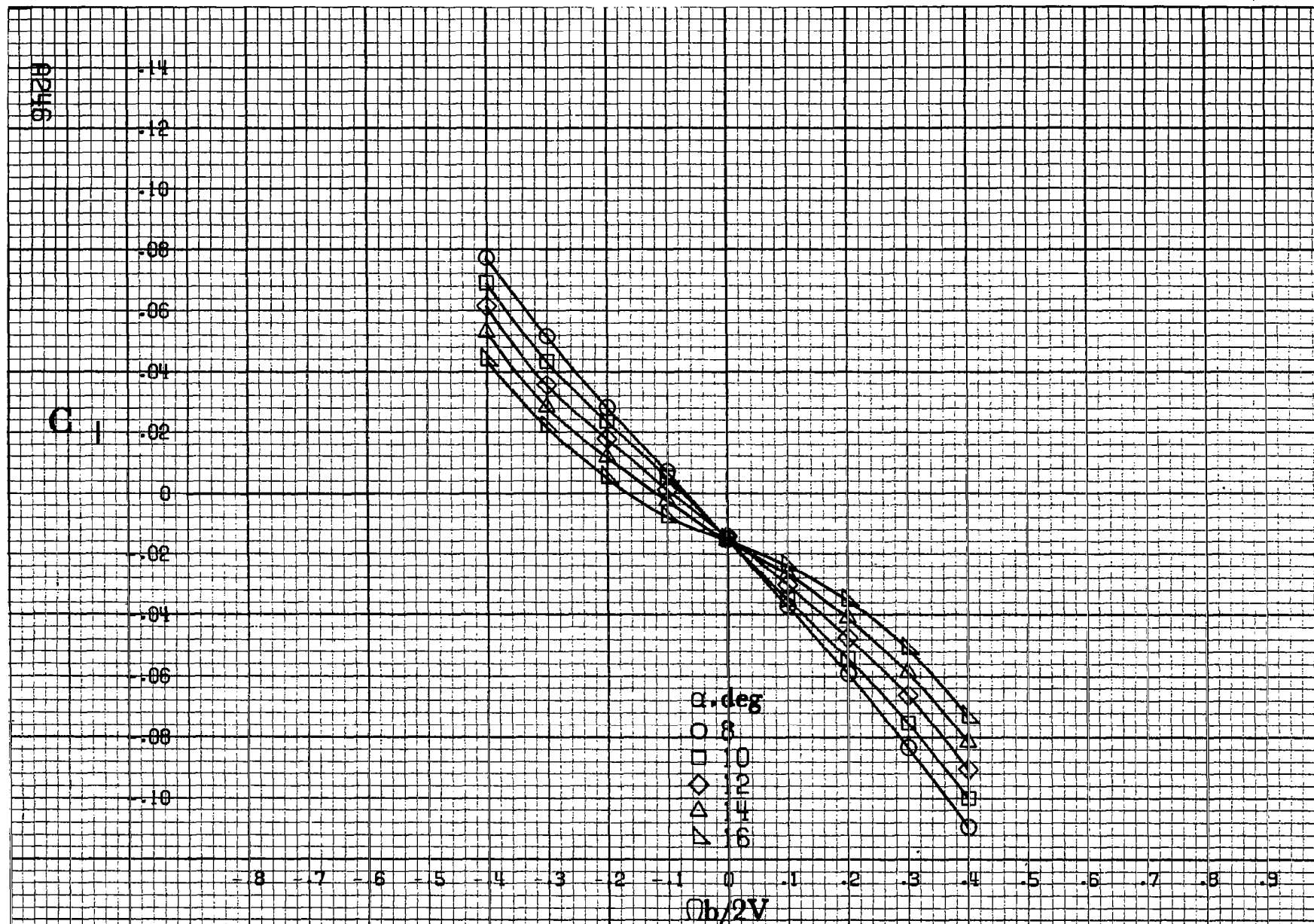
-8 -7 -6 -5 -4 -3 -2 -1 0 -1 -2 -3 -4 .5 .6 .7 .8 .9

$b/2V$

6245

(d) $\alpha=55$ to 90 deg, $SR=0$.
 Figure A67.-Concluded.





(a) $\alpha = 8$ to 16 deg, $SR = 182.9$ cm (72 in).

Figure A.68.- Effect of rotation rate and angle of attack on rolling-moment coefficient for basic configuration. $\delta_c = 0^\circ$, $\delta_a = 0^\circ$, $\delta_d = 11^\circ$, $\delta_r = 0^\circ$, $\delta = 0^\circ$.

C_1

-14
-12
-10
-08
-06
-04
-02
0
-02
-04
-06
-08
-10

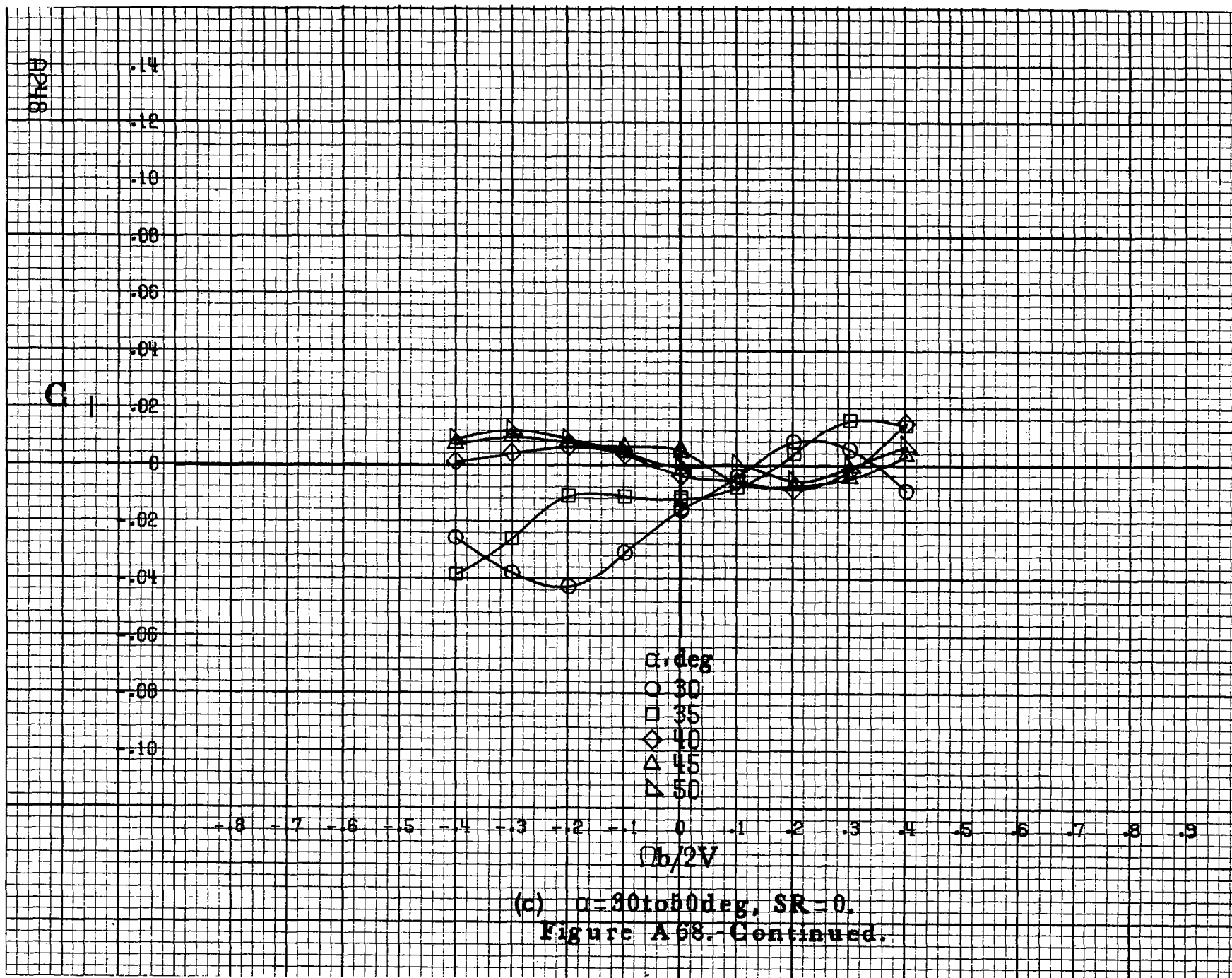
α, deg
○ 18
□ 20
◇ 25
△ 30
▽ 35

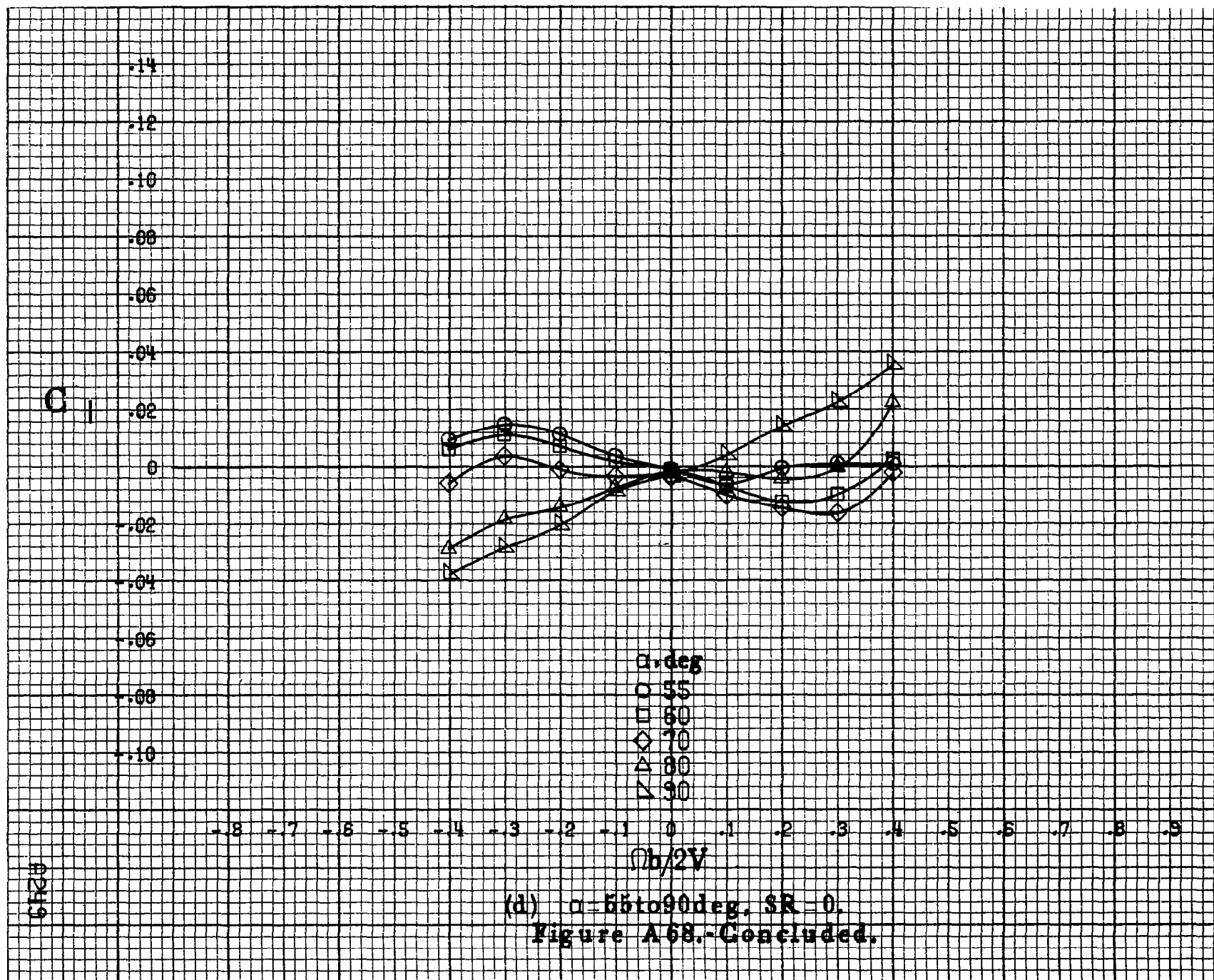
-8 -7 -6 -5 -4 -3 -2 -1 0 .1 .2 .3 .4 .5 .6 .7 .8 .9

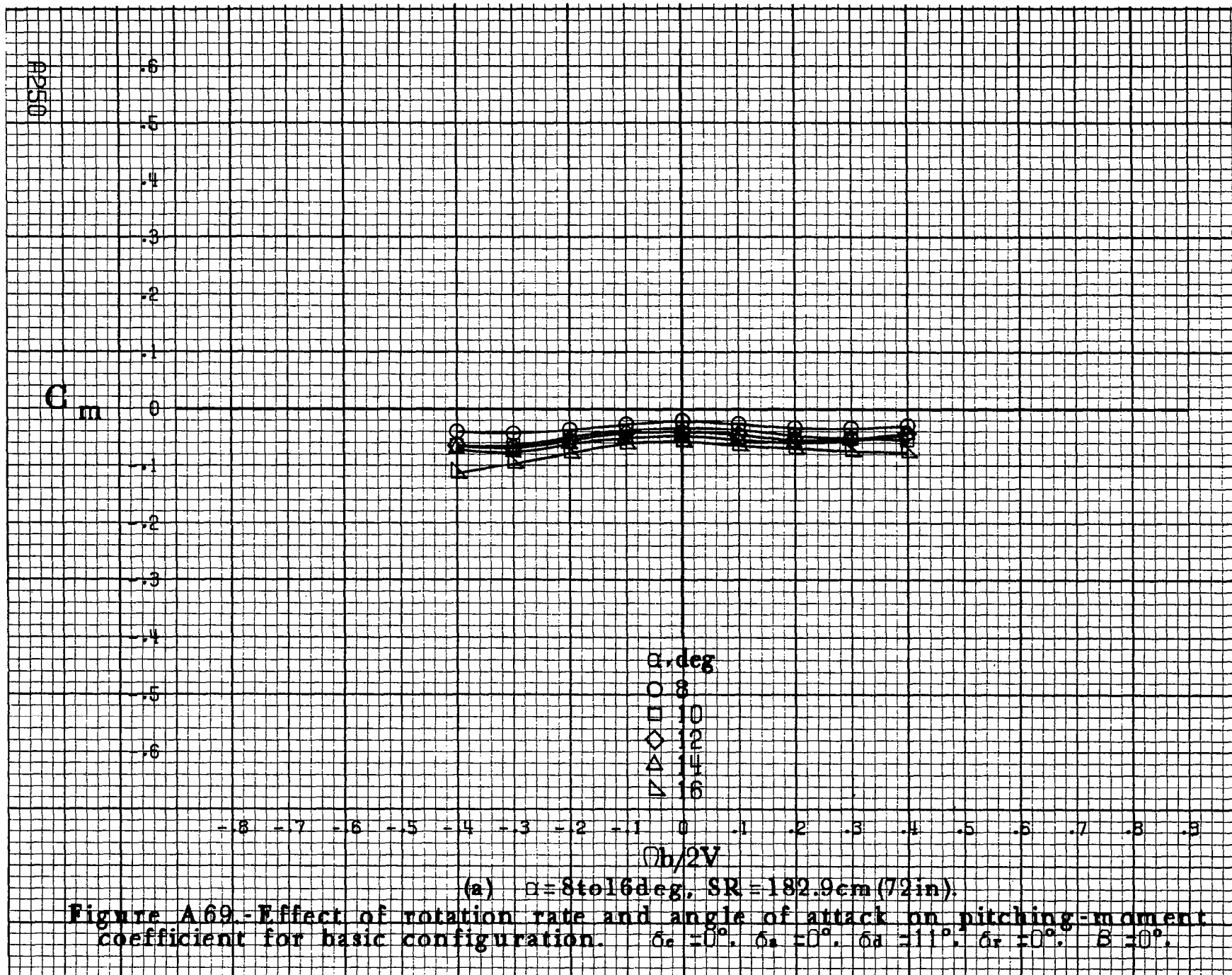
$\phi b/2V$

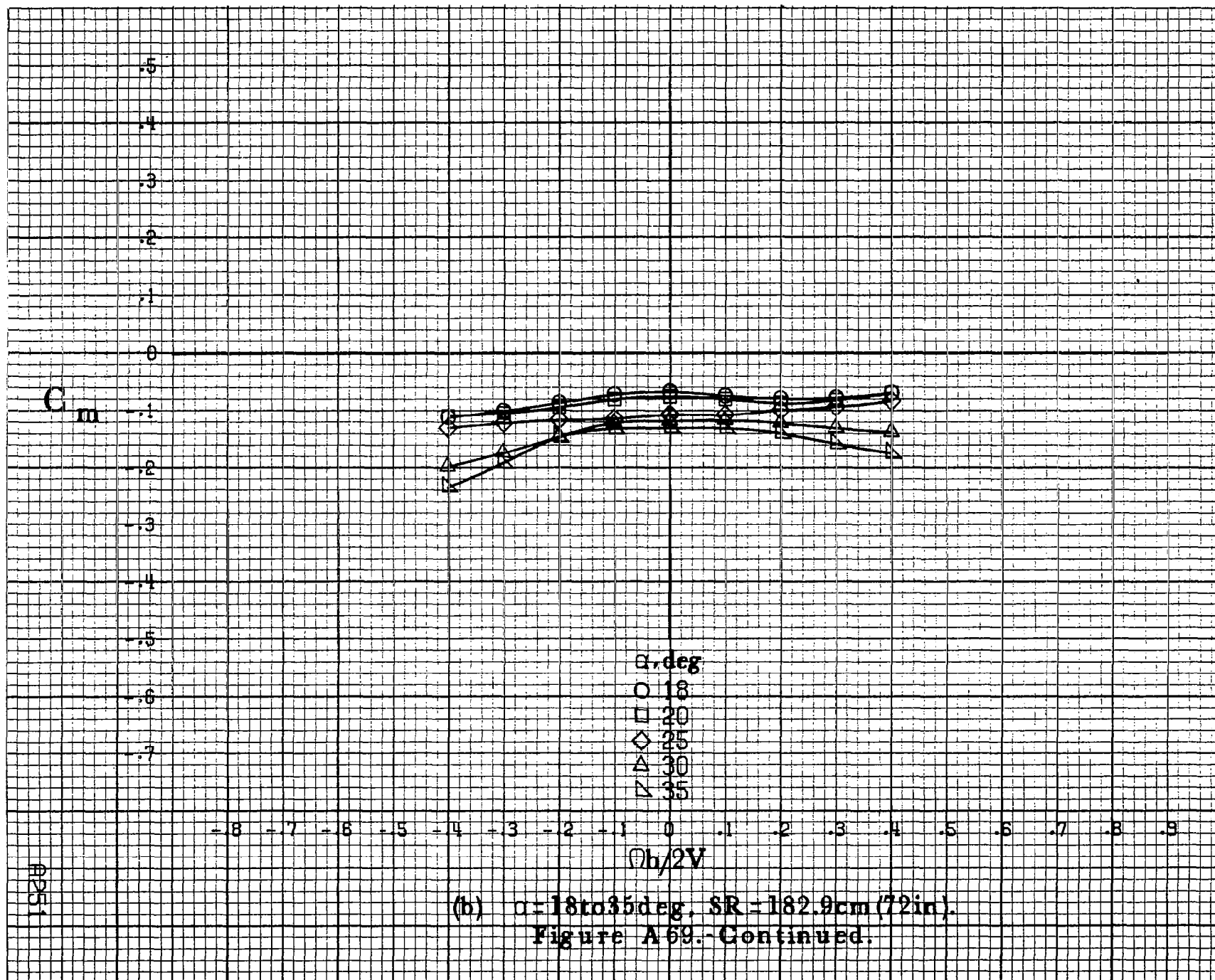
8247

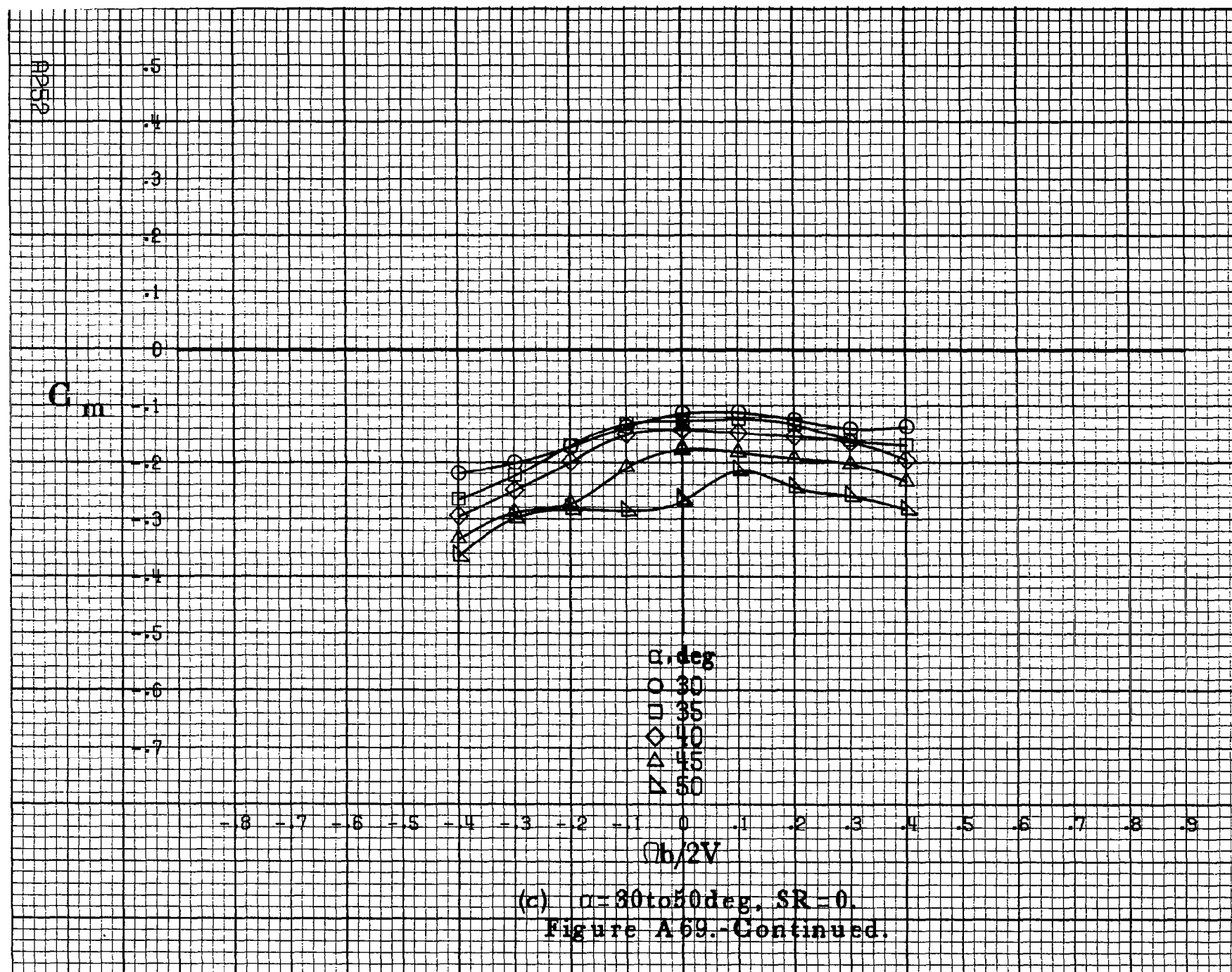
(b) $\alpha = 18 \text{ to } 35 \text{ deg}$, $SR = 182.9 \text{ cm (72 in)}$.
Figure A68.-Continued.











C_m

.3
.2
.1
0
-.1
-.2
-.3
-.4
-.5
-.6
-.7
-.8
-.9

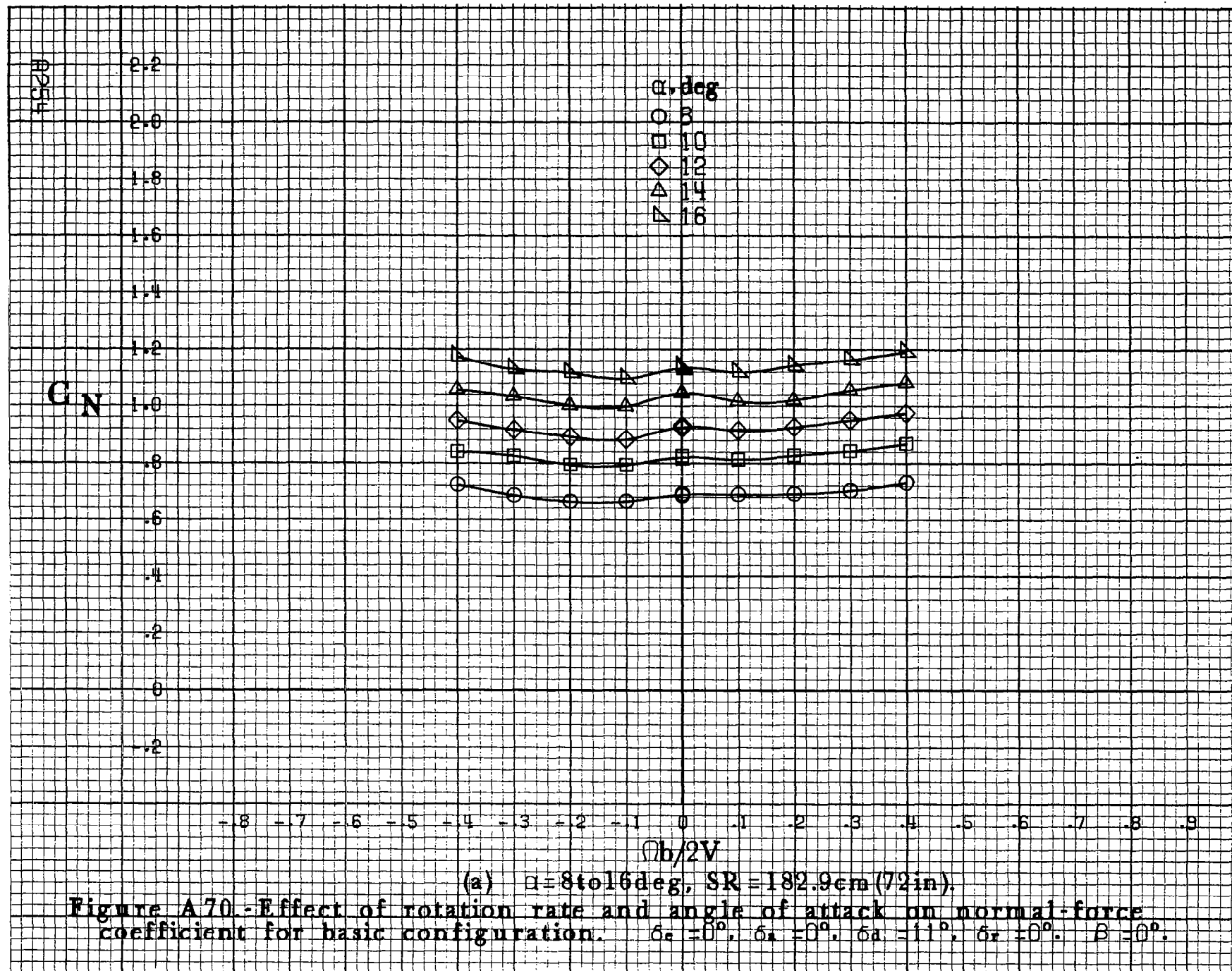
-.8 -.7 -.6 -.5 -.4 -.3 -.2 -.1 0 .1 .2 .3 .4 .5 .6 .7 .8 .9

α, deg
○ 55
□ 60
◇ 70
△ 80
▽ 90

$\Omega b/2V$

(d) $\alpha=55$ to 90 deg, $SR=0$.
Figure A69.-Concluded.

A253



C_N

α, deg

- 18
- 20
- ◇ 25
- △ 30
- ▽ 35

$\phi h/2V$

(b) $\alpha = 18 \text{ to } 35 \text{ deg}$, $SR = 182.9 \text{ cm (72 in)}$.
Figure A70.-Continued.

AP255

9256

C_N

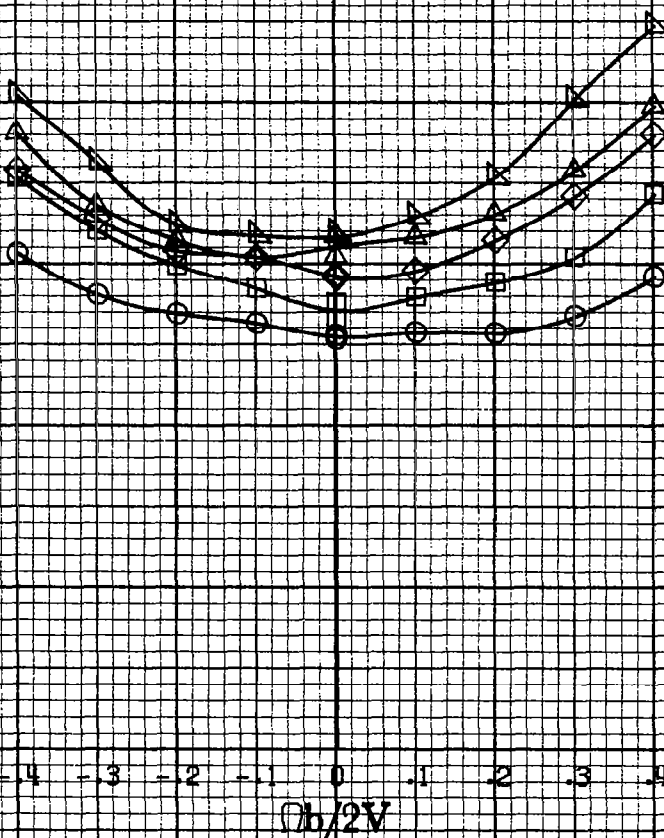
α, deg
 ○ 30
 □ 35
 ◇ 40
 △ 45
 ▽ 50

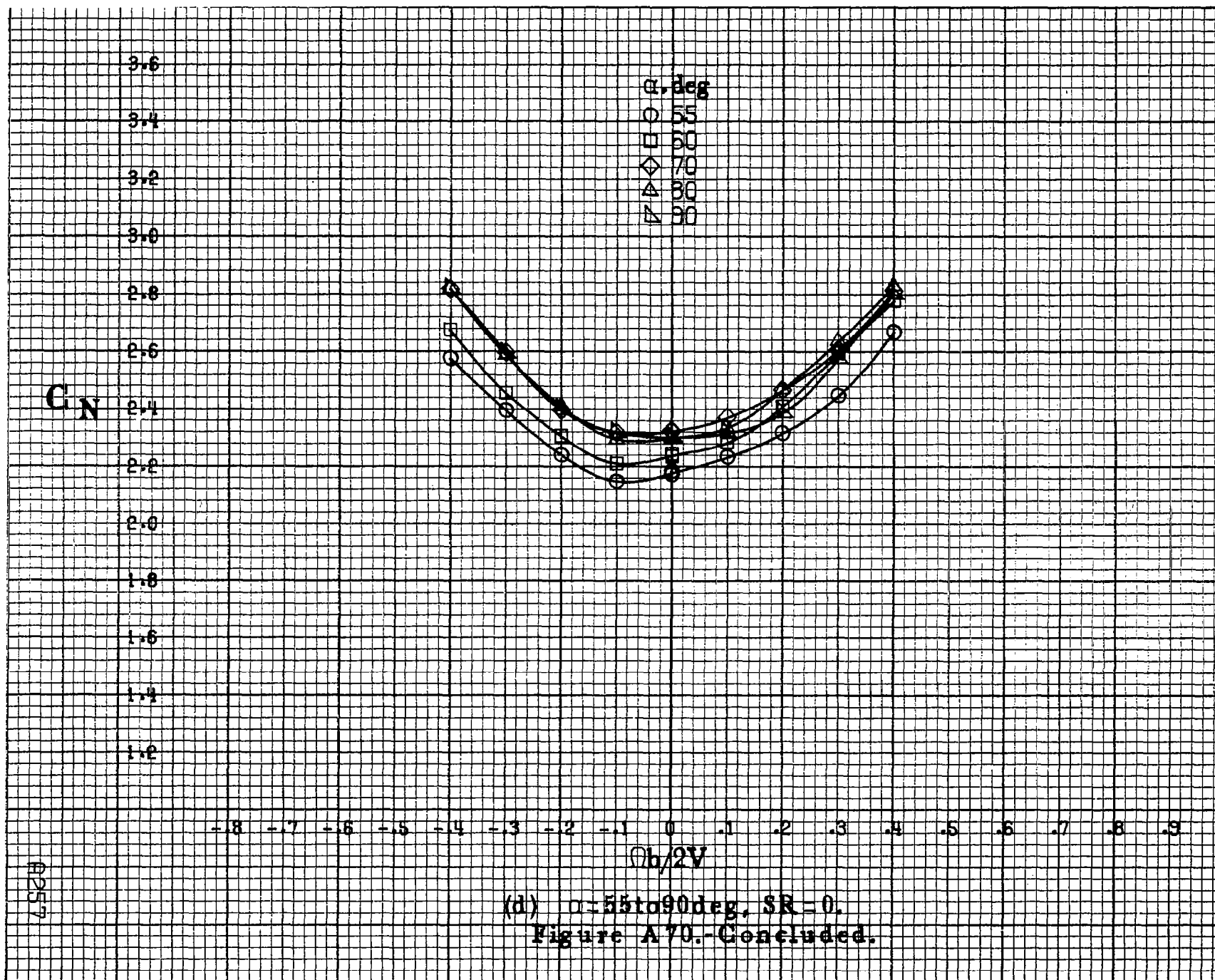
3.4
3.2
3.0
2.8
2.6
2.4
2.2
2.0
1.8
1.6
1.4
1.2
1.0

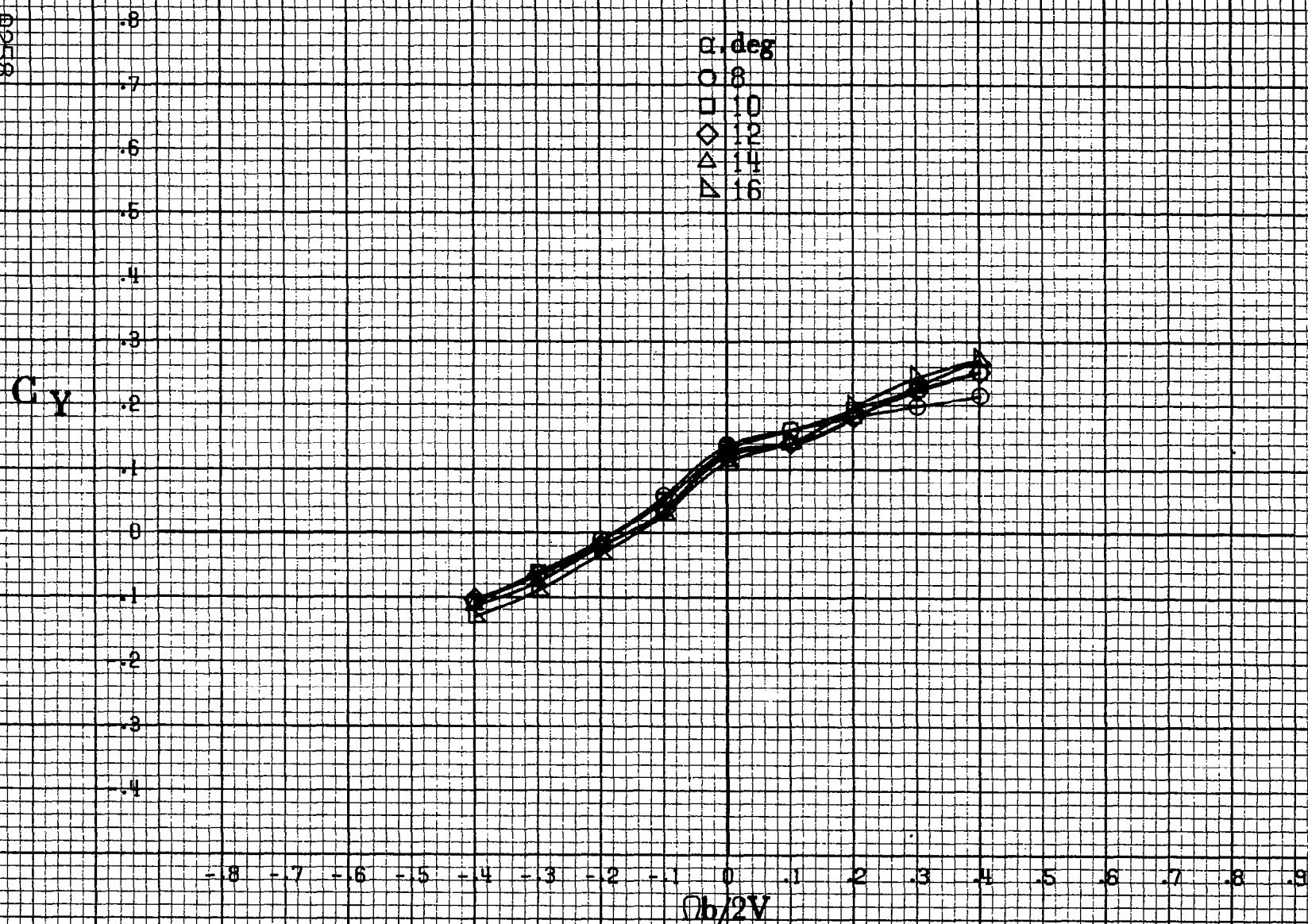
-8 -7 -6 -5 -4 -3 -2 -1 0 .1 .2 .3 .4 .5 .6 .7 .8 .9

$\phi b/2V$

(c) $\alpha=30\text{ to }50\text{deg}$, $SR=0$.
 Figure A70.-Continued.







(a) $\alpha = 8$ to 16° , $SR = 182.9 \text{ cm (72 in.)}$.

Figure A71.-Effect of rotation rate and angle of attack on side-force coefficient for basic configuration. $\delta_e = 0^\circ$, $\delta_a = 0^\circ$, $\delta_a = 11^\circ$, $\delta_r = 0^\circ$. $\beta = 0^\circ$.

C_Y

α, deg

○ 18

□ 20

◇ 25

△ 30

▽ 35

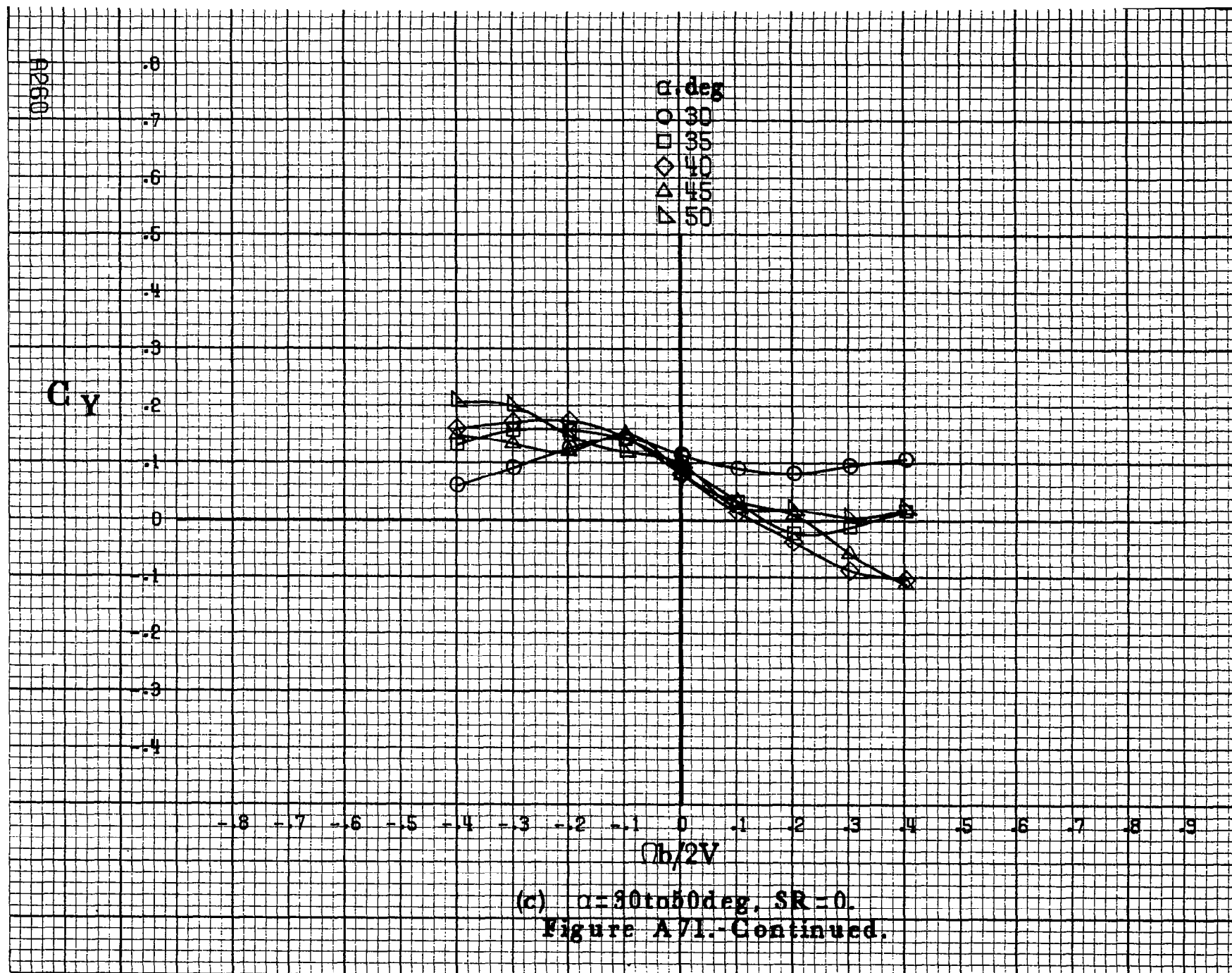
-8 -7 -6 -5 -4 -3 -2 -1 0 .1 .2 .3 .4 .5 .6 .7 .8 .9

$Ch/2V$

(b) $\alpha = 18 \text{ to } 35 \text{ deg}$, $SR = 182.9 \text{ cm (72 in)}$.

Figure A71.-Continued.

A259



C_y

α, deg

○ 55

□ 60

◇ 70

△ 80

▽ 90

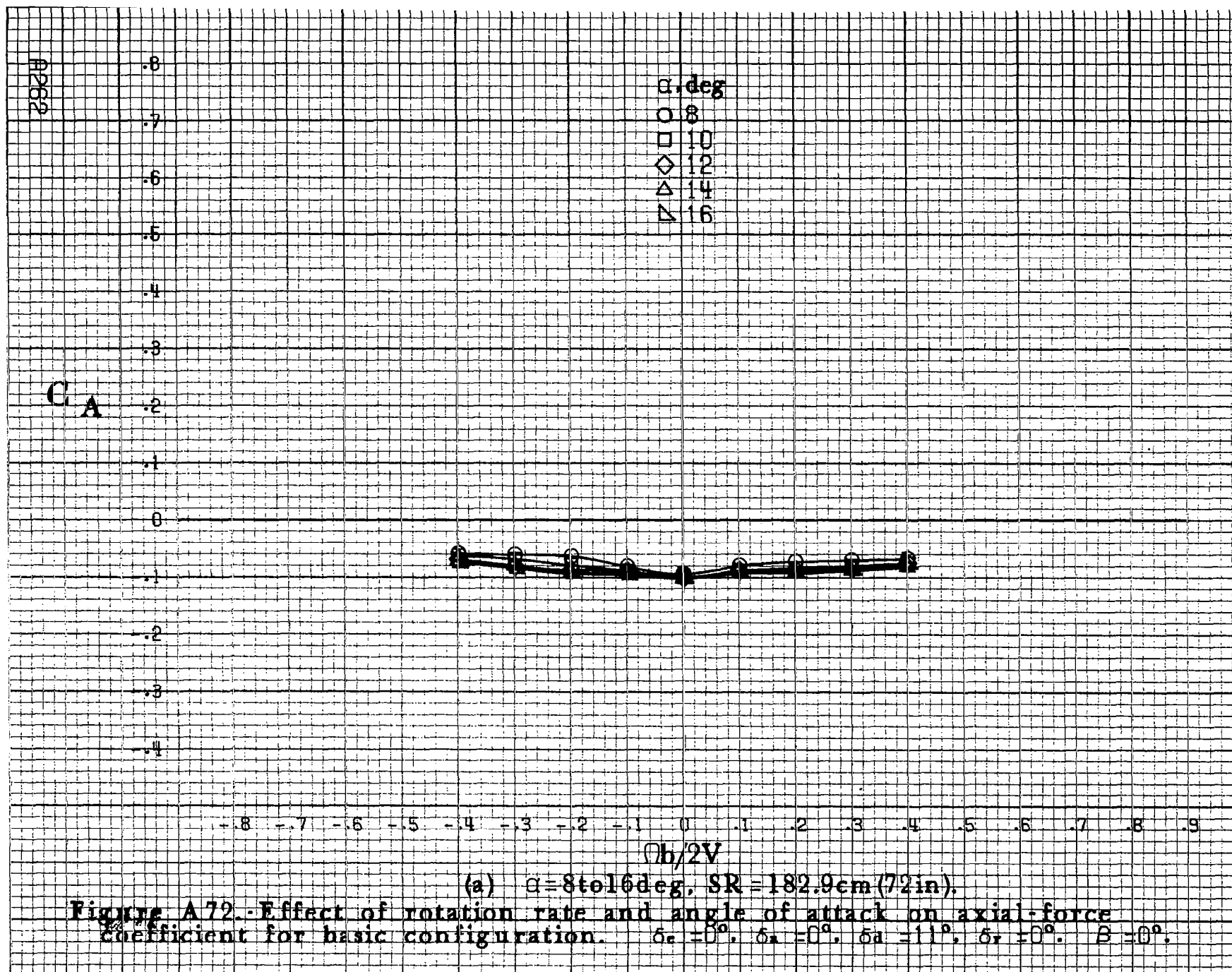
-0.8 -0.7 -0.6 -0.5 -0.4 -0.3 -0.2 -0.1 0 0.1 0.2 0.3 0.4 0.5 0.6 0.7 0.8 0.9

$\Omega b/2V$

(d) $\alpha = 55 \text{ to } 90 \text{ deg. } SR = 0.$

Figure A71.-Concluded.

A261



C_A

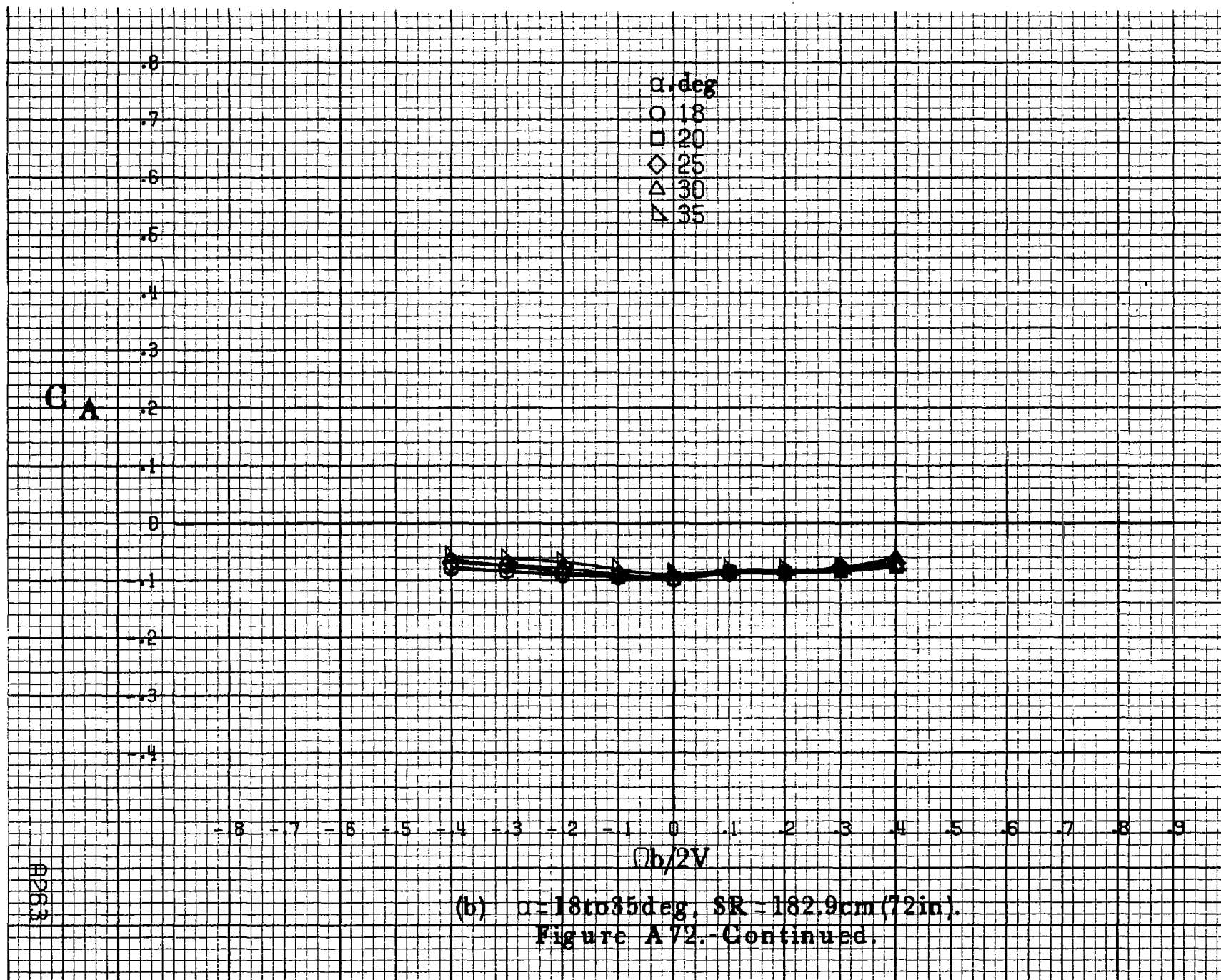
α, deg
 ○ 18
 □ 20
 ◇ 25
 △ 30
 ▴ 35

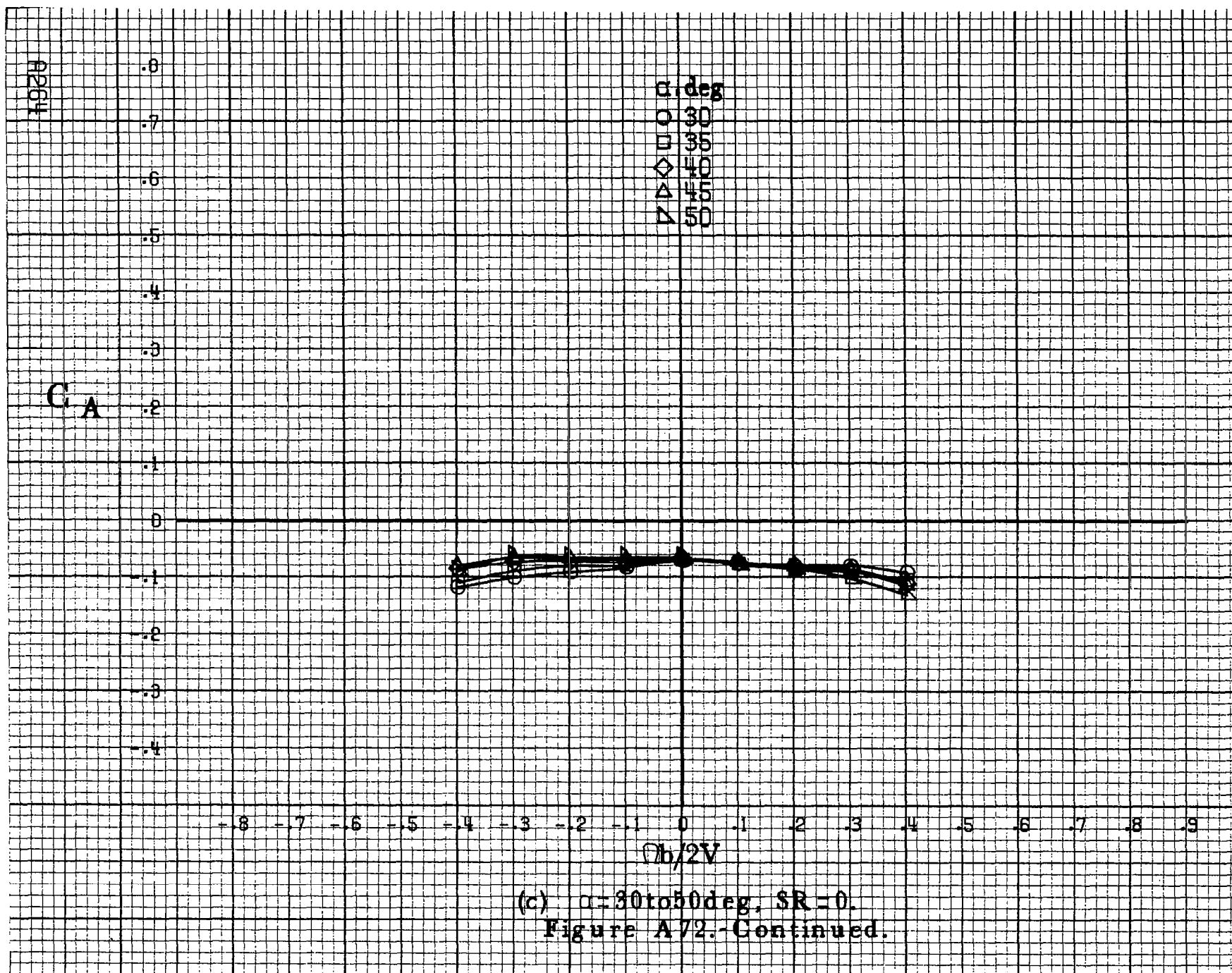
-8 -7 -6 -5 -4 -3 -2 -1 0 .1 .2 .3 .4 .5 .6 .7 .8 .9

$b/2V$

A263

(b) $\alpha = 18 \text{ to } 35 \text{ deg}$, $SR = 182.9 \text{ cm (72 in)}$.
 Figure A72.-Continued.





C_A

α, deg
 ○ 55
 □ 60
 ◇ 70
 △ 80
 ▽ 90

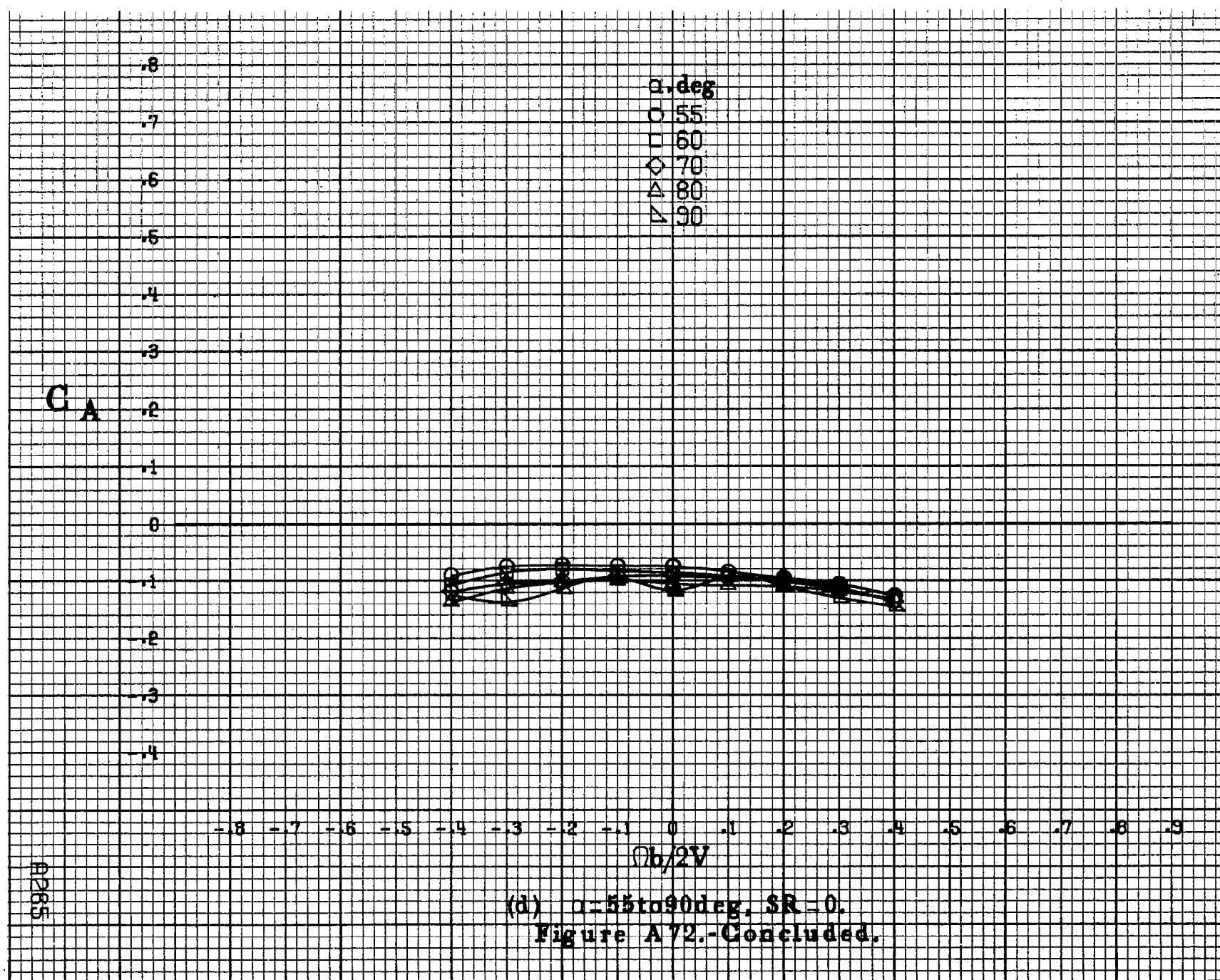
.8
.7
.6
.5
.4
.3
.2
.1
0
-.1
-.2
-.3
-.4

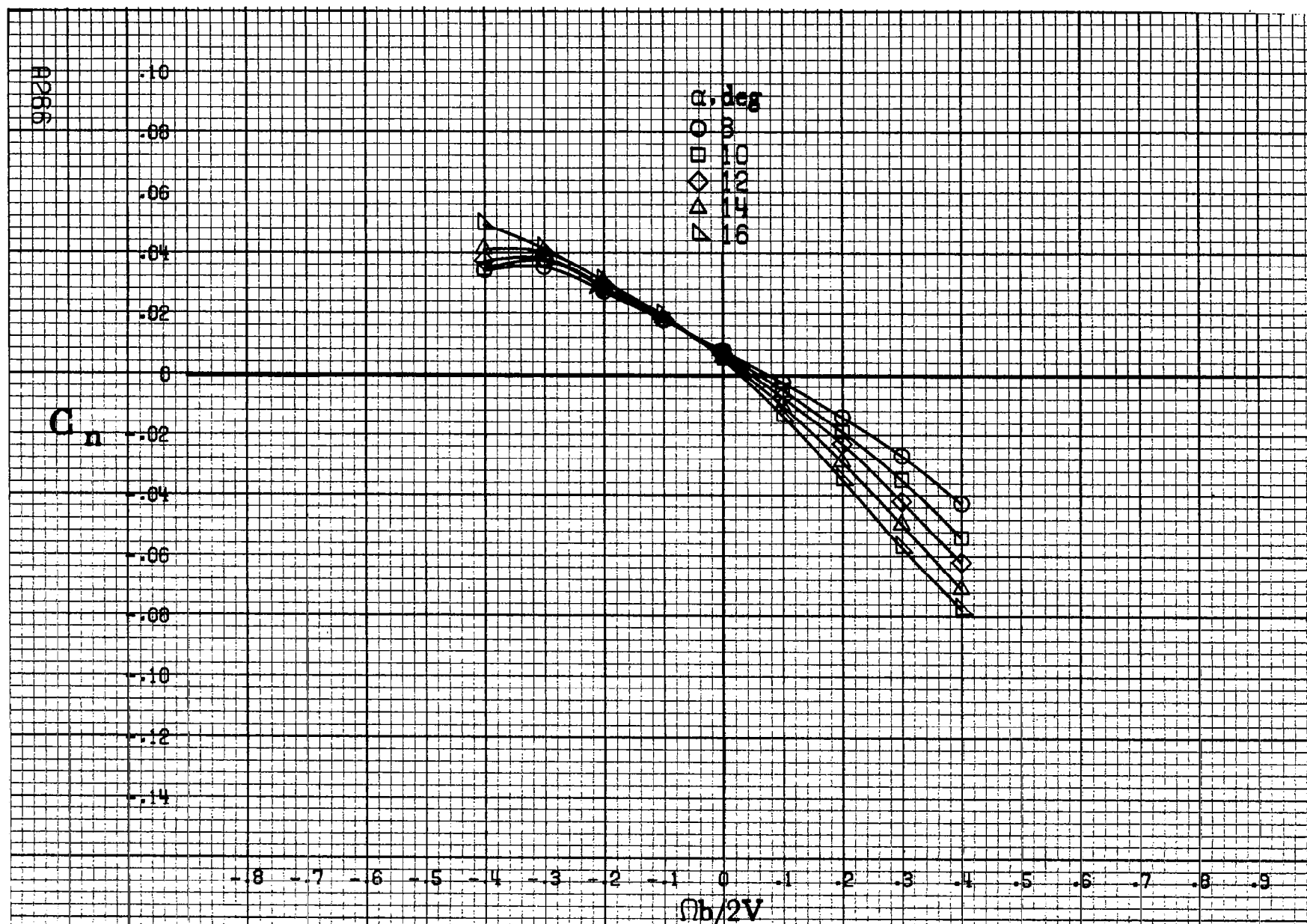
-.8 -.7 -.6 -.5 -.4 -.3 -.2 -.1 0 .1 .2 .3 .4 .5 .6 .7 .8 .9

$b/2V$

A265

(d) $\alpha=55\text{ to }90\text{deg}, SR=0.$
 Figure A72.-Concluded.





(a) $\alpha=8$ to 16° , $SR=182.9$ cm (72 in).

Figure A73.-Effect of rotation rate and angle of attack on yawing-moment coefficient for basic configuration. $\delta_e=0^\circ$, $\delta_a=0^\circ$, $\delta_d=11^\circ$, $\delta_r=0^\circ$, $\beta=10^\circ$.

C_n

α, deg

○ 18

□ 20

◇ 25

△ 30

▽ 35

.10

.08

.06

.04

.02

0

-.02

-.04

-.06

-.08

-.10

-.12

-.14

-.8

-.7

-.6

-.5

-.4

-.3

-.2

-.1

0

.1

.2

.3

.4

.5

.6

.7

.8

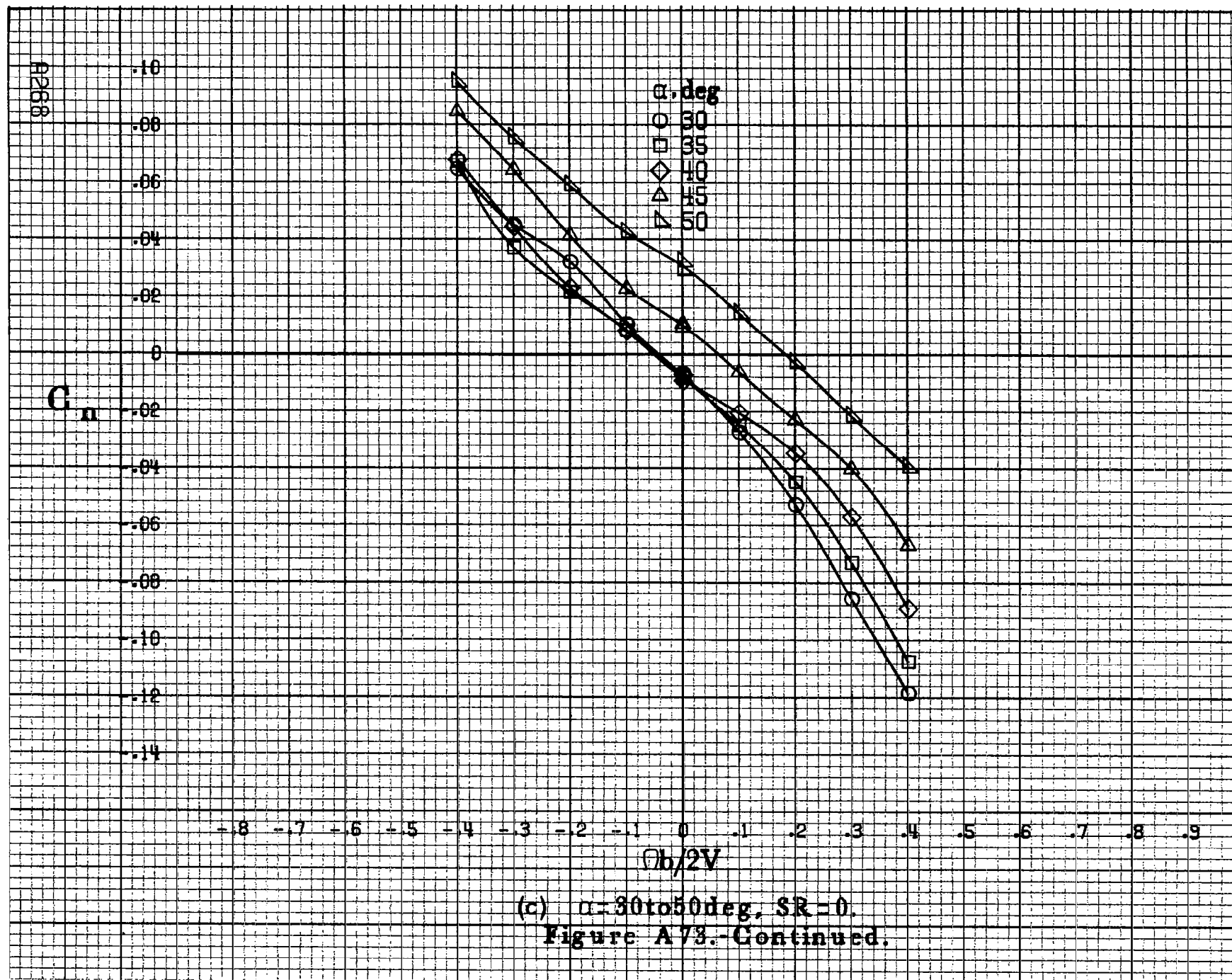
.9

$\Omega b/2V$

(b) $\alpha = 18$ to 35 deg, $SR = 182.9 \text{ cm (72 in.)}$.

Figure A73.-Continued.

A267



4263

C_n

.14
.12
.10
.08
.06
.04
0
-.02
-.04
-.06
-.08
-.10

α, deg

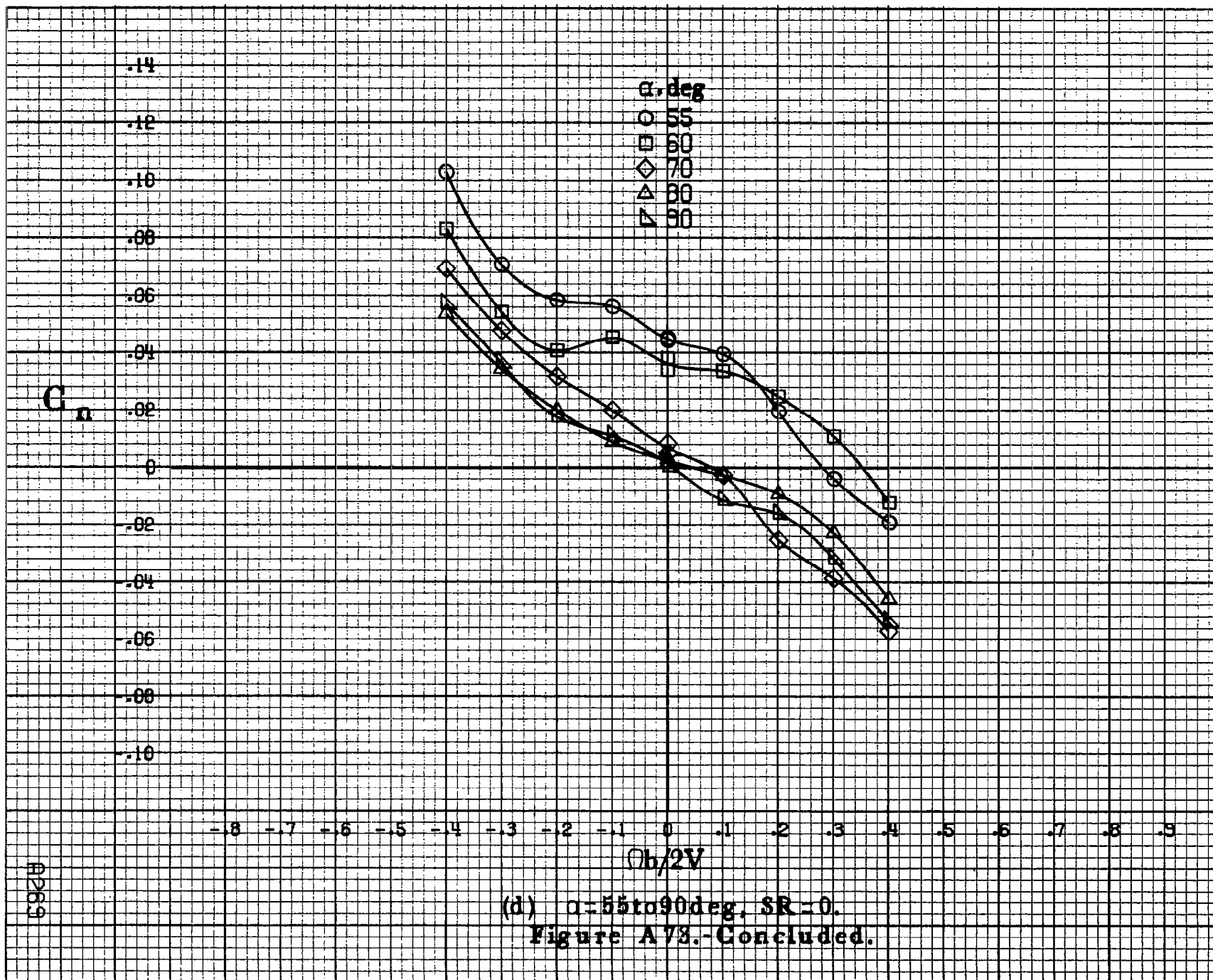
○ 55
□ 60
◇ 70
△ 80
▽ 90

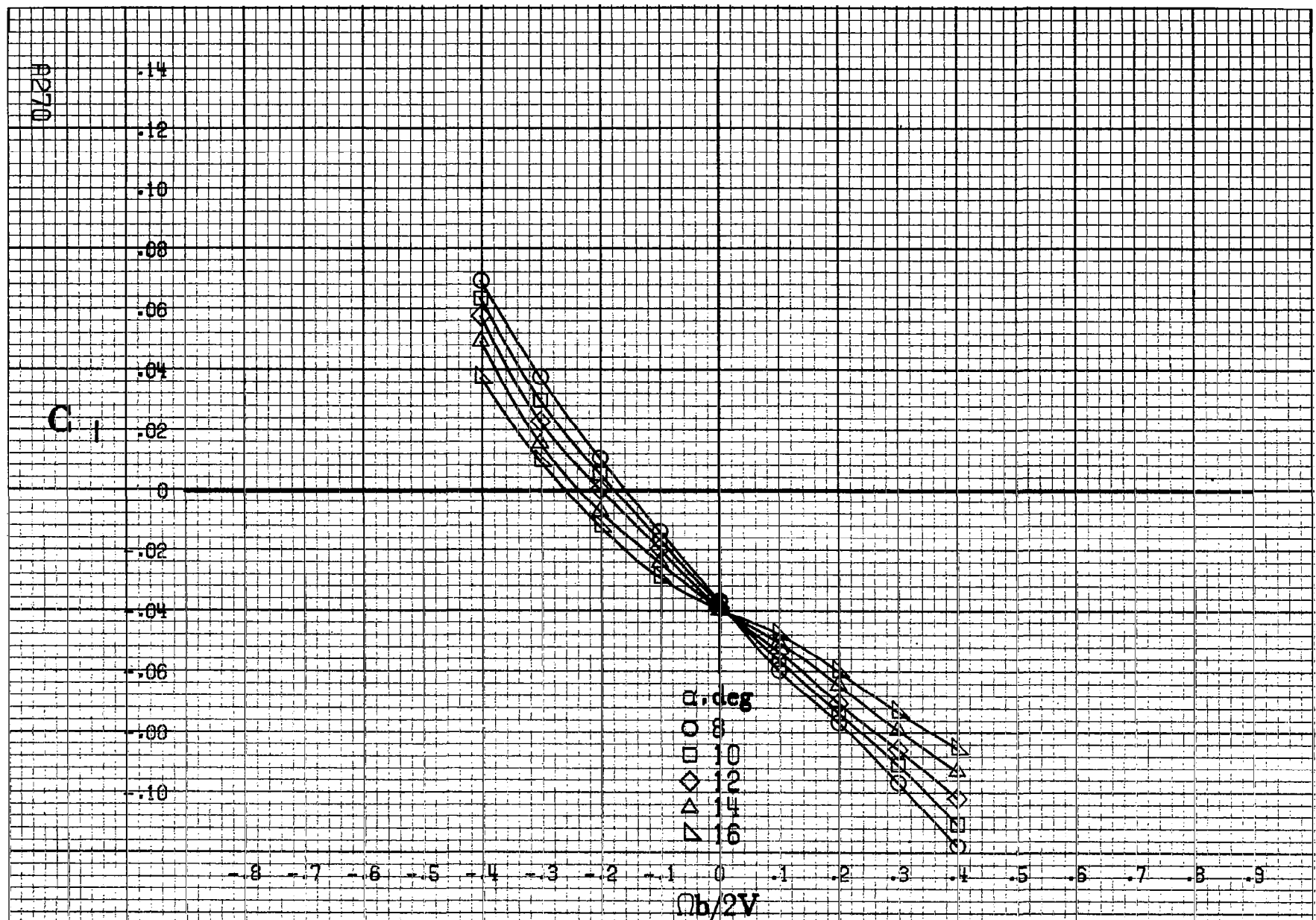
- .8 - .7 - .6 - .5 - .4 - .3 - .2 - .1 0 .1 .2 .3 .4 .5 .6 .7 .8 .9

$Ob/2V$

(d) $\alpha=55$ to 90 deg. $SR=0$.

Figure A73.- Concluded.





(a) $\alpha=8$ to 16° , $SR=182.9\text{cm}$ (72 in).

Figure A74.-Effect of rotation rate and angle of attack on rolling-moment coefficient for basic configuration. $\delta_e=0^\circ$, $\delta_a=0^\circ$, $\delta_d=11^\circ$, $\delta_r=0^\circ$, $\beta=10^\circ$.

C₁

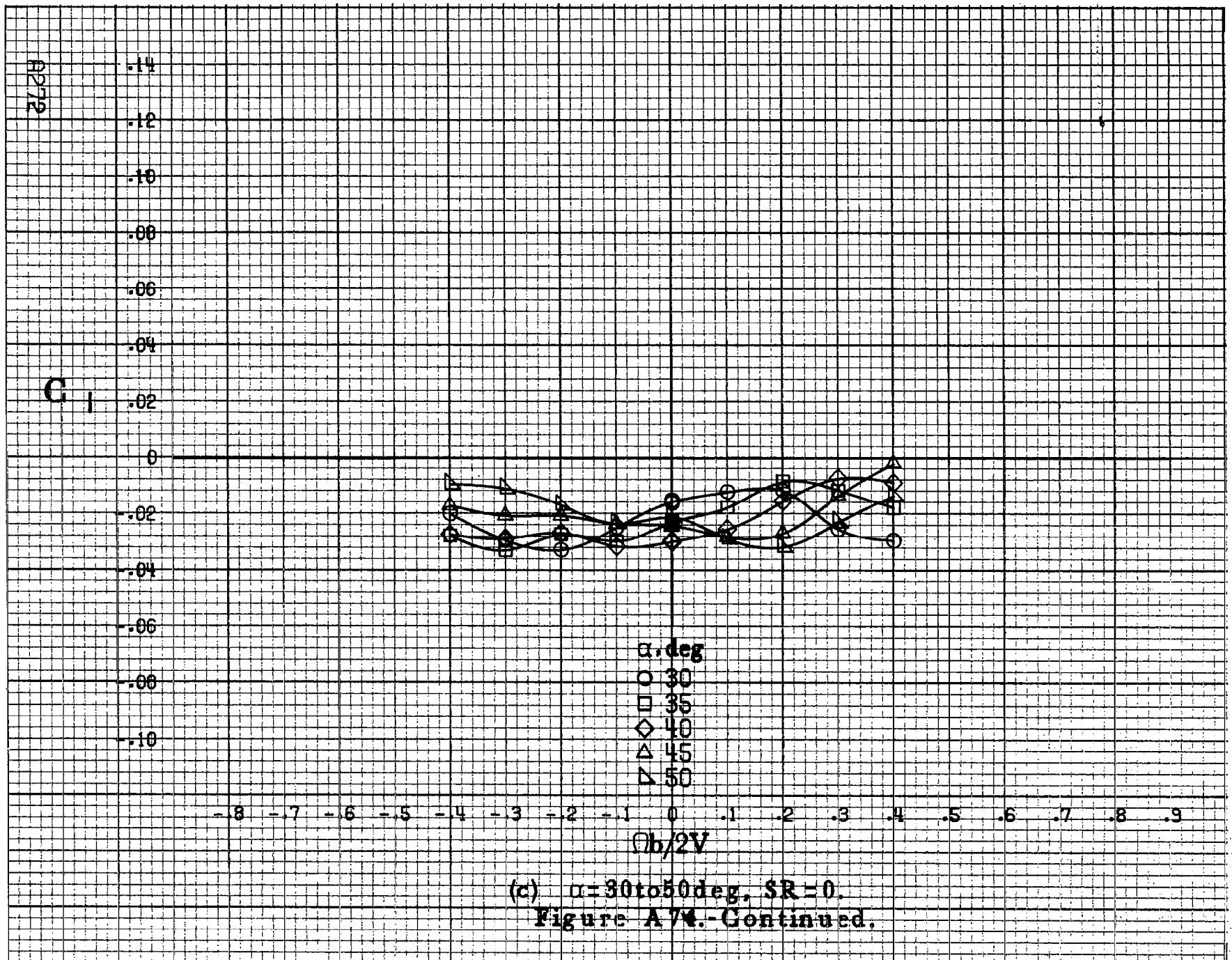
.14
.12
.10
.08
.06
.04
.02
0
-.02
-.04
-.06
-.08
-.10

α, deg
○ 18
□ 20
◇ 25
△ 30
▽ 35

-.8 -.7 -.6 -.5 -.4 -.3 -.2 -.1 0 .1 .2 .3 .4 .5 .6 .7 .8 .9
 $\phi b/2V$

(b) $\alpha = 18 \text{ to } 35 \text{ deg}$, SR = 182.9cm (72in).
Figure A74.-Continued.

A271



C_1

.14
.12
.10
.08
.06
.04
.02
0
-.02
-.04
-.06
-.08
-.10

α, deg
○ 55
□ 60
◇ 70
△ 80
▽ 90

-.8 -.7 -.6 -.5 -.4 -.3 -.2 -.1 0 .1 .2 .3 .4 .5 .6 .7 .8 .9
 $\phi b/2V$

(d) $\alpha=55\text{ to }90\text{ deg, SR}=0$.
Figure A74.-Concluded.

A273

8274

C_m

α, deg

- 8
- 10
- ◇ 12
- △ 14
- ▽ 16

-18 -17 -16 -15 -14 -13 -12 -11 -10 -9 -8 -7 -6 -5 -4 -3 -2 -1 0 1 2 3 4 5 6 7 8 9

$\Omega b/2V$

(a) $\alpha = 8 \text{ to } 16 \text{ deg}$, $SR = 182.9 \text{ cm (72 in)}$.

Figure A75.-Effect of rotation rate and angle of attack on pitching-moment coefficient for basic configuration. $\delta_e = 0^\circ$, $\delta_a = 0^\circ$, $\delta_d = 11^\circ$, $\delta_r = 0^\circ$, $\delta = 10^\circ$.

C_m

α, deg

○ 18

□ 20

◇ 25

△ 30

▽ 35

-8 -7 -6 -5 -4 -3 -2 -1 0 .1 .2 .3 .4 .5 .6 .7 .8 .9

$b/2V$

(b) $\alpha = 18 \text{ to } 35 \text{ deg}$, $SR = 182.9 \text{ cm (72 in)}$.

Figure A75.-Continued.

8975

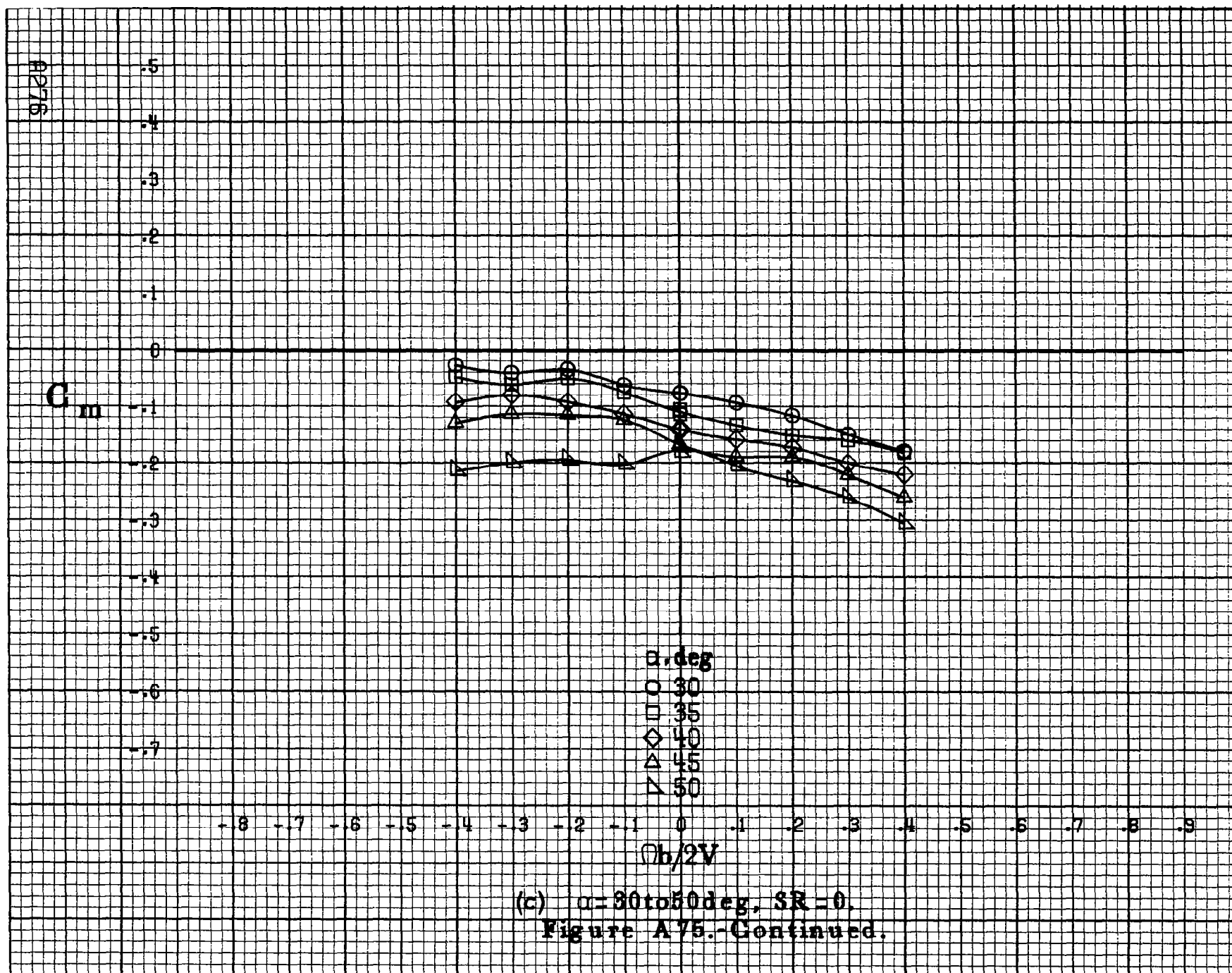
A276

 C_m α, deg

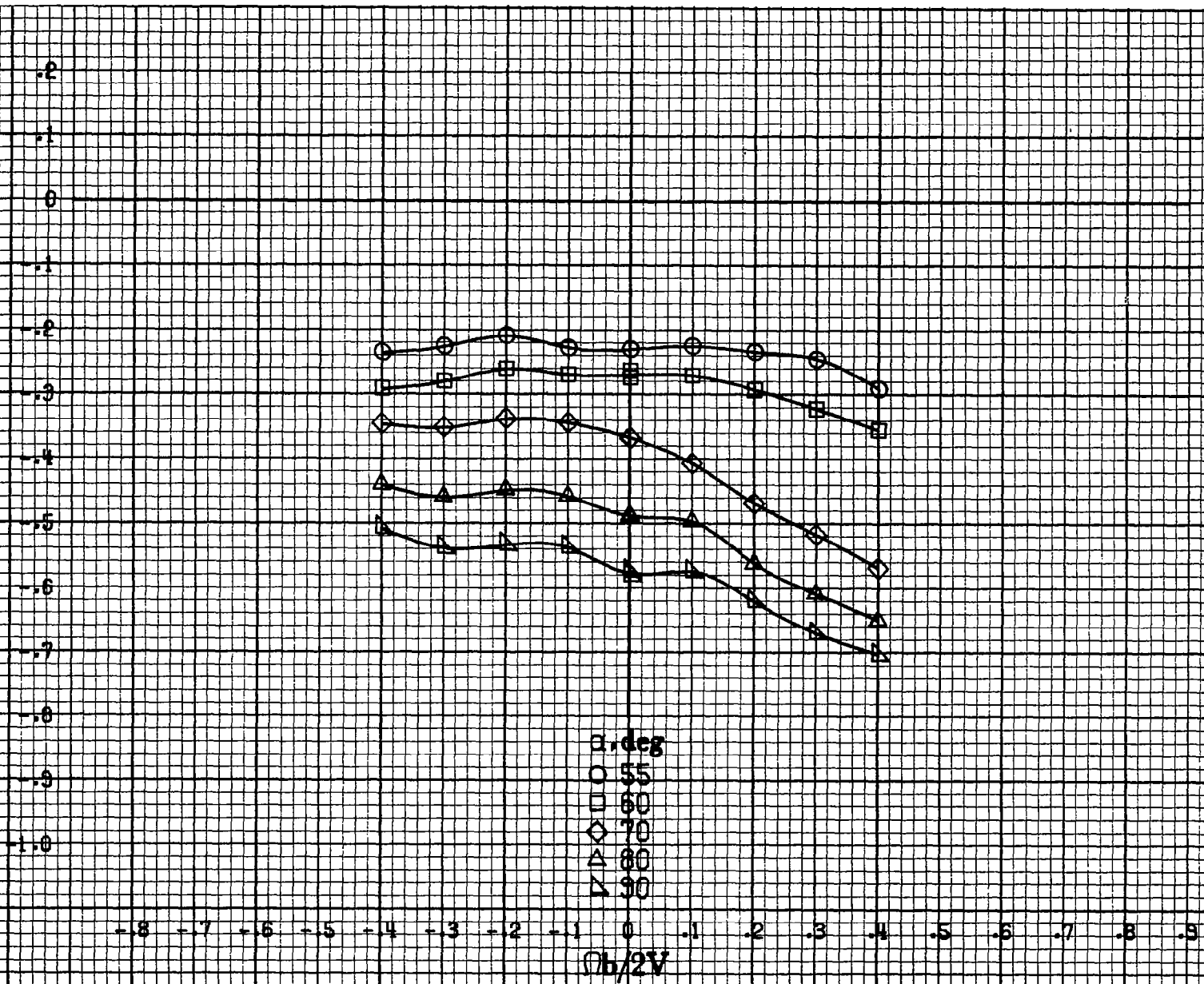
○ 30
□ 35
◇ 40
△ 45
▽ 50

 $b/2V$ (c) $\alpha = 30 \text{ to } 50 \text{ deg}, SR = 0.$

Figure A75.-Continued.



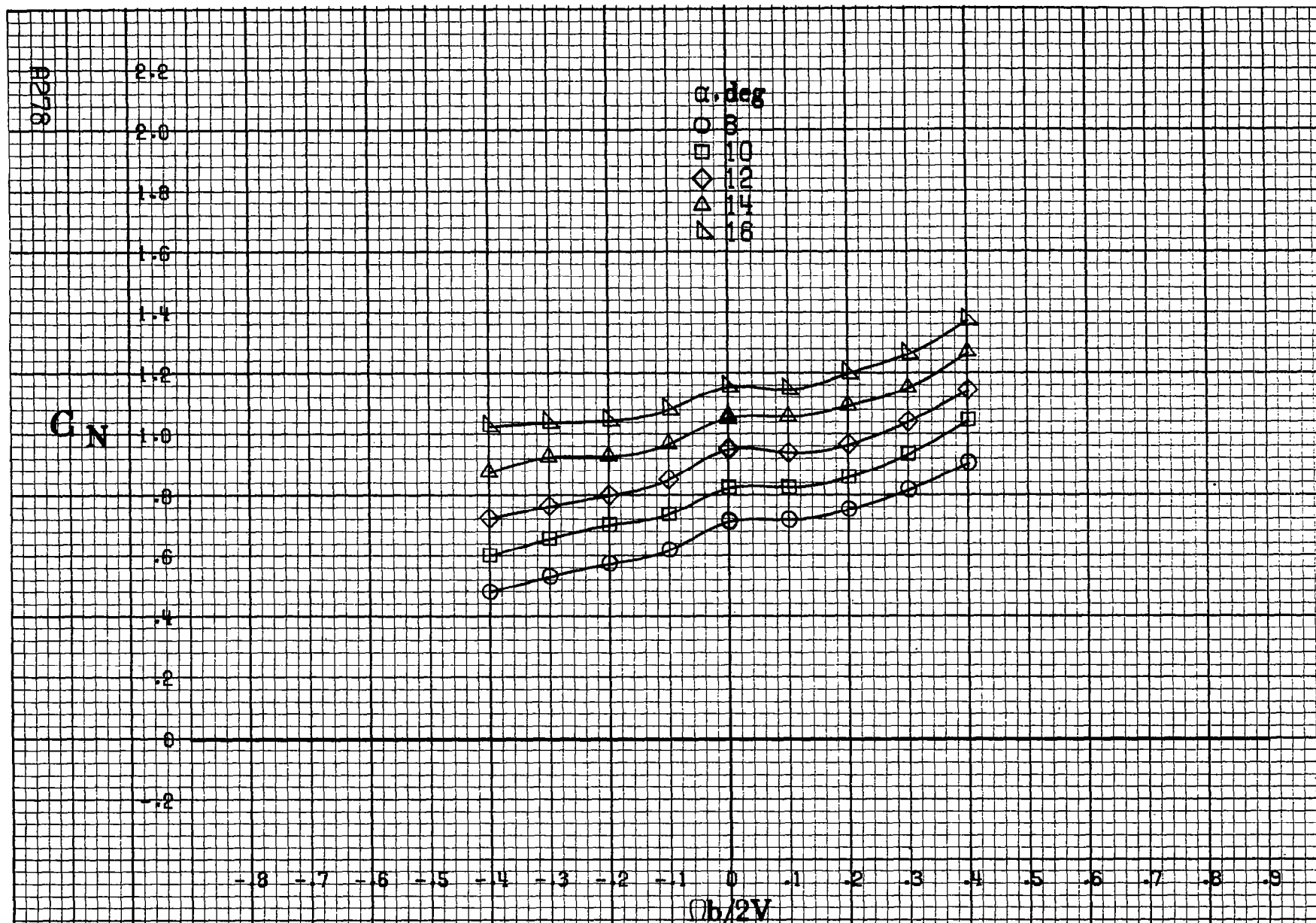
C_m



(d) $\alpha = 55$ to 90 deg, $SR = 0$.

Figure A75.-Concluded.

AP277



(a) $\alpha=8$ to 16° , $SR=182.9\text{cm}(72\text{in})$.

Figure A76.-Effect of rotation rate and angle of attack on normal-force coefficient for basic configuration. $\delta_e \pm 0^\circ$, $\delta_a \pm 0^\circ$, $\delta_{\alpha} \pm 11^\circ$, $\delta_r \pm 0^\circ$, $\beta \pm 10^\circ$.

C_N

α, deg
 ○ 18
 □ 20
 ◇ 25
 △ 30
 ▽ 35

$\phi b/2V$

(b) $\alpha = 18 \text{ to } 35 \text{ deg}$, $SR = 182.9 \text{ cm (72 in.)}$.
 Figure A76.-Continued.

A279

A280

 C_N

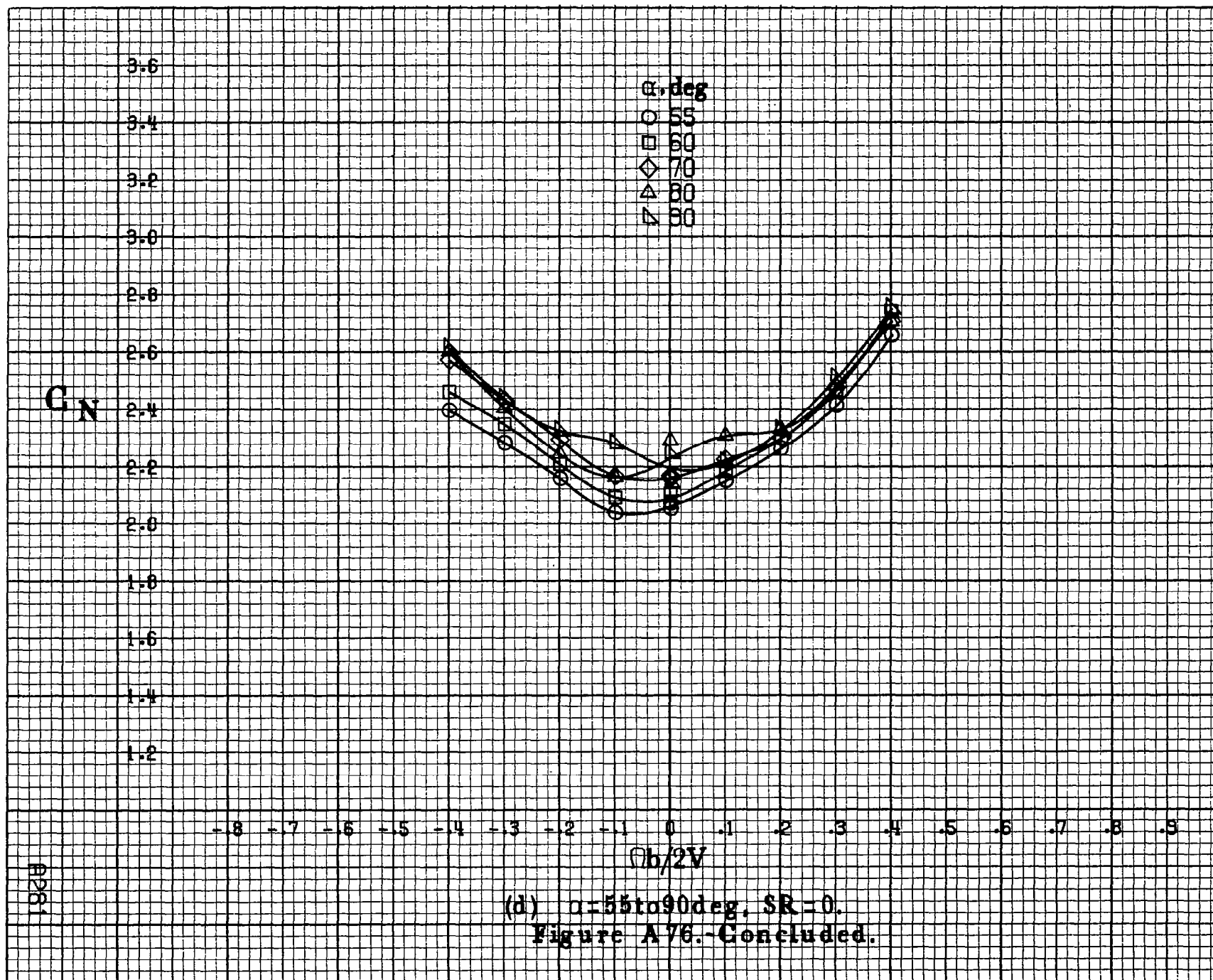
3.4
3.2
3.0
2.8
2.6
2.4
2.2
2.0
1.8
1.6
1.4
1.2
1.0

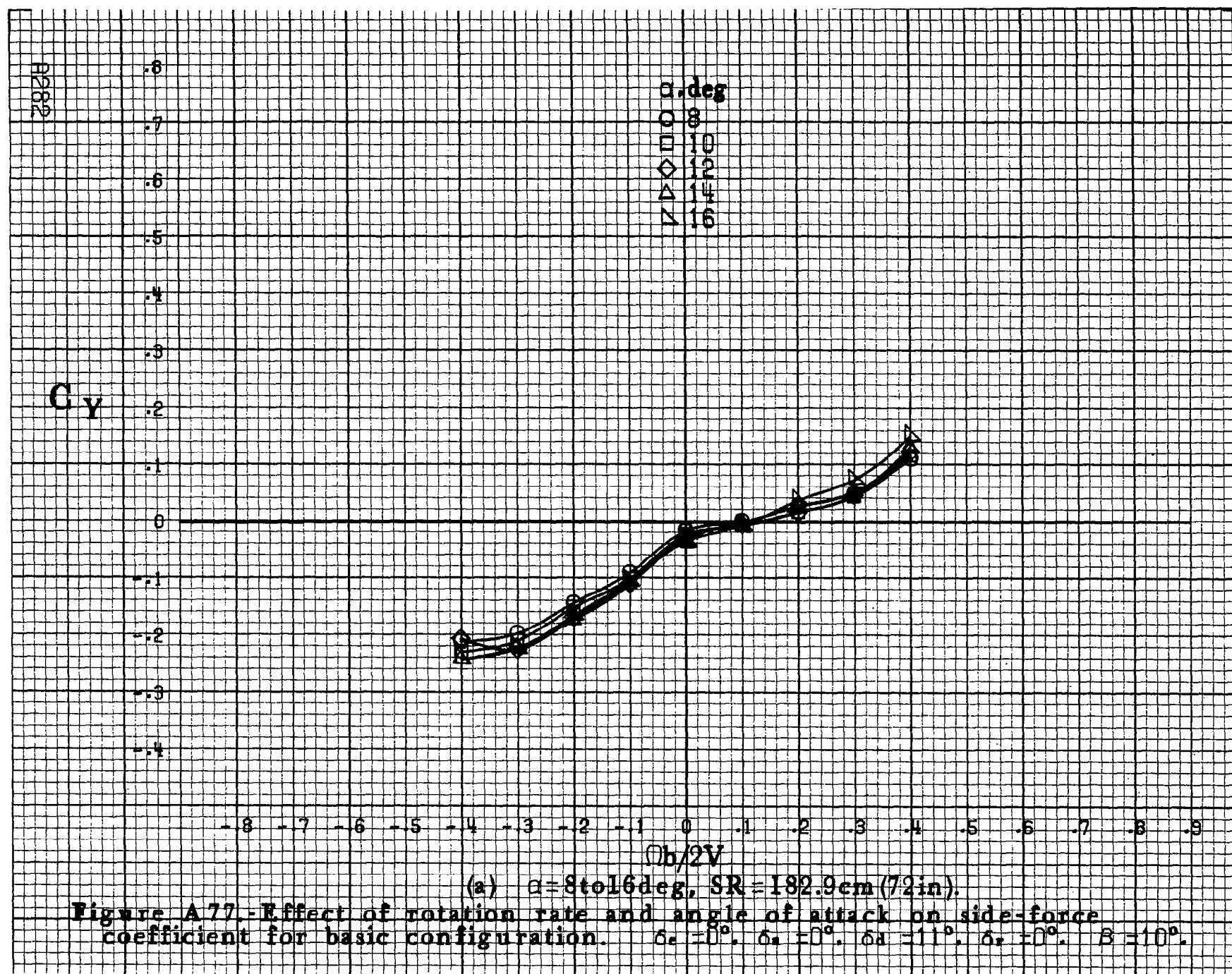
α, deg
○ 30
□ 35
◇ 40
△ 45
▽ 50

-8 -7 -6 -5 -4 -3 -2 -1 0 .1 .2 .3 .4 .5 .6 .7 .8 .9

 $\Omega b/2V$

(c) $\alpha=30$ to 50 deg, $SR=0$.
Figure A76.-Continued.





C_y

α, deg
 ○ 18
 □ 20
 ◇ 25
 △ 30
 ▽ 35

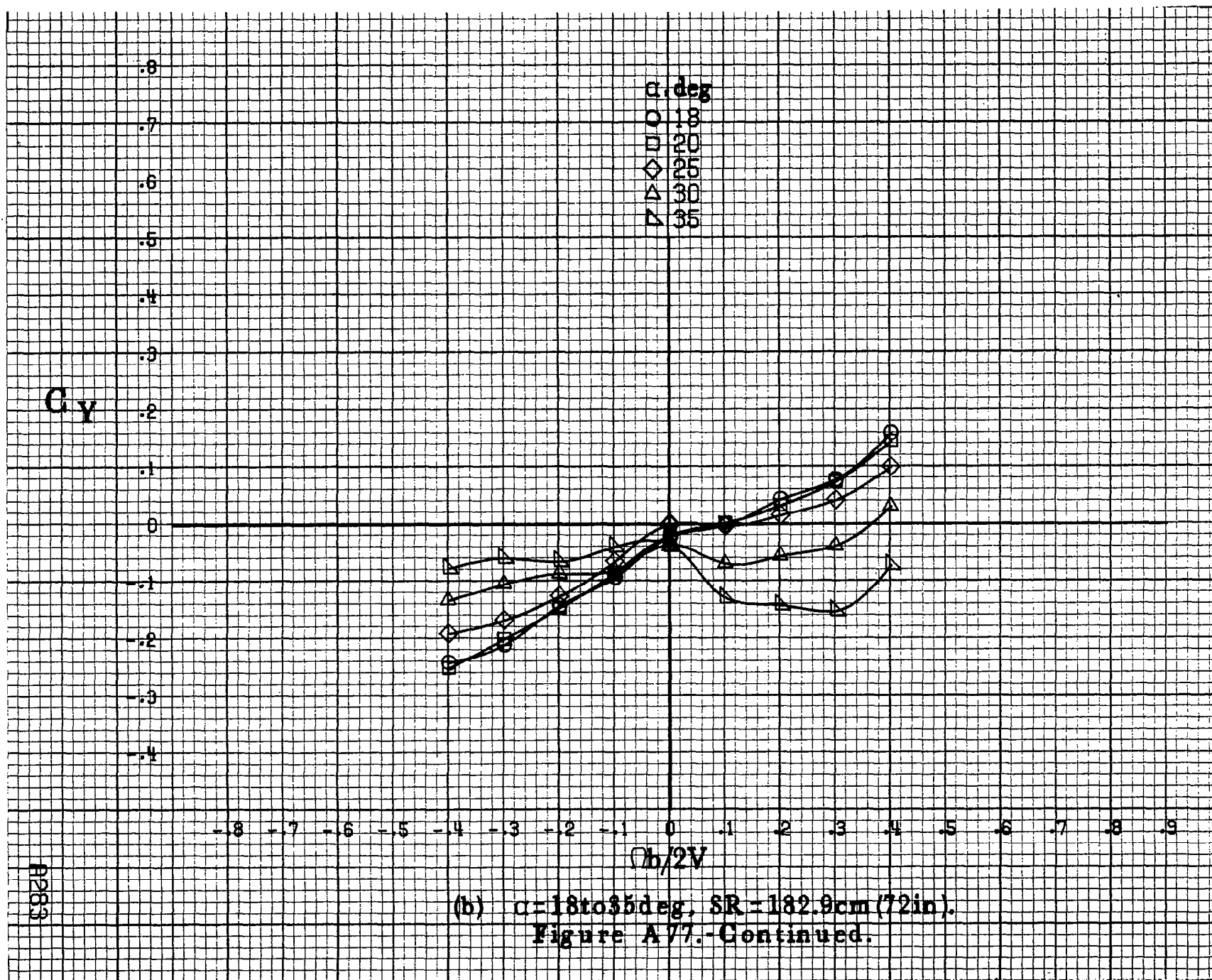
.8
.7
.6
.5
.4
.3
.2
.1
0
-.1
-.2
-.3
-.4

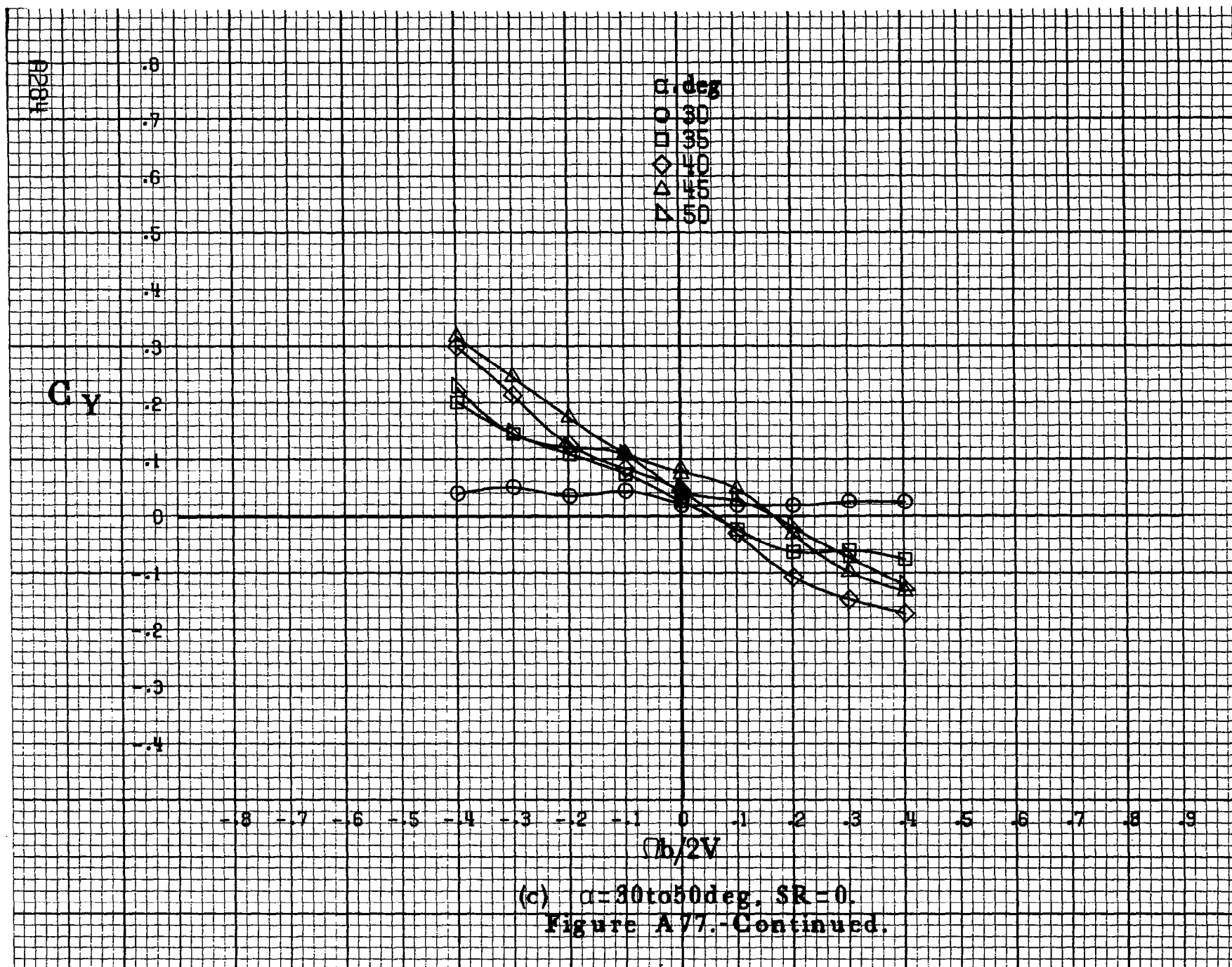
-.8 -.7 -.6 -.5 -.4 -.3 -.2 -.1 0 .1 .2 .3 .4 .5 .6 .7 .8 .9

$Ob/2V$

A263

(b) $\alpha=18\text{to}35\text{deg}$, $SR=182.9\text{cm}(72\text{in})$.
 Figure A77.-Continued.





C_y

α, deg

○ 55

□ 60

◇ 70

△ 80

▽ 90

0.8
0.7
0.6
0.5
0.4
0.3
0.2
0.1
0
-0.1
-0.2
-0.3
-0.4

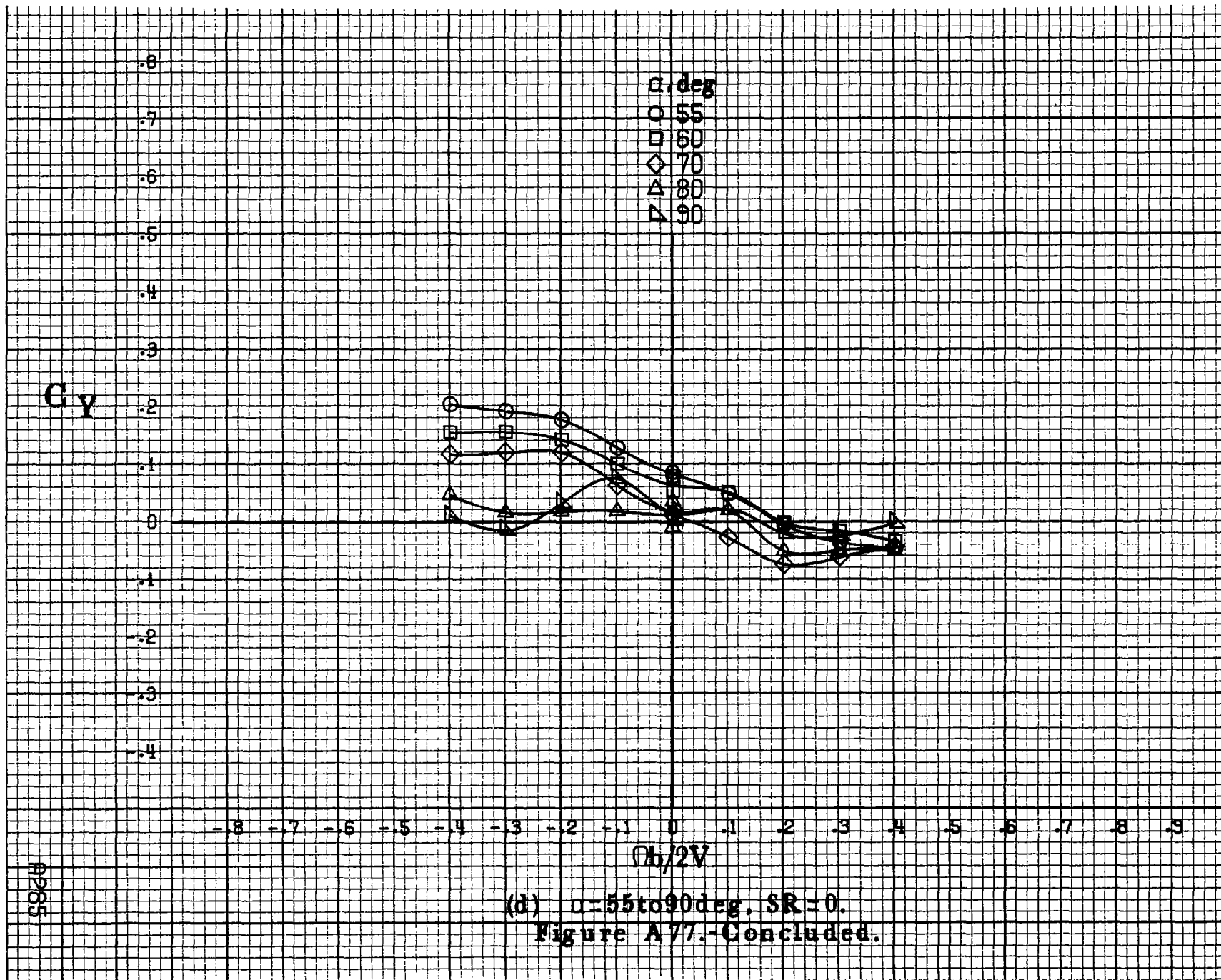
-0.8 -0.7 -0.6 -0.5 -0.4 -0.3 -0.2 -0.1 0 0.1 0.2 0.3 0.4 0.5 0.6 0.7 0.8 0.9

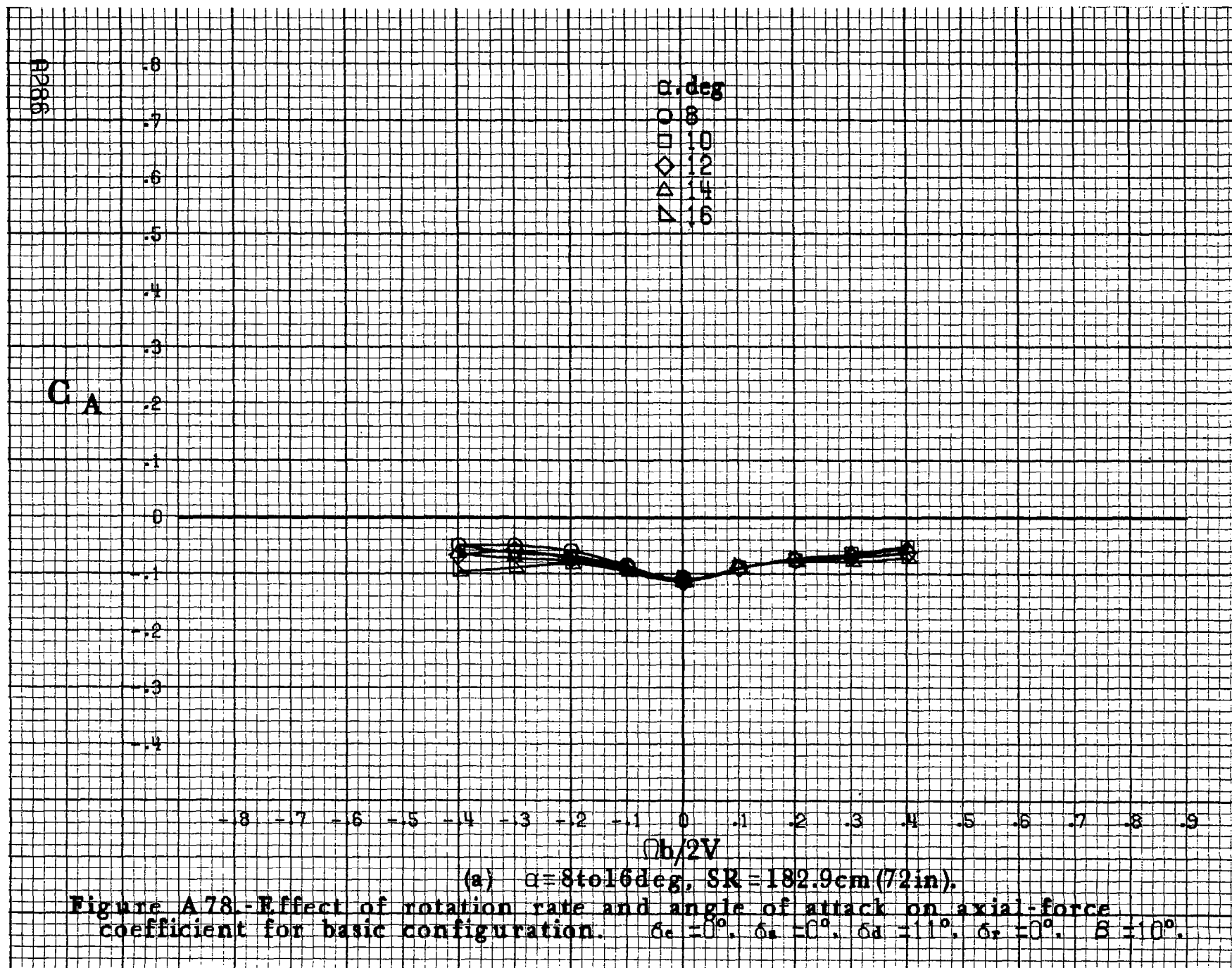
$\phi_b/2V$

0265

(d) $\alpha=55\text{to}90\text{deg. SR}=0.$

Figure A77.-Concluded.





G_A

.8
.7
.6
.5
.4
.3
.2
.1
0
-.1
-.2
-.3
-.4

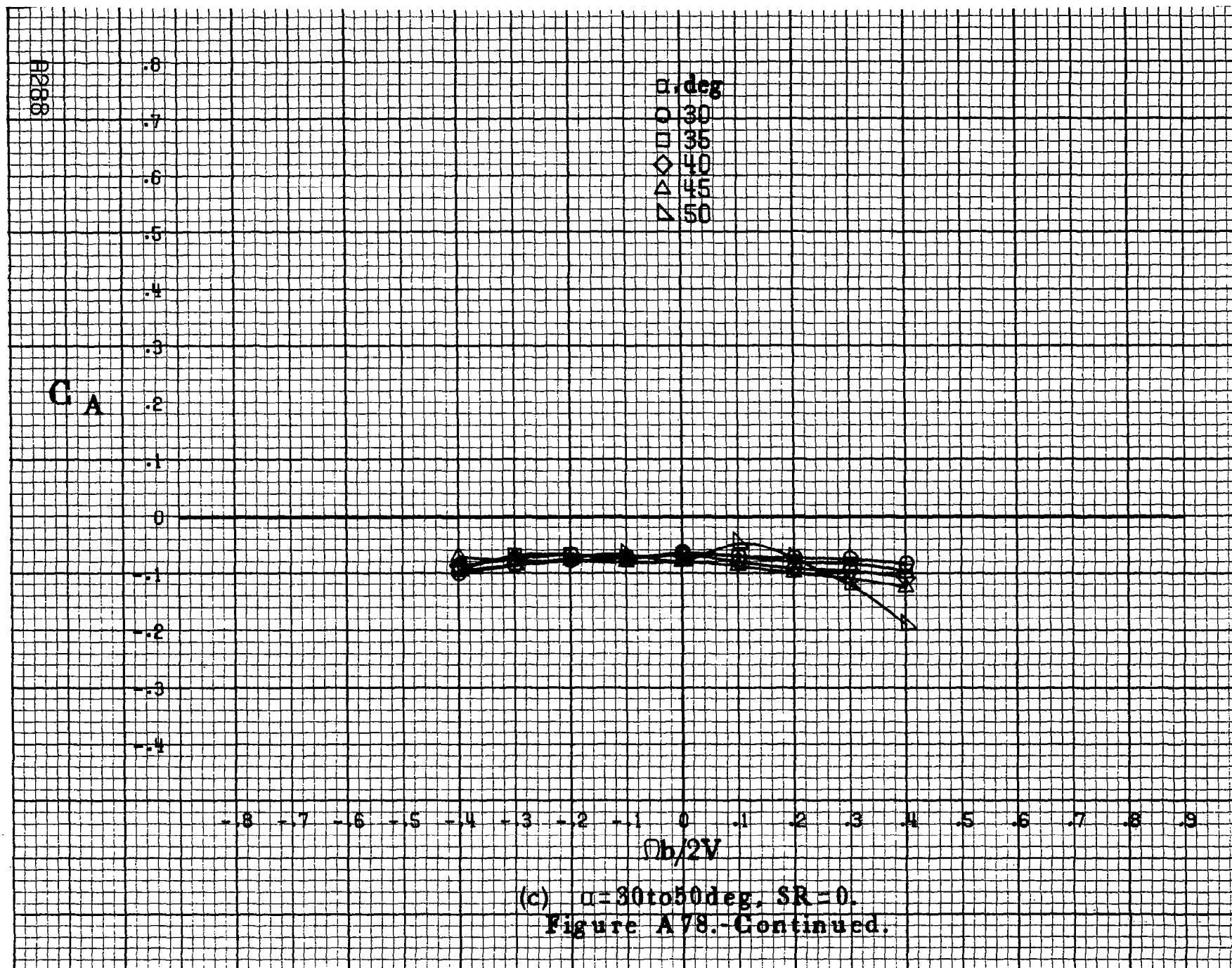
α deg
○ 18
□ 20
◇ 25
△ 30
▽ 35

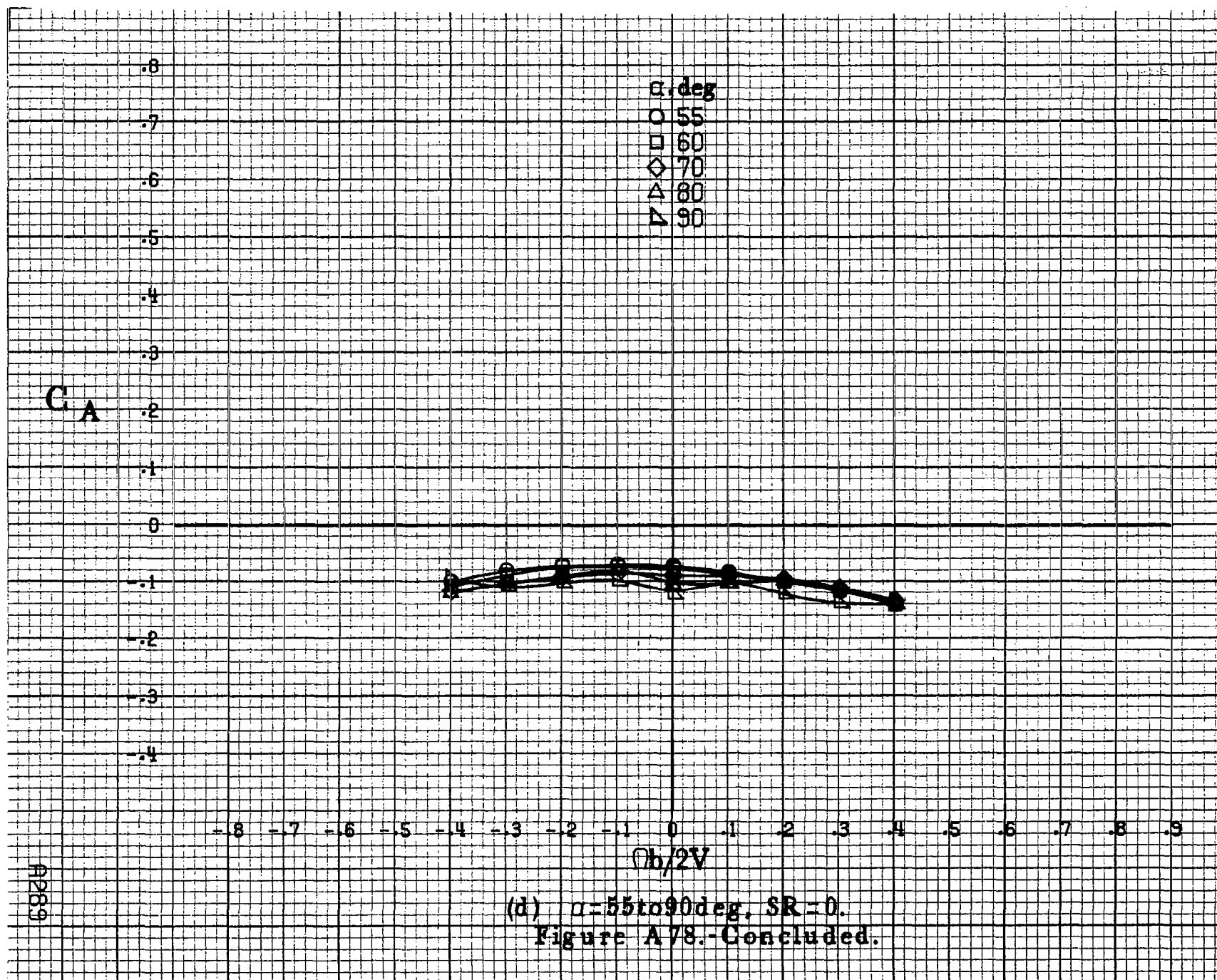
-.8 -.7 -.6 -.5 -.4 -.3 -.2 -.1 0 .1 .2 .3 .4 .5 .6 .7 .8 .9

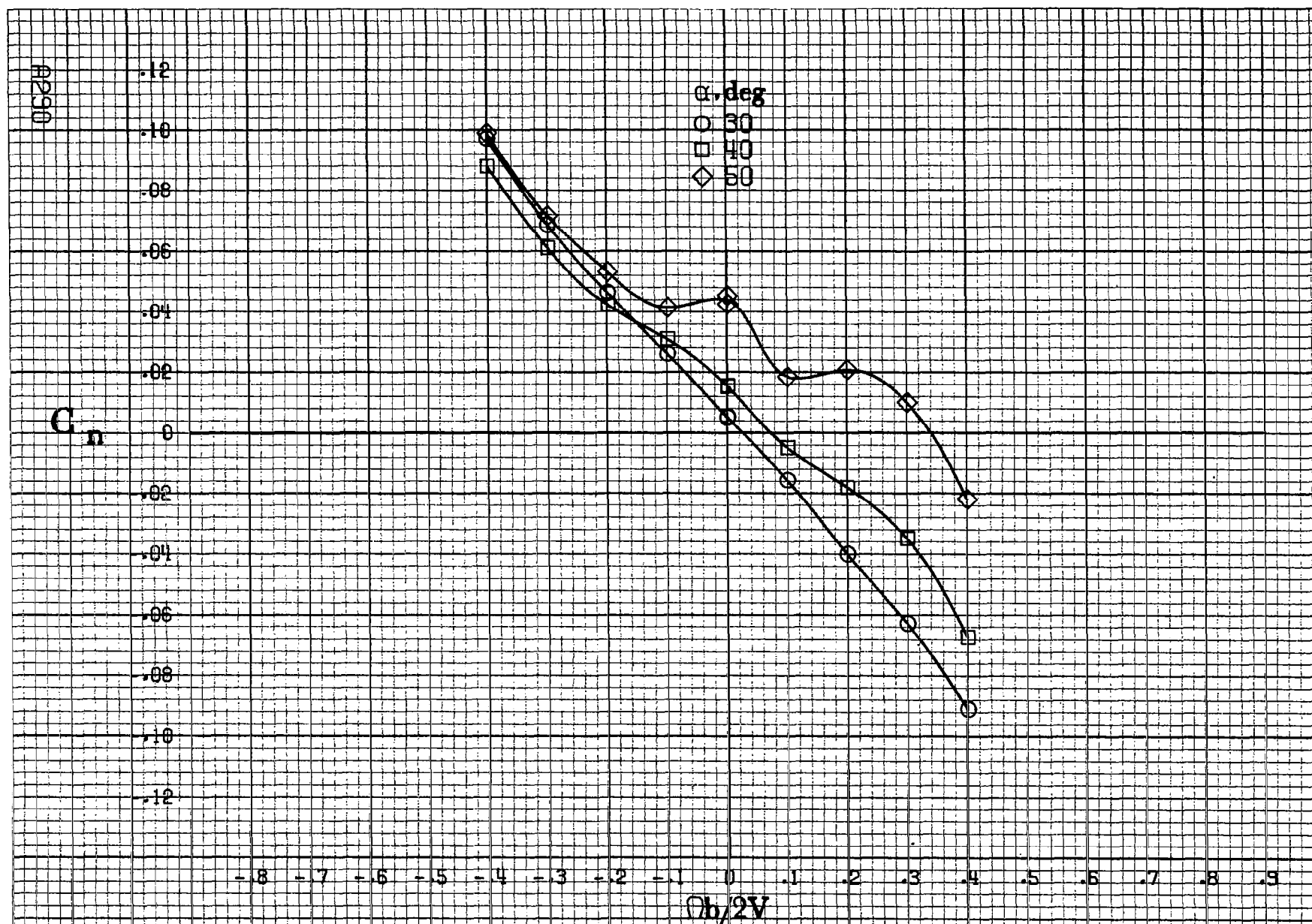
$b/2V$

(b) $\alpha = 18$ to 35 deg, $SR = 182.9$ cm (72 in).
Figure A78.-Continued.

9287

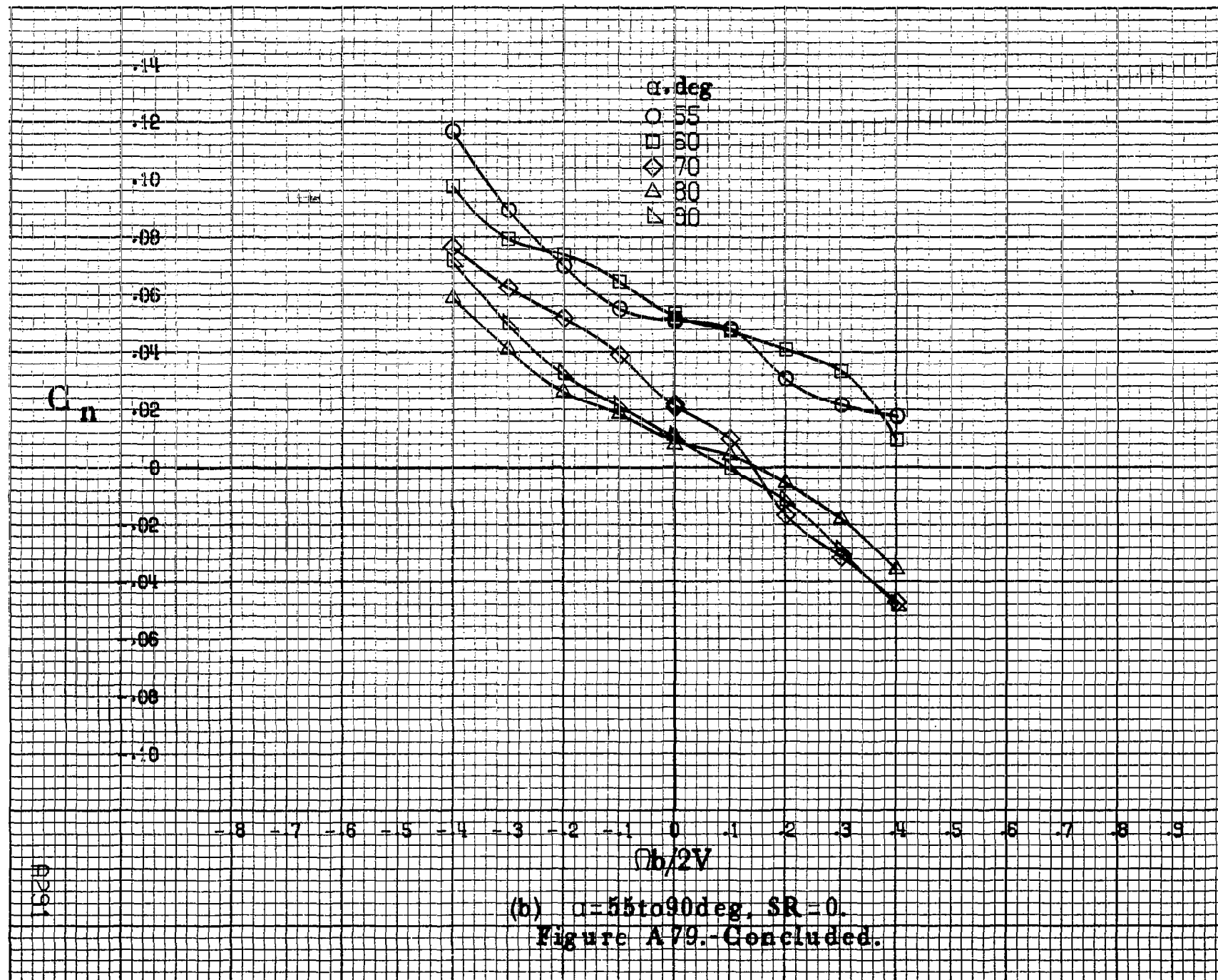






(a) $\alpha = 30$ to 50° , $SR = 0$.

Figure A79.- Effect of rotation rate and angle of attack on yawing-moment coefficient for basic configuration. $\delta_e = 0^\circ$, $\delta_a = -20.0^\circ$, $\delta_a = -6^\circ$, $\delta_r = 0^\circ$, $\beta = 0^\circ$.



(b) $\alpha=55$ to 90 deg, $SR=0$.
Figure A79.-Concluded.

8292

8292

C_l

.14
.12
.10
.08
.06
.04
.02
0
-.02
-.04
-.06
-.08
-.10

α , deg
○ 30
□ 40
◇ 50

-8 -7 -6 -5 -4 -3 -2 -1 0 .1 .2 .3 .4 .5 .6 .7 .8 .9
 $\Omega b/2V$

(a) $\alpha = 30$ to 50 deg, $SR = 0$.

Figure A80.-Effect of rotation rate and angle of attack on rolling-moment coefficient for basic configuration. $\delta_e = 0^\circ$, $\delta_a = 20.0^\circ$, $\delta_d = 6^\circ$, $\delta_r = 0^\circ$, $\beta = 0^\circ$.

C_1

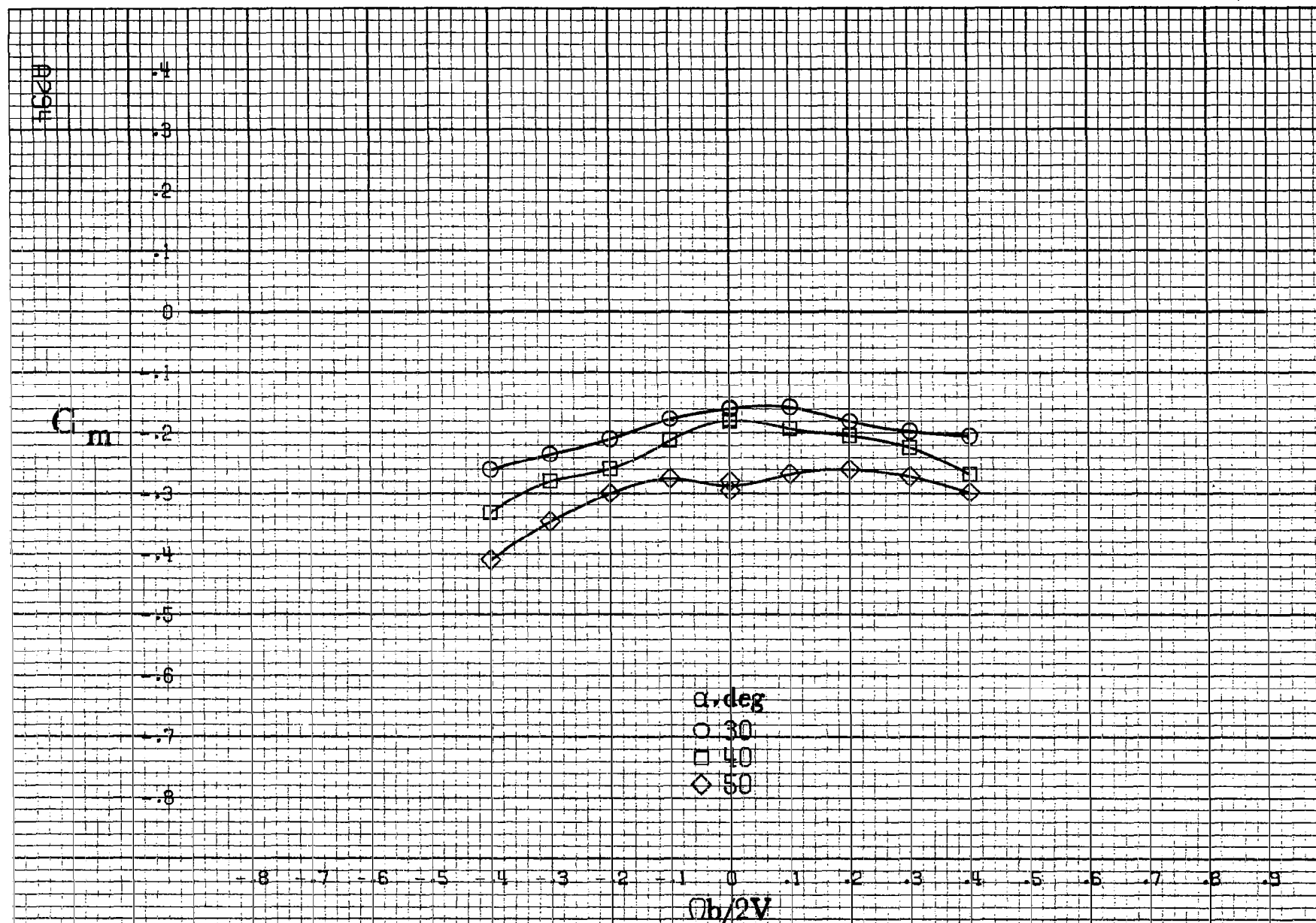
.14
.12
.10
.08
.06
.04
0
-.02
-.04
-.06
-.08
-.10

α, deg
○ 55
□ 60
◇ 70
△ 80
▽ 90

-8 -7 -6 -5 -4 -3 -2 -1 0 1 2 3 4 5 6 7 8 9
 $b/2V$

(b) $\alpha = 55 \text{ to } 90 \text{ deg}$, $SR = 0$.
Figure A80.-Concluded.

A293



(a) $\alpha = 30$ to 50° , $SR = 0$.

Figure A81. Effect of rotation rate and angle of attack on pitching-moment coefficient for basic configuration. $\delta_e = 0^\circ$, $\delta_a = 20.0^\circ$, $\delta_d = 6^\circ$, $\delta_r = 0^\circ$, $\beta = 0^\circ$.

C_m

.2
.1
0
-.1
-.2
-.3
-.4
-.5
-.6
-.7
-.8
-.9
-1.0

α, deg

○ 55
□ 60
◇ 70
△ 80
▽ 90

-8 -7 -6 -5 -4 -3 -2 -1 0 .1 .2 .3 .4 .5 .6 .7 .8 .9

$\Omega b/2V$

(b) $\alpha = 55 \text{ to } 90 \text{ deg}, SR = 0.$

Figure A81.-Concluded.

A295

A296

 C_N α, deg

○ 30

□ 40

◇ 50

3.0

2.8

2.6

2.4

2.2

2.0

1.8

1.6

1.4

1.2

1.0

.8

.6

-.8

-.7

-.6

-.5

-.4

-.3

-.2

-.1

0

.1

.2

.3

.4

.5

.6

.7

.8

.9

 $\Omega b/2V$ (a) $\alpha=30$ to 50 deg, $SR=0$.

Figure A82.- Effect of rotation rate and angle of attack on normal-force coefficient for basic configuration. $\delta_c = 0^\circ$, $\delta_s = 20.0^\circ$, $\delta_d = 6^\circ$, $\delta_r = 0^\circ$, $\beta = 0^\circ$.

C_N

α, deg

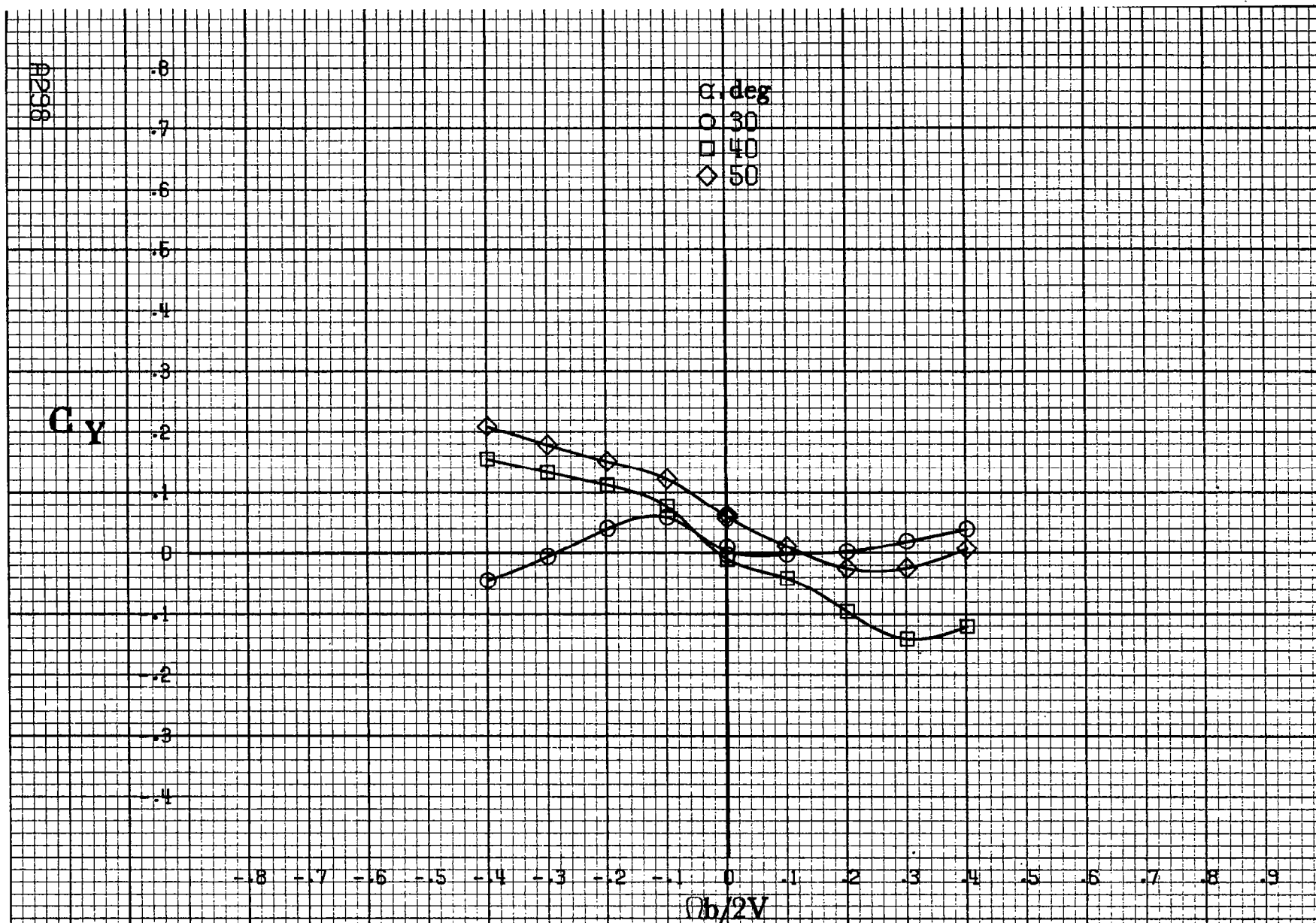
- 55
- 60
- ◇ 70
- △ 80
- ▽ 90

-8 -7 -6 -5 -4 -3 -2 -1 0 .1 .2 .3 .4 .5 .6 .7 .8 .9

$\Omega b/2V$

(b) $\alpha=55\text{to}90\text{deg}, SR=0.$
Figure A82.-Concluded.

A297



(a) $\alpha=30$ to 50° , $SR=0$.

Figure A83 - Effect of rotation rate and angle of attack on side-force coefficient for basic configuration. $\delta_c=0^\circ$, $\delta_a=20.0^\circ$, $\delta_d=6^\circ$, $\delta_r=0^\circ$, $\beta=0^\circ$.

C_y

α, deg

○ 55

□ 60

◇ 70

△ 80

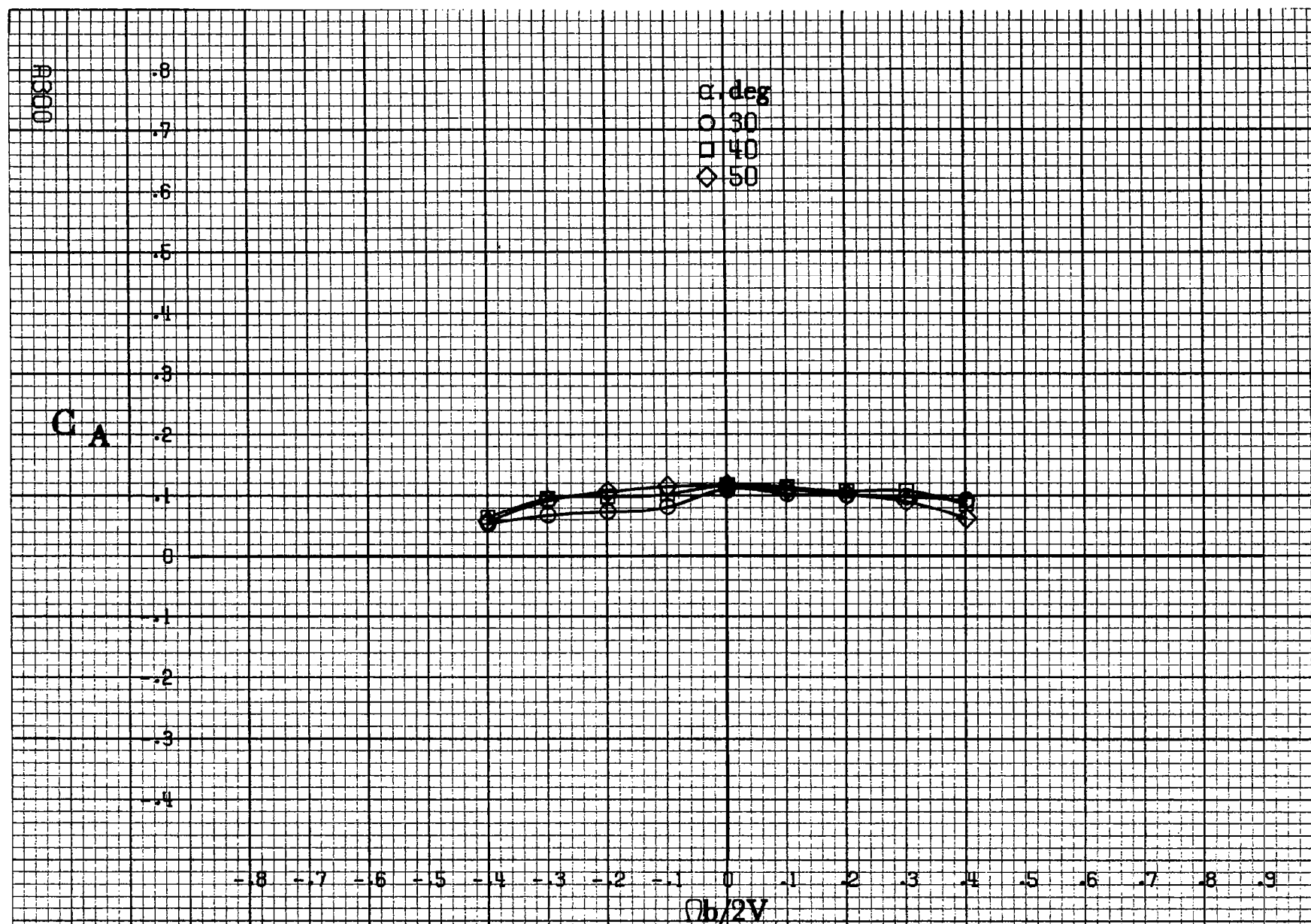
▽ 90

-0.8 -0.7 -0.6 -0.5 -0.4 -0.3 -0.2 -0.1 0 0.1 0.2 0.3 0.4 0.5 0.6 0.7 0.8 0.9

$Ob/2V$

0299

(b) $\alpha=55$ to 90 deg, $SR=0$.
Figure A83.-Concluded.



(a) $\alpha = 30$ to 50 deg, $SR = 0$.

Figure A84. Effect of rotation rate and angle of attack on axial-force coefficient for basic configuration. $\delta_c = 0^\circ$, $\delta_a = 20.0^\circ$, $\delta_d = 6^\circ$, $\delta_r = 0^\circ$, $\beta = 0^\circ$.

C_A

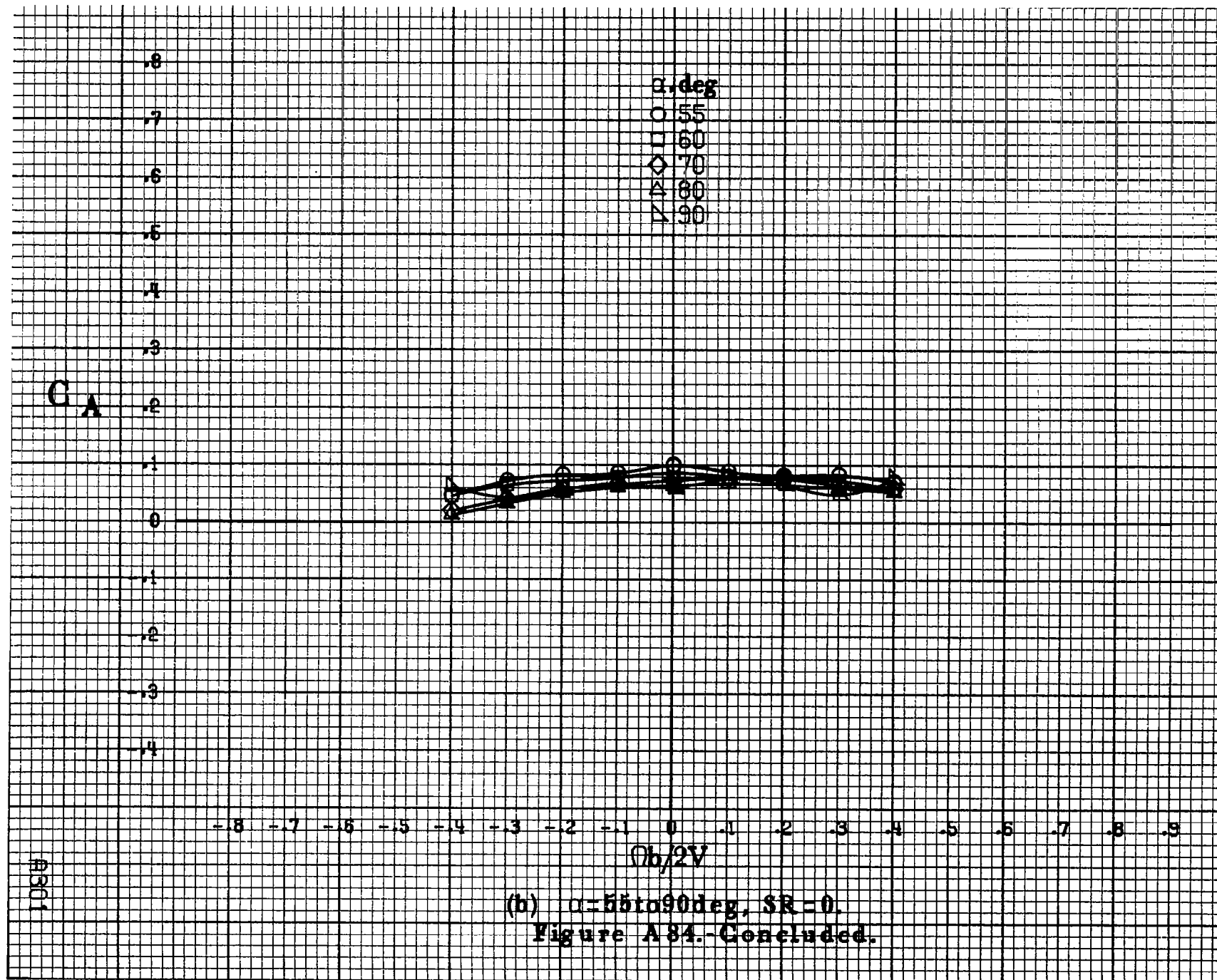
α, deg
 ○ 55
 □ 60
 ◇ 70
 △ 80
 ▽ 90

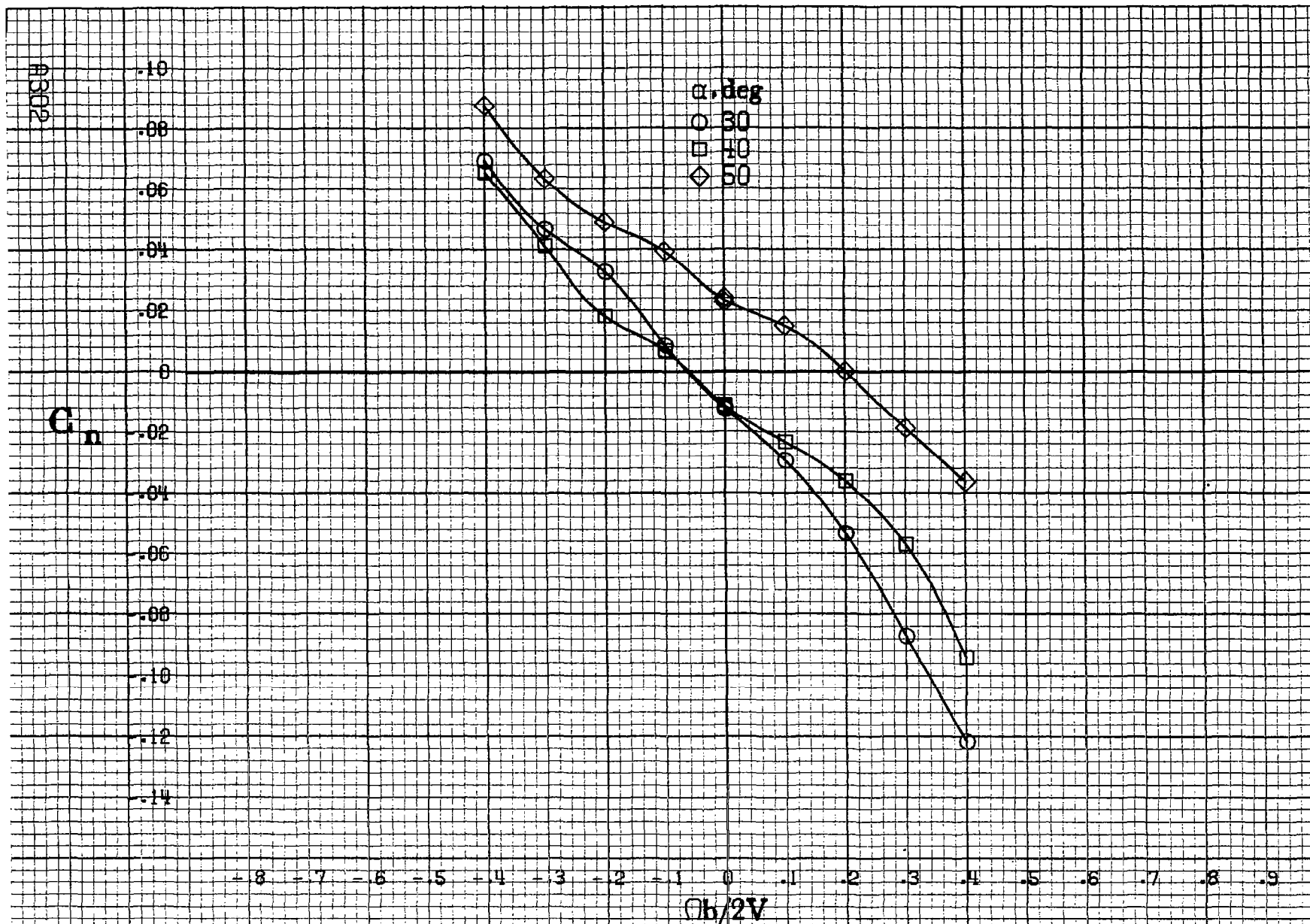
-0.8 -0.7 -0.6 -0.5 -0.4 -0.3 -0.2 -0.1 0 .1 .2 .3 .4 .5 .6 .7 .8 .9

$Ob/2V$

A801

(b) $\alpha=55\text{to}90\text{deg}$, $SR=0$.
 Figure A84.-Concluded.





(a) $\alpha = 30$ to 50 deg, $SR = 0$.

Figure A85.- Effect of rotation rate and angle of attack on yawing-moment coefficient for basic configuration. $\delta_e = 0^\circ$, $\delta_a = 20.0^\circ$, $\delta_d = 6^\circ$, $\delta_r = 0^\circ$, $\beta = 10^\circ$.

C_n

α, deg

- 55
- 60
- ◇ 70
- △ 80
- ▽ 90

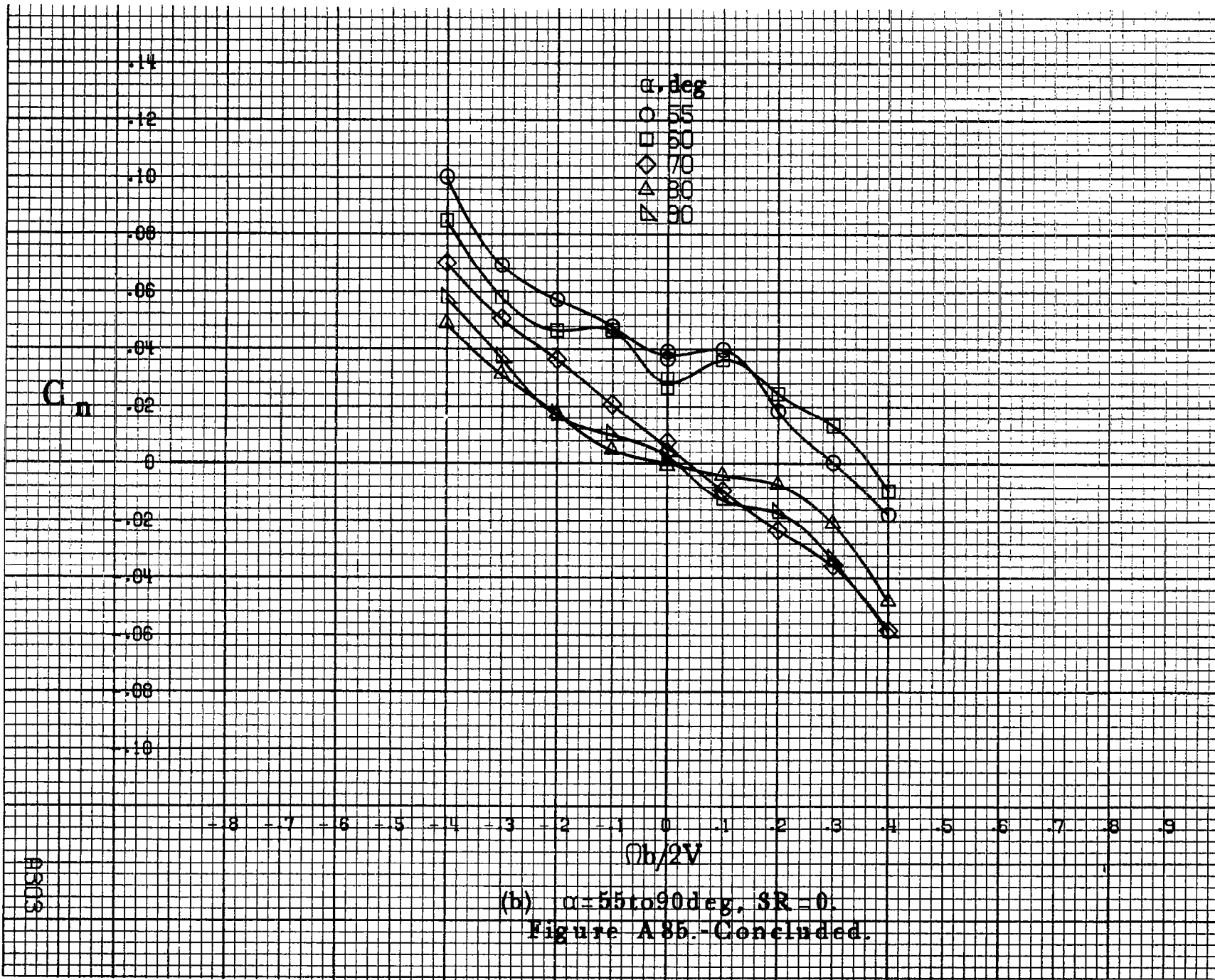
.14
.12
.10
.08
.06
.04
.02
0
-.02
-.04
-.06
-.08
-.10

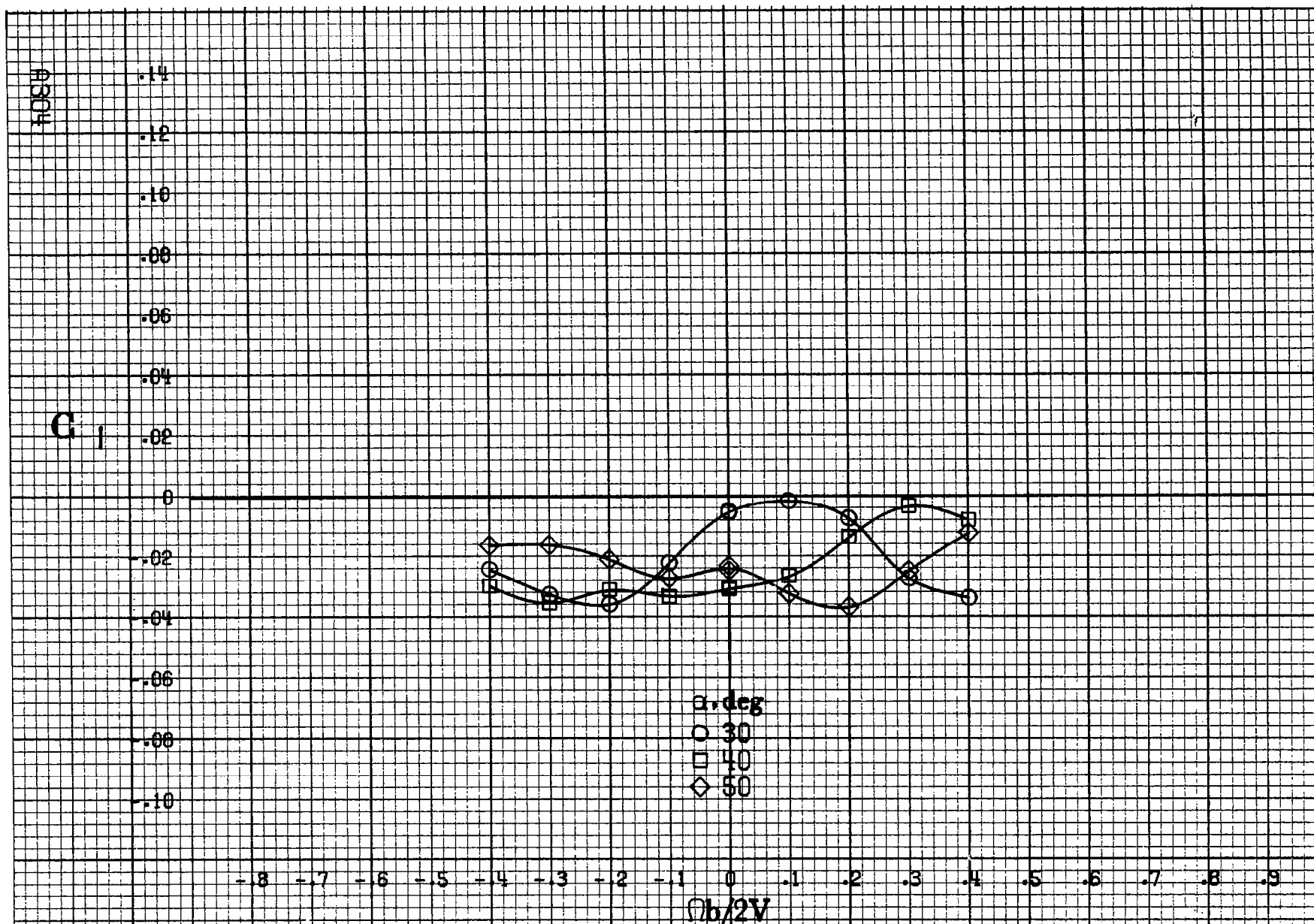
-8 -7 -6 -5 -4 -3 -2 -1 0 -1 -2 -3 -4 .5 .6 .7 .8 .9

$\phi b/2V$

FIG 5

(b) $\alpha=55$ to 90 deg, $SR=0$.
Figure A85.-Concluded.





(a) $\alpha = 30$ to 50° , $SR = 0$.

Figure A.86.- Effect of rotation rate and angle of attack on rolling-moment coefficient for basic configuration. $\delta_e = 0^\circ$, $\delta_a = 20.0^\circ$, $\delta_d = 6^\circ$, $\delta_r = 0^\circ$, $\beta = 10^\circ$.

C_{II}

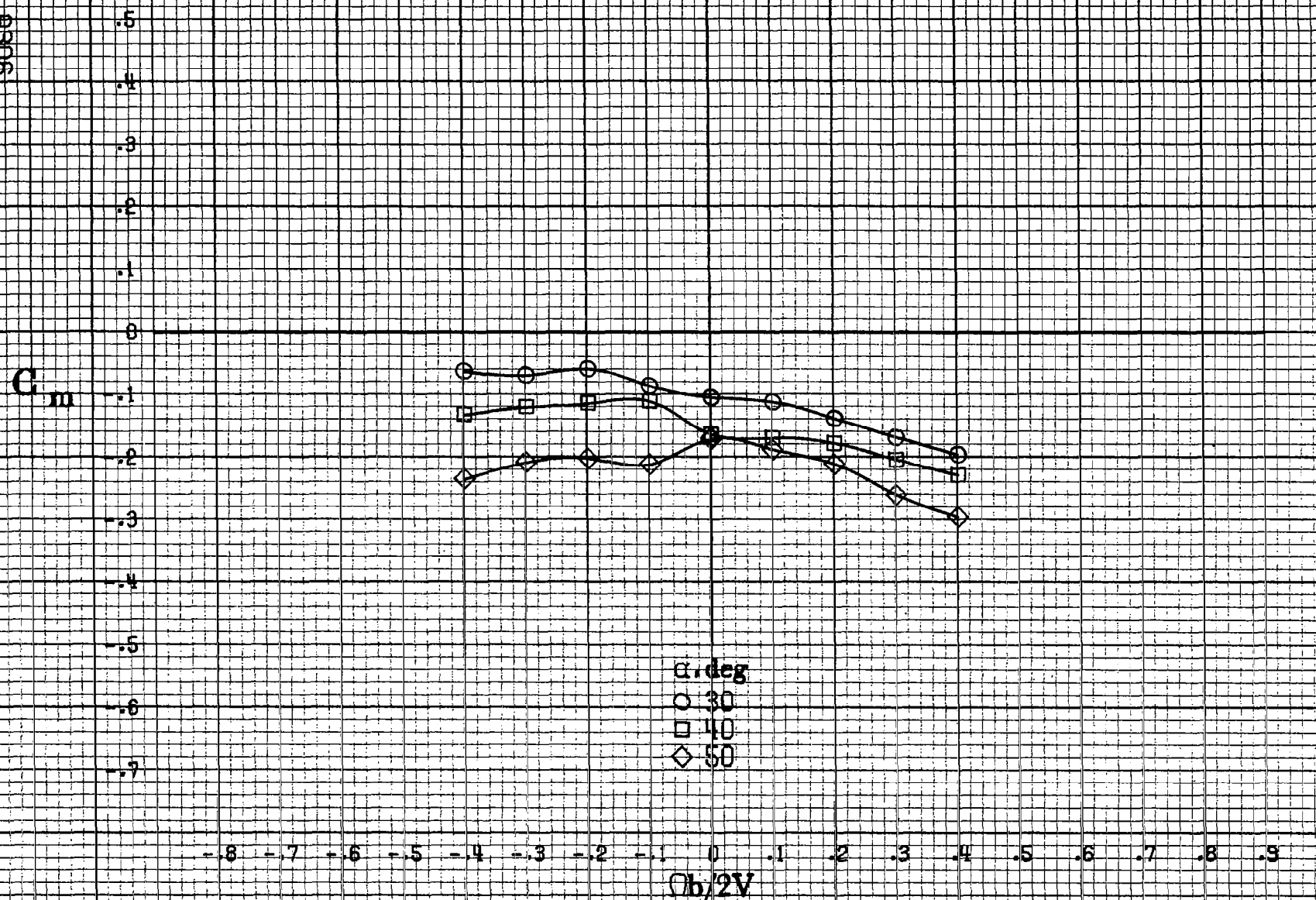
.14
.12
.10
.08
.06
.04
.02
0
-.02
-.04
-.06
-.08
-.10

α , deg
○ 55
□ 60
◇ 70
△ 80
▽ 90

-.8 -.7 -.6 -.5 -.4 -.3 -.2 -.1 0 .1 .2 .3 .4 .5 .6 .7 .8 .9
 $\phi b/2V$

(b) $\alpha=55$ to 90 deg, $SR=0$.
Figure A85.-Concluded.

A305



(a) $\alpha = 30$ to 50° , $SR = 0$.

Figure A87.-Effect of rotation rate and angle of attack on pitching-moment coefficient for basic configuration. $\delta_a = 0^\circ$, $\delta_s = 20.0^\circ$, $\delta_d = 6^\circ$, $\delta_r = 0^\circ$, $\beta = 10^\circ$.

C_m

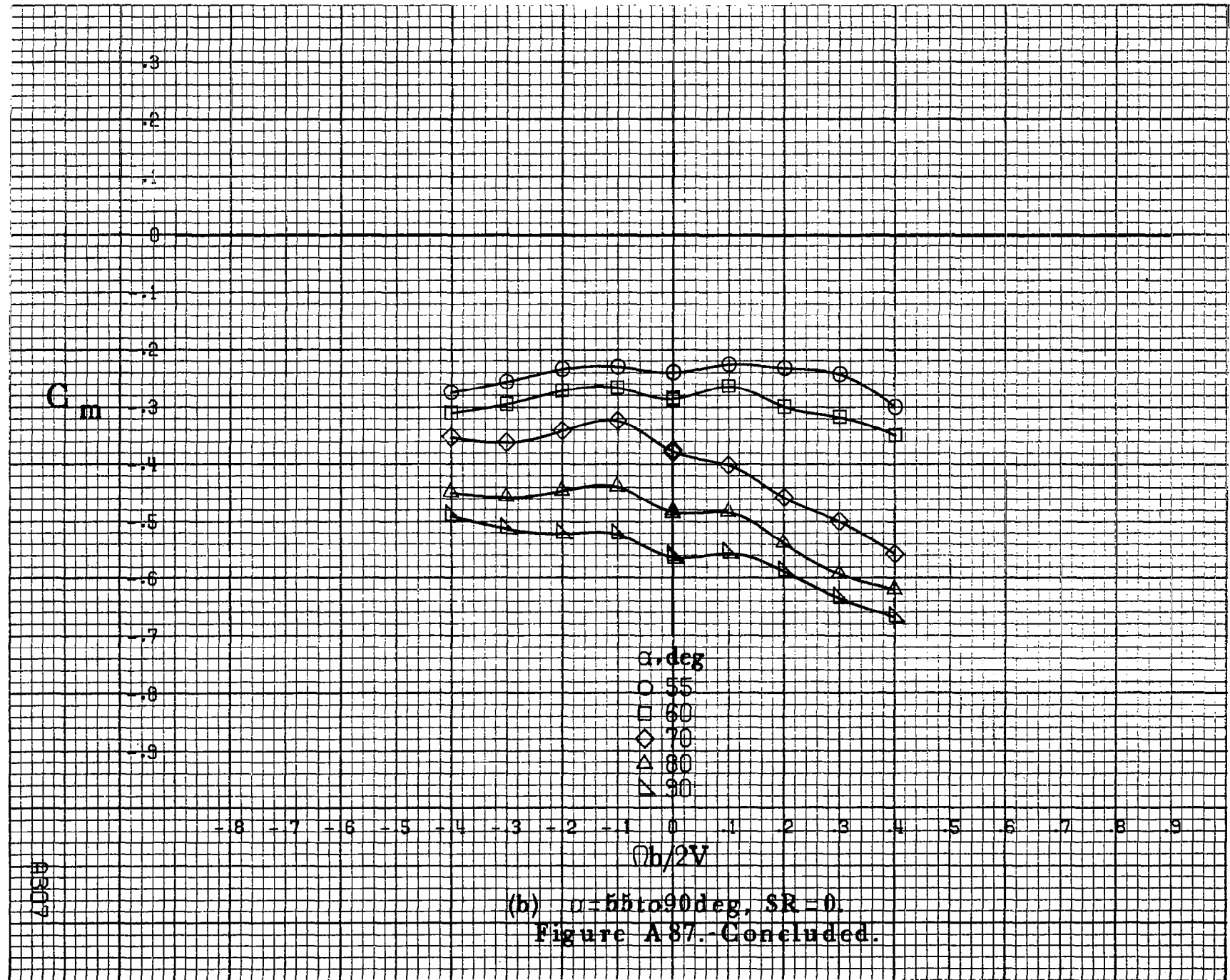
.3
.2
.1
0
-.1
-.2
-.3
-.4
-.5
-.6
-.7
-.8
-.9

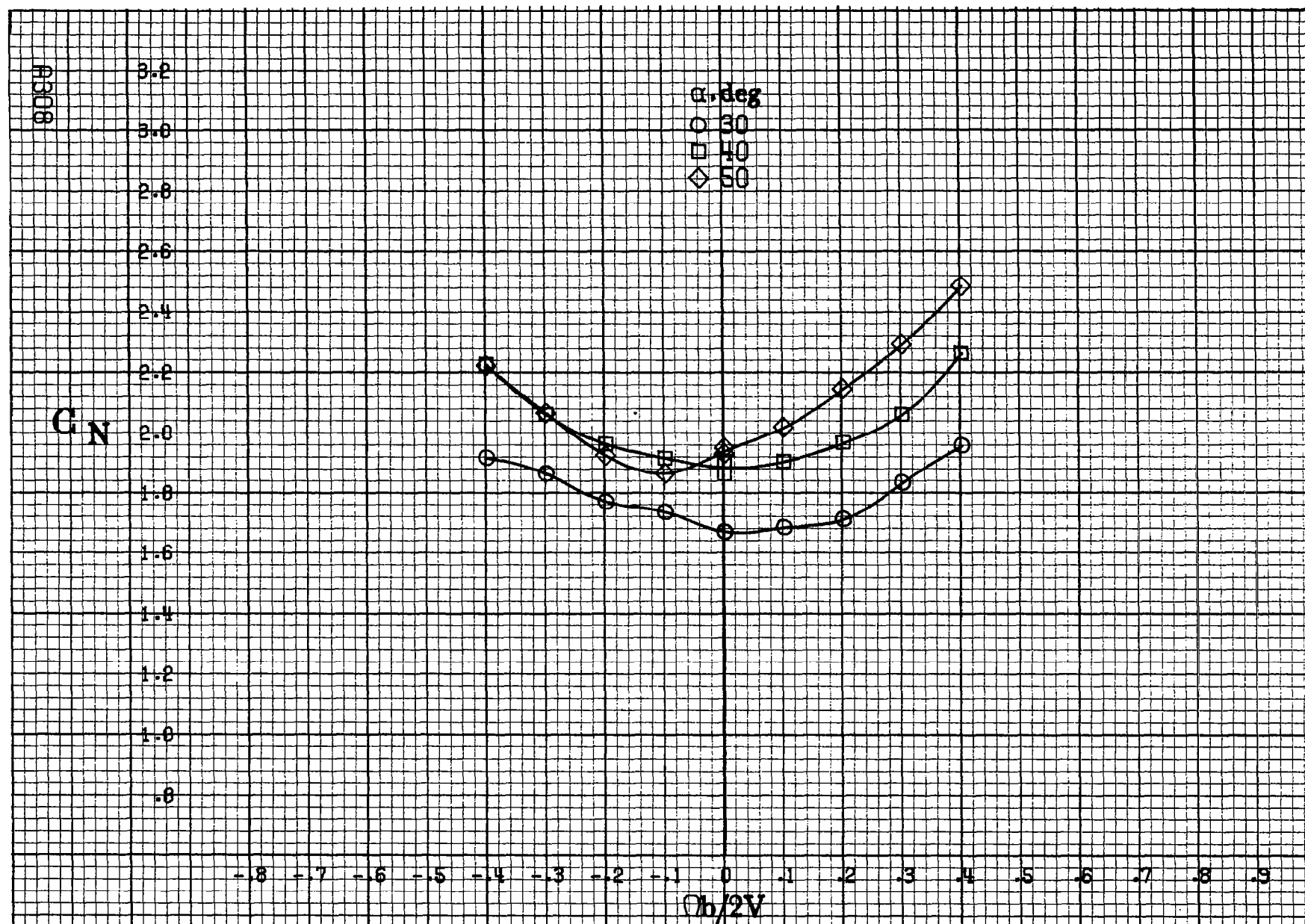
α, deg
○ 55
□ 60
◇ 70
△ 80
▽ 90

-8 -7 -6 -5 -4 -3 -2 -1 0 -1 -2 -3 -4 -5 -6 -7 -8 -9
 $b/2V$

A307

(b) $\alpha=55$ to 90 deg, $SR=0$.
Figure A87.-Concluded.





(a) $\alpha = 30$ to 50 deg, $SR = 0$.

Figure A88.-Effect of rotation rate and angle of attack on normal-force coefficient for basic configuration. $\delta_c = 0^\circ$, $\delta_a = 20.0^\circ$, $\delta_d = 6^\circ$, $\delta_r = 0^\circ$, $\delta = 10^\circ$.

C_N

α, deg
 ○ 55
 □ 60
 ◇ 70
 ▲ 80
 ▴ 85

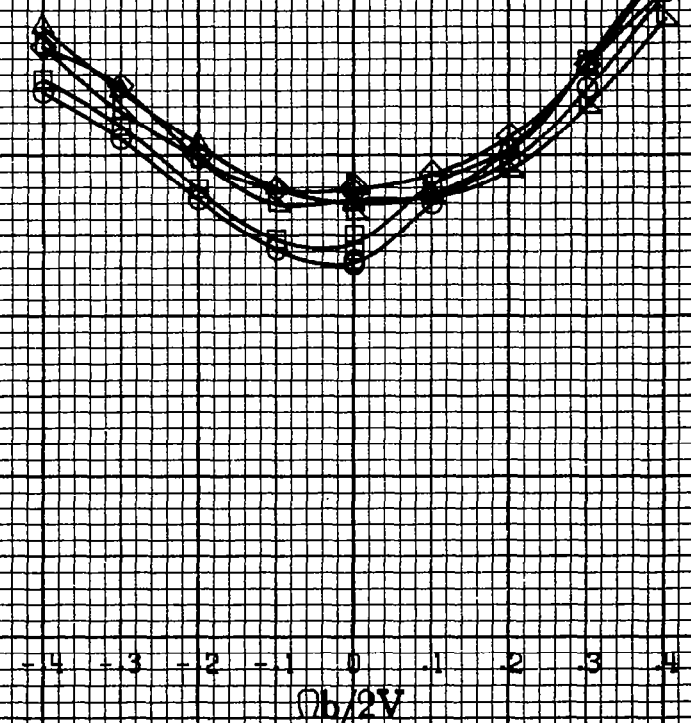
3.6
3.4
3.2
3.0
2.8
2.6
2.4
2.2
2.0
1.8
1.6
1.4
1.2

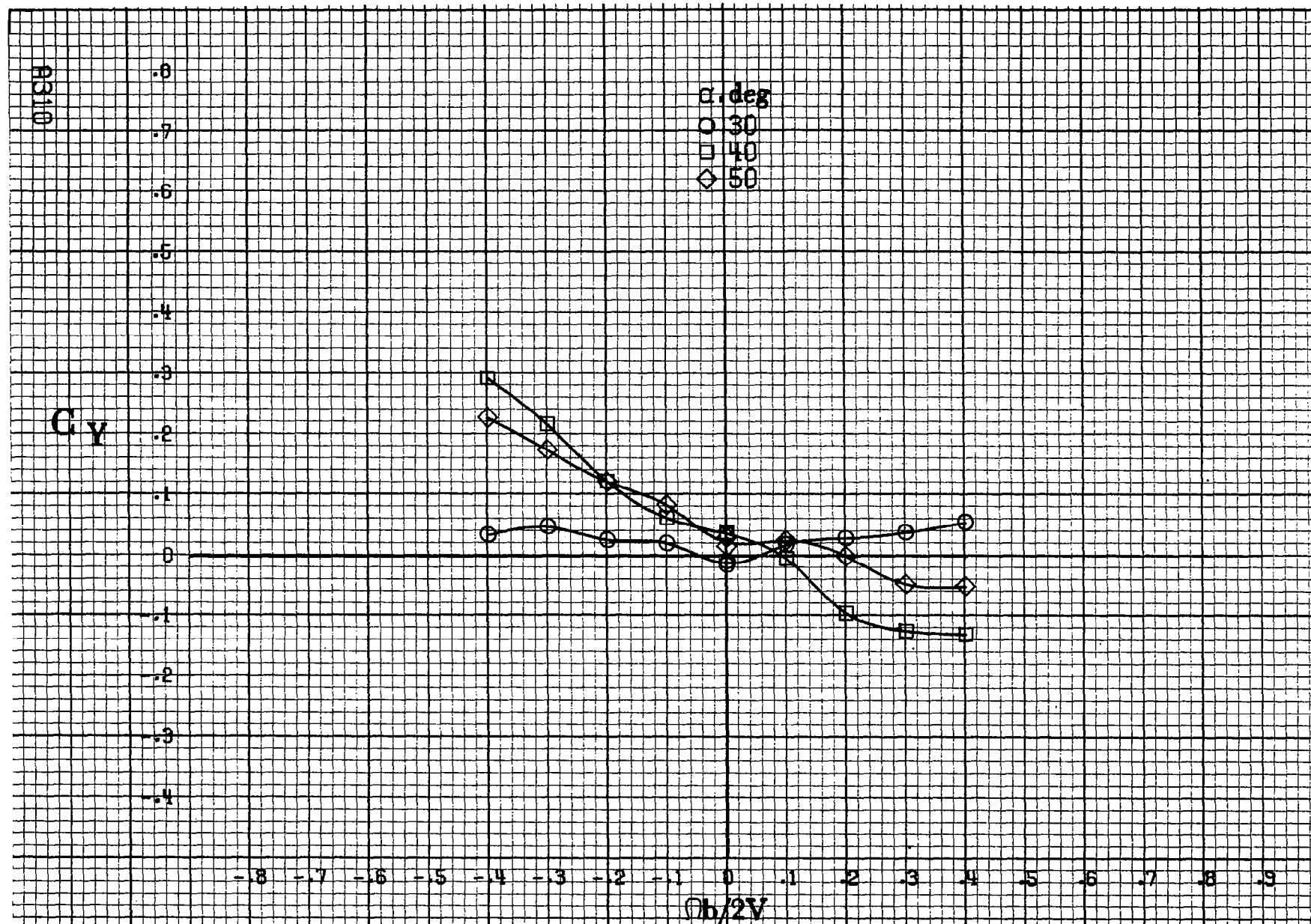
-8 -7 -6 -5 -4 -3 -2 -1 0 1 2 3 4 5 6 7 8 9

$\phi b/2V$

A509

(b) $\alpha=55\text{ to }90\text{deg}$, $SR=0$.
 Figure A88.-Concluded.





(a) $\alpha = 30$ to 50° , $SR = 0$.

Figure A89.-Effect of rotation rate and angle of attack on side-force coefficient for basic configuration. $\delta_e = 0^\circ$, $\delta_a = 20.0^\circ$, $\delta_{\dot{a}} = 6^\circ$, $\delta_r = 0^\circ$, $\beta = 10^\circ$.

C_Y

α, deg

○ 55

□ 60

◇ 70

△ 80

▽ 90

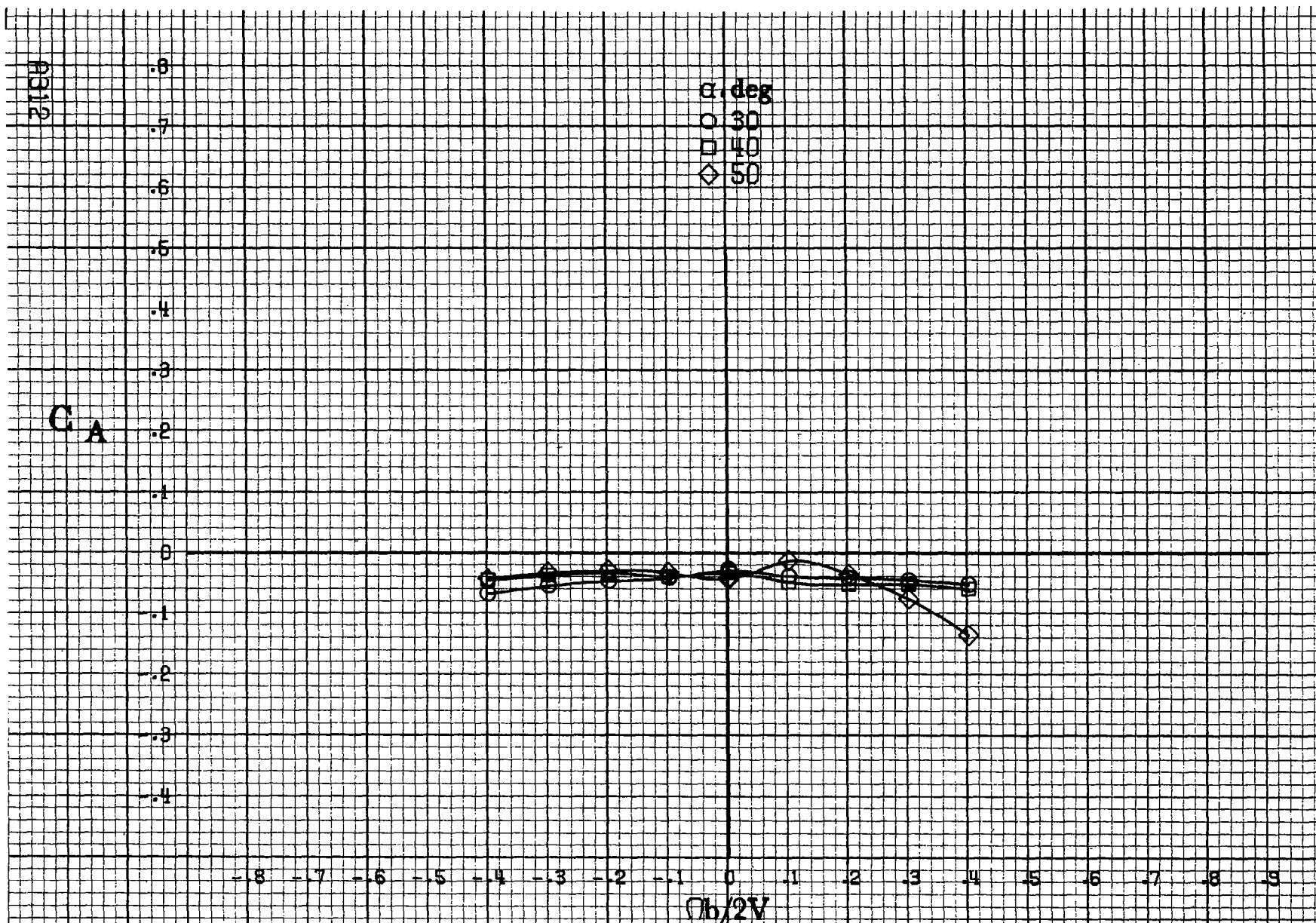
-0.8 -0.7 -0.6 -0.5 -0.4 -0.3 -0.2 -0.1 0 .1 .2 .3 .4 .5 .6 .7 .8 .9

$Ob/2V$

(b) $\alpha = 55 \text{ to } 90 \text{ deg}, SR = 0.$

Figure A 89.- Concluded.

A9311



(a) $\alpha = 30$ to 50 deg, $SR = 0$.

Figure A90 - Effect of rotation rate and angle of attack on axial-force coefficient for basic configuration. $\delta_e = 0^\circ$, $\delta_a = 20.0^\circ$, $\delta_s = 6^\circ$, $\delta_r = 0^\circ$, $\beta = 10^\circ$.

C_A

α, deg
 ○ 55
 □ 60
 ◇ 70
 △ 80
 ▽ 90

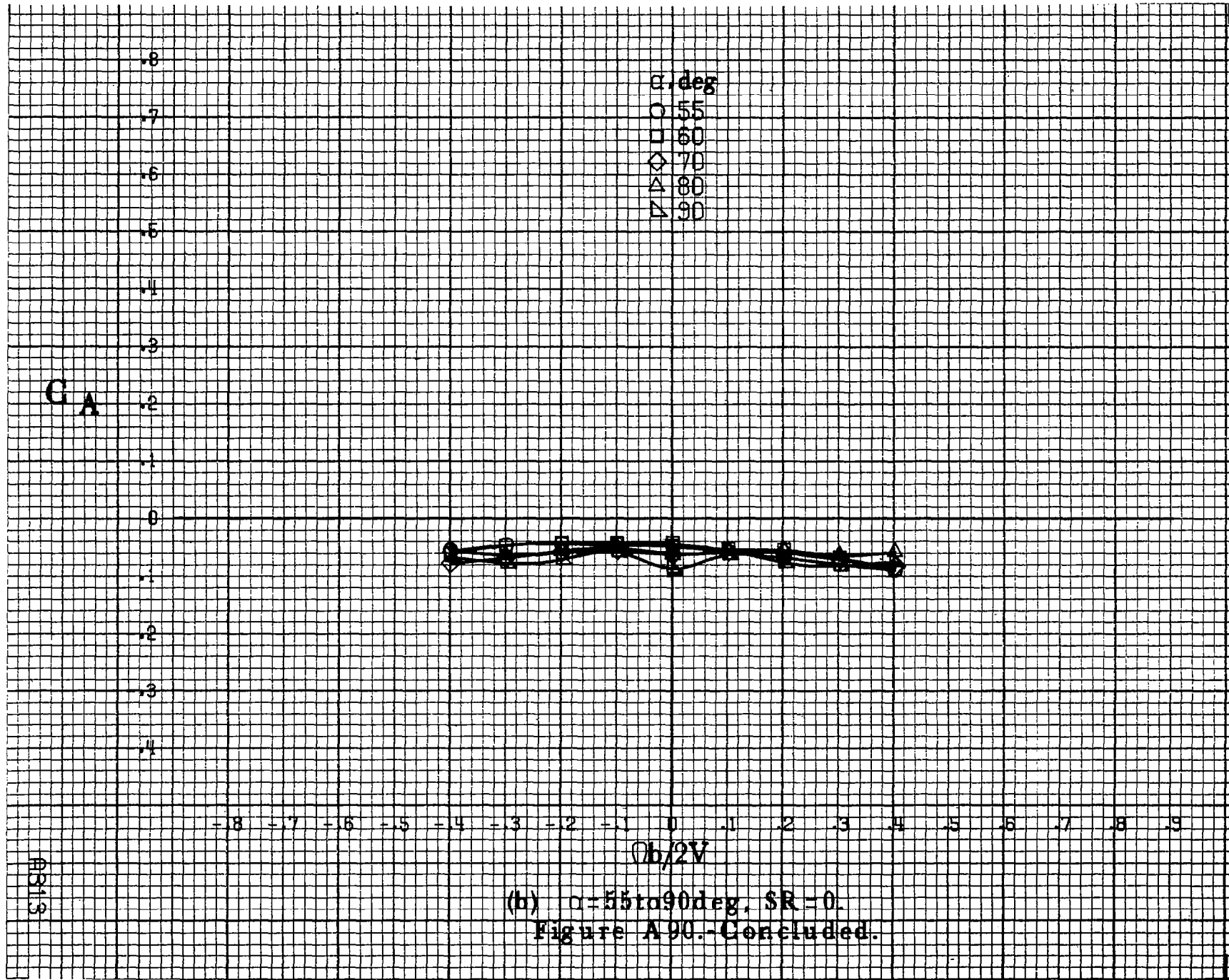
.8
.7
.6
.5
.4
.3
.2
.1
0
-.1
-.2
-.3
-.4

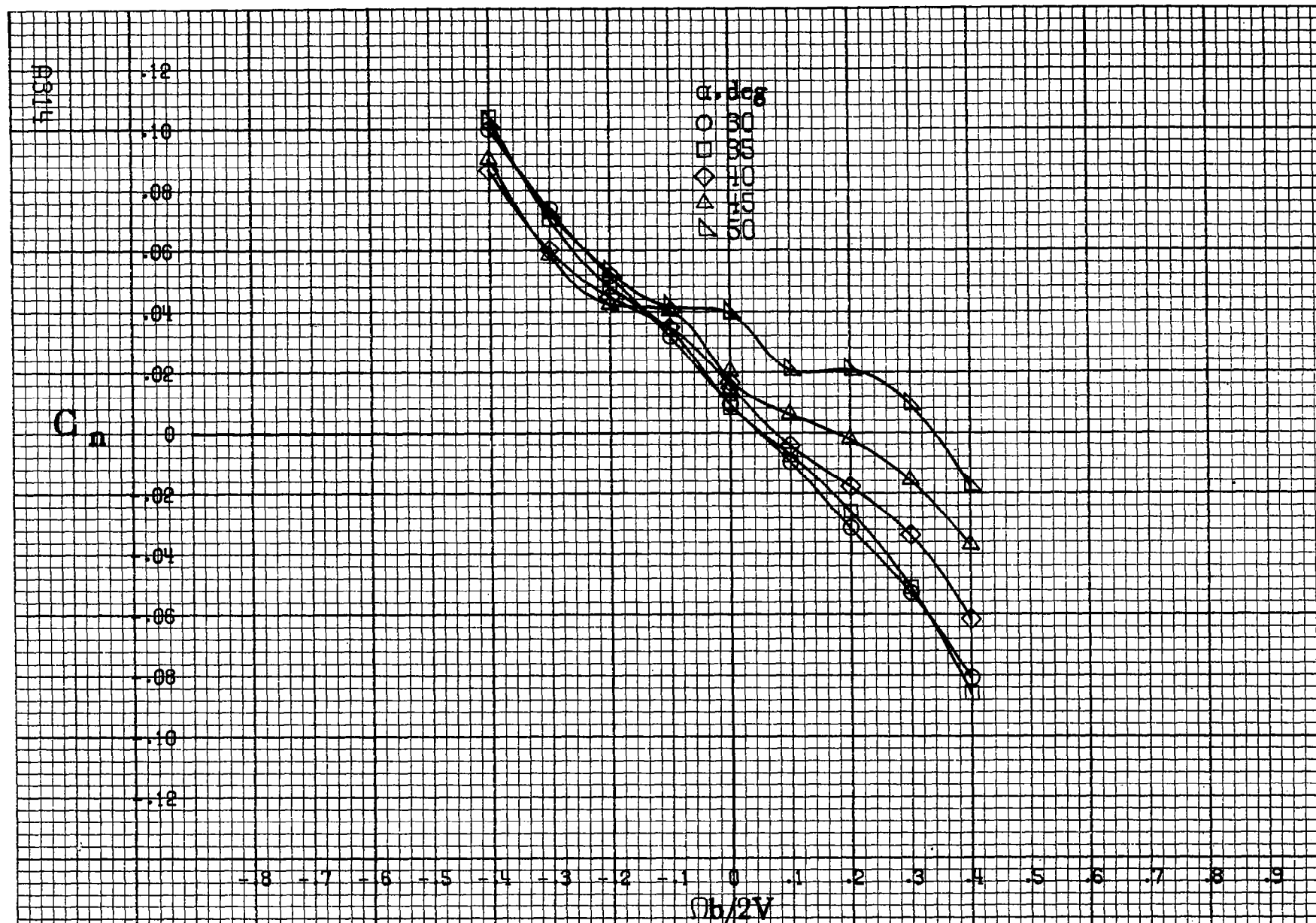
-.8 -.7 -.6 -.5 -.4 -.3 -.2 -.1 0 .1 .2 .3 .4 .5 .6 .7 .8 .9

$Ob/2V$

ASIS

(b) $\alpha=55\text{to}90\text{deg}$, $SR=0$.
 Figure A90.- Concluded.





(a) $\alpha = 30$ to 50 deg, $SR = 0$.

Figure A91.-Effect of rotation rate and angle of attack on yawing-moment coefficient for basic configuration. $\delta_a = 0^\circ$, $\delta_s = 20.0^\circ$, $\delta_d = 6^\circ$, $\delta_r = -15^\circ$, $\beta = 0^\circ$.

C_n

α, deg

- 55
- 60
- ◇ 70
- △ 80
- ▽ 90

.14

.12

.10

.08

.06

.04

.02

0

-.02

-.04

-.06

-.08

-.10

-.8

-.7

-.6

-.5

-.4

-.3

-.2

-.1

0

.1

.2

.3

.4

.5

.6

.7

.8

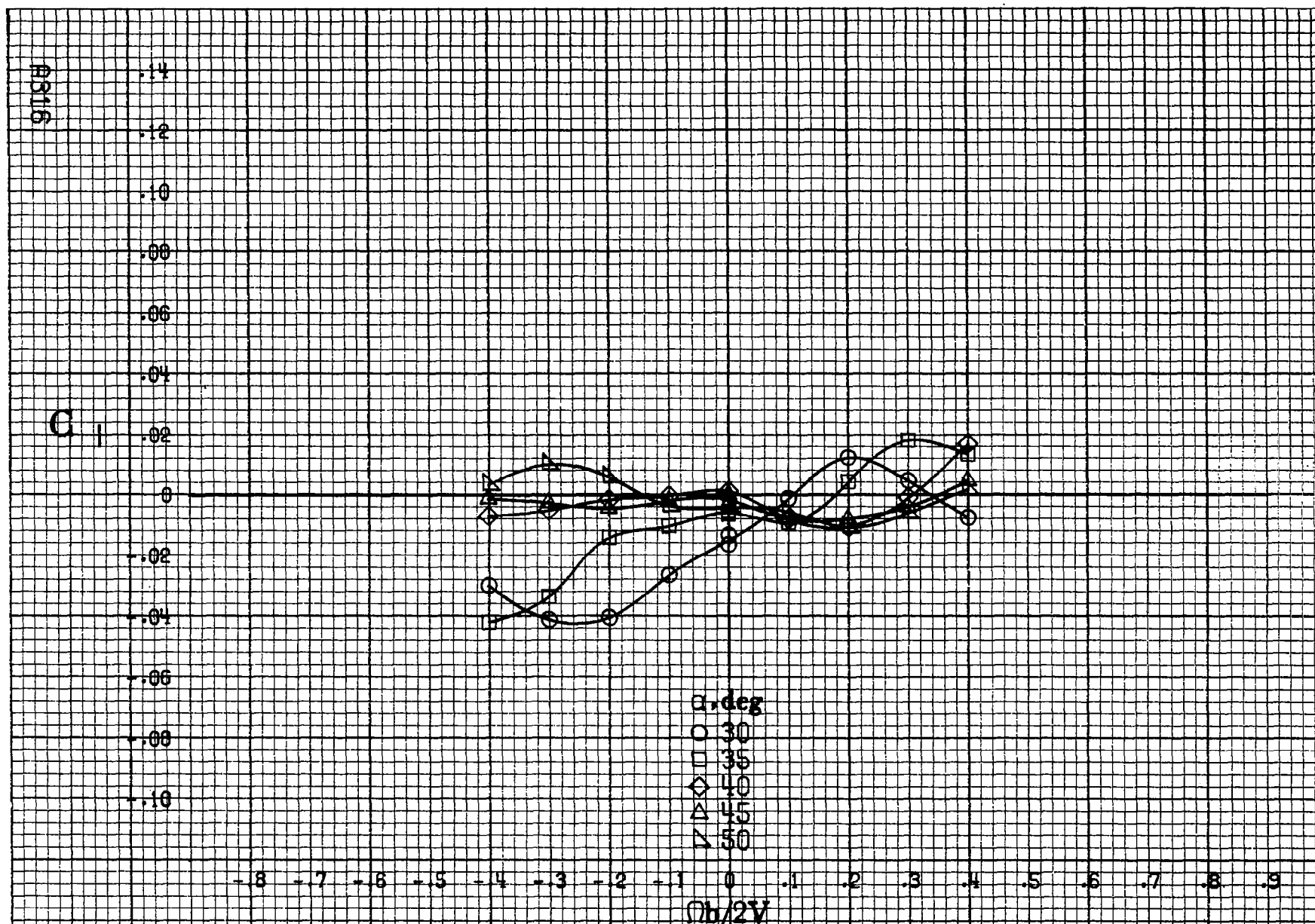
.9

$\phi b/2V$

(b) $\alpha=55$ to 90 deg, $SR=0$.

Figure A91.-Concluded.

A9315



(a) $\alpha = 30$ to 50 deg, $SR = 0$.

Figure A92.-Effect of rotation rate and angle of attack on rolling-moment coefficient for basic configuration. $\delta_a = 0^\circ$, $\delta_s = 20.0^\circ$, $\delta_a = 6^\circ$, $\delta_r = -15^\circ$, $\beta = 0^\circ$.

C₁

.14
.12
.10
.08
.06
.04
.02
0
-.02
-.04
-.06
-.08
-.10

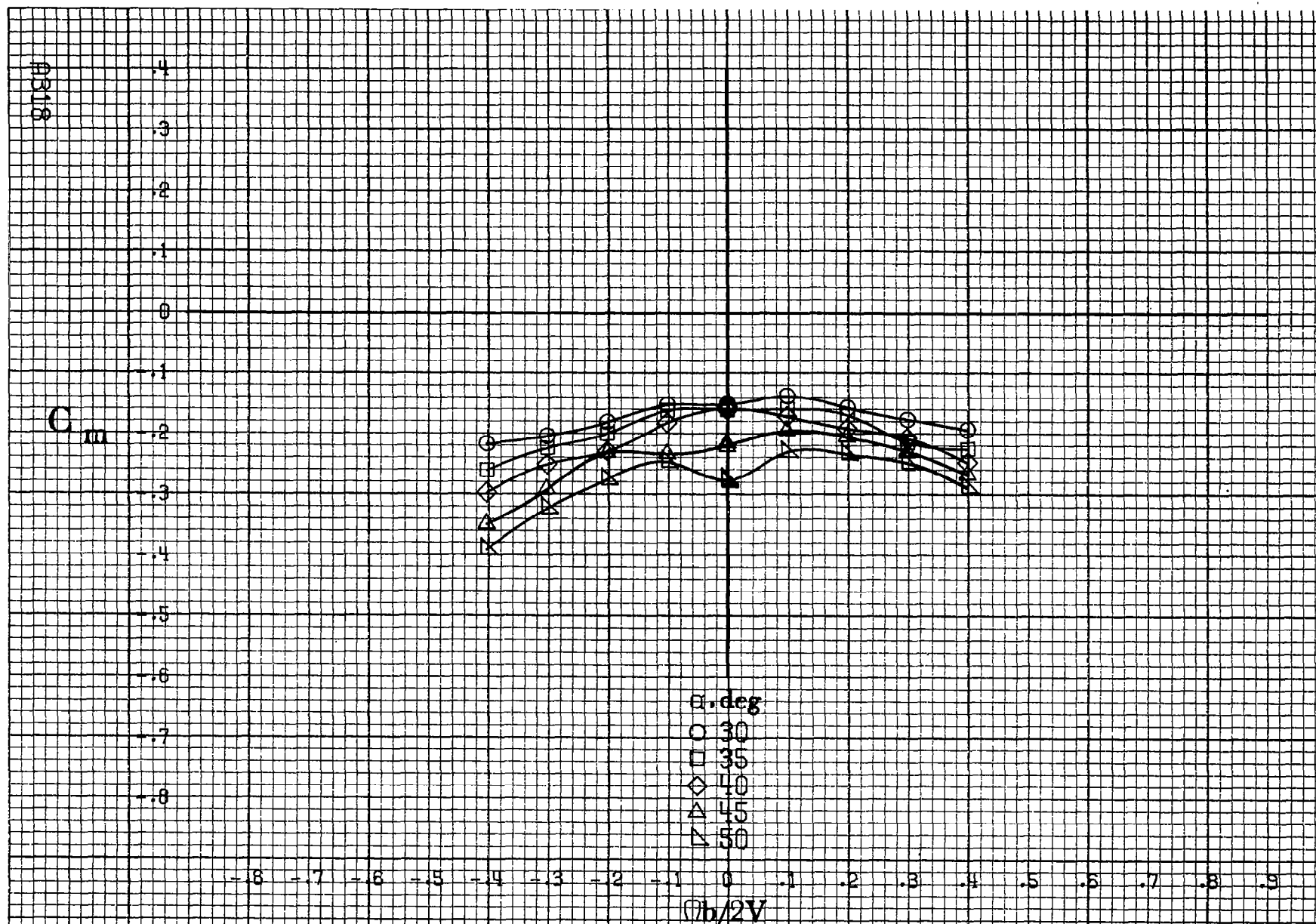
α , deg
○ 55
□ 60
◇ 70
△ 80
▽ 90

-8 -7 -6 -5 -4 -3 -2 -1 0 -1 -2 -3 -4 -5 -6 -7 -8 -9

$\Omega b/2V$

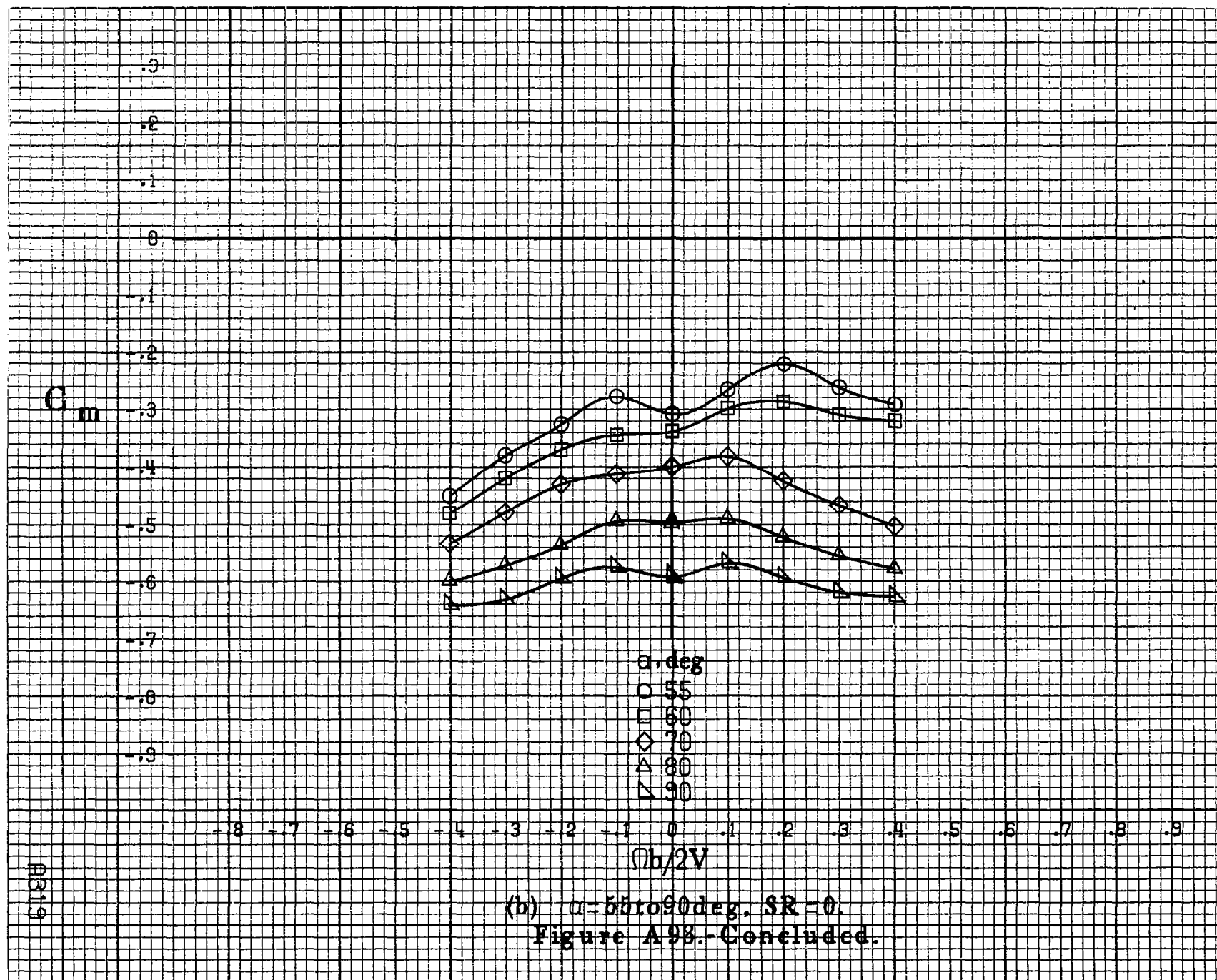
(b) $\alpha=55$ to 90 deg, $SR=0$.
Figure A92.-Concluded.

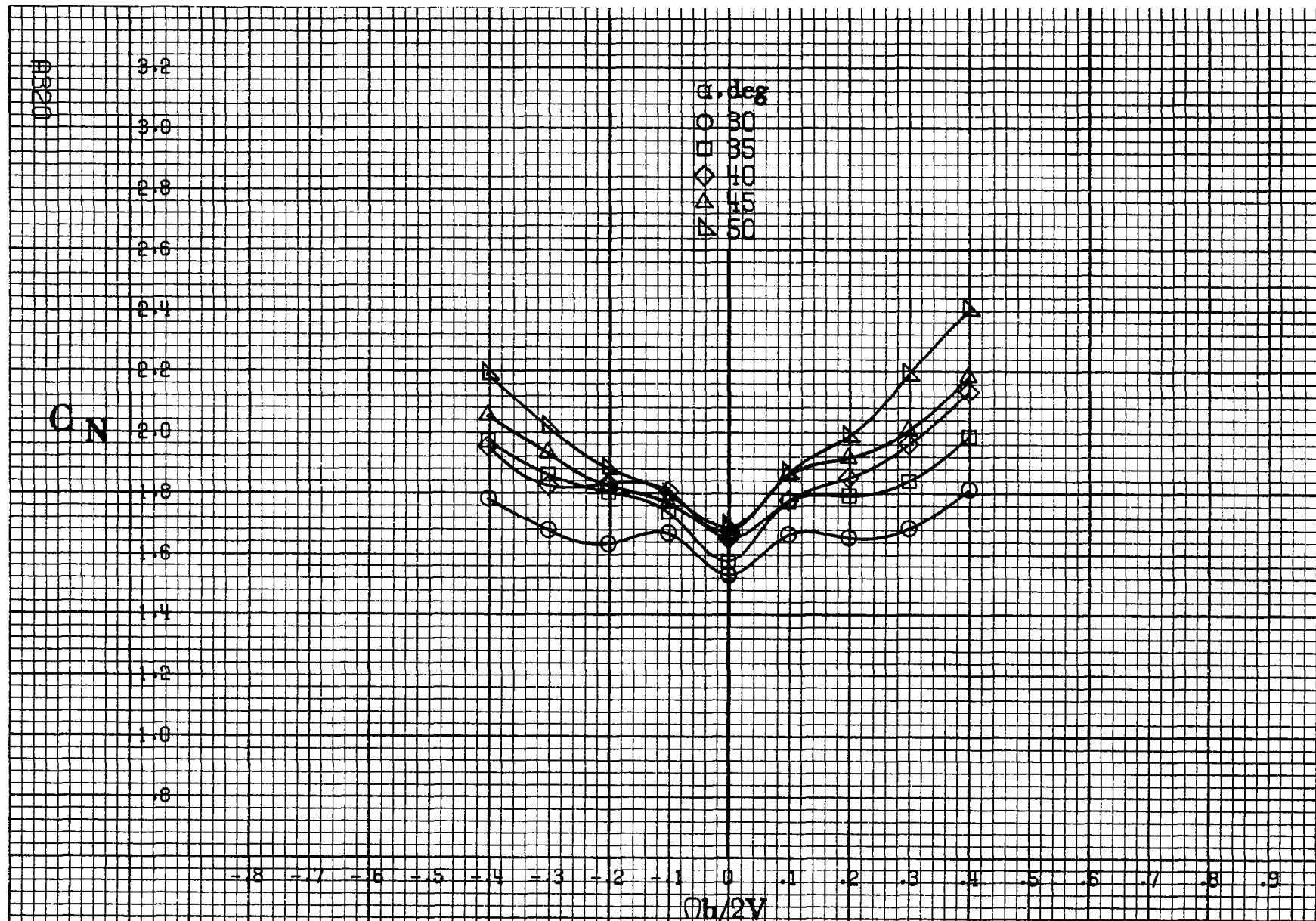
A817



(a) $\alpha = 30 \text{ to } 50 \text{ deg}$, $SR = 0$.

Figure A93.-Effect of rotation rate and angle of attack on pitching-moment coefficient for basic configuration. $\delta_c = 0^\circ$, $\delta_x = 20.0^\circ$, $\delta_d = 6^\circ$, $\delta_r = 15^\circ$, $\beta = 0^\circ$.





(a) $\alpha=30$ to 50 deg, $SR=0$.

Figure A 94.- Effect of rotation rate and angle of attack on normal-force coefficient for basic configuration. $\delta_a = 0^\circ$, $\delta_s = 20.0^\circ$, $\delta_a = 6^\circ$, $\delta_r = -15^\circ$, $\beta = 0^\circ$.

C_N

α, deg
 ○ 55
 □ 60
 ◇ 70
 △ 80
 ▽ 90

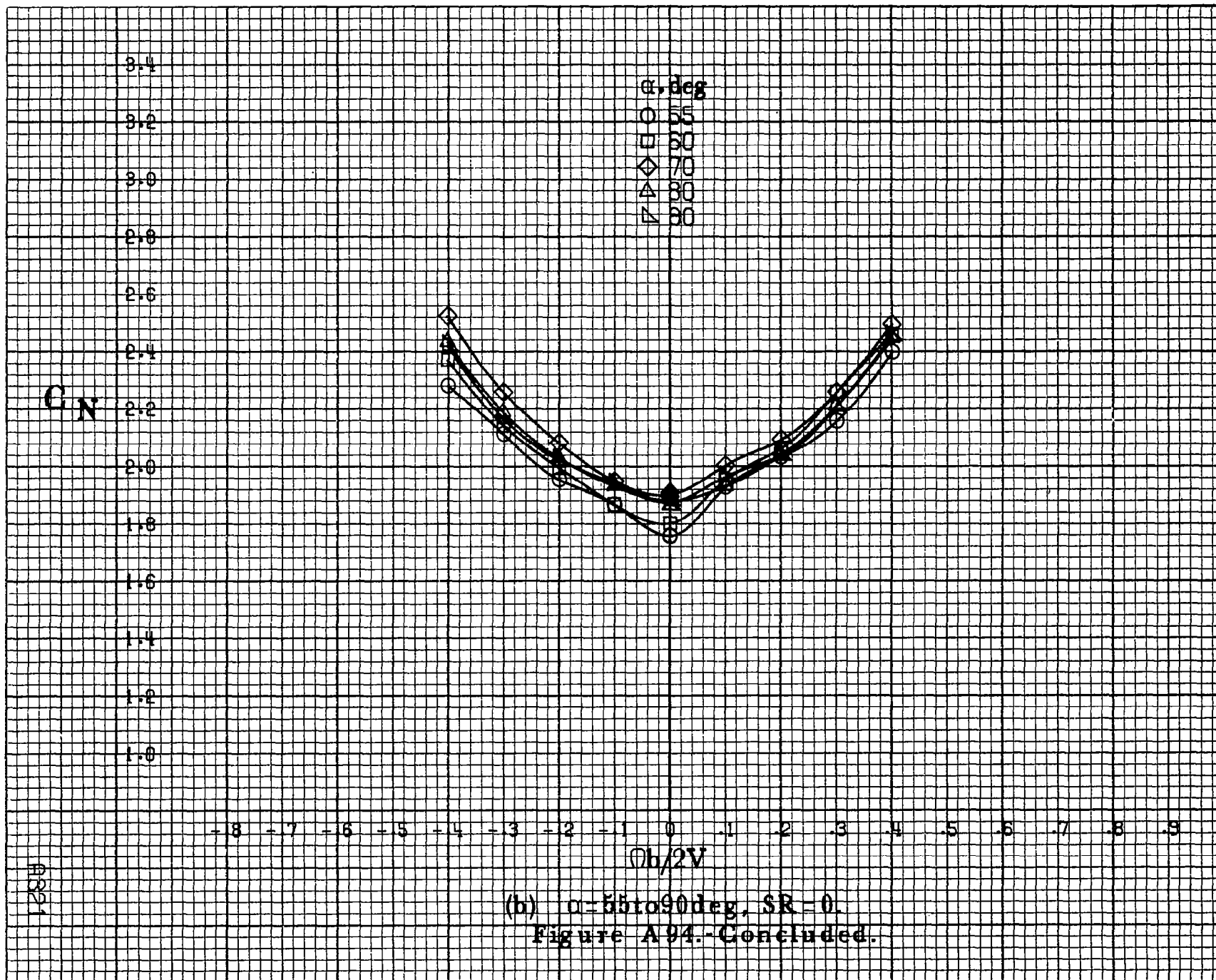
3.4
3.2
3.0
2.8
2.6
2.4
2.2
2.0
1.8
1.6
1.4
1.2
1.0

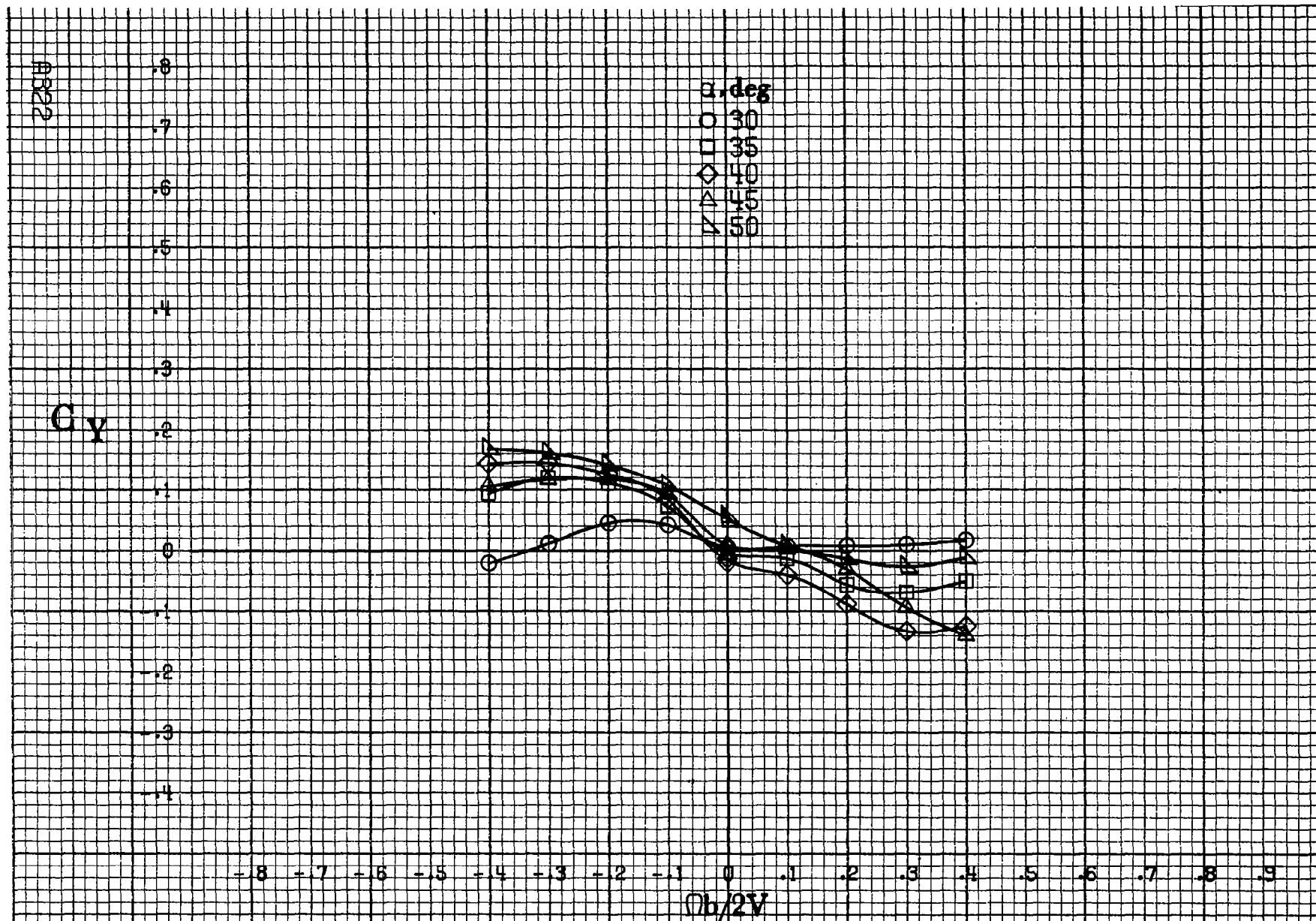
-8 -7 -6 -5 -4 -3 -2 -1 0 .1 .2 .3 .4 .5 .6 .7 .8 .9

$Ob/2V$

(b) $\alpha=55\text{to}90\text{deg}$, $SR=0$.
 Figure A94.-Concluded.

A921





(a) $\alpha=30$ to 50° , $SR=0$.

Figure A95.-Effect of rotation rate and angle of attack on side-force coefficient for basic configuration. $\delta_c = 0^\circ$, $\delta_a = 20.0^\circ$, $\delta_d = 6^\circ$, $\delta_r = -15^\circ$, $\beta = 0^\circ$.

C_y

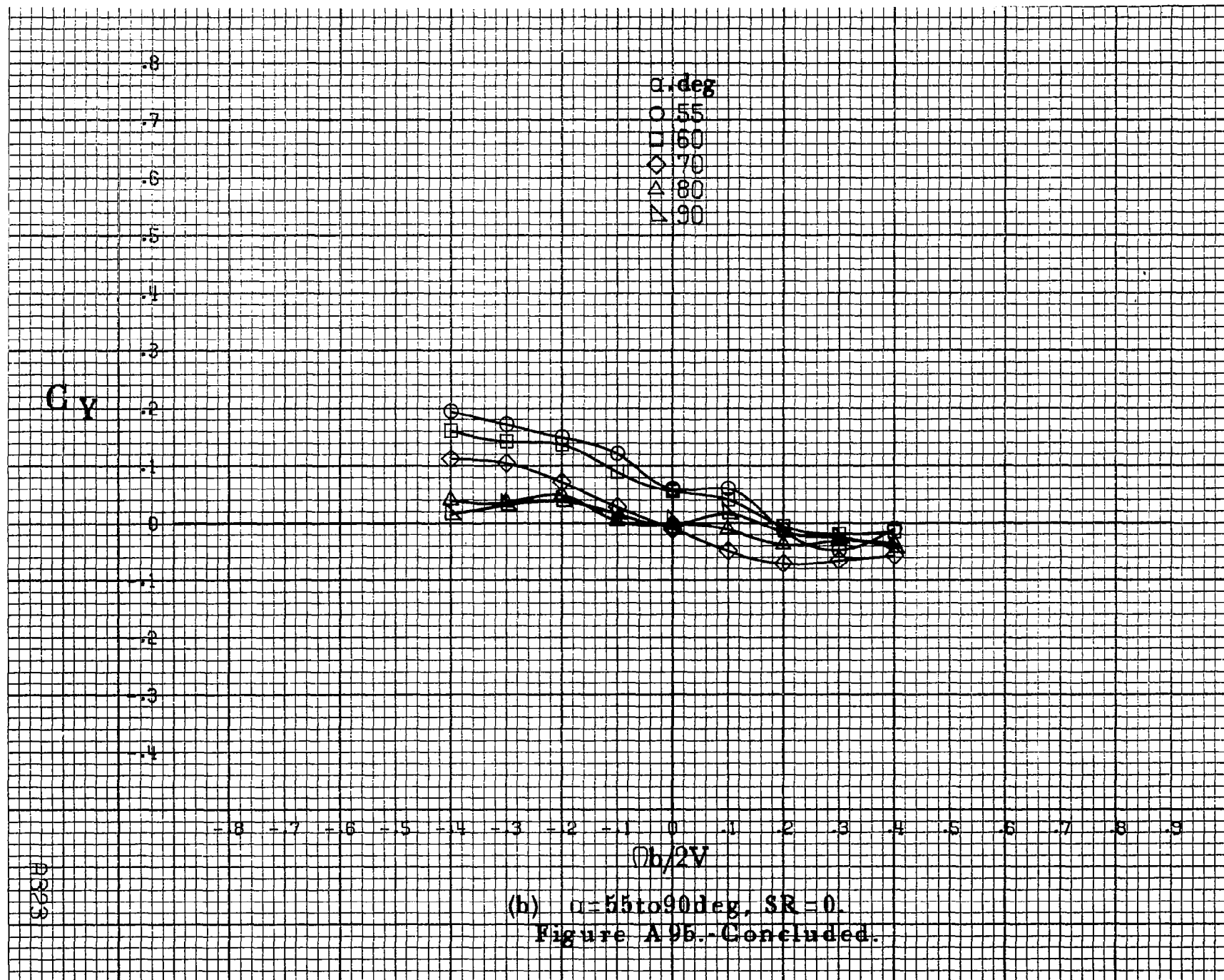
α, deg
 ○ 55
 □ 60
 ◇ 70
 △ 80
 ▽ 90

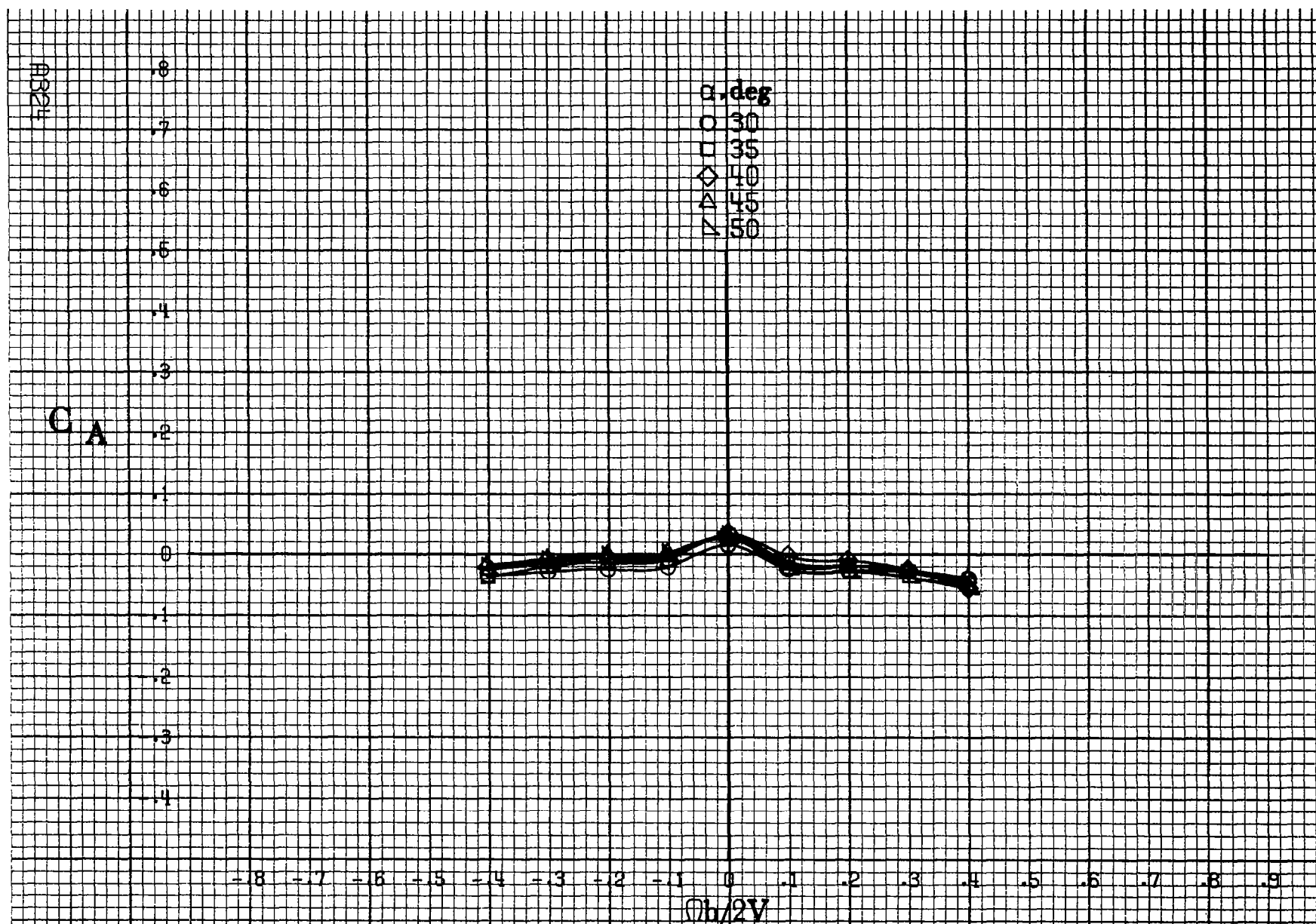
-8 -7 -6 -5 -4 -3 -2 -1 0 .1 .2 .3 .4 .5 .6 .7 .8 .9

$b/2V$

(b) $\alpha = 55 \text{ to } 90 \text{ deg, } SR = 0.$
 Figure A95.- Concluded.

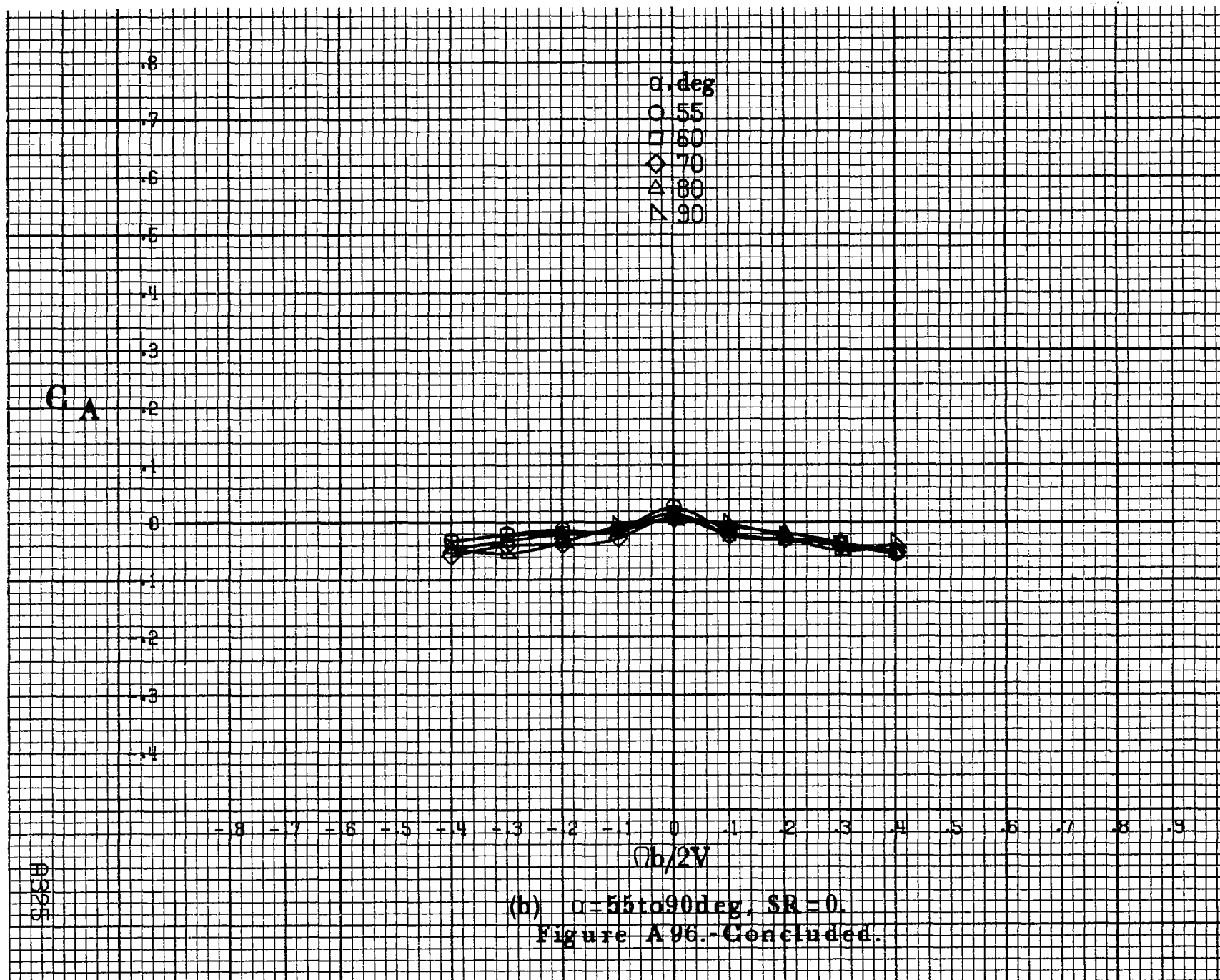
A923



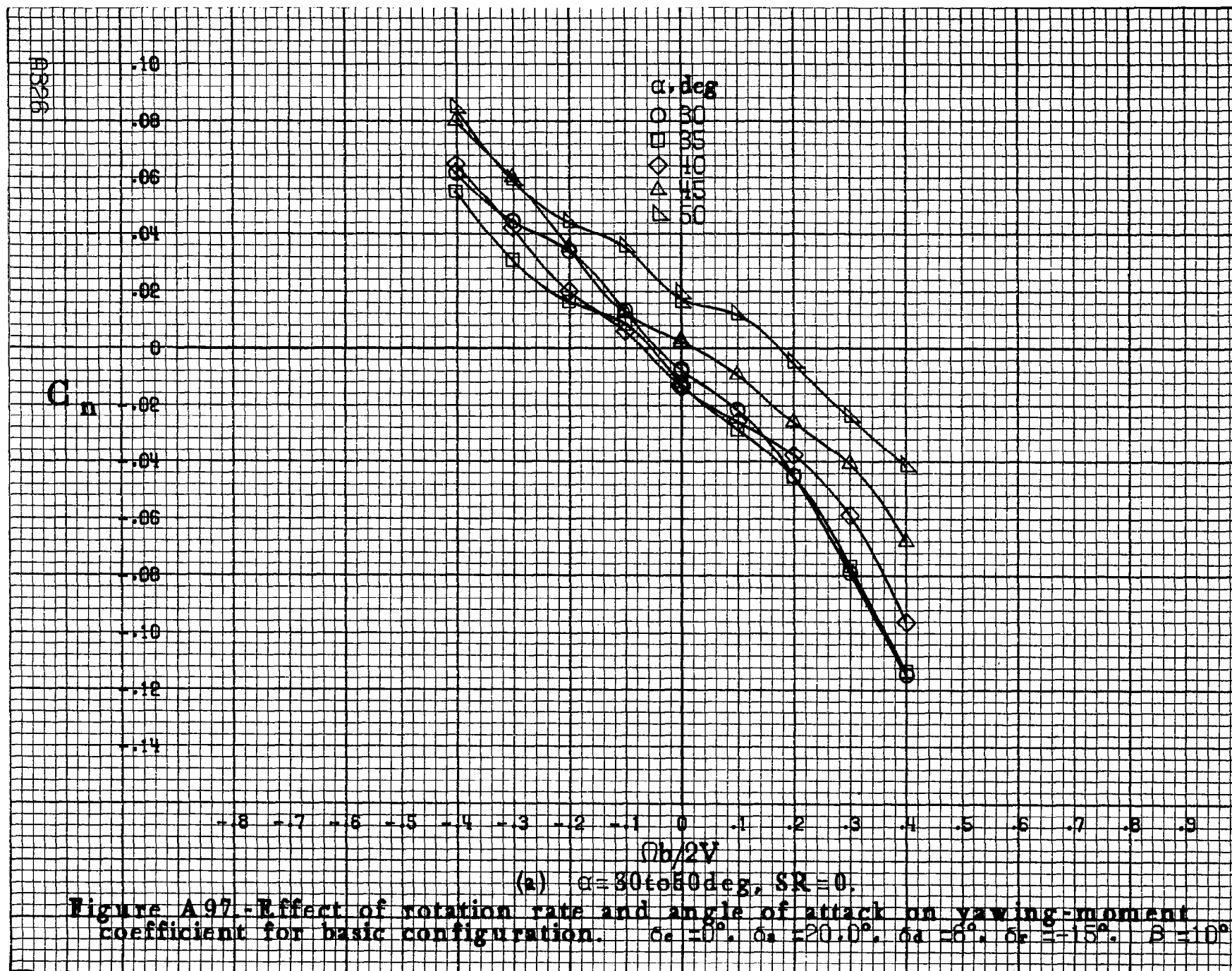


(a) $\alpha = 30$ to 50 deg, $SR = 0$.

Figure A96.-Effect of rotation rate and angle of attack on axial-force coefficient for basic configuration. $\delta_e = 0^\circ$, $\delta_a = 20.0^\circ$, $\delta_d = 6^\circ$, $\delta_r = -15^\circ$, $\beta = 0^\circ$.



(b) $\alpha = 55$ to 90 deg, $SR = 0$.
Figure A96.-Concluded.



C_n

α, deg

- 55
- 60
- ◇ 70
- △ 80
- ▽ 90

-8 -7 -6 -5 -4 -3 -2 -1 0 -1 -2 -3 -4 -5 -6 -7 -8 -9

$Ob/2V$

A927

(b) $\alpha=55$ to 90 deg, $SR=0$.
Figure A97.-Concluded.

.14
.12
.10
.08
.06
.04
.02
0
.02
.04
.06
.08
.10

A928

C

.14
.12
.10
.08
.06
.04
.02
0
-.02
-.04
-.06
-.08
-.10

α, deg
○ 30
□ 35
◇ 40
△ 45
▽ 50

-.8 -.7 -.6 -.5 -.4 -.3 -.2 -.1 0 .1 .2 .3 .4 .5 .6 .7 .8 .9
 $\Omega b/2V$

(a) $\alpha = 30 \text{ to } 50 \text{ deg}$, $SR = 0$.

Figure A98.-Effect of rotation rate and angle of attack on rolling-moment coefficient for basic configuration. $\delta_e = 0^\circ$, $\delta_a = 20.0^\circ$, $\delta_d = 6^\circ$, $\delta_r = -15^\circ$, $\beta = 10^\circ$.

C_1

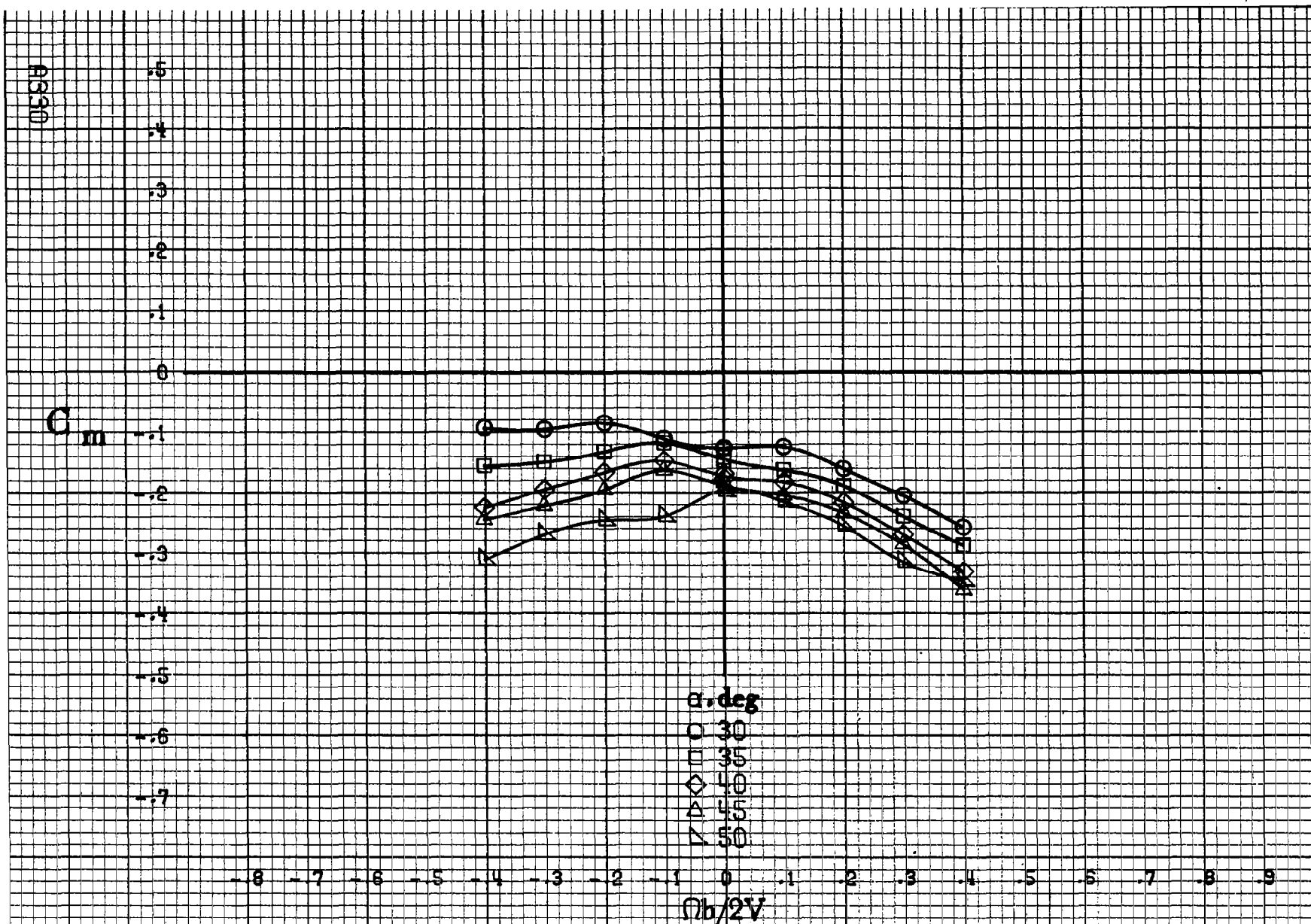
.14
.12
.10
.08
.06
.04
.02
0
-.02
-.04
-.06
-.08
-.10

α, deg
○ 55
□ 60
◇ 70
△ 80
▽ 90

-.8 -.7 -.6 -.5 -.4 -.3 -.2 -.1 0 .1 .2 .3 .4 .5 .6 .7 .8 .9
 $\Omega h/2V$

(b) $\alpha = 55 \text{ to } 90 \text{ deg}, SR = 0$
Figure A98.-Concluded.

A9829



(a) $\alpha = 30$ to 50° , $SR = 0$.

Figure A99.-Effect of rotation rate and angle of attack on pitching-moment coefficient for basic configuration. $\delta_e = 0^\circ$, $\delta_s = 20.0^\circ$, $\delta_d = 6^\circ$, $\delta_r = -15^\circ$, $\beta = 10^\circ$.

C_m

.2
.1
0
-.1
-.2
-.3
-.4
-.5
-.6
-.7
-.8
-.9
-1.0

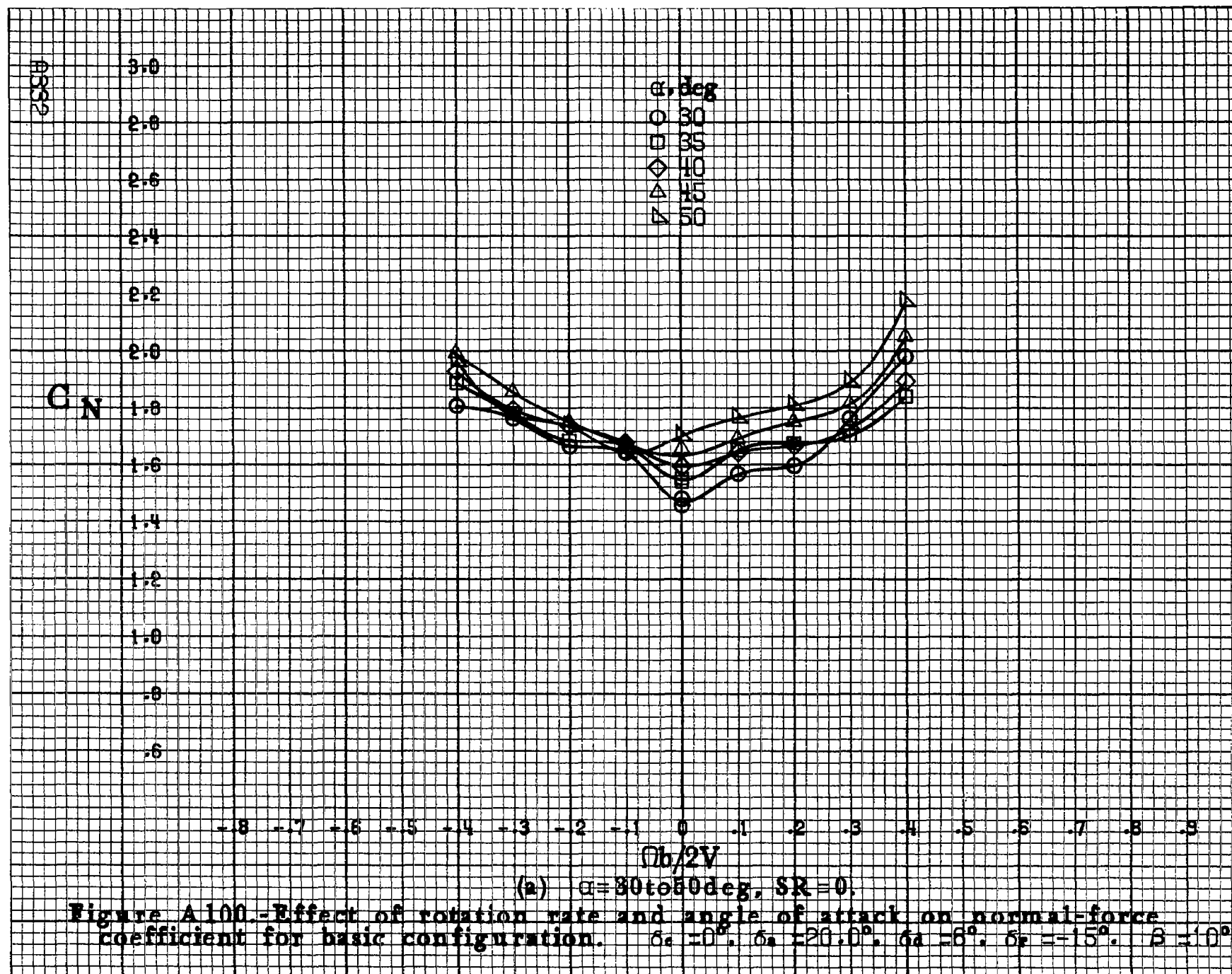
α, deg
○ 55
□ 60
◇ 70
△ 80
▽ 90

-8 -7 -6 -5 -4 -3 -2 -1 0 .1 .2 .3 .4 .5 .6 .7 .8 .9

$\Omega b/2V$

A331

(b) $\alpha=55\text{ to }90\text{deg}$, $SR=0$.
Figure A99.-Concluded.



C_N

α, deg

○ 55

□ 60

◇ 70

△ 80

▽ 90

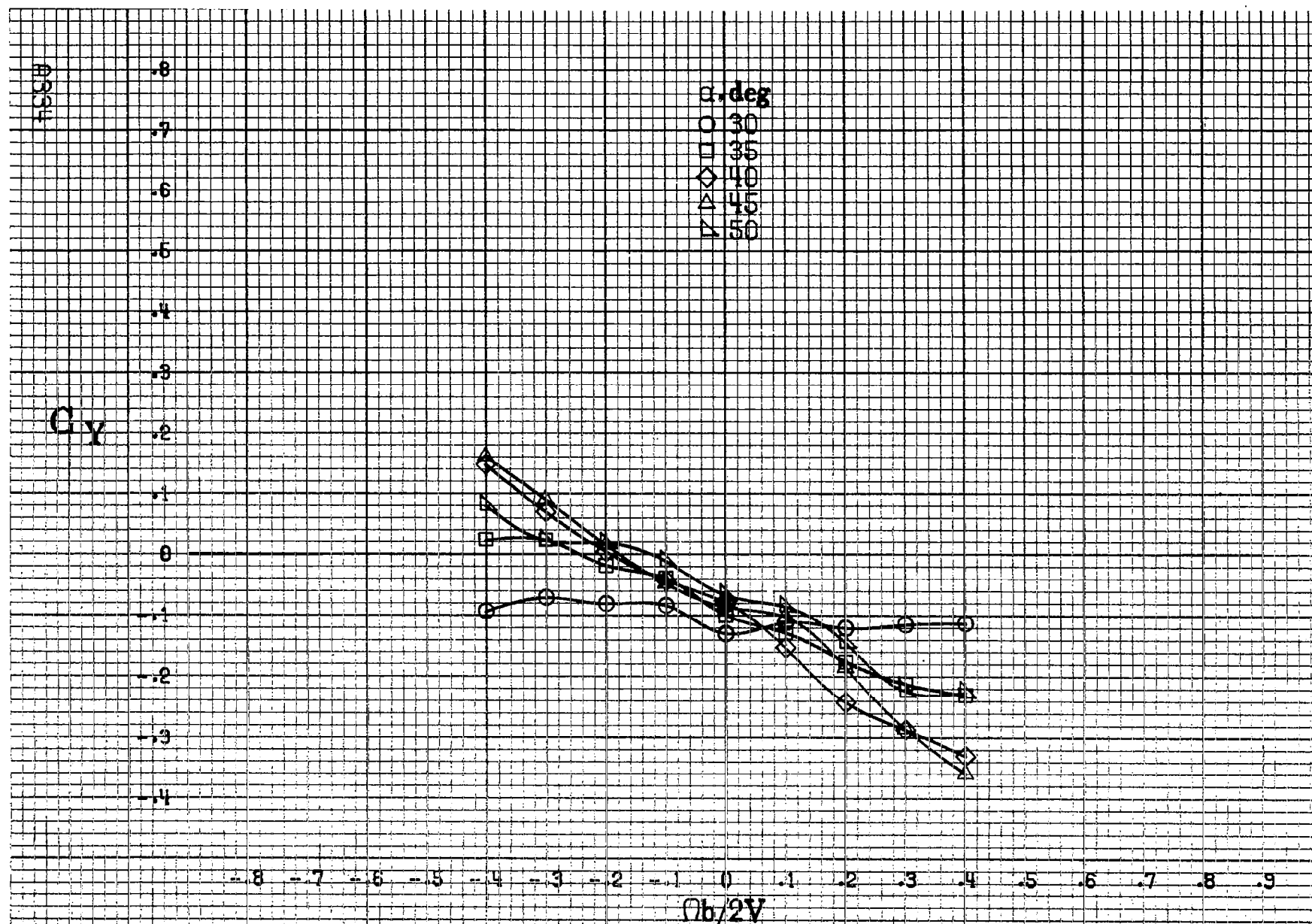
3.2
3.0
2.8
2.6
2.4
2.2
2.0
1.8
1.6
1.4
1.2
1.0
.8

-8 -7 -6 -5 -4 -3 -2 -1 0 -1 -2 -3 -4 -5 -6 -7 -8 -9

$b/2V$

(b) $\alpha=55$ to 90 deg, $SR=0$.
Figure A100.-Concluded.

4339



(a) $\alpha = 30$ to 50 deg, $SR = 0$.

Figure A101.-Effect of rotation rate and angle of attack on side-force coefficient for basic configuration. $\delta_e = 0^\circ$, $\delta_a = 20.0^\circ$, $\delta_d = 6^\circ$, $\delta_r = -15^\circ$, $\beta = 10^\circ$.

G_Y

α, deg

○ 55

□ 60

◇ 70

△ 80

▽ 90

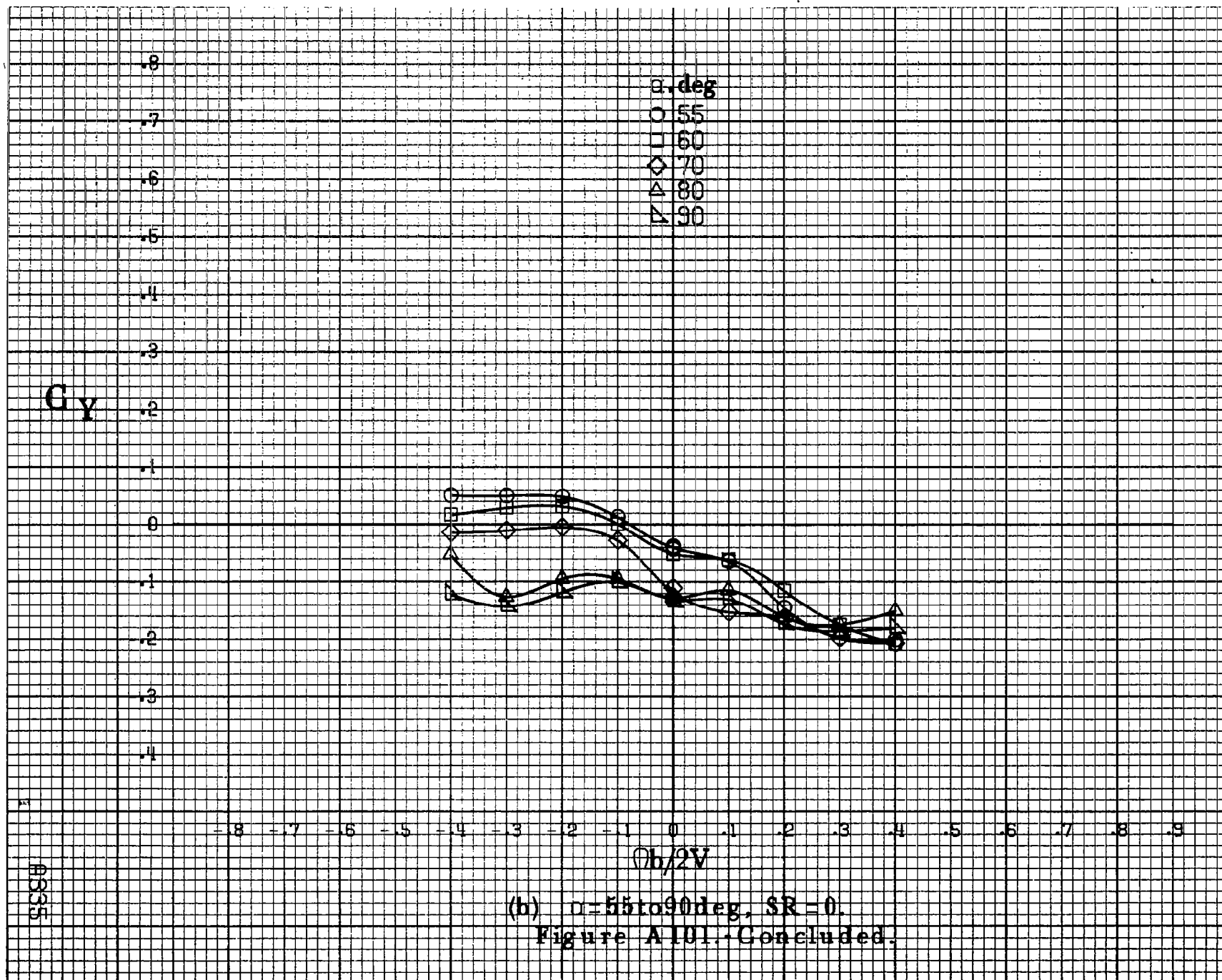
0335

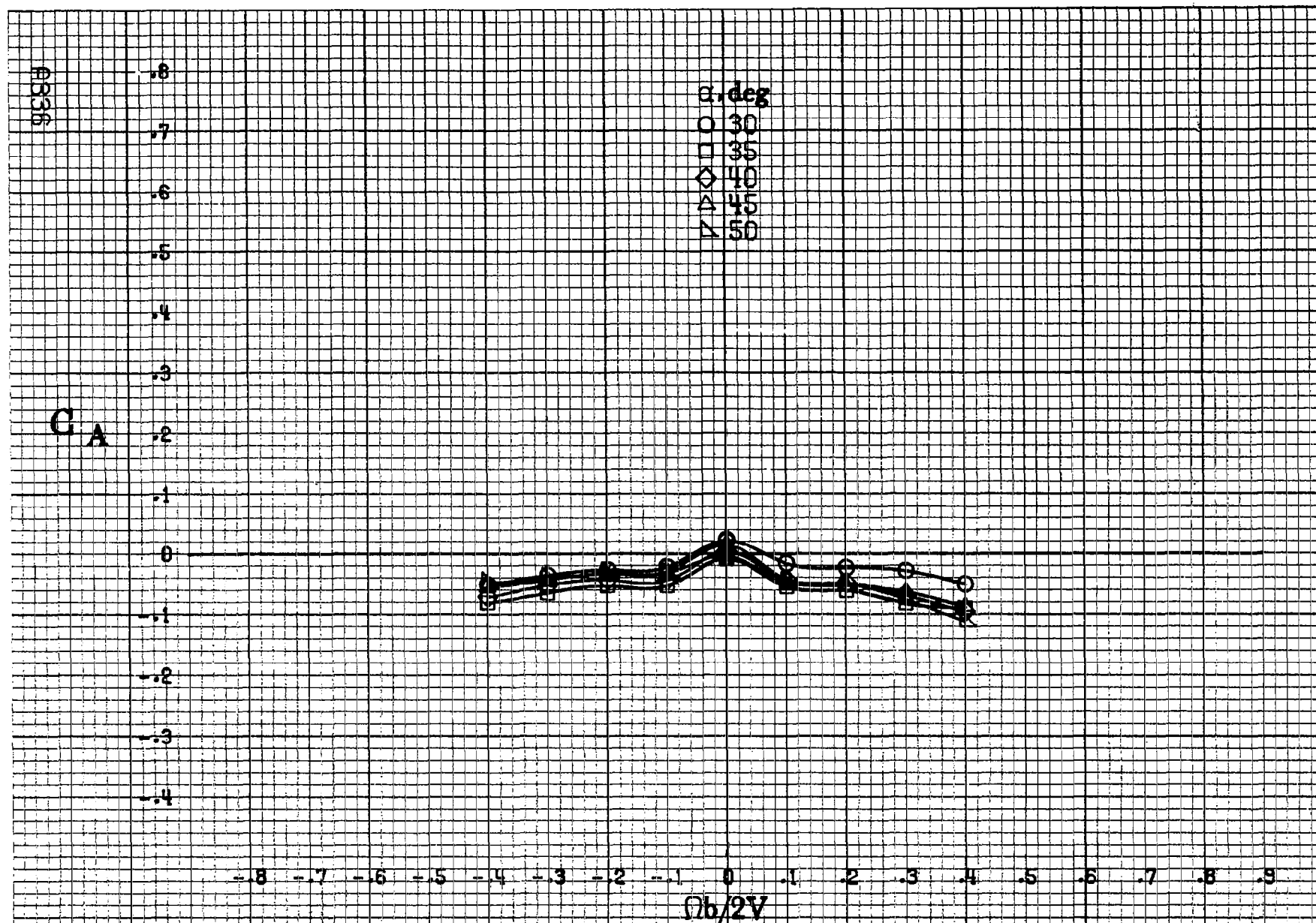
-0.8 -0.7 -0.6 -0.5 -0.4 -0.3 -0.2 -0.1 0 0.1 0.2 0.3 0.4 0.5 0.6 0.7 0.8 0.9

$Ob/2V$

(b) $\alpha = 55 \text{ to } 90 \text{ deg}, SR = 0.$

Figure A101.-Concluded.





(a) $\alpha=30$ to 50° , $SR=0$.

Figure A102.-Effect of rotation rate and angle of attack on axial-force coefficient for basic configuration. $\delta_c=0^\circ$, $\delta_s=20.0^\circ$, $\delta_d=6^\circ$, $\delta_r=-15^\circ$, $\beta=10^\circ$.

C_A

α, deg

○ 55

□ 60

◇ 70

△ 80

▽ 90

.8
.7
.6
.5
.4
.3
.2
.1
0
-.1
-.2
-.3
-.4

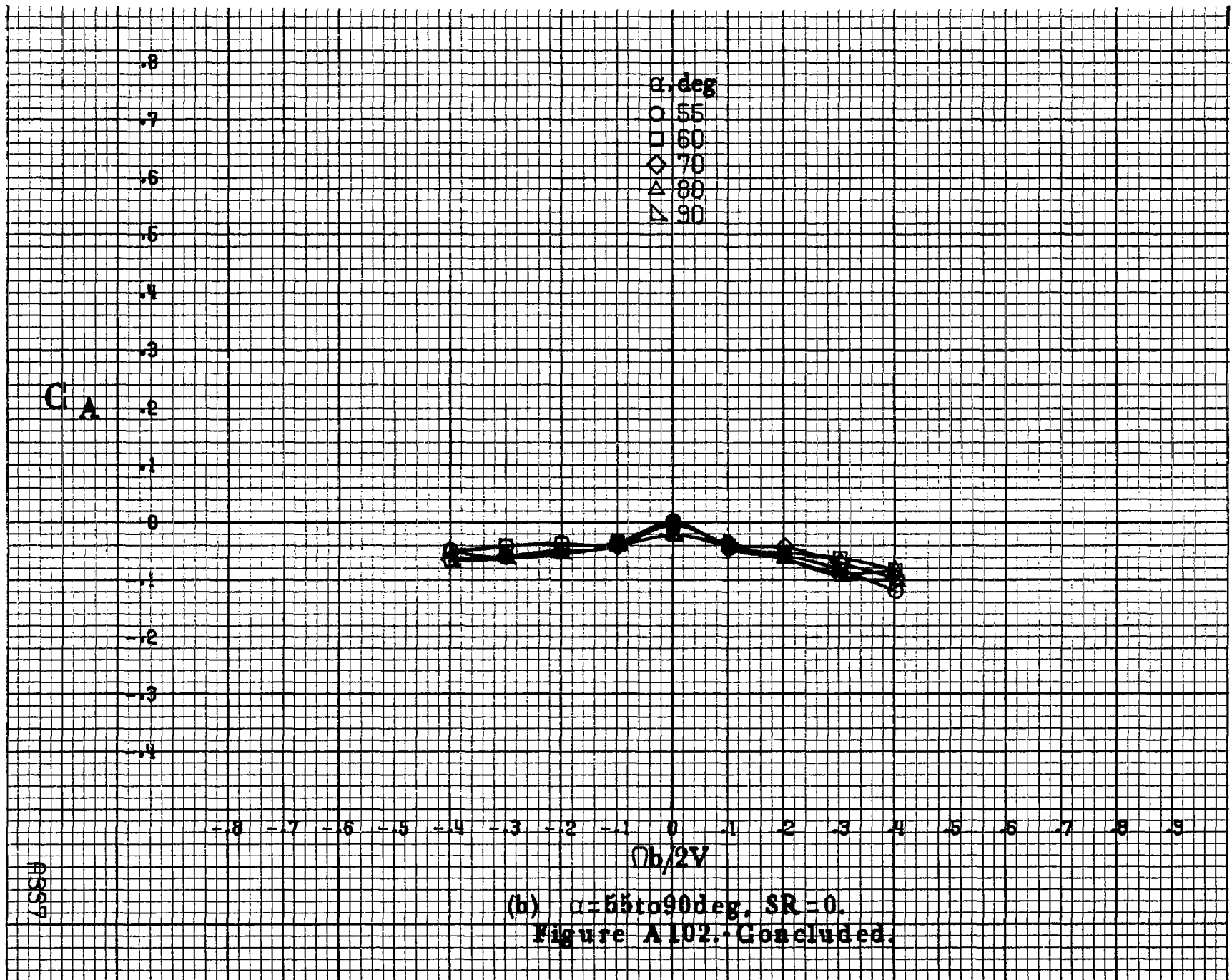
-.8 -.7 -.6 -.5 -.4 -.3 -.2 -.1 0 .1 .2 .3 .4 .5 .6 .7 .8 .9

$b/2V$

A357

(b) $\alpha = 55 \text{ to } 90 \text{ deg}$, $SR = 0$.

Figure A102.- Concluded.



0338

C_n

.08
.06
.04
.02
0
-.02
-.04
-.06
-.08
-.10
-.12
-.14
-.16

α, deg
○ 30
□ 35
◇ 40
△ 45
▽ 50

-8 -7 -6 -5 -4 -3 -2 -1 0 .1 .2 .3 .4 .5 .6 .7 .8 .9

$\Omega b/2V$

(a) $\alpha = 30 \text{ to } 50 \text{ deg}$, $SR = 0$.

Figure A103.-Effect of rotation rate and angle of attack on yawing-moment coefficient for basic configuration. $\delta_a = 0^\circ$, $\delta_s = -20.0^\circ$, $\delta_d = -6^\circ$, $\delta_r = 30^\circ$, $\delta = 0^\circ$.

C_n

.10
.08
.06
.04
.02
0
-.02
-.04
-.06
-.08
-.10
-.12
-.14

α, deg

○ 55
□ 60
◇ 70
△ 80
▽ 90

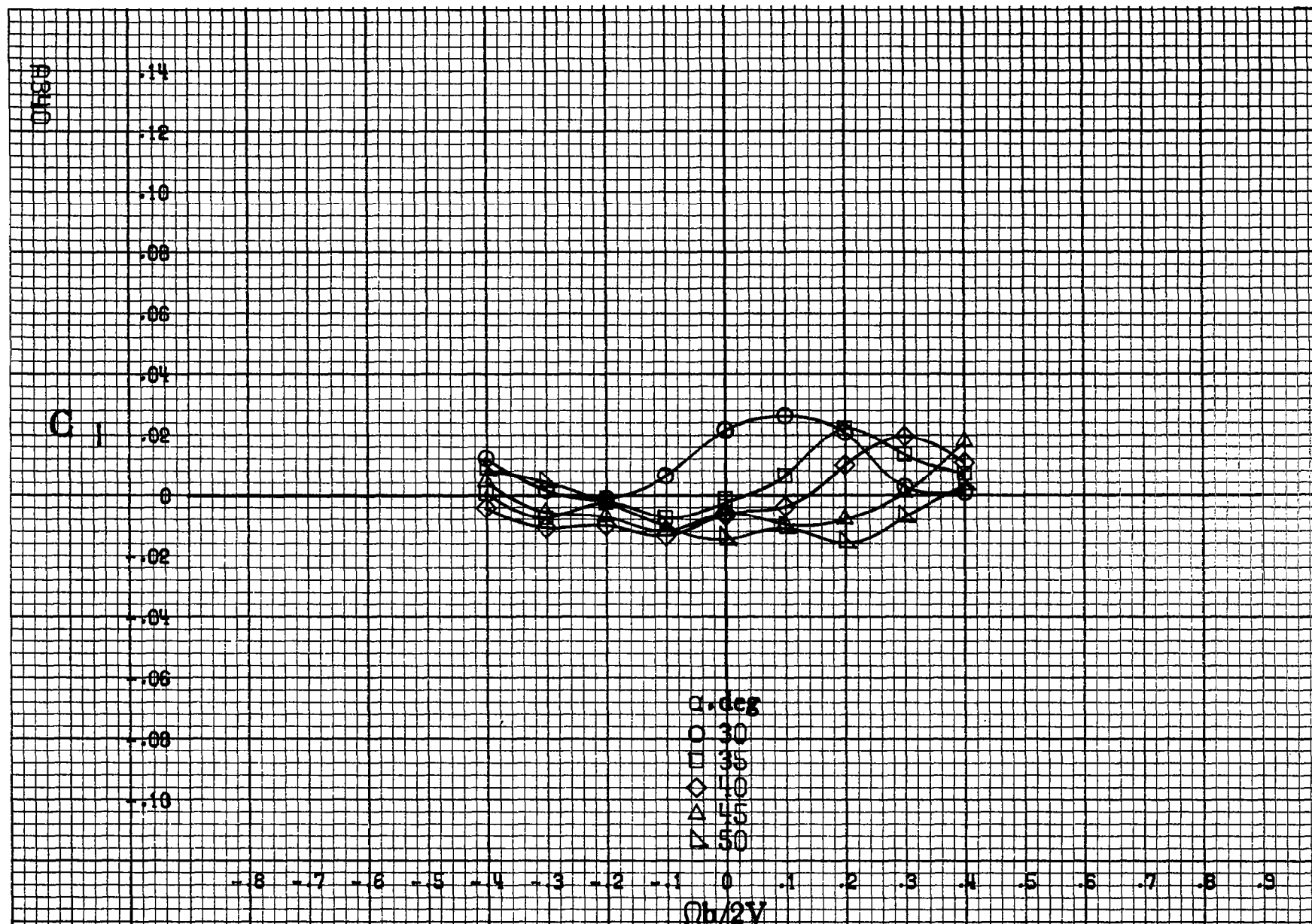
-8 -7 -6 -5 -4 -3 -2 -1 0 .1 .2 .3 .4 .5 .6 .7 .8 .9

$\Omega b/2V$

A339

(b) $\alpha=55$ to 90 deg, $SR=0$.

Figure A108.-Concluded.



(a) $\alpha = 30$ to 50 deg, $SR = 0$.

Figure A104.-Effect of rotation rate and angle of attack on rolling-moment coefficient for basic configuration. $\delta_e = 0^\circ$, $\delta_a = \pm 20.0^\circ$, $\delta_r = \pm 6^\circ$, $\delta_f = \pm 30^\circ$, $\delta = 0^\circ$.

C

A104.1

.14
.12
.10
.08
.06
.04
.02
0
-.02
-.04
-.06
-.08
-.10

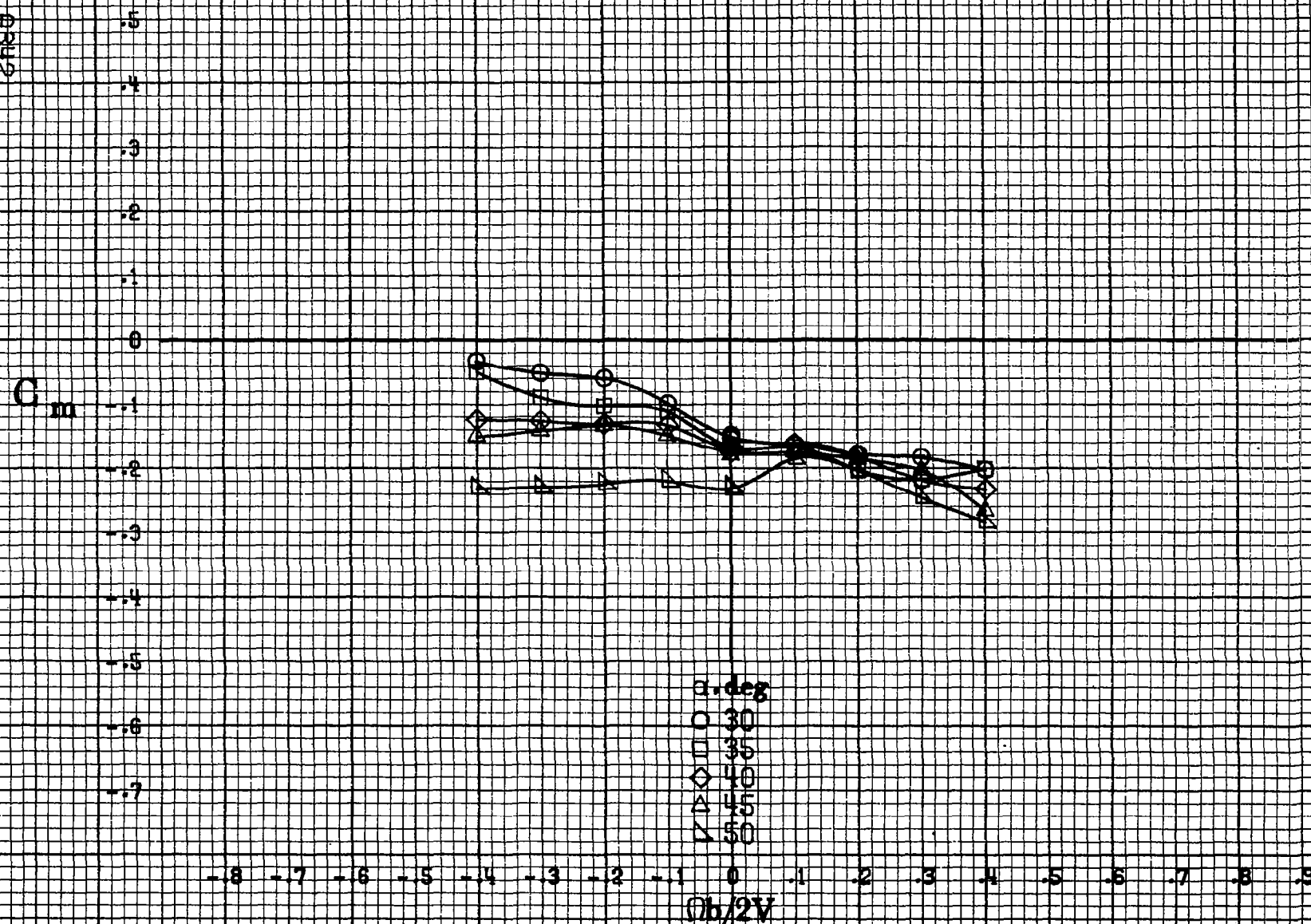
α, deg
○ 55
□ 60
◇ 70
△ 80
▽ 90

 $Ob/2V$

-.8 -.7 -.6 -.5 -.4 -.3 -.2 -.1 0 .1 .2 .3 .4 .5 .6 .7 .8 .9

(b) $\alpha = 55 \text{ to } 90 \text{ deg}, SR = 0.$
Figure A104.-Concluded.

AB42



(a) $\alpha = 30$ to 50 deg, $SR = 0$.

Figure A105.-Effect of rotation rate and angle of attack on pitching-moment coefficient for basic configuration. $\delta_e = 0^\circ$, $\delta_a = -20.0^\circ$, $\delta_s = -6^\circ$, $\delta_r = 30^\circ$, $\beta = 0^\circ$.

C_m

α, deg

○ 55

□ 60

◇ 70

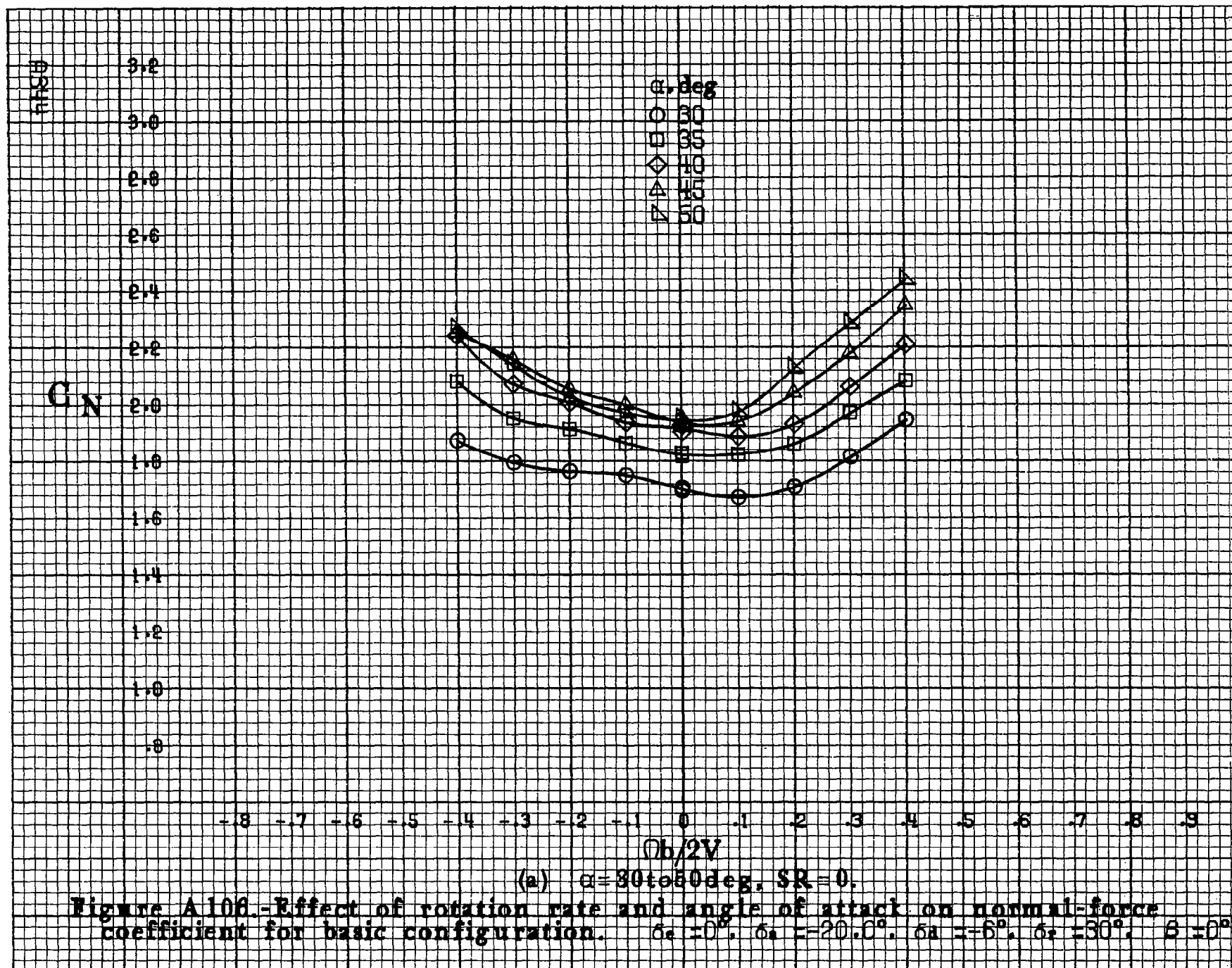
△ 80

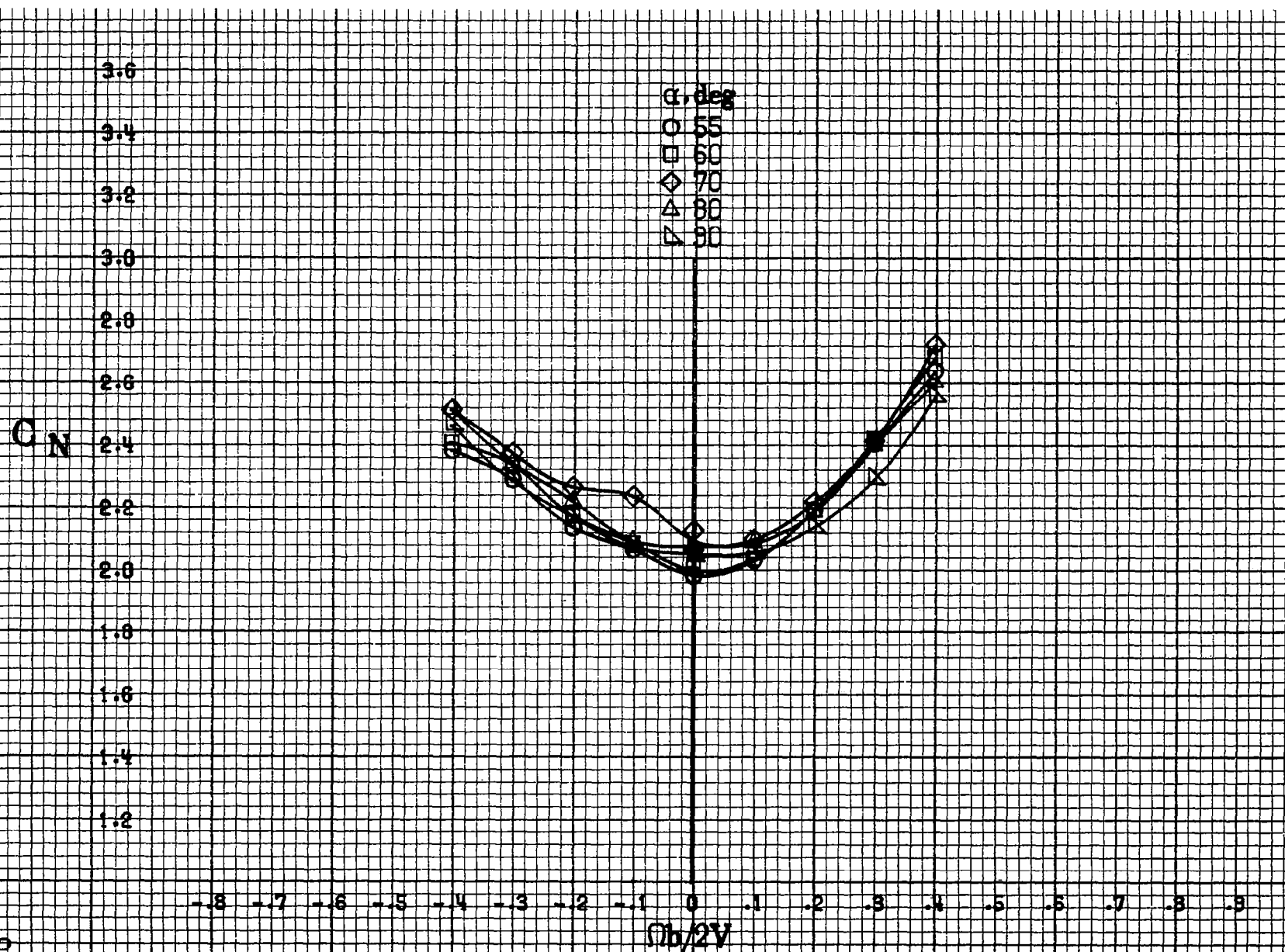
▽ 90

$\Omega b/2V$

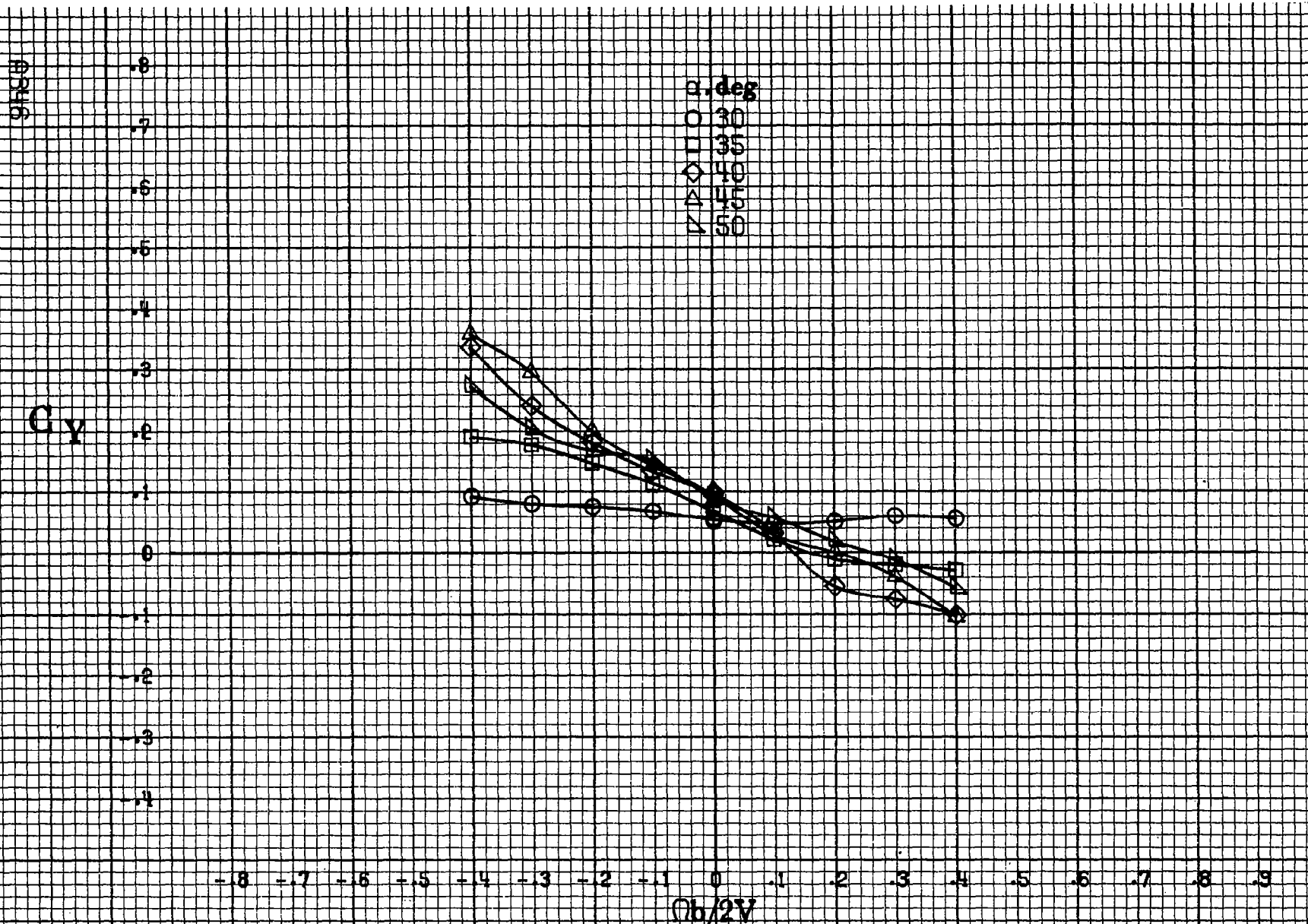
(b) $\alpha=55\text{ to }90\text{deg}, SR=0.$

Figure A105.-Concluded.





(b) $\alpha = 55$ to 90° , $SR = 0$.
Figure A106.-Concluded.



(a) $\alpha=30$ to 50° , $SR=0$.

Figure A107.-Effect of rotation rate and angle of attack on side-force coefficient for basic configuration. $\delta_e=0^\circ$, $\delta_a=-20.0^\circ$, $\delta_a=-6^\circ$, $\delta_r=30^\circ$, $\beta=0^\circ$.

C_y

α, deg
 ○ 55
 □ 60
 ◇ 70
 ▲ 80
 ▼ 90

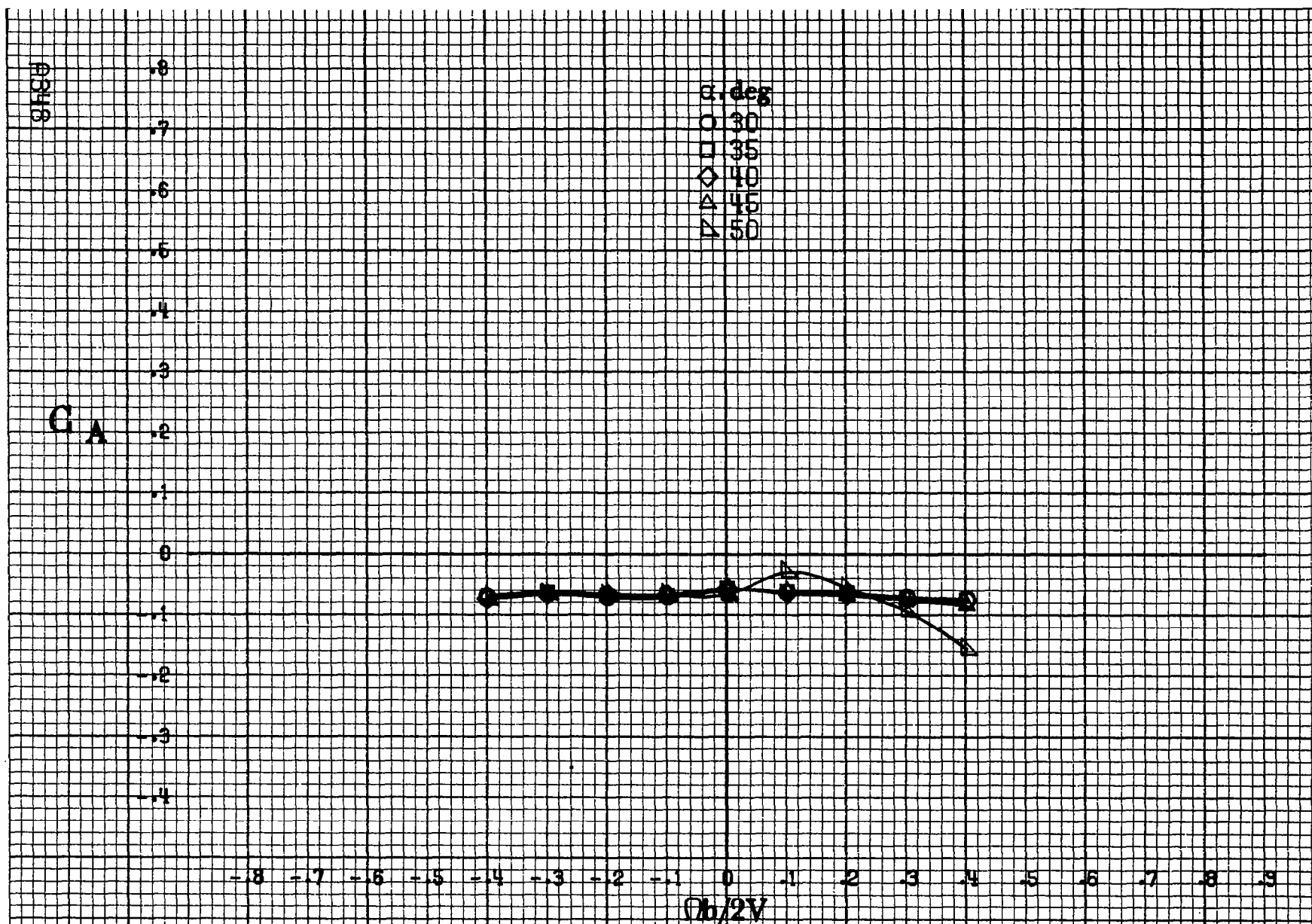
.8
.7
.6
.5
.4
.3
.2
.1
0
-.1
-.2
-.3
-.4

-.8 -.7 -.6 -.5 -.4 -.3 -.2 -.1 0 .1 .2 .3 .4 .5 .6 .7 .8 .9

$mb/2V$

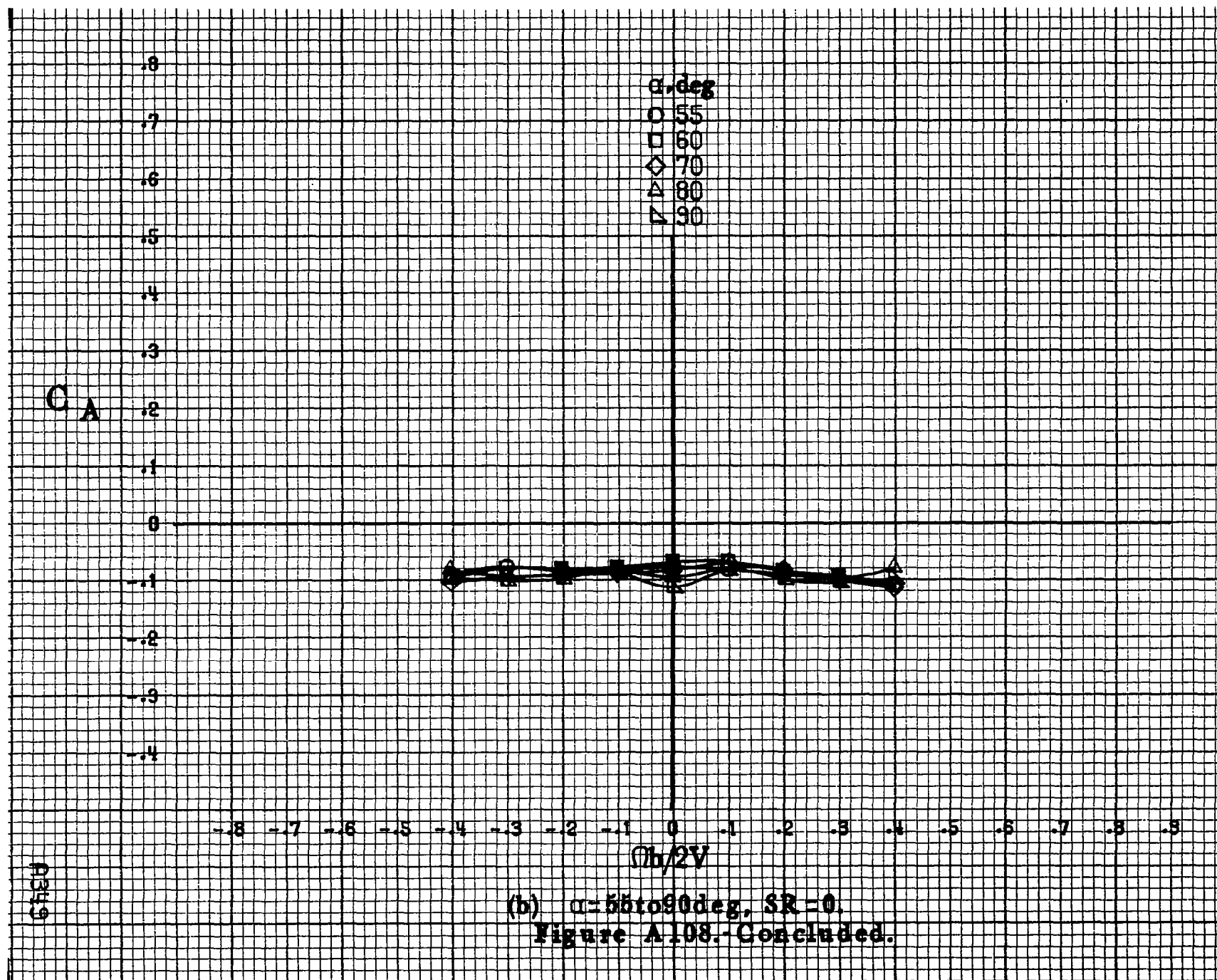
8347

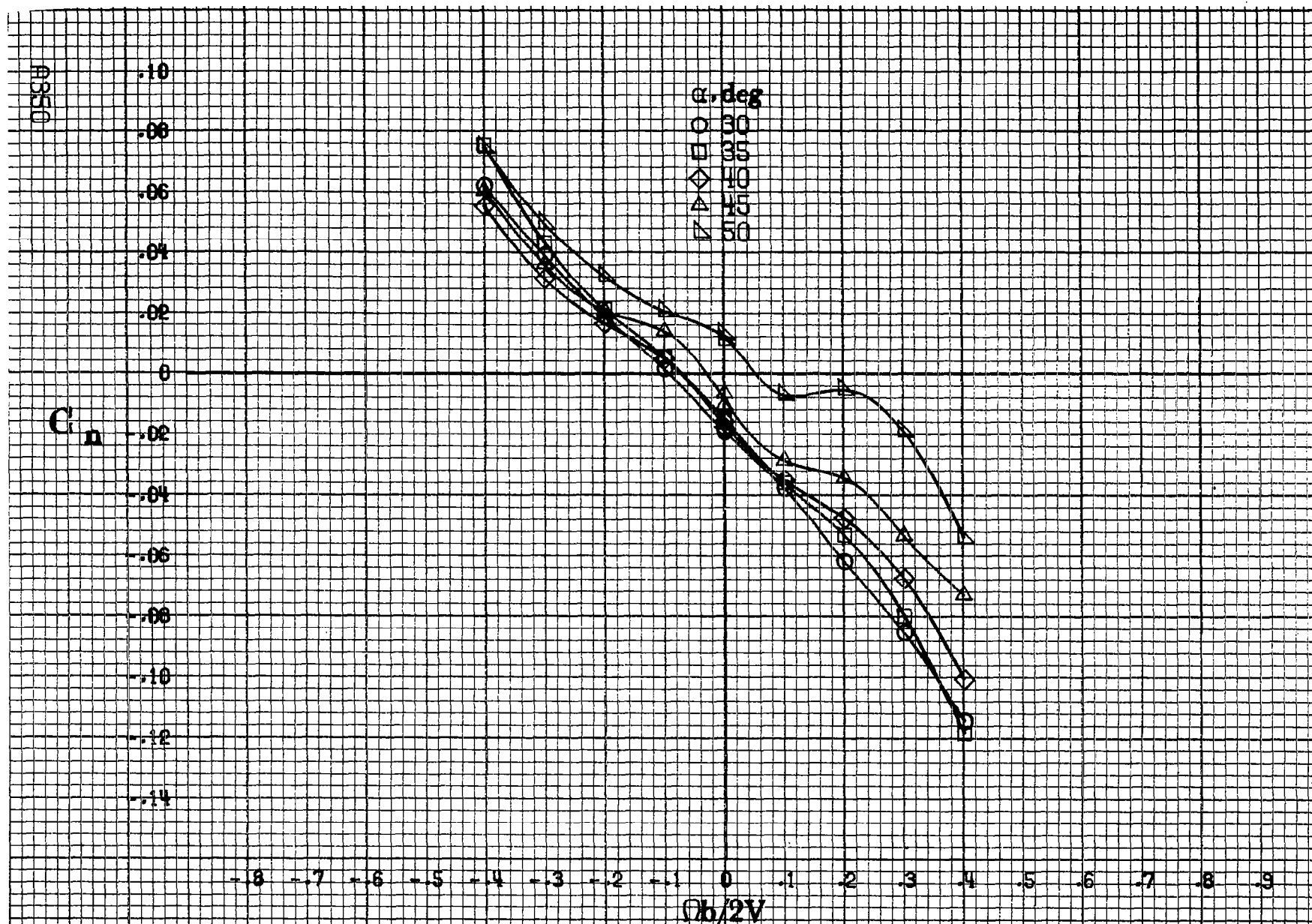
(b) $\alpha=55$ to 90 deg, $SR=0$.
 Figure A107.- Concluded.



(a) $\alpha = 30$ to 50 deg, $SR = 0$.

Figure A108.-Effect of rotation rate and angle of attack on axial-force coefficient for basic configuration. $\delta_e = 0^\circ$, $\delta_a = -20.0^\circ$, $\delta_{\bar{a}} = -6^\circ$, $\delta_r = 30^\circ$, $\theta = 0^\circ$.





(a) $\alpha=30$ to 50 deg, $SR=0$.

Figure A109.-Effect of rotation rate and angle of attack on yawing-moment coefficient for basic configuration. $\delta_e = 0^\circ$, $\delta_a = -20.6^\circ$, $\delta_d = -6^\circ$, $\delta_r = 30^\circ$, $\delta = 10^\circ$.

C_n

α, deg

- 55
- 60
- ◇ 70
- △ 80
- ▽ 90

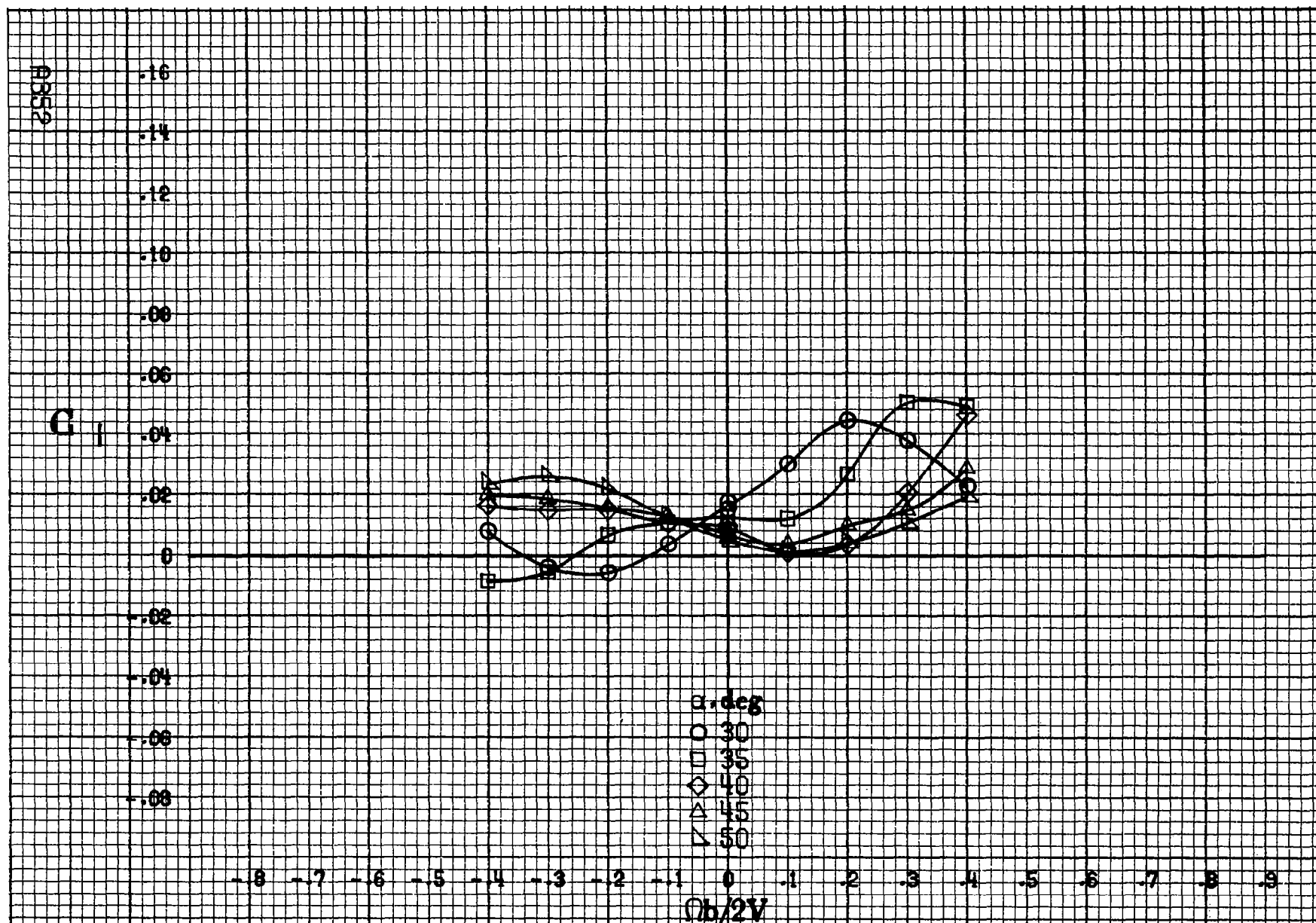
-0.8 -0.7 -0.6 -0.5 -0.4 -0.3 -0.2 -0.1 0 -0.1 -0.2 -0.3 -0.4 -0.5 -0.6 -0.7 -0.8 -0.9

$Ob/2V$

(b) $\alpha=55\text{ to }90\text{ deg, }SR=0.$

Figure A109--Concluded.

0351



(a) $\alpha = 30$ to 50° , $SR = 0$.

Figure A110.-Effect of rotation rate and angle of attack on rolling-moment coefficient for basic configuration. $\delta_s = 0^\circ$, $\delta_a = -20.0^\circ$, $\delta_1 = -6^\circ$, $\delta_2 = 30^\circ$, $\beta = 10^\circ$

C₁

.14
.12
.10
.08
.06
.04
.02
0
-.02
-.04
-.06
-.08
-.10

α, deg

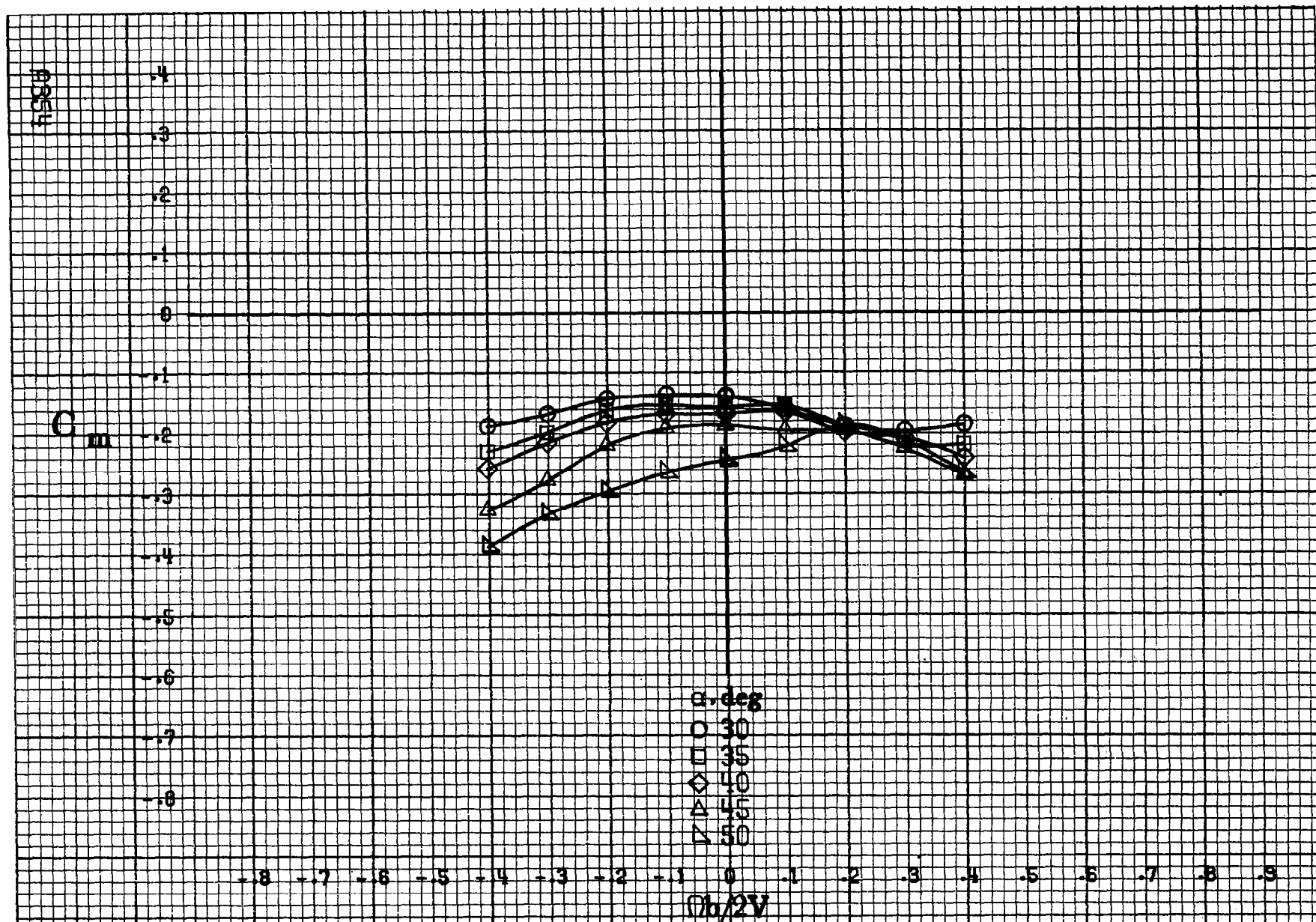
○ 55
□ 60
◇ 70
△ 80
▽ 90

-8 -7 -6 -5 -4 -3 -2 -1 0 .1 .2 .3 .4 .5 .6 .7 .8 .9

$Ob/2V$

(b) $\alpha = 55 \text{ to } 90 \text{ deg, } SR = 0.$
Figure A110. Concluded.

4355



(a) $\alpha = 30$ to 50° , $SR = 0$.

Figure A111.-Effect of rotation rate and angle of attack on pitching-moment coefficient for basic configuration. $\delta_a = 10^\circ$, $\delta_a = -20.0^\circ$, $\delta_a = -6^\circ$, $\delta_a = 30^\circ$, $\delta = 10^\circ$

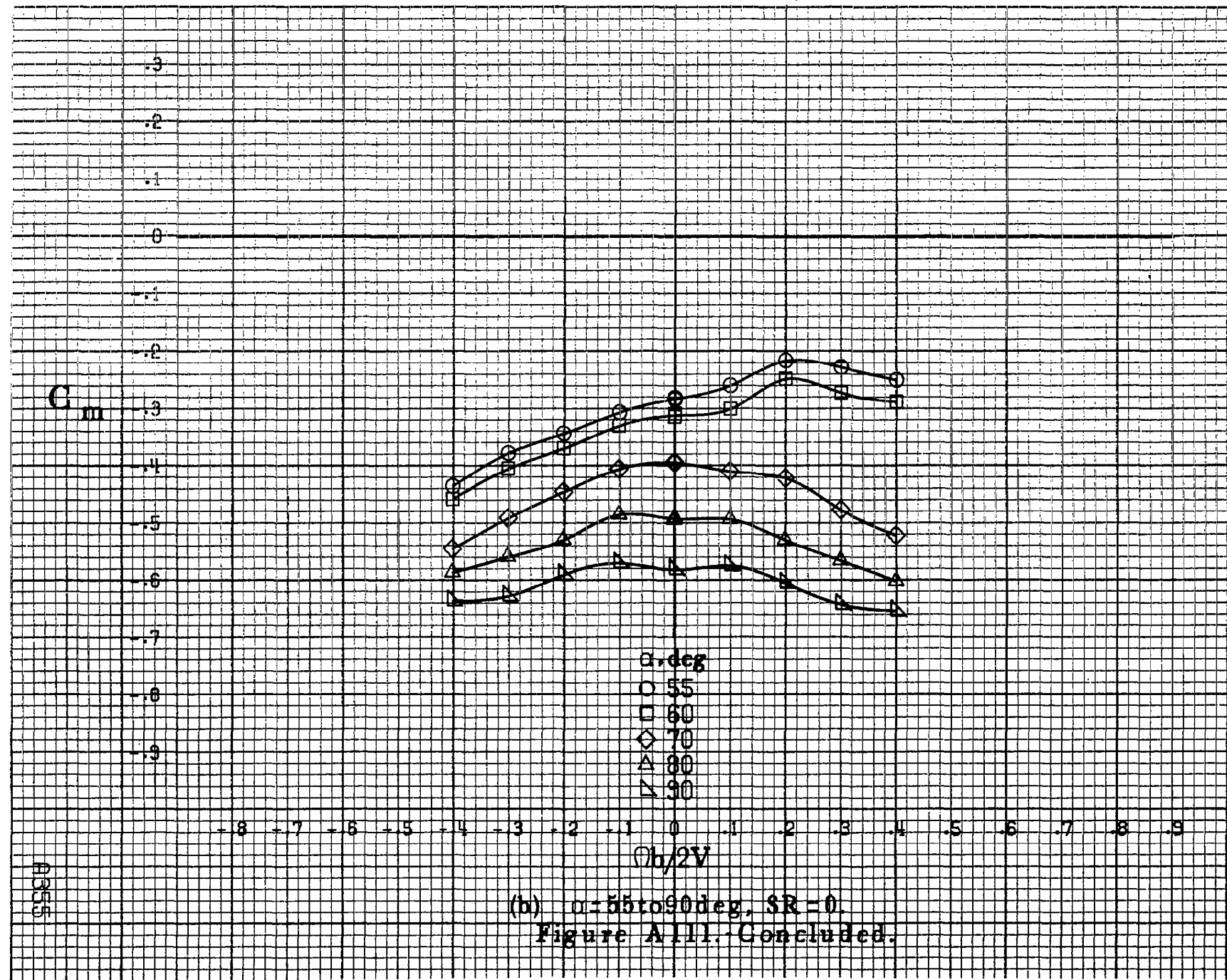
C_m

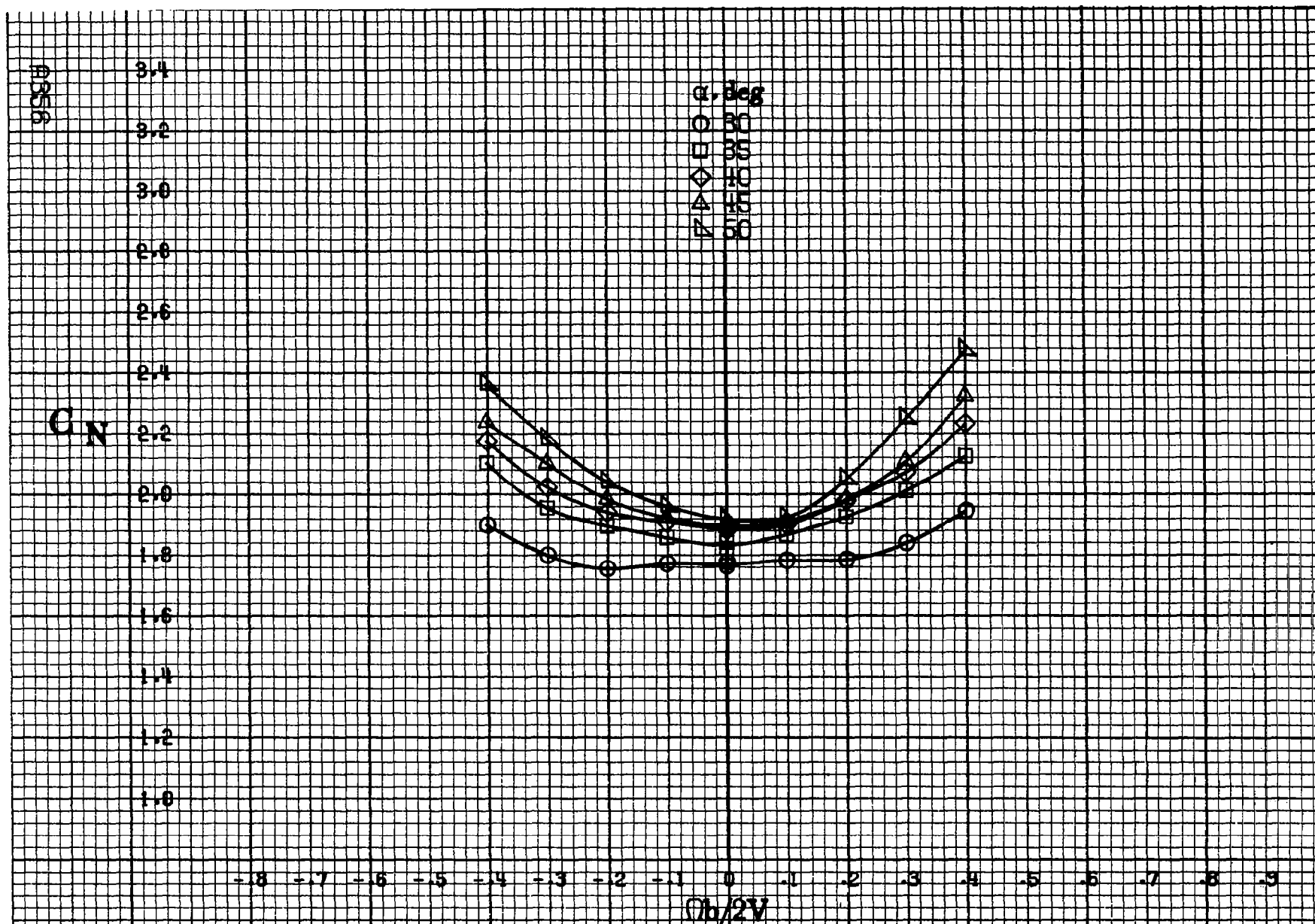
α, deg
 ○ 55
 □ 60
 ◇ 70
 △ 80
 ▽ 90

$\Phi h/2V$

(b) $\alpha = 55 \text{ to } 90 \text{ deg}, SR = 0$.
 Figure A111. Concluded.

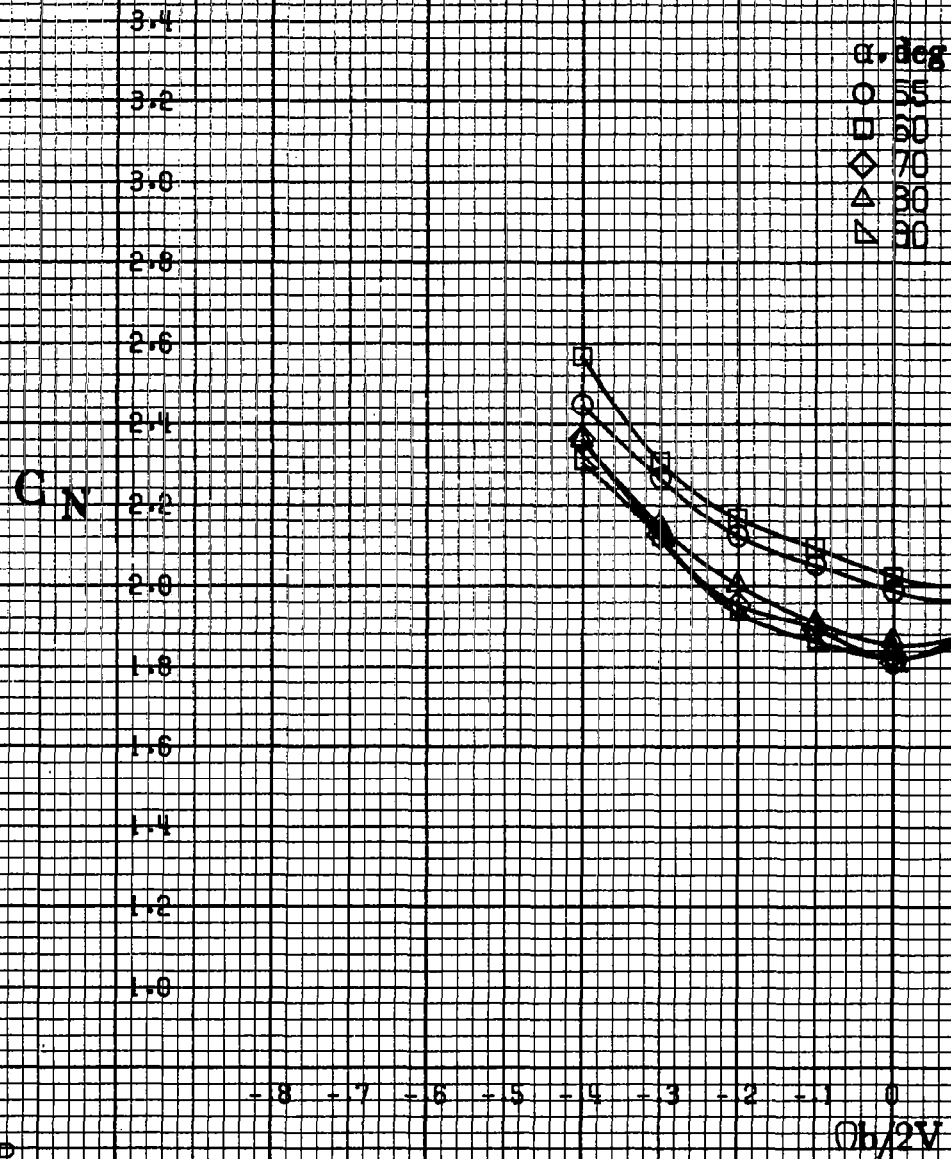
A355



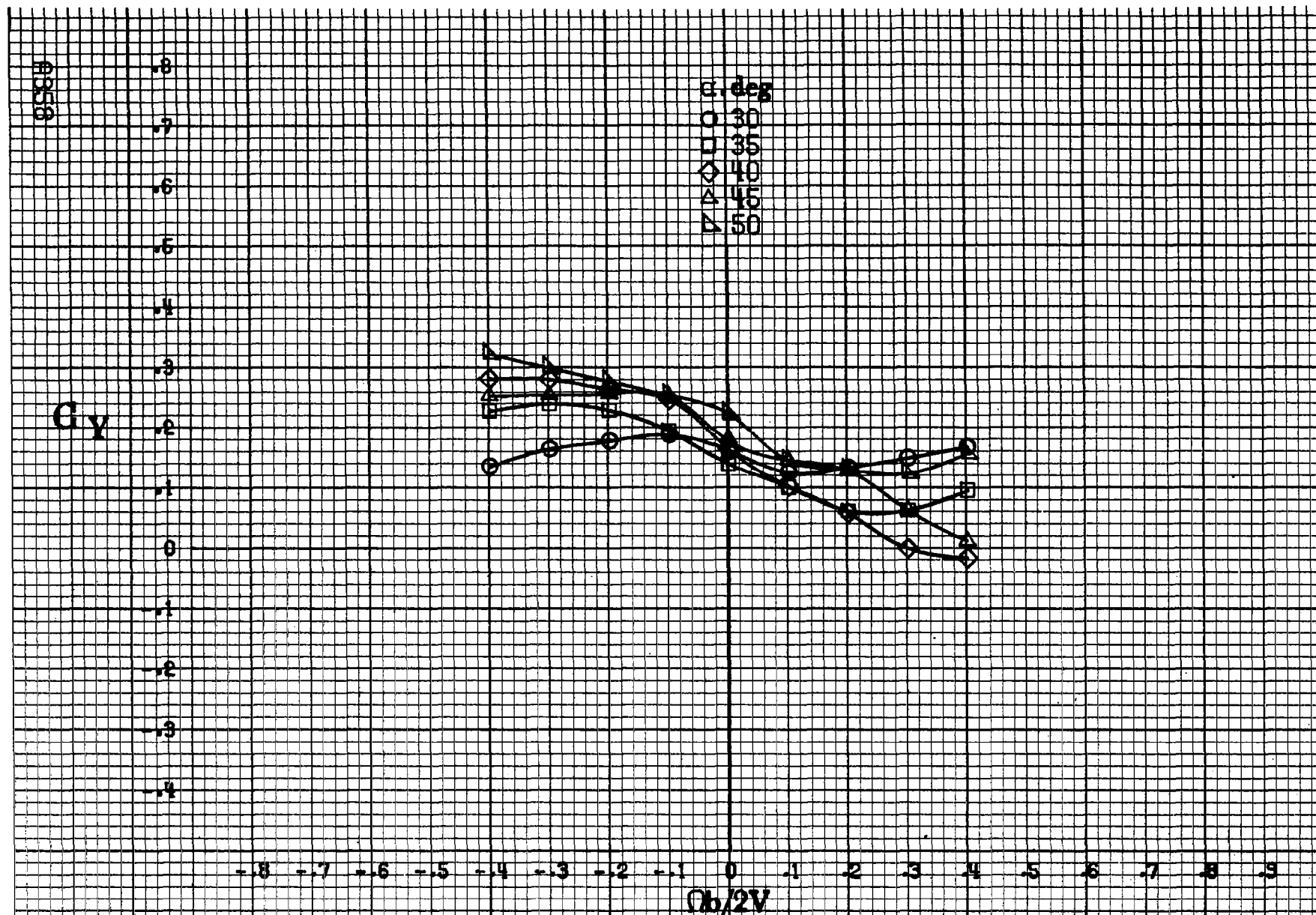


(a) $\alpha = 30$ to 50 deg, $SR = 0$.

Figure A112.-Effect of rotation rate and angle of attack on normal-force coefficient for basic configuration. $\delta_s = 0^\circ$, $\delta_a = -20.0^\circ$, $\delta_i = -6^\circ$, $\delta_r = 30^\circ$, $\delta = 10^\circ$

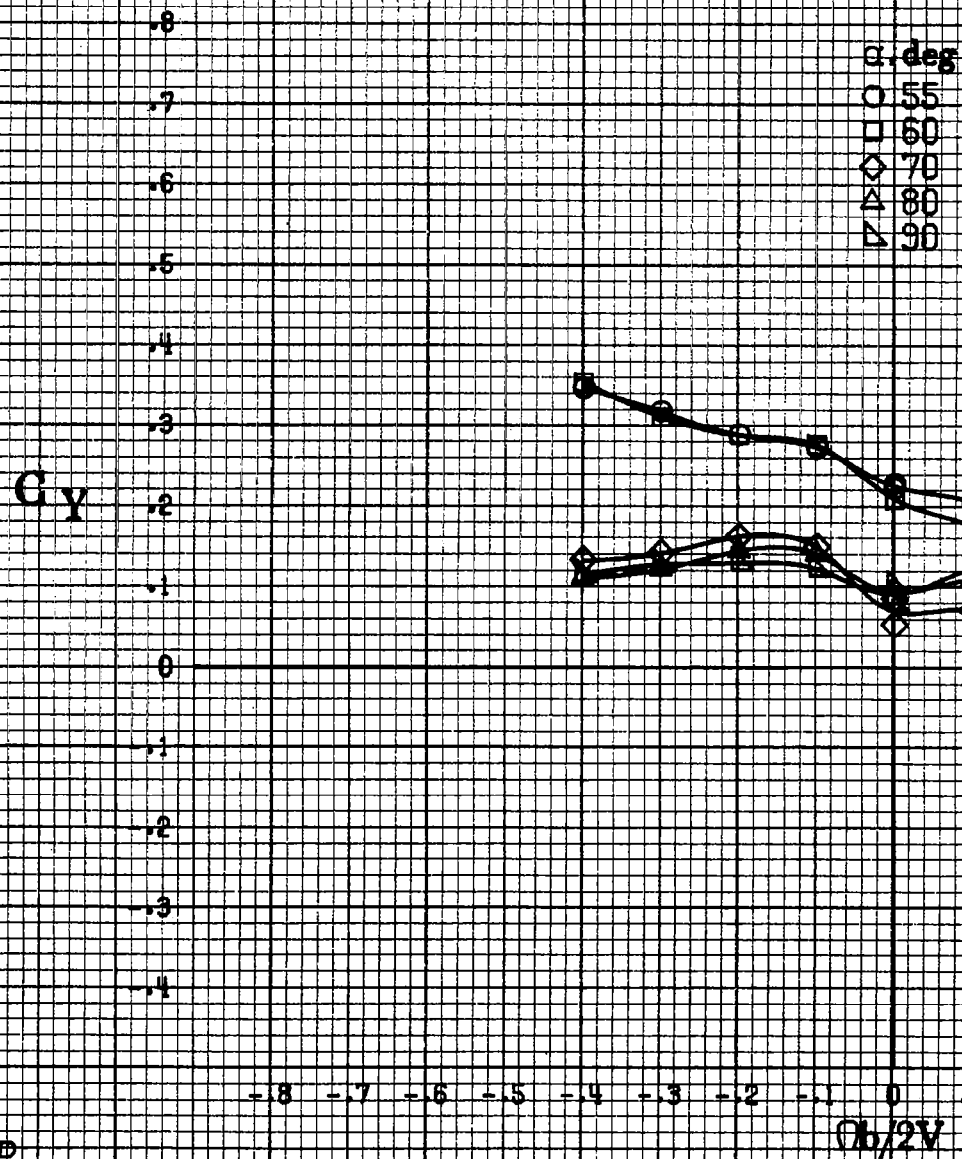


(b) $\alpha = 55$ to 90° , $SR = 0$.
Figure A112. Concluded.

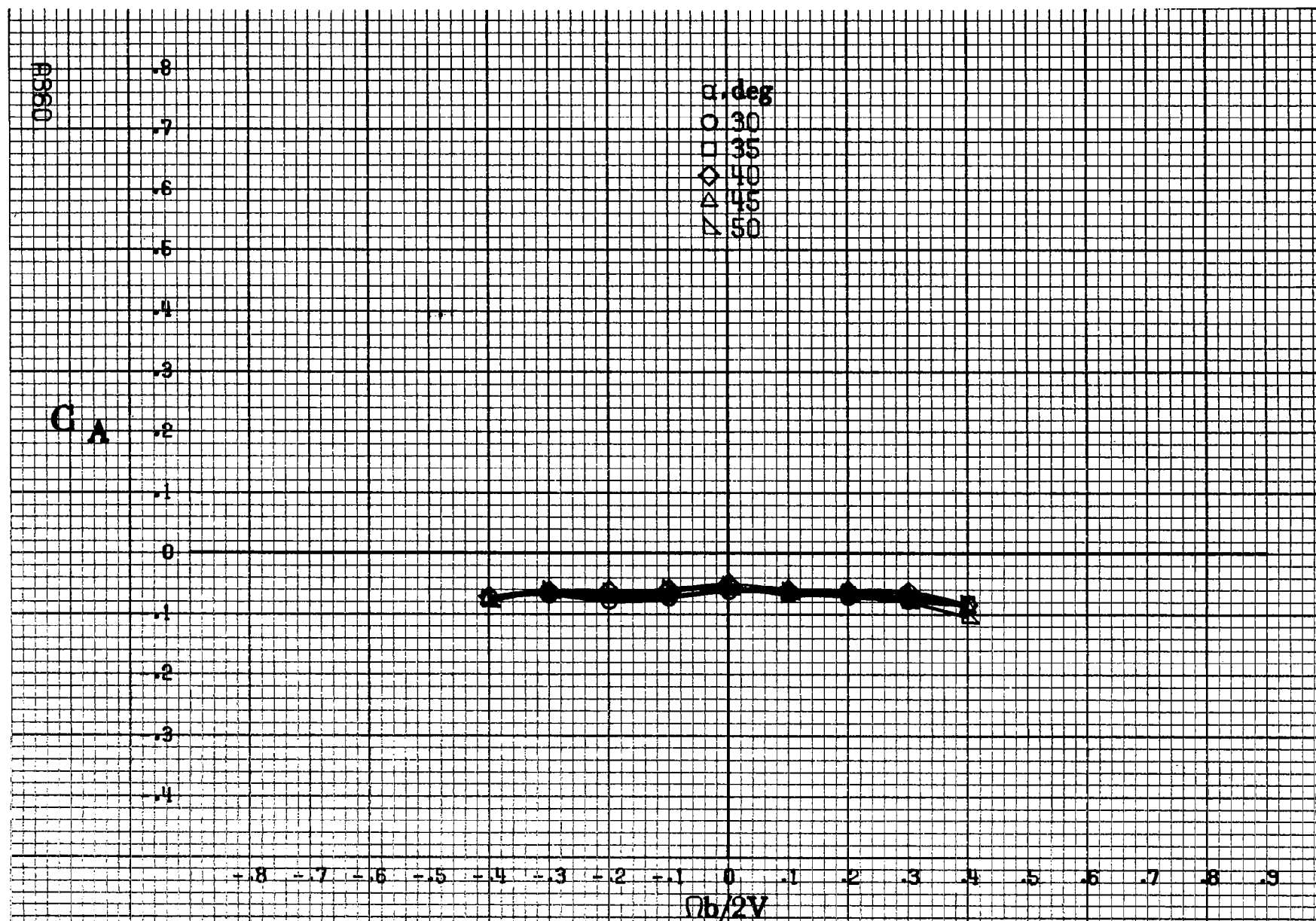


(a) $\alpha = 30$ to 50° , $SR = 0$.

Figure A118.-Effect of rotation rate and angle of attack on side-force coefficient for basic configuration. $\delta_e = 0^\circ$, $\delta_a = -20.0^\circ$, $\delta_s = -6^\circ$, $\delta_r = 30^\circ$, $\beta = 10^\circ$



(b) $\alpha = 55$ to 90 deg, $SR = 0$.
Figure A118. Concluded.



(a) $\alpha = 30$ to 50° , $SR = 0$.

Figure A114.-Effect of rotation rate and angle of attack on axial-force coefficient for basic configuration. $\delta_s = 0^\circ$, $\delta_a = -20.0^\circ$, $\delta_a = -6^\circ$, $\delta_r = 30^\circ$, $\beta = 10^\circ$.

C_A

α, deg
 ○ 55
 □ 60
 ◇ 70
 △ 80
 ▽ 90

.8
.7
.6
.5
.4
.3
.2
.1
0
.1
.2
.3
.4

-8 -7 -6 -5 -4 -3 -2 -1 0 .1 .2 .3 .4 .5 .6 .7 .8 .9

$\Omega b/2V$

(b) $\alpha = 55 \text{ to } 90 \text{ deg}, SR = 0$
 Figure A114. Concluded.

4361

1. Report No. NASA CR-3478		2. Government Accession No.		3. Recipient's Catalog No.	
4. Title and Subtitle F-15 ROTARY BALANCE DATA FOR AN ANGLE-OF-ATTACK RANGE OF 8° TO 90°				5. Report Date May 1982	
				6. Performing Organization Code	
7. Author(s) Billy Barnhart				8. Performing Organization Report No.	
				10. Work Unit No.	
9. Performing Organization Name and Address Bihrl Applied Research, Inc. 400 Jericho Turnpike Jericho, New York 11753				11. Contract or Grant No. NAS1-16205	
				13. Type of Report and Period Covered Contractor Report	
12. Sponsoring Agency Name and Address National Aeronautics and Space Administration Washington, DC 20546				14. Sponsoring Agency Code 505-43-13-01	
15. Supplementary Notes Langley Technical Monitor: James S. Bowman, Jr. Topical report					
16. Abstract Aerodynamic characteristics obtained in a rotational flow environment, utilizing a rotary balance located in the Langley spin tunnel, are presented in plotted form for a 1/12-scale F-15 airplane model. The configurations tested included the build-up of airplane components and the basic airplane with various control deflections. Data are presented for all configurations without analysis for an angle-of-attack range of 8° to 90°, and clockwise and counter-clockwise rotations covering an $\Omega b/2V$ range from 0 to 0.4. Selected configurations are presented over an extended $\Omega b/2V$ range from 0 to 0.9. Analysis of these data is presented in another report.					
17. Key Words (Suggested by Author(s)) Spinning Rotary balance High angle-of-attack wind tunnel data			18. Distribution Statement Unclassified - Unlimited Subject Category 02		
19. Security Classif. (of this report) Unclassified	20. Security Classif. (of this page) Unclassified	21. No. of Pages 376	22. Price* A17		